University of Strathclyde

Department of Civil Engineering

Numerical modelling of embankments on soft soils

by

Harald Krenn

A thesis presented

in fulfilment of the requirements

for the degree of Doctor of Philosophy

2008

Glasgow, 2008

Signed: 

Abstract

The design of embankments on soft soils requires a reliable estimate of deformations and stability of the embankment. Natural soft soils are structured materials, and as a consequence they exhibit anisotropy in their stress-strain-strength behaviour. The complex nature of soft soil makes it very difficult for designers to estimate deformations during construction and over time. The properties of very soft clays, silts and organic soils can be improved with deep mixing. Conventional design methods are very limited and do not account for the complex stress-strain-strength behaviour of the soft soil and/or the deep mixed soil. Numerical techniques, such as the finite element method provide a powerful tool, given the complex stress-strain-strength behaviour of the soft soil and/or the deep mixed material can be taken into account using advanced constitutive models.

The aim of the thesis is to investigate through 2D and 3D numerical simulations using advanced constitutive models the behaviour of embankments constructed on soft clays. In addition to embankments constructed on natural soils, embankments on deep mixed columns are studied. Simulations investigate the effect of anisotropy, apparent interparticle bonding and destructuration on the predicted response. It was found that ignoring anisotropy and destructuration leads to underprediction of surface settlements and horizontal displacements. However, although the effect of anisotropy was more pronounced than the effect of destructuration, the latter is needed to represent the measured remoulded and natural undrained strength in time. Constitutive models with a hyperbolic stress-strain relationship give a good representation of the non-linear behaviour of deep mixed material. 3D simulations of embankments on deep mixed columns showed that with increasing column spacing, differential settlements occur between column and soil. The results furthermore demonstrate that floating columns can be very effective in settlement reduction.

Glasgow, March 2008

Harald Krenn

Acknowledgments

First and foremost I would like to thank my supervisor Dr. Minna Karstunen for her support, interest and enthusiasm for my research. Without her guidance, assistance and freedom she gave me during the period of this work I would not have been able to produce the thesis in its present form. I am most grateful that the work i have carried out with her will be of great benefit for my future career in geotechnical engineering.

I would also like to thank Dr. Marcelo Sanchez for his co-supervision at the University of Strathclyde and Prof. Simon Wheeler at the University of Glasgow.

The research presented in this thesis was funded by scholarships from the Faculty of Engineering at the University of Strathclyde and the Faculty of Engineering at the University of Glasgow. I would also like to thank Donaldson Associates Ltd (UK) for their financial support in the first year of my study. The work was also sponsored by the Marie Curie Research Training Network on Advanced Modelling of Ground Improvement on Soft Soils (AMGISS) and Soft Clay Modelling for Engineering Practice (SCMEP) (Contracts MRTN-CT-2004-512120 and HPRN-CT-1999-00049). The funding and collaboration of all parties is gratefully acknowledged.

I would also like to thank Dr. Paul Bonnier from PLAXIS BV for his endless efforts in helping me to implement the user defined soil models into the PLAXIS 3D foundation code and for his help in other problems regarding the finite element code.

Many thanks to Andy Sloan and his team at Donaldson Associates Ltd. at the Glasgow office.

Special thanks go to my friends in the Department: Marcin, Urs, Daniela, Gráinne, Marco, Gavin, Gerry, Francis, Hossam and Kim for making my time special. With special thanks to Gráinne for reading and correcting the manuscript.

To my lovely girlfriend Heidi and my son Logan: I would like to thank you both for all the happiness in my life and all the energy you gave me to carry out this work.

To my family: thank you very much for your endless support and encouragement.

Contents

List of figures

List of tables

Chapter 1

Introduction

1.1 Background

Building embankments and other constructions on soft soil is still a major challenge for geotechnical engineers. In the past it was thought that most soft soils were unsuitable for construction due to the associated high construction costs and uncertainties in design. Nowadays designers and engineers can benefit from research on soft soils and the development of advanced constitutive models. Important characteristics of soft soils such as anisotropy, bonding and creep are now far better understood due to intensive research in these fields. When correctly applied these developments can contribute to safer and more economical designs than were produced in the past. The recent developments of advanced constitutive laws for soft clays have been made possible through intensive research work undertaken in the last two decades in soil mechanics laboratories all over the world. European research projects such as the SCMEP (Soft Clay Modelling in Engineering Practice) and the AMGISS (Advanced Modelling of Ground Improvement in Soft Soils) projects have provided major contributions to the recent advances in soft soil engineering and design.

Large settlements associated with soft soils create a lot of problems in foundation and infrastructure engineering. Consequently, ground improvement methods, such as deep mixing are greatly relied upon in such constructions. Deep mixing is a method which involves mixing lime and/or cement with the in-situ soft soil to create columnar rein-

forcements in the ground. The utilisation of deep mixed columns is often an economical and sustainable solution to improve the properties of very soft clays, silts and organic soils.

The conventional methods used to design embankments on soft soils with deep mixed columns are based on rigid-plastic solutions to predict ultimate loads and empirical (elastic) techniques to predict settlements. An alternative to the conventional design methods is given by numerical techniques, such as the finite element analysis. With the finite element method the true nature of the geometry of the problem and a realistic stress-strain-strength behaviour of the embankment, soil and deep mixed columns can be considered.

1.2 Aims and objectives

The overall aim of this thesis is to use the most advanced soil modelling expertise to simulate the stress-strain-strength behaviour of embankments constructed on soft soil or embankments constructed with deep mixed columns. The aim is to improve predictions and gain improved understanding of the behaviour of normally consolidated or slightly over-consolidated soft clays, and especially the pre-failure behaviour. Two cases of embankments have been considered. Embankments on natural soil and embankments constructed on deep mixed columns. The specific objectives are as follows:

Undrained shear strength: The undrained shear strength of the soft soil is not a soil constant as often assumed in conventional design. The strength is stress dependent and changes with consolidation. Undrained strength is also affected by the inherent and induced anisotropy, bonding and destructuration. This thesis presents a number of studies of laboratory test simulations and numerical simulations of embankments with different constitutive laws in which the influence of anisotropy and destructuration is studied to assess their influence on the prediction of the undrained strength in triaxial stress state and plane strain.

Settlements and horizontal displacements of embankments on natural ground: The objective is to assess the influence of anisotropy, bonding and destructuration of soft soils with different constitutive formulations on the settlement behaviour of embankments. The 2D finite element method is utilised to study the stress-strain behaviour of embankment on natural soft soils. The findings are used to give recommendations for numerical simulations of embankments and practical applications.

S-CLAY2S model: The findings of various studies and literature review are used to propose a new constitutive model. The S-CLAY2S model is an improved version of the S-CLAY1S model which accounts for large strain anisotropy, bonding and destructuration. A conditional plastic potential is introduced to enhance the model predictions of multistage triaxial tests simulations at different stress ratios η and the predictions of horizontal displacements below the slope of embankments.

Murro test embankment: The long term behaviour of the embankment is investigated through numerical studies. The results of the finite element simulations are compared with field monitoring results. The first part concentrates on the settlement predictions by using four different constitutive models. The second study examined the development of the undrained shear strength with time. The in-situ testing at Murro in 2001 below the embankment showed that in the top 7 m there had been an increase in the undrained strength, but below a depth of 7 m, the measured strength decreased. A parametric study is performed using an advanced constitutive model which accounts for anisotropy and destructuration to investigate the reduction in strength with time. Simulations show that is quantitatively possible to simulate this behaviour.

Embankments on deep mixed columns: The behaviour of embankments on deep mixed columns is examined through numerical studies. The observed stress-strain behaviour of deep mixed material is non-linear. 2D and 3D analyses using advanced constitutive models for the soil and the deep mixed material are employed during the research and predictions are compared to each other in terms of settlements and stresses to examine the suitability of the models to simulate embankments on deep

mixed columns. The influence of end bearing columns and floating columns on the settlement behaviour of the embankment and the stresses in the columns is examined. This improves our understanding of the soil column interaction.

The experience gained in the time of the research using the 2D and 3D PLAXIS finite element codes are used for a number of innovative and useful developments and improvements in terms of possible output.

1.3 Thesis Layout

In **Chapter 2** as an introduction, the main characteristics of soft soils are discussed. This begins with the definition of the terms anisotropy, destructuration and creep. Thereafter two well known constitutive models for soft soils are introduced and discussed. Special attention is given to the advanced constitutive models (S-CLAY1, S-CLAY1S and ACM), which account for anisotropy, destructuration and creep. This is followed by the introduction of two constitutive models which suitably present the stress-strain-strength behaviour of granular materials and deep mixed soils.

Chapter 3 discusses the construction of embankments on soft ground. In order to provide a better understanding of the problems encountered by building embankments on soft soils three case studies are reviewed and the field measurements are discussed. A review is presented regarding the modelling of embankments with the finite element technique. Factors such as basic boundary conditions and other important aspects of modelling embankments are considered.

In **Chapter 4** the importance of selecting the constitutive model which simulates the stress-strain-strength behaviour of the soft soil is evaluated. Two dimensional finite element analyses were carried out with five different constitutive models for soft soils. In particular it will be shown that accounting for anisotropy and/or destructuration is important when modelling embankments on soft soils. A special section is dedicated to a parametric study on the effect of the geometry on the results. In the last

part of this chapter a short study is undertaken to demonstrate the effect of anisotropy and destructuration on the bearing capacity of soft soils.

Chapter 5 discusses practical developments of the Fortran subroutines for the implementation of the user defined soil models into the PLAXIS 2D and 3D finite element code. Thereafter, a new plastic potential surface is proposed for the S-CLAY1S model to improve its predictive capabilities. In order to validate the proposed plastic potential, model simulations of drained triaxial tests on Murro clay are presented. This is followed by a two dimensional numerical simulation of an embankment constructed on soft soils using the new model.

Chapter 6 is dedicated to two-dimensional numerical simulations of the Murro test embankment. The numerical predictions are compared to measured vertical settlements, horizontal movements and pore pressures. Special attention is given to the measured and predicted undrained shear strength, prior to construction and 8 years after construction of the embankment. The results show that only a model that accounts for anisotropy and destructuration is able to predict the development of undrained strength as a function of time during primary consolidation.

Chapter 7 discusses the ground improvement method of deep mixing. First the basics of the method are introduced in terms of construction, design and material characteristics. The few case histories that can be found in the literature are reviewed. Furthermore, the stress-strain behaviour of the deep mixed material is described. Model simulations of drained triaxial tests of deep mixed Vanttila clay using different constitutive models are presented. Finally, the state-of-the-art in the two and three dimensional finite element modelling of deep mixed columns installed below embankments is reviewed.

Chapter 8 deals with finite element modelling of deep mixed columns below embankments. A two dimensional analysis of a single column and the surrounding soil (unit cell) demonstrates the influence of anisotropy and destructuration on the settlement behaviour of the soil column system. The column spacing is varied to study

the effect of spacing on the predicted settlements. Furthermore, a three dimensional model of a unit cell is developed and the simulations are compared to the axisymmetric unit cell. In order to model the true geometry of an embankment constructed on deep mixed columns, a full three dimensional model is then developed. The results by the three dimensional models are compared with the predictions of the 2D and 3D unit cell. In the last part of the chapter, simulations of an embankment constructed on floating columns are compared to end bearing columns by utilising full three-dimensional models. Both systems were found to be very effective in reducing the settlements although the predicted behaviour in terms of mechanisms are very different.

Chapter 9 summaries the main conclusions reached in the previous chapters and gives recommendations for future research.

1.4 Publications

This thesis has led to two journal publications and fourteen conference papers.

Journal publication I: Karstunen, M., Krenn, H., Wheeler, S.J., Koskinen, M. and Zentar, R. (2005). The effect of anisotropy and destructuration on the behaviour of Murro test embankment. Int. J. for Geomechanics (ASCE), 5(2), p 87-97

Journal publication II: Karstunen, M., Wiltafsky, C., Krenn, H., Scharinger, F. and Schweiger, H.F. (2006). Modelling the stress-strain behaviour of an embankment on soft clay with different constitutive models. International Journal of Numerical and Analytical Methods in Geomechanics 30(10): 953-982.

The journal publications and a list of the conference papers are appended at the end of this thesis.

Chapter 2

Constitutive modelling

This chapter gives an overview of the recent developments in the field of constitutive modelling of soft soils. The soft soil features of anisotropy, bonding and destructuration, and creep are introduced, and their importance in modelling realistically the stress-strain behaviour of soft soils is discussed. The second part of the chapter focuses on seven constitutive models and their formulations. The models covered in more detail are:

- Modified Cam Clay model (Roscoe & Burland, 1968)
- Soft Soil model (Brinkgreve, 2002)
- S-CLAY1 model (Wheeler et al. 2003)
- Multilaminate Model for Clay (Wiltafsky, 2003)
- S-CLAY1S model (Karstunen et al. 2005)
- Soft Soil Creep model (Vermeer et al. 1998)
- Anisotropic Creep model (Vermeer et al. 2007)

These models were selected in order to represent widely and extensively used constitutive models for soft soils, and models which incorporate recent developments and improvements in realistic modelling of stress-strain-strength behaviour of soft soils. The developers of the models enhanced their models while still keeping the formulations simple to allow the models to be potentially widely used in engineering practice on soft soils.

At the end of the chapter, two more constitutive models are introduced namely, the Hardening Soil model (Schanz, 1998) and the Matsuoka-Nakai Hardening Soil model (Benz, 2006). These models are not applied to simulate the soft soil behaviour but rather for granular type materials such as embankment fills, and for cohesive material such as dry crust and deep mixed material.

2.1 Background

Modern soil mechanics often uses the term "structure" to describe the state of the natural soil. Following Mitchell (1976) and Burland (1990), the term "structure" means the combination of fabric and interparticle bonding. Leroueil & Hight (2003) state that structure consists even of three components, the fabric, bonding and lithification. Lithification is the destruction of porosity through compaction and cementation.

Burland (1990) describes the fabric as the arrangement of the soil particles and the interparticle contacts. The fabric can be split into the arrangement caused by natural processes and any subsequent changes to fabric due to loading or unloading of the soil. The arrangement of the fabric by natural processes was developed during geological deposition and one dimensional consolidation. The anisotropy associated with these processes is referred to as induced anisotropy because the strains are a result of the applied stresses (Zdravkovic & Potts, 1999). During one dimensional consolidation in the field, the particles are arranged in such a way that the material properties are different in the horizontal and vertical directions. This type of phenomena is referred to as "cross-anisotropy". The anisotropy of the soil can also be seen in the yield characteristic of the natural soil. Diaz Rodriguez et al. (1992) summarised data from several natural soils and showed that anisotropy is demonstrated in an inclined yield surface in the p'-q -plane, where p' is the mean effective stress and q the deviatoric stress. During subsequent straining the particles are rearranged and the interparticle contacts will change. This causes the fabric anisotropy to change (Wheeler et al. 2003). Fabric anisotropy can influence the elastic and the plastic behaviour of natural soil. For engineering problems such as embankments on normally or slightly overcon-

solidated soft clays it is most likely that the plastic behaviour is dominant during loading of the soil. As discussed later, anisotropy of soft soils has an influence on the stress-strain-strength behaviour and is as such an important feature to be considered in the design of embankments and foundations on soft soils.

Burland (1990) and Leroueil & Vaughan (1990) indicated that most natural soils are bonded (microstructured). Furthermore Leroueil & Vaughan (1990) concluded that the microstructure of the soil is as important as any other initial state variable used to determine or describe a realistic stress-strain-strength behaviour. Development of bonds in the soil can be explained by several phenomena such as compression, cementation and thixotropy (Leroueil & Hight, 2003). However, the initial bonding of the soil can be destroyed during rearrangement of the fabric caused by straining. This process was termed destructuration by Leroueil et al. (1979). The term destructuration is often limited to describing the progressive damage of the bonds during plastic straining and this is the context in which it is used in this work. Most bonded soils can withstand higher yield stresses than the same unbonded material. It is best demonstrated in a one dimensional compression test (oedometer test) by comparing the compression curves of a natural sample with a reconstituted sample. Figure 2.1illustrates the type of behaviour that would be observed by comparing a good quality natural sample (with initial bonding) and a reconstituted sample (with no bonding) in an oedometer test. In the v-ln(p')-plane, where v is the specific volume and p' the mean effective stress, the reconstituted sample would follow the intrinsic compression line with the gradient λ_i. In contrast the natural sample would follow a line with a very low gradient until it reaches the yield stress, and the compression curve would then converge with the intrinsic compression line as bonding is gradually destroyed. The gradient λ of the virgin compression line of the natural sample at the onset of yielding is significantly greater than the gradient λ_i of the reconstituted sample and is also not constant.

The consolidation process is divided into two parts, namely primary consolidation and secondary consolidation. During primary consolidation the excess pore pressure

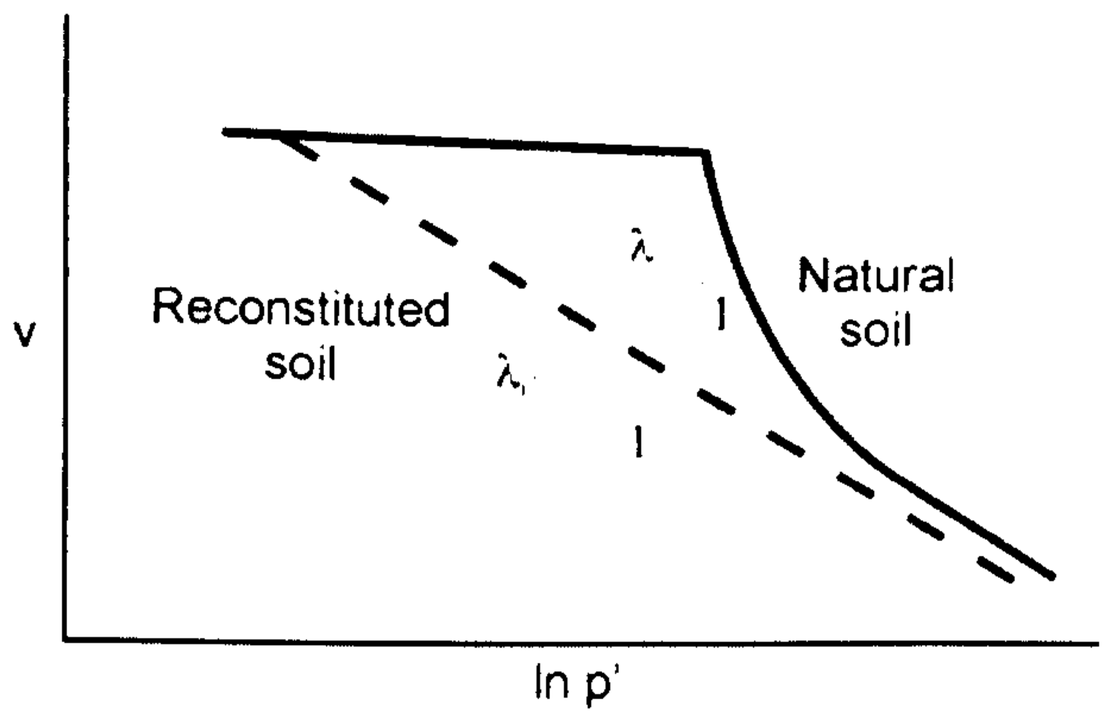

Figure 2.1: Influence of destructuration during oedometric loading

built up during undrained loading is transferred as load onto the soil skeleton, whereas during secondary consolidation all stresses are constant but a soil specimen under constant vertical stress would continue to strain. This process is also referred to as creep. Continuous settlements caused by creep can impose damage to embankments if not considered accordingly in the geotechnical design.

2.2 Modelling anisotropy, destructuration and creep

2.2.1 Modelling anisotropy

Tavenas & Leroueil (1977) indicated that the yield surface of natural clay samples is inclined and has an elliptical shape in the t'-s-plane. It was also found that the yield surface expands with time due to creep. Tavenas & Leroueil (1977) proposed a time dependent model with an inclined yield surface to represent initial anisotropy. The centre of the ellipse in their model is orientated around a stress path following the K_0 consolidation line (K_0 is the earth pressure at rest). Sekiguchi & Ohta (1977) proposed a constitutive model for normally consolidated clays which permits consistent descriptions of both stress induced anisotropy and time dependent stress-strain response of the soil. Diaz-Rodriguez (1992) reported similar findings to Tavenas & Leroueil (1977) based on laboratory tests on several clays.

The understanding of initial and plastic strain induced anisotropy led to the developments of enhanced constitutive model formulations. Nova (1986), Dafalias (1986 & 1987), Davies & Newson (1993) and Whittle and Kavvadas (1994) used a standard elasto-plastic framework to incorporate initial and plastic strain induced anisotropy. Rotational or distortional hardening laws were used in these models to describe the change in anisotropy with plastic straining. Di-Prisco et al. (1993) were the first to apply a kinematic (translational) hardening law instead of a rotational hardening law. Some of the models above, using a rotational hardening law to simulate development or erasure of the fabric, assume that the changes in the inclination of the yield surface is entirely related to the development of plastic volumetric strains. The role of plastic shear strains is ignored in the process of the change of fabric due to loading. Wheeler et al. (2003) argue that this seems physically unlikely and can cause unrealistic predictions under certain stress path directions. The MIT-S1 model (Pestana and Whittle, 1999) and the S-CLAY1 model (Wheeler et al. 2003), introduced later in this chapter, are some of the first to link the evolution and erasure of the fabric to both plastic volumetric and shear strains. The MIT-S1 is a very complex general model for uncemented materials such as sands and is also capable of representing stiff clays. The S-CLAY1 formulation is far less complex and the model itself was developed in parallel with an intense experimental programme which investigated the stress-strain behaviour of soft clays.

An alternative to the standard elasto-plastic framework is to account for plastic induced anisotropy by utilising the ideas of the so-called multilaminate framework. Zienkiewicz & Pande (1977) originally proposed the multilaminate framework for rocks and later it was extended to clays by Pande and Sharma (1983) and Pietruszczak and Pande (1987). In the multilaminate framework a number of contact planes is associated with each integration point. The orientation of the contact planes is defined by an integration rule. On each contact plane a local microscopic stress-strain relationship is formulated. The global strains are obtained by numerical integration of the plastic strains from each sampling plane and the global elastic strain. Wiltafsky (2003) developed an elasto-plastic constitutive model for soft clays (MMC) formu-

lated using the multilaminate framework. The MMC model is introduced in Section 2.4.2.

2.2.2 Modelling bonding and destructuration

Gens and Nova (1993) developed a very simple idea to incorporate initial bonding and destructuration in an isotropic elasto-plastic critical state model. In addition to the yield surface of the natural material, a second yield surface was introduced. The second yield surface, the so-called "intrinsic yield surface", represents the material with all its bonds destroyed or removed. It has the same shape as the natural yield surface but is different in size. The bonding effect of the natural material is expressed through the ratio of the different sizes of the yield surfaces. The increase in the size of the intrinsic yield surface is linked to the plastic volumetric strains via a hardening law. A second hardening law, often referred to as the destructuration law, is used to relate the reduction of the bonding effect to the plastic strains. The influence of the plastic volumetric and plastic shear strains on the rate of destructuration is controlled via two soil constants.

In the last two decades several different models have been developed and published, which incorporate bonding and destructuration. The main difference in the models is the form of the destructuration law and the reference model used for unbonded material. Rouainia and Muir Wood (2000) presented a "bubble" model based on the model by Al-Tabbaa and Muir Wood (1989). The destructuration law used in their model is similar to Gens and Nova (1993). The bonding effect due to the offset of the yield curve from the origin leads to "some" anisotropy of the yield surface of the natural material for large strains. The large strain anisotropy disappears once the bonding has been completely destroyed as the yield surface becomes isotropic. This assumption is in contrast to experimental evidence (Koskinen et al. 2002). The clay fabric orientation continues to change or evolve regardless if bonding is present or not. Kavvadas and Amorosi (2001) published another type of very complex "bubble" model accounting for bonding and destructuration. This model does not use an explicit intrinsic yield surface as presented by Gens and Nova (1993). Baudet and Stallebrass

(2004) introduced another model based on the 3-SKH model (Stallebrass and Taylor, 1997). The destructuration law implemented in their model is similar to Rouainia and Muir Wood (2000) but the influence of the plastic volumetric and plastic shear strain on the rate of the destructuration is assumed to be equal. Gajo and Muir Wood (2001) published a further development of a destructuration law by the inclusion of a third soil constant as an extra exponent. Many models incorporating bonding and destructuration put emphasis on small strain behaviour and ignore initial and plastic strain induced anisotropy, which is very important when modelling soft soil. A model which accounts for bonding and destructuration, in addition to plastic anisotropy is the S-CLAY1S model (Koskinen et al. 2002a, Karstunen et al. 2005). The formulation of this model is introduced in Section 2.5.

2.2.3 Modelling creep

Malvern (1951) introduced the so-called "overstress theory", which was an innovative development compared to the simplified rheological models and the isotache concept proposed by Suklje (1957). The one dimensional constitutive model developed by Malvern (1951) was enhanced by Perzyna (1966) to a three dimensional version. The 3D model forms the basis of most time dependent constitutive models developed in recent years. It assumes that the time dependent behaviour in the elastic region is negligible. Two yield surfaces form the basic principles of the model: a so-called static yield surface, similar to the yield surfaces used in the concept of time independent plasticity, and a dynamic yield surface which is bigger in size than the static yield surface. The area between the two yield surfaces is often referred to as the viscoplastic regime (Liingaard et al. 2004). The overstress is defined as the distance between the static and the dynamic yield surface. The total strain predicted is composed of an elastic part and a visco-plastic part. The formulation of the models using the overstress theory are mainly based on the isotropic Cam Clay model (Sekiguchi and Otha, 1977) or on the Modified Cam Clay model (Adachi and Okano, 1974; Nova, 1984). In the overstress models a change in the stress state does generate a visco-plastic strain. In contrast, true creep models such as proposed by Vermeer and Neher (1999) and Yin

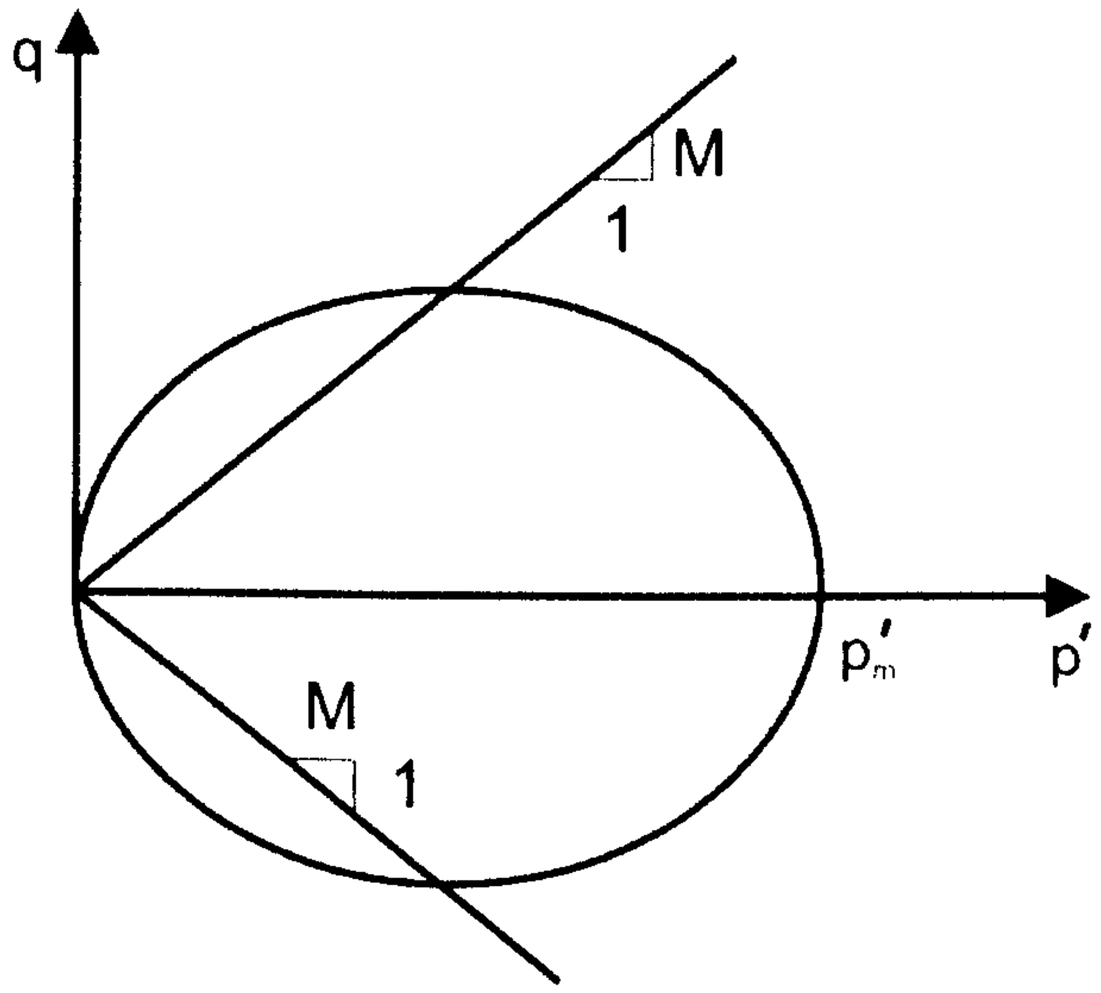

Figure 2.2: Modified Cam Clay model in the p'-q stress space

and Graham (2006) predict creep stresses even if there is no change in the stress state. Neher et al. 2003 demonstrated the importance of accounting for time dependent behaviour very sucessfully in the "Pisa Tower Stability" case study through the application of an isotropic creep model. As mentioned earlier initial and large strain anisotropy has an influence on the stress-strain-strength behaviour and as such it is also important to account for it in constitutive models for soft soils. Vermeer et al. (2007) published an advanced version of an isotropic creep model, the anisotropic creep model (ACM). The ACM uses rotated yield surfaces based on the S-CLAY1 model (Wheeler et al. 2003) as normal consolidation surfaces. The formulation of the ACM can be found in Section 2.6.2.

2.3 Isotropic models

2.3.1 Modified Cam Clay model (MCC)

Roscoe and Burland (1968) introduced the isotropic MCC model, which is a variation of the original Cam Clay model published by Roscoe and Schofield (1963). The model uses the Critical State concept as the failure criteria. The Critical State Soil Mechanics (CSSM) concept was developed by Roscoe et al. (1968) and Schofield and

Wroth (1968). The basis of the concept was formed mostly on tests conducted on reconstituted isotropically consolidated clay samples. Therefore no influence of the microstructure is present and the model thus describes an ideal soil. A soil element which has reached a critical state stress ratio η continues shearing under constant volume. M is the value of the stress ratio η=q/p' at critical state. It is assumed that the deformation at failure is so large that any possible bonding which might have led to cohesion is broken down. The concept also defines a limited area where the soil behaviour is elastic. The elastic domain is limited by the yield surface. MCC uses an ellipse to describe the yield surface in a p'-q plane (triaxial) stress space. The yield function of the MCC model is defined by:

$$f = q^2 - M^2 p'(p'_m - p') = 0 \qquad [2.1]$$

where the state parameter p'_m defines the size of the yield surface in the p'-q stress space. The state parameter p'_m can be evaluated based on the vertical pre-consolidation stress. The MCC model uses a Drucker-Prager criterion as the failure criteria with an associated flow rule. For numerical analysis the model has to be formulated in general stress space. The model was first generalised by Roscoe and Burland (1968). They assumed that the yield surface and the plastic potential in the deviatoric plane is a circle as shown in Figure 2.3 and hence the failure surface is a circle in the deviatoric plane. It is known that a circle does not present very well the failure conditions of soils in the deviatoric plane. In general stress space the yield surface has the form of an ellipsoid. Changes in size of the yield surface is solely related to plastic volumetric strains $d\varepsilon_v^p$ as defined by:

$$dp'_m = \frac{v p'_m d\varepsilon_v^p}{\lambda - \kappa} \qquad [2.2]$$

where v is the specific volume, κ is the gradient of the (pre-yield) elastic swelling line in the v:ln(p') plane. λ is the gradient of the post-yield compression curve for a constant η stress path in the v:ln(p') plane. MCC assumes isotropic elastic behaviour for stress states inside the yield surface.

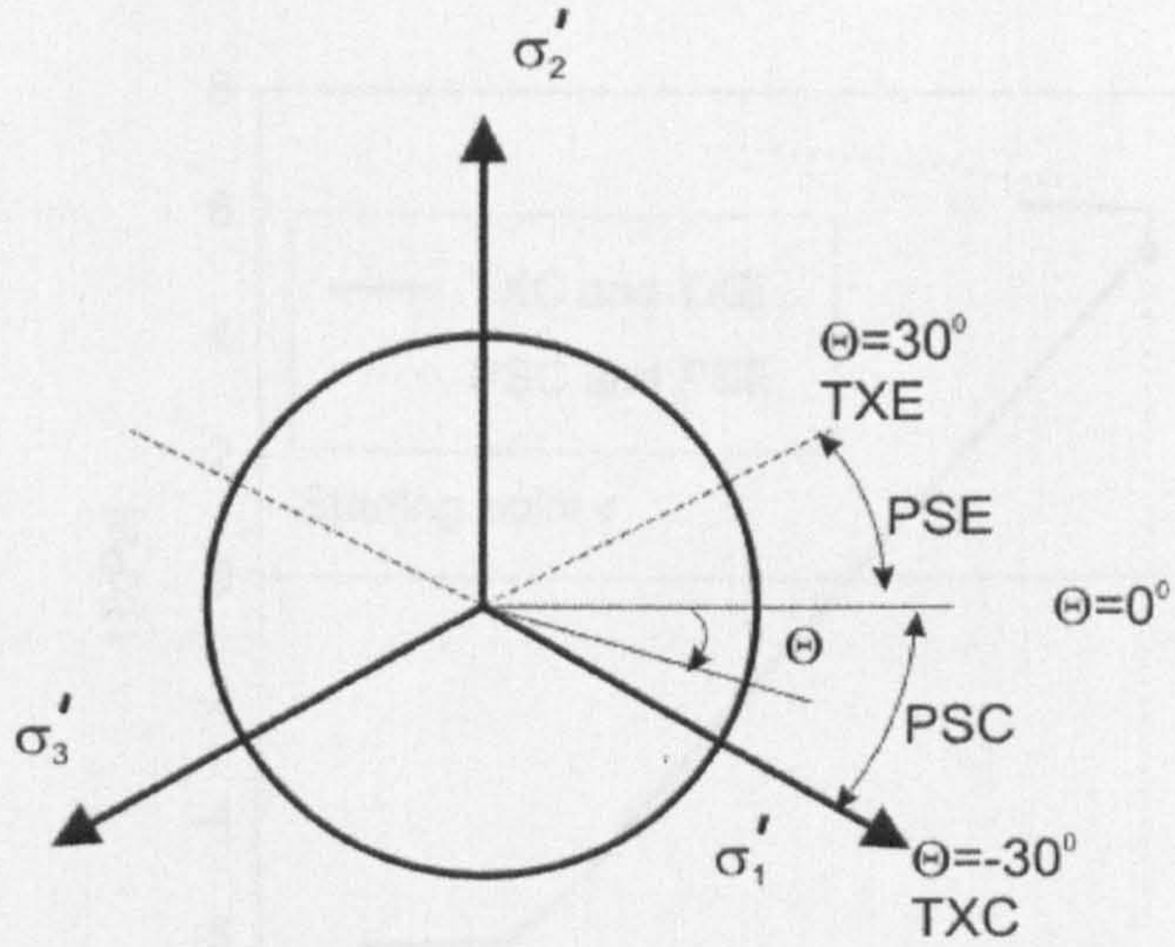

Figure 2.3: Drucker Prager criteria in the deviatoric plane

Inspection of Figure 2.2 reveals that an ultimate value of deviator stress q can be defined in the MCC model. This implies $q_{max} = Mp'$ and hence the peak undrained shear strength c_u can be defined by:

$$c_u = \frac{q_{max}}{2} = \frac{Mp'}{2}. \qquad [2.3]$$

As p' in *Eq. 2.3* is not known in a numerical analysis it is necessary to combine it with *Eq. 2.1* to derive c_u. Combining both equations results in a quadratic equation which can be written as:

$$2q^2 - Mqp'_m = 0. \qquad [2.4]$$

Applying the quadratic formula results in

$$2c_u = q_{max} = \frac{Mp'_m}{2} \quad . \qquad [2.5]$$

One of the two solutions is zero and the second is q_{max} which represents the interception of the critical state line with the MCC yield surface, see Figure 2.2. In the MCC

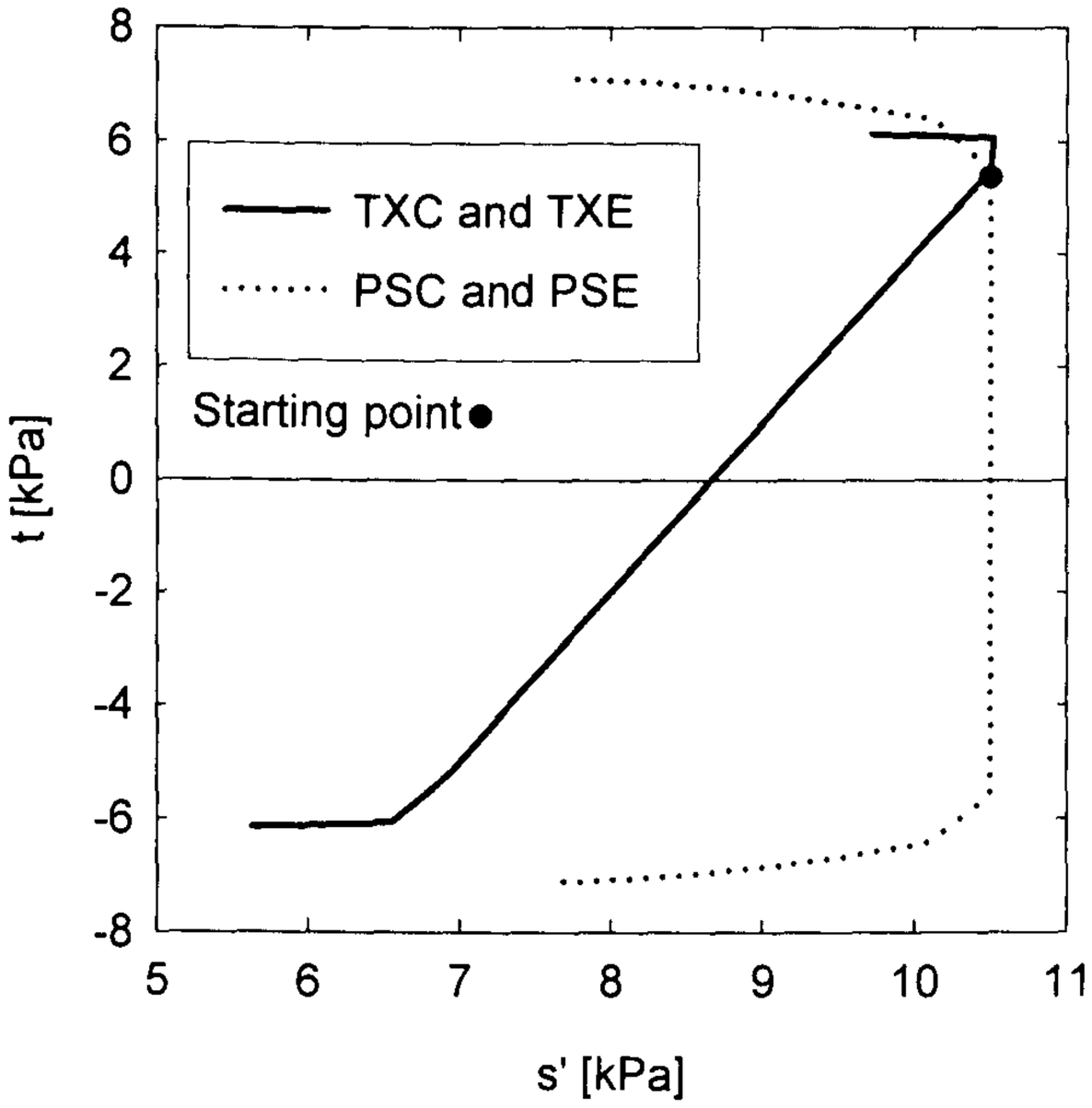

Figure 2.4: Predicted stress path for undrained shearing in triaxial compression and extension and plane strain compression and extension

model the c_u in compression and extension is of the same order due to the assumed shape of the yield surface.

For boundary value problems such as embankment simulations in plane strain conditions the predicted undrained strength in plane strain compression and extension is of interest. Triaxial compression TXC is predicted at a Lode angle of -30° (see Figure 2.3), triaxial extension TXC at +30°, plane strain compression PSC between 0° and -30° and plane strain extension PSE between 0° and +30°. To demonstrate the difference in the undrained strength in triaxial stress space and plane strain stress space model simulations with a single gauss point programme have been undertaken. The soil samples in the simulations represents Murro clay, a soft Finnish clay from Finland. Details about Murro clay are presented in Chapter 6. The results of the prediction are presented in Figure 2.4. The stress path is presented in the s'-t plane, where s' is defined as $(\sigma'_1+ \sigma'_3)/2$ and t as $(\sigma'_1- \sigma'_3)/2$. The definition ignores the intermediate stress σ'_2. The results show that the MCC model predicts a higher failure stress t in compression under plane strain conditions than for triaxial conditions. This was found

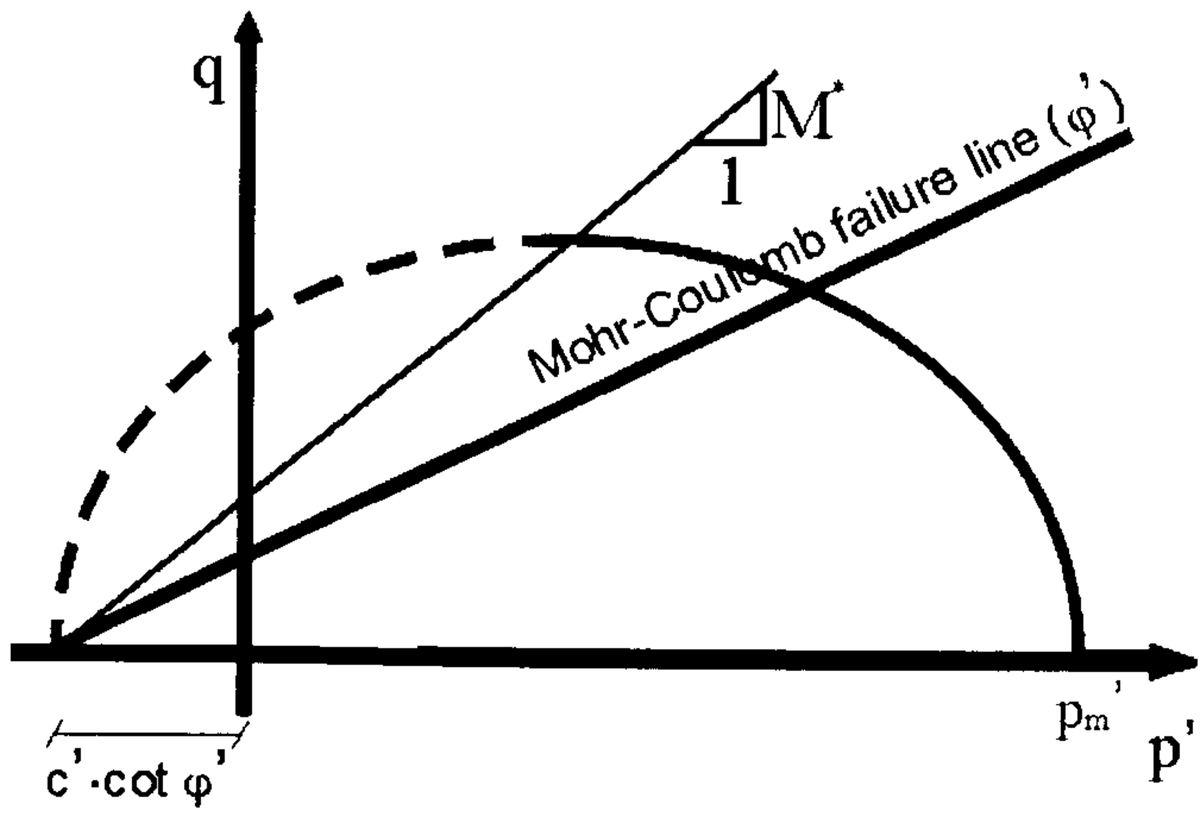

Figure 2.5: The yield surface of the Soft Soil model in the p'-q stress space

to be the case for both compression and extension paths. The maximum stress at failure is the same in extension and compression due to the assumed isotropic behaviour and Drucker Prager failure criteria.

2.3.2 Soft Soil model (SS)

The SS model (Brinkgreve, 2002) is a modification of the MCC model. The yield surface of the SS model is composed of two parts, the cap yield surface and the failure yield surface, as shown in Figure 2.5. The cap yield surface is defined by:

$$f = q^2 - M^{*2}(p'_m - p')(p + \cot\varphi') = 0. \qquad [2.6]$$

The size of the yield surface is defined by the state parameter p'_m and can be evaluated from the vertical pre-consolidation stress. The shape is described by the parameter M*, the soil constants c' (effective cohesion) and φ' (effective peak friction angle). The parameter M* should not be confused with the M in the MCC model. It is a parameter which is solely used to define the shape of the ellipse and not as a failure criterion. Failure in the p'-q stress space is defined with the Mohr-Coulomb failure criteria with a non associated flow rule as shown in Figure 2.5. The Mohr -Coulomb criteria in the deviatoric plane is shown in Figure 2.6. In contrast to the critical state criteria mentioned earlier the Mohr-Coulomb criteria assumes a failure condition on the plane and simply accounts for minor and major principal stresses (σ'_3 and σ'_1).

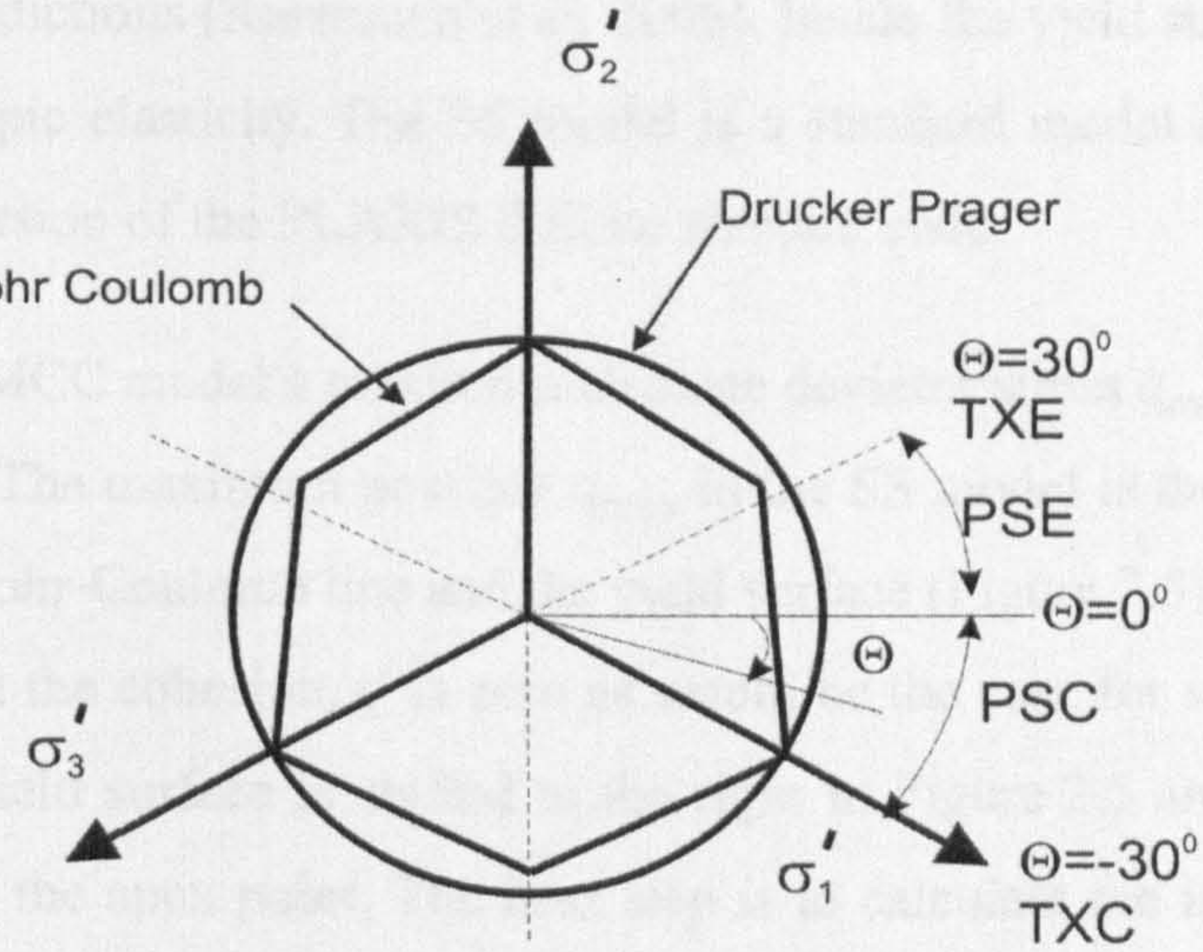

Figure 2.6: The Mohr-Coulomb failure surface in the deviatoric plane

The intermediate principal stress σ'_2 is ignored. By using M* to define the shape of the cap surface, the yield surface is totally independent of the failure surface. On the cap surface, the flow rule is associated. For the special case of triaxial compression the parameter M* can be calculated from *Eq. 2.7* (Brinkgreve, 1994).

$$M^* = 3\sqrt{\frac{(1-K_0^{NC})^2}{(1+2K_0^{NC})} + \frac{(1-K_0^{NC})(1-2\nu')(\lambda^*/\kappa^*-1)}{(1+2K_0^{NC})(1-2\nu')(\lambda^*/\kappa^*)-(1-K_0^{NC})(1+\nu')}} \quad [2.7]$$

where κ^* is the modified swelling index, λ^* is the modified compression index, both are defined in the ε_v:ln(p') plane and ν' is the Poisson's ratio. K_0^{NC} is the coefficient of lateral earth pressure at rest in the normally consolidated condition and can be estimated using Jaky's formula (*Eq. 2.8*).

$$K_0^{NC} = (1-\sin\varphi') \quad [2.8]$$

From *Eq. 2.7* it can be seen that the shape of the cap yield surface, apart from K_0^{NC}, also depends on the compression ratio λ^*/κ^* and on Poisson's ratio ν'. By using K_0^{NC} values between 0.3 to 0.9 (Brinkgreve, 1994) the model predicts realistic stress paths with stress ratios close to η_{K0} for normally consolidated soils. This feature is a substantial improvement when compared to the MCC model which is well known for

its poor K_0 predictions (Karstunen et al. 2006). Inside the yield surface the SS model assumes isotropic elasticity. The SS model is a standard model implemented in the commercial version of the PLAXIS 8 finite element code.

Similar to the MCC model a maximum ultimate deviator stress q_{max} can be defined in the SS model. The maximum possible q_{max} in the SS model is the interception point between the Mohr-Coulomb line and the yield surface (Figure 2.5). In the following it is assumed that the cohesion, c' is zero as would be the case for soft soils. With zero cohesion the yield surface is shifted to the right in Figure 2.5 and the yield surface intercepts with the apex point. The next step is to calculate the inclination M of the Mohr-Coulomb line in the p'-q stress space from the friction angle φ'. Knowing M and combining *Eq. 2.3* with the yield function (*Eq. 2.6*) of the SS model leads to:

$$0 = q^2\left(\frac{M^{*2}}{M} + 1\right) + q\frac{M^{*2}}{M}(\cot\varphi' - p_m) - M^{*2}p_m\cot\varphi' . \qquad [2.9]$$

Application of the quadratic formula results in:

$$q_{max} = \frac{\frac{M^{*2}}{M}(\cot\varphi' - p_m) \mp \sqrt{\left(\frac{M^{*2}}{M}(\cot\varphi' - p_m)\right)^2 - 4\left(\frac{M^{*2}}{M} + 1\right)(M^{*2}p_m\cot\varphi')}}{2\left(\frac{M^{*2}}{M} + 1\right)} \qquad [2.10]$$

The ultimate deviatoric stress q_{max} in the SS model needs to be interpreted with caution and has a different meaning compared to the q_{max} in the MCC model. During undrained loading a soil element may possibly fail at a much lower stress ratio because of the Mohr-Coulomb failure criteria used in the model.

As shown in Figure 2.6 the MC criteria and the DP criteria both predict the same maximum stress in undrained triaxial compression. As a consequence the MC criteria will predict a lower failure stress under plane strain conditions than in triaxial compression due to the shape of the MC criteria. It will also predict a lower stress at failure in plane strain than the DP criteria.

2.4 Anisotropic models

2.4.1 S-CLAY1 model

The S-CLAY1 model (Wheeler et al. 2003) is an extension of the MCC model. The anisotropy of plastic behaviour is represented through an inclined yield surface and a hardening law relates the development and evolution of the fabric of the soil to plastic straining. Accounting for anisotropy in the models means that the model can no longer be formulated solely in invariants. A so-called mixed formulation of the yield surface is required which consist of tensors and invariants. The yield surface in general stress space is defined as:

$$f = \frac{3}{2}[\{\underline{\sigma}'_d - p'\underline{\alpha}_d\}^T\{\underline{\sigma}'_d - p'\underline{\alpha}_d\}] - \left[M^2 - \frac{3}{2}\{\underline{\alpha}_d\}^T\{\underline{\alpha}_d\}\right](p'_m - p')p' = 0 \qquad [2.11]$$

where $\underline{\sigma}_d$ is the deviatoric stress tensor and $\underline{\alpha}_d$ is the so-called deviatoric fabric tensor. The deviatoric stress tensor is defined as:

$$\underline{\sigma}'_d = \begin{bmatrix} \sigma'_x - p' \\ \sigma'_y - p' \\ \sigma'_z - p' \\ \sqrt{2}\tau_{xy} \\ \sqrt{2}\tau_{yz} \\ \sqrt{2}\tau_{zx} \end{bmatrix} = \begin{bmatrix} \frac{1}{3}(2\sigma'_x - \sigma'_y - \sigma'_z) \\ \frac{1}{3}(-\sigma'_x + 2\sigma'_y - \sigma'_z) \\ \frac{1}{3}(-\sigma'_x - \sigma'_y + 2\sigma'_z) \\ \sqrt{2}\tau_{xy} \\ \sqrt{2}\tau_{yz} \\ \sqrt{2}\tau_{zx} \end{bmatrix}. \qquad [2.12]$$

The fabric tensor is a dimensionless second-order tensor that is defined analogously to the deviatoric stress tensor and is shown in *Eq. 2.13*.

$$\alpha_d = \begin{bmatrix} \frac{1}{3}(2\alpha_x - \alpha_y - \alpha_z) \\ \frac{1}{3}(-\alpha_x + 2\alpha_y - \alpha_z) \\ \frac{1}{3}(-\alpha_x - \alpha_y + 2\alpha_z) \\ \sqrt{2}\alpha_{xy} \\ \sqrt{2}\alpha_{yz} \\ \sqrt{2}\alpha_{zx} \end{bmatrix} = \begin{bmatrix} \alpha_x - 1 \\ \alpha_y - 1 \\ \alpha_z - 1 \\ \sqrt{2}\alpha_{xy} \\ \sqrt{2}\alpha_{yz} \\ \sqrt{2}\alpha_{zx} \end{bmatrix} \qquad [2.13]$$

where the components of the fabric tensor have the property as defined in *Eq. 2.14*.

$$\frac{1}{3}(\alpha_x + \alpha_y + \alpha_z) = 1 \qquad [2.14]$$

M is the stress ratio at critical state and the state parameter p'_m defines the size of the yield surface. A general version of the yield surface is required for numerical analysis of boundary value problems, where three dimensional stress states and rotation of the principal axis occurs. Figure 2.7 shows the S-CLAY1 model in three dimensional stress space for the case where the principal axes of the deviatoric stress tensor coincide with the axes of the deviatoric fabric tensor in x, y and z direction. The yield surface has the shape of an inclined ellipsoid. The special case shown represents for instance a soil element which has been one-dimensionally consolidated. The components σ'_{xy}, σ'_{yz} and σ'_{zx} of the deviatoric stress tensor $\underline{\alpha}_d$ and the components α_{xy}, α_{yz} and α_{zx} of the deviatoric fabric tensor $\underline{\alpha}_d$ are zero. It can be seen in Figure 2.7, however that the axis of the yield surface does not coincide with the hydrostatic axis due to the initial anisotropy of the soil.

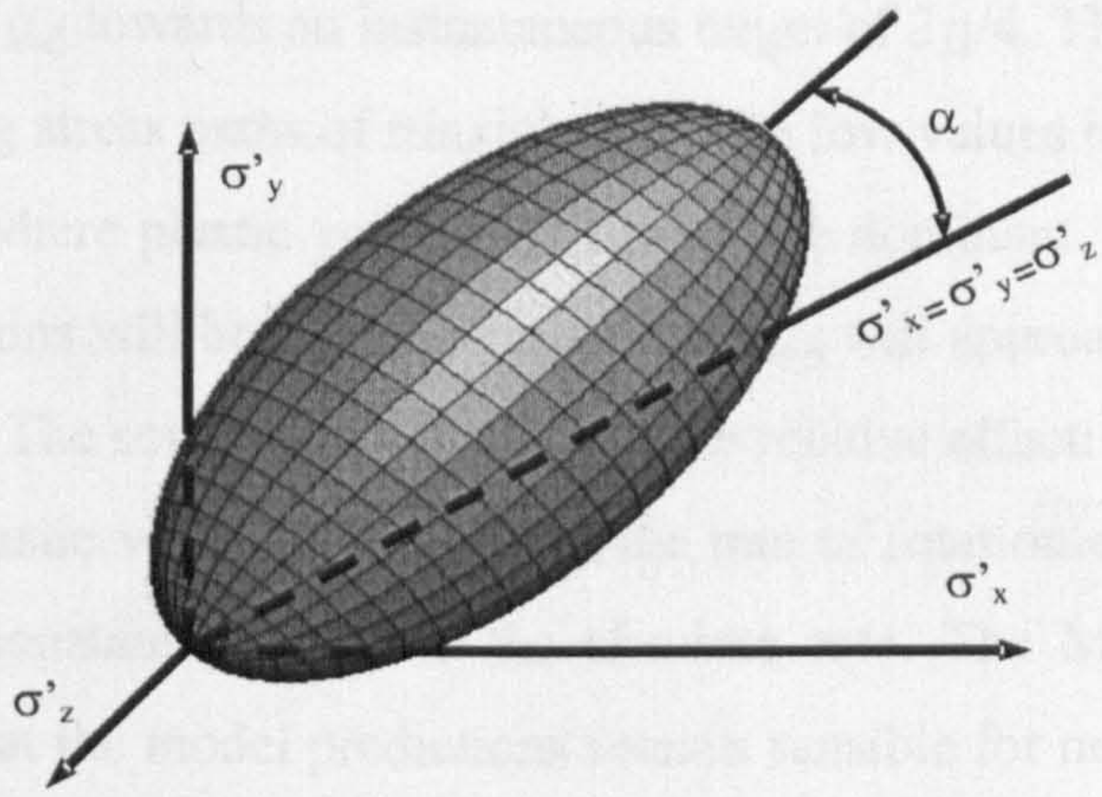

Figure 2.7: Yield surface of the S-CLAY1 model in 3D stress space

2.4.1.1 Hardening laws

The S-CLAY1 model incorporates two hardening laws. The first relates the change in size of the yield surface to the plastic volumetric strain increment $d\varepsilon_v^p$. It is of the same form as the equivalent hardening law in the MCC model and is defined by:

$$dp'_m = \frac{vp'_m d\varepsilon_v^p}{\lambda - \kappa} \qquad [2.15]$$

where v is the specific volume, κ is the gradient of the (pre-yield) elastic swelling line in the v:ln(p') plane and λ is the gradient of the post-yield compression curve for a constant η stress path in the v:ln(p') plane involving no change of the fabric anisotropy ($\underline{\alpha}_d$ is constant).

The second hardening law (the "rotational hardening law") describes the change of the orientation of the yield surface with plastic straining, representing the development and erasure of plastic anisotropy. The proposed form of the rotational hardening law is:

$$d\underline{\alpha}_d = \mu\left(\left[\frac{3\underline{\underline{\eta}}}{4} - \underline{\alpha}_d\right]\langle d\varepsilon_v^p\rangle + \beta\left[\frac{\underline{\underline{\eta}}}{3} - \alpha_d\right](d\varepsilon_d^p)\right) \qquad [2.16]$$

where $\underline{\eta}=\underline{\sigma}_d/p'$, $d\varepsilon_d^p$ is the increment of the plastic deviatoric strain increment and μ and β are additional soil constants. *Eq. 2.16* shows that positive volumetric strains

attempt to drag the $\underline{\alpha}_d$ towards an instantaneous target of $3\underline{\eta}/4$. This can be best illustrated by simulating stress paths of triaxial tests with low values of stress ratio $\eta=q/p'$ (close to p'-axis), where plastic volumetric strains are dominant. At higher values of η, plastic shear strains will be more dominant and $\underline{\alpha}_d$ will approach asymptotically a target value of $\underline{\eta}/3$. The soil constant β controls the relative effectiveness of the plastic shear strain and plastic volumetric strain on the rate of rotation of the yield surface, whereas the soil constant μ controls the absolute rate. The Macaulay bracket in *Eq. 2.16* ensures that the model predictions remain sensible for negative plastic volumetric strain increments on the dry side of the yield surface (see Wheeler et al. 2003 for details).

2.4.1.2 Triaxial stress space

For simplified conditions of a triaxial test on a previously one-dimensionally consolidated sample, it can be assumed that the horizontal plane of the soil specimen in the triaxial apparatus coincides with the plane of isotropy of the sample. In this case, the fabric tensor can be replaced by a scalar parameter α, defined as:

$$\alpha^2 = \frac{3}{2}\{\underline{\alpha}_d\}^T\{\underline{\alpha}_d\} \qquad [2.17]$$

which is a measure of the degree of anisotropy of the soil. In the triaxial stress space the deviator stress can be defined as the scalar value q.

$$q^2 = \frac{3}{2}\{\underline{\sigma}'_d\}^T\{\underline{\sigma}'_d\} \qquad [2.18]$$

The general version of the yield surface *Eq. 2.11* can be simplified to a formulation that is valid in triaxial stress space by using the scalar values as defined in *Eq. 2.17* and *Eq. 2.18*.

$$f = (q - \alpha p')^2 - (M^2 - \alpha^2)(p'_m - p')p' = 0 \qquad [2.19]$$

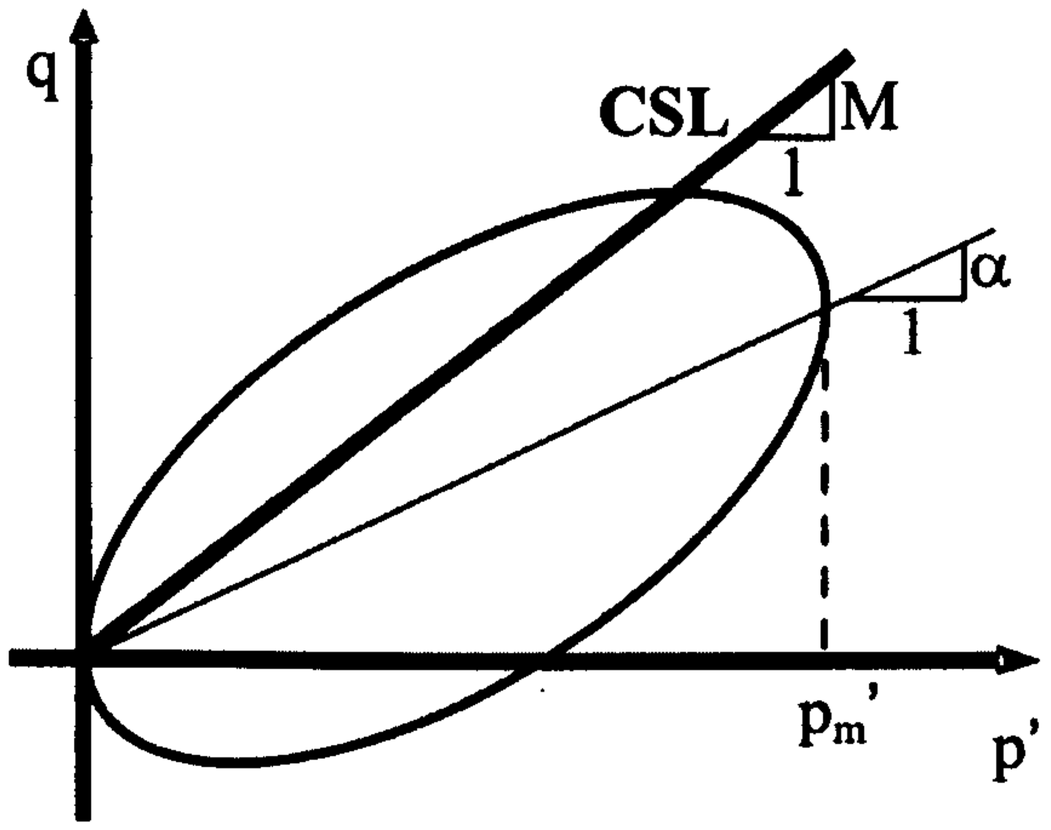

Figure 2.8: The yield curve of the S-CLAY1 model in triaxial stress space

The yield surface in the triaxial stress space has the shape of a sheared ellipse and is illustrated in Figure 2.8. As shown in Figure 2.8, the yield surface in triaxial stress space has an inclination of α and a maximum dimension of p'_m. The proposed shape of the curve is identical to the yield curve expressions proposed independently by Dafalias (2006) and Korhonen and Lojander (1987). The yield surface provides a good match to experimental data for a wide range of natural soils (Wheeler et al. 2003). Koskinen (2002b) showed for four different natural Finnish clays, that the yield curve expression (*Eq. 2.19*) is a reasonable fit to the experimental data, see Figure 2.9. Karstunen and Koskinen (2007) also showed that the yield surface provides an excellent fit for yield points at different stress ratios η on reconstituted samples of soft Finnish clays.

The rotational hardening law was originally developed and validated on the basis of an extensive testing programme on natural Otaniemi clay (Näätänen et al. 1999; Wheeler et al. 2003). Otaniemi clay is soft clay from southern Finland. Further validation of the proposed hardening law was provided by simulations of natural and reconstituted samples of POKO clay, Vanttila clay and Murro clay, all clays from Finland (Karstunen and Koskinen 2007, Koskinen et al. 2002b). In particular, model simulations of drained triaxial tests on reconstituted samples with different stress path directions demonstrated excellent agreement with test results.

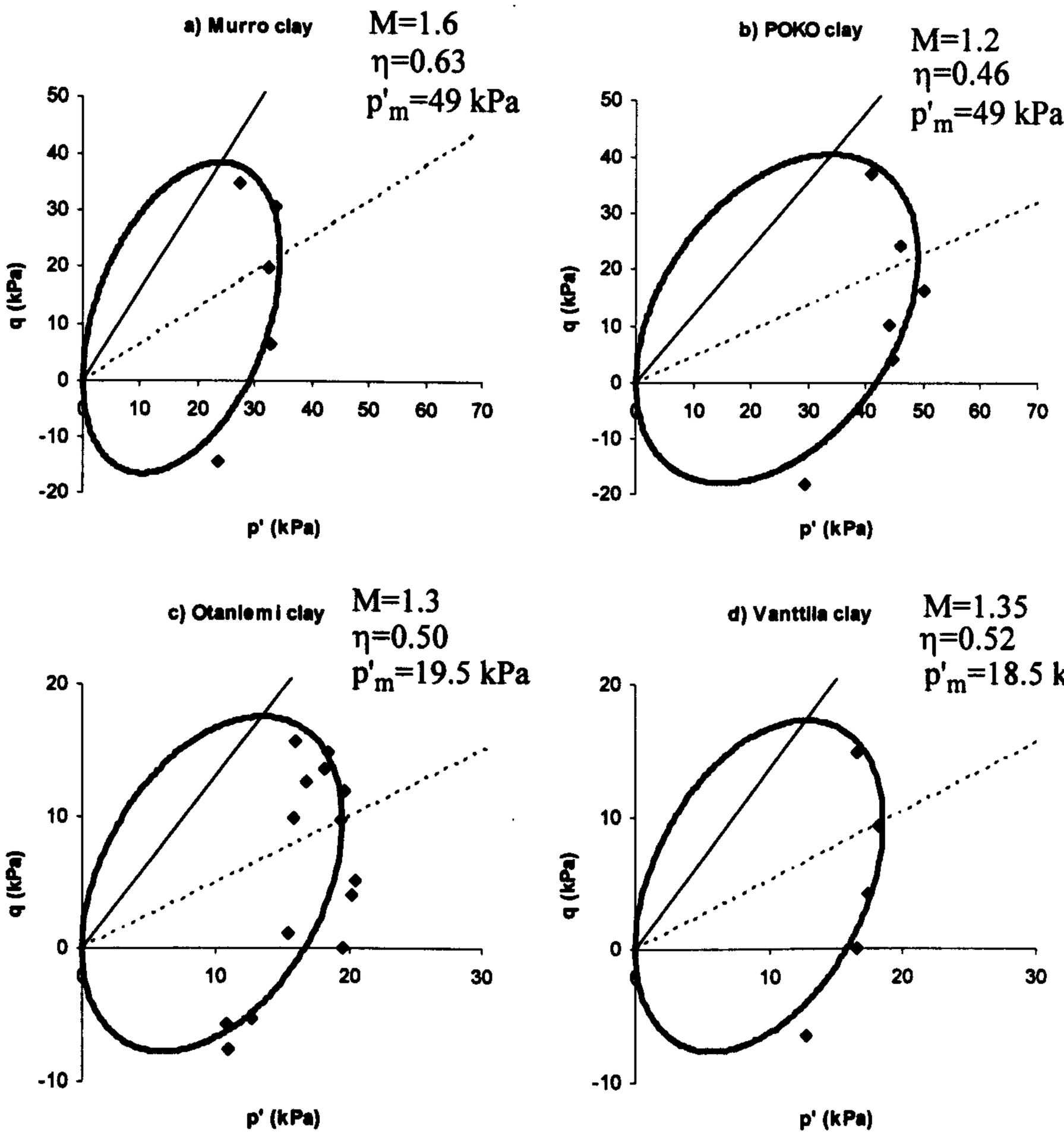

Figure 2.9: The initial yield curve for four natural Finnish clays (Koskinen 2002b)

The elastic behaviour of the S-CLAY1 model is assumed to be isotropic similar to that of the MCC model. It is a reasonable assumption for practical problems in soft clays such as the construction of embankments where deformations are dominated by plastic strains, in particular for cases under monotonic loading. The flow rule of the S-CLAY1 model is assumed to be associated. The model simulation of reconstituted samples of the Finnish clays demonstrated that an associated flow rule is a reasonable assumption (Karstunen and Koskinen, 2007).

2.4.1.3 Initial state parameters

Three state parameters are required to describe the initial state of the soil using the S-CLAY1 model. These parameters are the initial void ratio e_0, the initial size of the yield surface p'_m and the initial inclination of the yield surface α.

For high quality model simulations of laboratory tests it is very important to derive an appropriate yield point from stress-strain curves. The yield stress is used to calculate the initial size of the yield surface p'_m. Koskinen et al. (2003) reports that an aniso-tropic model, such as the S-CLAY1, predicts considerable curvature in the post-yield compression curve if the anisotropy of the soil is changing (i.e. rotation of the yield curve). The curvature is a result of the gradual rotation of the yield surface. Yield points estimated from the intersection point of lines fitted to the elastic swelling and post-yield compression curve in the ε_v:ln(p') diagram overestimate the true yield stress (Wheeler et al. 2003). Koskinen et al. (2003) proposed an alternative procedure to estimate the yield stress. The idea is to plot the stress-strain curve in an ε_v:p'-plot instead of ε_v:ln(p'). Again the yield stress is identified by the intersection point of two straight lines. The first line represents the tangent to the elastic swelling line at the point of the shallowest gradient of the elastic swelling line and the second is also a tangent but the tangent to the steepest gradient of the post-yield compression curve. This method results in a better prediction of the true yield stress (Koskinen et al. 2003).

The stress and strain history of the soil element determines not just the initial size of the yield surface p'_m but also the initial inclination α of the yield surface. If the soil in the past was restricted to one-dimensional straining and is in a normal or slightly over-consolidated state then the initial inclination α can be estimated via the proce-dure described by Wheeler et al. (2003). First the lateral earth pressure at rest, K_0 for normally consolidated soil, can be estimated by Jaky's formula (K_0=1-sinφ', φ' is the critical state friction angle). Knowing K_0, one can calculate the corresponding stress ratio η_{K0}. Model simulations show that for simulations of stress paths with a stress

ratio of η_{K0}, the model predicts one value of α which corresponds to one-dimensional straining. One-dimensional straining corresponds to:

$$\frac{d\varepsilon_d}{d\varepsilon_v} = \frac{2}{3}. \qquad [2.20]$$

Assuming that elastic strains are negligible during one dimensional depositions, the plastic strains can be estimated by:

$$\frac{d\varepsilon_d^p}{d\varepsilon_v^p} \approx \frac{2}{3}. \qquad [2.21]$$

The associated flow rule of the S-CLAY1 model leads to:

$$\frac{d\varepsilon_d^p}{d\varepsilon_v^p} = \frac{2(\eta - \alpha)}{M^2 - \eta^2}. \qquad [2.22]$$

By combining *Eq. 2.21* with the associated flow rule (*Eq. 2.22*) the initial inclination of the yield surface for normally consolidated soils can by derived by the following expression.

$$\alpha_{K0} \approx \frac{\eta_{K0}^2 + 3\eta_{K0} - M^2}{3} \qquad [2.23]$$

Eq. 2.23 suggests that the α_{K0} is related to the critical friction angle φ' of the soil. In the general version of the S-CLAY1 model the α_{K0} is used to calculate the fabric tensor $\underline{\alpha}_d$ (*Eq. 2.28*).

For a cross anisotropic soil, where the horizontal planes coincide with the plane of isotropy, the following can be defined (y-axis is the vertical axis in the ground):

$$\alpha_x = \alpha_z,\ \alpha_{xy} = \alpha_{yz} = \alpha_{xz}. \qquad [2.24]$$

This definition simplifies *Eq. 2.14* to:

$$\alpha_y = 3\text{-}2\alpha_x. \qquad [2.25]$$

By inserting *Eq. 2.24* and *Eq. 2.25* into *Eq. 2.13* the deviatoric fabric tensor $\underline{\alpha}_d$ can be expressed in terms of α_x:

$$\underline{\alpha}_d = \begin{bmatrix} \alpha_x - 1 \\ 2(1-\alpha_x) \\ \alpha_x - 1 \\ 0 \\ 0 \\ 0 \end{bmatrix}. \qquad [2.26]$$

To provide a relationship between α_x and scalar parameter α_{K0}, the *Eq. 2.24* and *Eq. 2.25* are inserted into *Eq. 2.17*:

$$\alpha_x = 1 - \frac{\alpha}{3}. \qquad [2.27]$$

The derivation of *Eq. 2.27* makes use of the fact that positive values of α refer to a soil with $\alpha_y > \alpha_x$, in order to be consistent with the fact that positive values of q refer conventionally to a stress with $\sigma'_y > \sigma'_x$ (Zentar, 2004).

Inserting *Eq. 2.27* into *Eq. 2.26* gives the deviatoric fabric tensor in terms of the scalar parameter for cross-anisotropic soil and for K_0 consolidated soil:

$$\underline{\alpha}_{d,0} = \begin{bmatrix} -\frac{\alpha}{3} \\ -\frac{2\alpha}{3} \\ -\frac{\alpha}{3} \\ 0 \\ 0 \\ 0 \end{bmatrix} = \begin{bmatrix} -\frac{\alpha_{K0}}{3} \\ -\frac{2\alpha_{K0}}{3} \\ -\frac{\alpha_{K0}}{3} \\ 0 \\ 0 \\ 0 \end{bmatrix}. \qquad [2.28]$$

The theoretical background to the initial anisotropy holds for one-dimensional consolidation history of slightly overconsolidated soil with horizontal soil layers. In many practical problems the ground surface is not horizontal, consider for example slopes,

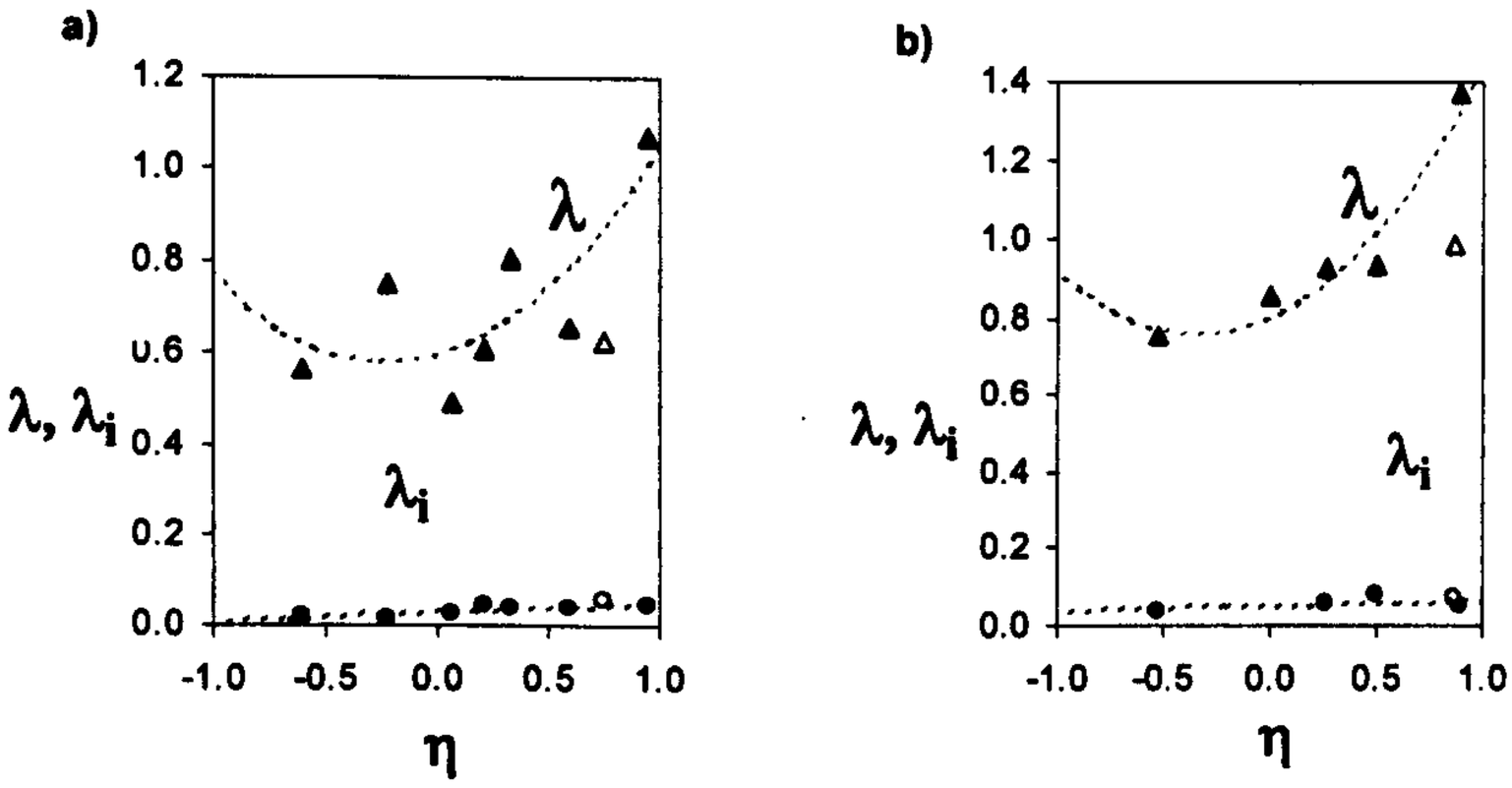

Figure 2.10: The influence of η on the apparent value of λ and λ_i: a) Poko clay and b) Vanttila clay (Koskinen and Karstunen, 2004)

but the underlying soil layers are. If the slope has been built by river erosion or wind erosion, which is very often the case, one can assume that the above assumption will be valid.

2.4.1.4 Model parameters

The S-CLAY1 model involves six soil parameters (constants). Four are conventional parameters from the MCC model (κ, λ, M and Poisson's ratio ν') that can be determined from conventional laboratory tests.

Koskinen and Karstunen (2004) demonstrated using two different Finnish clays that due to the presence of bonding and destructuration in natural soil, the value of the apparent slope of the natural compression line λ depends on the stress ratio η of the stress path, see Figure 2.10. Koskinen and Karstunen (2004) argue that the stress path direction influences the rate at which destructuration proceeds. For any model simulations a representative average value of λ is recommended. In simulations of boundary value problems where loading is likely to dominate, a value should be used which corresponds to the K_0 condition.

The two additional model parameters, μ and β, relate to the rotational hardening law. The parameter μ can not be derived through a direct method. A solution would be to conduct several model simulations with different values of μ and compare the pre-

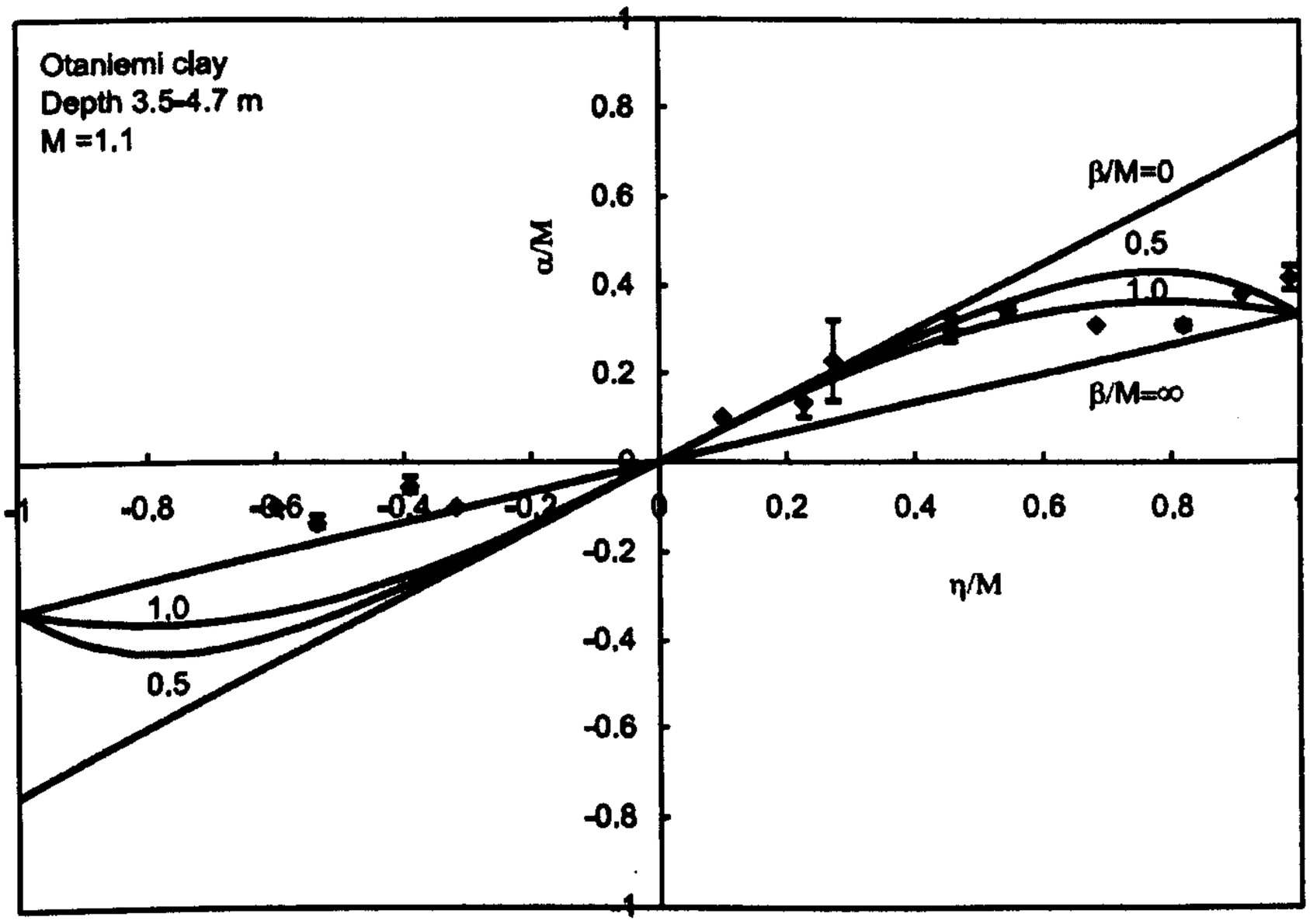

Figure 2.11: Equilibrium values of η/M for radial stress paths on Otaniemi clay. (Wheeler et al. 2004)

dicted behaviour with the observed behaviour. Alternatively, Zentar et al. (2002) suggest, based on parametric studies, that a practical range of μ lies somewhere between $10/\lambda < \mu < 20/\lambda$. Näätänen et al. (1999) and Wheeler et al. (2003) showed that the numerical simulations of triaxial tests with different stress path directions are not very sensitive to μ values within the proposed limits. With μ within the proposed limits the model predicts that a soil element must be subjected to an isotropic stress state three times larger than the yield stress before the anisotropy of the fabric is totally erased.

The model parameter β defines the relative effectiveness of plastic shear strains and volumetric strains in the rotational hardening (*Eq. 2.16*). Loading a soil element with any constant stress ratio η, the rotational hardening law will predict a final equilibrium value of α, as shown by Figure 2.11. Consequently, when loading the soil with a normally consolidated stress ratio η_{K0}, shows that only one value of β will result in a value of α corresponding to α_{K0}. Wheeler et al. (2003) suggest that the soil parameter β corresponding to the α_{K0}, can be calculated from a simple expression. By setting $d\underline{\alpha}_d$ in the simplified triaxial version of *Eq. 2.16* to zero it can be shown that just one unique β value will correspond to α_{K0}. Combining *Eq. 2.16* with *Eq. 2.23* will lead to the following expression:

$$\beta = \frac{3(4M^2 - 4\eta_{K0}^2 - 3\eta_{K0})}{8(\eta_{K0}^2 - (M^2 + 2\eta_{K0}))}. \qquad [2.29]$$

Eq. 2.29 suggests that β is related to φ' (given that both M and η_{K0} are related to φ' (Wheeler et al. 2003)). By setting the constant μ and the initial values of all terms of the fabric tensor $\underline{\alpha}_d$ to zero, the S-CLAY1 model reduces to the isotropic MCC model.

2.4.1.5 Peak undrained shear strength

In the same manner as in the MCC model, a peak undrained shear strength c_u is defined in the S-CLAY1 model in the p' -q stress space. The peak is defined at the interception point between the critical state line and the yield curve (Figure 2.8). Inserting *Eq. 2.3* in the yield curve (Figure 2.19) leads to a quadratic equation:

$$2q^2 + q\left(\frac{\alpha p'_m}{M} - \frac{2\alpha}{M} - Mp'_m\right) = 0 \qquad . \qquad [2.30]$$

Applying the quadratic formula results in:

$$2c_u = q_{max} = \frac{\alpha p_m - Mp'_m}{4} \qquad . \qquad [2.31]$$

The derived c_u presented above is just a simple interpretation of the peak undrained shear strength c_u of the S-CLAY1 model in triaxial compression and not the true peak strengths at undrained failure in compression. The predicted strength is only valid at the moment the c_u value is calculated. Under continuous undrained loading the yield curve will continue to rotate and this will change the peak value continuously until the stress ratio at critical state is reached. To calculate the strength in extension, M needs to be replaced with the M at extension. In the S-CLAY1 model the M in extension is the same as in compression as no Lode angle dependency is implemented. To calculate the undrained shear strength in extension with *Eq. 2.31* the minus sign is replaced with a plus sign. Due to the rotated yield surface (ellipse) the peak strength in extension is significantly lower than in compression.

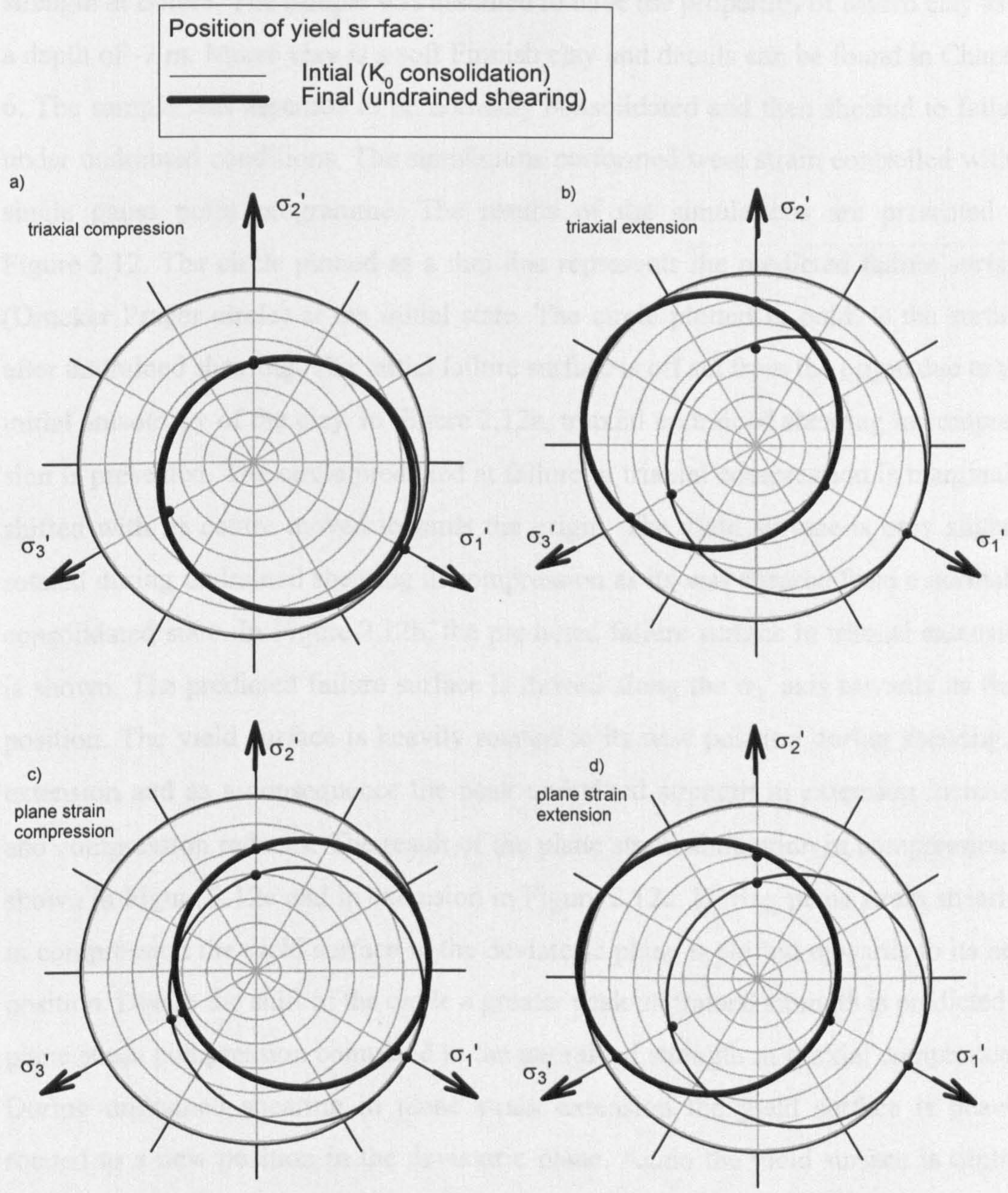

Figure 2.12: Failure surface of the S-CLAY1 model on the deviatoric plane for initial state (K_0 consolidation) and at the end of undrained shearing: a) Triaxial compression, b) Triaxial extension, c) Plane strain compression and d) Plane strain extension

The difference in the predictions of the S-CLAY1 model for triaxial conditions and plane strain conditions are better observed on the deviatoric plane. Undrained triaxial compression and extension tests and plane strain compression and extension tests have been simulated to highlight the difference in the predicted undrained shear

strength at failure. The sample was assumed to have the properties of Murro clay as at a depth of -7 m. Murro clay is a soft Finnish clay and details can be found in Chapter 6. The sample was assumed to be normally consolidated and then sheared to failure under undrained conditions. The simulations performed were strain controlled with a single gauss point programme. The results of the simulations are presented in Figure 2.12. The circle plotted as a thin line represents the predicted failure surface (Drucker Prager circle) at the initial state. The circle plotted in bold, is the surface after undrained shearing. The initial failure surface is off set from the origin due to the initial anisotropy of the clay. In Figure 2.12a, triaxial undrained shearing in compression is presented. The circle predicted at failure in triaxial compression is marginally shifted with its centre moved towards the origin. The yield surface is only slightly rotated during undrained shearing in compression as its was sheared from a normally consolidated state. In Figure 2.12b, the predicted failure surface in triaxial extension is shown. The predicted failure surface is moved along the σ_1' axis towards its final position. The yield surface is heavily rotated to its new position during shearing in extension and as a consequence the peak undrained strength in extension increases and compression reduces. The result of the plane strain simulation in compression is shown in Figure 2.12c and in extension in Figure 2.12d. During plane strain shearing in compression the yield surface in the deviatoric plane is shifted upwards to its new position. Due to the shift of the circle a greater peak undrained strength is predicted in plane strain compression compared to the undrained strength in triaxial compression. During undrained shearing in plane strain extension the yield surface is heavily rotated to a new position in the deviatoric plane. Again the yield surface is centred around a new position with the centre of the circle close to the axis of the Lode angle of zero degrees.

The corresponding stress paths in the s'-t plane are presented in Figure 2.13. The predictions by the S-CLAY1 model are compared to the simulations using the isotropic MCC model. In triaxial compression the S-CLAY1 model predicts an initial higher stress level before finally reaching a stress level at critical state which is marginally

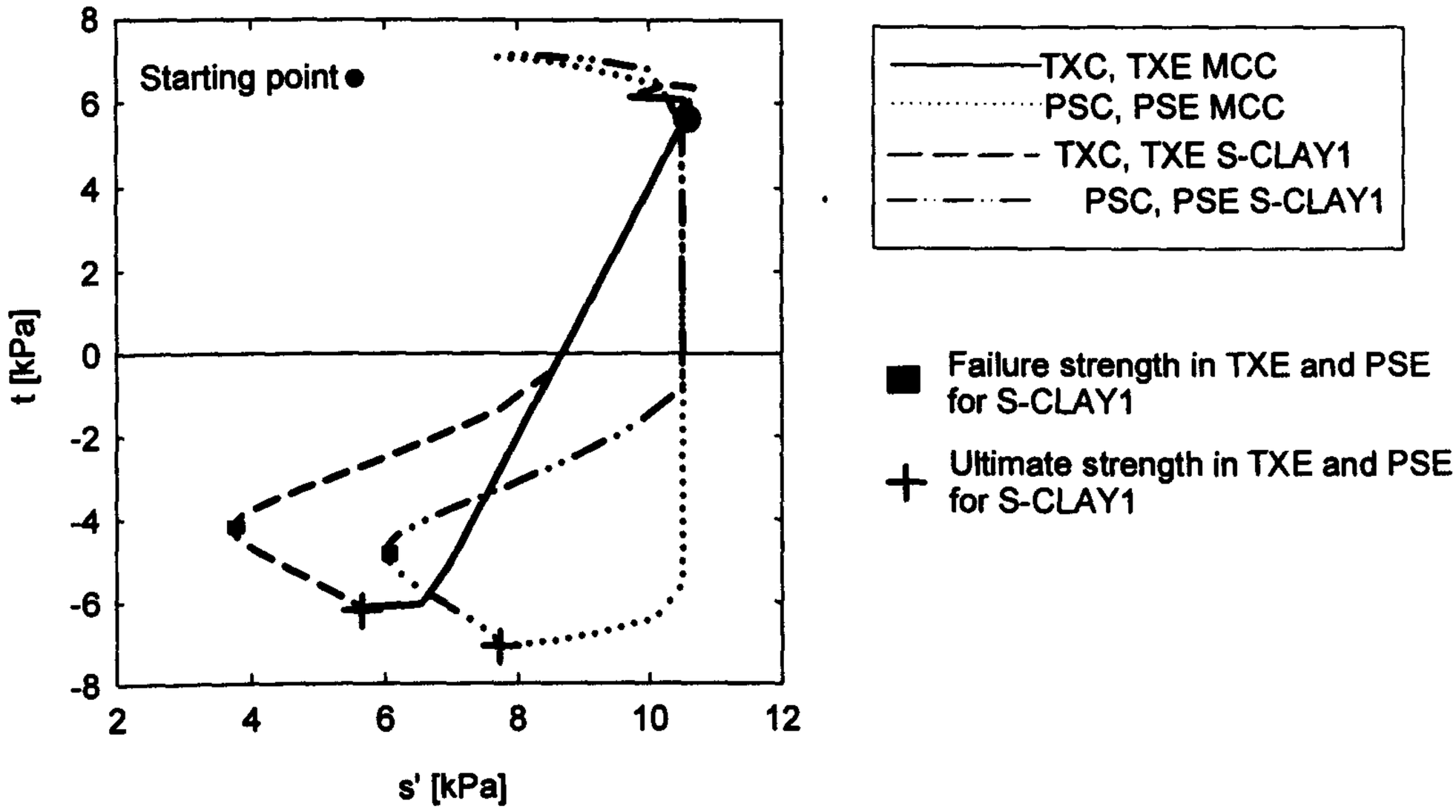

Figure 2.13: Predicted stress path for triaxial compression and extension, and plane strain compression and extension by the S-CLAY1 and MCC model

higher than that predicted using MCC. Similar behaviour is observed for plane strain compression. In extension both models predict the same stress level at critical state but the stress paths towards the final point are totally different. The S-CLAY1 path diverges from the MCC path at a point where the S-CLAY1 model starts yielding in extension. Once S-CLAY1 reaches a stress level close to the critical state in extension the stress path heavily bends and continues to move downwards to the failure line. This is defined as the failure strength of the S-CLAY1 model in extension. At this point of the stress path the corresponding strain level is very large and the sample has failed. For practical applications and in boundary value problems this is the maximum strength in extension. In the model simulations the yield surface continues to rotate until the fabric is completely rearranged (ultimate strength in extension). Again it can be seen that the maximum stress predicted in PSE is greater than in TXE.

2.4.2 Multilaminate Model for Clay (MMC)

The multilaminate framework (Zienkiewicz and Pande, 1973) can be used to model anisotropy of plastic behaviour. The framework was originally introduced to model rocks with different joint directions. Pande and Sharma (1983) extended the basic framework (Zienkiewicz and Pande, 1973) to model clays. A formulation that enables the use of multilaminate models in combination with an elasto-plastic tangent stiffness algorithm was first presented by Pietrusczak and Pande (1987). In the multilaminate framework each stress integration point is associated with a number of sampling planes of different direction. On each sampling plane a local stress-strain relation is formulated (microscopic level). The local stress on the sampling plane is derived from the global stress state (macroscopic state) via a stress transformation. The elastic part is formulated on the global level (macroscopic level). The total global strains, which consist of an elastic strain plus a plastic strain, are obtained by numerical integration of the plastic strains from each sampling plane and the global elastic contribution.

An anisotropic global stress state will produce a different combination of local stress states on each sampling plane of the multilaminate model. Hence an anisotropic stress history will result in different sizes of yield surfaces on each sampling plane. However, an isotropic global stress state will generate the same local stress state on each sampling plane. Each yield curve on each individual sampling plane will have the same size.

Wiltafsky (2003) describes the Multilaminate Model for Clay (MMC). In the MMC, the yield curve is based on a double hardening formulation by Vermeer (1978). The yield curve is formulated in terms of σ'_n and τ on the σ'_n - τ plane, where σ'_n is the effective normal stress and τ the shear stress. It consists of three parts, an elliptical volumetric cap (f_c), a deviatoric hardening section (f) and a tension cut off (f_t) section.

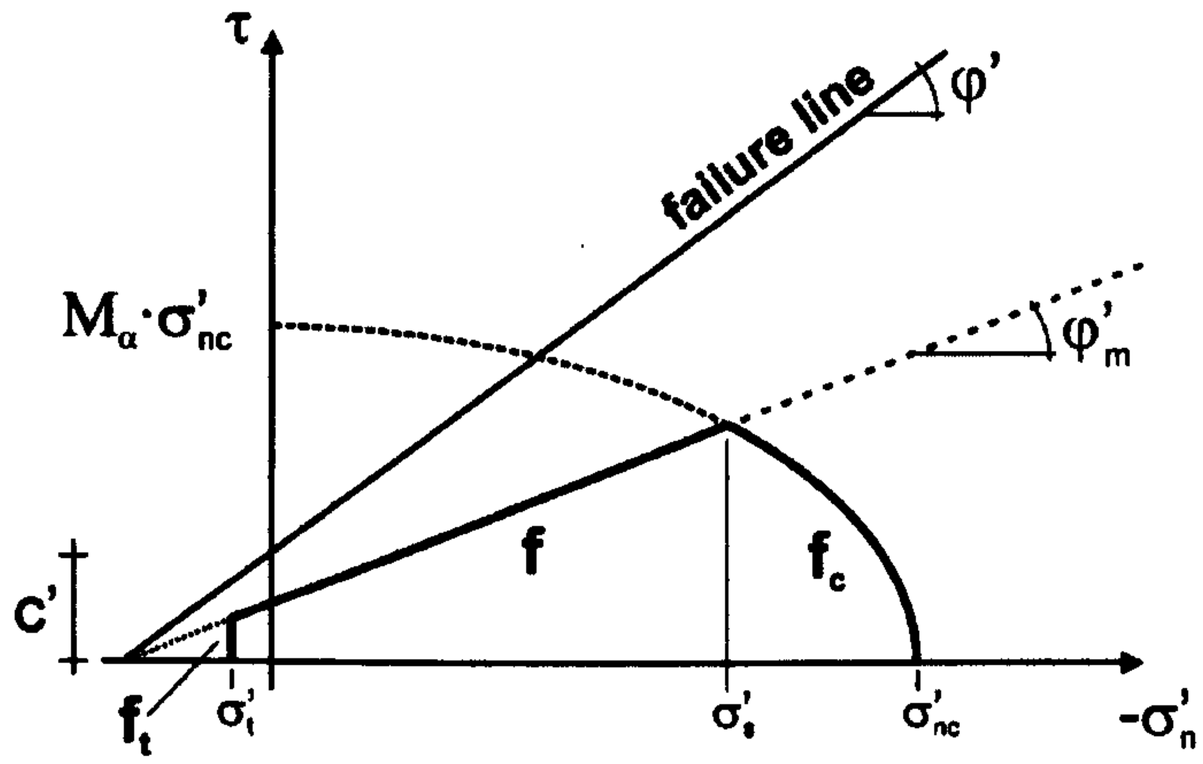

Figure 2.14: Yield surface of the MMC on each sampling plane

Figure 2.14. shows the yield surface on the σ'_n - τ plane. The formulation of the volumetric cap is given by:

$$f_c = \left(\frac{\sigma'_n}{\sigma'_{nc}}\right)^2 + \left(\frac{\tau}{M_\alpha \sigma'_{nc}}\right)^2 - 1 = 0. \qquad [2.32]$$

where the normal preconsolidation stress σ'_{nc} defines the current size of the yield surface and M_α defines the aspect ratio of the yield curve. Note that M_α is not the same as M at the critical state stress ratio. M_α defines the shape of the yield curve and thus influences the predicted global K_0-value, similar to the definition in the Soft Soil model (Brinkgreve, 2002). The value of M_α is calculated as:

$$M_\alpha = \alpha(\sin\varphi'). \qquad [2.33]$$

where α is a material constant and can be estimated by $\alpha = 1-\sin(2/3\varphi')$ for normally consolidated clays (Wiltafsky, 2003). The parameter α should not be confused with the parameter α in the S-CLAY1 model. Volumetric hardening is related to the increment of the plastic normal strain $d\varepsilon^p_{n,cap}$ on the sampling plane. The volumetric hardening law is given by:

$$d\sigma'_{nc} = \frac{\nu \sigma'_{nc} d\varepsilon^p_{n,cap}}{\lambda - \kappa}. \qquad [2.34]$$

and is defined analogous to the volumetric hardening law of the MCC model (*Eq. 2.2*). An associated flow rule is used for the yielding on the cap side and to give the ratio for the plastic normal strain increment $d\varepsilon^p_{n,cap}$ and plastic shear increment $d\varepsilon^p_{\gamma,cap}$ on each sampling plane.

The yield curve of the deviatoric hardening section is given by the following equation:

$$f = \tau - \sigma'_n \tan\varphi'_m - \frac{c' \tan\varphi'_m}{\tan\varphi} = 0. \qquad [2.35]$$

where φ'_m is the mobilised friction angle and a hardening parameter, c' is the effective cohesion and φ' the friction angle of the Mohr Coulomb failure line (Figure 2.14). Hardening of the deviatoric section is related to the plastic shear strain increment $d\varepsilon^p_{\gamma,cap}$ on the sampling and given by:

$$d(\tan\varphi'_m) = \frac{(\tan\varphi' - \tan\varphi'_m)^2}{A \tan\varphi'} d\varepsilon^p_{\gamma,\,cone}. \qquad [2.36]$$

where A is a soil constant controlling the rate of deviatoric hardening of the cone. The parameter A is found by optimising model simulations with experimental data on triaxial tests reaching compressive failure. The influence of parameter A is best observed in q-e_q diagram (Wiltafsky, 2003). The value has a large influence on the predicted stress strain behaviour and the results are very sensible against the A value. Back calculation of triaxial tests of Finnish clays (Wiltafsky, 2003) showed that a large number of tests at different stress ratios η are required to derive sensible values for it. A non-associated flow rule is used on the deviatoric hardening section, using a mobilised dilatancy angle ψ, based on the stress theory of Rowe (1972).

The third part of the yield curve is the tension cut off criterion according to:

$$f_t = \sigma'_n - \sigma'_t = 0. \qquad [2.37]$$

where σ'_t is the maximum allowable tension stress on the sampling plane. An associated flow rule is assumed for the tension cut off.

The parameters of the MMC are derived from conventional laboratory tests with the exception of parameter A as mentioned above. The model was implemented as an User defined soil model into the 2D PLAXIS 8 code by Wiltafsky (2003). Wiltafsky (2003) presented numerical simulations, using the MMC model, of Vanttila clay and POKO clay, both clays from Finland. Each test was performed at different values of η. The results of the simulations showed high quality matches with the experimental data, with yield points well predicted. In tests, where the second loading stage was very different to the previous loading stage, MMC simulations resulted in progressive yielding on the various sampling planes, and hence a gradual change in soil compressibility. This leads to a significant curvature of the post-yield compression curve in a ε_v:ln(p') plot (Wiltafsky, 2003). The behaviour is similar to what is observed in numerical simulations with the S-CLAY1 model.

A global peak undrained shear strength similar to that which has been defined in the MCC and S-CLAY1 model can not be described in the MMC model. The peak strength is different on each of the integration planes and as such represents a local peak on the individual plane.

2.5 Destructuration model: S-CLAY1S

The S-CLAY1S model (Karstunen et al. 2005) is an extension of the S-CLAY1 model, which incorporates large strain anisotropy via a rotational hardening law. Additionally the S-CLAY1S model accounts for bonding and destructuration. The yield surface of the natural soil is given by the same expression as in S-CLAY1, *Eq. 2.11* for the general stress state and *Eq. 2.19* for the special case of the triaxial stress state. The effect of bonding is described by an intrinsic yield surface (Gens and Nova, 1993), which represents the equivalent unbonded soil. It is assumed that the unbonded soil has the same fabric as the natural soil and hence the intrinsic yield surface has the same shape and orientation as the natural yield surface (Figure 2.15). The size of the intrinsic yield surface p'_{mi} is related to the size of the natural yield surface p'_m through the following expression:

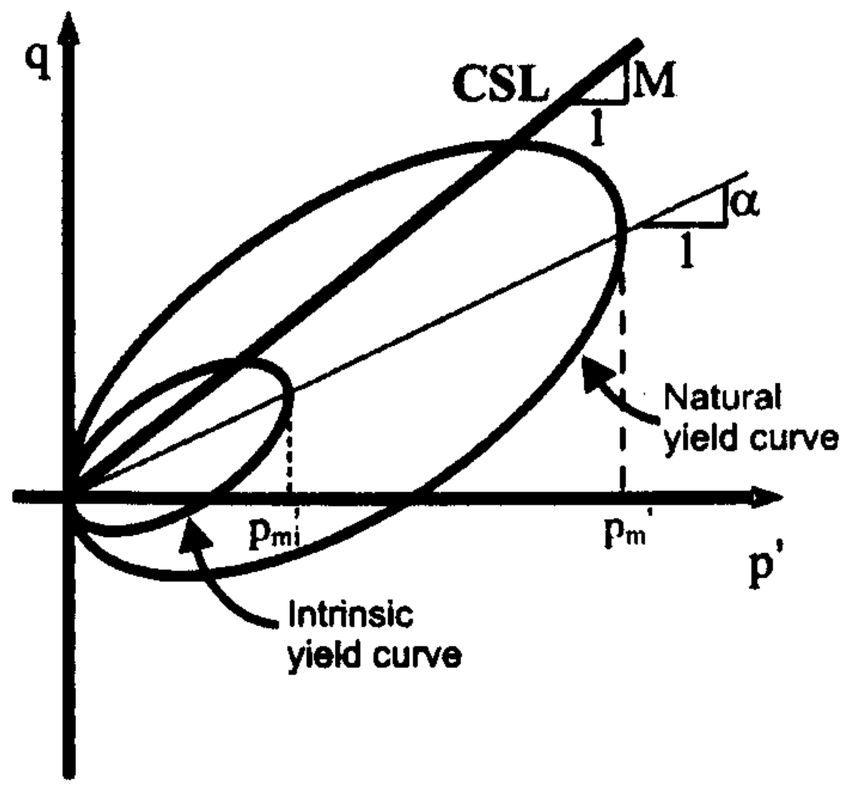

Figure 2.15: Yield surface of the S-CLAY1S in triaxial stress space

$$p'_m = (1+x)p'_{mi} \qquad [2.38]$$

where x defines the current degree of bonding. In the S-CLAY1S model not only the size of the intrinsic yield surface is important for the formulation of the model but also the rotation of the intrinsic yield surface. The intrinsic yield surface is not directly used to derive partial derivatives for the direction of the plastic strains but it represents the remoulded soil and as such the maximum deviatoric stress q_{max} of the remoulded soil.

Elastic behaviour inside the yield surface is provided with the same equations as in S-CLAY1 and MCC. The model assumes an associated flow rule to derive the ratio of the plastic volumetric stains and plastic deviatoric strains.

2.5.1 Hardening laws

The S-CLAY1S model incorporates three hardening laws. The first one is related to the change in the size of the intrinsic yield surface. The size is related to the plastic volumetric strain increment $d\varepsilon_v^p$ by the hardening law for the unbonded (reconstituted) material:

$$dp'_{mi} = \frac{vp'_{mi}d\varepsilon_v^p}{\lambda_i - \kappa} \qquad [2.39]$$

where λ_i is the gradient of the intrinsic normal compression line of a reconstituted soil in the v:ln(p') plane. The first hardening law is of the same form to that of the S-CLAY1 model but with p'_m replaced by p'_{mi} and λ replaced by λ_i. The second hardening law, describing the rotation of the surface (i.e. evolution of anisotropy), is the same as in the S-CLAY1 model (*Eq. 2.16*).

The third hardening law of the S-CLAY1S model, the so-called destructuration law, describes the degradation of bonding with plastic straining. It is assumed that both plastic volumetric strain and plastic deviatoric strain, whether positive or negative, tend to reduce the bonding parameter x to zero:

$$dx = -ax(\left|d\varepsilon_v^p\right| + b\left|d\varepsilon_d^p\right|). \qquad [2.40]$$

Soil constant, a, controls the absolute rate of destructuration and b controls the relative effect of plastic deviatoric strain increment $d\varepsilon_q^p$ in destroying the bonding. As discussed in Section 2.5 many of the previously proposed destructuration models assume b = 1.

2.5.2 Initial state parameters

Four state parameters are required to describe the initial state of the soil using the S-CLAY1S model. The first three, the initial void ratio e_0, the initial size of the yield surface p'_m and the initial inclination of the yield surface α_0, are the same as in the S-CLAY1 model. The fourth parameter required is the bonding parameter, x. Koskinen et al. (2002a) suggest a procedure for determining the initial value of x. The value of x can be best derived from the sensitivity S_t measured from a fall cone test. S_t provides an estimate for the bonding parameter x.

$$x = S_t - 1 \qquad [2.41]$$

2.5.3 Model parameters

The S-CLAY1S model involves eight soil parameters. Five are the same as in the S-CLAY1 model (κ, M, ν', μ, β). The parameters a and b are derived via an optimisation

procedure in doing model simulations of laboratory tests (Koskinen et al. 2002a). First a value for parameter a is selected. This is best achieved by simulating a drained triaxial test involving a low value of η, for example a stress path close to isotropic compression, where the shear strains are small and hence the influence of parameter b is negligible. Once parameter a has been selected, a test involving a high value of η should be modelled, where the contribution of shear strains to destructuration is dominant. These simulations are then used to select an appropriate value for parameter b. Model simulations of Finnish natural clays (Koskinen et al. 2002a) have indicated that typically a = 9-11 and b = 0.2-0.3. It seems to be the case that these values can be used as default values for soft clays from Finland. Magnet (2006) reported similar value of a and b based on back calculation of triaxial tests on Bothkennar clay. It was found through an optimisation procedure that a = 10-12 and b = 0.4. Often specialist stress path controlled tests are not available and then a typical default value could be chosen for b (e.g. b = 0.2). Following that the value of a could be optimised by simulating any compression test for which test data is available.

By setting the initial value of the state parameter x to zero and using an apparent value of λ from a natural sample, instead of λ_i from a reconstituted sample, the model reduces to the S-CLAY1 model, which accounts for anisotropy only. If in addition the initial value of α is set to zero, and the soil constant μ are set to zero, the model reduces further to the isotropic MCC model.

The model was originally implemented by Zentar (2004) in the SAGE Crisp finite element code using an explicit forward Euler algorithm. In 2003 Wiltafsky (2003b) implemented the model into the PLAXIS 8 code as a user defined soil model using an implicit backward integration scheme. During this work the model implementation by Wiltafsky (2003b) was extended and further improved. As part of this work the model was also implemented into the PLAXIS 3D foundation and a limited version has been implemented into the PLAXIS 3D tunnel code.

Koskinen et al. (2002a) presented S-CLAY1S simulations of natural POKO clay with each test involving two loading stages at different η values. The simulations were

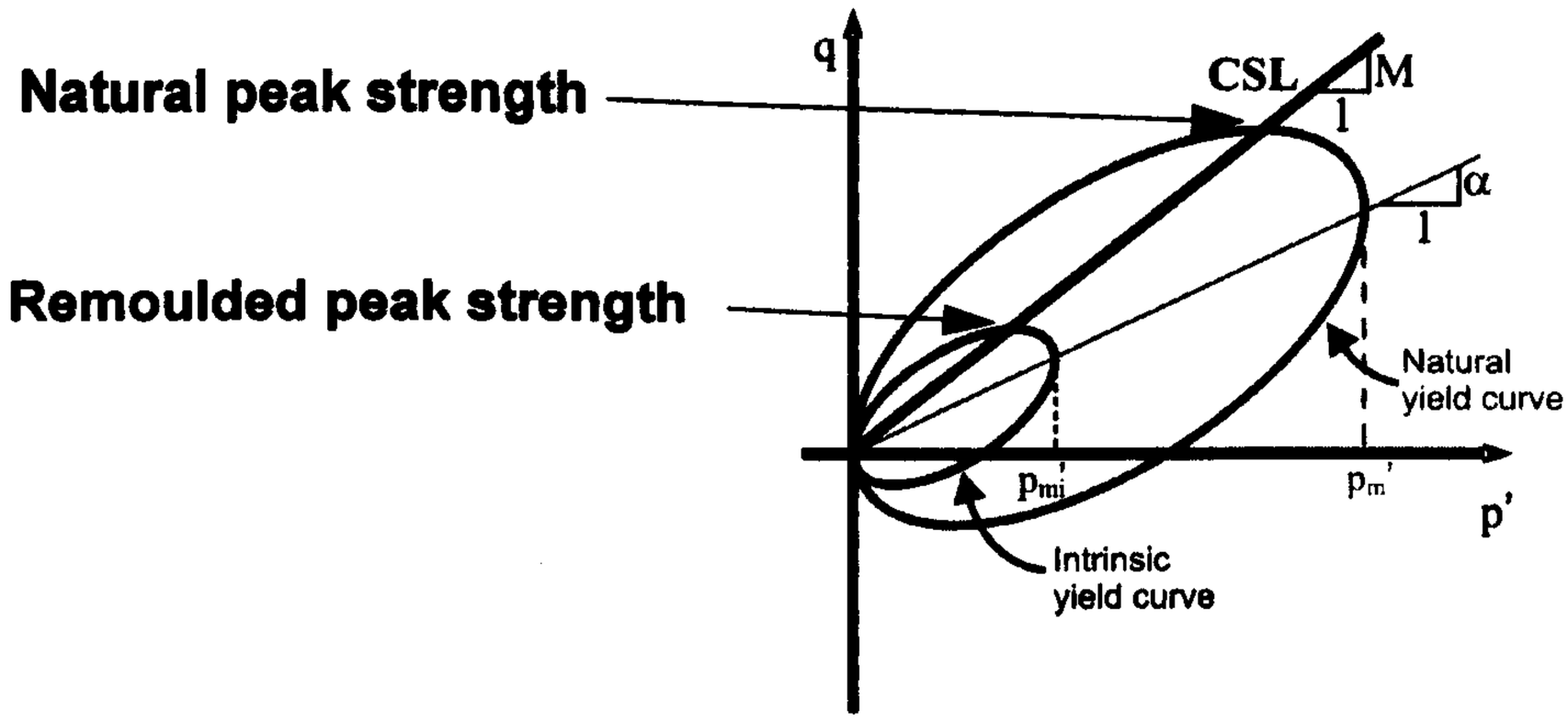

Figure 2.16: Natural and remoulded peak undrained shear strength

generally a good match to the experimental data. In addition simulations have been performed of experimental tests on natural samples of Otaniemi clay, Murro clay and Vanttila clay (Koskinen et al. 2002d, Koskinen et al. 2004, Zentar et al. 2004). These test simulations also show good agreement for a range of η values and over both loading stages.

2.5.4 Peak undrained shear strength

The peak undrained shear strength of the natural material is defined in the same way as in the S-CLAY1 model (Section 2.4.1.5). The definition of the natural peak strength in the p'-q stress space is shown in Figure 2.16.

2.5.5 Remoulded peak undrained shear strength

Similar to the natural strength in the S-CLAY1S model the remoulded strength can be described in the p'-q stress space. The second yield surface, the intrinsic yield curve smaller in size represents the unbonded material which has the same void ratio and the same fabric as the natural material. The q_{max_i} of the unbonded material (the interception point between the critical state line and the intrinsic yield surface) is smaller than the q_{max} of the natural material (see Figure 2.16). The q_{max_i} of the unbonded material describes the remoulded peak shear strength c_{ur} during undrained loading or consolidation.

For the mathematical definition of the remoulded strength c_{ur}, the same principal as used for the natural strength can be applied. Inserting *Eq. 2.3* in the intrinsic yield curve function (Figure 2.19) leads to a quadratic equation.

$$2q^2 + q\left(\frac{\alpha p'_{mi}}{M} - \frac{2\alpha}{M} - p'_{mi}\right) = 0 \qquad [2.42]$$

Applying the quadratic formula results in:

$$2c_{ur} = q_{max\neg i} = 2c_u = q_{max} = \frac{\alpha p_{mi} - M p'_{mi}}{4} \quad . \qquad [2.43]$$

Eq. 2.43 is the same as *Eq. 2.31* for the natural strength. Only the variable p'_m which defines the size of the natural yield curve in the p'-q stress space is replaced with p'_{mi} the variable which defines the size of the intrinsic yield surface.

It is well known that during consolidation the remoulded and natural shear strength will increase but in special circumstances a different phenomena is observed. A change in natural and remoulded strength means that both yield surfaces increase in size and/or a rotation of the yield surfaces takes place. An increase in the remoulded strength is not necessarily always linked to an increase of the natural strength. In some circumstances an expansion of the intrinsic yield curve can be observed without an increase of the natural yield curve. Thus the remoulded strength increases but the natural strength does not. Another phenomena can be observed using the S-CLAY1S model: an increase in the size of the intrinsic yield curve while at the same time the natural yield curve undergoes a reduction in size.

The predicted stress paths in the s'-t plane for triaxial undrained shearing in compression and extension, and plane strain undrained shearing in compression and extension using the S-CLAY1S model are shown in Figure 2.17. The samples are assumed to represent natural Murro clay at a depth of -7 m. Details about the clay can be found in Chapter 6. The simulations are performed with a single Gauss point programme. For

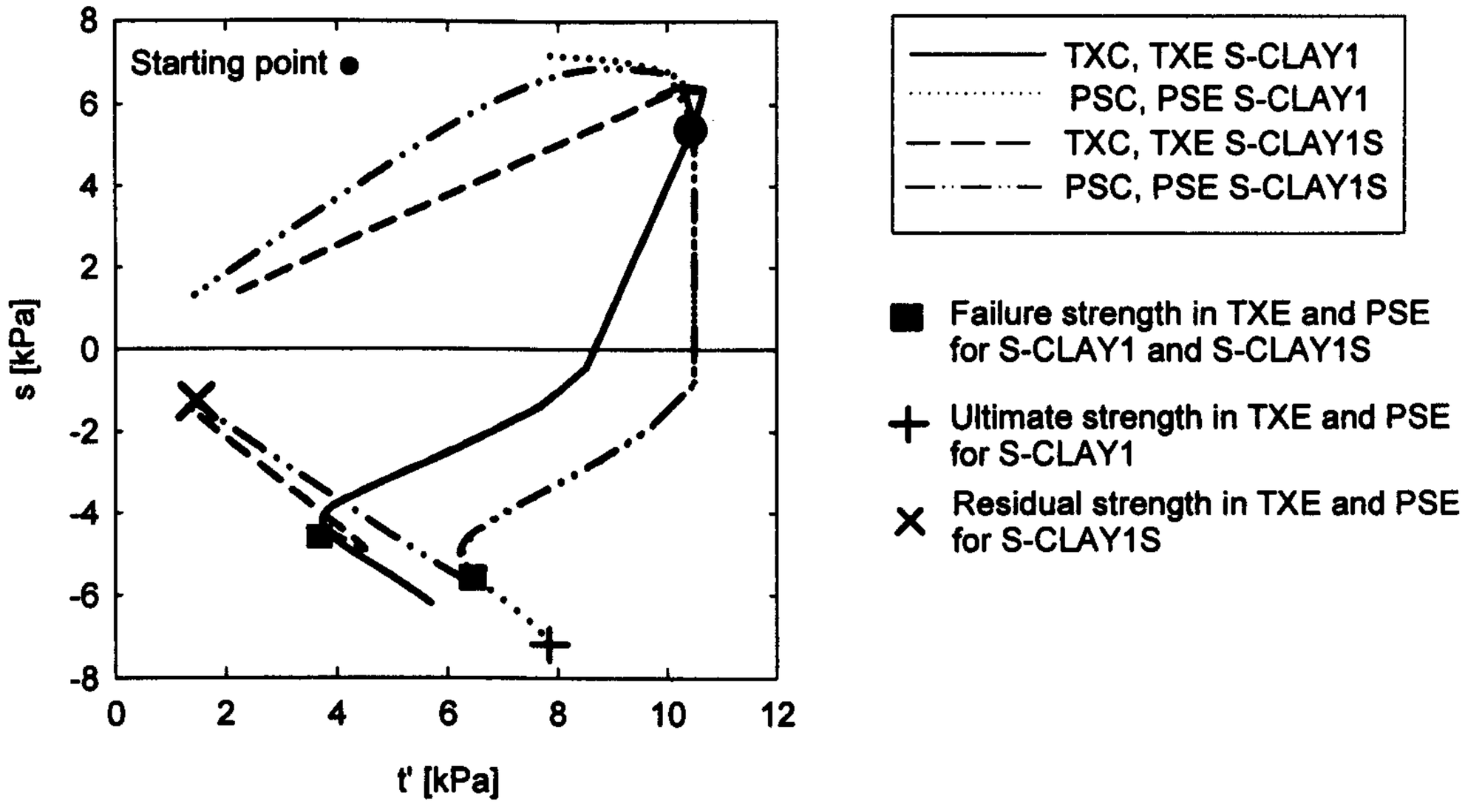

Figure 2.17: Predicted stress paths for triaxial compression and extension, and plane strain compression and extension using the S-CLAY1S and S-CLAY1 model

comparison, the paths predicted using the S-CLAY1 model are also presented here. Initial inspection of the stress paths reveals that the S-CLAY1S model predicts strain softening once it reaches the critical state stress ratio. The S-CLAY1 model predicts a marginally higher peak stress t in triaxial compression than the S-CLAY1S before reaching the critical state stress ratio. This is more pronouced in plane strain compression. Both paths diverge after a certain amount of yielding. The S-CLAY1 predicts an increase in the stress level t up to the critical state stress ratio but the S-CLAY1S predicts a reduction in t before reaching the critical state stress ratio. The same is observed in extension but is less pronounced. In triaxial extension both models predict similar stress paths up to a point close to a stress ratio at critical state before they diverge. The S-CLAY1 path is moving upwards to the failure line (ultimate strength in TXE and PSE) whereas the path by the S-CLAY1S turns, reverses the direction and moves downwards as strain softening happens (residual strength in TXE and PSE). Interestingly the path of the S-CLAY1S model swings outwards for triaxial extension but inwards for plane strain before softening. Again the maximum t in extension for the S-CLAY1S is lower than for S-CLAY1 model. Accounting for destructuration reduces the maximum possible t in triaxial stress space and plane strain conditions.

2.6 Creep models

2.6.1 Soft Soil Creep model (SSC)

The isotropic SSC model (Vermeer et al. 1998, Vermeer & Neher 1999, Neher et al. 2001) is a general three-dimensional creep model based on the isotropic Modified Cam Clay ellipse. In the SSC model the total strain increment $d\varepsilon$ is divided into two components, namely the elastic part $d\varepsilon_e$ and the viscoplastic part $d\varepsilon_{cr}$ (creep component).

$$d\varepsilon = d\varepsilon^{e} + d\varepsilon^{cr} \qquad [2.44]$$

In order to be able to conveniently describe the SSC in terms of stress invariants in the p'-q plane the volumetric strain increment $d\varepsilon_v$ is introduced.

$$d\varepsilon_{v} = d\varepsilon_{v}^{e} + d\varepsilon_{v}^{cr} \qquad [2.45]$$

For triaxial stress states *Eq. 2.45* can be expanded to *Eq. 2.46*:

$$d\varepsilon_{v} = \frac{\kappa^{*} dp'}{p'} + \frac{\mu^{*}}{\tau}\left(\frac{p'_{eq}}{p'_{p}}\right)^{\frac{\lambda^{*}-\kappa^{*}}{\mu^{*}}} \qquad [2.46]$$

where the first term of the equation is the elastic volumetric strain increment expressed by a simple hypoelastic law. κ^* is the modified swelling index, defined in the ε_v:ln(p') plane and dp' is the change in mean effective stress. The elastic increment is directly linked to the rate of increase of the mean effective stress p'. The second term in *Eq. 2.46* is the volumetric creep strain increment. μ^* is the modified creep index, defined in a ε_v:ln(t) plot. It can also be related to the conventional creep index C_α by:

$$\mu^{*} = \frac{C_{\alpha}}{(1+e)\ln 10} \quad . \qquad [2.47]$$

τ in *Eq. 2.46* is the reference time which is usually taken as 1 day when the position of the normally consolidation line is defined through 24 hour oedometer tests. The 1 day

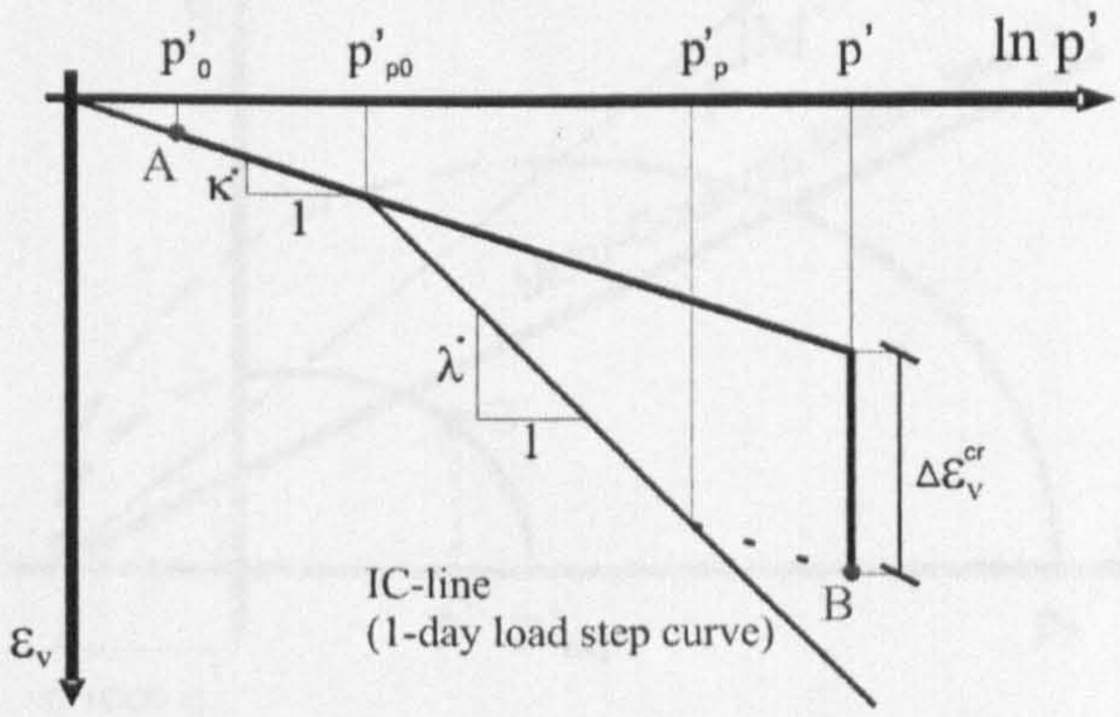

Figure 2.18: Idealised stress strain curve from an oedometer test

compression line is usually used to determine the preconsolidation pressure. λ^* is the modified compression index and defines the gradient of the normal consolidation line in the ε_v:ln(p'), shown in Figure 2.18. The normal consolidation line in Figure 2.18 corresponds to a test where the reference time τ for each load step has been held constant. p'_p in *Eq. 2.46* and shown in Figure 2.18 is defined by reference to the normal consolidation line. The projection of p'_p on to the normal consolidation line can be expressed via the following relation:

$$p'_p = p'_{p0} \exp\left(\frac{\Delta\varepsilon_v^{cr}}{\lambda^* - \kappa^*}\right) \qquad [2.48]$$

where p'_{p0} is the initial value of p'_p, the intersection of the normal consolidation line with the elastic swelling line, see Figure 2.18. The increase of p'_p with time is related to the increase of the volumetric creep strain. Inspection of *Eq. 2.46* and Figure 2.18 shows that the ratio of p'/p'_p determines the rate of creep strain. A stress state p' which plots on the normal consolidation line would yield large creep strains. Creep strains decrease exponentially for stress state p' with distance from the isotropic line, i.e. all stress states which plot above the normal consolidation line.

To represent the creep model in triaxial stress space (Figure 2.19), ellipses are introduced similar to the ellipses used in the MCC model. The ellipses of the SSC model are shifted off the apex point and the elastic domain is limited by Mohr-Coulomb fail-

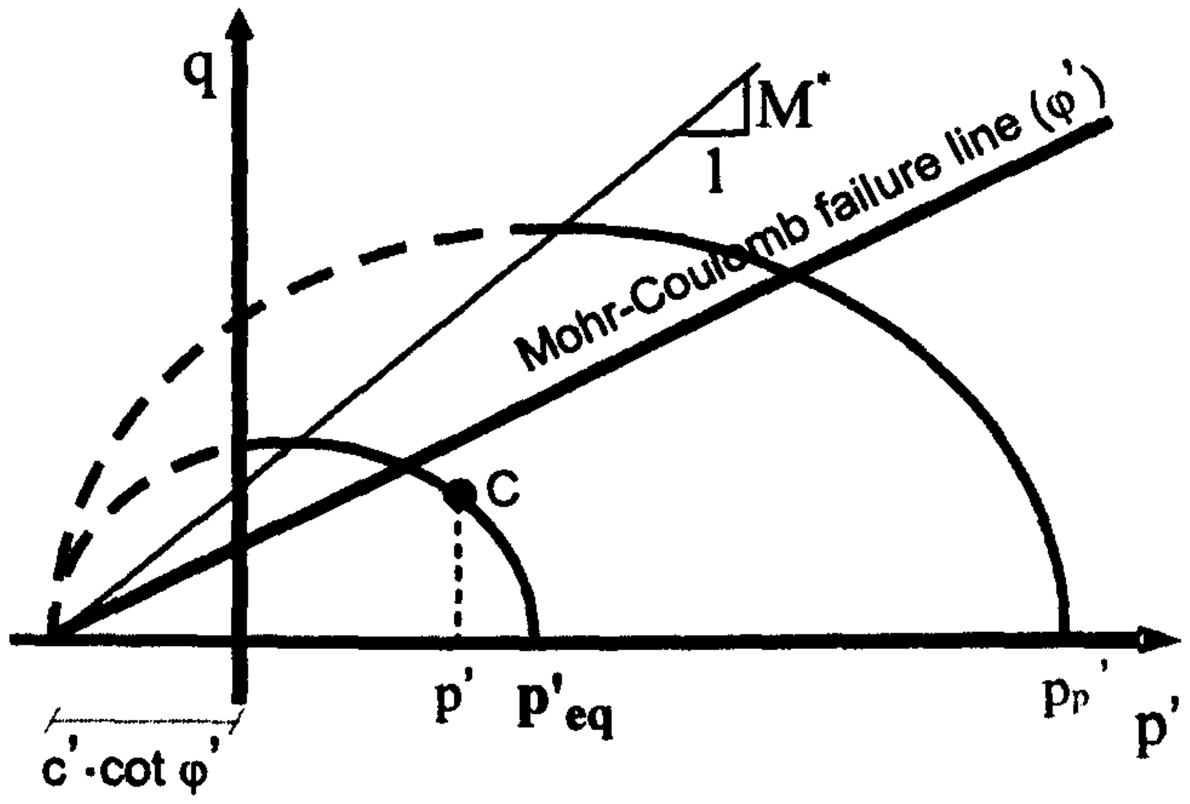

Figure 2.19: Soft soil creep model in triaxial stress space

ure criteria. The current stress state p' lies on the inner ellipse, which has a size of p'_{eq}. The shape of the ellipse is defined through the soil constant M* which is not the same as the stress ratio M at critical state (see SS model for details). p'_{eq} is given by:

$$p_{eq}' = p' - \frac{q^2}{M^{*2}(p' - c\cot\varphi)} \qquad [2.49]$$

The second ellipse, the viscoplastic surface, represents the stress state on the normal consolidation line. The size of the viscoplastic surface is defined by p'_p and increases in time as creep strain occurs, according to *Eq. 2.48*. p'_{eq} presents the current stress state. The ratio controlling the creep in the triaxial stress state is p'_{eq}/p'_p (*Eq. 2.18*). The ratio:

$$\frac{p'^{eq}}{p'_p} = \frac{1}{OCR^*} \qquad [2.50]$$

where OCR* is the apparent overconsolidation ratio, which should not be confused with the overstress in Penzana (1962) type models. Unlike the overstress models the SSC model predicts creep strains at any stress level thus there is no pure elastic state.

An associated flow rule is assumed to provide the magnitude of the deviatoric creep strain. The model uses a Mohr Coulomb failure line with a non associated flow rule to describe shear failure. No creeps strains occur on the failure line.

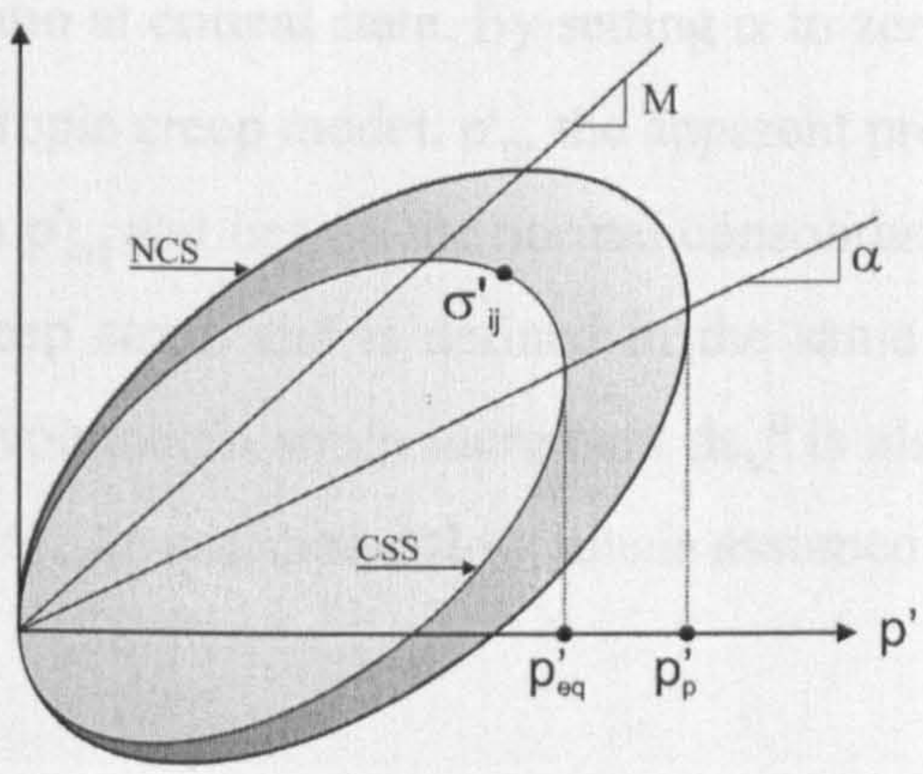

Figure 2.20: ACM model in triaxial stress space (Leoni et al. (in press))

The model was tested on drained and undrained compression tests using reconstituted samples (Vermeer and Neher, 1999) and is able to represent the experimentally observed time dependent behaviour, reasonably well.

2.6.2 Anisotropic creep model (ACM)

Vermeer et al. (2007) and Leoni et al. (in press) point out that the assumption of an isotropic yield surface as used in isotropic creep models does not represent the observed behaviour of natural soft clays. A more realistic model must account for the initial anisotropy and changes in the fabric anisotropy due to plastic straining. Leoni et al. (in press) at the University of Stuttgart developed an anisotropic creep model, the so-called ACM in collaboration with the University of Strathclyde.

To define the ACM in the simplified triaxial stress state (where the axis of cross anisotropy coincides with an axis of the specimen in the test apparatus), the model uses the yield surface of the S-CLAY1 model (Wheeler et al. 2003) for the current stress surface (CSS) and normal consolidation surface (NCS), see Figure 2.20. The two surfaces are assumed to have the same inclination, α. The mean stress state p'_{eq}, is defined by:

$$p'_{eq} = p' + \frac{(q - \alpha p')^2}{(M^2 - \alpha^2)p'} \qquad [2.51]$$

where M is the stress ratio at critical state. By setting α to zero in *Eq. 2.51* the model would reduce to an isotropic creep model. p'_p, the apparent pre-consolidation stress is defined in analogy with p'_{eq} and lies on the normal consolidation line. p'_p is evolving with the volumetric creep strain and is defined in the same manner as in the SSC model (*Eq. 2.48*). The volumetric strain increment $d\varepsilon_v^c$ is also defined according to the SSC model (*Eq. 2.46*). An associated flow rule is assumed for the rate of the deviatoric creep strain $d\varepsilon_d^c$.

The rotation of the NCS and the CSS is controlled by the rotational hardening law, similar to that proposed by Wheeler et al. 2003 for the S-CLAY1 model and is given by:

$$d\alpha = \omega\left[\left(\frac{3q}{4p'} - \alpha\right)d\varepsilon_v^c + \omega_d\left(\frac{q}{3p'} - \alpha\right)(d\varepsilon_d^c)\right] \qquad [2.52]$$

where ω and ω_d are soil constants that control the rate of rotation. Both parameters fulfil a similar function in the rotational law to the parameters μ and β used in the S-CLAY1 model (Section 2.4.1.1). ω_d is defined similarly to the parameter β in the S-CLAY1 model. For the estimation of the parameter ω the reader is referred to Leoni et al. (in press).

Numerical simulations of undrained compression and extension tests of Hong Kong clay show a good agreement with the experimental results (Leoni et al. (in press)) and a notable improvement compared to the SCC model.

2.7 Comments about model implementation

In the subsequent chapters of this thesis not all the constitutive laws introduced here were used in numerical simulations. For the majority of the 2D simulations the S-CLAY models were used and only in simulations of the benchmark embankment in Chapter 4 was the MMC utilised. In the following discussion only the models implemented as user defined soil models into the 2D finite element code PLAXIS 8 are considered. The S-CLAY models and the MMC model were originally implemented

by Wiltafsky (2003a, 2003b) into the PLAXIS 8 finite element code. Wiltafsky did some pioneering work in 2003 as the first to implement the MMC into the code via the user defined soil model interface. At that time there was not much documentation available other than personal guidance by the software developers. At this point the discussion will mainly focus on the original implementation and later in Chapter 5 new developments regarding the implementation are introduced.

2.7.1 User subroutine

When using a user defined soil model all the soil constants and state variables related to the model are inputted via a so-called user defined model interface. The model interface has a simple tabular layout with an empty box for the input next to the name of the input parameter. The user defined subroutine is called by the calculation kernel whenever information regarding the constitutive model is required. In the PLAXIS code this information demand is split into different so-called ID tasks. In total there are six tasks. In the following a general introduction to the ID tasks is given.

2.7.1.1 Initialise state variables (ID Task=1)

The initialisation is used to determine the initial values of the state variables such as the size of the yield surface, the initial void ratio and any other state variable related to the yield surface position or shape. The initialisation process will be activated only once. Between ongoing calculation stages the state variables are transferred from one stage to another. This initialisation stage is also used to calculate any other important variables or constants stored as state variables which will be later used as a reference in the output stage.

2.7.1.2 Calculating the constitutive stresses (ID Task=2)

This task contains the calculation procedure used to evaluate the constitutive stresses corresponding to a given strain increment. As mentioned before the S-CLAY models and the MMC model have been implemented using the implicit forward integration scheme. In this scheme the trial stress is modified as long as convergence is satisfied.

In general the convergence criteria is reached when the iterative stress state is returned to the yield surface by using a stress return algorithm. For a comprehensive summary and detailed discussion about the integration scheme and the return algorithm the reader is referred to Potts and Zdravkovic (1999).

2.7.1.3 Create material stiffness matrix (ID Task=3&6)

As an implicit forward integration scheme is used for both model implementations the ID Task 3 and 6 are the same. In both cases the elastic material stiffness matrix is derived. For details when the ID Task 3 is different to ID Task 6 the reader is referred to Brinkgreve (2002).

2.7.1.4 Number of state variables (ID Task=4)

This is a minor task which simply returns the number of state variables used in the constitutive model to the calculation kernel. The maximum number of state variables in the PLAXIS code is practically unlimited (Brinkgreve, 2002).

2.7.1.5 Matrix attributes (ID Task=5)

In this task the type of material stiffness matrix is defined. The material stiffness matrix can be stress dependent, time dependent, symmetric or non-symmetric. Both the MMC and S-CLAY models use a symmetric stress-dependent stiffness matrix.

2.7.2 Discussion of the implementation

In the S-CLAY1S model user subroutines, 11 state variables are stored. The state variables are the six components of the fabric tensor $\underline{\alpha}_d$, the scalar value of the fabric tensor α, the size of the intrinsic yield surface p'_{mi}, the bonding parameter x, the size of the natural yield surface p'_m and the void ratio e. The values of α and p'_m are only stored for output purposes. In the MMC model the storage requirements are much more demanding due to the large number of integration planes. Four state variables per integration plane are stored. Namely, the size of the local yield surface σ'_{nc}, the local mobilised friction angle φ'_m, the plastic shear strain increment $d\varepsilon^p_{\gamma,cone}$ and the

plastic volumetric strain increment $d\varepsilon^{p}_{n,cap}$. Wiltafsky (2003a) uses a 33-plane integration rule and that means a total of 132 state variables are stored just for the local information on the planes for each Gauss point. The rest of the state variables such as the void ratio e are stored globally. This large number of state variables requires a significant larger memory space than the S-CLAY1S model which is embedded in a standard elasto-plastic framework. Consequently, MMC requires more run time than the other models. For the simple benchmark embankment problem presented in Chapter 4, the run time for the models implemented in the standard elasto-plastic framework is less than 10 min whereas the calculation time using the MMC model is at least 3 hours.

The S-CLAY models and the MMC models are non-linear models. The accuracy of the calculation results depends significantly on the size of the strain increment. The size of the trial strain increment is controlled by the user via a sub-stepping procedure. Through an input parameter called 'step size' the user can manually control the size of the strain increment. The sub-stepping procedure has been implemented to avoid convergence problems and inaccuracies. Further details about the substepping procedure can be found in Section 5.2. For most boundary value problems a value of -0.01 is recommended based on the experience of the author.

2.7.3 Global iteration and control procedure

The iterative procedure at the global level needs to satisfy the constitutive relations and the equilibrium conditions. PLAXIS uses a so-called automatic step-size procedure (Brinkgreve, 2002). The size of the first load step is either chosen manually by the user or automatically by the software. For each load step a series of iterations is carried out. The number of iterations is limited to a so-called desired minimum and maximum which is a default setting or can be changed by the user to an appropriate value. If equilibrium is reached in less iterations than the desired minimum the software automatically increases the load step by two in the next calculation step. However, if the equilibrium is not reached within the maximum number of iterations the load increment is divided by a factor of two. In the case of equilibrium being reached

within a number of iterations which lies between the minimum and maximum, the load size is kept constant for the next load increment.

Other important control parameters for the iterative procedure are the tolerated error, the over-relaxation and the maximum number of iterations per calculation step. Any non-linear analysis tends to drift from the exact solution (Potts and Zdravkovic, 1999). To keep the drift within an acceptable limit a tolerated error can be specified. For most applications the default setting of 0.01 is recommended. In order to reduce the number of iterations needed for convergence the software uses a so-called over-relaxation procedure. For all calculation undertaken in this work a default value of 1.2 was used. The reader is referred to Vermeer and Van Langen (1989) and Van Langen and Vermeer (1990) for more details about the over-relaxation parameter. The maximum number of iterations limits the number of iterations per calculation step to avoid excessive running time. If the solution does not converge within the set limit the calculation is aborted. A standard setting is 50 but it is recommend to use 100 when highly non-linear models such as the S-CLAY1S are used in an analysis where large strains are expected.

2.8 Review of soft soil constitutive models

The constitutive models discussed and introduced in this chapter are divided into four main classes of models: isotropic models (MCC and SS model), anisotropic models (S-CLAY1 and MMC), destructuration model (S-CLAY1) and creep models (SSC and ACM model).

The two isotropic models are nowadays widely used in engineering practice for numerical simulations for all sorts of boundary value problems in soft soils. Both models have also been tested in drained and undrained compression tests by various researchers, showing an overall good performance. Nevertheless, the assumption of isotropic yield surfaces does not match the experimental data of natural and reconstituted soils. Inclined yield surfaces have been observed and reported for a wide range of natural soft soils, which is an indication of initial anisotropy of the fabric of the

soil. For practical problems in soft soils, where loading is likely to be dominant, it is important to account for large strain anisotropy, whereas anisotropy at small strains may have a minor influence. Accounting for initial and strain induced anisotropy does not just improve the quality of numerical simulations of laboratory tests but also has a big influence on numerical predictions of the stress-strain-strength behaviour of soft soil deposits in boundary value problems.

Two recently proposed advanced constitutive models accounting for initial and strain induced anisotropy, namely S-CLAY1 and MMC have been introduced. The S-CLAY1 is an extension of a standard elasto-plastic model, with initial anisotropy expressed via an inclined (sheared) ellipse in triaxial stress space. Erasure or development of the anisotropy of the fabric is related to a rotational hardening law. In contrast the MMC model is formulated and embedded in the so-called multilaminate framework. Each stress integration point is associated with a certain number of sampling planes at different orientations. The elasto-plastic stress-strain relation is formulated locally on each plane and the global behaviour is obtained by numerical integration of the plastic contribution from each sampling plane. Both models have been validated by experimental data from laboratory tests on reconstituted and natural samples. Simulations of drained reconstituted tests are qualitatively better than those of the natural samples. That can be explained with the existence of structure in the natural soils. The MMC model has some advantages and disadvantage compared to the S-CLAY1 model. The benefit of the multilaminate model is that plastic anisotropy is a natural outcome of the model formulation and no additional hardening law is required. However, there are some significant shortcomings. Computational the MMC is very demanding and already needs a lot of run time for simple embankment problems (Karstunen et al. 2006). Some run time consumption can be explained by the deviatoric hardening law which is not accounted for in the other models. This feature is not very important for embankment loadings but plays an important role in situations such as excavations and tunnels. Another point is the shape of the global yield surface, which does not represent the findings of the experimental data. Indeed, determi-

nation of an appropriate shape for the yield surface in the multilaminate framework is not a trivial task (Reza and Karstunen, 2004).

Structure can be divided into the fabric and the bonding between the particles. The bonding between the particles provides an additional resistance against yielding but will be progressively destroyed during plastic straining. A constitutive model which accounts for both, anisotropy and destructuration will improve the predictions of drained tests on natural samples. The S-CLAY1S model, a further development of the S-CLAY1 model, accounts for anisotropy combined with destructuration. In addition to the yield surface of natural clay, a rotational intrinsic yield surface is introduced, it represents the soil without bonding. The difference in the size of the yield surfaces is a measure of the amount of bonding. Reduction of bonding is related to the plastic strain via a so-called destructuration law (hardening law). Simulations of laboratory tests on natural samples of Finnish clays show an improvement compared to the S-CLAY1 model. However, in numerical simulation some problems may arise with the S-CLAY1S model. The model predicts strain softening during undrained loading which may cause numerical problems during simulations.

The stress-strain-strength behaviour of soft soils is not just dependent on fundamental features such as anisotropy and destructuration but also on creep (time-dependent). Creep strongly influences the soil response under foundation loading. Constitutive models incorporating creep are not explicitly used in this research but for the sake of completeness and the importance for this subject, two creep models have been introduced in this chapter. The choice of the models reflects the recent developments in creep models and also covers a creep model widely used in practical applications by geotechnical engineers all over the world. First an introduction to the isotropic SSC model was given followed by a detailed description of the fundamental features of the model. Then a new creep model, the ACM model, was presented. The model accounts for initial anisotropy, via a sheared elliptical yield surface. The change in the fabric anisotropy is related to volumetric creep strains and shear strains via a rotational hardening law.

The advanced models show substantial improvements to the well know isotropic models. All of the advanced models above, with the exception of MMC have one important aspect in common, the additional features do not make the models to over-complicated and most additional parameters have either a physical meaning, can be derived by numerical simulations or a default value can be used. This gives the models great potential for widespread practical application.

2.9 Constitutive models for granular and cohesive material

So far constitutive models for soft soils have been introduced and discussed. In the following two more isotropic constitutive models will be introduced, as they are not standard models for granular material or stiff cohesive material, such as the well known Mohr-Coulomb model. The two models are called the Hardening Soil model (Brinkgreve, 2002) and the Matsuoka-Nakai Hardening model (Benz, 2006). Both models will be used to describe the stress-strain behaviour of granular type embankment fills and deep mixed material.

2.9.1 Hardening Soil model

The Hardening Soil model (HS model) is a non-linear double hardening model which aims to describe the soil behaviour in the pre-failure state. The model adopts a stress-dependent stiffness formulation following the basic ideas by Ohde (1951). The stiffness either increases or decreases with increasing or decreasing pressure.

2.9.1.1 Hyperbolic stress-strain relationship

Soil which is subjected to deviatoric loading follows a stress-strain curve similar to the one shown in Figure 2.21. Kondner (1963) formulated a stress-strain relationship for the special case of a drained triaxial test. Later Duncan and Chang (1963) presented a hyperbolic model which was able to replicate the curve observed in the triax-

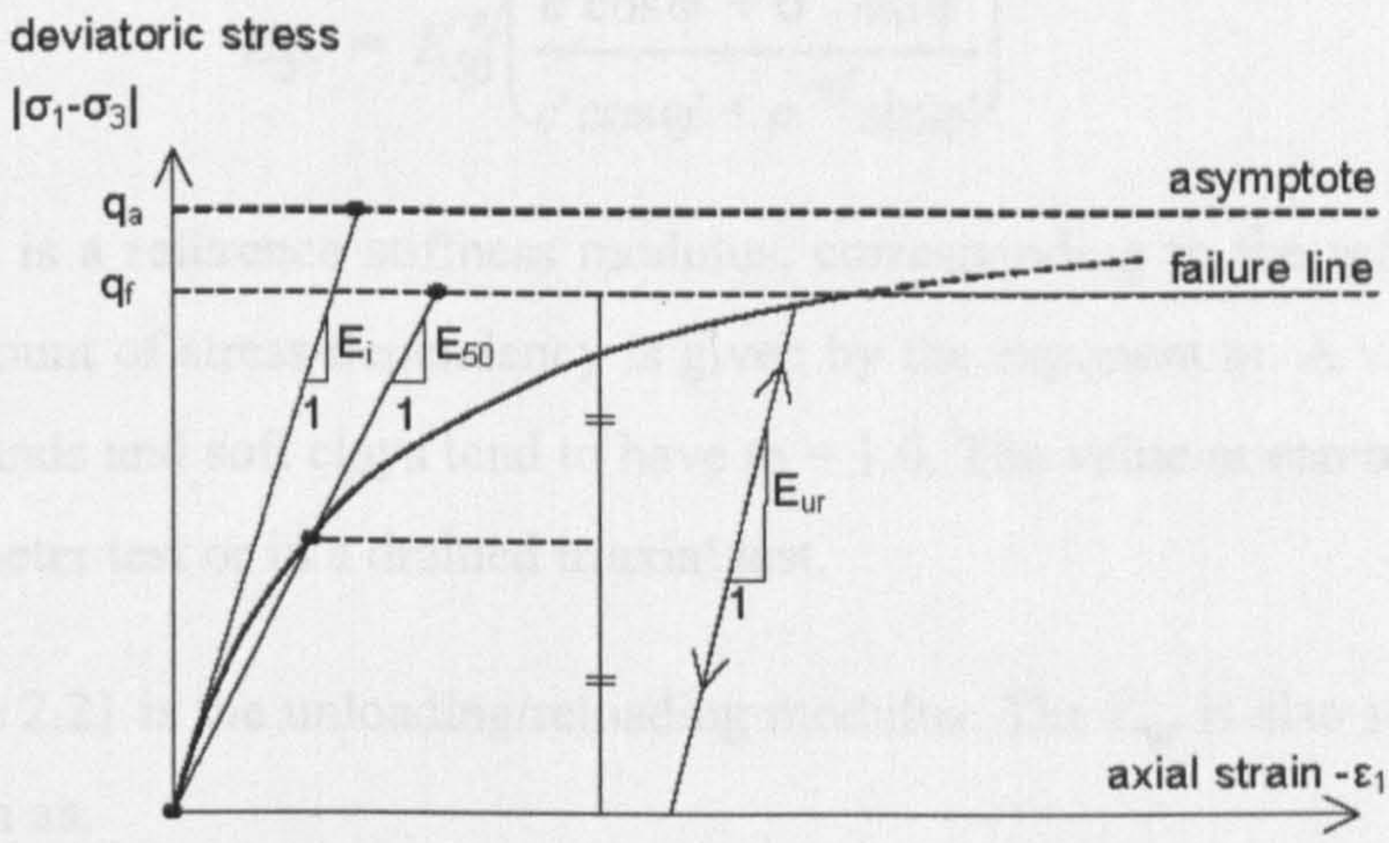

Figure 2.21: Hyperbolic stress strain relationship observed in a drained triaxial test (Brinkgreve, 2002)

ial test. The HS model uses the following hyperbolic stress-strain formulation to describe the behaviour observed in the drained triaxial test:

$$\varepsilon_1 = \frac{q_a}{2E_{50}} \cdot \frac{q}{q_a - q} \qquad [2.53]$$

where q_a is the asymptotic deviatoric failure stress and E_{50} is the secant stiffness modulus at 50% of the q_f. When soil is subjected to primary deviatoric loading, plastic strains develop and a stiffness decrease is observed as shown in Figure 2.21. *Eq. 2.53* describes such a non-linear behaviour up to the Mohr Coulomb failure stress q_f. q_f is defined by:

$$q_f = R_f \cdot q_a . \qquad [2.54]$$

R_f is found to be 0.9 for most soils. The detailed formulation of q_a is as follows:

$$q_a = (c' \cot\varphi' + \sigma'_3) \cdot \frac{2\sin\varphi'}{R_f(1-\sin\varphi')} . \qquad [2.55]$$

The above relationship is derived from the Mohr-Coulomb failure criteria. The stress dependent E_{50} used in *Eq. 2.53* is defined as:

$$E_{50} = E_{50}^{ref}\left(\frac{c'\cos\varphi' + \sigma'_3\sin\varphi'}{c'\cos\varphi' + p^{ref}\sin\varphi'}\right)^m \qquad [2.56]$$

where E_{50}^{ref} is a reference stiffness modulus, corresponding to the reference stress p^{ref}. The amount of stress-dependency is given by the exponent m. A value of 0.5 is typical for sands and soft clays tend to have m = 1.0. The value m can be determined in the oedometer test or in a drained triaxial test.

E_{ur} in Figure 2.21 is the unloading/reloading modulus. The E_{ur} is also stress dependent and given as:

$$E_{ur} = E_{ur}^{ref}\left(\frac{c'\cos\varphi' + \sigma'_3\sin\varphi'}{c'\cos\varphi' + p^{ref}\sin\varphi'}\right)^m \qquad [2.57]$$

where E_{ur}^{ref} is a reference stiffness modulus, corresponding to the reference stress p^{ref}.

2.9.1.2 Hardening laws and yield functions

The HS model distinguishes between two types of hardening, shear hardening and compression hardening. The yield function adopted for the shear hardening formulation is:

$$f = f_s + \gamma^p \qquad [2.58]$$

where:

$$f_s = \frac{1}{E_{50}}\frac{q}{1 - q/q_a} - 2\frac{q}{E_{ur}}. \qquad [2.59]$$

The hardening parameter γ^p is the measure of the plastic shear strain according to:

$$\gamma^p = 2\varepsilon_1^{\,p} - \varepsilon_v^{\,p} \approx 2\varepsilon_1^{\,p}\ . \qquad [2.60]$$

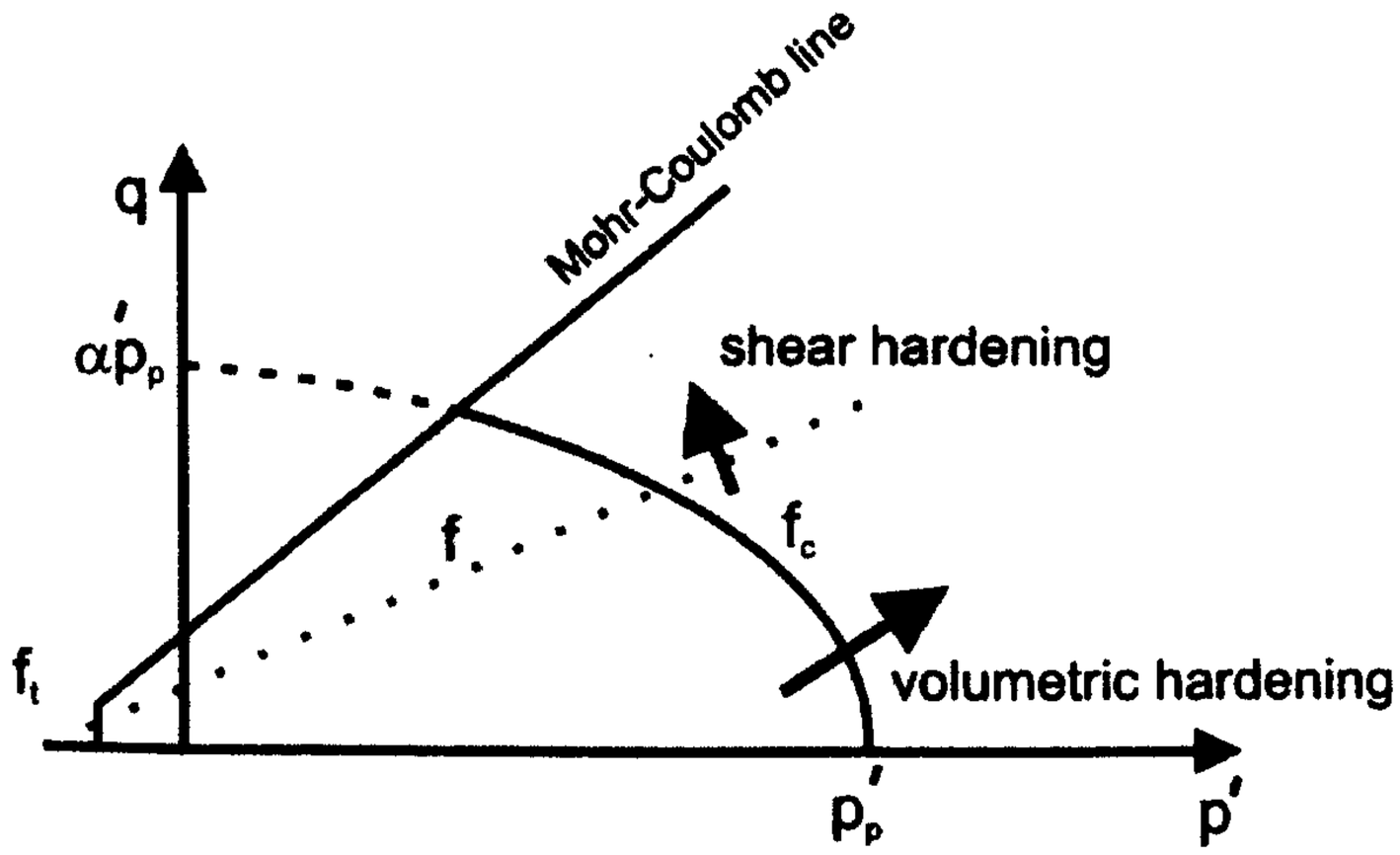

Figure 2.22: Yield surface of the Hardening Soil model in p'-q stress space

Plastic volumetric strains ε_v^p will never be zero, but for hard soils or granular materials plastic volume changes tend to be small compared to the axial strain (Schanz 1998).

To make the model suitable for modelling soft soils and over-consolidated soils, a compression hardening law has been introduced. The compression law is linked to a cap type yield surface as shown in Figure 2.22. The yield function of the yield surface is formulated as:

$$f_c = \frac{q^2}{M^2} + (p' + c\cot\varphi') - (p'_p + c\cot\varphi')^2 \qquad [2.61]$$

where:

$$M = \frac{6\sin\varphi'}{3 - \sin\varphi'}. \qquad [2.62]$$

The size of the cap yield surface is defined by the pre-consolidation pressure p'_p. The change of the size of the cap yield surface is linked to the plastic volumetric strain ε_v^p and defined by:

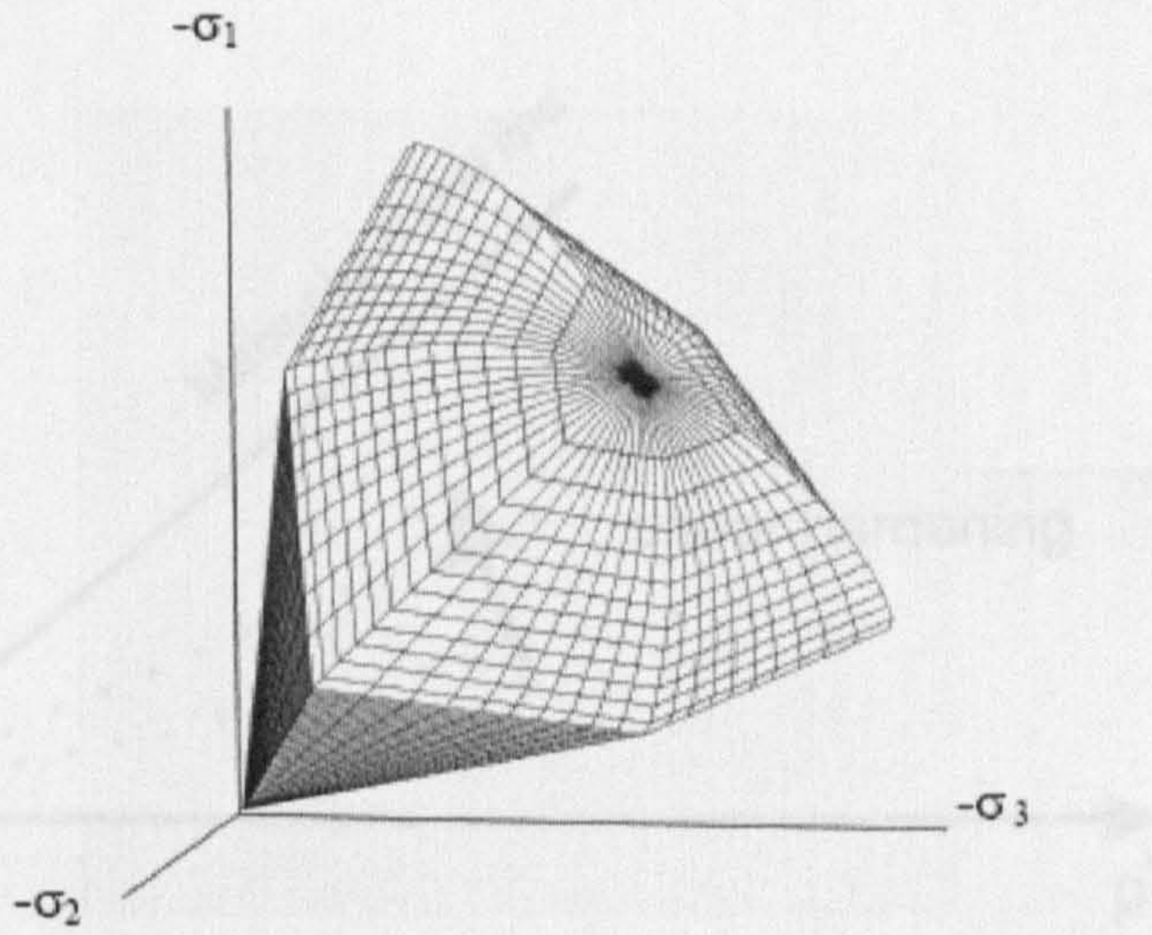

Figure 2.23: Yield surface of the Hardening Soil model in the general stress space for the special case c'=0 kPa (Brinkgreve, 2002)

$$\varepsilon_v^p = \frac{\beta}{1-m}\left(\frac{p'_p}{p^{ref}}\right)^{1-m} \quad . \qquad [2.63]$$

The parameter β is linked to the oedometer stiffness E_{oed}. In the HS model the oedometer stiffness is also stress-dependent and is defined according to:

$$E_{oed} = E_{oed}^{ref}\left(\frac{c'\cos\varphi' + \sigma'_1\sin\varphi'}{c'\cos\varphi' + p^{ref}\sin\varphi'}\right)^m \quad . \qquad [2.64]$$

where E_{oed}^{ref} is the reference modulus for the axial reference stress p^{ref}. An associated flow rule is used to determine the plastic strains on the cap yield surface. The model also includes a so-called tension cut off criterion with a yield surface f_t (Figure 2.22). For details on the tension cut off, the reader is referred to Brinkgreve (2002). The yield surface of the HS model in general stress space for cohesionless soil is presented in Figure 2.23. The model is implemented as a standard model in the PLAXIS finite element code. For more detailed information on the formulation of the model the reader is referred to Schanz (1998) and Brinkgreve (2002).

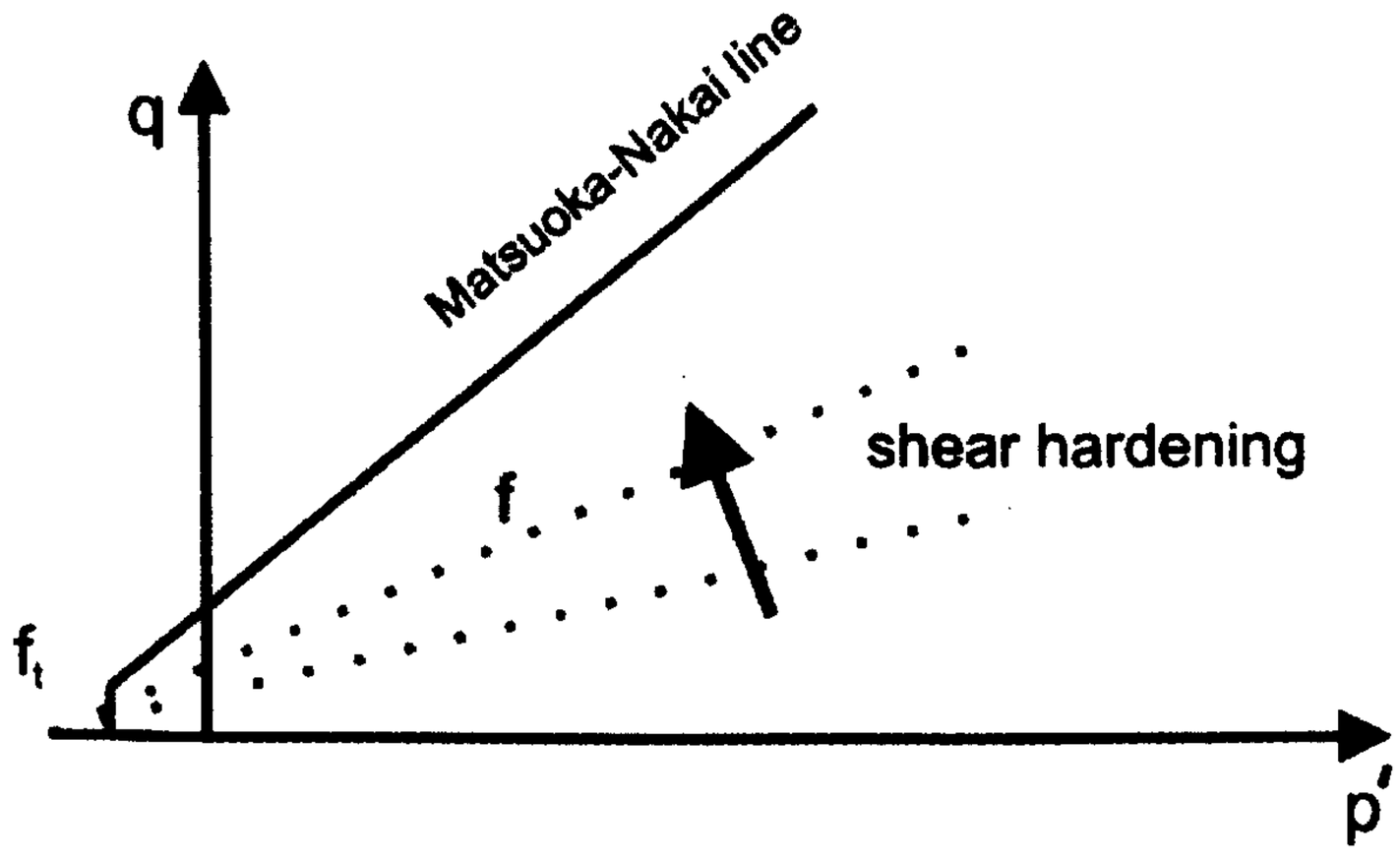

Figure 2.24: Yield surface of the Matsuoka-Nakai Hardening model in the p'-q stress space

2.9.2 Matsuoka-Nakai Hardening model

The Matsuoka-Nakai Hardening (MNhard) model is similar to the HS model which has been introduced in Section 2.9.1. It follows the same principle of stress-dependent stiffness and hyperbolic stress-strain relationship as the HS model (Section 2.9.1.1 and Figure 2.21). The model is a single hardening model with a shear hardening criterion implemented to model irreversible plastic strains due to primary deviatoric loading (see Figure 2.24). Instead of using the well known Mohr-Coulomb criteria it adopts the failure criteria after Matsuoka (1974) and Matsuoka-Nakai (1982).

Lade and Duncan (1973) showed that the failure surface of Monterey sand does not coincide with the Mohr-Coulomb failure surfaces in the deviatoric plane except at the corner points of the principal stresses (see Figure 2.25). The shear capacity in triaxial compression and extension is greater than anticipated in the Mohr-Coulomb criteria. Matsuoka (1974) and Matsuoka-Nakai (1982) introduced a failure criterion which accounts for the intermediate principal stress and is in better agreement with experimental results in the deviatoric plane than the Mohr-Coulomb criterion. They introduced the so-called Spatial Mobilised Plane (SMP) concept which is defined in the

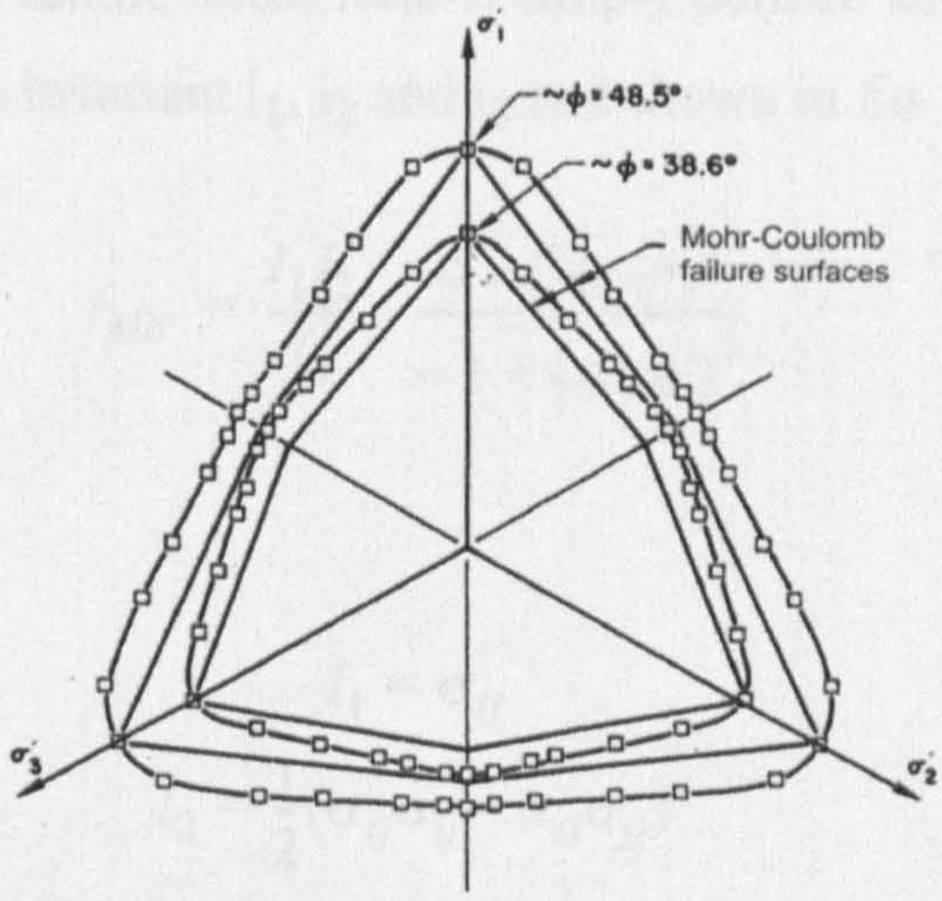

Figure 2.25: Failure surface for dense and loose Monterey sand in relation to Mohr-Coulomb failure surface (Lade & Duncan, 1973)

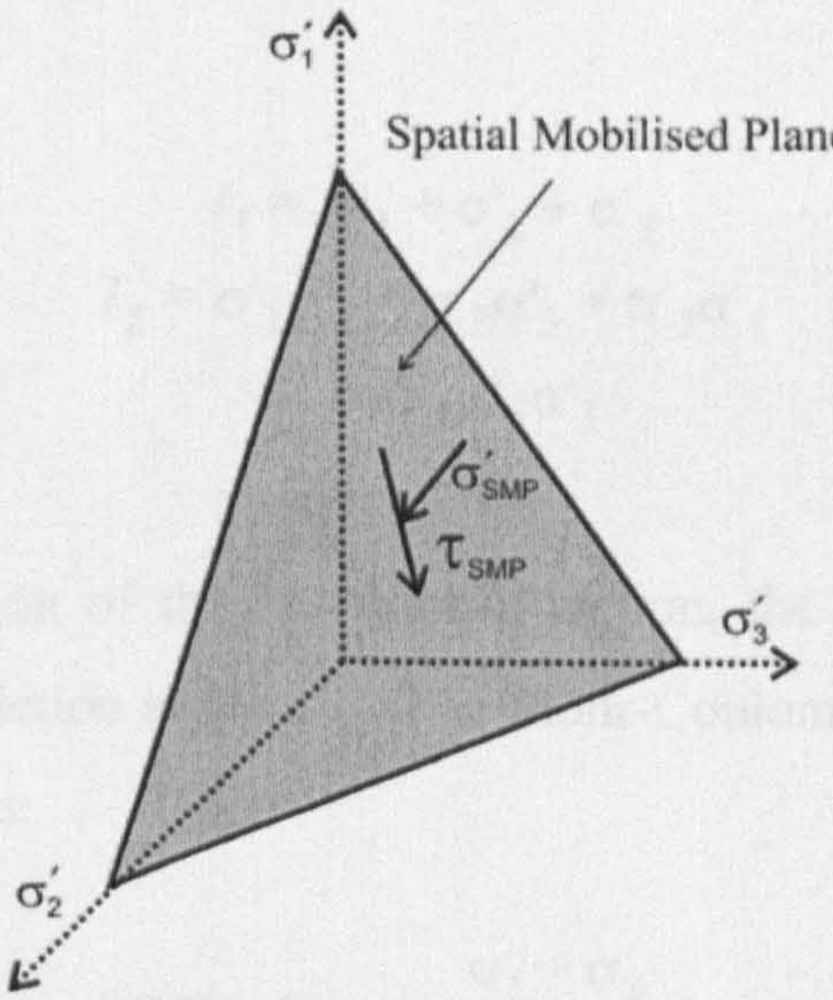

Figure 2.26: Spatial Mobilised Plane concept in general stress space

general stress space (Figure 2.26). The SMP defines the plane of maximum spatial averaged particle mobilisation. For each principal stress combination (σ'_1-σ'_2, σ'_2-σ'_3, σ'_3-σ'_1) the mobilised Mohr-Coulomb friction angle is derived. The SMP is the projection of the three planes into the general stress space, as shown in Figure 2.26.

In the Matsuoka-Nakai criteria (MN) the failure stress is defined by limiting the averaged ratio of spatial normal stress to averaged spatial shear stress.

In the MN criteria the failure stress ratio is simply defined as a function of the first, second and third stress invariant I_1, I_2 and I_3 and shown in *Eq. 2.65*.

$$f_{MN} = \frac{I_1 I_2}{I_3} - \frac{9 - (\sin\varphi')^2}{-1 + (\sin\varphi')^2} \qquad [2.65]$$

where

$$I_1 = \sigma_{ii}$$

$$I_2 = \frac{1}{2}(\sigma_{ij}\sigma_{ij} - \sigma_{ii}\sigma_{jj}) \qquad [2.66]$$

$$I_3 = \frac{1}{6}(\sigma_{ii}\sigma_{jj} + 2\sigma_{ij}\sigma_{jk}\sigma_{ki} - 3\sigma_{ij}\sigma_{jki}\sigma_{kk})$$

In principal space these invariants simplify to:

$$I_1 = \sigma'_1 + \sigma'_2 + \sigma'_3$$

$$I_2 = \sigma'_1\sigma'_2 + \sigma'_2\sigma'_3 + \sigma'_3\sigma'_1 \qquad [2.67]$$

$$I_3 = \sigma'_1\sigma'_2\sigma'_3$$

For the implementation of the MN yield function, the function is reformulated in terms of mobilised friction angle φ'_m. The Mohr-Coulomb criterion in triaxial conditions can be written as:

$$\sin\varphi'_m = \frac{\sigma_1 - \sigma_3}{\sigma_1 + \sigma_3 + 2c\cot\varphi'} \qquad [2.68]$$

and combining it with *Eq. 2.54* yields to:

$$\frac{q_f}{q_a} = R_f\left(\frac{1 - \sin\varphi'}{\sin\varphi'}\right)\left(\frac{\sin\varphi'_m}{1 - \sin\varphi'_m}\right). \qquad [2.69]$$

The yield function of the MNhard model can be written as:

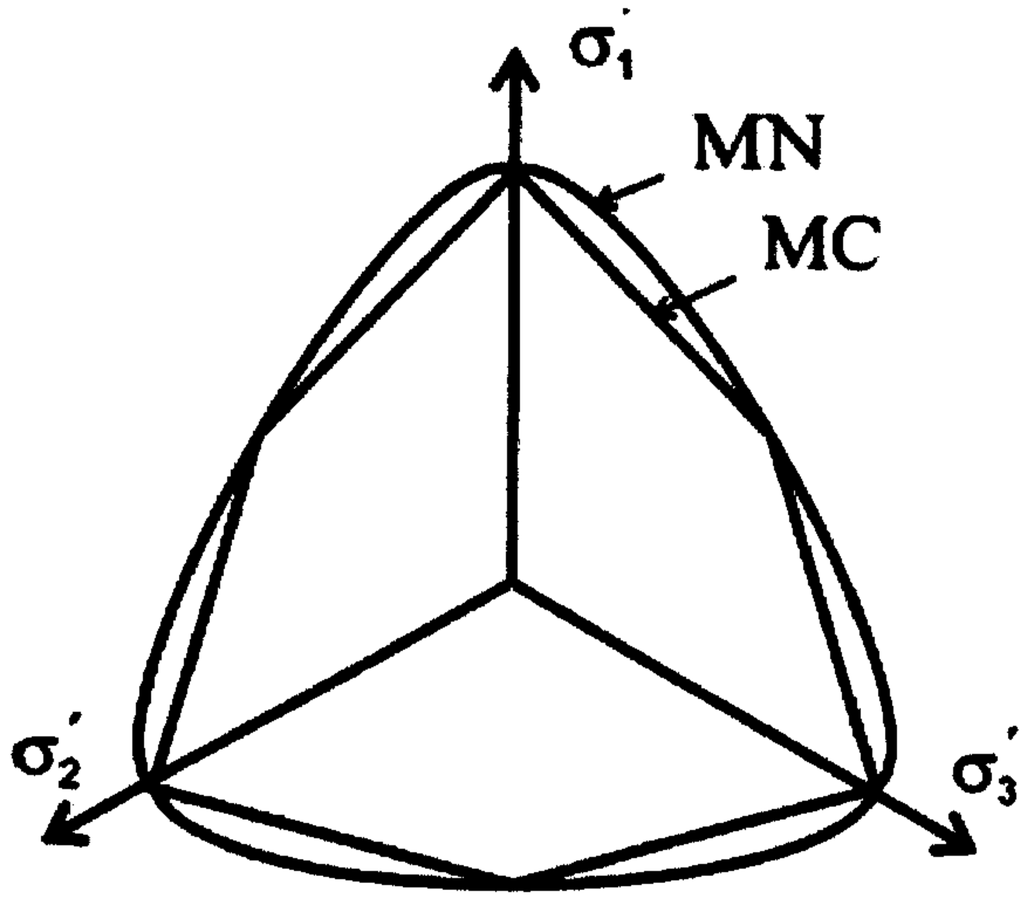

Figure 2.27: Matsuoka-Nakai criterion compared to Mohr-Coulomb criterion on the deviatoric plane

$$f = \frac{3}{2}\frac{1}{E_{50}} \cdot \frac{\dfrac{1-\sin\varphi'_m}{\sin\varphi'_m}}{\dfrac{1-\sin\varphi'_m}{\sin\varphi'_m} - R_f \cdot \dfrac{1-\sin\varphi'}{\sin\varphi'}} - \frac{3}{2}\frac{1q}{E_{ur}} - \gamma_s^p \qquad [2.70]$$

where φ'_m is the friction angle in triaxial compression and γ_s^p is the hardening parameter. By rearranging *Eq. 2.65* the mobilised friction angle φ'_m can be expressed through the MN criteria.

$$\sin\varphi'_m = \frac{9 - \dfrac{I_1 \cdot I_2}{I_3}}{1 - \dfrac{I_1 \cdot I_2}{I_3}} \qquad [2.71]$$

In Figure 2.27 the MN criterion is compared to Mohr-Coulomb criterion. The MN failure criterion has a rounded shape in the deviatoric plane. For further details on the MNhard model the reader is referred to Benz (2006). The MNhard model was originally implemented by Benz as a user defined soil model in the 2D finite element code PLAXIS 8 code. For this work the model was also implemented in PLAXIS 3D foundation.

2.9.3 Summary

Two advanced constitutive models for granular and cohesive material have been introduced. The HS model is a standard model in the 2D PLAXIS and PLAXIS 3D foundation finite element code. In this work the HS model is used to represent the stress strain behaviour of embankment fill and deep mixed materials. The MNhard model was developed by Benz (2006) and is implemented as a user defined soil model in the PLAXIS finite element codes. The model is used in this work to represent the stress-strain behaviour of deep mixed material in simulations of embankments constructed on deep mixed columns.

Chapter 3

Embankments on soft soils

In this Chapter the behaviour of embankments constructed on soft soils are reviewed and discussed. At the beginning a short overview summarises the type of embankments built, the various functions of embankments and the difficulties that geotechnical engineers encounter during design and construction. In the second part some well documented case histories are revisited. The discussion on the case histories focuses on the monitoring results. At the end of the chapter the modelling and design is covered with special emphasis on numerical modelling.

3.1 Overview

Embankments have been built for centuries by engineers for different purposes. Constructions of embankments are required for road networks, motorways, railways, water retention, flood control works and airports, just to list a few of the many different purposes. One of the oldest embankments mentioned in history is the Sadd-el-Kafara embankment (www.simsience.org). It is estimated that it was built around 2600 BC. The embankment is 14 m high and has a 113 m long crest. The purpose of the embankment was to retain water from floods.

Embankments are best built on sites with good ground conditions, in order to reduce and avoid stability problems during construction, large settlements and costs associ-

ated with technical difficulties. It is often found that regions along the coast and river estuaries are covered with young, shallow to deep deposits of soft clays, muds and compressible silts. The ever growing population in urban areas, along rivers and coast lines pushes city boundaries outwards to areas with low quality land. In the last 50 to 60 years more and more structures have been built on highly compressible soils particularly for transport, housing and industrial projects.

3.2 Design considerations

Design and construction of embankments on soft compressible soils is a challenge for geotechnical engineer. The main problems are the high compressibility and low permeability of the underlying deposit together with very low undrained shear strength c_u. The low c_u can cause stability problems during the undrained construction of the embankment and the designer has to use adequate care to address this issue in the design. In cases where the designer can not achieve the required factors of safety (FoS) for stability or limit the settlements to an acceptable degree, different ground improvement or reinforcement methods can be used. The acceptable degree of settlements and required minimum FoS depends on the function of the structure. For details on minimum FoS and limits of settlements, the reader is referred to national codes or any recommendations by authorities such as national railway or highway standards. In the United Kingdom the design of embankments on soft soils has to be undertaken in accordance with British Standard 6031 (BS 6031:1981). In 2010 the BS 6031 will be replaced permanently with the European standard number 7 part 1 (EC7, EN1997-1:2004), in practice this is often referred to as Eurocode 7. Up to 2010 both codes can be used in parallel but in 2010 the use of Eurocode 7 will become compulsory.

The high compressibility of soft soil makes it difficult to ensure that deformations are within the acceptable limits, which have to be defined to account for the entire working or design life of an embankment. Understanding the influence of the soil properties and fundamental characteristics on the primary and secondary consolidation is crucial for an adequate serviceability limit state (SLS) design. For embankment on

soft soils it can be expected that the majority of the settlements will occur after construction as the excess pore pressures dissipate. Special attention should always be paid to time dependent creep. A suitable SLS design will contribute to minimise the long term maintenance costs of a structure which can be substantial for big structures. Creep is often just associated with the SLS design of an embankment but it may also influence the ultimate limit state design (ULS). If there is a build up of excess pore pressures Δu as creep continues under constant load, the mean effective stress p' will be reduced as Δu increases. The allowable deviatoric stress q_{max} can be reached as the effective stress state is pushed towards the undrained shear limit of the soil. Once the undrained shear limit is reached along a potential slip surface the resisting shear forces do not continue to provide resistance and failure can occur. Bauduin et al. (1999) performed a back analysis of an embankment dyke and showed how the creep effects contributed to the instability of the embankment. It was concluded that the pore pressures continued to grow after the end of the undrained loading stage and this phenomenon was most likely, partly the cause of the failure.

3.3 Case histories

In the past 40 to 50 years numerous case histories of constructed embankments were reported in journal papers, conference papers or special reports by authorities or research institutions. Trial embankments have been constructed in different countries all over the world, including Canada, Finland, Sweden, France, Malaysia, China, US, Brazil and Japan. Some are well known by researchers, such as the Haarajoki (Aalto et al. 1998) and Vaasa test embankments (Vepsäläinen et al. 1991) in Finland, Boston trial embankment (Davies and Poulos, 1975) in the United States, Cubzac A and B trial embankments (Magnan et al. 1982) in France, Muar Flats embankments (Nakase and Takemura, 1989) in Malaysia and Skå-Edeby (Larsson and Mattsson, 2003) in Sweden.

The quality and usefulness of the information on the trial embankments for researchers or geotechnical engineers can be categorised from not useful to highly recom-

mended. Limited access to high quality site investigations, laboratory testing and data monitoring alongside poorly documented data do not make all published cases valuable. However, in the last two decades more and more case histories have been utilised to verify the use of constitutive models for soft soils (e.g. Cudny et al. 2003, Karstunen et al. 2005, Neher et al. 2001, Nakai and Matsuoka, 1987) and test the constitutive models in different boundary value problems (e.g. Krenn & Yildiz, 2006, The et al. 1998, Sun et al. 2001). The majority of trial embankments have been built to study either the maximum failure height (ULS) or the long term behaviour (SLS). The embankments constructed to investigate the long term behaviour can be divided into two groups. Most have been monitored for 250 to approximately 2000 days after completion of the embankment (Mestat et al. 2004) and just a few cases reported have been monitored up to 50 years or more (e.g. Larsson & Mattsson, 2003). Monitoring embankments for such a long time is difficult and costly. Measurements are usually frequent in the first couple of years after construction but often less frequently taken over later years (Larsson & Mattsson, 2003, Karstunen et al. 2005). In the past many technical difficulties with monitoring devices have been reported, particularly related to piezometers and the instruments used to measure lateral deformations (Larsson & Mattsson, 2003). Improvement and developments of modern monitoring devices will certainly help in the future.

A practical source for information about trial embankments and case histories is the MOMIS database (Mestat, 2001; Mestat et al. 2004). MOMIS has been developed by the French Public Works Research Laboratory (LCPC) for several years. The database was collated for numerical modelling of boundary value problems and the comparisons between computational results and in-situ measurements (Mestat, 2001). Up to 86 embankments built on natural soft soils and 35 embankments on improved soils are recorded in this data base. The information available includes measurements compared to predictions, geometry details, statistical information about model geometries, the quality of the predictions, constitutive models applied etc.

Studying all the information available on embankments, Mestat (2004) concluded that in the last 10 to 15 years the trend has gone towards using more advanced constitutive models for soft soils. Recent developments of advanced constitutive models for soft soils and the implementation of some of the models into commercial finite element codes make them more available to more engineers and researchers working in geotechnical engineering. Models used included the Matsuoka-Nakai model (Nakai and Matsuoka, 1987), Sekiguchi and Ohta model (Nakase and Takemura, 1989), Melanie model (Magnan et al., 1982), extended Cam Clay model (The et al. 1998), anisotropic Sekiguchi and Ohta model (Sun et al. 2001) and Soft Soil Creep model (Neher et al. 2001).

The quality of the long term predictions of the settlements at the centre line is far better than the short term predictions (after the completion of construction). Simplification of the construction process in the model and poorly documented construction procedures might well contribute to less accurate short term predictions. However, it has been found that the lateral displacements at the toe of the embankment are generally poorly predicted for both, long term and short term predictions. This agrees with findings by other researchers (e.g. Karstunen et al. 2005, Koskinen & Karstunen, 2006). The shape of the yield surface and the shape of the plastic potential of the constitutive model will influence the prediction of the horizontal displacements.

3.4 Selected Case histories

The selected case histories reviewed and discussed are chosen because of their quality and detailed documentation in the literature. More importantly some of the embankments chosen have been monitored for over 50 years and this is extraordinary and outstanding for trial embankments. Furthermore the embankments selected are of similar height to the Murro test embankment (Koskinen et al. 2002e), which will be extensively investigated in Chapter 6.

3.4.1 Lilla Mellösa test site

From 1945 to 1947 three test embankments were built at the farm of Lilla Millösa (Larsson & Mattsson, 2003) in Sweden. The test embankments were constructed to investigate the suitability of the site for a new airport runway just outside the city of Stockholm. Two out of the three embankments were constructed on natural ground; the other was built on ground improved using vertical drains. One of the embankments on natural ground was made out of a low weight fill. In the following, only the embankment built on natural ground with the standard fill material will be discussed. The embankment base measures 30 m by 30 m. It is 2.5 m high and the slopes have a gradient of 1:1.5. The total time of construction was approximately 25 days.

The ground consists of a 10 to 15 m deep soft soils deposit. At the top of the deposit a 2 m deep dry crust can be found. The ground water level is estimated to be at a depth of 0.8 m.

The embankment was instrumented with settlement devices and piezometers to record the excess pore pressures. Over the years the measurements have continued but only limited information about the settlements is available. The piezometers have ceased to function with time. However, in 2002 retractable piezometers were installed temporally for two months in conjunction with a site investigation (Larsson & Mattsson, 2003).

At the end of the undrained construction the measured settlements were in the order of 0.05 m. In 1966, the measured vertical settlements at the centre line of the embankment were 1.4 m and the maximum excess pore pressure Δu were of the order of 30 kPa at a depth of 6 m. In the next ten years the settlements increased to maximum of 1.65 m and Δu decreased to approximately 22 kPa at a depth of 7m. The latest measurements were taken in 2002. The settlements have been report to have reached approximately 2 m and the Δu has decreased to 12 kPa. Nowadays, the embankment still settles an average rate of 10mm per year.

The large compression measured causes overconsolidation in the top layers (Larsson & Mattsson, 2003) and slows down the settlements of the upper layers. Hence, the compression of the deeper layers is more recognisable, and this is also visible in the undrained shear strength profile. In the past the shear strength increased primarly in the shallow layers, where as in the last years the shear strength also increased in the deeper layers (see Larsson & Mattsson, 2003 for further details).

3.4.2 Skå-Edeby test site

In 1957 the Swedish Geotechnical Institute was commissioned to construct a test field at Skå-Edeby to investigate the possibility of the construction of another airport runway (Larsson & Mattsson, 2003). The site consists of 10 to 15 m soft clay above a bedrock formation. Four circular test fills with a diameter between 35 and 70 m were constructed. Only one out of the four test fills was placed on natural ground and will be discussed in the following. The embankment was constructed with a diameter of 35 m and to maximum height of 1.5 m. Slopes were built with a gradient of 1:1.5. The average load at the top of the ground surface due to the weight of the fill was 27 kPa.

The monitoring devices installed included settlement markers, piezometers and vertical pipes to measure horizontal deformation. In 2002, retractable piezometers were installed temporally for two months. After completion of the construction of the embankment the measured vertical displacements were approximately 0.06 m. 25 years after construction in 1982, the measured settlements at the centre of the fill were 0.95 m and the Δu had decreased to 20 kPa. In 2002, 45 years after construction, the total settlements have reached 1.45 m and the Δu has further decreased to approximately 12 kPa. Larsson and Mattsson (2003) report that the fill continues to settles by an average rate of 5 to 6 mm per year. The dry crust and part of the fill are largely submerged. Over the years it has been observed that the settlement rate varies seasonally and between the layers. Snow fall, temperature variation, ground freezing and ground water level variation are almost certainly the reasons for these observed variations in settlement rates (Larsson and Mattsson, 2003).

The importance of the findings from these test fields for research and construction of road projects led to the construction of another test embankment. In 1961, four years after the construction of the original circular test fields at Skå-Edeby, another embankment was constructed (Larsson and Mattsson, 2003). The trial embankment was built with a crest width of 4 m and total length of 40 m. The slopes were 1:1.5 and the height of the fill was 1.5 m. The maximum total load at the ground surface was 27 kPa.

At the end of construction the settlement reached 0.06 m similar to that which was observed at the circular fill. For the first time the importance of the shear deformation was reported. It was recognised that due to the undrained stress-strain behaviour after construction or beginning of consolidation the horizontal displacements at the toes are related to vertical displacements. This phenomenon becomes less relevant with ongoing consolidation as the vertical displacements become dominant. Larsson and Mattsson (2003) reported that the total settlements at the centre line of the fill in 2004 had reached 1.0 m with a maximum Δu of 6 kPa.

3.5 Modelling of embankments

By designing an embankment the engineer takes on responsibility and reliability for its stability during construction and must prove that the embankment will not suffer damage or collapse during its working life. Thus, modelling the reality is necessary in order to predict the behaviour of the embankment during its construction and over its life time. Design methods and recommendations have been developed in almost every country. Before modelling can actually begin, a considerable amount of information must be assembled, regarding e.g. geometry, loading conditions, geology and soil properties.

Design models for predicting settlements and overall stability which have been developed for the use in geotechnical design, include a variety of closed form solutions, limit equilibrium, stress field solutions, limit analysis and numerical analysis. Analytical solutions have to be simple and as such a number of simplifications such as

homogeneous ground conditions or simple cross sections are introduced in the models. Elastic settlement calculations are an example of a closed form solution. To increase the accuracy of the predictions the engineer will necessarily turn to more complex solutions which allow them to account for soil features such as over-consolidation, more soil layers and consolidation, e.g. Larsson (1997). The engineer will use a software package or spreadsheet program to support them.

Stability assessments of embankments are commonly undertaken by programmes which utilise the limit equilibrium method. Most programmes have a user friendly interface which make it easy to use and have almost no limit in terms of geometry or structural parts. An alternative design model is the full numerical analysis of an embankment. This category of analysis attempts to satisfy all theoretical requirements, including realistic stress-strain modelling and boundary conditions. There are a wide range of full numerical tools available: e.g. Finite Element Method, Finite Difference Methods, and Boundary Element Method, etc. Approaches based on Finite Element Method and Finite Difference Methods are the most widely used by geotechnical engineers. The present thesis uses the Finite Element Method. For detailed description about the Finite Element Method the reader is referred to literature. (e.g. Zienkiewicz and Taylor (1991), Smith (1993), Potts and Zdravkovic (1999)). All results from numerical simulations presented in this thesis have been obtained by using the two – and three- dimensional versions of the Finite Element code PLAXIS.

3.6 Modelling aspects of embankments in plane strain

Finite element modelling of an embankment constructed on soft soil requires some judgement regarding the size of the geometry of the model, the coarseness of the mesh, the in-situ stress conditions, the boundary conditions, the constitutive model, simplification of the construction process etc. Modelling will always involve some engineering judgement and more importantly experience is required as to how to apply the above and what is relevant to each individual boundary value problem. Some of the aspects listed above are covered in the literature (e.g. Potts et al. 2004,

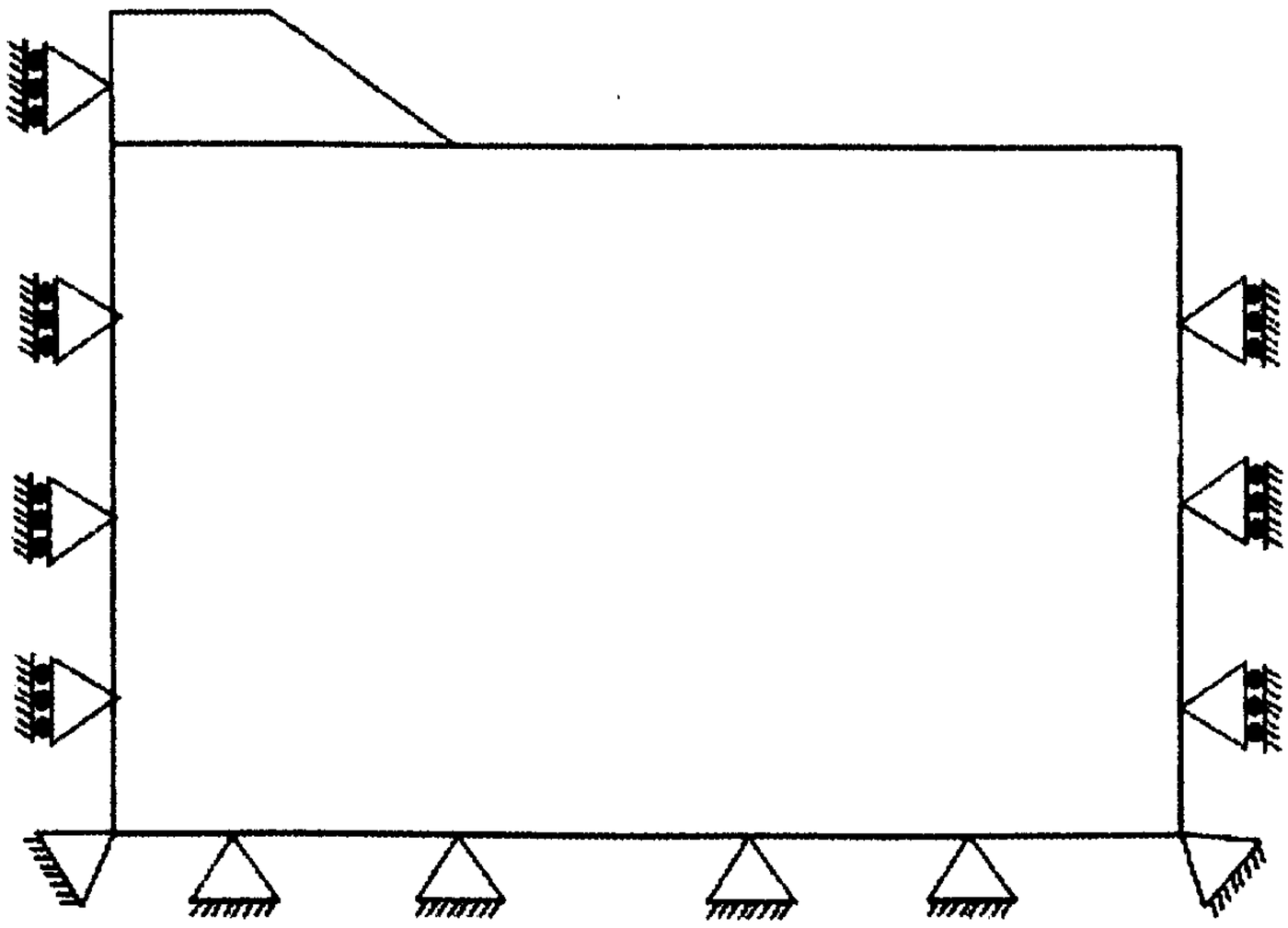

Figure 3.1: Deformation boundaries (Default setting in PLAXIS 2D)

Chai 1993) others are not and it is recommended that the influence of each aspect on the result is illustrated via trial and error runs. In the following some of the issues are discussed in more detail.

3.6.1 Boundary conditions

Boundary conditions relevant for models of embankments on soft soils can be divided into two categories, the deformation boundaries and the so-called consolidation boundaries. Both types of boundaries have to be defined for the vertical and horizontal boundaries of the proposed finite element model.

3.6.1.1 Deformation boundaries

At the horizontal deformation boundaries, often referred to as lateral boundaries, the horizontal displacement u_x is restrained and the vertical displacement u_y is left free. This boundary condition, allowing only for normal stress and no shear stress, also satisfies the symmetry conditions which are commonly applied along the centreline of symmetrical embankments. The upper boundary formed by the embankment and the existing ground surface are left free to displace. In contrast, the bottom boundary is

usually fully restrained in both direction, u_x =0 and u_y =0. Hence normal and shear stress may occur. The above boundary conditions are a default setting in the PLAXIS code (Brinkgreve, 2002) as shown in Figure 3.1. However, if the bottom boundary is rock, overlain by a soft soil layer, the boundary conditions should allow for displacements in the horizontal direction u_x (Azizi, 2000). To investigate the influence of the bottom boundary on the settlement behaviour, two simple models were developed. The model consists of a 2 m high embankment with a crest width of 16 m. The gradient of the embankment slope is 1 to 3. The embankment itself is assumed to be constructed on a (a) 12 m deep and (b) 36 m deep soft soil deposit. Just one half of the embankment was considered due to the symmetry conditions applied. The S-CLAY1S model was utilised to simulate the stress-strain behaviour of the soft soil and the elasto-plastic Mohr Coloumb model to represent the embankment fill. Parameters for the soft soil correspond to the so-called POKO clay (Koskinen et al. 2002a, Koskinen et al. 2002b). Embankment fill and clay parameters are listed in Chapter 4, Table 4.1 to 4.4. The construction of the embankment was simulated as fully undrained followed by a consolidation stage to allow the excess pore pressure to dissipate.

The predicted vertical displacements versus time at the centre line of the embankment are presented in Figure 3.2. In Figure 3.2a, the results for the 12 m deposit are shown. It can be seen that the model with the nodes free to move in the horizontal direction at the bottom predicts notably higher vertical displacements with time. For the 36 m deposit, presented in Figure 3.2b, the difference between the two time settlement curves is negligible. The importance of the correct choice of bottom boundary can also be illustrated by examining the horizontal displacements at the toe of the embankment. Figure 3.3 shows the horizontal displacements at the end of the consolidation stage. For the 12m deposit (Figure 3.3a) the model with free boundary conditions predicts significant larger horizontal displacements at the top and at the

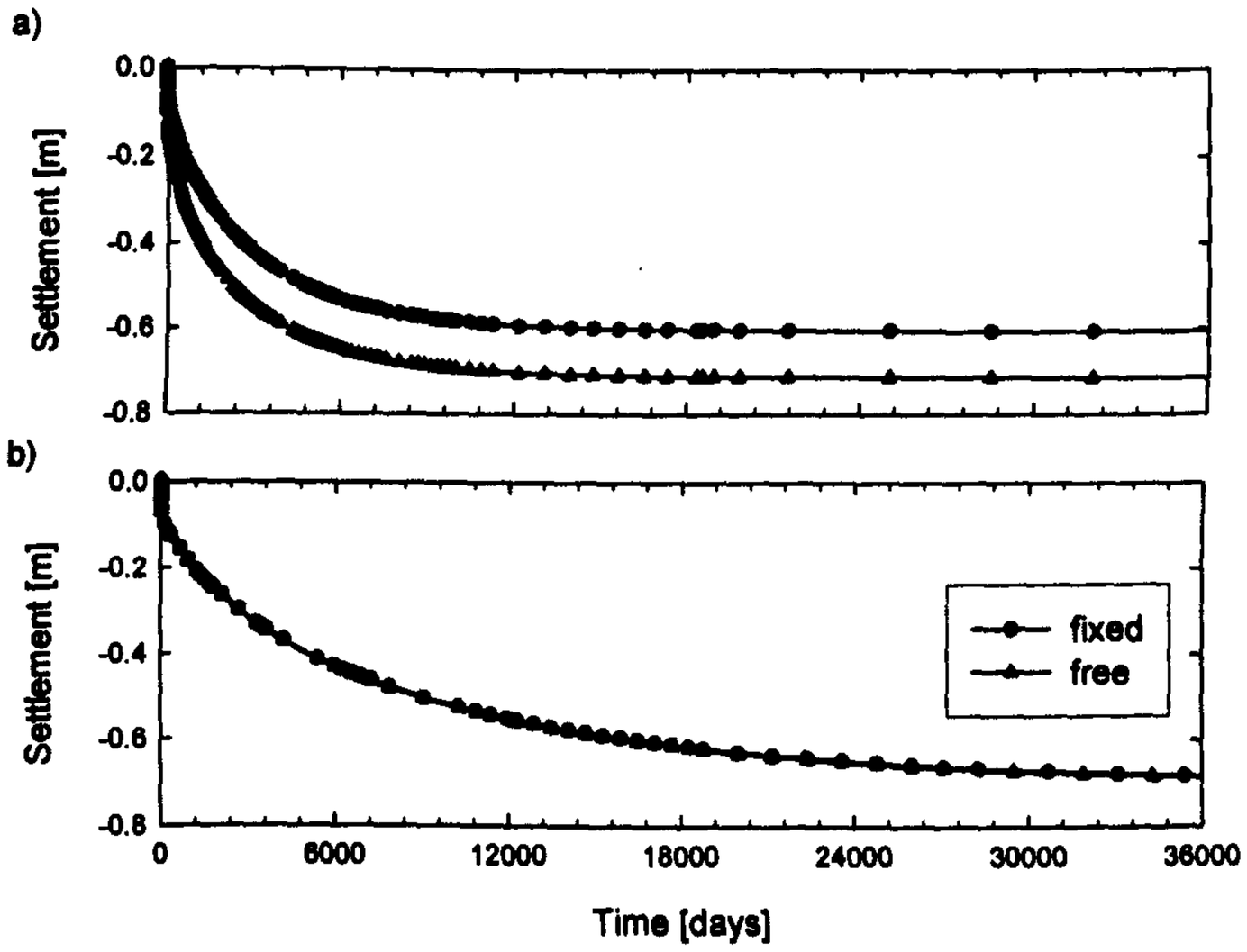

Figure 3.2: Time settlement curve: a) 12 m and b) 36 m deep deposit

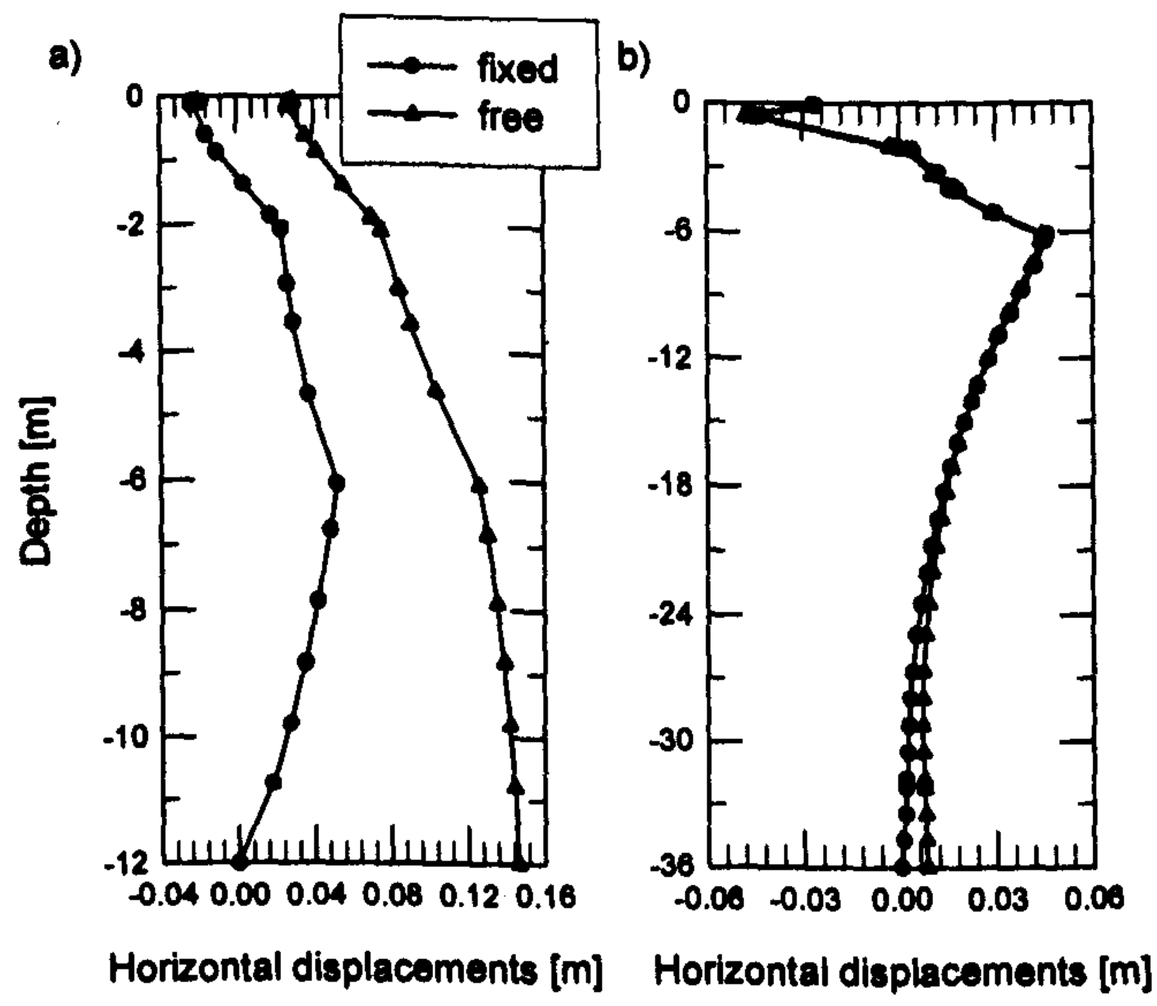

Figure 3.3: Horizontal displacements underneath the toe of the embankment after 100 years of consolidation: a) 12 m and b) 36 m deep deposit

bottom of the model. In fact the displacements at the bottom of the model are even bigger than the maximum displacements predicted by the model with the fixed conditions. Both models predict a substantially different straining behaviour. The influence of the bottom boundary conditions is less significant for the 36 m deposit, as shown in Figure 3.3b. The significant difference in the predictions for the shallow

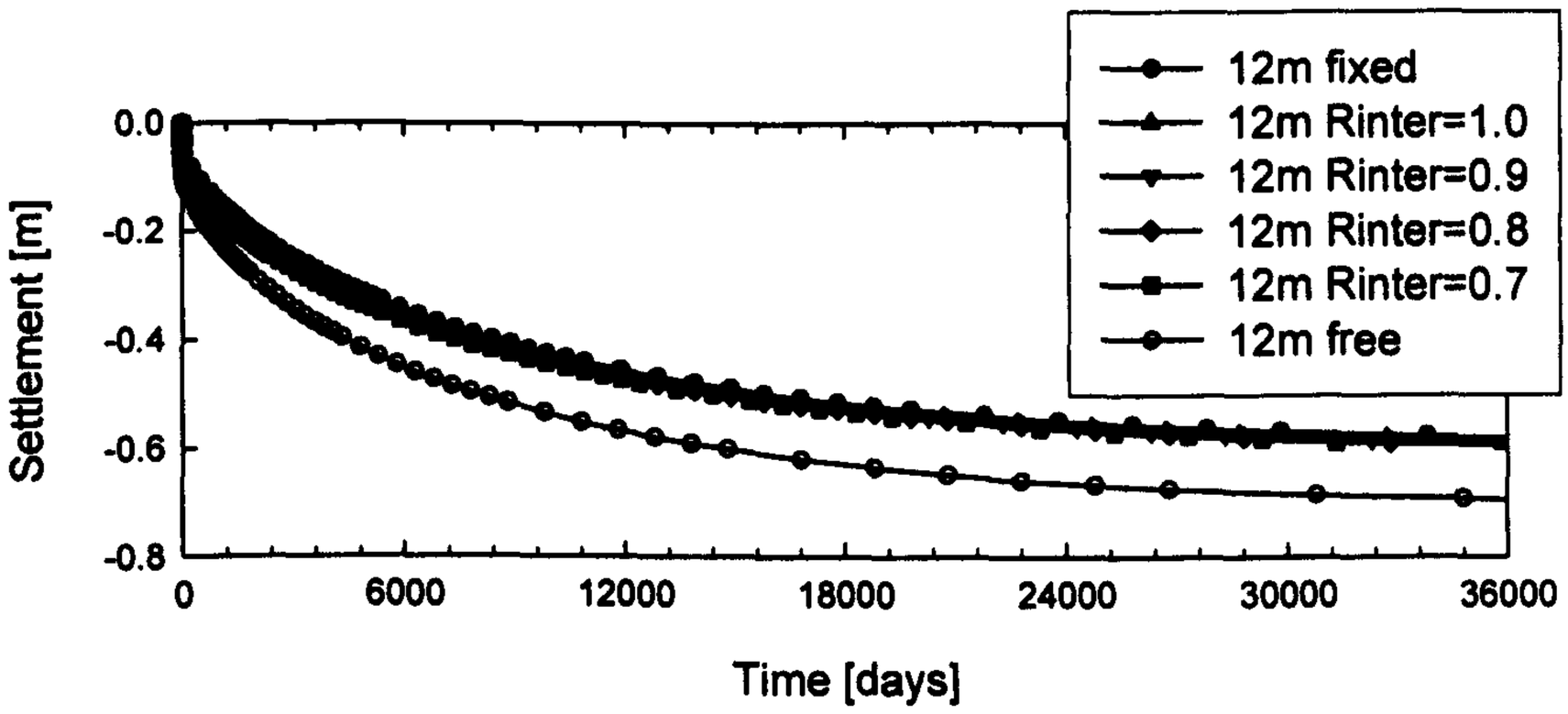

Figure 3.4: Time settlement curve: Influence of the interface

deposit implies that the modeller has to think carefully about which boundary conditions needs to be applied along the bottom of the model.

An alternative method to the fixed and free bottom boundary conditions is an interface along the rock surface. Direct soil-rock interaction can be simulated by a Mohr-Coulomb interface implemented into the PLAXIS code (Brinkgreve, 2002). The strength properties of the interface are related to strength properties of the soil layer. Each interface has an associated strength reduction factor R_{inter}. For the reduction of the friction angle φ' of the soil the following rule is applied:

$$\tan\varphi'_i = R_{inter}\tan\varphi'_{soil} \qquad [3.1]$$

where φ' is the friction angle of the interface. For the detailed formulation of the interface the reader is referred to Brinkgreve (2002) and Satibi et al. (2007).

The interface has been applied in the model with the soft soil to a depth of 12 m to simulate the boundary between the soft soil and the rock. Different values of R_{inter} were applied to study the influence of the interface on the strain behaviour of the soft soil.

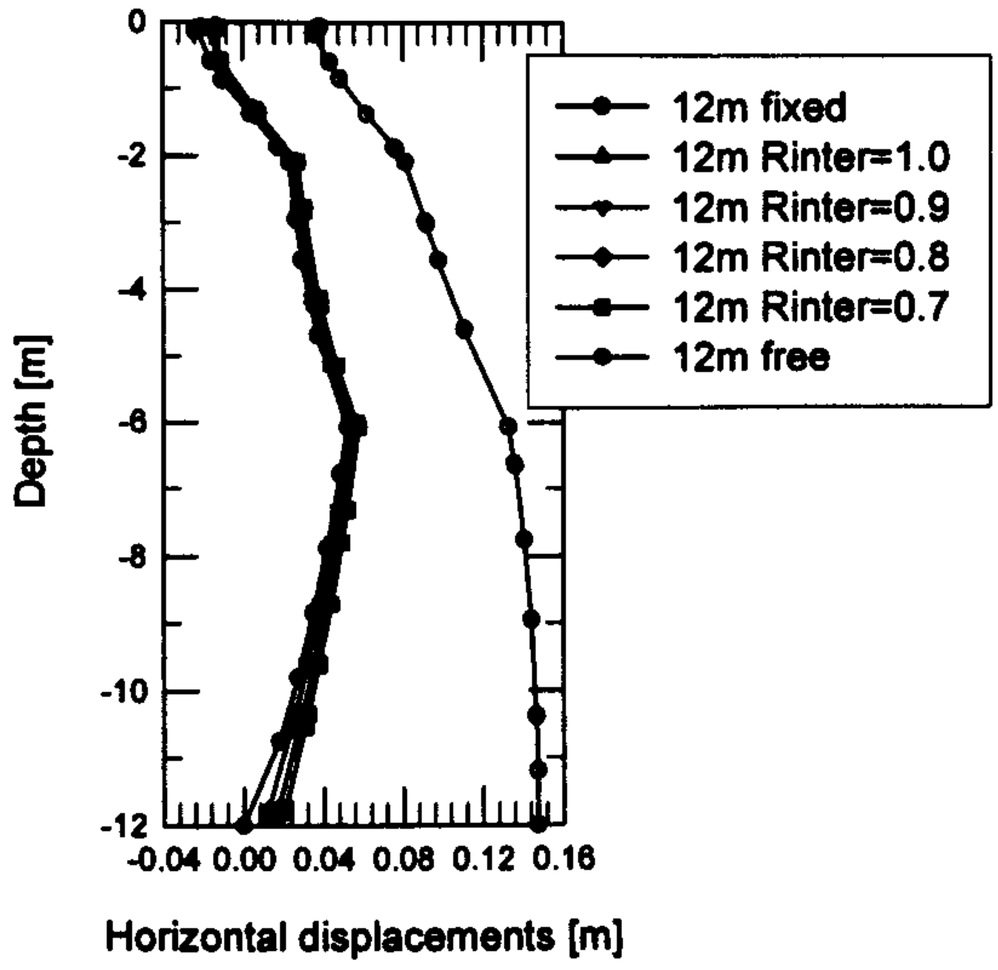

Figure 3.5: Horizontal displacements underneath the toe of the embankment after 100 years of consolidation

In Figure 3.4 the time settlement curve for a point at the centre line at the bottom of the embankment is shown. The results of 6 simulations are compared, one without an interface at rock surface, four with an interface and different R_{inter} values and the model with free boundary conditions in the horizontal direction. The different R_{inter} values can be interpreted as a variation of the roughness of the rock surface. A smaller value represents a smoother surface. It can be seen that the interface has a negligible influence on the predicted vertical displacements. Horizontal displacements with depth under the toe of the embankment after 100 years of consolidation are illustrated in Figure 3.5. An influence of the interface on the predicted shape of the profile with depth can be seen. The magnitude of the horizontal displacements is similar at the surface but different at the bottom of the soft soil. Small movements at the interface between soft soil and rock surface seems to be more realistic considering the small embankment simulated compared to larger movements predicted by the model with the free boundary condition. A reduction of the R_{inter} value results in a small increase of the horizontal displacements at the top of the rock.

Instead of an interface along the bottom boundary one can also increase the depth of the model and explicitly model the underlying rock. The horizontal displacements at

the bottom of the soft clay will then be influenced by the apparent ratio of rock/soil stiffness and the Poisson's ratio of the rock.

3.6.1.2 Hydraulic boundaries and finite elements for consolidation analysis

In the finite element code, two different types of finite elements are available, the consolidating elements and non-consolidating elements. It is the degree of freedom which distinguishes the two elements and not the shape. A non-consolidating element has just two displacement degrees of freedom at the nodes. With such an element only a drained analysis or an undrained analysis in terms of total stress can be performed. Real soil behaviour is normally time dependent, with the excess pore pressure response dependent on the soil permeability. To account for such behaviour another degree of freedom must be added to the elements used. A consolidating element has in addition to the two displacement degrees of freedom a pore fluid pressure degree of freedom. The non-consolidating element would be used for drained material behaviour such as sand (bulk modulus of water set to zero) and the consolidating element for clays (bulk modulus of water activated). When using the PLAXIS software, the user does not choose between the element type. The user just chooses a material behaviour (drained or undrained) for each soil layer and the software will automatically use the correct element type for the layer.

After the definition of the elements for the different layers, the hydraulic boundary conditions for the consolidation analysis at the nodes along the model boundaries and the interfaces between the different layers need to be set. Depending on the drainage condition required, the excess pore pressure at the nodes along the boundaries can be set to zero. In the PLAXIS software Δu is set to zero by default at the boundaries and at the interface between a drained and undrained layer. By applying special conditions, the so-called consolidation boundary, this setting can be changed by the user. When applying a consolidation boundary, the boundary is practical impermeabable and no pore pressure can dissipate through the boundary (Δu is greater than zero).

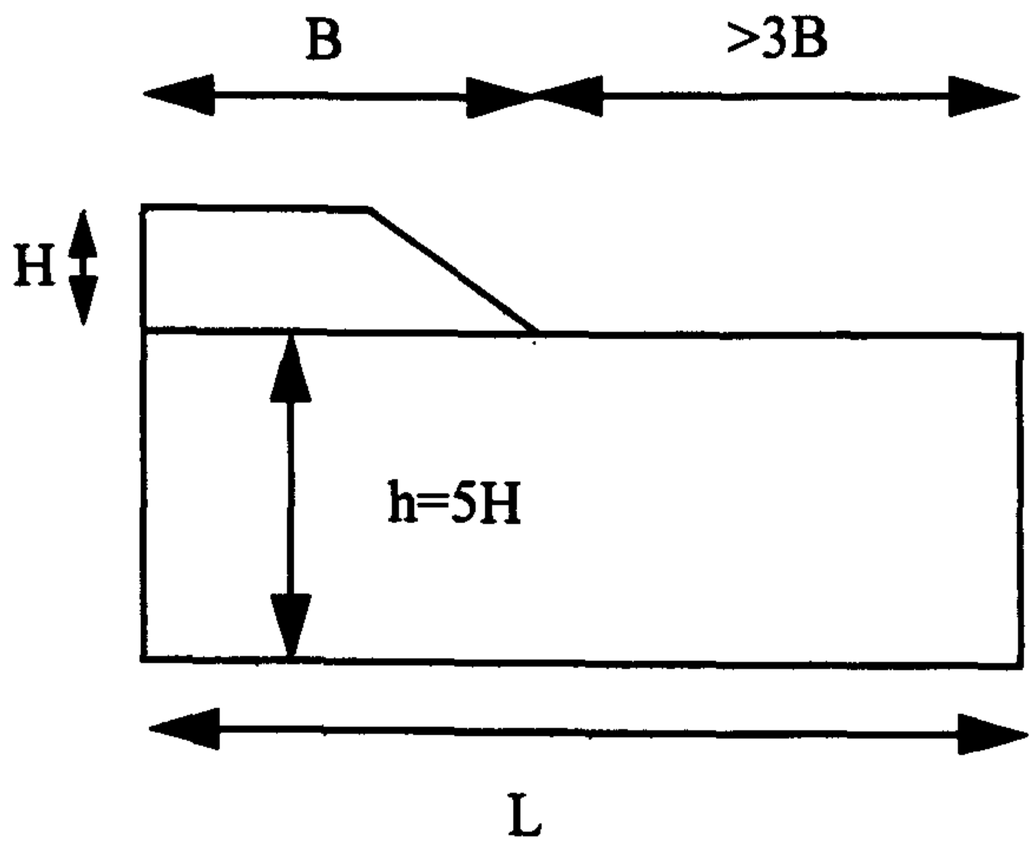

Figure 3.6: Geometry of the finite element mesh (Azizi, 2000)

3.6.1.3 Concluding remarks on the boundaries

The results of a study on the boundaries have been obtained with a particular set of parameters, constitutive model and geometry. No doubt all the factors have an influence and a detailed and thorough investigation into the effect of the interface would be required to provide solid recommendations on the subject. It can be summarised that for a shallow deposit, the 12 m deposit simulated in the model, and a 2 m high embankment (h/H=2/12=0.16) the application of the interface at the surface of the rock resulted in a more realistic horizontal displacement profile than the free boundary conditions. The horizontal displacements at the surface or within a few meters of the ground surface were not noticeably affected by the interface. The relation between the height of the embankment and the depth of the deposit is an important factor.

3.6.2 Geometry of the finite element mesh

The mesh dimension is an important component in finite element analysis but it is not well documented in the literature. Ideally the mesh should cover the areas where the stress increases and displacements are generated. According to Azizi (1999) the mesh should be characterised by a lateral dimension L which should be at least four times

the embankment width B and a minimum depth h of five times the height of the embankment H for a homogeneous soil (see Figure 3.6). The recommendations compare well with conclusions and recommendations given by Mestat et al. (2004) based on research on modelling embankments on soft soil. According to Mestat et al. (2004), the model needs to have a minimum geometry, three times the embankment width L and a minimum depth h of four times the embankment height H. These dimensions are slightly smaller than those proposed by Azizi (1999). Based on the experience gained during this research project it can be summarised that the documented horizontal geometries are well justified but the depth recommendation should be applied with caution. It is recommended that several trial and error runs are carried out to investigate the depth at which the increase of the vertical stress due to embankment loading extends in combination with the volumetric strains. This is best achieved through inspection of contour plots.

3.6.3 Coarseness of the finite element mesh

As it is difficult to describe the ideal coarseness of a finite element mesh, Mestat et al. (1997) recommend using a mesh with approximately 1500 nodes for a symmetric embankment. This recommendation is a bit vague. In order to demonstrate the influence of the finite element mesh coarseness four different simulations using the S-CLAY1S model with different degrees of coarseness are presented. The mesh coarseness for plane strain simulations of embankments on soft soil, which are not close to failure, does not have an influence on the predicted vertical displacements, as shown in Figure 3.7. It can be seen that the time settlement curve does not diverge at any point. However, it is recommended that the mesh should be sufficiently refined in areas of high stress and stress rotation. The degree of necessary refinement will be dependent on the type of element used. Elements with more nodes, such as a 15-noded triangular element, allow for a coarser mesh compared to a mesh generated with 6-noded triangular elements in the areas of interest.

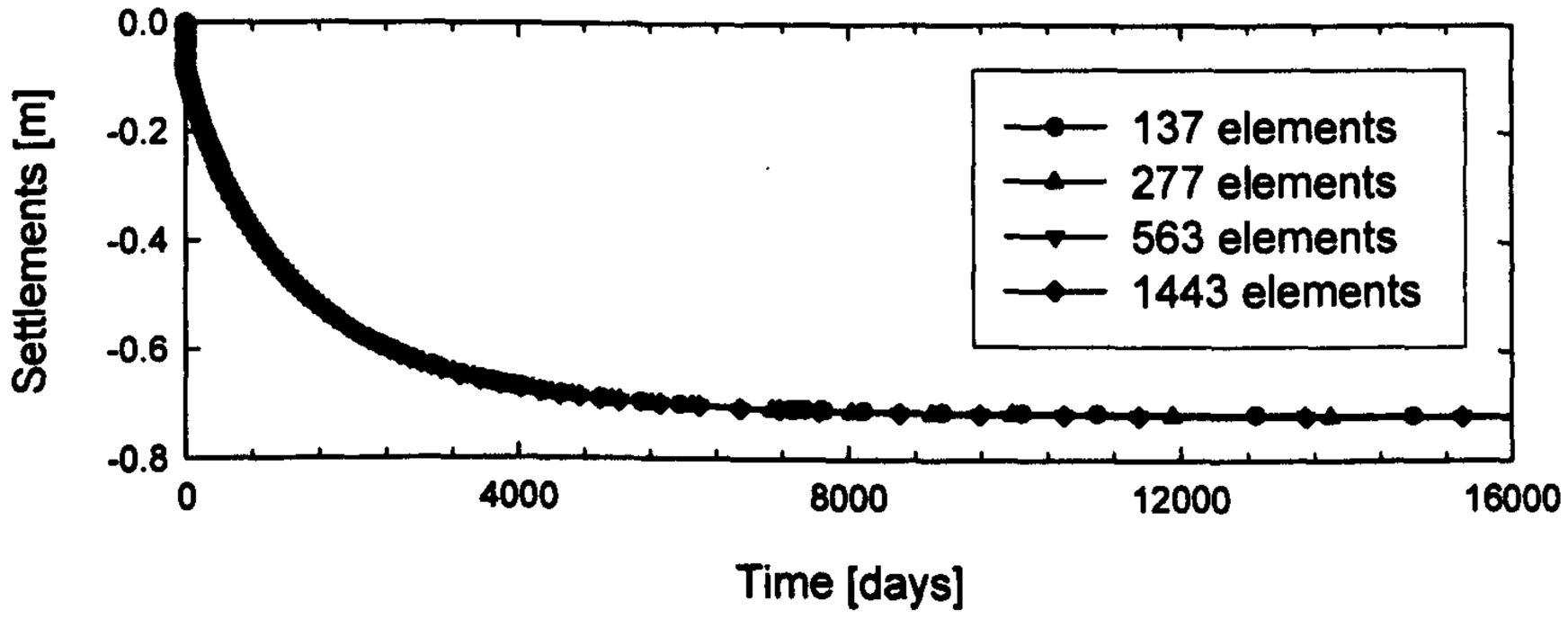

Figure 3.7: Influence of the finite element mesh coarseness on the time settlement curve

3.6.4 Large strain versus small strain analysis

Construction of embankments on soft soil is no doubt a large deformation problem. The Skå-Edeby trial embankment with a construction height of just 1.5 m settled approximately 1.4 m in 45 years (Larsson and Mattsson, 1993). Nowadays most of the fill is submerged. This embankment is relatively small compared to the trial embankment of Muar in Malaysia reported by Brand and Premchitt (1989) which had a total height of 8 m. It settled excessively 1.5 m during the construction period of 398 days (Chai and Bergado, 1993). For both cases the deformation had a significant influence on the shape and geometry.

For most geotechnical problems a small strain formulation is used. This means that the integration processes are made with respect to the initial geometry and changes in the dimension of the geometry are not taken into account. However, in situations like those mentioned above, it is not appropriate to use a small strain formulation as the geometrical changes are ignored. Thus, a large strain formulation has to be used (Potts and Zdravkovic, 1999; Chai and Bergado, 1992; Chambon, 1994). In a large strain formulation some additional terms in the stiffness matrix need to be included to

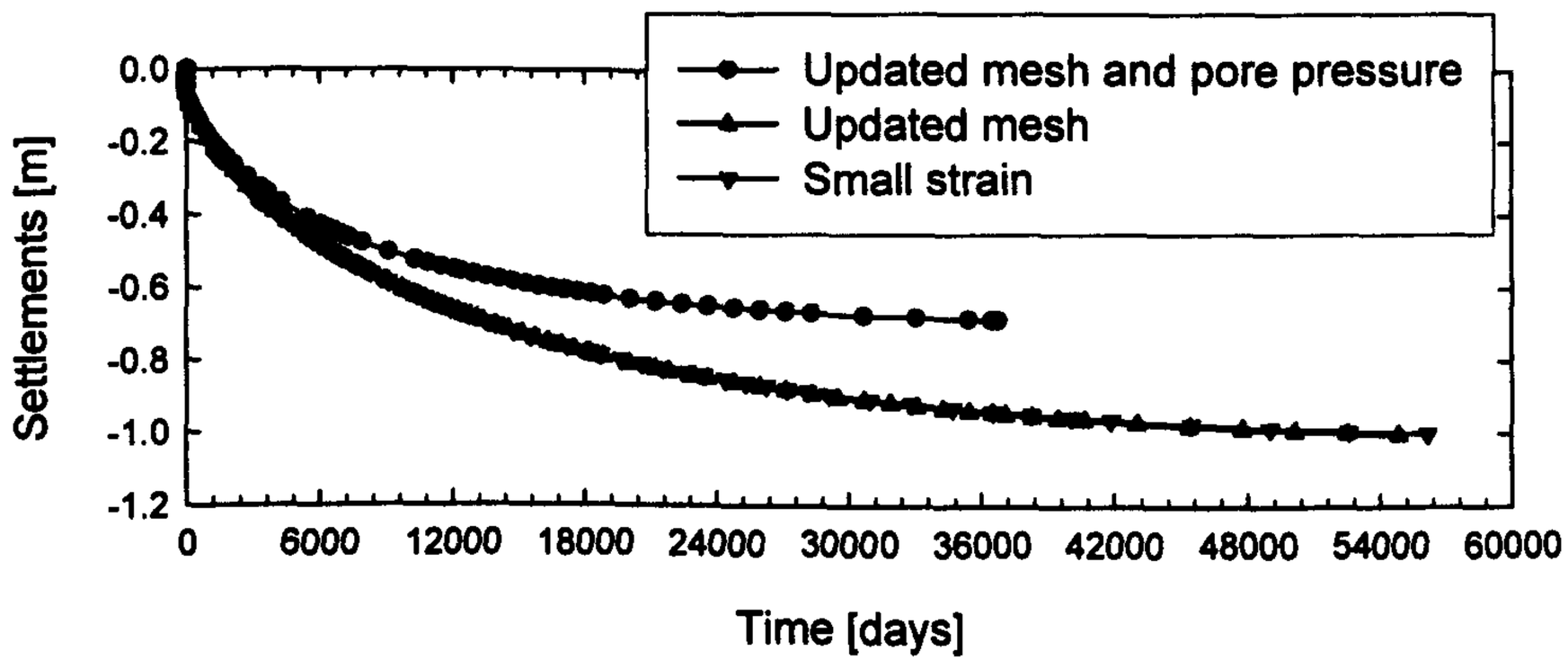

Figure 3.8: Influence of analysis type on the time settlement curve

account for large distortions. Secondly, attention must be given to the stress tensor. As the body configuration changes, the stress tensor must be continuously updated with respect to the deformed body.

In the PLAXIS code a so-called "updated mesh" calculation can be used to account for large strains (Brinkgreve, 2002). The method is based on an updated Lagrangian formulation (Bathe, 1982) with a Kirchhoff stress tensor. It is recommended to combine the large strain analysis with a so-called "updated water pressure" analysis (Brinkgreve, 2002) for embankment simulations on soft clay. The "updated water pressure" analysis continuously recalculates the water pressures at the new nodal position as the node settles below the water level. For further details about the large strain formulation in the PLAXIS code the reader is referred to Van Langen (1991).

The influence of the analysis type on the time settlement predictions is illustrated in Figure 3.8. The simulated embankment is 2 m high and constructed on a slightly over-consolidated POKO clay deposit. Performing an updated mesh analysis without updating the pore pressure has no influence on the predicted time settlement behaviour, as shown in Figure 3.8. Combining both an "updated mesh" and an "updated water pressure" analysis, results in a shorter consolidation time and a lower settle-

ment, as inspection of Figure 3.8 demonstrates. Koskinen & Karstunen (2006) published numerical simulations of the Murro test embankment using the updated mesh and water pressure analysis. The importance of large strain analysis was also demonstrated by Krenn & Yildiz (2006) in back calculations of the Vaasa trial embankment. Most embankment simulations on soft soils in the literature have been modelled as small strain analyses. As they are large strain problems modelled as small strain problems usually a good match between model predictions using isotropic models and field measurements is achieved.

3.6.5 Embankment construction

When modelling embankments, a realistic simulation of the construction of the embankment fill is important, particularly for simulations of embankments of substantial height. The significance of realistic simulation of the construction was shown by Chai & Bergado (1993).

Basically three different methods are available for modelling construction processes. A very simple method is to replace the embankment fill by surface loads. The method does not account for the stiffness of the fill and as such the lateral load spread, observed in embankment fills (Chai & Bergado, 1993), is ignored. Nowadays, the method is seldom used due to the development of easy to use finite element codes. Another method is to include the full height (geometry) of the embankment fill in the finite element mesh. The weight of the embankment fill is gradually increased until the full load is reached. Applying the load in small increments has the advantage that a constitutive model can be used to model the stress strain behaviour of the embankment fill. In this method the practical construction steps (e.g. fill layer heights) are ignored as in the first method. The most relevant and recommended method to model the construction of the fill layers, is placing or activating the fill layers according to the construction of the embankment. In this method the embankment fill is also included in the finite element mesh. The mesh of the fill is divided into several sections according to the construction and geometry of the embankment. The layers of the embankment are activated per calculation phase according to the construction

schedule of the embankment. With this method it is also possible to account for the time between the construction of each embankment layer or section. Chai and Bergado (1993) compared the last two methods with field trials, and showed that the latter method results in a much more realistic settlement trough.

3.6.6 Initial stress field

For any finite element analysis, a reasonable assumption of the initial vertical and horizontal stress profile over depth is needed. For normally consolidated ground, a soil which has never been subjected to a higher loading than the present condition, the coefficient of lateral earth pressure at rest K_0 is best estimated using Jaky's formula ($K_0^{nc}=1-\sin\varphi'$). φ' is the critical state friction angle and superscript nc stands for normally consolidated.

In overconsolidated ground, a soil which has been unloaded in the past, or soil which has been subjected to intensive creep (Bjerrum, 1967), the K_0 is usually higher. An empirical formula to estimate the K_0 of an overconsolidated soil was proposed by Mayne and Kulhawy (1982).

$$K_0^{oc} = (1-\sin\varphi')OCR^{\sin\varphi'} \qquad [3.2]$$

where OCR is the Overconsolidation ratio of the soil, which is defined as the ratio between the vertical preconsolidation stress σ'_{vp} and the initial vertical stress σ'_v.

The initial size of the yield surface of the constitutive models discussed in Chapter 2 is related to the overconsolidation of the soil. In PLAXIS the overconsolidation of each soil layer can be defined by OCR or alternatively with the so-called Pre-Overburden Pressure (POP). The POP is defined as the difference between the vertical preconsolidation stress σ'_{vp} and the initial vertical stress σ'_v:

$$POP = \sigma'_{vp} - \sigma'_v. \qquad [3.3]$$

It can be seen from *Eq.3.3* that POP is a constant which is independent of depth. The difference between the two definitions of vertical preconsolidation stress σ'_{vp} is illus-

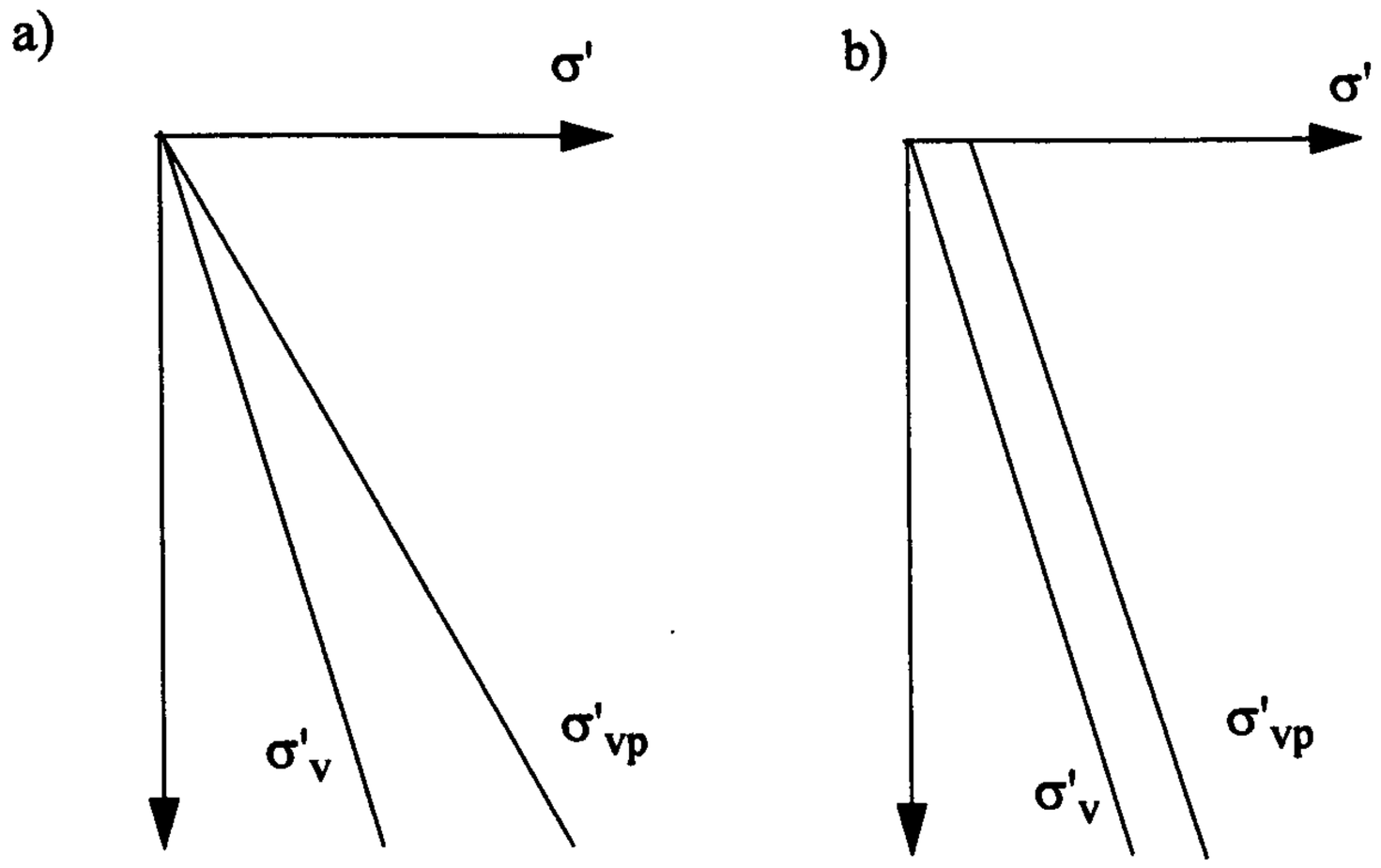

Figure 3.9: Preconsolidation pressure as a function of depth a) defined with OCR and b) with POP

trated in Figure 3.9. In many cases it is convenient to use a combination of OCR and POP with depth to simulate realistically the preconsolidation state of the soil. As seen from Figure 3.9, OCR and POP are constant with depth. Ideally the definition of both would be a function of depth. To model a smooth change of OCR or POP with depth, the user can introduce very shallow soil layers of the same material.

3.7 Summary

A short overview has been given about case histories and about modelling aspects of embankments constructed on soft soil. The discussion of the three case histories highlighted the long term problems associated with building and maintaining embankments on soft clays. Extensive vertical and lateral movements with time are the main issues which are difficult to predict with conventional methods. Numerical modelling can be a useful tool to predict settlements with time. The basics of modelling in terms of boundaries, modelling of the construction of the embankment fill and in-situ ground conditions were discussed.

Chapter 4

Benchmark embankment

This chapter studies the influence of constitutive models on the predicted response of an embankment constructed on soft clay. In the investigation five constitutive models have been used: the Modified Cam Clay model (MCC), Soft soil model (SS), S-CLAY1 model, S-CLAY1S model and the Multilaminate Model for Clay (MMC) all of which have been introduced in Chapter 2. The soft clay is assumed to have the properties of POKO clay from Finland. In the second part of this chapter the influence of the depth of the deposit, the width of the crest, the slope gradient and the constitutive model of the embankment fill on the predicted settlement behaviour of the embankment is discussed.

4.1 Benchmark

The original benchmark embankment was developed for a Benchmark Exercise as part of the SCMEP research project (Wiltafsky et al. 2003). The benchmark was used to investigate the influence of the different constitutive models on the settlement behaviour of the embankment during construction and subsequent consolidation. Wiltafsky et al. (2003) highlighted the effects of the different methods of modelling advanced soft soil features such as anisotropy and destructuration on the soft clay response. Karstunen et al. (2006) considered these issues which are related to the stress-strain behaviour on a slightly modified version of the original benchmark

embankment in much greater detail. Both studies concluded that anisotropy and destructuration increase the predicted settlements of the embankment. Furthermore, Karstunen et al. (2006) showed that the ratio between the predicted maximum horizontal displacement below the toe of the embankment and the maximum vertical displacement at the centre line of the embankment is to a certain degree dependent on the constitutive model. Obviously, the shape of the yield surface of the constitutive model influences the predicted ratio of displacements in simulations of normally or slightly overconsolidated soft clays. The benchmark presented in this chapter is a modification of the benchmark presented by Karstunen et al. (2006). In the original benchmark the constitutive models used for the dry crust were the same as for the soft clay deposit. Therefore, it was possible that the predicted behaviour of the dry crust influenced the overall predictions. For this set of simulations the dry crust was modelled with a so-called Hardening Soil model (Brinkgreve, 2002) which is a more realistic model to represent the dry crust. The dry crust was divided into two layers, a drained and an undrained layer. This is a simplified method used in order to simulate the change from an unsaturated soil at the top, to a fully saturated soil towards the bottom of the dry crust.

4.2 Numerical model

The geometry of the embankment is shown in Figure 4.1. Due to symmetry of the embankment just half of the geometry is presented in Figure 4.1. The embankment fill is 2 m high and is constructed with slopes of a gradient of 1:3. The groundwater table is assumed to be located at a depth of -2 m. Zero initial pore pressures are assumed above the water table. Fully drained ground conditions (no excess pore pressures are generated) using non-consolidating finite elements are applied to a depth of -0.5 m and fully undrained conditions (excess pore pressure generated) using consolidating elements are applied to each layer deeper than -0.5 m. The embankment has been analysed under plane strain conditions extending 50 m horizontally from the symmetry axis and 36 m vertically. A mesh with 298, 15-noded triangular elements has been used in all simulations, consisting of non-consolidating and consolidating elements.

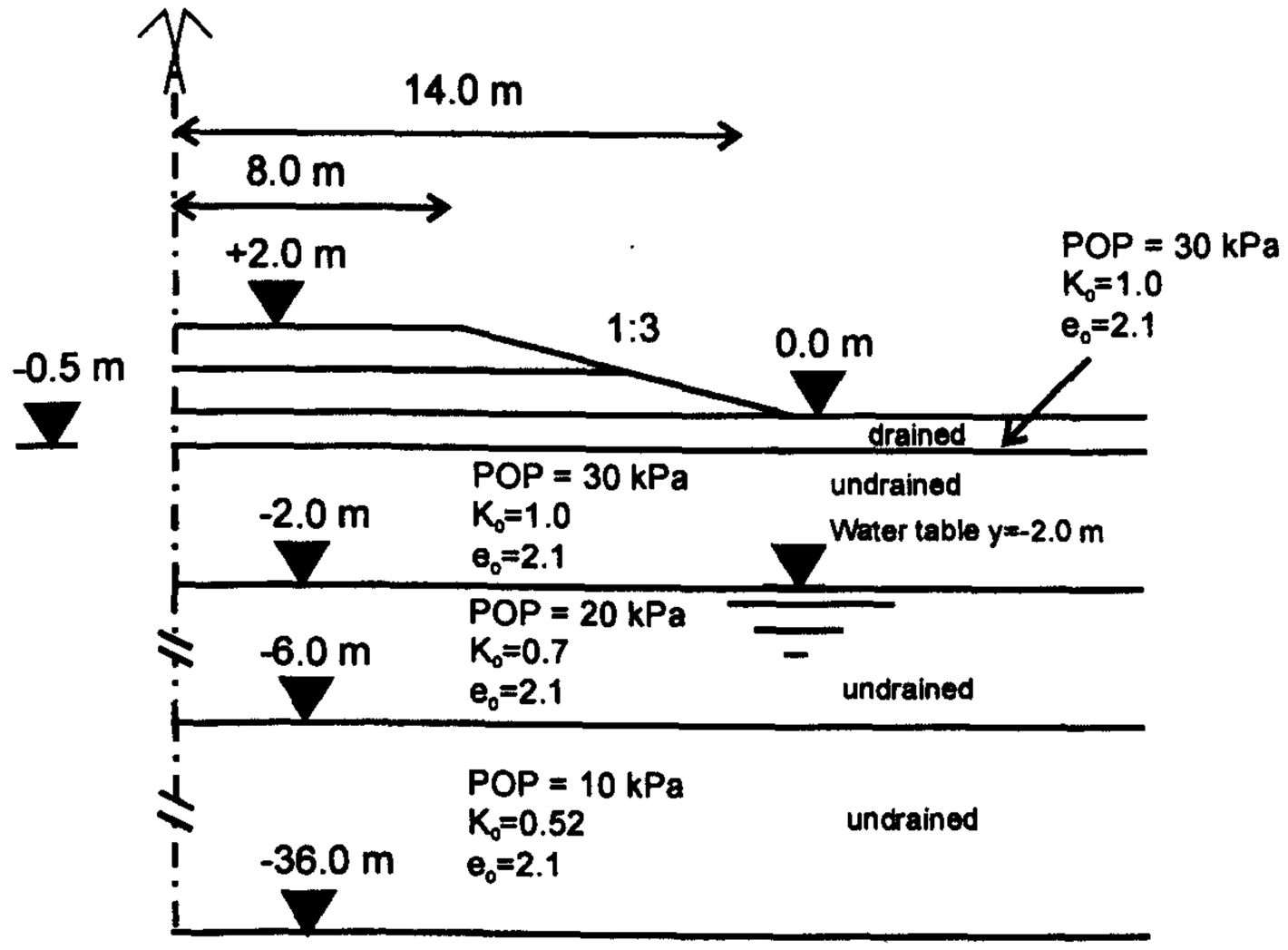

Figure 4.1: Embankment geometry and assumed soil profile

Drainage boundaries (hydraulic boundaries) are simulated by setting the excess pores pressure to zero at the corner nodes at a depth of -0.5 m and at the bottom of the model during the consolidation analysis.

The construction of the embankment was simulated in two stages, with layers of 1m each. It was simulated under fully undrained conditions not allowing for any excess pore pressure dissipation. This was followed by a consolidation phase simulated via a fully coupled static consolidation analysis. Instead of applying a maximum number of calculation steps or time, a maximum excess pore pressure of 1 kPa was applied as the simulation end criterion. When the excess pore pressure in the soil dissipated to the applied maximum, the calculation was stopped. All simulations were modelled with an "updated mesh" and "updated water pressure" analysis (Brinkgreve 2002).

4.3 Input values

4.3.1 Embankment fill and dry crust

The embankment fill was assumed to be made of granular material and was modelled with the simple Mohr Coulomb model, assuming the parameters shown in Table 4.1.

Table 4.1: Embankment fill parameters

E' [kN/m^2]	ν'	φ'	ψ'	c'	γ [kN/m^3]
40000	0.3	38	0	0	20

E' is Young's modulus, ν' is Poisson's ratio, ψ' is the dilatancy angle and γ the unit weight of the embankment material. The material behaviour was assumed to be fully drained.

The dry crust was modelled with the Hardening Soil model (see Section 2.9.1) and the parameters are shown in Table 4.2.

Table 4.2:Dry crust parameters

Type	E_{50}^{ref} E_{oed}^{ref} [kN/m^2]	E_{ur}^{ref} [kN/m^2]	φ'	ν'	m	γ [kN/m^3]	$k_x = k_y$ [m/day]
drained	1080	16822	30	0.2	1	15	-
undrained	1080	16822	30	0.2	1	15	8.64e-5

* p_{ref} = 100 kPa

It was assumed that the reference young modulus E_{50}^{ref} is of the same order of magnitude as the reference oedometer modulus E_{oed}^{ref}. The reference unloading/reloading modulus E_{ur}^{ref} is approximately 16 times greater than the E_{50}^{ref}. The critical state friction angle φ' was choosen to be 30 degrees. Possion's ratio ν_{ur} is 0.2. The exponent m is 1, which is a typical value for soft clays.

The dry crust was modelled as an overconsolidated soil by using a vertical pre-overburden pressure (POP). The value of POP and the predicted OCR are shown in Figure 4.2. The K_0 values assumed for each layer are shown in Figure 4.1.

4.3.2 Input values and initial state of the soft clay

The soft clay profile corresponds to the so-called POKO clay (Koskinen et al. 2002a, Koskinen et al. 2002b). The abbreviation POKO stands for Porvoo-Koskenkylä, which was a 25 km stretch of motorway close to the town of Porvoo. In the bench-

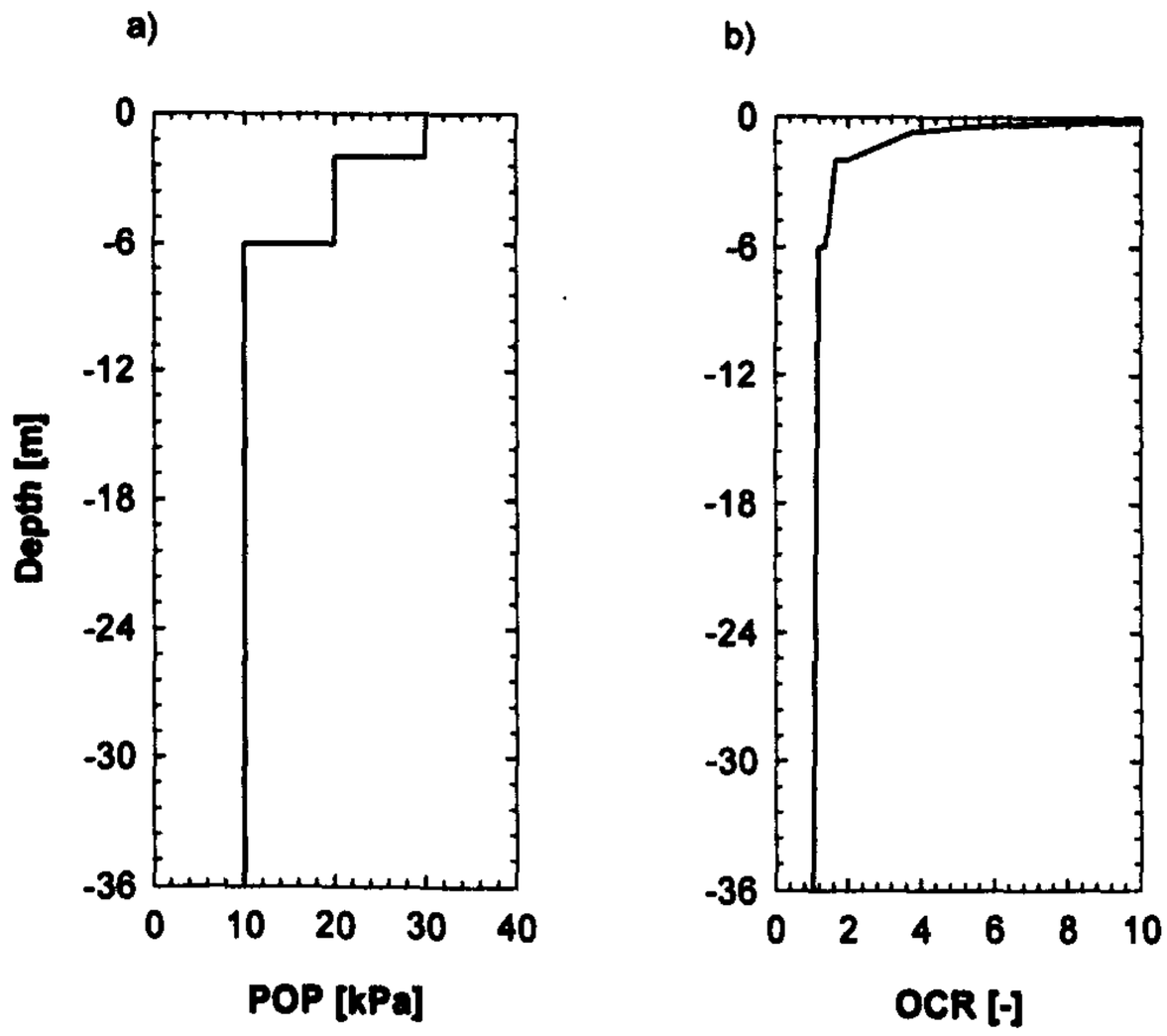

Figure 4.2: Overconsolidation profile: a) POP and b) OCR

mark the deep soft clay deposit was divided into two layers with a single set of clay parameters for the 36 m. The input values have been determined from oedometer and triaxial tests on natural and reconstituted samples (Koskinen et al. 2002a, Koskinen et al. 2002b). An overconsolidation profile which approximates the slightly overconsolidated deposit with depth was chosen. The POP values with depth are shown in Figure 4.2a. Because it is not possible to provide a continuous profile of POP with depth in PLAXIS (Section 3.6.6), the assumed initial state will have some small discontinuities at the interface between the layers. The calculated OCR profile is presented in Figure 4.2b. Small discontinuities in OCR values at the interfaces between the layers at a depth of -2 m and -6 m can be seen in the profile. The K_0 values shown in Figure 4.1 were calculated with the formula of Mayne and Kulhawy (1982) (*Eq. 3.2*) at the middle of each layer. In general if the K_0 value is high (greater than 1) each stress state should be plotted in a p'-q diagram to check that the stress state lies within the yield surface at the beginning of the calculation. Certain stress states which have a negative q value due to a high K_0 value or a stress state with an initial low η value and p' close to p_m can potentially be located outside the yield surface because of the different shapes of yield surfaces of the constitutive models.

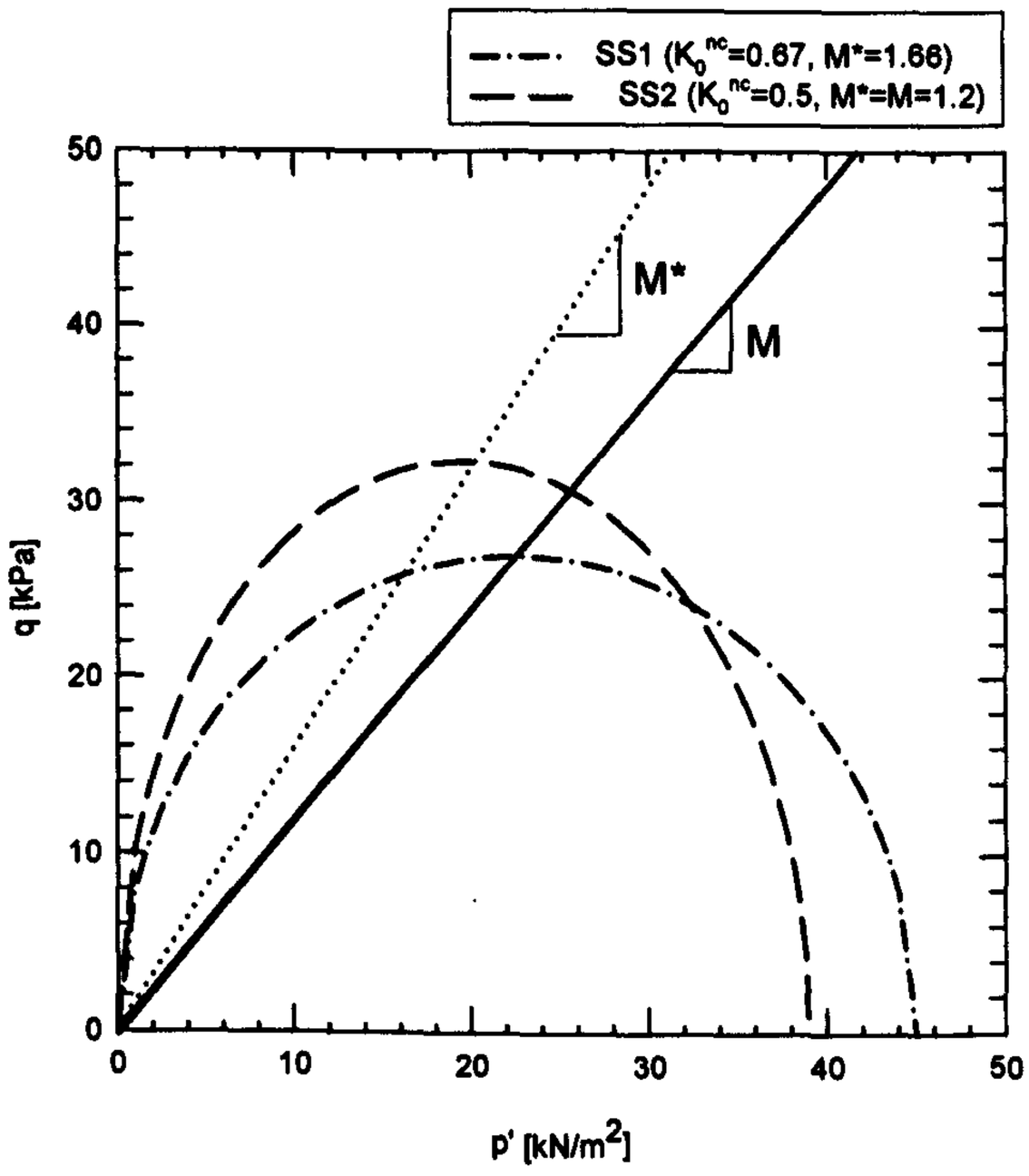

Figure 4.3: Yield surface of the Soft Soil models in the p'-q diagram at a stress point at a depth of -5.4 m

The initial void ratio e_0 has been kept constant for each layer and is shown in Figure 4.1. The permeability k (hydraulic conductivity) of the POKO was assumed to be 10^{-9} m/s in both vertical and horizontal direction.

4.3.2.1 Soft Soil models

The SS model has been used twice in the simulations, each with a different shape and size of the volumetric cap yield surface. As explained in Section 2.3.2 the shape of the yield surface of the SS model is related to the K_0^{nc} value (input value) of the soil. By using a K_0^{nc} of 0.67 for normally consolidated POKO clay the SS model corresponds to the MCC model because the cap yield surface of the SS model has the same shape as the yield surface of the MCC model. The model matching the MCC model yield surface is referred to as SS1 in the results. The input parameters and initial state parameters are shown in Table 4.3. In contrast in the model referred to as SS2, the value of K_0^{nc} has been calculated using Jaky's formula (Section 3.6.6). The difference

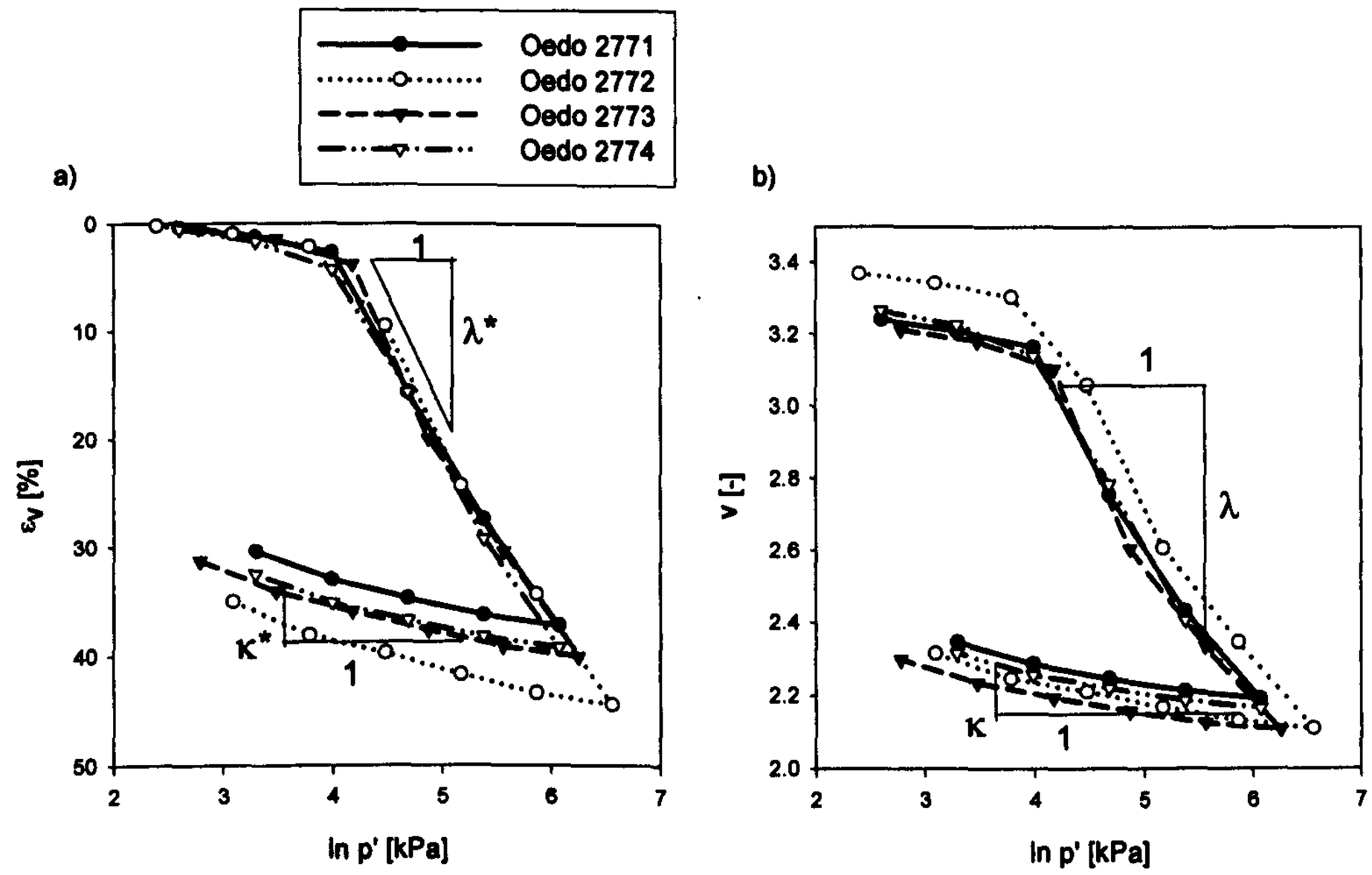

Figure 4.4: Oedometer test results on POKO clay: a) ε_v-lnp' plot and b) v-lnp' plot (Krenn, 2002)

in the shape and size of the yield surfaces is illustrated in Figure 4.3. Both model's yield surfaces have been plotted for a depth of -5.4 m.

Table 4.3: Input parameters and initial state of the soil

Model	λ^*	κ^*	ν'	φ'	c' [kPa]	ψ'	K_0
SS1	0.24	0.01	0.2	30	0	0	0.67
SS2	0.24	0.01	0.2	30	0	0	0.5

λ^* and κ^* were directly estimated from ε_v-lnp' plots of oedometer tests on natural POKO clay samples (Figure 4.4a). The κ^* was estimated from the gradient of the unloading-reloading part of the oedometer results. For determing λ^* the steepest part of the curves was used. The same criterion was used to estimate λ and κ from v-lnp' plots.

4.3.2.2 MCC, S-CLAY1 and S-CLAY1S model

The soil constants and initial state parameters for the Modified Cam Clay model (MCC), the S-CLAY1 model and the S-CLAY1S model are shown in Table 4.4. λ and κ were estimated from v-lnp' plots of oedometer tests on natural POKO clay samples

(see Figure 4.4b). The initial inclination of the yield surface α and the parameter β were derived following the procedure outlined in Section 2.4.1.1. The initial value of x_0 was estimated based on the sensitivity of the soil (Koskinen et al. 2002a). For the soil constants μ, a and b typical values for POKO clay have been assumed.

Table 4.4: Input parameters and initial state of the soil

Model	λ (or λ_i)	κ	ν'	M	μ	β	a	b	α_{K0}	x_0
MCC	0.71	0.03	0.2	1.2	-	-	-	-	-	-
S-CLAY1	0.71	0.03	0.2	1.2	20	0.76	-	-	0.46	-
S-CLAY1S	0.26	0.03	0.2	1.2	20	0.76	9	0.2	0.46	12

4.3.2.3 Multilaminate Model for Clay

The input values for the MMC are shown in Table 4.5. α which is related to the critical state friction angle φ' of the POKO clay, was estimated using the equations presented in Section 2.4.2. The value for A was found through simulations of drained triaxial tests on POKO clay (Wiltafsky, 2003).

Table 4.5: Input parameters and initial state of the soil

Model	λ	κ	ν'	φ'	c' [kPa]	α	A
MMC	0.71	0.03	0.2	30	0	0.67	0.015

4.4 Results of the numerical analyses with different models

In the following the results of the simulations with the different constitutive models are presented. In each category of results three diagrams per figure are shown if not stated otherwise. Figures a, present the results of all six models used. Figures b show the predicted results of the three isotropic models (MCC, SS1 and SS2), while figures c compare the three advanced models (S-CLAY1, S-CLAY1S and MMC) to the isotropic MCC model. The comparisons aim to highlight the effect of anisotropy and the combination of anisotropy and destructuration on the soft clay response and to demonstrate the differences between the alternative modelling approaches.

4.4.1 Vertical displacements

The predicted time-settlement curves at a node at the centreline of the embankment are presented in Figure 4.5. The average total consolidation time predicted by the models for primary consolidation was approximately 115 years, whereas the MCC and the S-CLAY1S predict a slightly longer time of 116 years. The S-CLAY1S model gives the highest prediction for vertical displacements, at 0.79 m, while in comparison the lower bound estimate was given by the isotropic MCC model at 0.55 m. If the predictions by the isotropic models are compared only (Figure 4.5b), it can be seen that the SS1 which attempts to match the MCC model gives notably higher displacements than the MCC, approximately 0.79 m. The difference in the predictions of the two models can be explained by the difference in the compression relationships (Karstunen et al. 2006). The original MCC uses the void ratio as a state parameter, whereas the Soft Soil model does not. Investigation of void ratio plots at the end of consolidation, estimated by the MCC suggest that the void ratios change from an initial value of 2.1 to a minimum of about 1.95 in the POKO clay layers. The changes in the void ratio are notable and contribute to the difference in the volumetric strain prediction of the two models (MCC and SS1), which attempt to match each other in the simulations. As mentioned in Section 4.3.2.1 the elasto-plastic stiffness of the Soft Soil models was estimated directly from laboratory data (ε_v-lnp' curve). It is important to estimate the values of λ^* directly from laboratory data, rather than using the simple relationship ($\lambda^*=\lambda/(1+e)$) to estimate realistic compression behaviour.

The huge influence of the shape of the yield surface can be seen by comparing the predictions of the SS1 and the SS2 models. The SS2 uses a shape which predicts a realistic value for normally consolidated K_0. Simulations with the SS2 show smaller final vertical displacements than the SS1 (0.6 m vs. 0.74 m). This highlights how small differences in the shape of the yield surface (see Figure 4.3) can lead to notably different responses by the same constitutive model. SS2 predictions are by coincidence, relatively close to those of the MCC model, about 0.55 m.

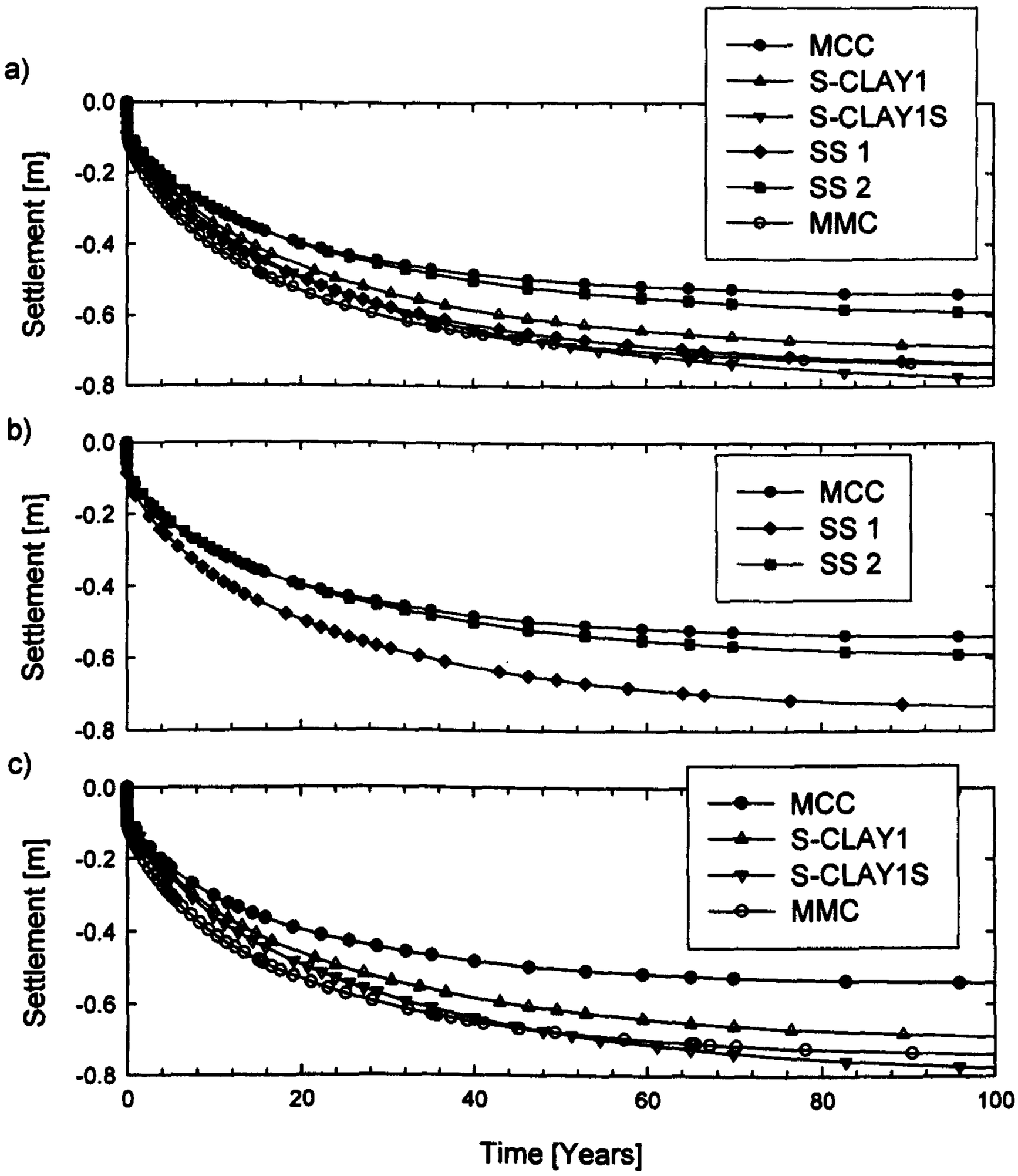

Figure 4.5: Time settlement curve for 100 years of consolidation

In Figure 4.5c the advanced models are compared to the reference model MCC. Accounting for anisotropy in the simulations increases the predicted vertical displacement from 0.55 m, predicted by the MCC, to 0.7 m predicted by the S-CLAY1, and 0.75 m estimated by the MMC. The two different approaches of modelling anisotropy predict maximum vertical displacements with time differently. The MMC model gives somewhat similar predictions to the S-CLAY1S model, which accounts in addition to anisotropy for destructuration. The predictions of MMC are influenced by the shape of the yield surface on the integration plane. The shape is dependent on the

parameter α, which can be estimated via the critical state friction angle φ'. A slight variation of the shape would change the prediction. Comparing S-CLAY1 and S-CLAY1S only, the results demonstrate that the incorporation of destructuration seems to increase the predicted final vertical displacements.

The predicted surface settlement troughs after the construction of the embankment are shown in Figure 4.6. All models predict a similar small surface heave outside the embankment, except the SS1 which predicts marginally greater heave than the other models. The maximum vertical displacement of 0.086 m was also predicted by SS1. The other models all show somewhat similar results of around 0.066 m. The point of zero displacement is about 14 m from the symmetry axis for all models, corresponding to the width of the embankment. All the models have identical elastic relationships and as such similar predictions are expected. The higher predictions of the SS1 can be explained by the different shape of the yield surface, which results in a marginal decrease of the elastic domain during the undrained construction (see Figure 4.3).

The predicted settlement troughs after 100 years of consolidation of the embankment are shown in Figure 4.7. The MCC, S-CLAY1 and S-CLAY1S models estimate the point of zero settlement at the surface at a distance of 42 to 43 m from the symmetry axis. The three other constitutive models predict settlements at the surface over the whole width of the model. In Figure 4.7b it can be seen that SS1 predicts marginally greater settlements towards the model boundary than MCC and SS2. All the models predict a rather sharp discontinuity at about 14 m from the symmetry line of the embankment (position of the toe of the embankment). MMC predicts a more gradual deflection of the settlement trough compared to all the other models (Figure 4.7 a and c). Overall it can be seen that anisotropy and the combination of anisotropy and destructuration result in marginally wider and steeper settlement troughs than predicted by the isotropic models after 100 years of consolidation.

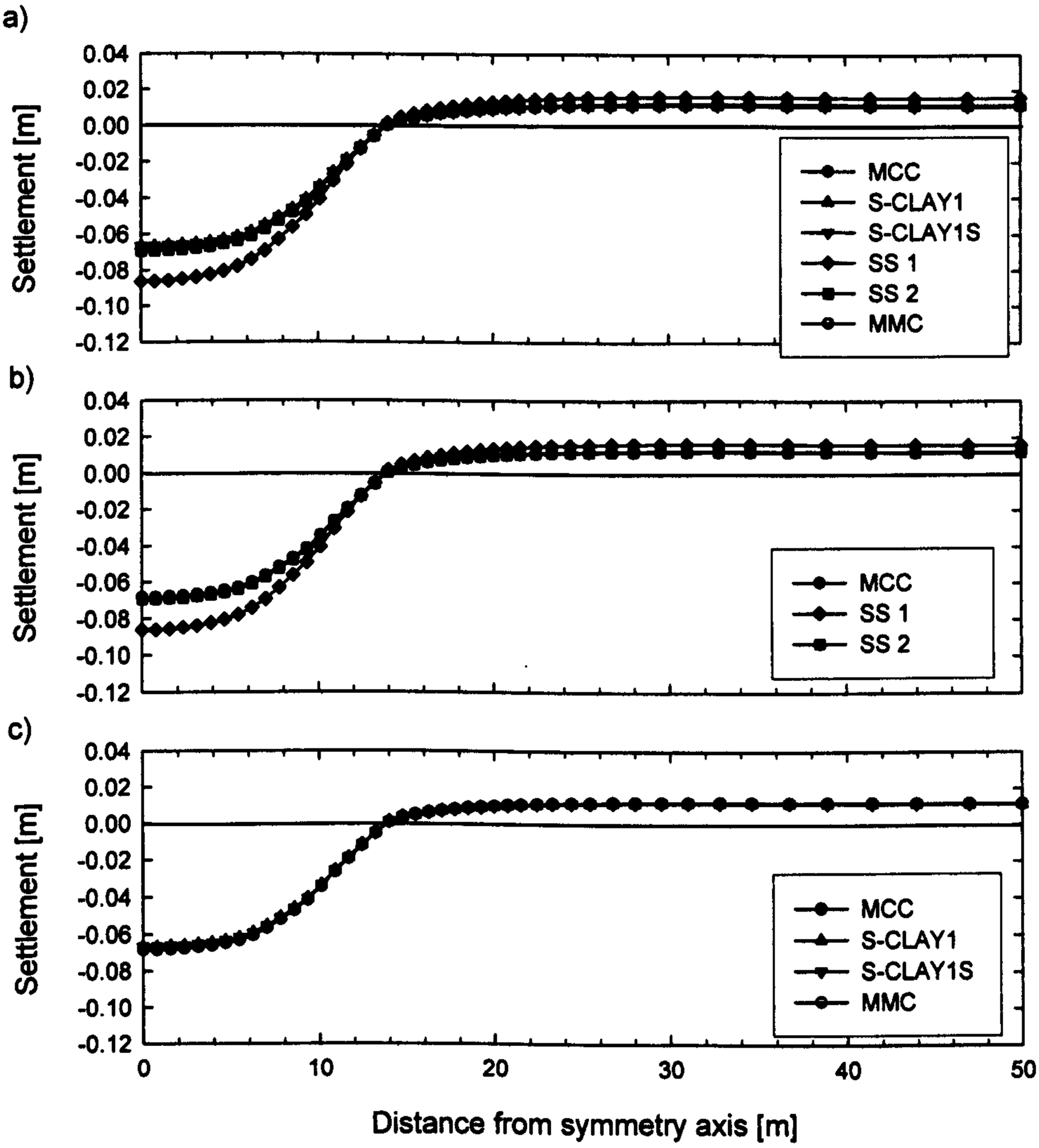

Figure 4.6: Surface settlements immediately after construction of the embankment

4.4.2 Horizontal displacements

The predicted horizontal displacements profile versus the depth underneath the toe of the embankment are shown in Figure 4.8. After construction of the embankment most models give similar predictions (~0.021 m) with the exception of the SS1 (0.028 m) and the MMC model (0.038 m). Both predict significantly larger horizontal displacements than the others. Again it is demonstrated that the attempt to match the original MCC model with the SS1 leads to different results. Inspection of the plastic point

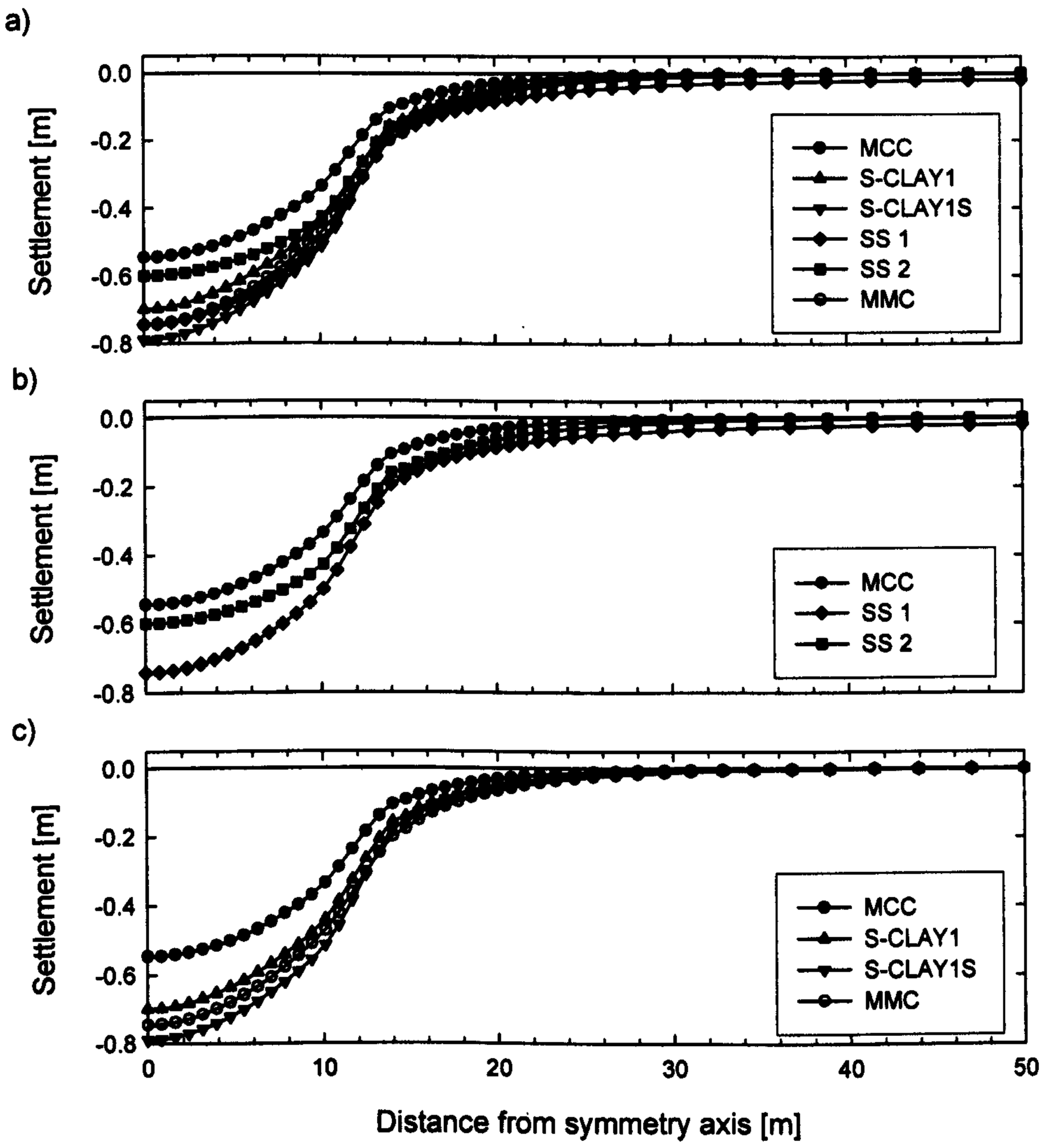

Figure 4.7: Surface settlements after 100 years of consolidation

plots of the MCC and SS1 provides some explanation to the difference in the predictions. In the predictions with the SS1 models in the area below the embankment yielding has occurred in most stress integration points whereas the MCC does not predict yielding in the shallow layers during the undrained construction. This can partly be attributed to the different formulation of the models on the so-called dry side of the failure line. In the MCC model, stress states above the critical stress ratio are allowed whereas in the SS model any stress above the failure criterion is prevented by perfectly plastic yielding.

The significantly larger predictions of horizontal displacements by the MMC than the other models can be attributed to the shear hardening law used in the model. Evaluation of the plastic point plots clearly show that shear hardening is activated in the shallow layers below the embankment.

The calculated u_x/u_y ratios of the maximum horizontal displacements u_x underneath the toe of the embankment to the maximum vertical displacements u_y at the centreline is presented in Table 4.6. u_x/u_y ratio is around 34% for the MCC and the S-CLAY models. MMC predicts a much higher u_x/u_y ratio of 56 %. The ratios are somewhat higher than the ratios predicted by Karstunen et al. (2006), which are also shown in Table 4.6. This clearly demonstrates the effect of the constitutive model used for the dry crust in the soil-embankment interaction. Secondly, it demonstrates the importance of the material behaviour assigned to the dry crust. In this case the majority of the dry crust is modelled as an undrained material whereas Karstunen et al. (2006), in their simulation modelled it as a drained material. The predicted ratios by Karstunen et al. (2006) are in the range suggest by Leroueil et al. (1990). Leroueil et al. (1990) suggest in their book, which is considered as the reference text for embankments on soft soil, that the ratio is dependent on the geometry of the embankment and the factor of safety. The results of the simulations indicate that it is dependent on the degree of predicted plasticity, the constitutive models and the material behaviour (drained / undrained) applied.

Table 4.6: u_x/u_y - ratio after construction

	MCC	S-CLAY1	S-CLAY1S	SS1	SS2	MMC
Current work	34 %	34 %	34 %	34 %	33 %	59 %
Karstunen et al. (2006)	19 %	14 %	16 %	17 %	15 %	22 %

The predicted horizontal displacements after 100 years of consolidation underneath the toe of the embankment are presented in Figure 4.9. The largest horizontal displacements are predicted by the SS1 (0.061 m) and the MMC (0.062 m) models. SS2 simulations predict the smallest horizontal displacement (0.027 m), which is signifi-

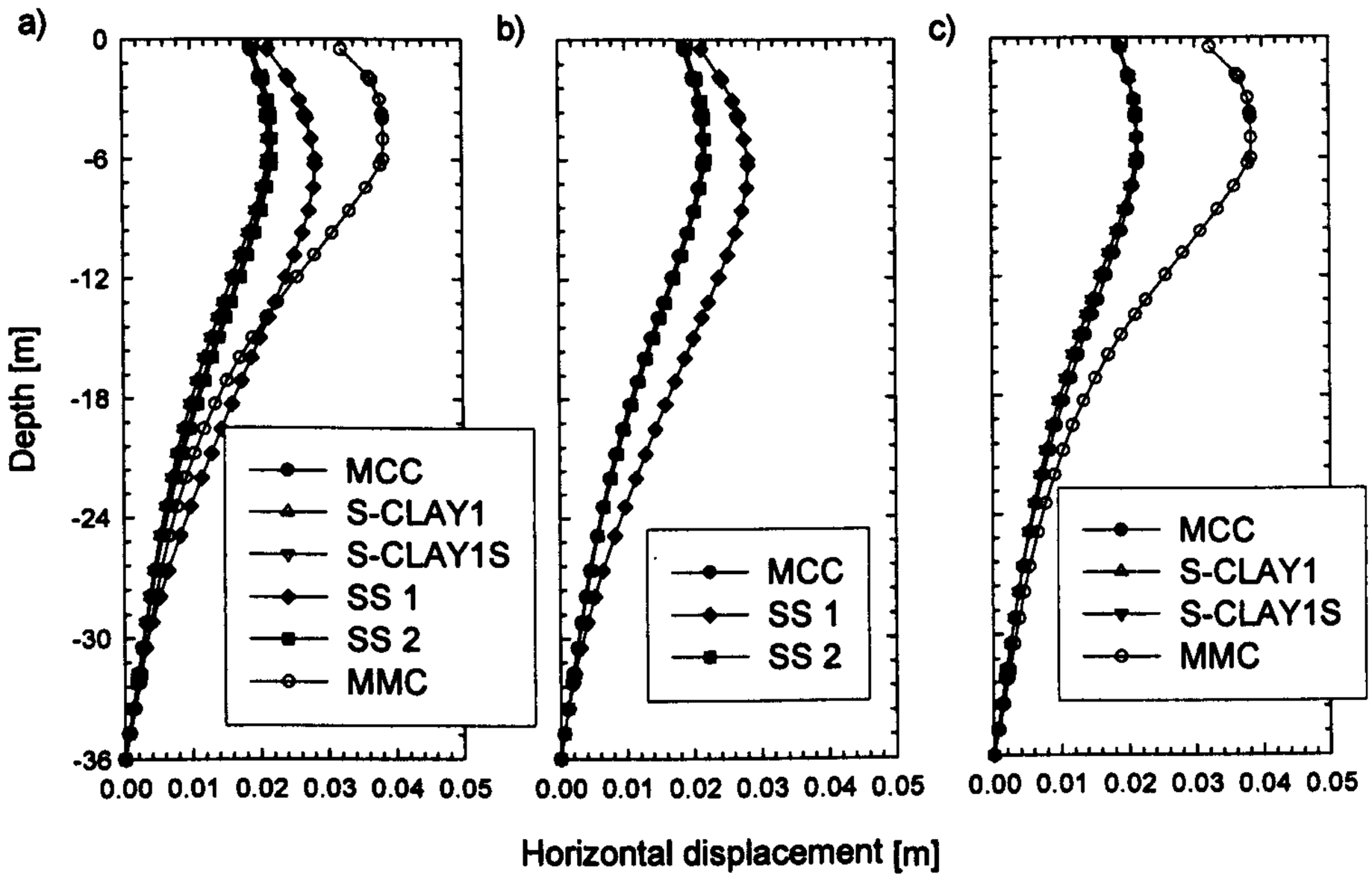

Figure 4.8: Horizontal displacements underneath the toe of the embankment immediately after construction

cantly lower than all the other predictions. The predictions of MCC and SS1 are almost identical at the surface but diverge to a depth of 6 m. All models estimate the maximum horizontal movement to occur at a depth of approximately 6 m, which coincides with the discontinuity of the K_0 and the POP values. At the surface (at the soil-embankment interface), all the model simulations predict some negative displacements (movements towards the symmetry axis) due to large vertical displacements. The predicted u_x/u_y - ratios are shown in Table 4.7.

Table 4.7: u_x/u_y - ratio after 100 years of consolidation

MCC	S-CLAY1	S-CLAY1S	SS1	SS2	MMC
9 %	7 %	7 %	8 %	5 %	8 %

The highest ratio of about 9 % is given by MCC, followed by the anisotropic MMC and SS1 at about 8 %. Both S-CLAY models estimate 7 %, suggesting that destructuration has a minor influence on the u_x/u_y-ratio. The lowest u_x/u_y ratio of 5% is predicted by SS2. The predicted ratios between the anisotropic and isotropic models is similar to that reported by Karstunen et al. (2006). The HS model used for the dry

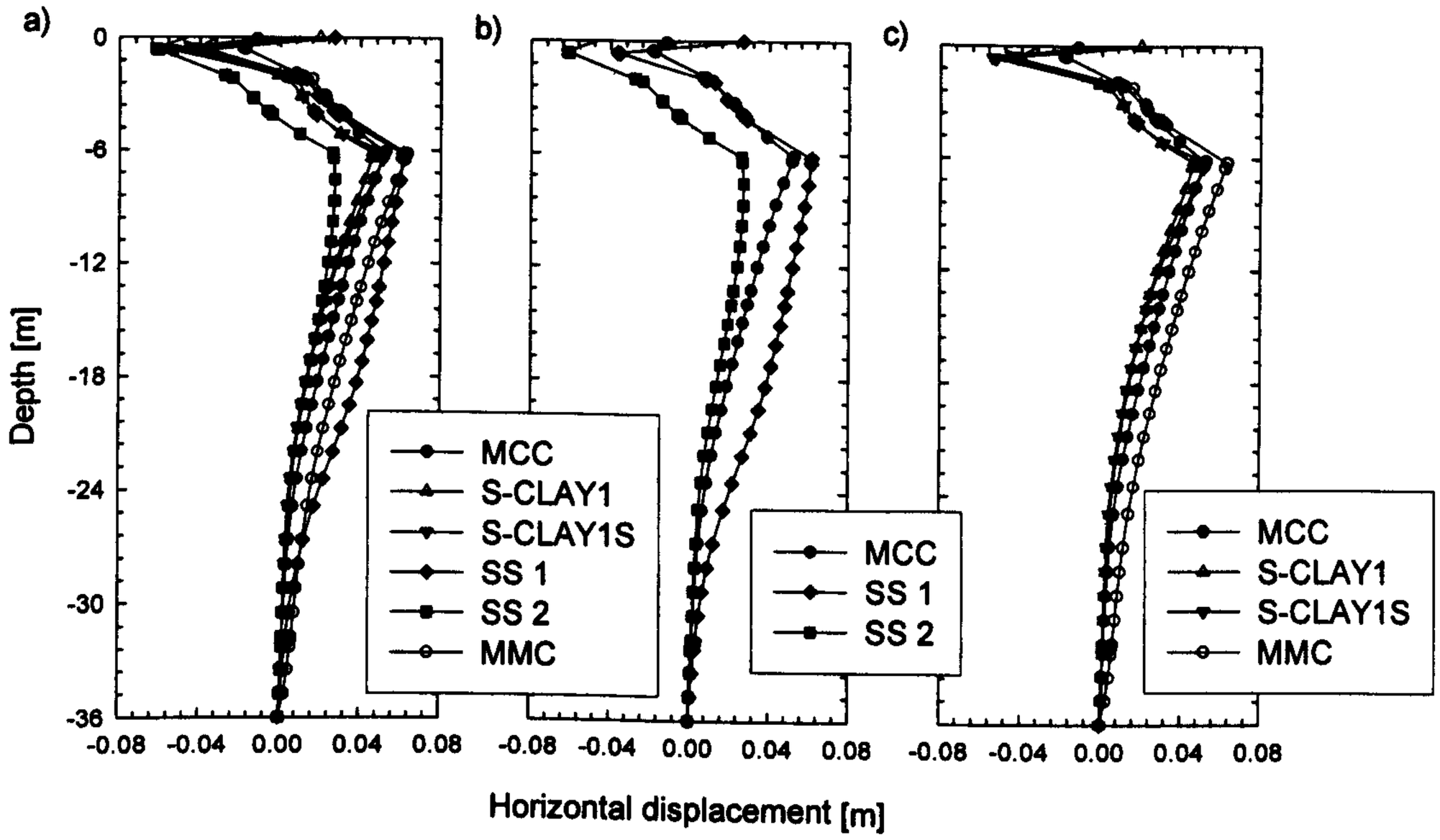

Figure 4.9: Horizontal displacements underneath the toe of the embankment after 100 years of consolidation

crust and the different material behaviour applied to the dry crust does not have a great influence on the overall predictions after 100 years of consolidation.

As an alternative to displacement profiles with depth, contour plots of horizontal displacements after the end of the construction of the embankment are shown in Figure 4.10. Inspection of the results shows that the MCC, S-CLAY1 and S-CLAY1S show similar horizontal displacement contours, with maximum centre located at a distance of about 12 m from the symmetry axis and at a depth of about 5 m. SS1 estimates the centre of the maximum contours at about the same distance but marginally deeper at a depth of 7 m. In addition, SS1 contours extend further in both the vertical and lateral directions. Similar predictions are suggested by the simulations of the MMC model. Its centre of the maximum is predicted at the same location as that of the S-CLAY models.

The horizontal displacement contour plots after 100 years of consolidation are presented in Figure 4.11. Initial inspection reveals that each model predicts a somewhat different overall contour line shape. The MCC and the two S-CLAY models predict

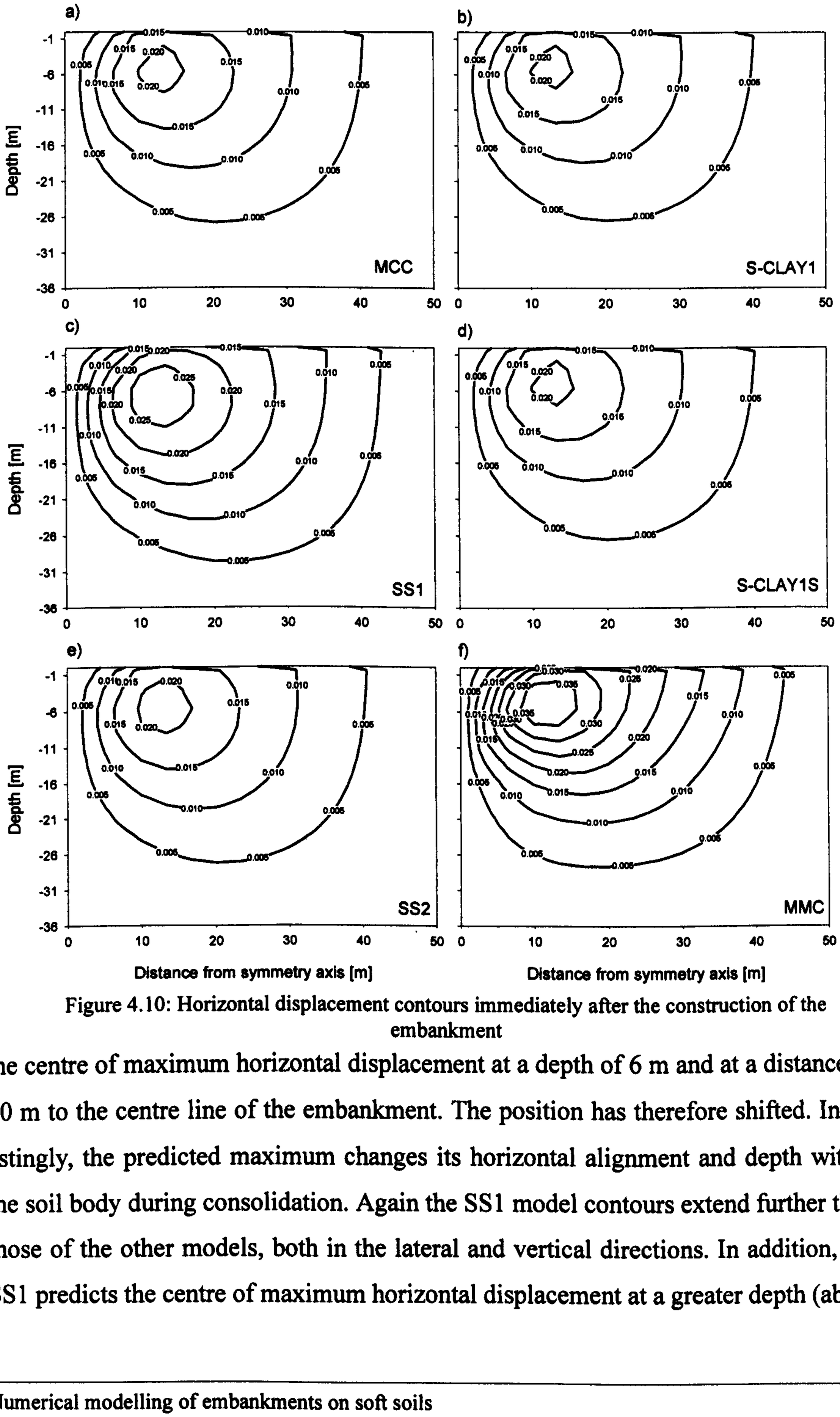

Figure 4.10: Horizontal displacement contours immediately after the construction of the embankment

the centre of maximum horizontal displacement at a depth of 6 m and at a distance of 10 m to the centre line of the embankment. The position has therefore shifted. Interestingly, the predicted maximum changes its horizontal alignment and depth within the soil body during consolidation. Again the SS1 model contours extend further than those of the other models, both in the lateral and vertical directions. In addition, the SS1 predicts the centre of maximum horizontal displacement at a greater depth (about

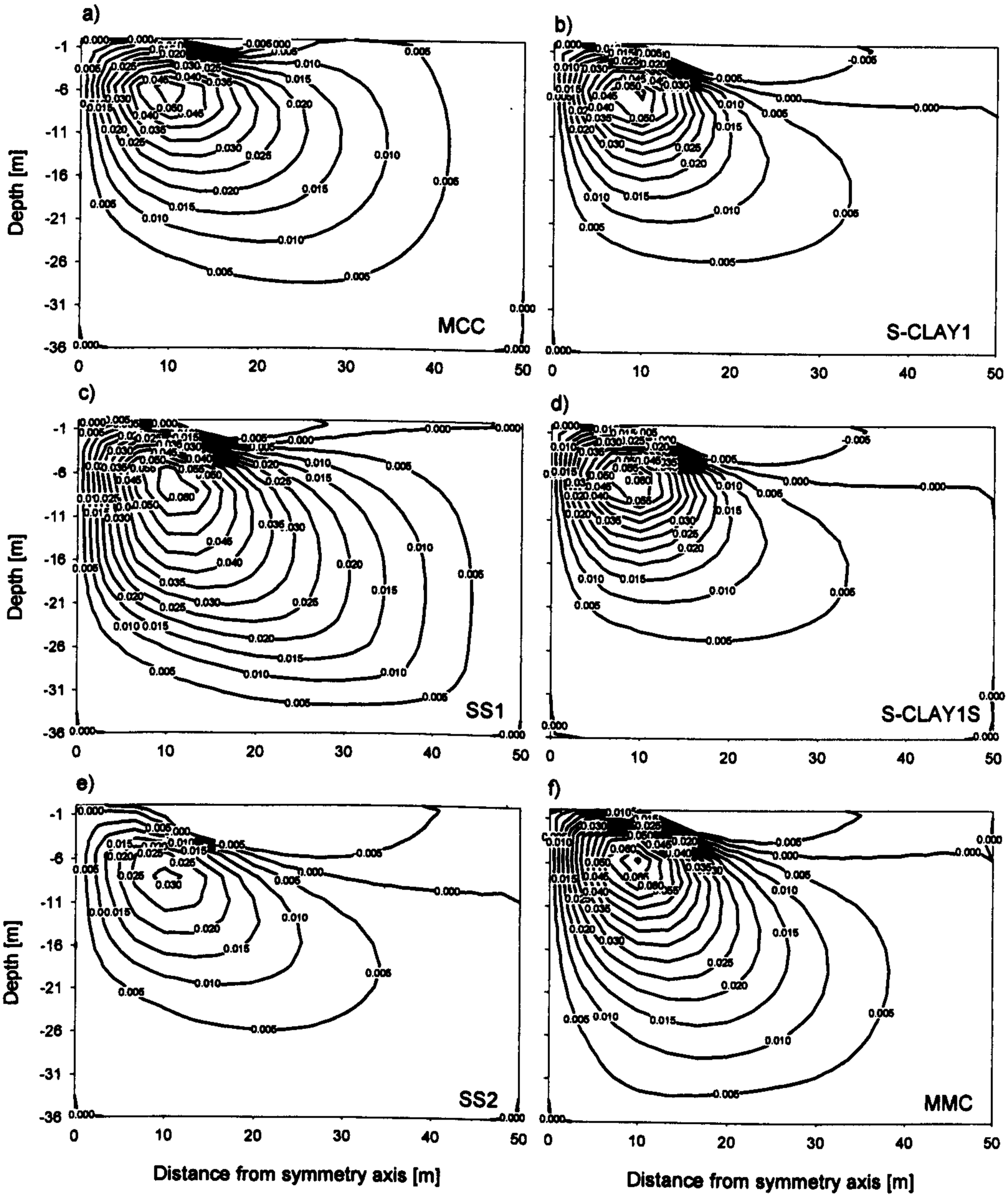

Figure 4.11: Horizontal displacements contours after 100 years of consolidation

7 m) and distance from symmetry axis (about 11 m from symmetry axis). SS2 predicts its maximum at the same depth as the SS1 but its contour lines extend much less, similar to the S-CLAY models. By comparing only the two anisotropic models, it can be seen that the displacements predicted by the MMC extend further, both laterally and with depth. However, both models predict the maximum at the same depth and dis-

tance from the symmetry axis. Even the overall shape of the contour lines is very similar despite the difference in size.

4.4.3 Strain contours

In Figure 4.12, the volumetric strain contours immediately after construction of the embankment have been plotted. The figures are scaled to display only a width of 14 m and a maximum depth of -10 m. It can be seen that the different constitutive models used for POKO clay have only a marginal influence on the predicted volumetric strains in the dry crust. In all cases the maximum volumetric strains are predicted only within the dry crust above the water table as expected.

The volumetric strain contour plots after 100 years of consolidation are shown in Figure 4.13. All models predict a similar shape of contour lines. However, the lateral and vertical extent of the contours differs from model to model. The MMC model predicts by far the deepest extent of the volumetric strain contour lines to a depth of about -26 m. All models show a discontinuity in volumetric contours at a depth of approximately -6 m. The discontinuity coincides with the stepwise increase of the POP in the model at this depth. This suggests that the method used to model overconsolidation of the soil has an influence on the volumetric strain pattern. Karstunen et al. (2006) reported similar findings.

Deviatoric strain plots after construction of the embankment are presented in Figure 4.14. The plots are scaled to a maximum depth of -10 m and a maximum width of 14 m. Inspection of the plots clearly shows that the predictions by MMC are notably different to all the other models. Due to the deviatoric hardening law implemented in the MMC model, the plot shows deviatoric strain contours in areas at a depth greater than -2.5 m. All models predict deviatoric strains of about 4 % in the area of the dry crust. It seems that the deviatoric strains of the dry crust are not influenced by the different constitutive models used for the POKO clay.

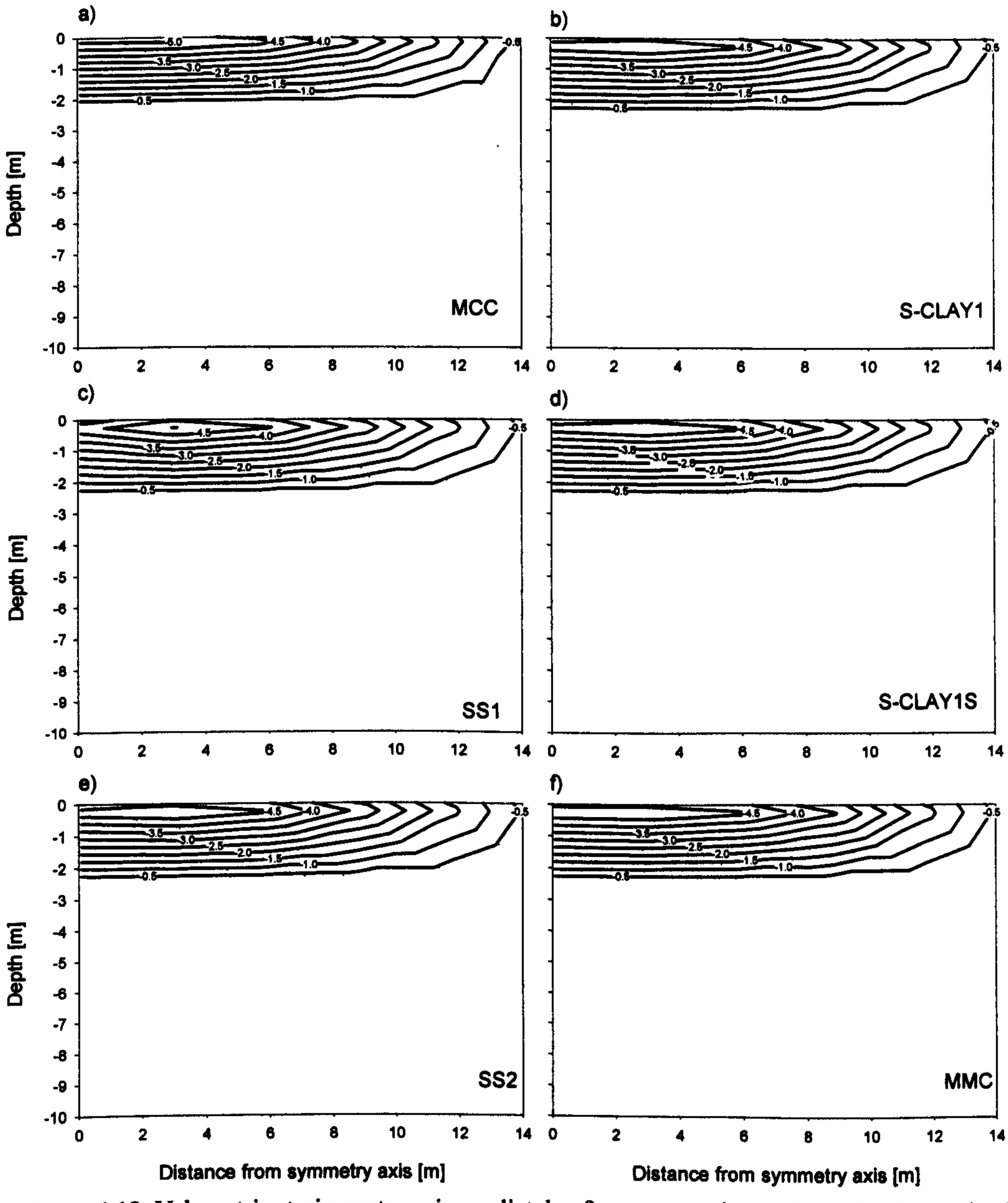

Figure 4.12: Volumetric strain contours immediately after construction of the embankment (scaled: max. depth 10 m and max. width 14 m)

Deviatoric strains after 100 years of consolidation are shown in Figure 4.15. The differences in the deviatoric contour line patterns in Figure 4.15 is more pronouced than was observed for the undrained construction stage. Each model predicts peak deviatoric strains close to the surface below the embankment and a second peak at a depth of -6 m. Again the predictions by the MMC extent much further vertically than for the

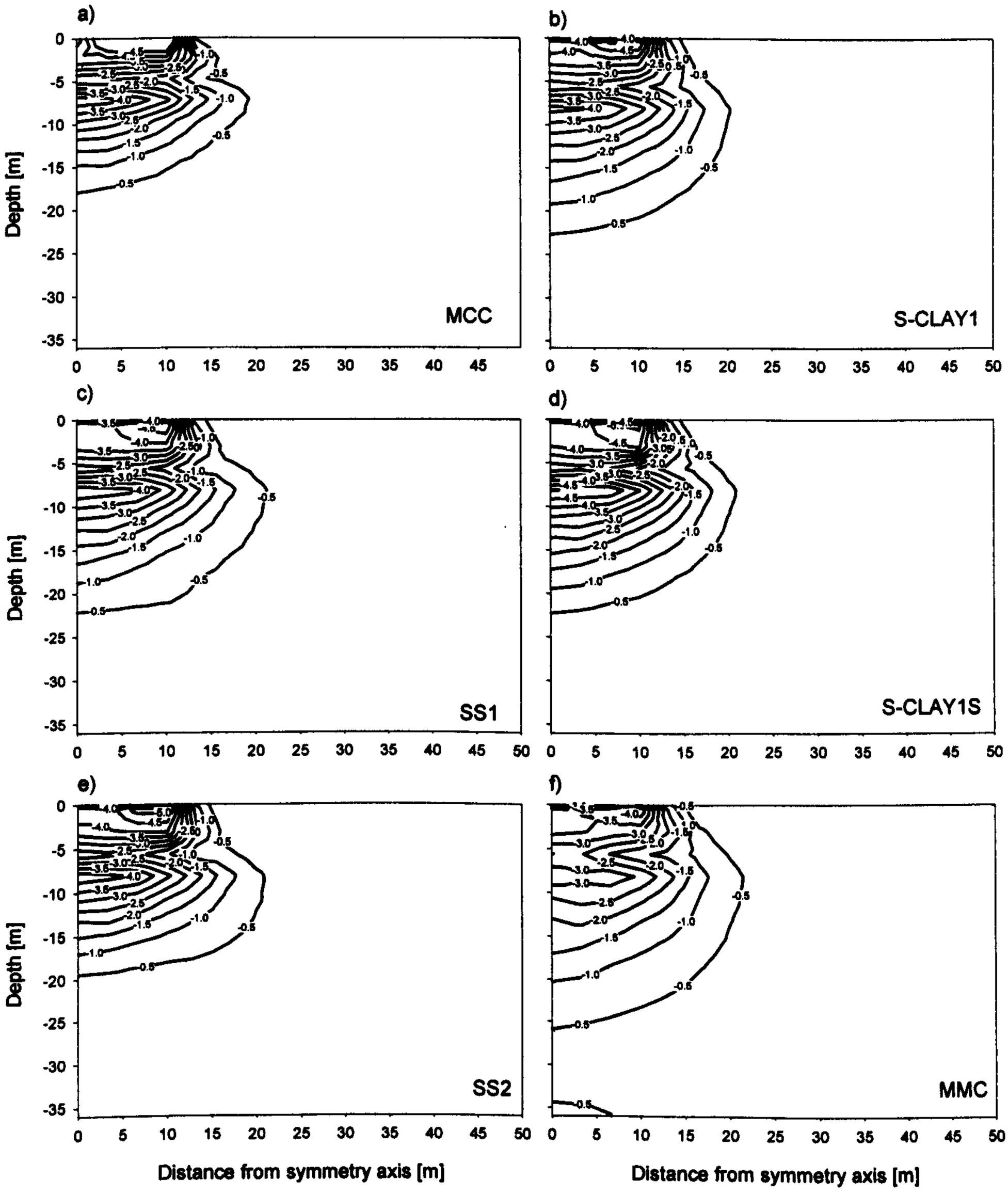

Figure 4.13: Volumetric strain contours after 100 years of consolidation

other models. By comparing only the advanced models, it can be seen that both S-CLAY models, show similar deviatoric strain behaviour, which is different to that predicted by the MMC. The totally different formulation of the models can explain the difference.

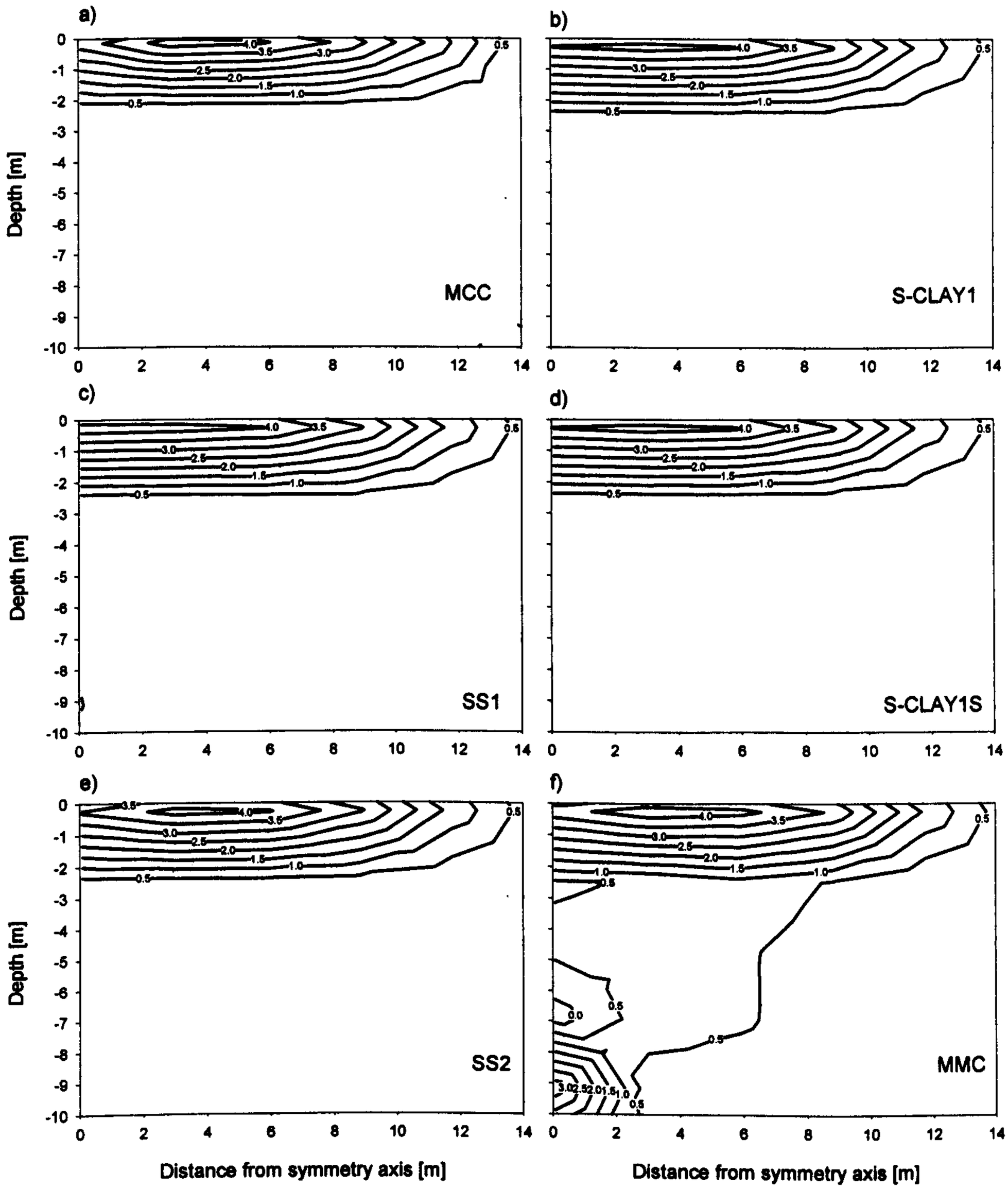

Figure 4.14: Deviatoric strain contours immediately after construction of the embankment (scaled:

4.4.4 Excess pore pressures

The predicted excess pore pressure distributions at the end of construction have been presented in Figure 4.16. In Figure 4.16 pressure is shown as negative due to the sign convention used in the finite element analysis. Because the construction of the embankment was modelled as undrained, non-zero excess pore pressure are predicted

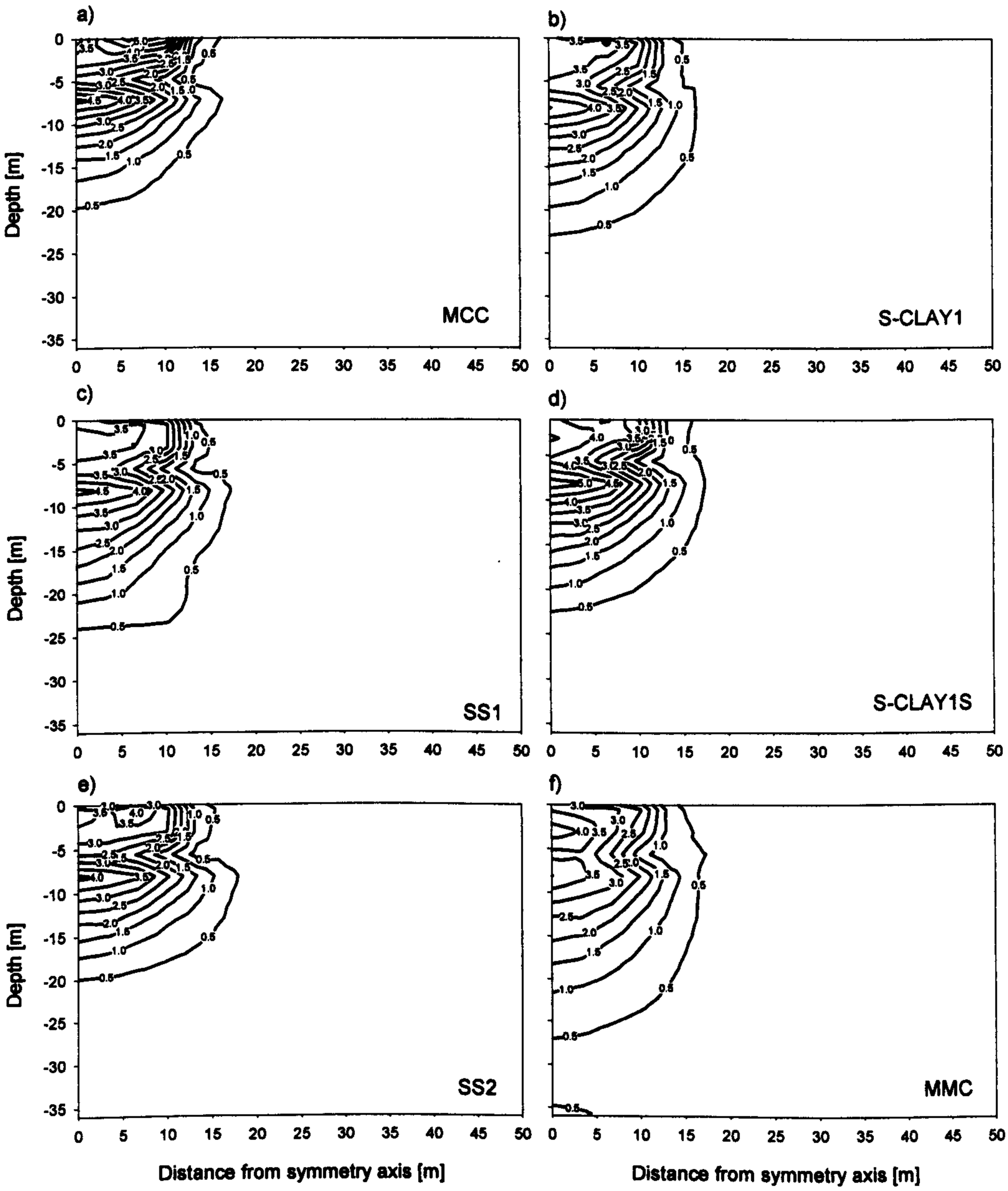

Figure 4.15: Deviatoric strain contours after 100 years of consolidation

at the bottom of the models. As soon as the fully coupled consolidation analysis starts the excess pore pressure at the bottom will be set to zero due to the boundary conditions applied (see Section 4.2). Overall it can be seen that the contour line patterns are similar for all models. The MMC model predicts the highest excess pore pressure in the order of - 36 kPa at a depth of about -5 m and a distance of 4 m from the symmetry axis. All the other models predict their maximum in the range of -28 to -32 kPa

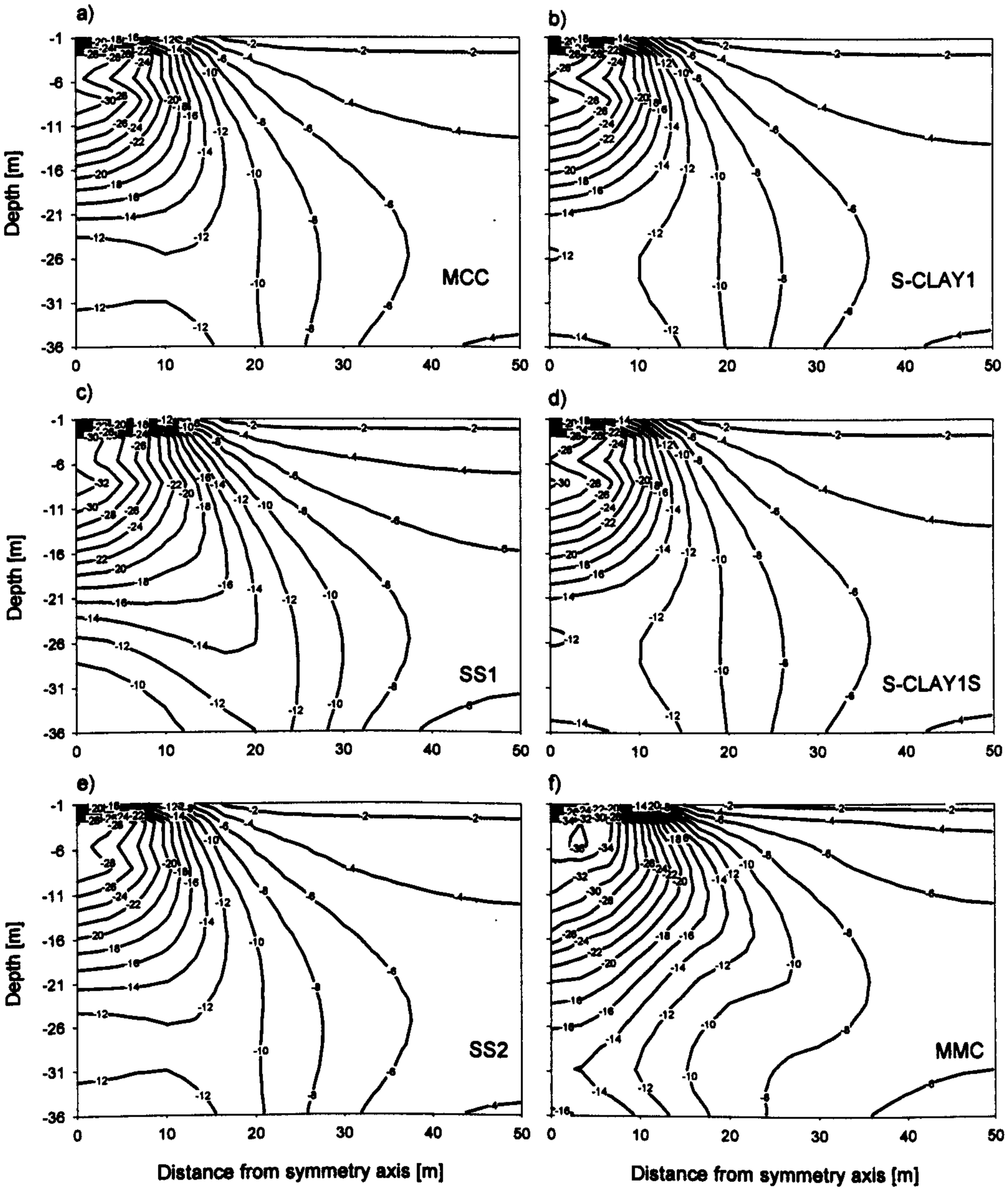

Figure 4.16: Excess pore contours immediately after construction of the embankment

at the centre line at a depth of - 8 m. The SS1 model which attempts to match the original MCC model predicts slightly higher excess pore throughout the deposit than the MCC model.

The excess pore pressures 5 years after construction are presented in Figure 4.17. Again pressure is plotted as negative. Due to the open consolidation boundaries

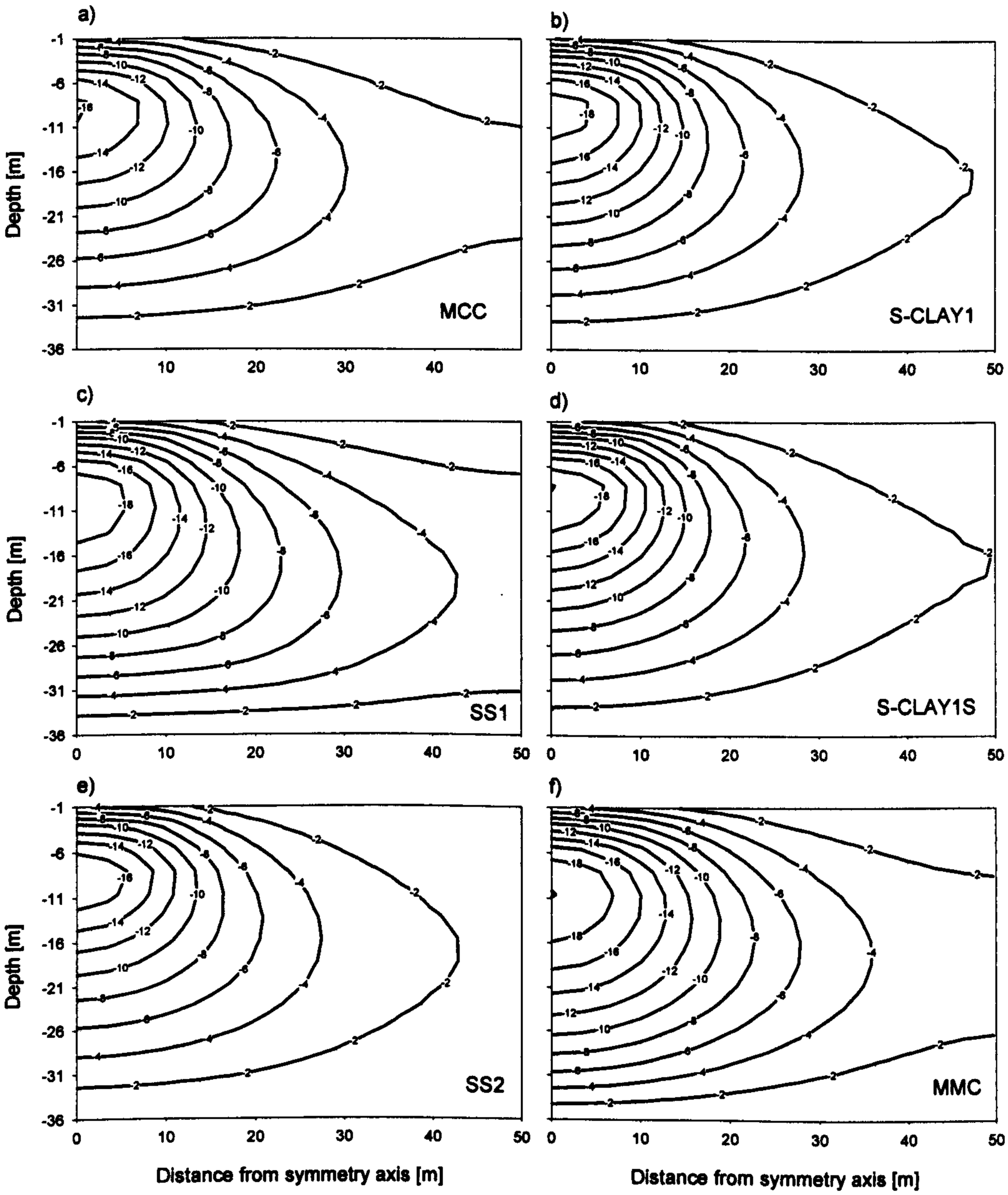

Figure 4.17: Excess pore pressure contours after 5 years of consolidation

applied at the bottom and 0.5 m below the ground surface of the models the contour lines have the shape of half circles symmetrical around the symmetry axis. Most models predict the maximum excess pressure at a depth of -8 m in the range of 16 to 18 kPa, but MMC predicts the maximum at a depth of -11 m. After 5 years the percentage of consolidation reached in terms of settlements by the models is about 42 % and about 63% in terms of excess pore pressure.

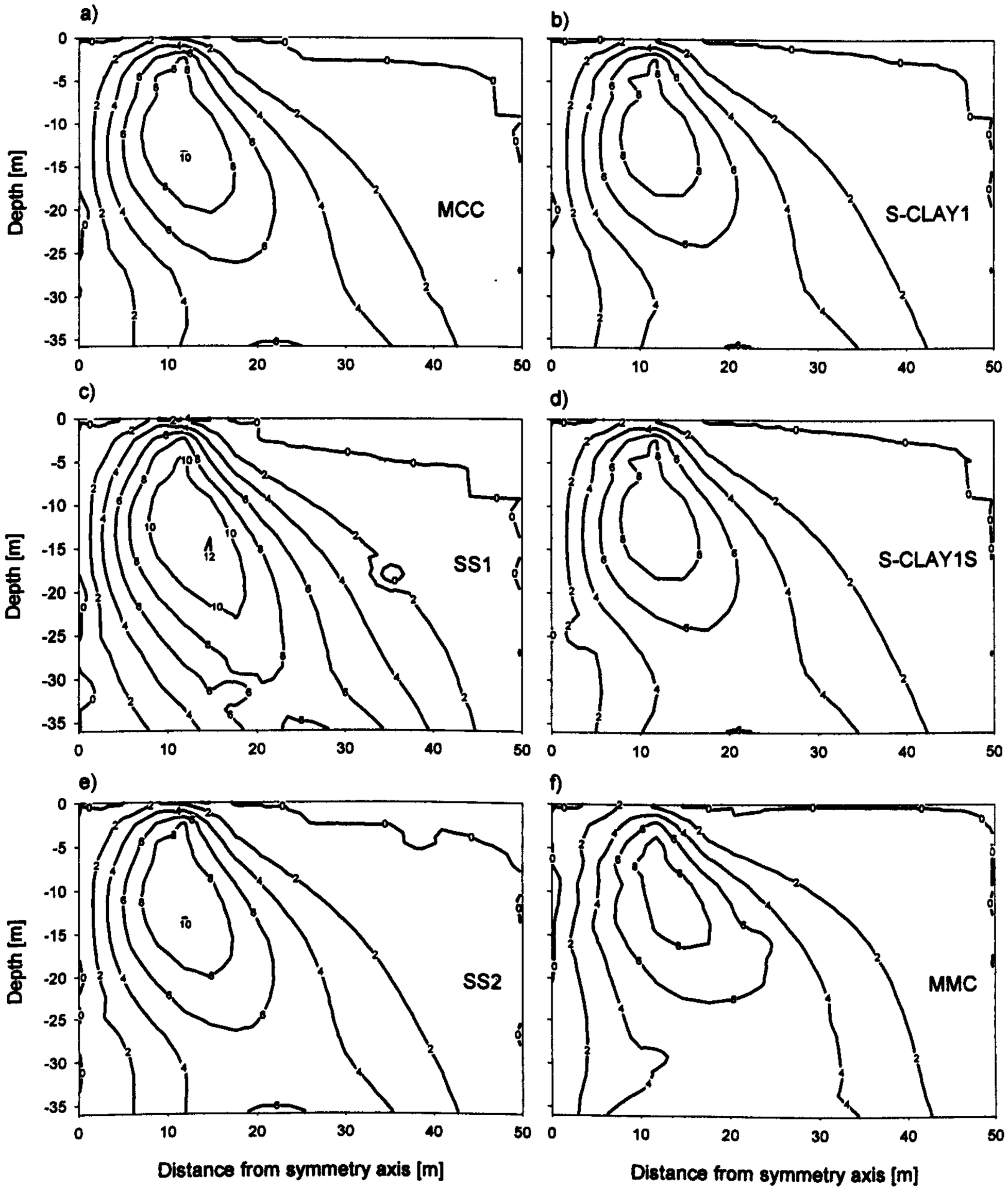

Figure 4.18: Shear stress contours immediately after construction of the embankment

4.4.5 Shear stress contours

Shear stresses immediately after construction of the embankment are presented in Figure 4.18. MCC, the S-CLAY models and the SS2 model predict an almost indentically shear stress contour pattern. SS1 predicts a slightly higher peak shear below the

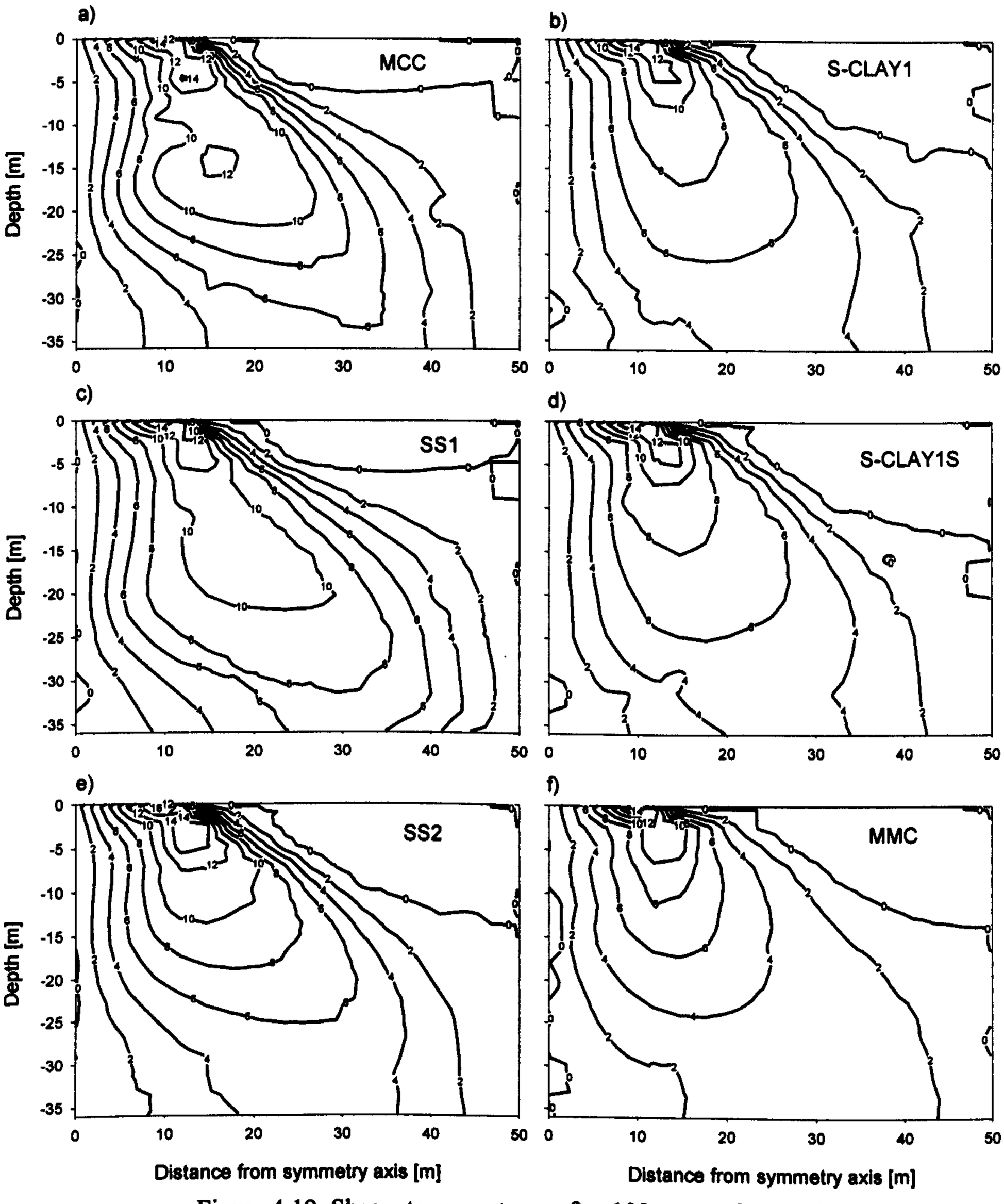

Figure 4.19: Shear stress contours after 100 years of consolidation

toe of the embankment at a depth of -15 m. The MMC model shows a somewhat similar contour pattern to the S-CLAY models.

In Figure 4.19 the shear stress distribution after 100 years of consolidation is shown. The maximum shear stress estimated by all the models is in the range of 14 to 16 kPa, below the toe of the embankment. The simulations clearly show that the isotropic

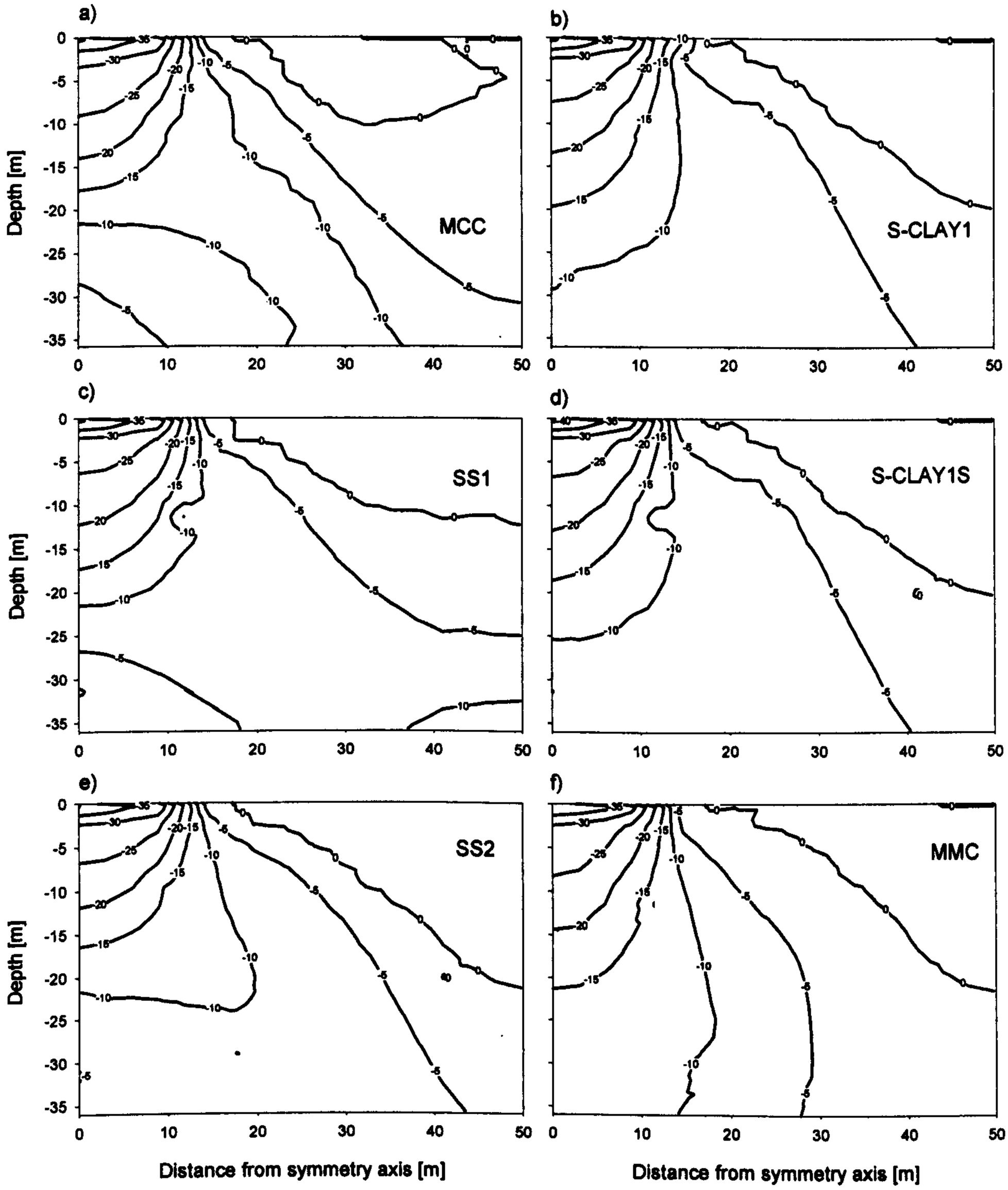

Figure 4.20: Differential vertical stress contours after 100 years of consolidation

models (MCC, SS1 and SS2) predict a overall higher shear stress distribution with depth than the advanced models (S-CLAY1, S-CLAY1S and MMC).

4.4.6 Differential vertical stresses

The predicted differential vertical stresses after 100 years of consolidation are presented in Figure 4.20. Differential vertical stresses are defined as the difference

between the initial vertical stresses and the final vertical stress at the gauss points. Figure 4.20 shows that all the models predicted a similar magnitude of stress increase in the range of 35 kPa underneath the embankment but different levels of increase of vertical stress with depth. The increase of vertical stress predicted by the MCC model and the SS1 model between a depth of -20 m and the bottom of the model is different to the other models. Both models show a diagonal band of constant stress increase from the lower part of symmetry axis to the left side of the bottom boundary with almost zero stress increase in the corner. This is not found in the result of the other models which predict a stress increase of about 10 kPa in the lower right corner of the model. Comparing the advanced models only, it can be seen that both S-CLAY models predict similar stress increases with depth. The simulation with the MMC model shows a higher level of stress increase with depth than the S-CLAY models. In the MMC model even the 10 kPa contour line intercepts the bottom boundary, compared to the 5 kPa contour line in the S-CLAY models.

4.4.7 Selected stress path

Figure 4.21 and Figure 4.22 show selected stress paths in the POKO clay deposit at four different locations below the embankment. The figures displayed in each column correspond to each other. The diagram at the top of each column presents stress paths from all models, the diagram in the centre of each column presents the isotropic models only and the diagram at the bottom of each column compares the advanced models to the reference model (MCC model).

In Figure 4.21 a-c the stress paths at the depth of -3.69 m and at a distance of 0.15 m from the symmetry axis of the embankment are presented. Inspection of Figure 4.21 a-c shows that each model predicts an individual stress path but that some paths follow a similar pattern. Comparing the isotropic models only it becomes clear that the SS2 estimates a somewhat more realistic stress path than the MCC and the SS1. After the end of the undrained construction (vertical part of the stress path) during consolidation, the SS2 models predict a gradient close to the K_0-stress ratio of 0.75. The

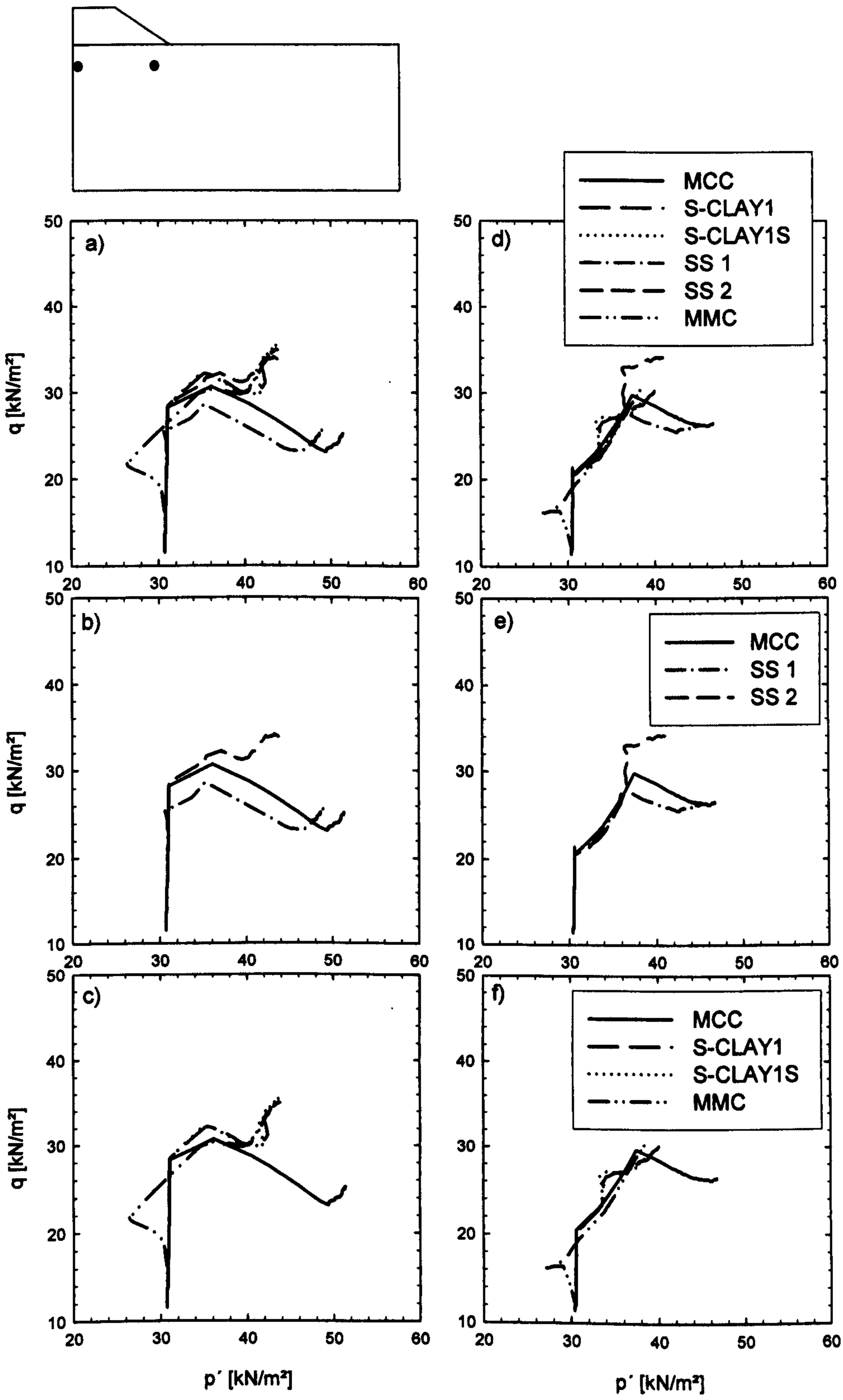

Figure 4.21: Stress path: a-c) x=0.18 m y=-3.67m and d-f) x=11.99 m y=-3.61 m

stress ratio of 0.75 is calculated for the 1D-consolidation. Stress points close to the symmetry axis will almost experience 1D-consolidation. In contrast the MCC and SS1 initially follow a K_0-path but than diverge during a large part of the consolidation phase. Just towards the end of the consolidation both models change direction again to a gradient similar to the K_0-path predicted by the MCC model. The MCC model is well known for its poor K_0 predictions and by attempting to match the MCC with the SS1, the SS1 also gives a similar K_0 prediction. Evaluation of the advanced models in the diagram at the bottom (Figure 4.21c) shows an interesting behaviour of the MMC model. During the undrained loading the stress state at one or more of the integration planes exceeds the elastic domain and yielding occurs. The yielding forces the stress path to follow the cap yield surface towards the critical state line. Once the undrained loading is finished and consolidation starts, the cap yield surface expands in size and the stress path follows a K_0-path. Both S-CLAY models predict similar stress paths.

In Figure 4.21 d-f the stress paths at depth of -3.61 m and a distance of 11.99 m from the symmetry axis of the embankment are presented. This location is only two meters from the toe of the embankment and in an area where shearing can be expected to dominate the stress strain behaviour. Inspection of the stress paths shows that the vertical part of the stress paths is short compared to the stress path discussed earlier. The increase in deviatoric stress due to the embankment loading is less at this location than at a point at the same depth along the centre line. All models predict a similar stress ratio after the undrained loading and just at the end of consolidation some stress paths deviate from the stress path direction. The models which deviate are the isotropic models. Evaluation of the MMC path shows again that yielding occurs during undrained loading on one or more of the integration planes but at a lower stress level than at the centre line.

The predicted stress paths at a point at a depth of -7.18 m and a distance of 0.15 m from the symmetry axis are shown in Figure 4.22 a-c. Evaluation of the paths demonstrates that each model predicts a unique stress path during undrained loading and that the difference is even more pronounced during the consolidation stage. Inspection of

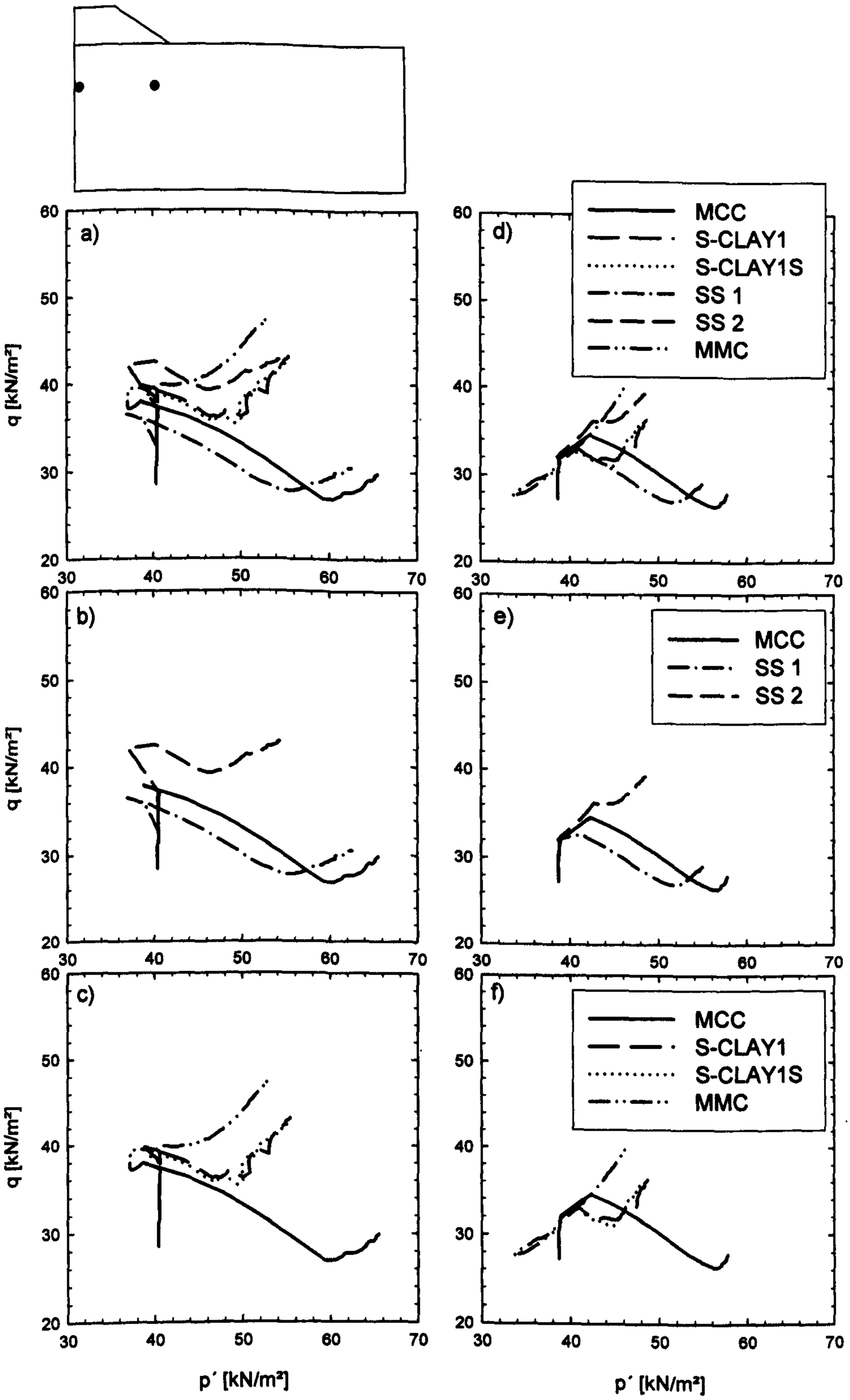

Figure 4.22: Stress path: a-c) x=0.15 m y=-7.18m and d-f) x=11.80 m y=-7.37 m

the paths estimated by the isotropic models only shows that the SS1 model, which attempts to match the original MCC, predicts yielding much earlier. Interestingly, the SS2 model predicts yielding at almost the same stress level as the MCC model but the predicted deviatoric stress level of the stress path at the end of the undrained loading stage suggests that SS2 might be close to failure. However, the SS2 stress path shows overall a similar pattern to the stress path estimated by the advanced models and predicts the same stress ratio at the end of consolidation as both of the S-CLAY models. Examination of the MMC path also highlights interesting behaviour. The model predicts yielding almost at the same stress ratio as both the S-CLAY models but shows some unloading in the form of a loop before it predicts a K_0 stress ratio during the consolidation phase. The MMC estimates a stress ratio of about 0.87 compared to the theoretical 0.75 at the end of the consolidation phase.

In Figure 4.22 d-f the stress paths at a depth of -7.37 m and a distance of 11.8 m are shown. Figure 4.22d presents clearly the difference in the stress ratio predictions by the different models. Both the S-CLAY models converge towards the same stress ratio at the end of consolidation, close to 0.75. The SS2 and the MMC, both predict a higher stress ratio of 0.8 and 0.87, respectively. In contrast the MCC and the SS1, (which attempts to match the MCC), estimate 0.48 and 0.52 respectively. All models with exception of the MMC yield at approximately the same stress level during the undrained loading phase of the soil. MCC yields again at a lower stress level and even shows a reduction of the stress ratio at the beginning of the consolidation phase. It is not clear what causes the unloading but most likely it is related to the deviatoric part of the model (Karstunen et al. 2006). The stress ratio predictions of the MMC model can be varied by changing the value of the input parameter α (see Section 2.4.2), which determines the shape of the yield surface on the sampling planes.

4.4.8 The peak undrained shear strength

To investigate the increase in undrained shear strength predicted by the different constitutive models, the undrained peak shear strength in triaxial compression, TXC

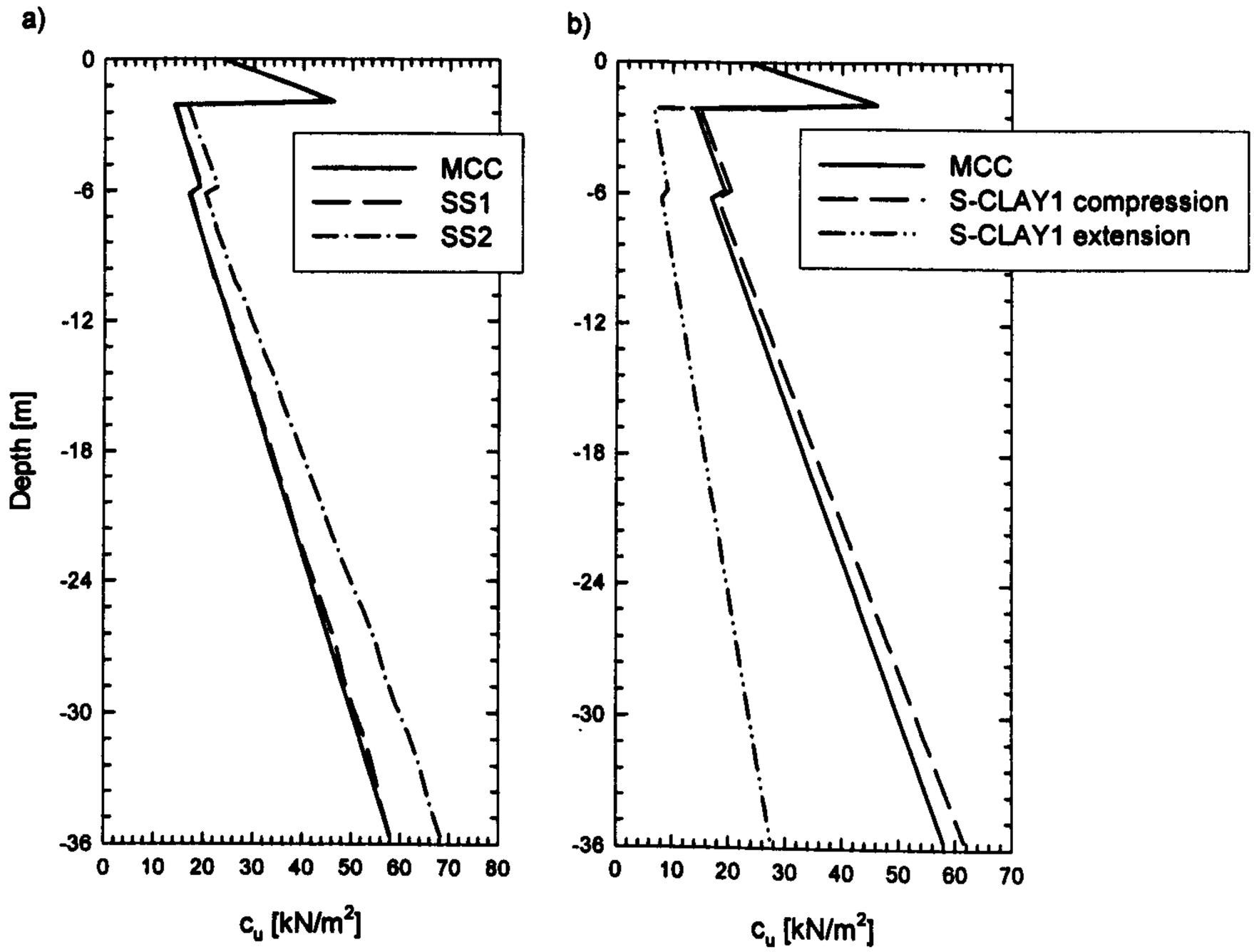

Figure 4.23: Initial peak undrained shear strength profile at the centre line of the embankment: a) isotropic and b) anisotropic models

(MCC, SS models and S-CLAY1) has been calculated for the greenfield conditions and after 100 years of consolidation. The failure strength triaxial extension, TXE (S-CLAY1) is shown just for the initial stress state. The definition of the undrained strength in the context of this work was introduced in Chapter 2 for each individual constitutive model. For the MMC model a peak undrained shear strength cannot be calculated, as a global equivalent of a peak undrained shear strength does not exist in the multilaminate framework. In the following only the MCC, S-CLAY1, SS1 and SS2 are included in the study of the peak undrained shear strength profile. The initial profile predicted by the S-CLAY1 and S-CLAY1S is the same due to the same size of the yield surface.

In Figure 4.23 the predicted initial undrained shear strength profile in TXC is presented. It can be seen that all profiles have discontinuities at a depth of -2 m and -6 m. This corresponds to the change of the POP and K_0 values (see Figure 4.1 for details) from one layer to the next layer. The profile in the dry crust is the same for all models as the HS model was used to simulate the dry crust. The MCC and the SS1, (which

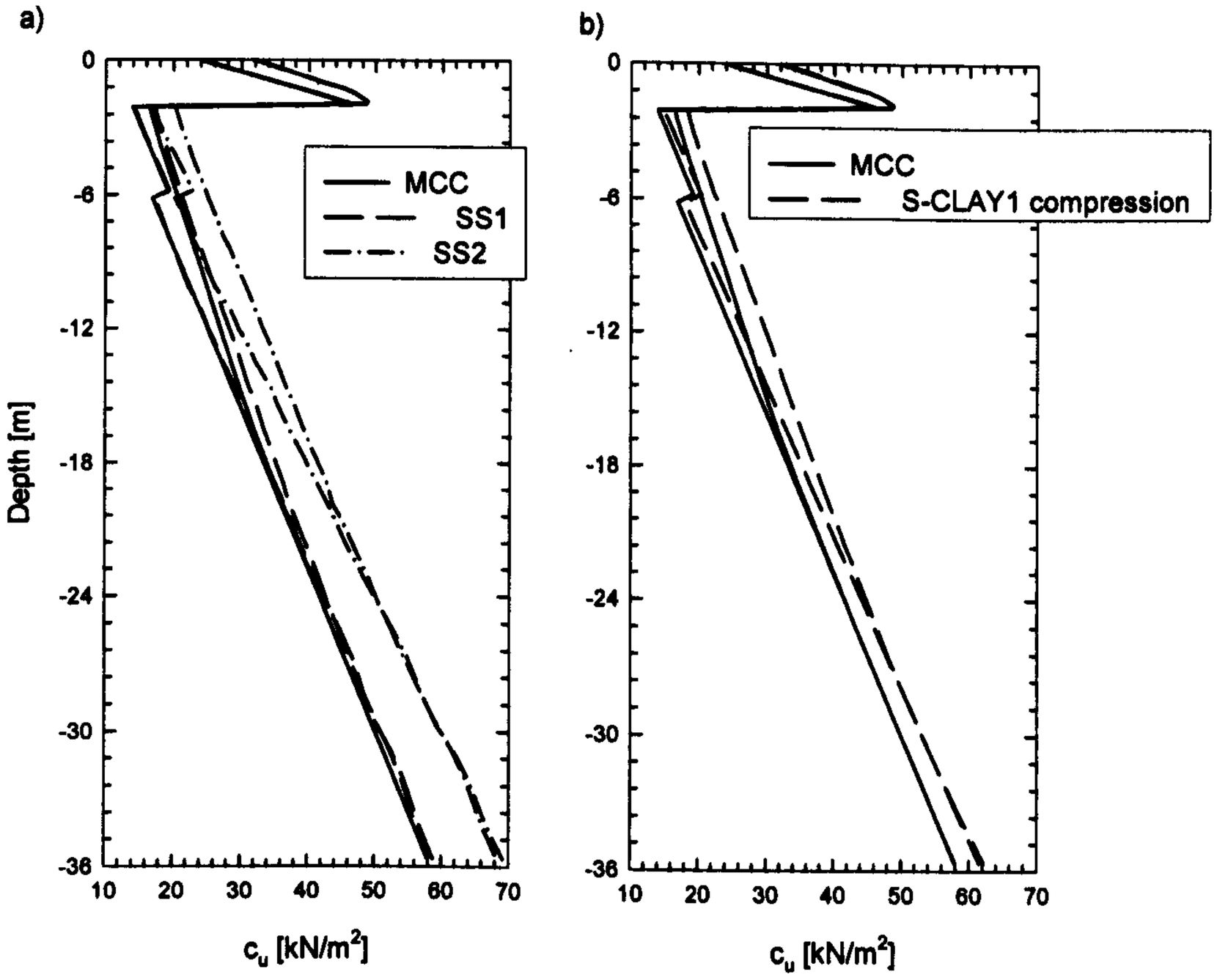

Figure 4.24: Initial and final undrained peak shear strength profile at the centre line of the embankment: isotropic and b) anisotropic models

attempts to match MCC), predict similar profiles with depth. The SS2 predicts substantially higher strength with depth than the MCC and the SS1 because of the different shape of the yield surface (see Figure 4.3). In contrast the S-CLAY1 model predicts an initial strength with depth which lies between the MCC and the SS2 models. All the isotropic models predict the same strength in compression and extension. Only the S-CLAY1 model predicts a different strength in compression and extension. The predicted failure strength in extension is lower than the strength in compression. The predicted strength profiles are directly related to the POP profile used and the shape of the yield functions of the models in the p'-q plane.

In Figure 4.24 the initial undrained shear strength profile of each model is compared to the predicted strength profile after 100 years of consolidation. The increase of undrained shear strength in the dry crust is about 8 kPa at the surface and 2 kPa at the bottom of the dry crust at a depth of -2 m. The SS2 predicts an average increase in shear strength of about 2 kPa to depth of about -24.5 m and a maximum increase of about 6

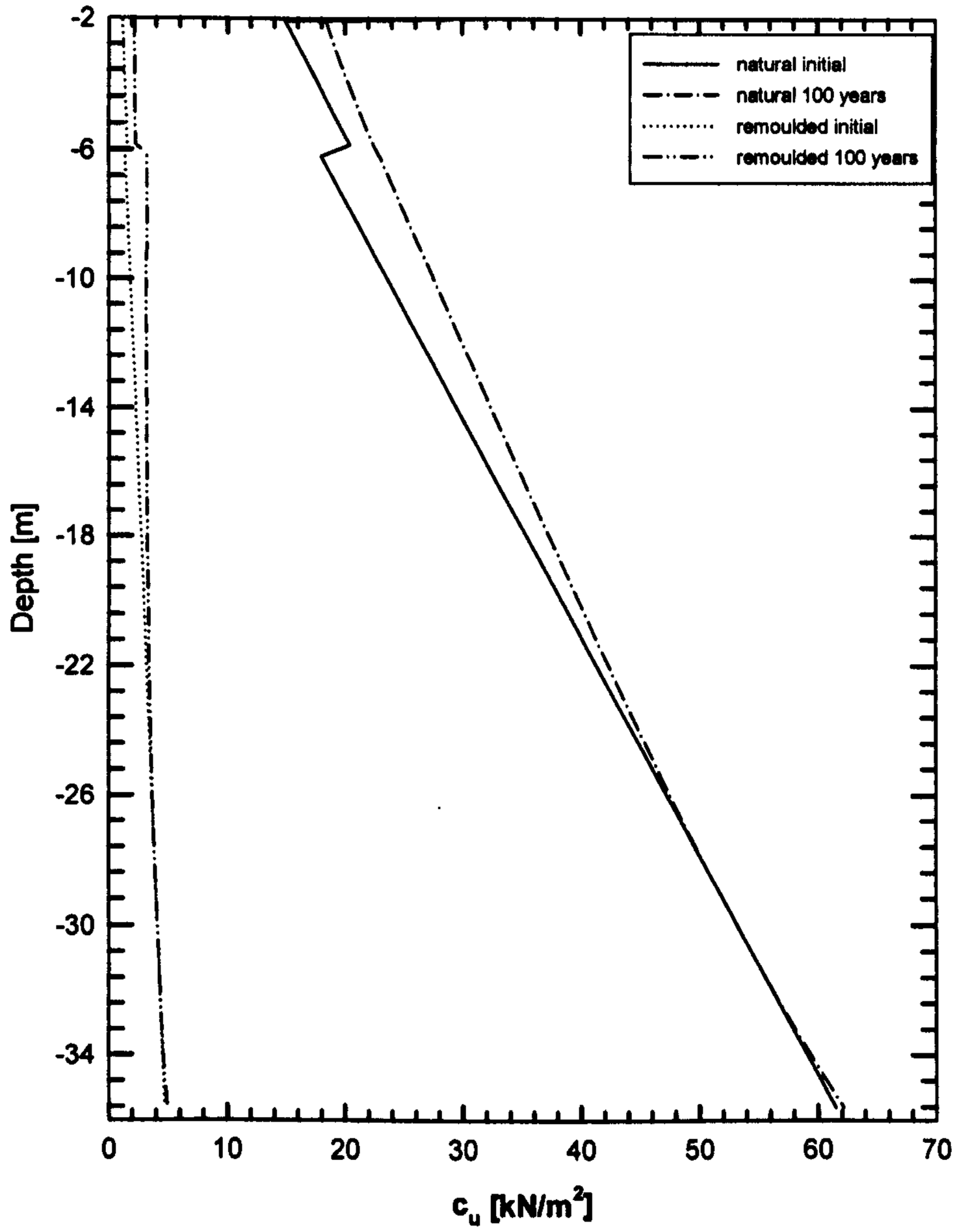

Figure 4.25: Natural and remoulded undrained peak undrained strength profile at the centre line of the embankment predicted by the S-CLAY1S model

kPa at a depth of -6.5 m. The MCC model estimates an increase of undrained strength of similar magnitude but only to a depth of -19.5 m. The SS1, (which attempts to match the MCC), predicts a similar increase in strength with depth as the SS2. Comparing the S-CLAY1 model to the MCC shows that the advanced model gives about the same magnitude of increase in strength but to a depth of -26.0 m instead of -19.5 m. The predicted ratio in the increase in undrained strength in compression Δc_u to vertical stress $\Delta\sigma_v$ is in the order of 0.25 at a depth of -6.0 m.

4.4.9 Remoulded shear strength

The predicted natural and remoulded undrained peak shear strength at the centre line of the embankment is presented in Figure 4.24. Both strength profiles predicted by the S-CLAY1S model are shown for greenfield conditions and after 100 years of consolidation. The strength profile is just shown from a depth of -2 m to the bottom of the model at a depth of -36 m. For the definition of the remoulded strength the reader is referred to Section 2.5.5. The initial remoulded strength increases with depth. During consolidation the intrinsic yield surface expands with plastic straining and the remoulded shear strength increases but the observed increase is not constant with depth.

4.4.10 Conclusion on the results predicted by the different models

All of the models assumed an identical initial state in terms of in-situ stress and vertical preconsolidation stress. The models gave a range of predictions in terms of settlements, horizontal displacements and stress increase. The results of the numerical analyses showed that for this problem accounting for anisotropy and destructuration increases the predicted vertical displacements. Karstunen et al. (2006) and Wiltafsky (2003) showed similar findings. Both anisotropic models showed that accounting for anisotropy increases the final vertical displacements. In contrast the horizontal displacements are more influenced by the pre-yield behaviour and the shape of the yield surface than anisotropy. The MMC model predicts the biggest horizontal displacement below the toe of the embankment followed by the SS1 model. Both S-CLAY models show similar predictions of horizontal displacements suggesting that the effect of bonding and destructuration is less significant than the effect of anisotropy. Similar findings have been reported by Karstunen et al. (2006) and Wiltafsky et al. (2003). All simulations showed that the area of maximum horizontal displacement is not underneath the toe of the embankment as suggest by Leroueil et al. (1990). The area is located below the slope of the embankment and its location moves with consolidation time, i.e. moving deeper and marginally closer to the centre line of the embankment.

All models predict similar volumetric contours after construction and consolidation with the exception of the MMC model. Similar behaviour was observed for the deviatoric strain predictions. The deviatoric hardening part of the MMC most likely contributes to the different straining behaviour predicted by the model.

The difference in the predicted excess pore pressure, shear stresses and differential vertical stresses by the different models is less pronouced than it was for the settlements. Again the MMC showed somewhat different results than the other models.

Inspection of the stress paths showed that both S-CLAY models and the SS2 predict similar values of K_0 close to the normally consolidated K_0, while MCC and SS1 predict unrealistic high values. The MMC gives overall the lowest values. In the MMC and the SS models the final K_0 value is dependent on the shape of yield surface and this can be influenced by the input of the user. It demonstrates the importance of using realistic input values to predict correct K_0 values. The use of the Soft Soil model and the Multilaminate model is therefore not as straightforward as some publications might suggest.

The peak undrained shear strength profile with depth of the MCC model, SS1 model, SS2 model and S-CLAY1 model has been evaluated before construction and after 100 years of consolidation. The predicted initial profiles differ somewhat from each other due to the different shapes of the yield surfaces. Anyone using advanced models should really check what the initial predicted strength is. Because the predicted values for undrained strength depend on the initial stress state, undrained shear strength can not be considered as a soil constant. All models predict a similar increase of peak undrained shear strength with time.

4.4.11 Other aspects influencing the behaviour of an embankment

In this section several aspects previously not mentioned influencing the settlement behaviour are studied and discussed. First, the depth of the deposit and the effect of anisotropy and bonding is explored. This is followed by a study on the embankment geometry and the effect of different constitutive models used to represent the stress-strain behaviour of the embankment fill. The results presented and discussed are based on a total of 83 finite element simulations.

4.4.11.1 Influence of the depth of the deposit

The geometry of the embankment and the soil layers are the same as shown in Figure 4.1. The stress-strain behaviour of the assumed underlain soft soil deposit is modelled with the MCC and the two S-CLAY models.

The predicted consolidation time versus the depth of the deposit is presented in Figure 4.26a. It is important to recall the drainage condition applied for the presented case before discussing the findings. Drainage at the surface and at the bottom of the model was applied. Inspection of the Figure 4.26a shows that with increasing depth of the deposit the consolidation time increases, as expected. From an 8 m to an 18 m deposit the increase in consolidation time appears to be non linear. In contrast, the increase from 18 m to 36 m could be represented with a linear relationship. The increase in consolidation time from the 8 m to a 12 m deposit predicted by the MCC is about 87 %, the S-CLAY1 predicts about 100 % and the S-CLAY1S 80 %. From 12 m to 18 m the predicted increase by the MCC is about 13 %, S-CLAY1 about 25 % and the S-CLAY1S predicts 8.5 %. The increase from 18 m to 36 m estimated by the MCC is 16% and both S-CLAY models predict an increase of 15%. Anisotropy contributes to a small increase in predicted consolidation time for the shallow deposits but this increase becomes negligible for deeper deposits. For the case considered it appears that including bonding and destructuration reduces the consolidation time for shallow deposits.

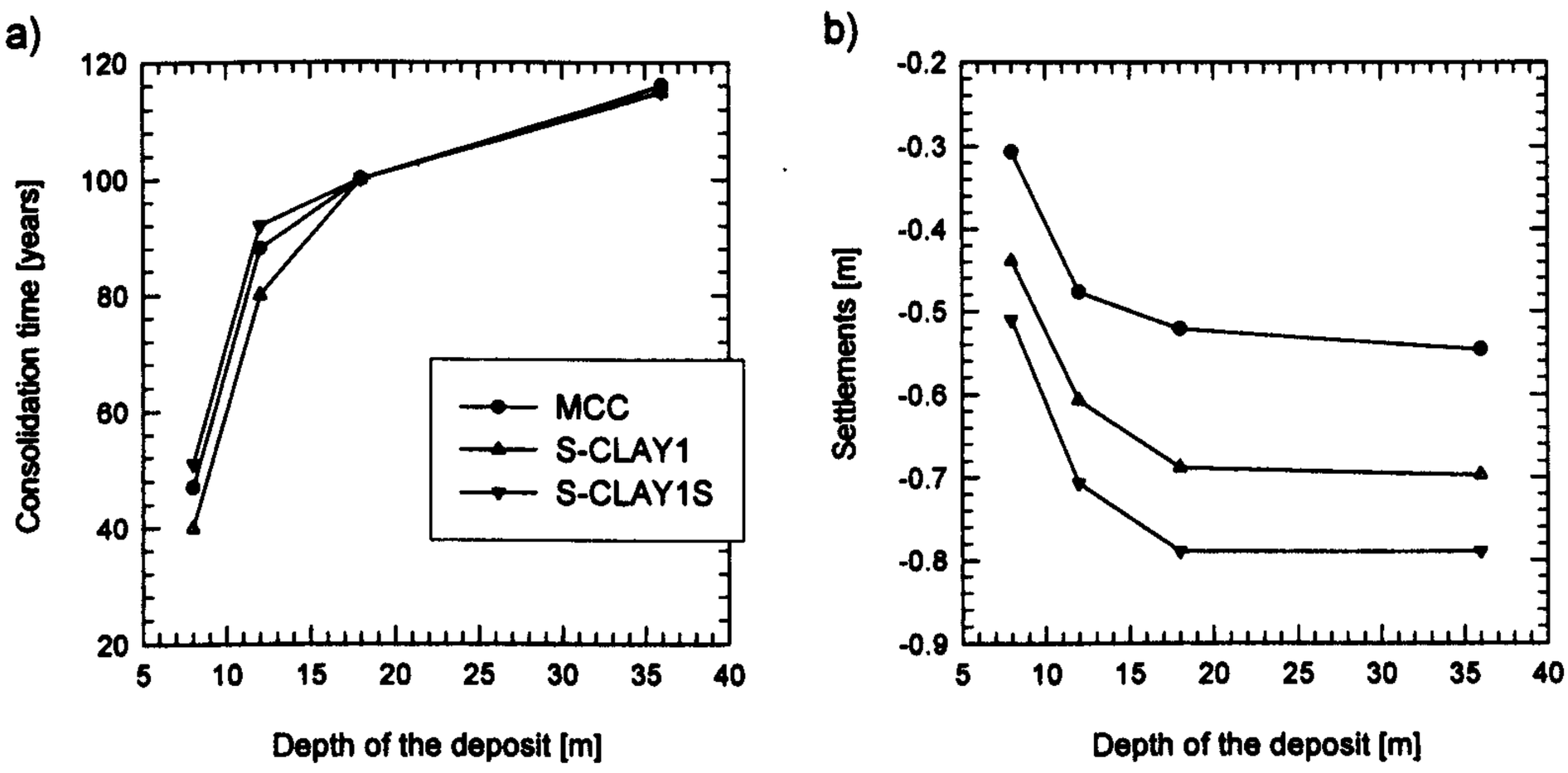

Figure 4.26: Influence of the depth of the deposit a) on the consolidation time and b) on the predicted final settlement

The predicted vertical settlements after the end of consolidation versus the depth of the deposit is illustrated in Figure 4.26b. Evaluation of the graph shows that the predicted curves are non-linear. All models predict the largest increase in displacement from 8 m to 12 m. The MCC predicts an increase of settlements of 55 % and both S-CLAY models somewhat less, around 38 %. Thereafter, the increase in settlement becomes smaller and smaller and there is almost no increase predicted between 18 m and 36 m. Comparing the predictions between the models shows that for an 8 m deposit the S-CLAY1 gives 43 % higher settlements than the MCC and the S-CLAY1S gives a 66 % increase in settlement. The increase due to anisotropy and destructuration is less apparent for the deeper deposits. For a 36 m deposit the S-CLAY1 shows a 30 % increase and the S-CLAY1S a 45 % increase compared to the MCC predictions. The results show that the influence of the depth is limited as expected.

The influence of the depth of the deposit on the predicted u_x/u_y - ratio is presented in Figure 4.27. Figure 4.27a compares the estimated ratio after the construction of the embankment and after 100 years of consolidation. The u_x used to calculated the ratio is the maximum u_x underneath the toe of the embankment. The u_x/u_y - ratio after con-

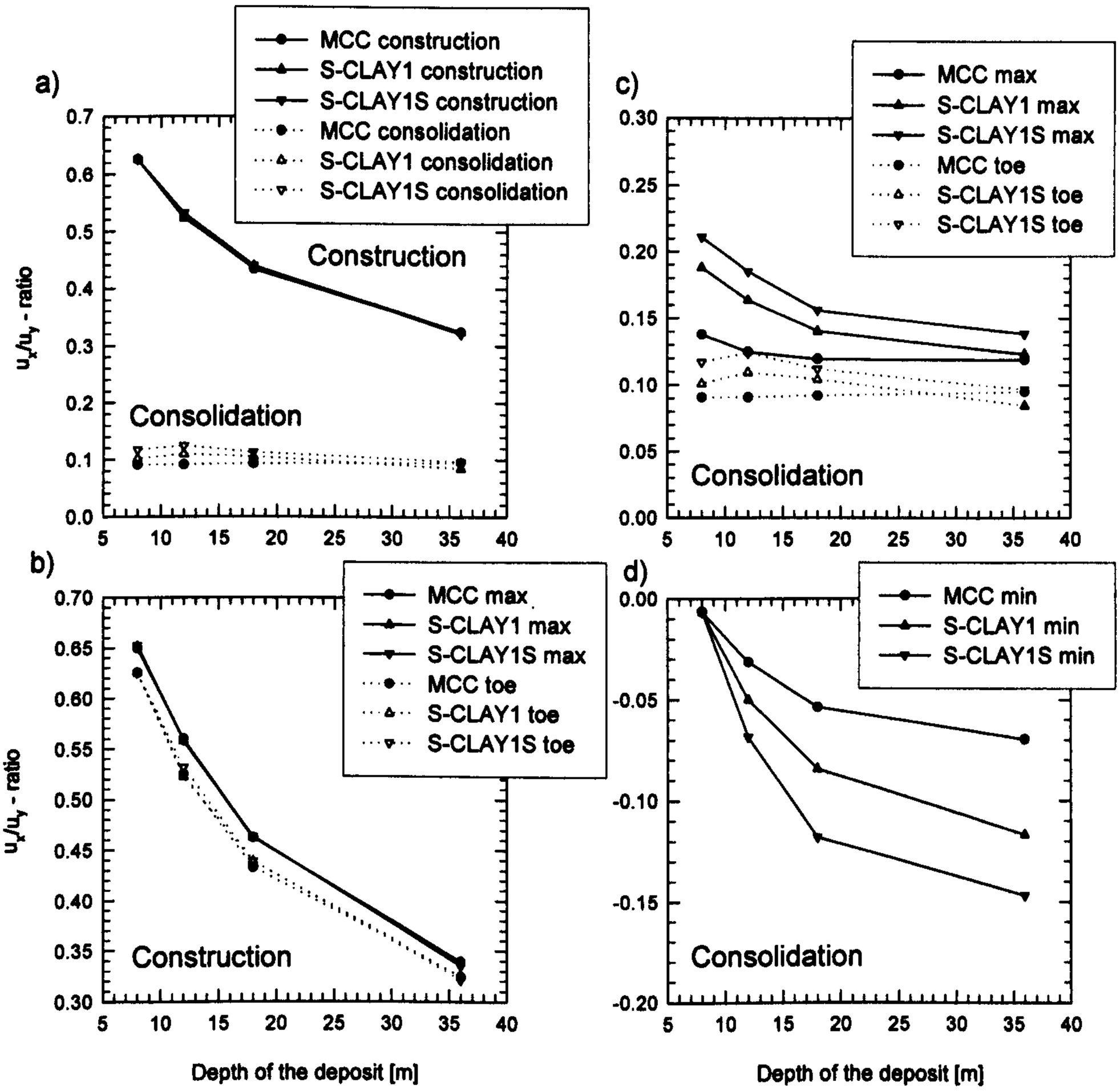

Figure 4.27: Influence of the depth of the deposit on the u_x/u_y - ratio a) after construction and consolidation (maximum u_x at the toe) b) after construction (maximum u_x at the toe compared to absolute maximum u_x below embankment) c) after consolidation (maximum u_x at the toe compared to absolute maximum u_x below embankment) d) after consolidation (minimum u_x at the toe)

struction is clearly dependent on the depth of the deposit. With increasing depth the ratio decreases from a maximum of 63 % for a depth of 8m to a minimum of 0.33 % for a 36 m deep deposit. Inspection of the curve shows that the decrease of the u_x/u_y - ratio certainly decreases with increasing depth. All three models (MCC, both S-CLAY models) used in the simulations predict similar ratios for all deposits simulated. The ratio drops significantly to about 10% at the end of 100 years of consolidation.

Inspection of the horizontal displacement contour plots (Figure 4.11) in Section 4.4.2 showed that the maximum horizontal displacements are not predicted underneath the toe of the embankment, as is very often incorrectly assumed. The location of the maximum is dependent on the degree of the consolidation and is located below the slope of the embankment. In Figure 4.27b and c the predicted absolute maximum value of u_x is used to calculate the $u_{x\,max}/u_y$ - ratio and compared to the u_x/u_y - ratio calculated with the maximum u_x at the toe. Figure 4.27b shows the prediction after the construction of the embankment. The estimated $u_{x\,max}/u_y$ - ratio is slightly higher than the u_x/u_y - ratio for all deposits and constitutive models. The $u_{x\,max}/u_y$ - ratio after 100 years of consolidation of the deposit is shown in Figure 4.27c. The simulations show that the $u_{x\,max}/u_y$ - ratio decreases with increasing depth of the deposit. This observed behaviour is somewhat different to the u_x/u_y - ratio which is not much influenced by the depth of the deposit.

In Figure 4.27d the minimum u_x below the toe of the embankment is used to calculate the $u_{x\,min}/u_y$ - ratio. The predicted $u_{x\,min}/u_y$ - ratio is negative due to the fact that the area below the toe of the embankment is pulled towards the centre line of the embankment due large vertical settlements. Inspection of Figure 4.27d shows that the $u_{x\,min}/u_y$ - ratio is dependent on the depth of the deposit and the constitutive model used. For an 8 m deposit all three models predict a ratio in around -0.8 %. With the increasing depth of the deposit, the influence of anisotropy becomes more obvious. Accounting for destructuration further decreases the $u_{x\,min}/u_y$ - ratio.

4.4.11.2 Influence of the width of the crest of the embankment

The influence of the width of the crest of the embankment is shown in Figure 4.28. In the simulations the S-CLAY1S model was used to represent the stress-strain behaviour of the deposit. Three different finite element models were used for the predictions. The first model was used to model a crest of width between 2 and 20 m. The second model, from 20 to 40 and the third from 40 to 58 m. The u_x/u_y-ratio (u_x at the toe) is presented immediately after construction of the embankment and after 100

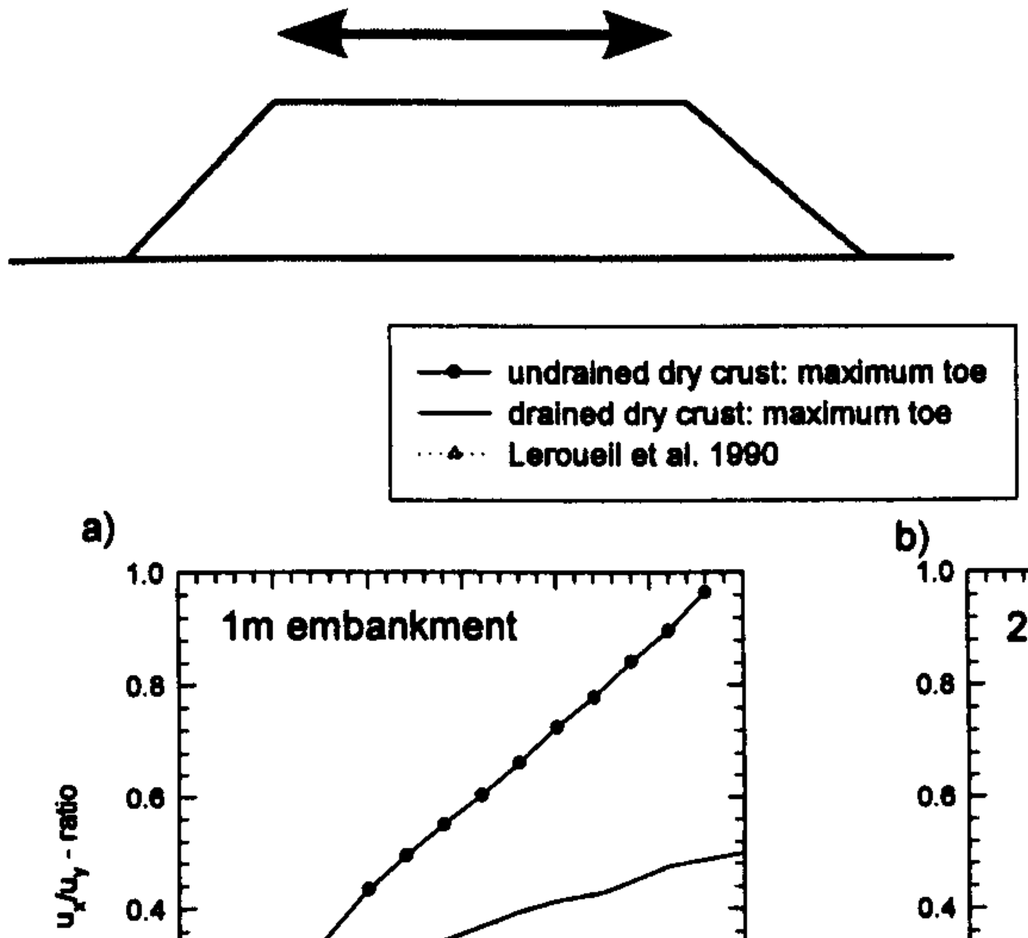

Figure 4.28: Influence of the width of the crest of the embankment on the u_x/u_y - ratio a) 1m embankment after construction b) 2m embankment after construction c) 1m embankment after 100 years consolidation d) 2m embankment after 100 years of consolidation

years of consolidation. In the study, embankments with different crest widths and a height of 1 m (Figure 4.28a and c)or 2 m (Figure 4.28b and d) were used. The crest width was varied from a minimum of 4 m to a maximum of 56 m for the 1m embankment and from 2 m to 56 m for the 2m embankment. All calculations were performed with just ten finite element models by activating the required size of the embankment. Numerically this is not ideal as the coarseness of the finite element mesh will influence the results to some extent. In the first set of simulations the dry crust was modelled as an undrained material and in the second set of simulations it was modelled as

a drained material. The material behaviour of the dry crust was varied to investigate the influence of the dry crust on the predicted u_x/u_y-ratios.

In Figure 4.28a the u_x/u_y - ratios are presented for the 1m embankments after the construction of the embankments. The u_x/u_y - ratio is presented for the simulations with the drained and the undrained dry crust. In addition the predictions are compared to a u_x/u_y - ratio suggest by Leroueil et al. 1990. The u_x/u_y - ratio for the case when the dry crust is assumed to be undrained is somewhat higher than when it is assumed to be drained and increases with increasing width of the embankment. The predicted increase is almost linear. The u_x/u_y - ratio for the drained case also increases with the embankment width but the gradient is smaller than that of the undrained. Only for the smaller width, is the u_x/u_y - ratio similar to that which was suggested by Leroueil et al. (1990).

In Figure 4.28b the predictions for the 2m embankments are shown. The predicted u_x/u_y - ratios for the undrained case are again higher than for the drained case. In general the u_x/u_y - ratios are lower than the u_x/u_y - ratios shown in Figure 4.28a. Again for the embankments with smaller widths the predictions are in agreement with the u_x/u_y - ratio by Leroueil et al. (1990). Measurement at the Murro test embankment a couple of days after construction resulted in a u_x/u_y - ratio of 18 %. At Murro the dry crust had a thickness of about 1.8 m and the average level of the water is located at a depth of 0.8 m. The width of the crest is 10 m. The measured ratio of the Murro embankment lies well within the values suggested in Figure 4.28b for a 10 m crest.

The predictions after 100 years of consolidation are shown in Figure 4.28c and d. As the influence of the material behaviour of the dry crust has been found to be neglible after 100 years of consolidation only one set of simulations is presented. In addition to the u_x/u_y - ratio at the toe, the $u_{x\,min}/u_y$ - ratio calculated based on the minimum u_x at the toe is presented. Figure 4.28c shows that the u_x/u_y - ratio and the $u_{x\,min}/u_y$ - ratio predicted for a 1m embankment decreases almost linearly with increasing width. A somewhat different behaviour for the u_x/u_y - ratio is evident in Figure 4.28d. The pre-

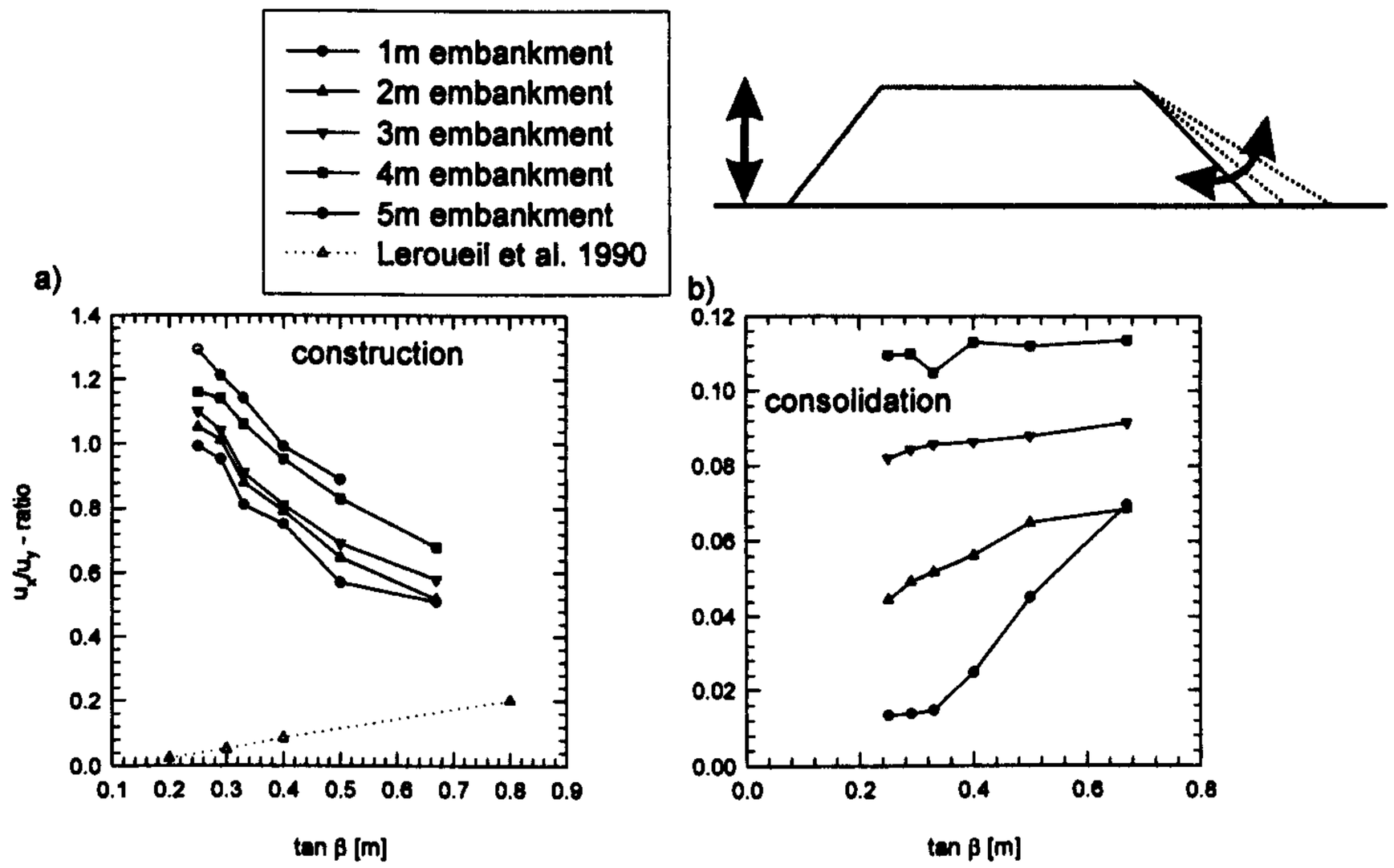

Figure 4.29: Influence of the embankment height and the gradient of the slope on the u_x/u_y - ratio a) after construction and b) after 100 years of consolidation

dicted u_x/u_y - ratio suggests that the ratio does not change with an increase of the width. In contrast the estimated $u_{x\,min}/u_y$ - ratio decreases with width.

4.4.11.3 Influence of the slope gradient and the embankment height

The results presented in this section are used to study the effect of the slope gradient and the embankment height on the u_x/u_y - ratio. The S-CLAY1S model was used to simulate the stress-strain of the soil and all simulations were performed with a single finite element model. The u_x used is the local maximum below the toe of the embankment. In this study the dry crust was simulated as an undrained material. The influence of the material behaviour (drained or undrained) of the dry crust was shown in Figure 4.28. In Figure 4.29a the results immediately after construction are presented. The slope gradients considered in the simulations are listed in Table 4.8, where β is the angle of the slope.

Table 4.8: Slope gradients used in the simulations

Slope gradient	1:1.5	1:2.0	1:2.5	1:3.0	1:3.5	1:4.0
tanβ	0.67	0.50	0.40	0.33	0.29	0.25

The predictions of the u_x/u_y - ratios after the construction of the embankments are shown in Figure 4.29a. An almost linear reduction of the u_x/u_y - ratio with an increase of slope steepness is observed. An increase of the height of the embankment results in an increase of the u_x/u_y - ratio. For comparision, the u_x/u_y - ratios suggested by Leroueil et al. 1990 are plotted. These are much lower compared to the predicted values. It has been shown before that the material behaviour of the dry crust and the width of the embankment have a strong influence on the predicted values. As a consequence the values suggested by Leroueil et al. 1990 can not be directly compared to the predictions. Measurements presented by Larsson and Mattsson (2003) from the Skå-Edeby embankment about 45 days after construction suggest a u_x/u_y - ratio of 70 %, respectively. The slope of the embankment is 1:1.5 ($\tan\beta$=0.67) and the height is 1.5 m. The depth of the dry crust is 0.5 m. The measured value lies reasonably well within the ratios predicted in Figure 4.29a.

The predictions of the u_x/u_y - ratios after 100 years of consolidation are presented in Figure 4.29b. An increase in the embankment height results in a decrease of the u_x/u_y - ratio. The influence of the slope gradient on the predicted ratio is more pronouced for low embankments. Measurements presented by Larsson and Mattsson (2003) from the Skå-Edeby embankment 25 years after construction suggest a u_x/u_y - ratio of 20 %. Final consolidation had not yet been reached, but the u_x/u_y - ratio dropped substantially and appears that it will continue to decrease.

4.4.11.4 Pratical aspects of u_x/u_y-ratio versus time

In Figure 4.30 the u_x/u_y -ratio versus the consolidation time is plotted for four different embankment heights. The results shown in Figure 4.30 were simulated with the S-CLAY1S model. The u_x/u_y -ratio continuously decreases with time towards a lower bound value which is similar for all four embankment heights considered and confirms the findings presented in Figure 4.27 and Figure 4.28. In Figure 4.30b the time is plotted as a percentage of the maximum consolidation time. Inspection of Figure 4.30b shows that after 10% of the total consolidation time, the u_x/u_y - ratio has

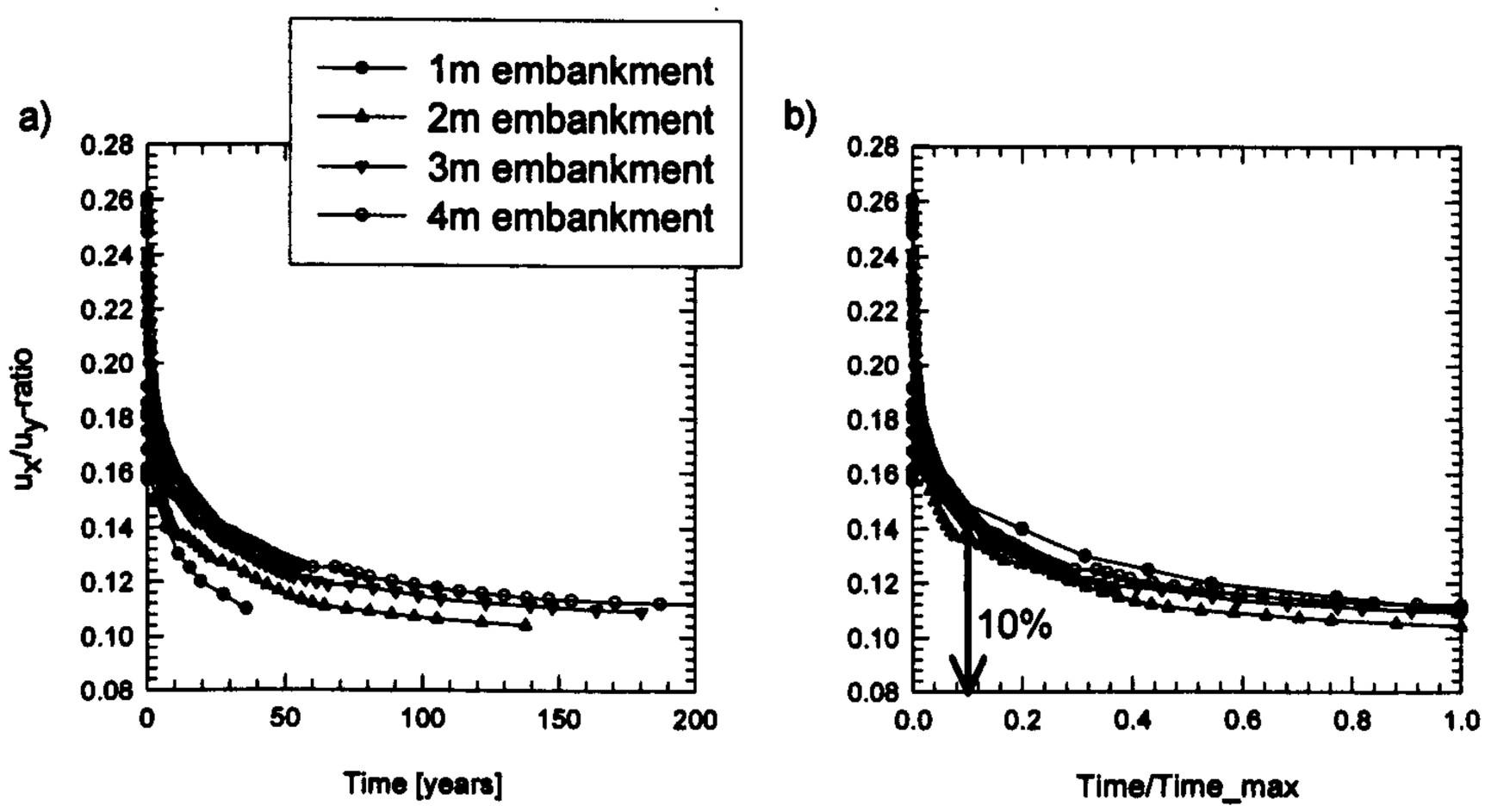

Figure 4.30: Influence of the consolidation time on the u_x/u_y - ratio a) time [years] b) time[%]

almost reached its final value. In all four cases the degree of consolidation in terms of settlement was ~40% after 10% of the consolidation time. From a practical perspective this finding is important. It would suggest that an embankment just requires the u_x/u_y - ratio to be monitored for 10% of its consolidation time. Secondly, monitoring the u_x/u_y - ratio would show clearly if the embankment settles as expected and any change in the u_x/u_y - ratio with time could be used as a trigger value for further investigation.

4.4.11.5 The influence of the constitutive model for the embankment fill

The following study investigates the influence of the constitutive model used to represent the stress-strain behaviour of the embankment fill on the settlement behaviour of the embankment. Three constitutive models were used in the simulations. A linear elastic model, the Mohr Coulomb model and the HS model (Brinkgreve 2002). The parameters for the models are summarised in Table 4.9.

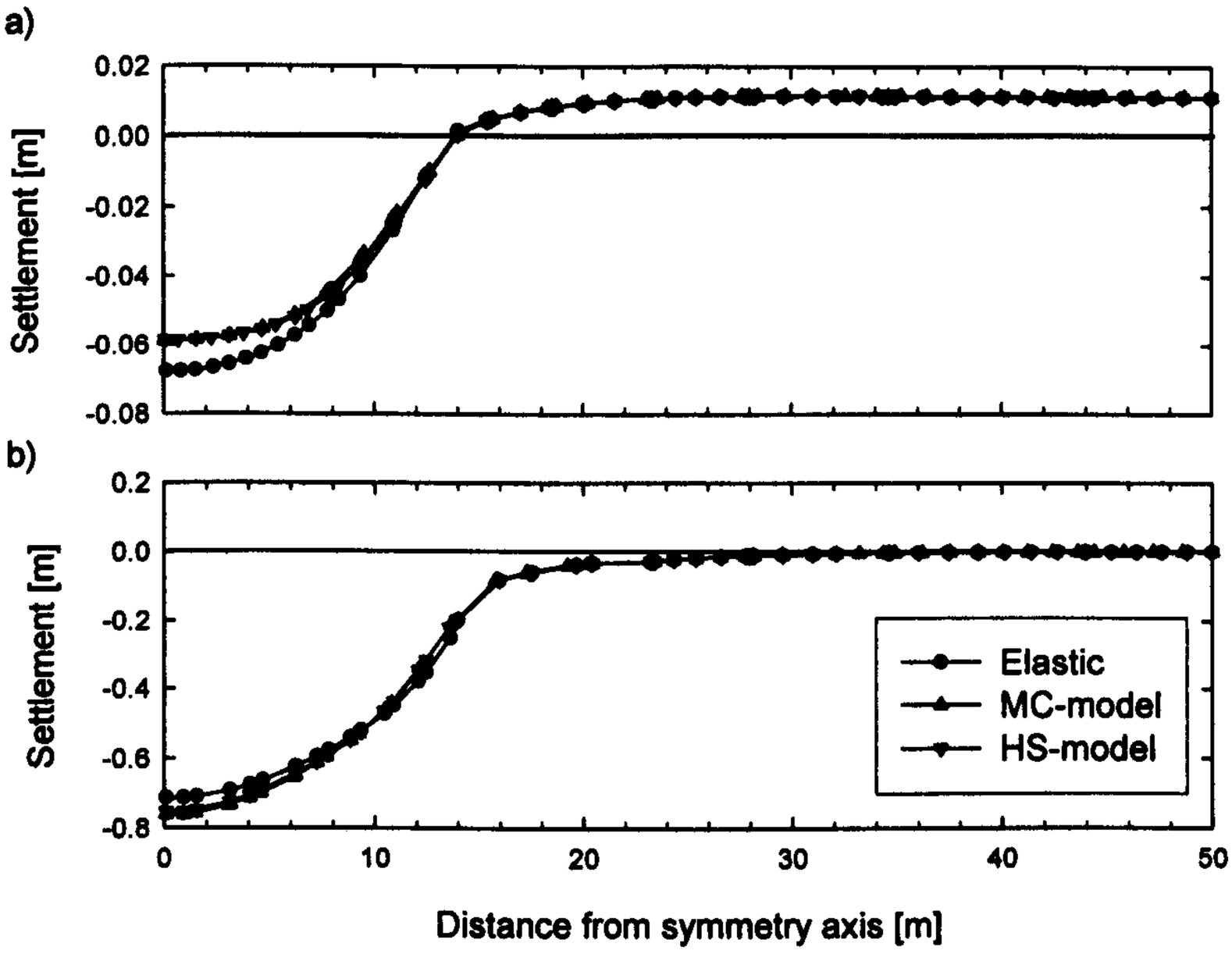

Figure 4.31: Influence of the constitutive model of the embankment fill on the surface settlements a) after construction and b) after 100 years of consolidation

Table 4.9: Input parameters of the embankment fill for the different constitutive models

Model	E_{50}^{ref} E_{oed}^{ref} [kN/m²]	E_{ur} or E_{ur}^{ref} [kN/m²]	φ'	ν'	m	γ' [kN/m³]	p_{ref} [kN/m²]
Elastic	-	40000	-	0.3	-	20	-
MC model	-	40000	38	0.3	-	20	-
HS model	40000	120000	38	0.3	0.5	20	10

The embankment used in the simulations is shown in Figure 4.1. The surface settlements after construction of the embankment predicted by the different models is shown in Figure 4.31a. The MC and HS model estimated a similar settlement trough with a maximum of -0.06 m at the centre line of the embankment. The elastic model predicts marginally bigger vertical displacements of about -0.068 m. All three models predict a similar magnitude of soil heave at a distance of 12 m to 50 m from the centre line of the embankment. The settlements after 100 years are presented in Figure 4.31b. Again the MC model and the HS model predict settlements of similar

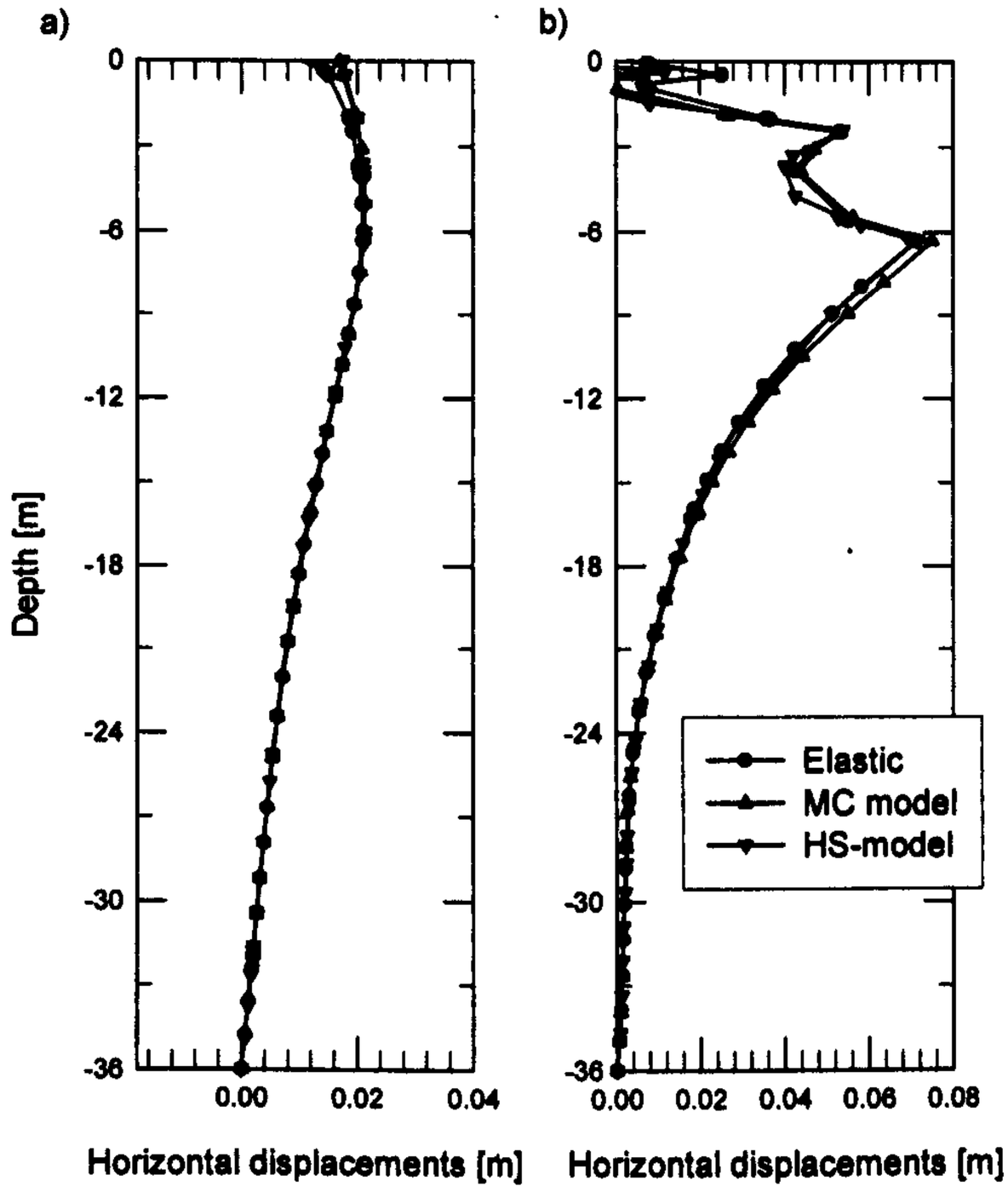

Figure 4.32: Influence of the constitutive model of the embankment fill on the horizontal displacements at the toe a) after construction and b) after 100 years of consolidation

maginitude, -0.77 m respectively. The elastic model predicts marginally lower settlements at the symmetry line of the embankment.

The horizontal displacements profile with depth below the toe of the embankment after construction is shown in Figure 4.32a. Predictions of horizontal displacements with depth by the MC and HS model are similar. The elastic model estimates marginally smaller displacements close to the surface but shows the same profile with increasing depth. Horizontal displacements after 100 years of consolidation are presented in Figure 4.32b. All the models predict similar displacement profiles with depth. The HS model predicts a marginally bigger peak at a depth of -6 m than the elastic and the MC model.

The simulations presented with the different constitutive models showed that the influence on the settlement behaviour is neglible for the horizontal displacements. As the MC and the HS model predict similar settlement troughs after construction and

consolidation the use of the MC model in simulations of embankments not close to failure can be justified.

4.4.11.6 Conclusion on the presented study

The evaluation of the effect of the geometry was divided into three parts. Firstly the predicted short term and long term behaviour of soft clay deposits of different depths was investigated through numerical simulations using MCC, S-CLAY1 and S-CLAY1S. Secondly the influence of the width of the embankment was simulated. Finally the effect of the slope gradient and the embankment height was studied.

a) Effect of the depth of the deposit (height of embankment 2 m, 16 m wide, slope gradient 1:3)

Anisotropy and destructuration have a marginal influence on the predicted consolidation time for deposit with a depth between 8 and 18 m. For deposits deeper than 18 m the influence on the consolidation time is negligible.

Anisotropy and destructuration increase the predicted surface settlements for deposits with a depth between 8 and 36 m.

The predicted $u_{x\text{-}toe}/u_y$-ratios (max. horizontal at the toe/max. vertical displacements) after construction of the embankment decrease in a non-linear manner from 65 % for a 8 m deposit to 34 % for a 36 m deposit.

The predicted $_{x\text{-}toe}/u_y$-ratios (max. horizontal at the toe/max. vertical displacements) after construction are marginally lower than the predicted $u_{x\text{-}max}/u_y$-ratios (max. horizontal /max. vertical displacements) after construction for all deposit depths investigated.

The predicted $u_{x\text{-}toe}/u_y$-ratios (max. horizontal at the toe/max. vertical displacements) at the end of consolidation are in the order of 10 % and are not dependent on the depth of the deposit.

The predicted $u_{x\text{-}max}/u_y$-ratios (max. horizontal/max. vertical displacements) after consolidation of the embankment decrease in a non-linear manner from about 18 % for a 8 m deposit to 14 % for a 36 m deposit using the S-CLAY1 model. S-CLAY1S predicts on average 23 % higher ratios than S-CLAY1 (22% to 18%).

b) Effect of the width (4 to 56 m), height (1 to 5 m) and the slope of the embankment (1:1.5 to 1:4)

The predicted $u_{x\text{-}toe}/u_y$-ratios (max. horizontal at the toe/max. vertical displacements) after construction are dependent on the material behaviour assumed for the dry crust. Modelling the dry crust as a drained material decreases the predicted $u_{x\text{-}toe}/u_y$-ratios by an average of 50 % compared to assuming an undrained dry crust for a 6 m wide embankment. The difference increases with increasing width of the embankment.

Predictions by the model simulations showed an increase of $u_{x\text{-}toe}/u_y$-ratios after construction with increasing width of the embankment. Leroueil et al. (1990) suggest a $u_{x\text{-}toe}/u_y$-ratios which is only dependent on the slope of the embankment. Model simulations are in good agreement with ratios suggested by Leroueil et al. (1990) for small embankment widths (up to 6 m) but suggest larger ratios with increasing embankment width.

The predicted $u_{x\text{-}toe}/u_y$-ratios after construction are dependent on the gradient of the slope of the embankment. For a gradient of 1:1.5 a ratio between 100 % and 136 % was predicted depending on the height of the embankment. The ratios decreased to between 58 % to 76 % with the increase of the gradient of the slope to 1:1.4.

The predicted $u_{x\text{-}toe}/u_y$-ratios decrease with consolidation time. It was found that after 10 to 20 % of the maximum consolidation the ux-toe/uy-ratio has reached its final value. This conclusion is of practical importance for the instrumentation and monitoring of an embankment. It suggests that the horizontal deformations of an embankment need only to be monitored for a certain period of time during the life time of the embankment.

4.5 The influence of anisotropy and destructuration on the ultimate vertical load

To study the influence of anisotropy and destructuration on the undrained shearing capacity, a simple boundary value problem was used instead of an embankment. The soil consists of a single layer with the parameters representing POKO clay (Table 4.4). At the ground surface of the soil layer a distributed vertical load was simulated over a width of 1 m. The load was applied in terms of displacements instead of forces at the nodes of the finite elements. The displacements were gradually increased in a controlled manner under undrained conditions. In the plane strain simulations a finite element mesh consisting of about 150 15-noded triangular elements was used. The mesh was very fine in the area of the load and becoming very coarse towards the boundaries. This is a large strain problem but the simulations were performed as small strain simulations. This was carried out to allow for the comparison to 3D simulations with the PLAXIS 3D foundation code which is limited to small strain analysis (Kamrat-Pietraszewska et al. 2008; Krenn and Karstunen, 2007).

4.5.1 Influence of OCR on undrained shear strength

In the analysis the OCR was assumed to be constant with depth but three different OCR values were considered, 1, 1.5 and 3.0, respectively. The OCR values chosen predict the undrained shear strength profiles shown in Figure 4.33. Four different soil models were used in the simulations, MCC1, MCC2, S-CLAY1 and S-CLAY1S. The profile predicted by the S-CLAY1S is not shown in Figure 4.33 as it is the same as predicted by the S-CLAY1. In order to study the effect of soil anisotropy on the ultimate load, the strength of the MCC1 and S-CLAY1 were matched in compression. The OCR values of the MCC1 were varied to match the strength of the S-CLAY1 model in compression. The required OCR values to match the strength are shown Table 4.10.

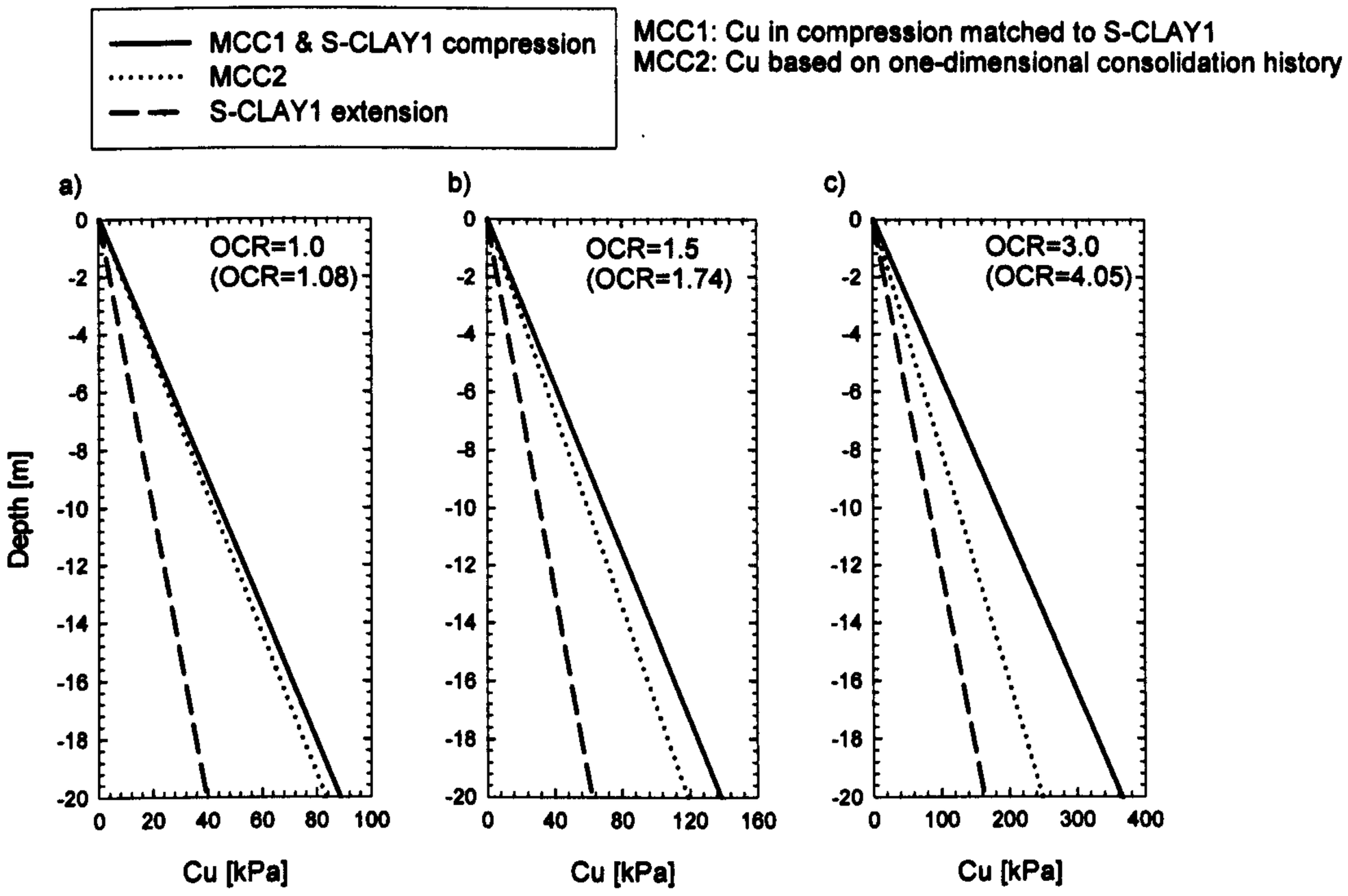

Figure 4.33:Undrained strength profiles, comparison of the MCC and S-CLAY1 predictions a) OCR=1.0 b) OCR=1.5 and c) OCR=3.0

Table 4.10: OCR values

MCC2 & S-CLAY1	1	1.5	3.0
MCC1	1.08	1.74	4.05

The OCR values for the S-CLAY1 and MCC2 are referred to as the reference values because the values are determined from the stress history. In Figure 4.33a the predicted strength for the reference value of OCR=1 is presented. The difference between MCC2 and S-CLAY1 is marginal at the top of the model and linearly increasing with depth. Inspection of Figure 4.33b and c shows that the difference between MCC2 and S-CLAY1 is increasing with increasing OCR values. The magnitude of the difference of the predicted undrained strength in compression is most obvious at the bottom of the model. For OCR=1, the difference in strength is 5.9%. OCR=1.5, the predicted difference is 14.2% and for the case with OCR=3, 31.8%, respectively. The right choice of the constitutive model is important for a correct representation of the strength if the strength is based on the stress history. Basing the strength of the soft soil on the stress history is the recommended choice. In the absence of an advanced

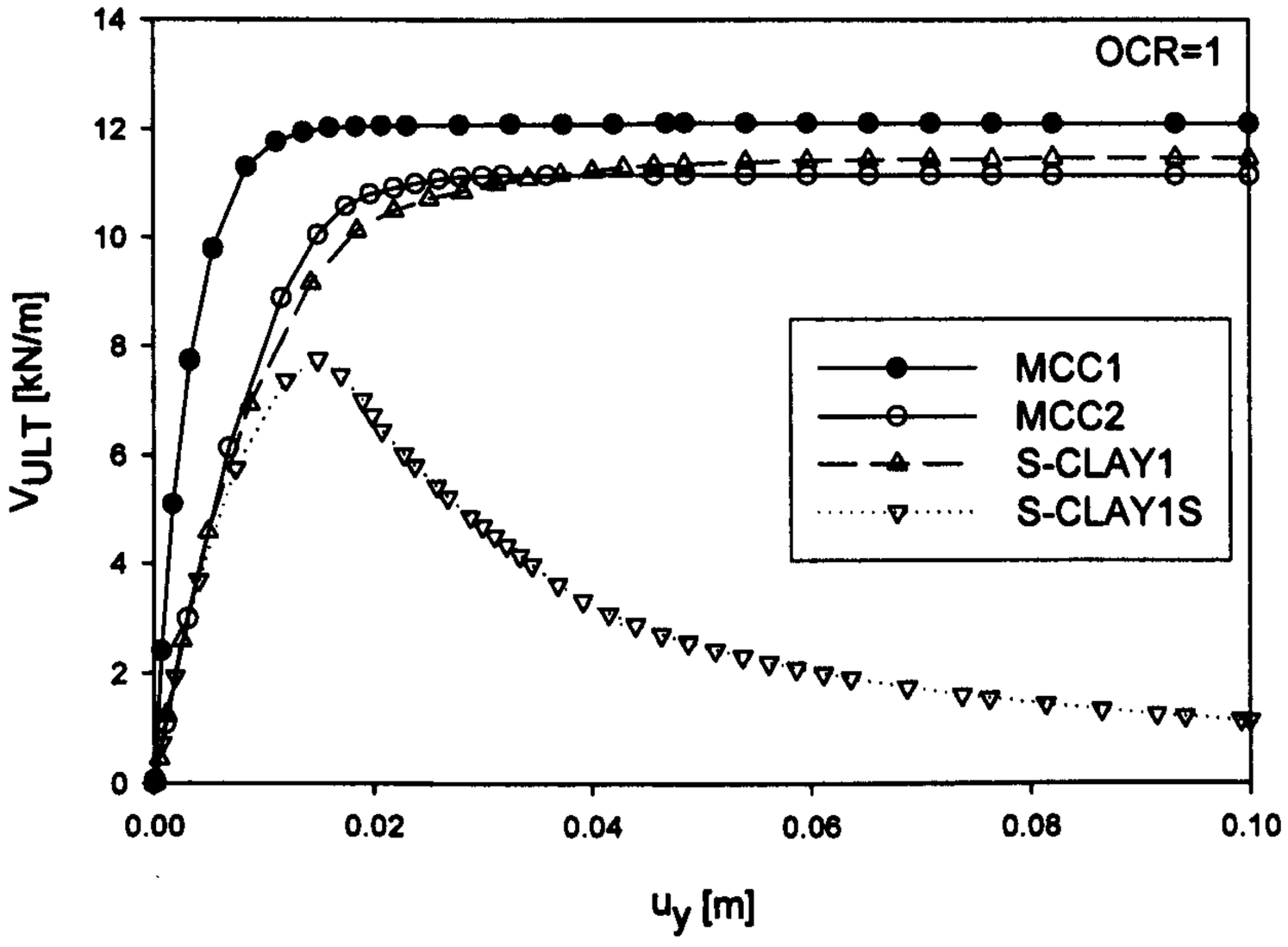

Figure 4.34: Load settlement curve for OCR=1

constitutive model, the strength can be matched in compression, by increasing the value of the OCR.

4.5.2 Predicted ultimate vertical loads

As a typical example the load settlement curve for OCR=1 is presented in Figure 4.34. The MCC1 model predicts the highest ultimate vertical load V_{ULT} of 12.12 kN/m, followed by the S-CLAY1 with 11.48 kN/m, respectively. The MCC2 predicts a marginally lower value of about 11.10 kN/m. The lowest vertical load over-all, is predicted by the S-CLAY1S model. The peak load is 7.76 kN, respectively. After the peak, the model predicts substanial softening and as a consequense the ulti-mate load is descreasing.

Closer inspection of the loading curve shows that all models predict a different gradi-ent before converging to an almost constant value. During undrained loading the size of the yield curve of the MCC model and the S-CLAY1 model can not change much, as no volume change is predicted and elastic volumetric strains are small. The differ-

ent gradients predicted by the two MCC models can be explained with the different sizes of the yield surface and as such the different magnitude of plastic straining involved. Obviously, the yield surface of MCC1 is bigger than that of MCC2. The elastic domain is bigger and less plastic strains are predicted. There is also a difference in the gradient of the loading curve of the MCC2 and S-CLAY1, despite assuming the same undrained shear strength in compression. The yield surface of the S-CLAY1S does not expand much during undrained loading but it can rotate because plastic straining gradually changes the fabric. A large degree of rotation is observed in areas where pure shearing or extension is observed.

In numerical simulations where strain softening is involved there is always to some degree mesh dependency involved and convergence problems may occur in the simulations. A limited study on the influence of the mesh size on the predicted response by the S-CLAY1S was performed. The number of elements directly below the loaded area and close to the expected slip surface was varied. The results of the exercise are presented as load displacement curves (Figure 4.35). In the simulations an intial state with OCR=1 was assumed. Both the peak load and the post-peak behaviour are influenced by the number of the elements. The influence on the peak load is more pronouced if the load applied is displacement controlled rather than load controlled (Kamrat-Pietraszewska et al. 2008). There is no clear trend for the peak load with the number of elements. It seems that with an increasing number of elements the peak load is reduced but this is not true for the simulation with 1858 elements. The number of elements obviously strongly influence the predicted post-peak softening gradient. An increase in the number of elements clearly shows a steepening in the gradient. For the case with 1858 elements the gradient is almost vertical. It was also found that the simulation with 1858 elements did not converge. For detailed discussion and research on softening the reader is referred to Toncone (2005) and Crawford et al. (1995). In the following discussion only the predicted peak values are considered.

In Figure 4.36 the influence of OCR on the predicted ultimate vertical loads is shown. To account for a realistic stress history in the simulations, the K_0 was altered together

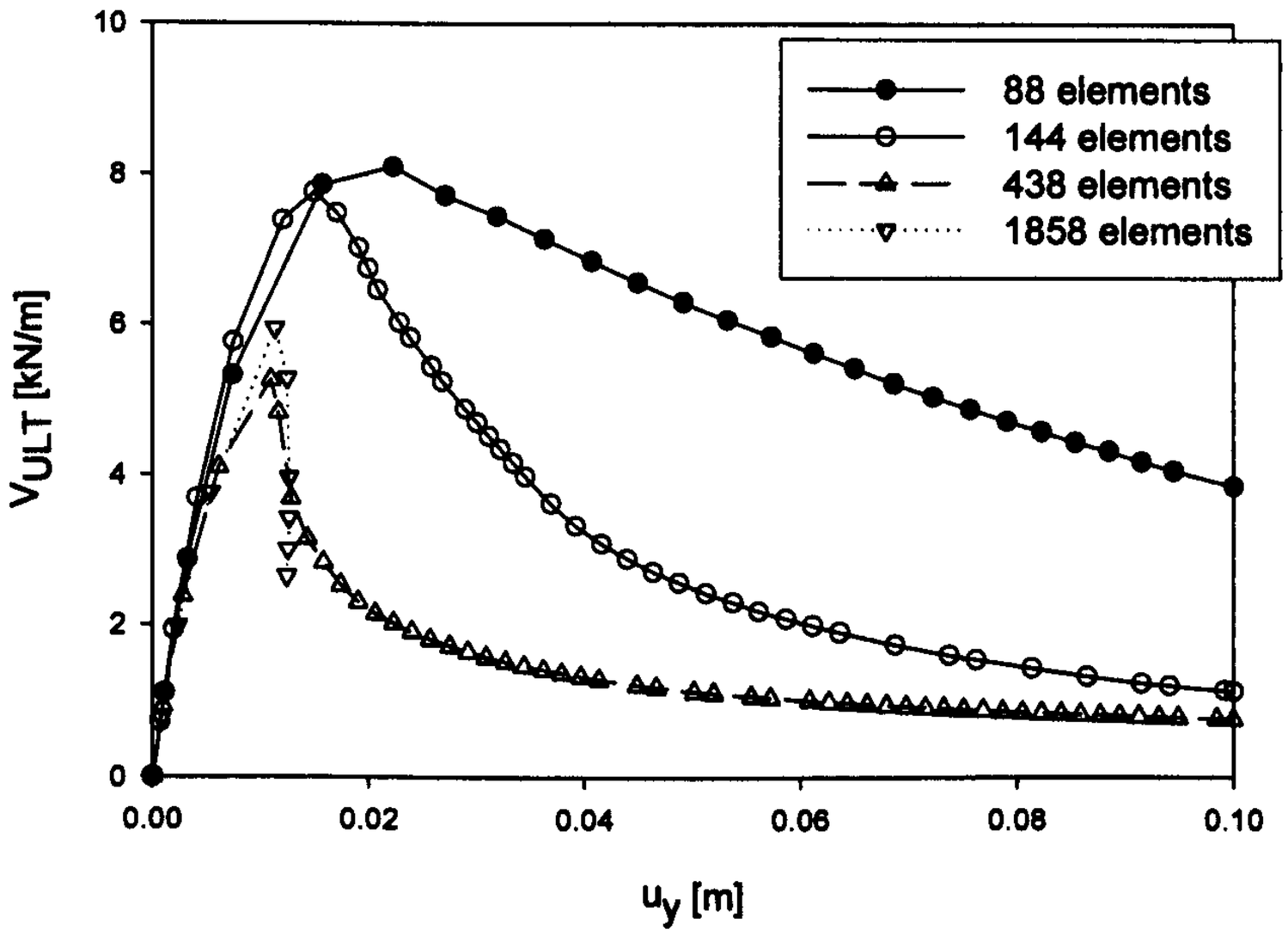

Figure 4.35: Load settlement curves predicted by S-CLAY1S model with different numbers of elements

with the OCR using the formula of Mayne and Kulhawy (1982) (*Eq. 3.3*). For the simulations with the MCC1 model, the K_0 was also calculated using the reference values of OCR rather than the OCR assumed to define the size of the yield surface. The predicted K_0 - OCR relation is shown in Figure 4.36a. In Figure 4.36b the ultimate vertical load V_{ULT} is presented as a function of the OCR and the constitutive model used. For the S-CLAY1S model the peak values have been plotted and due to the mesh dependency should be viewed with caution. With increasing OCR each models predicts an increase in V_{ULT}, as expected. The difference between the V_{ULT} predicted by the MCC1 and the S-CLAY1 increases with increasing OCR. In contrast the difference between S-CLAY1 and S-CLAY1S appears to be fairly constant with increasing OCR. MCC2 predicts similar V_{ULT} values for each OCR considered to the S-CLAY1. In Figure 4.36c the difference in V_{ULT} is presented as ΔV_{ULT} in percentage, using the predictions by the MCC1 model as a reference. The reduction of V_{ULT} predicted by S-CLAY1 for OCR=1 is 8%. With increasing OCR the reduction increases to a maximum of 23% for OCR=3. The difference between S-CLAY1 and MCC2 is in the

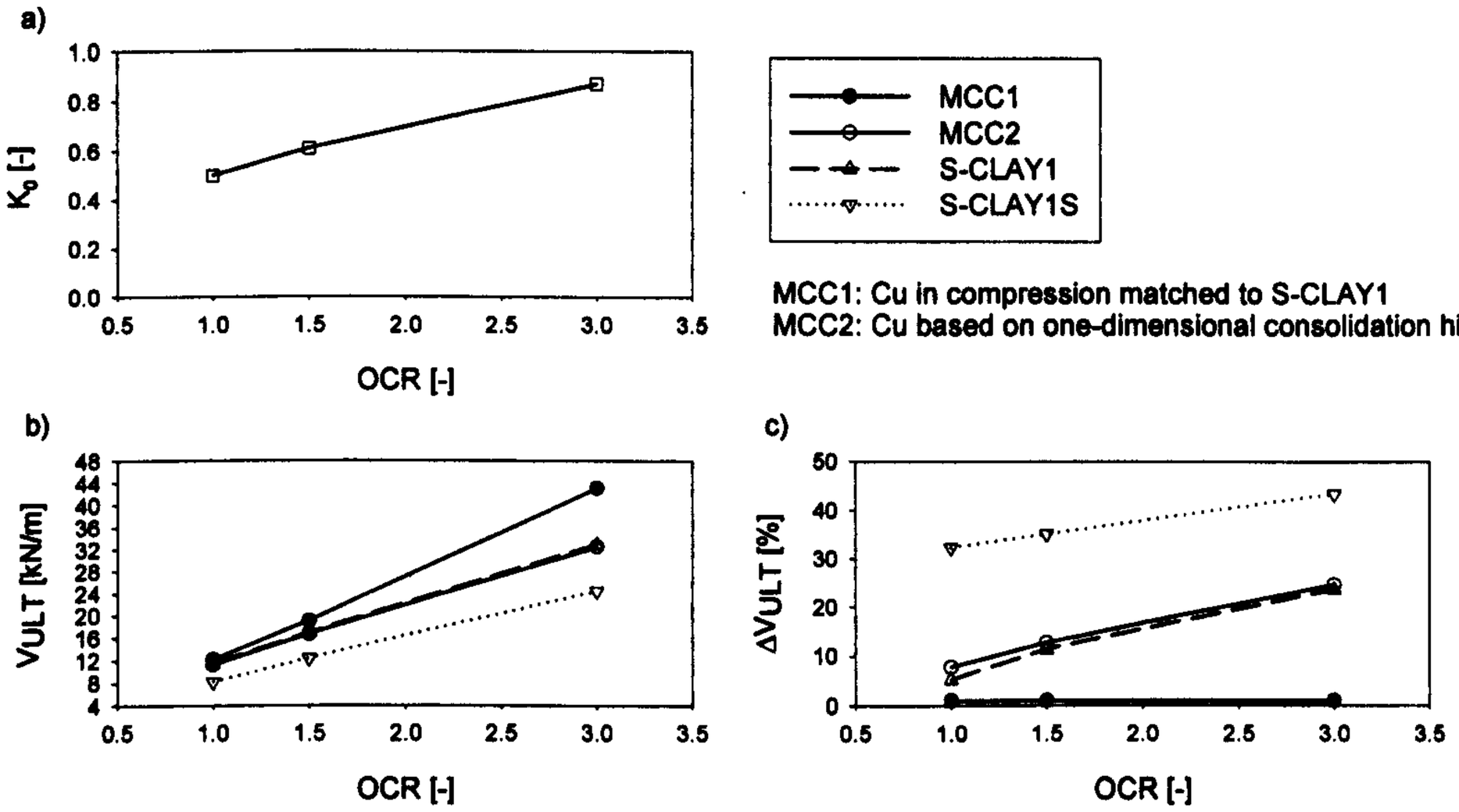

Figure 4.36: Influence of OCR on the ultimate vertical load: a) OCR versus K0 b) Vult versus OCR and c) ΔVult versus OCR

order of 1% for all three cases considered. The reduction in load predicted by the S-CLAY1S is substantial and is 32% for OCR=1 and 43% for OCR=3. The difference between S-CLAY1 and S-CLAY1S is significant, approximately 20% for OCR=1. Again, the results of S-CLAY1S should be viewed with caution due to mesh dependency.

Zdravkovic and Potts (1999) performed similar simulations of a strip footing and circular footing with the MIT-E3 model (Whittle, 1993) and MCC model on stiff normally consolidated clay. The MIT-E3 was developed for overconsolidated clays and is a bounding surface model which accounts for anisotropy via a sheared ellipsoid. It uses a critical state cone as the failure citerion and distinguishes between critical state in extension and compression. It also accounts for small strain non-linear plasticity and strain softening. In the simulations, Zdravkovic and Potts (1999) also matched the undrained strength in triaxial compression for both models, MCC and MIT-E3. The soil was assumed to be normally consolidated (OCR=1). The simulations by Zdravkovic and Potts (1999) showed that accounting for anisotropy reduced the vertical failure loads in the order of 20%. This reduction is bigger than predicted by the S-CLAY1

model, which predicts a reduction of about 8% for OCR=1. The difference can also be contributed to the fact that the MIT-E3 model is using a different critical state friction angle in compression and extension. Furthermore, the model predicts an undrained shear strength profile which is dependent on the direction of the principal stresses. All of the above will contribute to a lower ultimate load.

Zdravkovic et al. (2002) performed a number of plane strain analyses of test embankments constructed on soft clays. The behaviour of the soft clay was modelled with the MIT-E3 to simulate the anisotropic strength and with the MCC to represent isotropic strength. The failure height of the embankment was predicted correctly with the anisotropic model but overestimated by the isotropic MCC. Simulations of the test embankment by Grammatikopoulou et al. (2007) demonstrated the influence of the shape of the yield surface and the plastic potential on the predicted failure height. Grammatikopoulou et al. (2007) used different isotropic models with different yield surfaces and plastic potentials to represent the stress-strain behaviour of the soil. In the simulations the shear strength in triaxial compression was matched by all models used but each model predicted a different strength in plane strain which was dependent on the yield surface and the plastic potential. They concluded that using an isotropic model and choosing a suitable yield surface and plastic potential will allow the prediction of the correct anisotropic strength in plane strain.

4.5.3 Concluding remarks on the ultimate load

The influence of anisotropy and destructuration on the ultimate load was studied with plane strain simulations. To demonstrate the influence of anisotropy the undrained shear strength in compression was matched for MCC and S-CLAY1 by increasing the size of the yield surface of the MCC. For the prediction of the ultimate load it has been shown that the results are strongly influenced by the choice of the constitutive model and the initial state parameters, most importantly K_0 (earth pressure at rest) and OCR (vertical overconsolidation ratio).

When the model parameters were chosen such that MCC and S-CLAY1 predict the same undrained strength in triaxial compression, S-CLAY1 predicts a 5 % lower ultimate load.

When the undrained strength was based on the stress history, both models predict an ultimate load of similar magnitude. Accounting for destructuration substantially reduces the ultimate load but the absolute values have to be examined with caution. The S-CLAY1S model predicts strain softening during undrained loading. In finite element simulations where strain softening at the material point level is involved, the ultimate load and the magnitude of global strain softening is strongly influenced by the size, geometry, type and number of finite elements used in the simulations.

Chapter 5

Developments regarding S-CLAY1S

This chapter introduces developments regarding the implementation of the S-CLAY1S model as a user defined soil model into the PLAXIS finite element code. It summarises the extension of the implementation into a comprehensive tool in terms of possible output. Secondly, a sub-stepping procedure with a continuously updated D-matrix is introduced which predicts more accurate yielding when used with the automatic step size procedure in the PLAXIS code. In the last part of this Chapter an extension of the S-CLAY1S model, the S-CLAY2S model is introduced and verified against drained triaxial tests at different stress ratios. Embankment simulations with the S-CLAY2S model are compared to results predicted by the S-CLAY1S model.

5.1 User defined output

In the original implementation of the S-CLAY1S model (Wiltafsky, 2003b) the output was restricted to the standard output in terms of stresses, strains and displacements provided by the output programme of the PLAXIS 2D and PLAXIS 3D foundation code. Although with the original implementation some of the most relevant state variables can be displayed in the output programme, there was a need to graphically display more information about the predicted behaviour. The aim of this part of the work was to develop an output tool which makes it possible to present information about the predicted stress-strain-strength behaviour of the S-CLAY1S model differently.

5.1.1 Original implementation

In the original implementation of the S-CLAY1S model (Wiltafsky, 2003b) 11 state variables are stored (see also Section 2.7.2), as listed in Table 5.1.

Table 5.1: State variables stored for the output programme (original implementation)

Number	Symbol	Name
1	α_x	First component of fabric tensor
2	α_y	Second component of fabric tensor
3	α_z	Third component of fabric tensor
4	α_{xy}	Fourth component of fabric tensor
5	α_{yz}	Fifth component of fabric tensor
6	α_{zx}	Sixth component of fabric tensor
7	α_0	Scalar value of fabric tensor
8	p_{mi}	Current size of intrinsic yield surface
9	x	Bonding parameter
10	p_m	Current size of natural yield surface
11	e	Current void ratio
12	init	Initialisation

The values of the stored state variables can be viewed in the PLAXIS output programme. The state variables can be activated in the Stresses menu (see Figure 5.1). In the output programme all variables are called state variables even if they are not true state variables such as the Initialisation for example. The Initialisation is a variable which is set to a certain value once the finite element code has called the user defined soil model for the first time for each gauss point. It signals to the finite element code that all state variables are set up for the initial stress state. The name state variable in the programme should not be confused with the true meaning of a state variable in a constitutive model. Due to a limitation in the current version of the output programme only the number of the state variable is shown instead of the symbol.

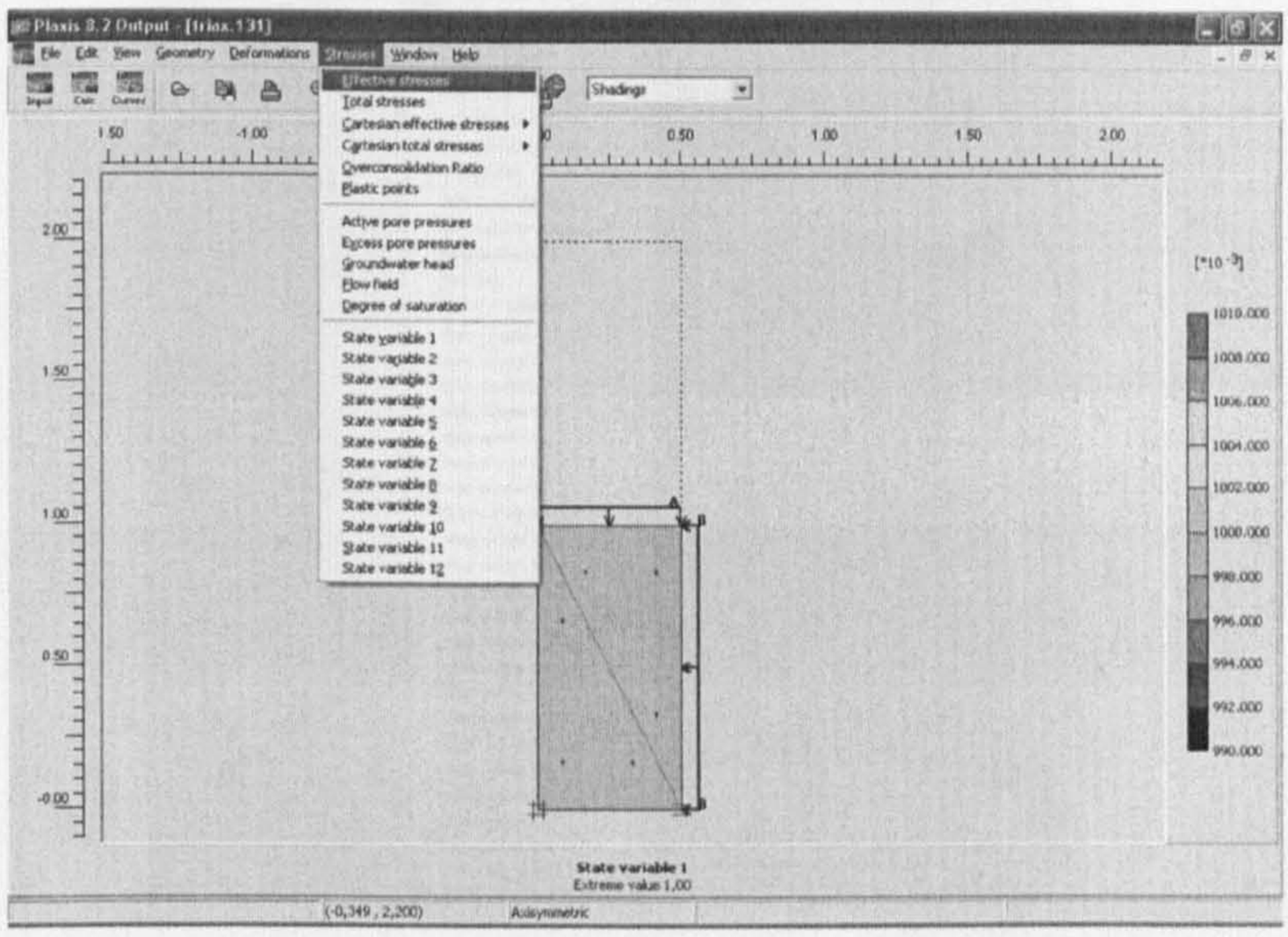

Figure 5.1: Submenu for state variables in the PLAXIS 2D output programme (original implementation)

5.1.2 Extended implementation

In the extended implementation developed as part of this work 10 more variables can be displayed in the output programme (Table 5.2). Not all additional variables are useful as such for the output, but are stored for calculation purposes. For the definition of state variable 13, 14 and 16 (natural and remoulded peak undrained shear strength) the reader is referred to Section 2.4.1.1 and 2.5.5. Number 15 is not used and is reserved for further development.

State variables 17 to 22 are used to calculate the differential effective stresses in the x,y and z-direction. In variables 20, 21, and 22 the initial effective stresses in x,y,z-directions are stored as reference for the calculation of the differential effective stresses at any later stage. The differential effective stresses in x,y,z-directions ($d\sigma_x$, $d\sigma_y$, $d\sigma_z$) are defined as

$$\begin{bmatrix} d\sigma_x \\ d\sigma_y \\ d\sigma_z \end{bmatrix} = \begin{bmatrix} \sigma_x - \sigma_{xi} \\ \sigma_y - \sigma_{yi} \\ \sigma_z - \sigma_{zi} \end{bmatrix} \quad [5.1]$$

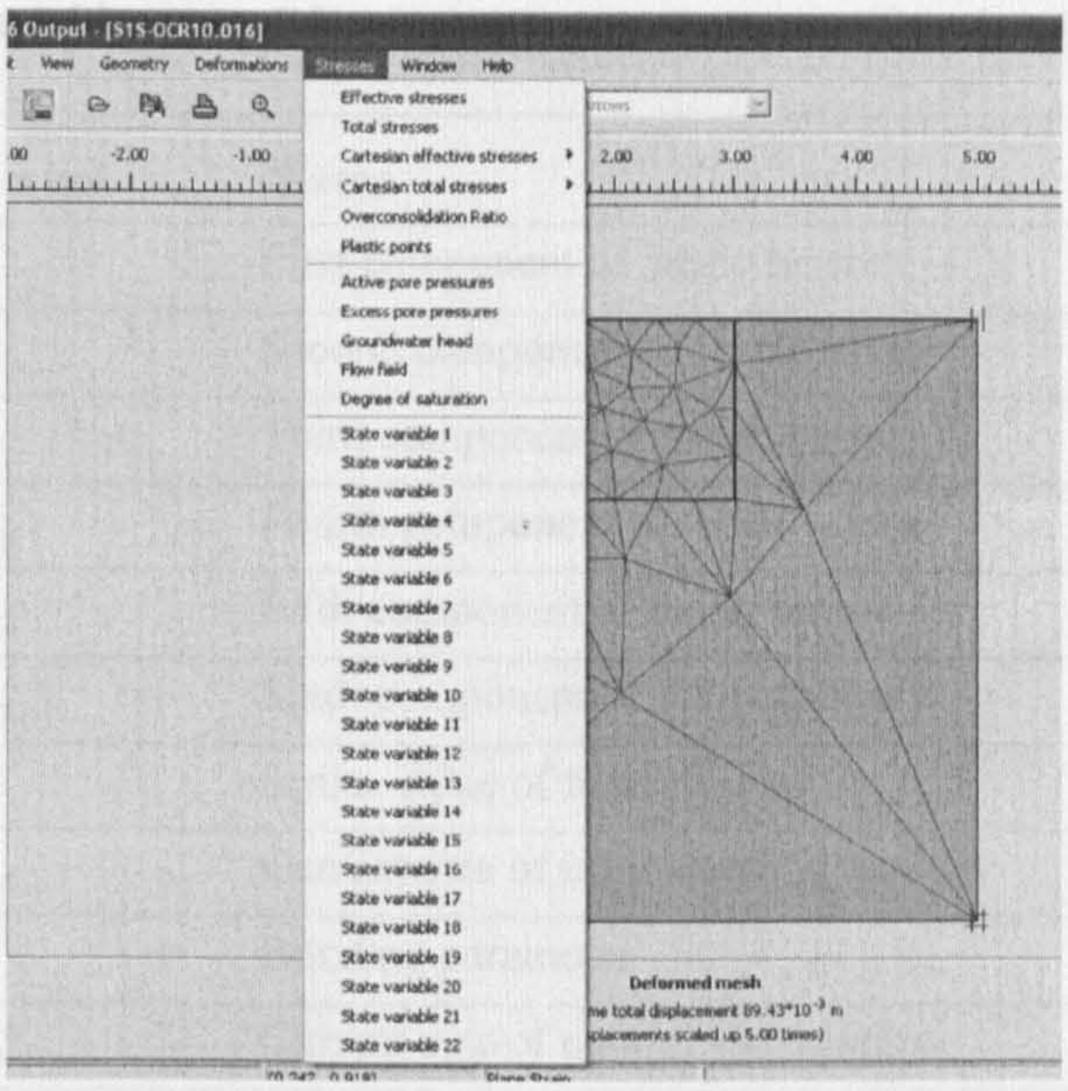

Figure 5.2: Submenu for state variables in the PLAXIS 2D output programme (new implementation)

where σ_{xi}, σ_{yi} and σ_{zi} are the initial effective stresses in the x,y,z-directions. In the 2D PLAXIS Software y is the vertical axis, x is the horizontal axis and z is the out of plane axis. In PLAXIS 3D Foundation, y defines the vertical axis, x and z the two horizontal axes. In the output programme of PLAXIS 2D the state variables can be activated in the Stresses menu as shown in Figure 5.2. To display the state variables in the PLAXIS 3D Foundation software, one needs to go to the Stresses menu and activate the submenu for State Parameters. In this submenu a second submenu lists all the available user defined state variables (see Figure 5.3 for details). A so-called plastic nil step needs to be added to the calculation as a first calculation step, to enable the display of the initial differential stresses or undrained shear strength with depth in the output programme.

Table 5.2: State variables stored for the output programme (new implementation)

Number	Symbol	Name
1	α_x	First component of fabric tensor
2	α_y	Second component of fabric tensor
3	α_z	Third component of fabric tensor
4	α_{xy}	Fourth component of fabric tensor
5	α_{yz}	Fifth component of fabric tensor
6	α_{zx}	Sixth component of fabric tensor
7	α_0	Scalar value of fabric tensor
8	p_{mi}	Current size of intrinsic yield surface
9	x_0	Bonding parameter
10	p_m	Current size of natural yield surface
11	e	Current void ratio
12	init	Initialisation .
13	c_{u_TXC}	Natural peak undrained shear strength in triaxial compression (see Section 2.4.1.1)
14	c_{ur}	Remoulded peak undrained shear strength (see Section 2.5.5)
15	-	reserved for future developments
16	c_{u_TXE}	Natural peak undrained shear strength in triaxial extension (see Section 2.4.1.1)
17	$d\sigma_x$	Differential effective vertical stress in x-direction
18	$d\sigma_y$	Differential effective vertical stress in y-direction
19	$d\sigma_z$	Differential effective vertical stress in z-direction
20	σ_x	Initial effective vertical stress in x-direction
21	σ_y	Initial effective vertical stress in y-direction
22	σ_z	Initial effective vertical stress in z-direction

5.1.3 Differential stresses in conjunction with other soil models

The differential stresses are only a practical output if they are calculated for all soil layers or embankment layers even if they are not modelled with the S-CLAY1S model. As mentioned before the differential stresses are a user defined output and are not available as standard in the PLAXIS software. To make the output as flexible as possible for a range of different boundary value problems, three more constitutive models have been implemented into the PLAXIS codes as User defined soil models.

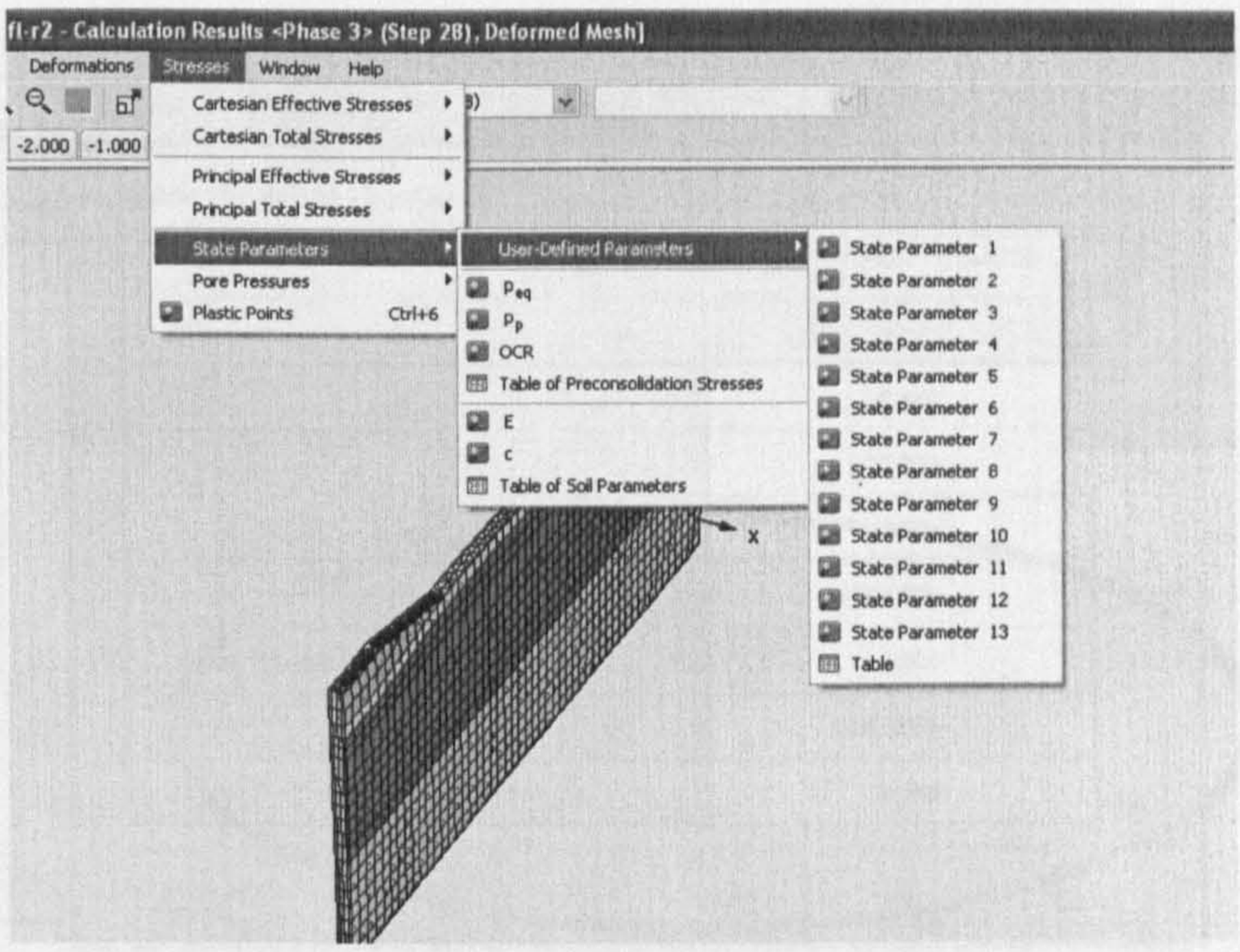

Figure 5.3: Submenu for state variables in the 3D PLAXIS Foundation output programme (new implementation)

Namely, an Elastic model, the Mohr Coulomb model and the Matsuoka-Nakai Hardening model which has been introduced in Section 2.9.2. In this work the Mohr Coulomb model is used to represent the embankment fill and the Matsuoka-Nakai Hardening model to represent the deep mixed material below the embankments. The elastic model is implemented for future application purposes such as piled embankments or similar. All three models store the differential stresses in x,y and z-directions in the state variables 17, 18 and 19. This enables a uniform output of the differential stresses in the output programme of the PLAXIS 2D and PLAXIS 3D Foundation software. Inspection of the differential stresses allows the detailed study of the load transfer with depth from the embankment to the soil. For examples of such studies in 2D and 3D, the reader is referred to Chapter 5, 6 and 8.

5.1.4 Stepwise or time-dependent storage of the state variables

In the PLAXIS code the state variables of the constitutive models which are implemented as user defined soil models are not stored automatically by the software for each load increment. The state variables of interest can only be viewed in the output programme in contour plots and are not plotted against time or calculation steps. To

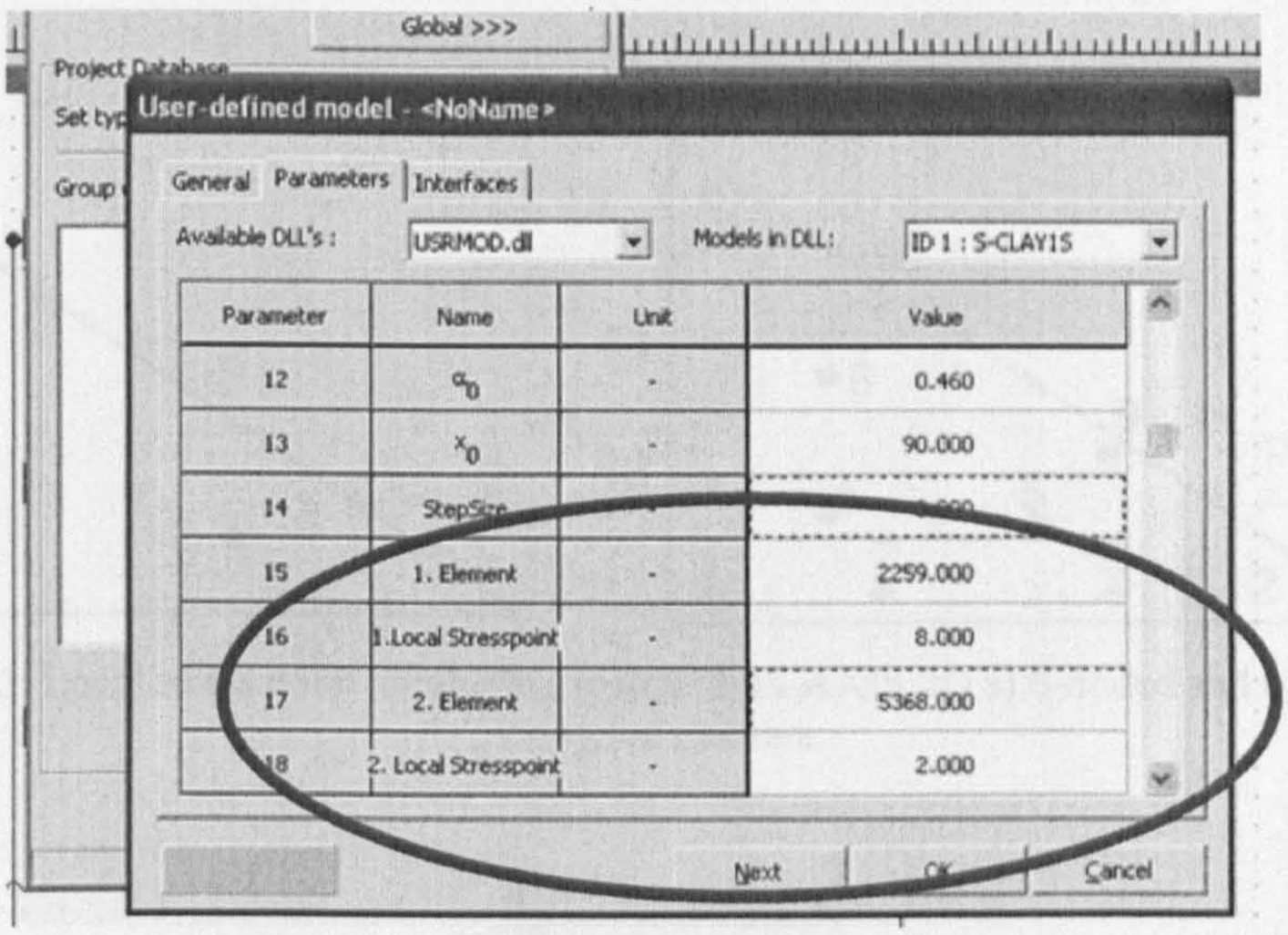

Figure 5.4: Input of global element number and local stress point number (PLAXIS 2D and PLAXIS 3D Foundation)

overcome this substantial shortcoming of the software a subroutine is implemented in the S-CLAY1S model which allows the user to store state variables with time and/or per calculation step in an ASCII file. This file can then be imported into any other data processing program to plot the state variables against time and/or calculation step. The user can choose up to 10 gauss integration points per soil layer for which the information is stored. This facility can be used with PLAXIS 2D and PLAXIS 3D Foundation.

The gauss point of interest is defined via the global element number and the local stress point number and not via the coordinates of the point. This information requires input into the parameter table (material database) of the input programme (see Figure 5.4). The two numbers can be found by graphically viewing the finite element mesh. In the finite element mesh the global element numbers and global stress point numbers are displayed. As the local stress point number is required as input, the global stress point number has to be related to the local stress point number. In PLAXIS 2D a 6-noded or 15-noded triangular finite element is available. The local numbering system of the gauss points is shown in Figure 5.5. The gauss points are numbered in an anti-clockwise direction. In PLAXIS 3D Foundation 15-noded wedge elements are

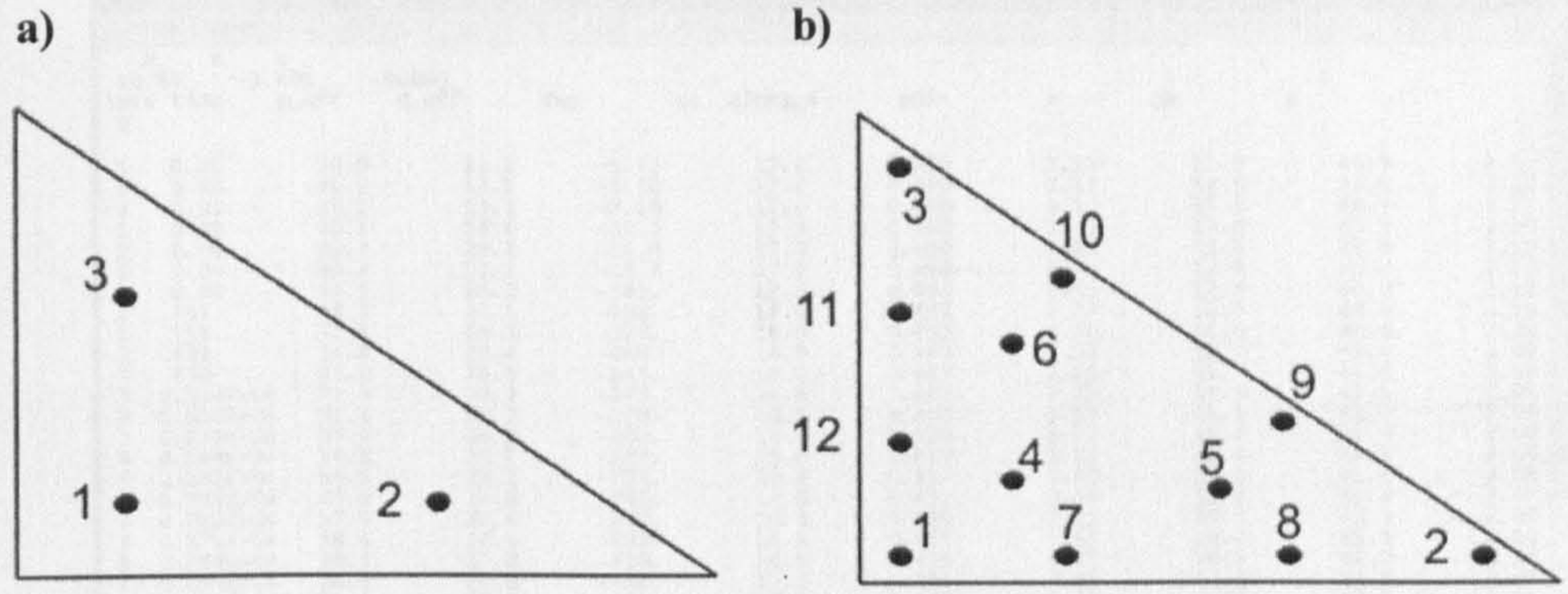

Figure 5.5: Local stress point numbering system in PLAXIS 2D a) 6-noded and b) 15 noded triangular element

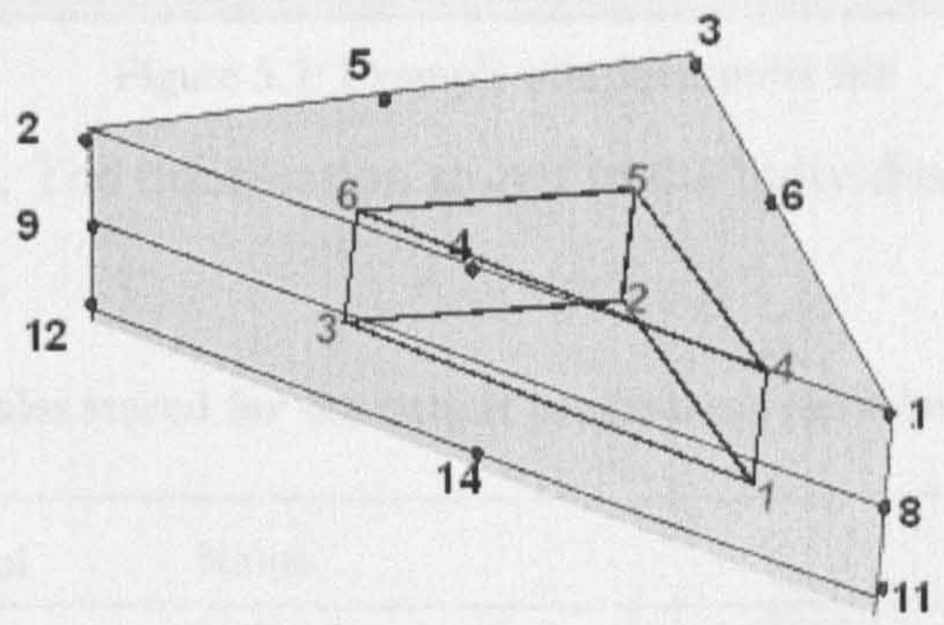

Figure 5.6: Local node and stress point numbering system of the 15-noded wedge element in PLAXIS 3D Foundation

used for the finite element mesh. The element consists of 15 nodes and is shown in Figure 5.6. The nodes are numbered clockwise and from top to bottom. Each element has 6 gauss points. The gauss points are numbered anti-clockwise from bottom to top.

The input of the required information for the stepwise or time dependent state variable storage requires three input steps which do not follow the standard step by step model generation in the 2D and 3D code. First, a material set for the soil layer with the S-CLAY1S model is set up. Secondly, the 2D and 3D finite element mesh is generated with the mesh generator. Once the mesh is built the Global element number is noted and the global gauss point number is related to the local gauss point number. Thirdly, the global element numbers and the corresponding local gauss point number are input into the material database table. An example of an output file generated during the analysis is shown in Figure 5.7. In the top left corner of the file the coordinates of the

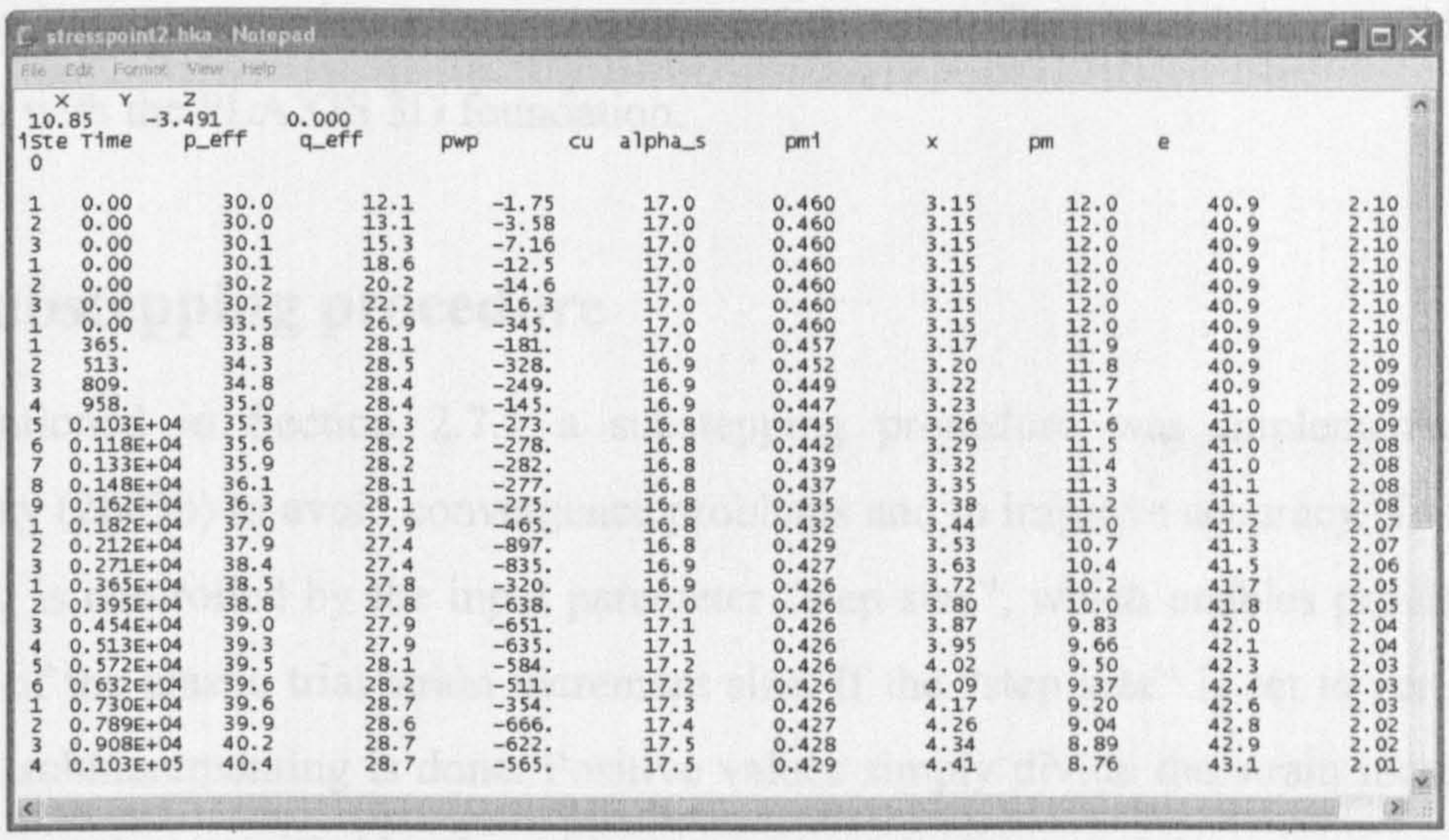
stresspoint2.hka - Notepad

File Edit Format View Help

	X	Y	Z								
10.85		-3.491		0.000							
iSte	Time		p_eff	q_eff	pwp	cu	alpha_s	pmi	x	pm	e
0											
1	0.00		30.0	12.1	-1.75	17.0	0.460	3.15	12.0	40.9	2.10
2	0.00		30.0	13.1	-3.58	17.0	0.460	3.15	12.0	40.9	2.10
3	0.00		30.1	15.3	-7.16	17.0	0.460	3.15	12.0	40.9	2.10
1	0.00		30.1	18.6	-12.5	17.0	0.460	3.15	12.0	40.9	2.10
2	0.00		30.2	20.2	-14.6	17.0	0.460	3.15	12.0	40.9	2.10
3	0.00		30.2	22.2	-16.3	17.0	0.460	3.15	12.0	40.9	2.10
1	0.00		33.5	26.9	-345.	17.0	0.460	3.15	12.0	40.9	2.10
1	365.		33.8	28.1	-181.	17.0	0.457	3.17	11.9	40.9	2.10
2	513.		34.3	28.5	-328.	16.9	0.452	3.20	11.8	40.9	2.09
3	809.		34.8	28.4	-249.	16.9	0.449	3.22	11.7	40.9	2.09
4	958.		35.0	28.4	-145.	16.9	0.447	3.23	11.7	41.0	2.09
5	0.103E+04		35.3	28.3	-273.	16.8	0.445	3.26	11.6	41.0	2.09
6	0.118E+04		35.6	28.2	-278.	16.8	0.442	3.29	11.5	41.0	2.08
7	0.133E+04		35.9	28.2	-282.	16.8	0.439	3.32	11.4	41.0	2.08
8	0.148E+04		36.1	28.1	-277.	16.8	0.437	3.35	11.3	41.1	2.08
9	0.162E+04		36.3	28.1	-275.	16.8	0.435	3.38	11.2	41.1	2.08
1	0.182E+04		37.0	27.9	-465.	16.8	0.432	3.44	11.0	41.2	2.07
2	0.212E+04		37.9	27.4	-897.	16.8	0.429	3.53	10.7	41.3	2.07
3	0.271E+04		38.4	27.4	-835.	16.9	0.427	3.63	10.4	41.5	2.06
1	0.365E+04		38.5	27.8	-320.	16.9	0.426	3.72	10.2	41.7	2.05
2	0.395E+04		38.8	27.8	-638.	17.0	0.426	3.80	10.0	41.8	2.05
3	0.454E+04		39.0	27.9	-651.	17.1	0.426	3.87	9.83	42.0	2.04
4	0.513E+04		39.3	27.9	-635.	17.1	0.426	3.95	9.66	42.1	2.04
5	0.572E+04		39.5	28.1	-584.	17.2	0.426	4.02	9.50	42.3	2.03
6	0.632E+04		39.6	28.2	-511.	17.2	0.426	4.09	9.37	42.4	2.03
1	0.730E+04		39.6	28.7	-354.	17.3	0.426	4.17	9.20	42.6	2.03
2	0.789E+04		39.9	28.6	-666.	17.4	0.427	4.26	9.04	42.8	2.02
3	0.908E+04		40.2	28.7	-622.	17.5	0.428	4.34	8.89	42.9	2.02
4	0.103E+05		40.4	28.7	-565.	17.5	0.429	4.41	8.76	43.1	2.01

Figure 5.7: Example of a stresspoint file

gauss point are shown. The information stored in the individual columns of the file is presented in Table 5.3.

Table 5.3: State variables stored for the output programme (new implementation)

Column	Symbol	Name
1	iSte	Global integration step per calculation step
2	Time	Time in seconds
3	p'	Mean effective stress
4	q	Deviatoric stress as defined in *Eq. 5.2*
5	pwp	Excess pore pressure
6	c_u	Natural peak undrained shear strength in triaxial compression
7	α_0	Scalar value of fabric tensor
8	p_{mi}	Current size of intrinsic yield surface
9	x_0	Bonding parameter
10	p_m	Current size of natural yield surface
11	e	Current void ratio

$$\sqrt{\frac{1}{2}((\sigma'_{xx}-\sigma'_{yy})^2+(\sigma'_{yy}-\sigma'_{zz})^2+(\sigma'_{zz}-\sigma'_{xx})^2+6(\sigma^2_{xy}+\sigma^2_{yz}+\sigma^2_{zx}))} \quad [5.2]$$

There is no restriction in the number of steps which can be stored, however if the number of steps becomes too large the calculation time can be excessive. It is recom-

mend to limit the number of stored gauss points to 10 for a coupled consolidation analysis with the PLAXIS 3D foundation.

5.2 Substepping procedure

As mentioned in Section 2.7.1 a substepping procedure was implemented by Wiltafsky (2003b) to avoid convergence problems and to improve accuracy. The substepping is controlled by the input parameter "step size", which enables provisional control of the elastic trial strain increment size. If the "step size" is set to zero or 1 then no subincrementing is done. Positive values simply divide the strain increment with the number specified by the subincrement.

$$d\varepsilon_{sub} = \frac{d\varepsilon}{stepsize} \qquad [5.3]$$

Negative values of the "step size" limit the size of the strain increment during iteration. The size of the strain increment is related to the following condition:

$$d\varepsilon_{norm} = \sqrt{d\varepsilon_1{}^2 + d\varepsilon_2{}^2 + d\varepsilon_3{}^2 + d\varepsilon_4{}^2 + d\varepsilon_5{}^2 + d\varepsilon_6{}^2} > \left|\frac{stepsize}{1000}\right|. \qquad [5.4]$$

The strain increment $d\varepsilon_{norm}$ is used as a measure in the above condition. If $d\varepsilon_{norm}$ is greater than ABS(stepsize/1000) the number of subincrements n_{sub} with the size ABS(stepsize/1000) is calculated by:

$$n_{sub} = d\varepsilon_{norm} / \left|\frac{stepsize}{1000}\right|. \qquad [5.5]$$

The schematic of the sub-incrementing is presented as a flow chart in Figure 5.8. The details of the convergence loop are shown in Figure 5.9. In the original convergence loop by Wiltafsky (2003b) only the state variables are updated. To reduce the drift from the true solution during substepping the stiffness matrix D is added to the convergence loop. In the implementation by Wiltafsky (2003b) the stiffness matrix D is only updated after the total strain increment (all subincrements) has been applied. In the extended version the D matrix is updated together with the state variables as

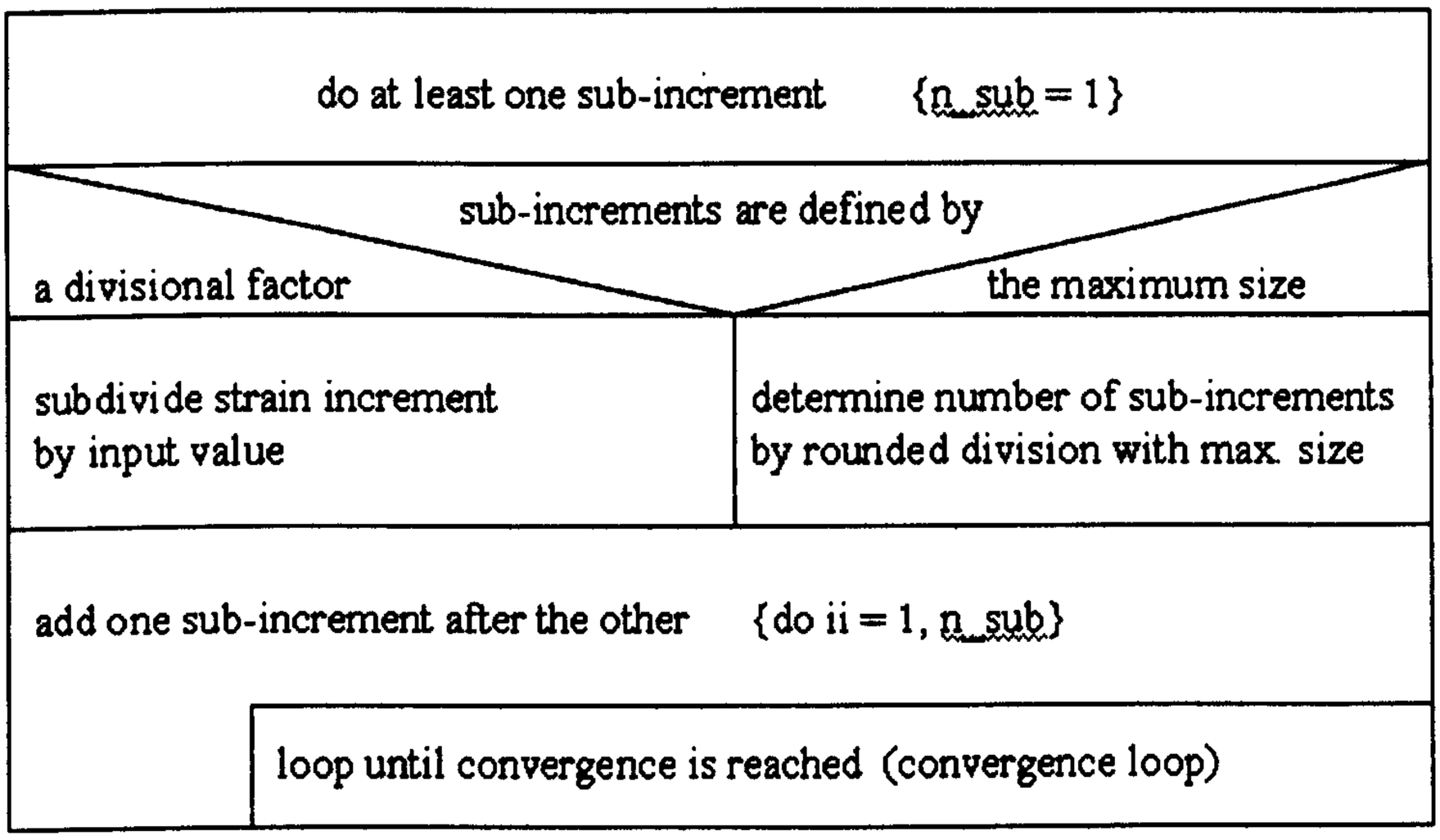

Figure 5.8: Flow chart of sub-incrementing (Wiltafsky, 2003b)

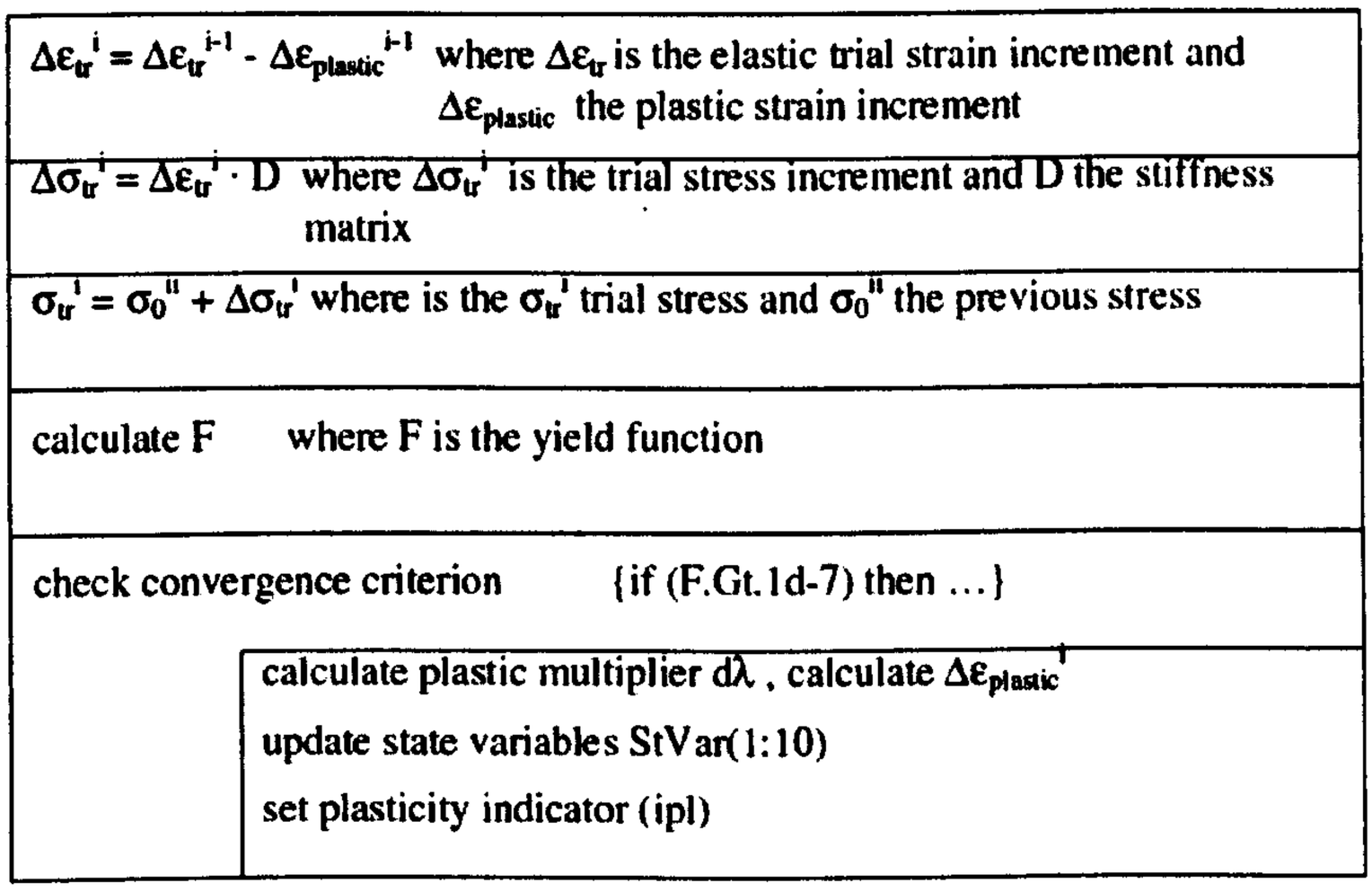

Figure 5.9: Flow chart of convergence loop (Wiltafsky, 2003b)

shown in the flow chart of the convergence loop in Figure 5.10. In the following the effect of including the D matrix in the convergence loop is explored in two examples. The first one is a simulation of an oedometer test and the second one is a simulation of an embankment constructed on soft clay. In both simulations POKO clay was used as the soft clay. The parameters of the POKO clay are listed in Table 4.4. In the Oedometer test a preconsolidation pressure of 20 kPa was assumed. In the simulations the loads were applied in large steps with an automatic step size procedure (Brinkgreve,

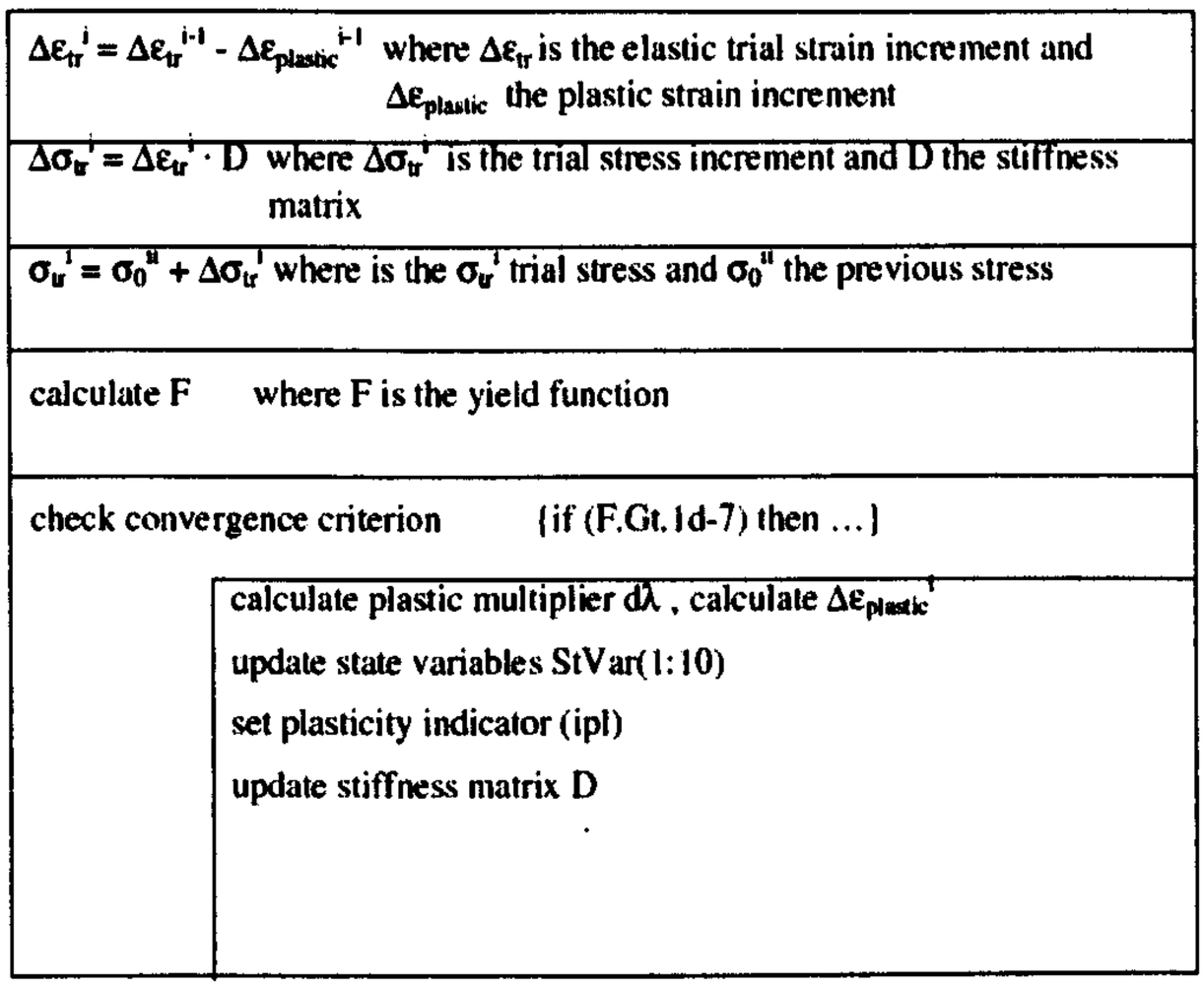

Figure 5.10: Flow chart of new convergence loop

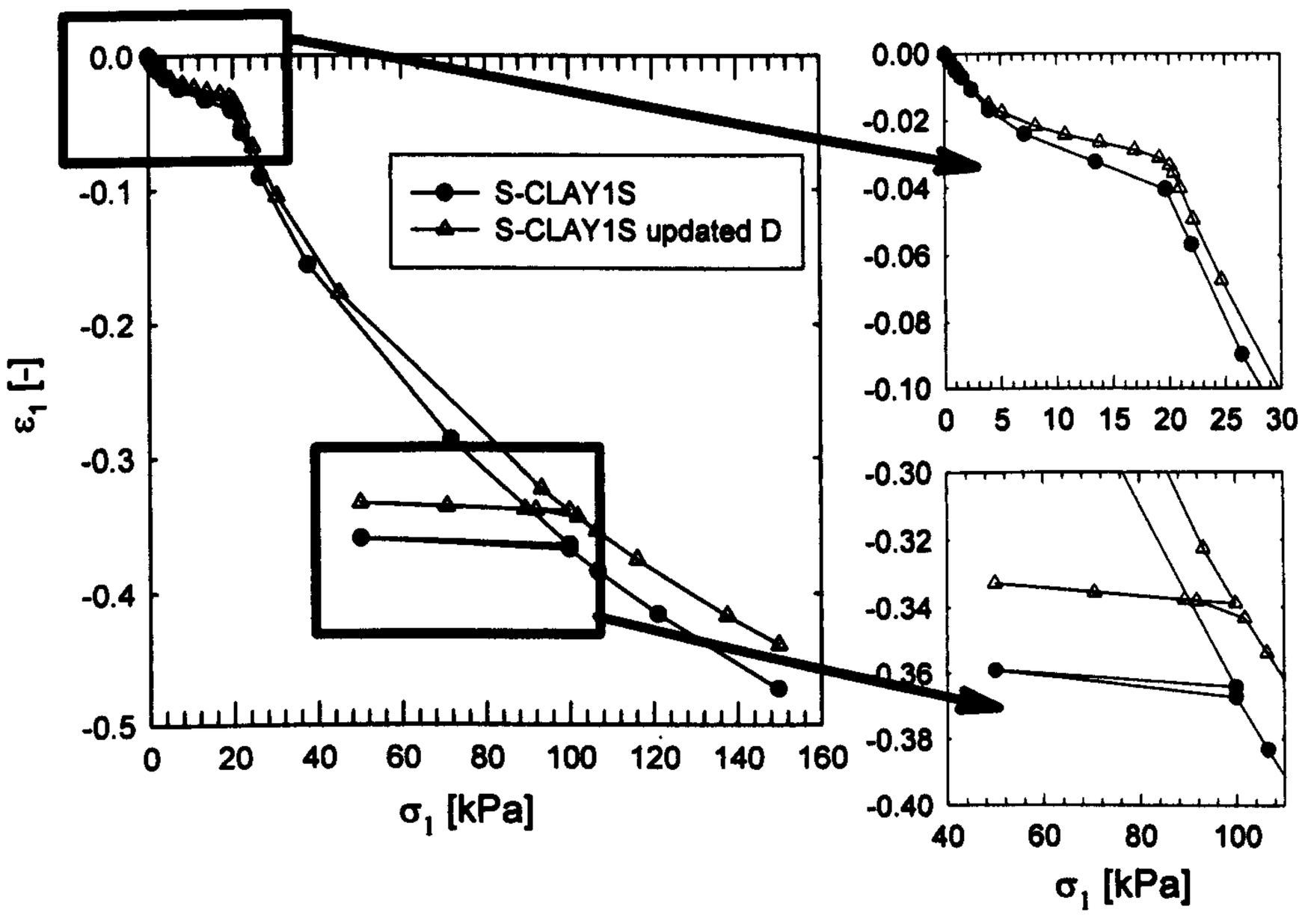

Figure 5.11: Stress strain curve from oedometer test simulations

2002). The results of the simulation of the oedometer test are shown in Figure 5.11. The simulation was undertaken as stress controlled with PLAXIS 2D and the global tolerance was set to 0.001. In Figure 5.11 the convergence loop using the D-matrix is referred to as "S-CLAY1S updated D". It is clearly demonstrated that both curves diverge with increasing vertical stress. Both predict the yield point at 20 kPa very

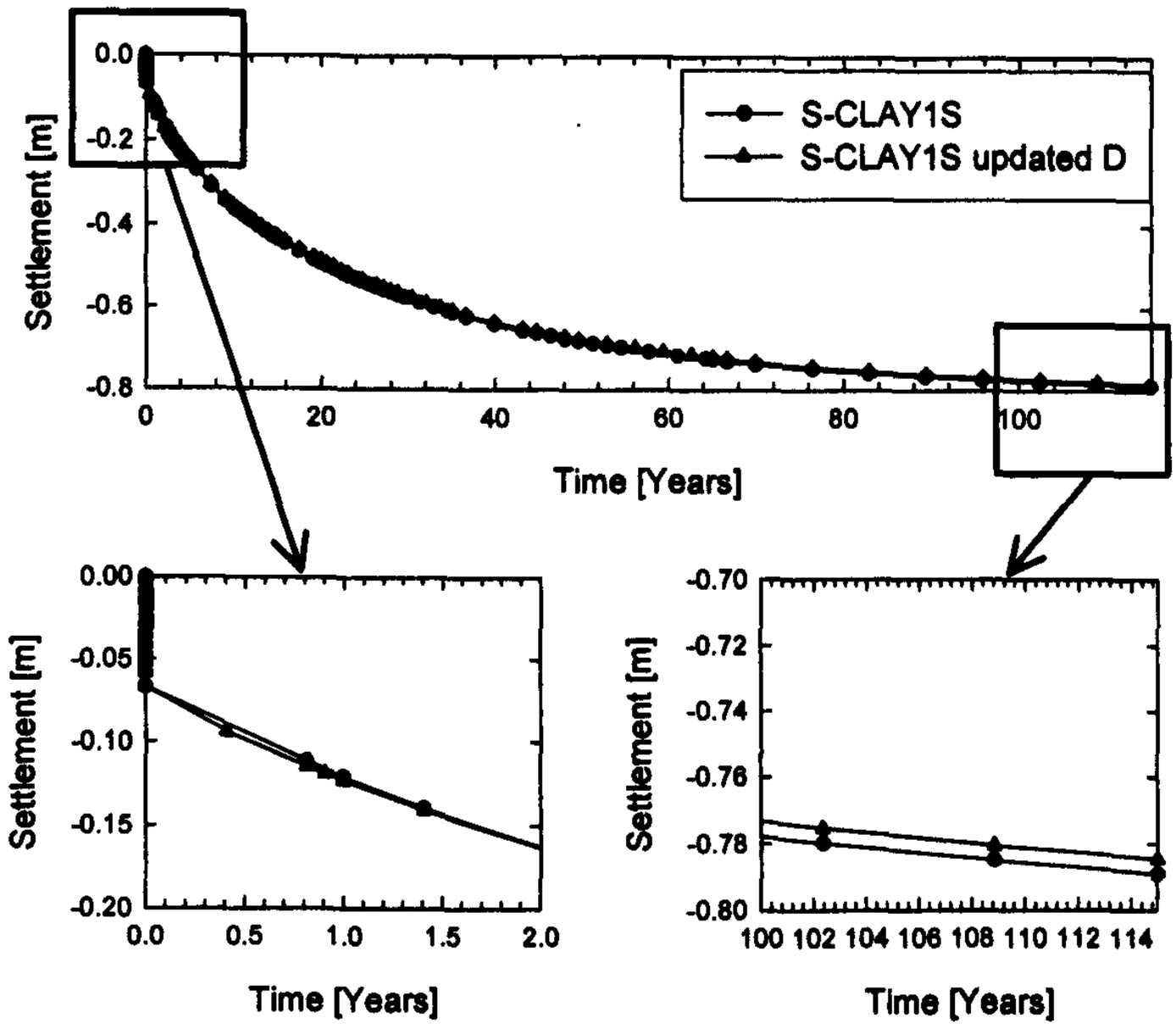

Figure 5.12: Time-settlement curve

accurately, as expected but the S-CLAY1S updated D predicts a smoother curve. Also the stress level of 100 kPa at the start of the unloading/reloading is predicted accurately by both versions but the predicted vertical strain level is different. The version with the updated D-matrix predicts a lower strain level at the point at which the sample is unloaded.

The embankment used in the second demonstration example is the same as introduced in Chapter 4 in the benchmark simulations. The global tolerance in the simulation was set to 0.1. The predicted time-settlement curves are shown in Figure 5.12. Inspection of the curve reveals hardly any difference in the predictions. Both versions predict the same order of settlements after construction of the embankment. Over the years the curves marginally diverge in the order of about 0.5 cm or less. This small difference is negligible for embankment simulations with S-CLAY1S.

The implementation of updating the D-matrix in the convergence loop does not improve predictions of the settlements of the chosen boundary value problem. As such it can be neglected in boundary value simulations. Simulations of an Oedometer

test showed somewhat greater differences in the predictions despite using a very small global tolerance of 0.001. Despite this findings it is recommended to use a one-point gauss programme for accurate simulations (Wiltafsky, 2003b) instead of the PLAXIS code. In case the user does not have access to the one point gauss programme it is recommend that the load be applied in small increments.

5.3 The S-CLAY2S model

5.3.1 Introduction

Karstunen and Koskinen (2004) presented triaxial test simulations with the S-CLAY1S model on natural samples of Murro clay. Murro clay is a soft, silty clay from the western coast of Finland. Murro is a site of a well instrumented test embankment, which has been monitored for years. Details about the test embankment can be found in Chapter 6. The specialised triaxial tests were multistage tests with two loading/ unloading cycles with different stress ratios per cycle. It was found that the S-CLAY1S predicts well the observed behaviour for stress ratios close to the normally consolidated stress ratio η_{K0} but underestimates the deviatoric strains ε_q for stress ratios η close to the hydrostatic axis.

The S-CLAY1S model uses an associated flow rule. Inspection of the strain plots shows that the plastic potential which determines the direction of the plastic strains in the S-CLAY1S model overestimates the ratio between plastic volumetric strains ε_v^p and plastic deviatoric strains ε_q^p. The introduction of a non-associated flow rule can potentially improve the prediction at low stress ratios η.

The motivation of the S-CLAY2S model was to introduce a non-associated flow rule without introducing more complexity to the model or an additional parameter to the model formulation.

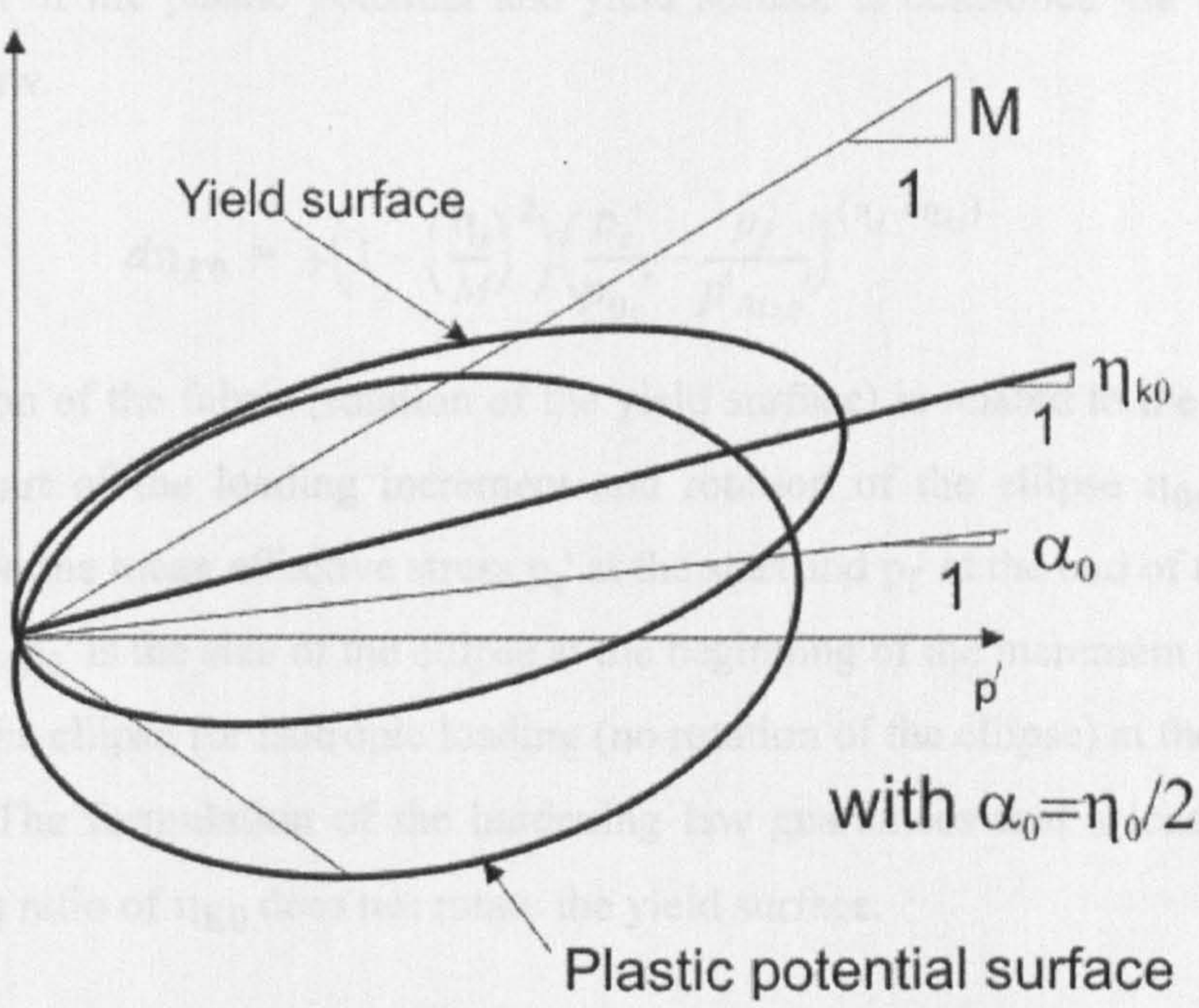

Figure 5.13: Anisotropic model (Davies and Newson, 1992)

5.3.2 Review of anisotropic models for soft clays with non-associated flow rules

Davies and News (1992) introduced an anisotropic model where the anisotropy is expressed as an inclined yield surface (Figure 5.13). The initial orientation of the yield surface in triaxial stress space is centred around the normally consolidated stress ratio η_{K0}. The yield function in triaxial stress space is

$$f = (1-\eta_{K0}^3 M^3)(q-\eta_{K0}\cdot p')^2 - (M-\eta_{K0})^2(p_0'-p')p' = 0 \quad . \qquad [5.6]$$

The plastic potential is also a rotated ellipse as shown in Figure 5.13. The gradient of the plastic potential α_0 is linked to the orientation of the yield surface via the relationship $\alpha_0=\eta_{K0}/2$. The plastic potential is given by

$$g = p'^2 - p'\cdot\beta + \frac{q^2 + -2\alpha_0 q p' - \alpha_0^2 p'\beta}{M^2} = 0 \qquad [5.7]$$

where β is the size of the plastic potential.

The rotation of the plastic potential and yield surface is controlled via a rotational hardening law.

$$d\eta_{K0} = \mp\left(1-\left(\frac{\eta_s}{M}\right)^2\right)\left(\frac{p_s'}{p_{0s}'}-\frac{p_f'}{p'_{0iso}'}\right)^{(\eta_s-\eta_{0s})} \qquad [5.8]$$

The evolution of the fabric (rotation of the yield surface) is related to the stress ratio η_s at the start of the loading increment and rotation of the ellipse η_{0s}. It is also dependent on the mean effective stress p_s' at the start and p_f' at the end of the loading, respectively. p_0' is the size of the ellipse at the beginning of the increment and $p_0'_{iso}$ is the size of the ellipse for isotropic loading (no rotation of the ellipse) at the end of the increment. The formulation of the hardening law guarantees that a load increment with a stress ratio of η_{K0} does not rotate the yield surface.

Dafalias et al. (2003) introduced an anisotropic model with a non-associated flow rule to simulate softening under undrained triaxial loading. The evolution of the fabric (rotation of the plastic potential) is linked to a rotational hardening law. Only the effect of volume change is considered in the rotational hardening law. A similar law is used for the rotation of the yield surface. The rotation of the yield surface is also related to volumetric strain and to the derivative of the plastic potential in order to keep the model stable once a critical state stress ratio is reached. Dafalias et al. (2006) presented a modified version of the previously proposed anisotropic model they named SANICLAY (Figure 5.14). The rotational hardening law for the plastic potential is extended by one term to introduce a dependency of the rotation on the stress ratio. The term also improves stability if the inclination of the plastic potential is close to the critical state in compression or extension. It also makes sure that the model is stable for stress ratios greater than the stress ratio at critical state in compression.

Dafalias et al. (2006) argue that a model for soft clays should be able to simulate the softening behaviour observed during undrained compression shearing of normally consolidated soils. Only a model such as the SANICLAY with a non-associated flow

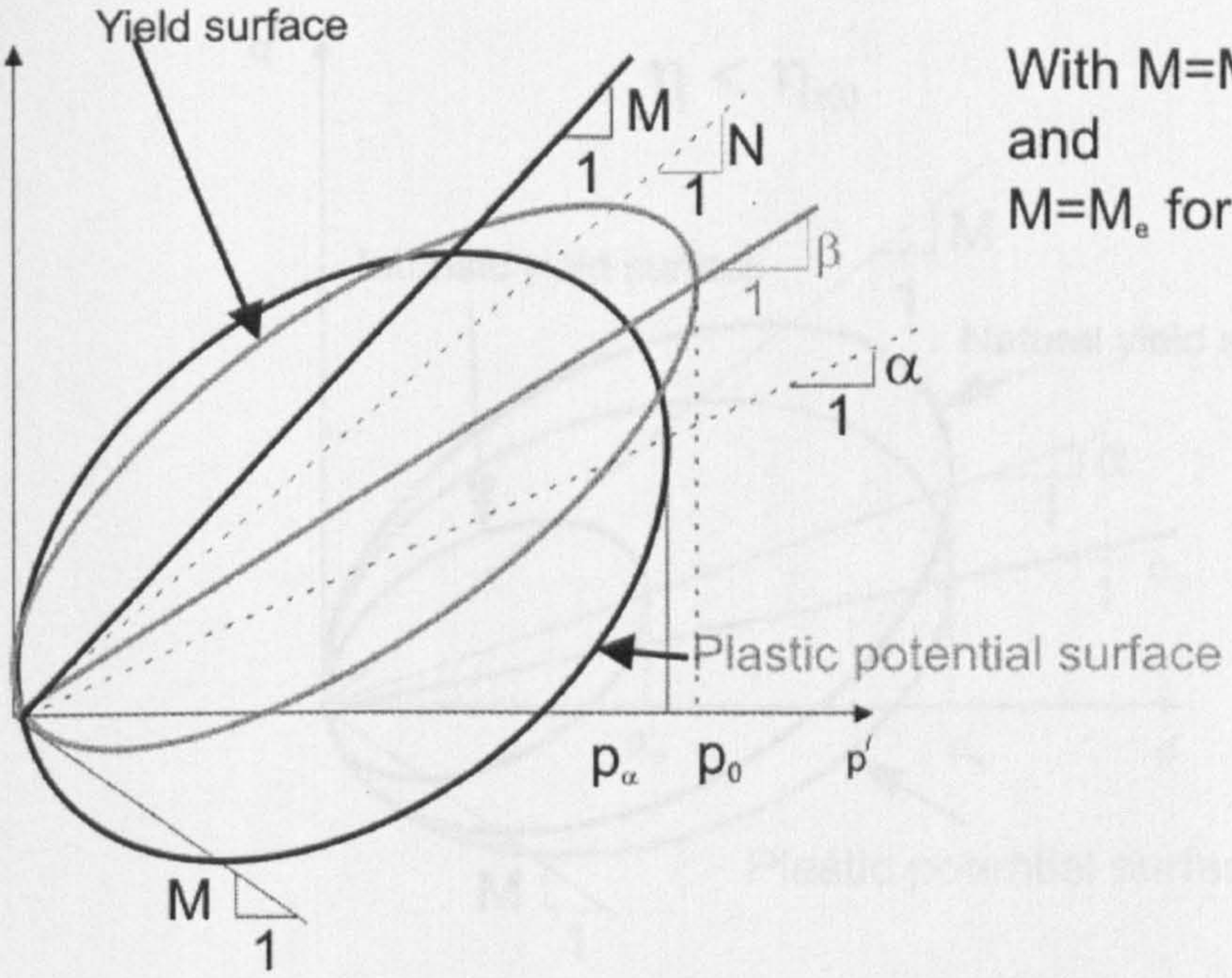

With $M=M_c$ for $\eta>\alpha$
and
$M=M_e$ for $\eta<\alpha$

Figure 5.14: SANICLAY model (Dafalias et al. (2006))

rule is capable of simulating this response. They emphasise that the softening response can not be attributed to destructuration if the corresponding drained loading after K_0 does not yield softening. Destructuration would have induced softening under drained and undrained shearing. Karstunen (2007) argues that such a softening phenomena is not observed in undrained compression tests of reconstituted samples and as such the softening behaviour can be attributed to destructuration.

5.3.3 Formulation of the S-CLAY2S

As mentioned before it was the aim to enhance the S-CLAY1S model without adding further complexity. This restriction will improve the model predictions but will not allow the ideal solution to be implemented.

In the S-CLAY1S model the initial state of the soil is defined by the stress state, the void ratio e, the initial values of the parameters p_m' and α_0 the soil constants μ and β. The size of the natural yield surface p_m' can be determined from laboratory tests using standard procedures. The detailed evaluation of soil constant μ and β and initial value of α_0 is explained in Section 2.4.1.1. However, it is important to recall the meaning of

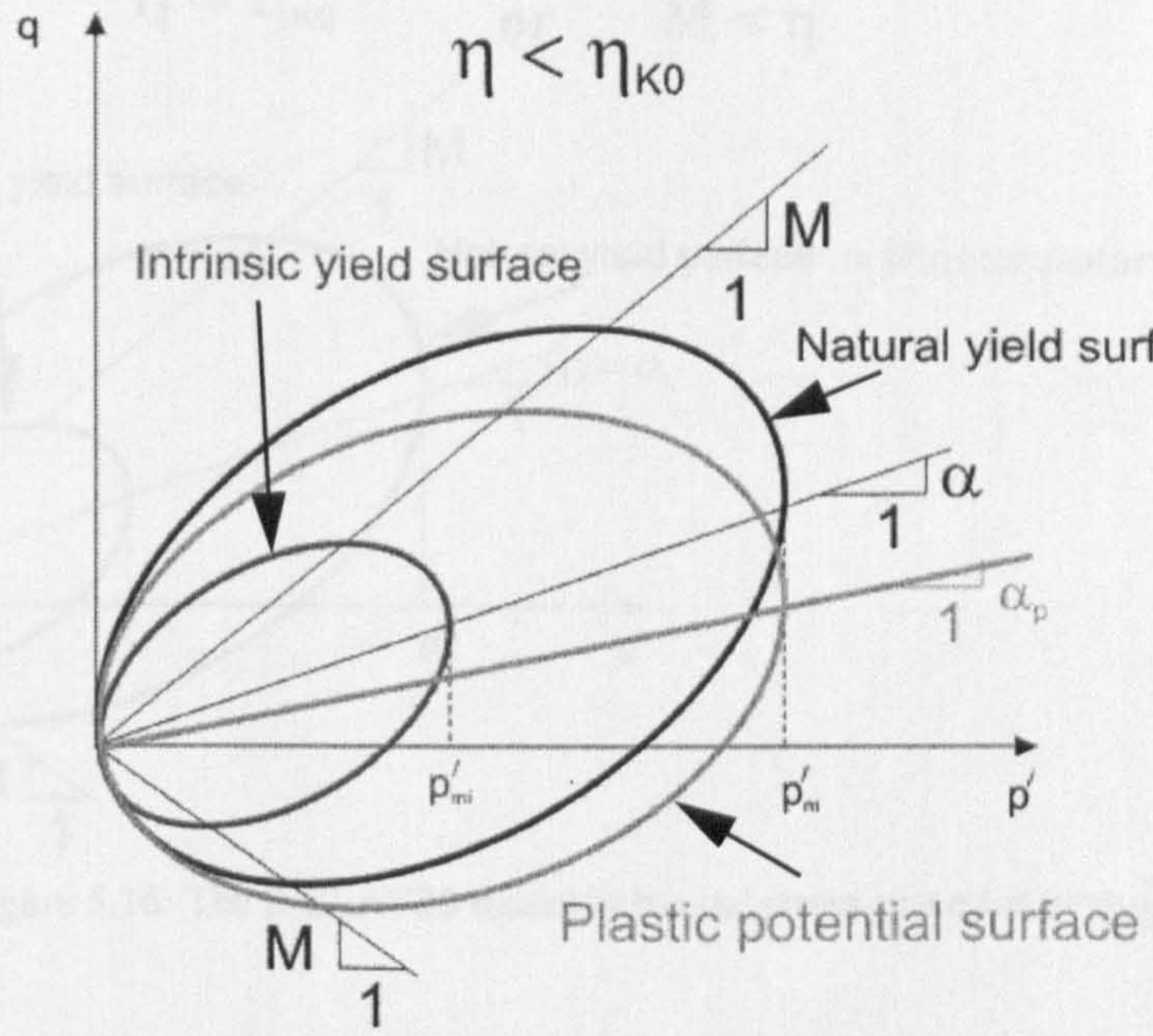

Figure 5.15: The S-CLAY2S model in triaxial stress space for $\eta<\eta_{K0}$

α_0 and β at this point. α_0 is a scalar and defines the initial inclination of the yield surface in triaxial stress space. It is related to the stress and strain history of the soil element and assumes that the soil was restricted to one-dimensional straining to a normally or slightly overconsolidated state. Secondly, it is assumed that during one-dimensional straining the plastic strains are much larger than the elastic strains and the direction and the ratio of the strains follows the principles of an associated flow rule. The soil constant β defines the relative effectiveness of plastic shear strains and volumetric stains in rotating the yield curve. Wheeler et al. (2003) (also see Section 2.4.1.2) showed that for loading along a normally consolidated K_0 stress ratio η_{K0}, only one value of β results in a value of α corresponding to α_0. Knowledge of the critical state friction angle φ' and of the normally consolidated state of the soil is therefore used to determine an appropriate value of α_0 and β.

The aim was to use the same procedures to determine α_0 and β in the S-CLAY2S model and thereby avoid introducing an additional procedure for the initial inclination of the yield surface in the case of a non-associated flow rule. Dafalias et al. (2006) use two different procedures to determine the initial inclination of the plastic potential and

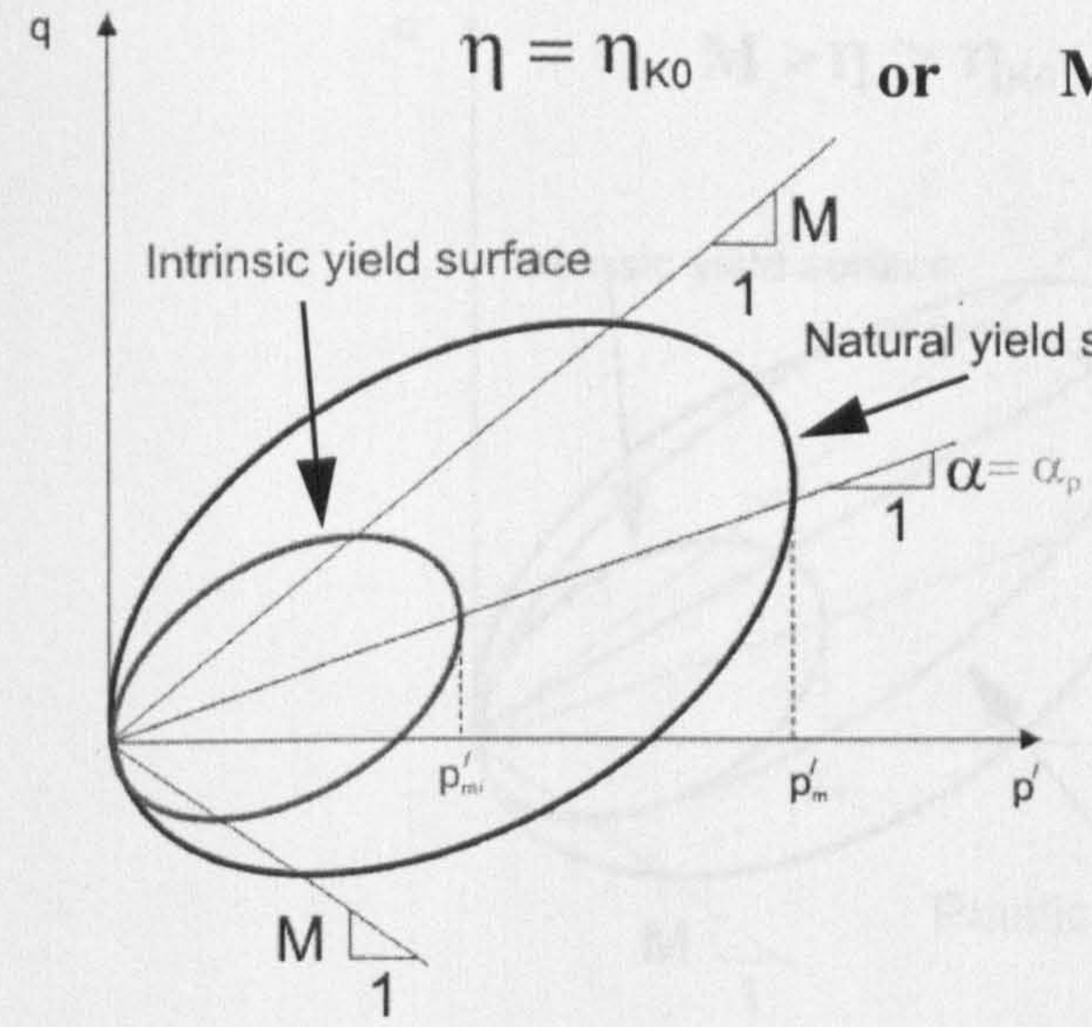

Figure 5.16: The S-CLAY2S model in triaxial stress space for $\eta=\eta_{K0}$ or $\eta>M$

the initial inclination of the yield surface. To be able to continue using the procedure introduced by Wheeler et al. (2003) a conditional plastic potential is introduced (Figure 5.15). The plastic potential will be activated just under certain stress ratios η to improve the prediction of the ratio between plastic deviatoric strains ε_q^p and plastic volumetric strains ε_v^p. Davies and Newson (1992) used a stress ratio η dependency for the rotational hardening law. The inclination α_p of the plastic potential g in triaxial stress space in the S-CLAY2S model is defined by:

$$\alpha_p = \alpha - \alpha\left(\eta_{K0} - \frac{q}{p'}\right) \qquad [5.9]$$

where η_{K0} is the normally consolidated K_0 stress ratio. For stress paths with a gradient of η_{K0} the plastic potential g has the same inclination as the yield surface and as such an associated flow rule applies (Figure 5.16). If the stress ratio η follows a predicted gradient smaller than η_{K0} the inclination α_p of the plastic potential will be less than that of the yield surface (see for instance Figure 5.15). For cases with η between M and α, the predicted inclination α_p of the plastic potential is greater than α. (Figure 5.17). If the predicted stress gradient η is greater than M the inclination α_p is set back to α to avoid numerical instabilities on the dry side of the yield curve (see for

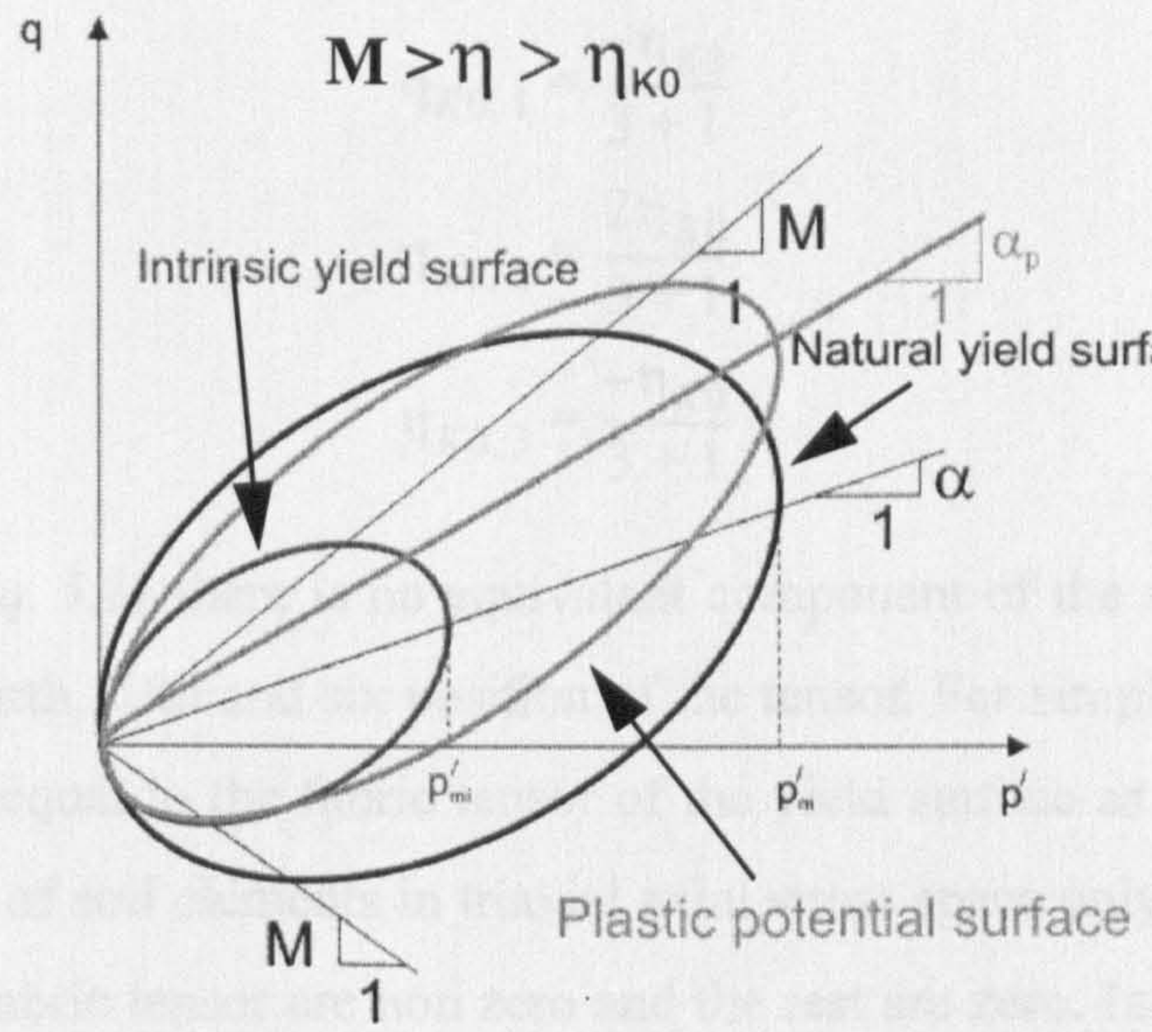

Figure 5.17: The S-CLAY2S model in triaxial stress space for $M>\eta>\eta_{K0}$

instance Figure 5.16). This artificial measure insures that the size of the plastic potential (ellipse) is reasonable at any time and does not collapse to a very slender ellipse which would cause numerical problems. For the triaxial test simulations the formulation of the model in triaxial stress space is reasonable. For calculation of boundary value problems the inclination α_p of the plastic potential needs to be formulated in general stress space. In the triaxial stress space the inclination α_p is a scalar. In general stress space the scalar is replaced with a tensor $\underline{\alpha}_p$. This tensor is special because just 3 out of the 6 components follow the logic of *Eq. 5.9*.

$$\underline{\alpha}_p = \begin{bmatrix} \alpha_{p1} \\ \alpha_{p2} \\ \alpha_{p3} \\ \alpha_{p4} \\ \alpha_{p5} \\ \alpha_{p6} \end{bmatrix} = \begin{bmatrix} \alpha_1 - \alpha_1\left(\eta_{K0,1} - \dfrac{\sigma'_1}{p'}\right) \\ \alpha_2 - \alpha_2\left(\eta_{K0,2} - \dfrac{\sigma'_2}{p'}\right) \\ \alpha_2 - \alpha_3\left(\eta_{K0,3} - \dfrac{\sigma'_3}{p'}\right) \\ \alpha_4 \\ \alpha_5 \\ \alpha_6 \end{bmatrix} \qquad [5.10]$$

with:

$$\eta_{K0,1} = \frac{-\eta_{K0}}{3+1}$$

$$\eta_{K0,2} = \frac{2\eta_{K0}}{3+1} \quad . \qquad [5.11]$$

$$\eta_{K0,3} = \frac{-\eta_{K0}}{3+1}$$

As shown in *Eq. 5.11* there is no equivalent component of the so-called stress ratio $\eta_{K0,i}$ for the fourth, fifth and six position of the tensor. For simplification these components are set equal to the fabric tensor of the yield surface as shown in *Eq. 5.10*. For simulations of soil elements in triaxial axial stress space only the first three components of the fabric tensor are non zero and the rest are zero. In plane strain simulations the fourth component is also non zero and only the fifth and the sixth components are zero. As a consequence of the simplified formulation of the plastic potential tensor a small error is introduced. The same is true for full three-dimensional simulations.

The model is implemented in a one point gauss programme (Wiltafsky, 2003b) and is also available as a user defined soil model for the PLAXIS codes. The plastic potential can be easily switched on by setting the parameter n to zero or one. With zero the associated flow rule is activated and by setting n to 1, the non-associated flow rule is activated.

5.3.4 Simulations of drained triaxial tests with S-CLAY2S

In the following results of simulations of multistage stress path controlled triaxial tests on natural Murro Clay from Finland using S-CLAY1S and S-CLAY2S are presented. The original simulations can be found in Karstunen and Koskinen (2004). The simulations are performed with the S-CLAY1S and S-CLAY2S implemented in the one point gauss programme (Wiltafsky, 2003b). The input parameters and initial state of both models, determined using procedures outlined in Karstunen and Koskinen (2004), are presented in Table 5.4.

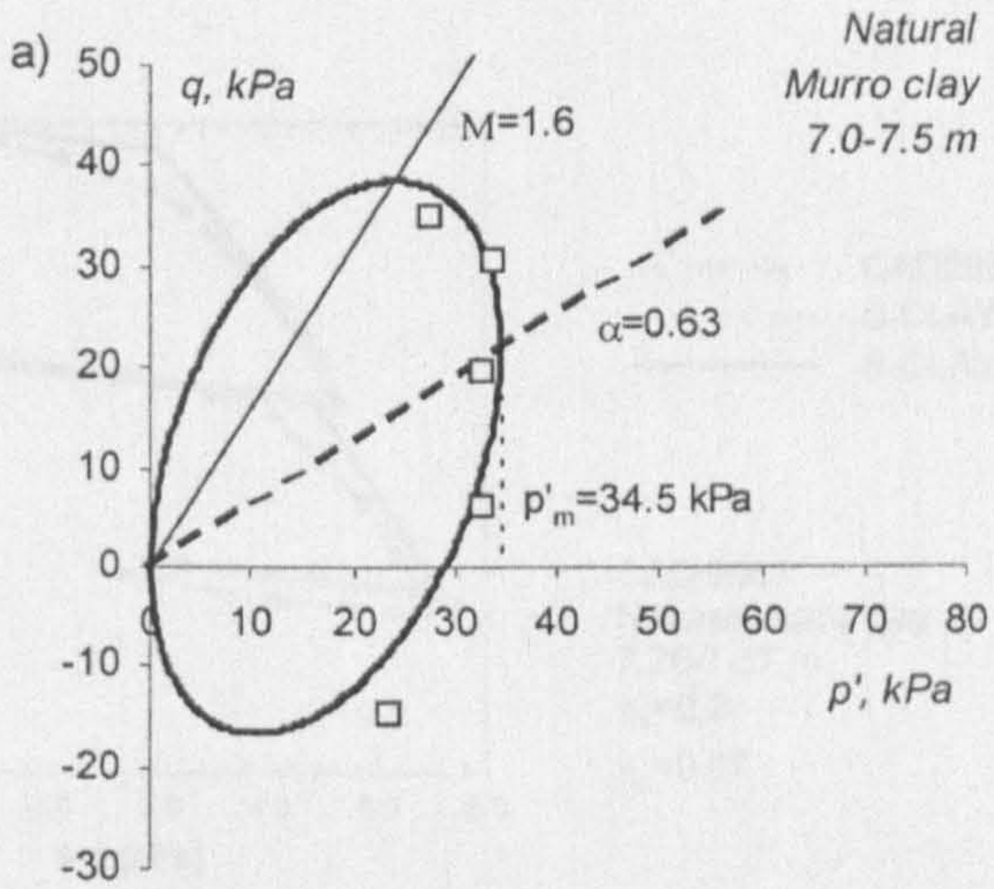

Figure 5.18: Initial yield curve for natural Murro Clay (Karstunen and Koskinen, 2004)

Table 5.4:Parameters and initial state for natural Murro Clay from a depth of 6.9-7.6 meters

Model	λ_i	κ	ν'	M	μ	β	a	b	α_{K0}	x_0
S-CLAY1S	0.21	0.03	0.3	1.6	20	1.02	10	0.2	0.63	9.5
S-CLAY2S	0.21	0.03	0.3	1.6	20	1.02	10	0.2	0.63	9.5

The value of x_0 was chosen on the basis of sensitivity test measurements of natural Murro clay. Parameters a and b were obtained by Karstunen and Koskinen (2004) by performing an optimisation procedure. The values are very similar to values of POKO clay (Section 4.3.2.1) and Bothkennar Clay (McGinty, 2006). The initial yield curve describes the anisotropy of the soil and the preconsolidation of the soil. The predicted natural yield curve by S-CLAY1S and S-CLAY2S model of Murro clay from a depth of 7.0 to 7.5m is shown in Figure 5.18. The predicted yield curve is a very good match of the predicted yield points. The details of the simulated tests are summarised in Table 5.5. Each loading stage listed in Table 5.5 is followed by unloading along the same stress ratio η. All simulations performed are load controlled with load steps in the size of 0.1 kPa or less.

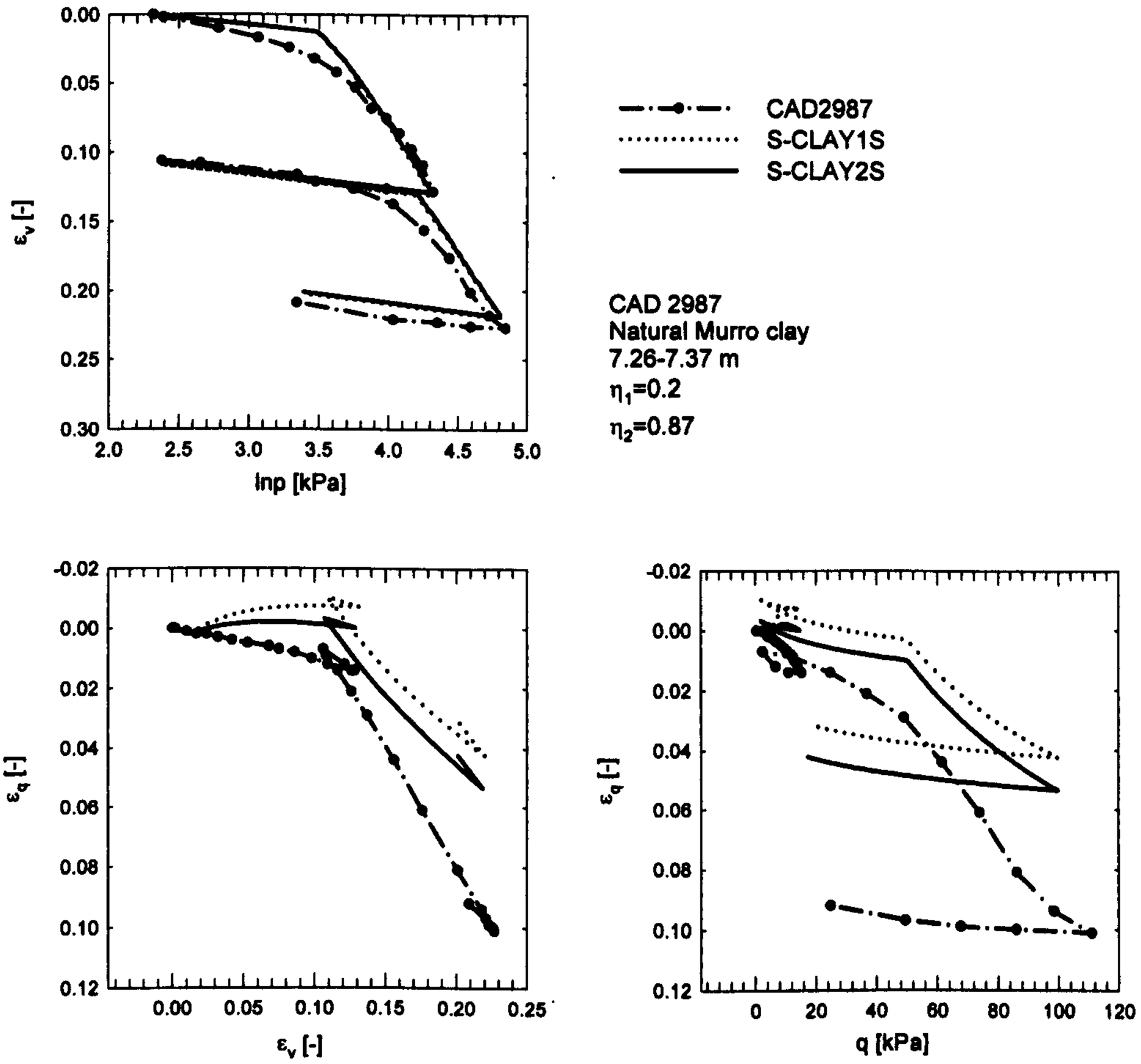

Figure 5.19: Test CAD 2987 on natural Murro Clay

Table 5.5: Simulated triaxial test on natural Murro Clay from a depth of 6.9-7.6 meters

Test number	Depth [m]	e_0	w_0 [%]	η_1	η_2
CAD 2987	7.26-7.37	1.962	74.1	0.20	-0.87
CAE 2989	7.15-7.26	1.945	73.4	0.61	-0.66
CAE 3312	7.36-7.47	2.113	79.0	1.27	-0.42

5.3.4.1 Test CAD 2987 (Figure 5.19)

The test was first loaded with a stress ratio η_1=0.2 (close to the hydrostatic axis) and after unloading reloaded with a stress ratio η_2=0.87. 0.87 is greater than the normally consolidated stress ratio η_{K0} of 0.78. Both models predict the volumetric strain very

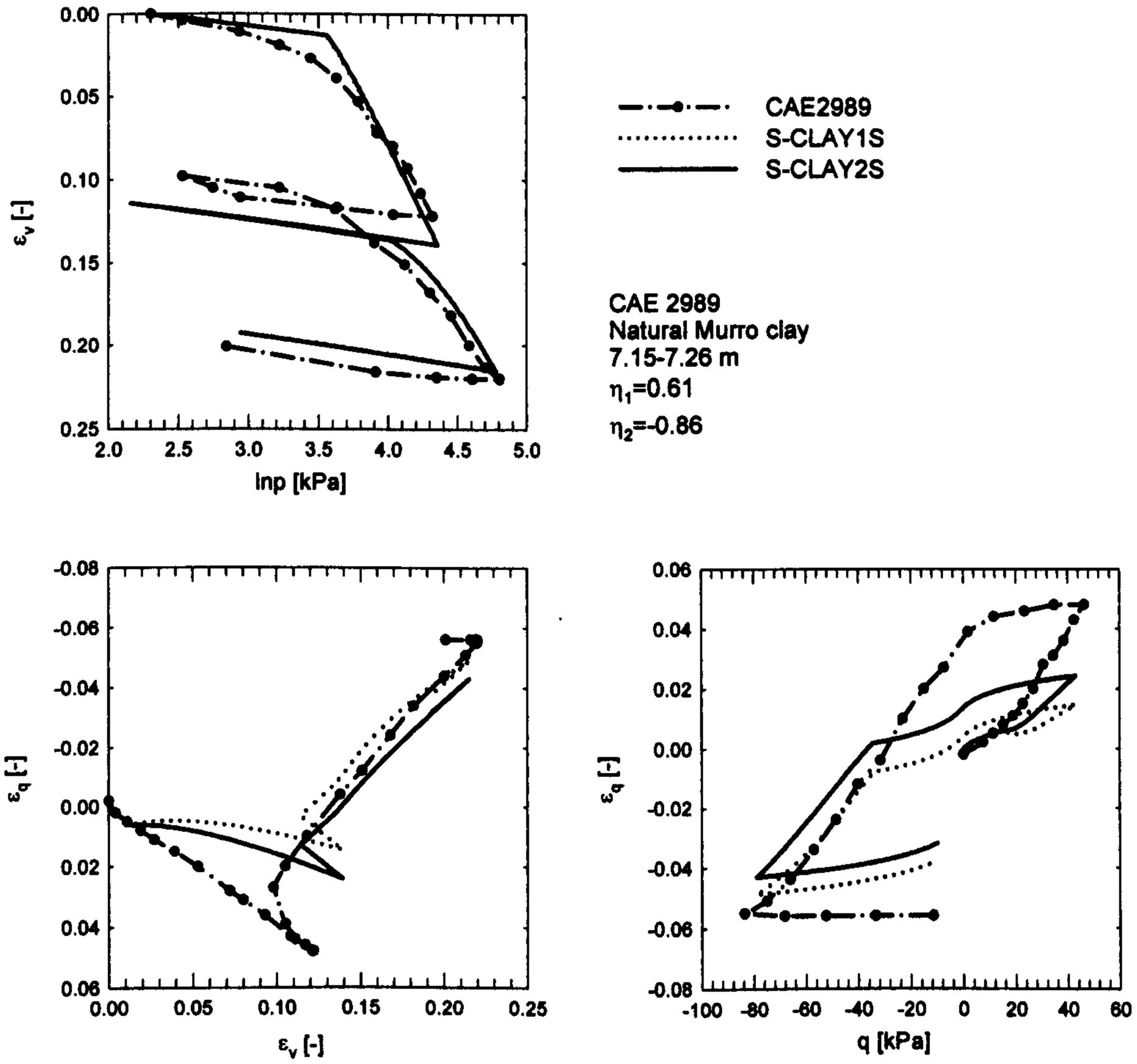

Figure 5.20: Test CAE 2989 on natural Murro Clay

well for both loading/reloading stages. In the first loading stage (η_1=0.2) both models predict negative shear strains whereas the test results show a positive strain. However, the S-CLAY2S predicts far less negative deviatoric strains than the S-CLAY1S. The different shape of the plastic potential in S-CLAY2S reduces the deviatoric strains. In the loading stage both models underestimate the maximum deviatoric strain. Again the S-CLAY2S shows improvement compared to the predictions by the S-CLAY1S.

5.3.4.2 Test CAE 2989 (Figure 5.20)

The test was first loaded with a stress ratio η_1=0.61 followed by a stress ratio η_2=-0.86. Both models overestimate in the first stage the volumetric strain and underesti-

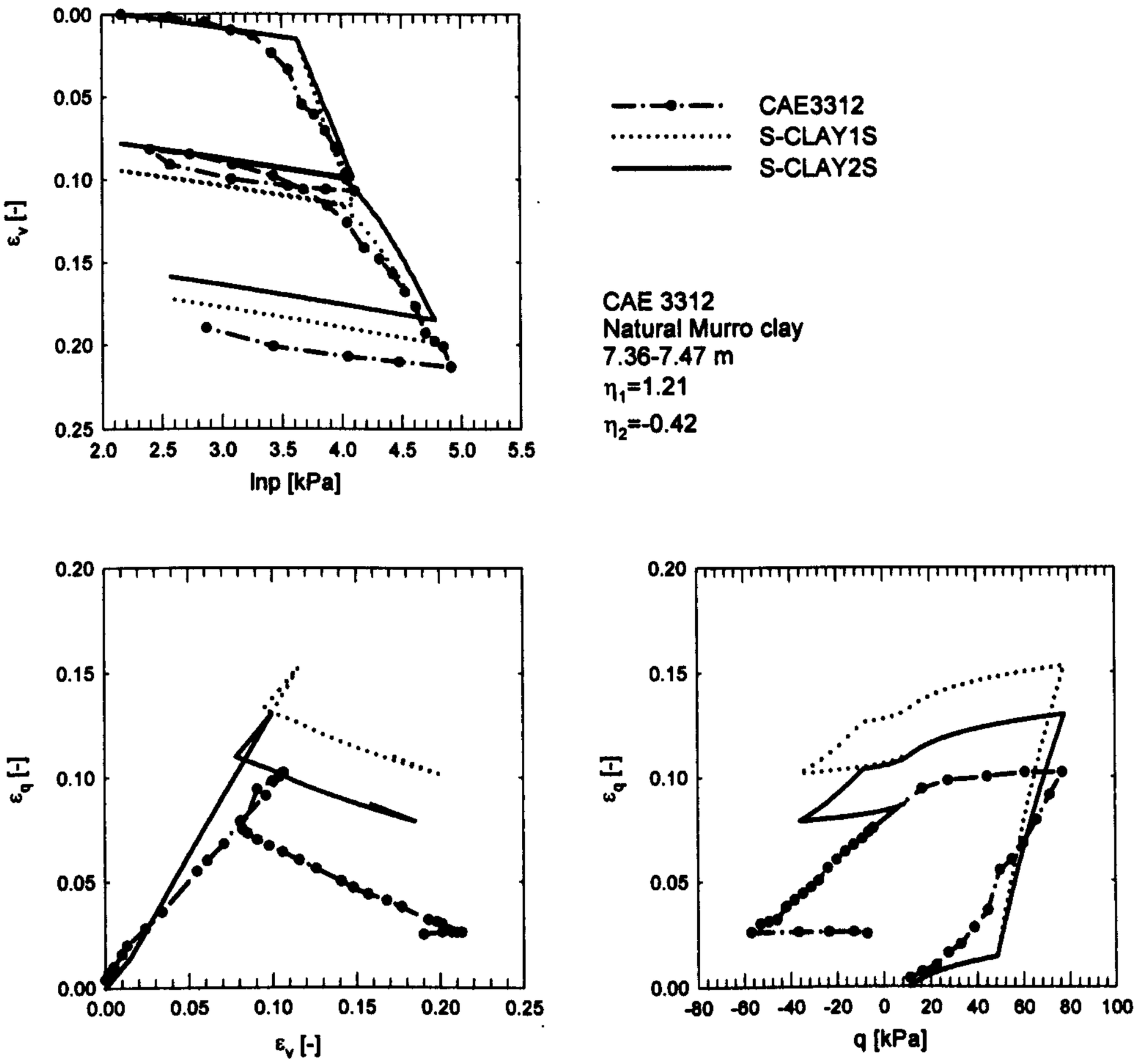

Figure 5.21: Test CAE 3312 on natural Murro Clay

mate the volumetric strain during the second loading stage. S-CLAY1S underpredicts the deviatoric strain in the first stage with S-CLAY2S showing an improvement. Both models also underestimate the deviatoric strain in the second stage. Overall the strain pattern is better predicted by the S-CLAY2S than by the S-CLAY1S model.

5.3.4.3 Test CAE 3312 (Figure 5.21)

The S-CLAY1S model overestimates the volumetric strain for the first loading stage whereas the S-CLAY2S predicts it very well. In the second loading stage both models underpredict the volumetric strains. Both models significantly overpredict the deviatoric strain with S-CLAY2S showing an improvement compared to the S-CLAY1S

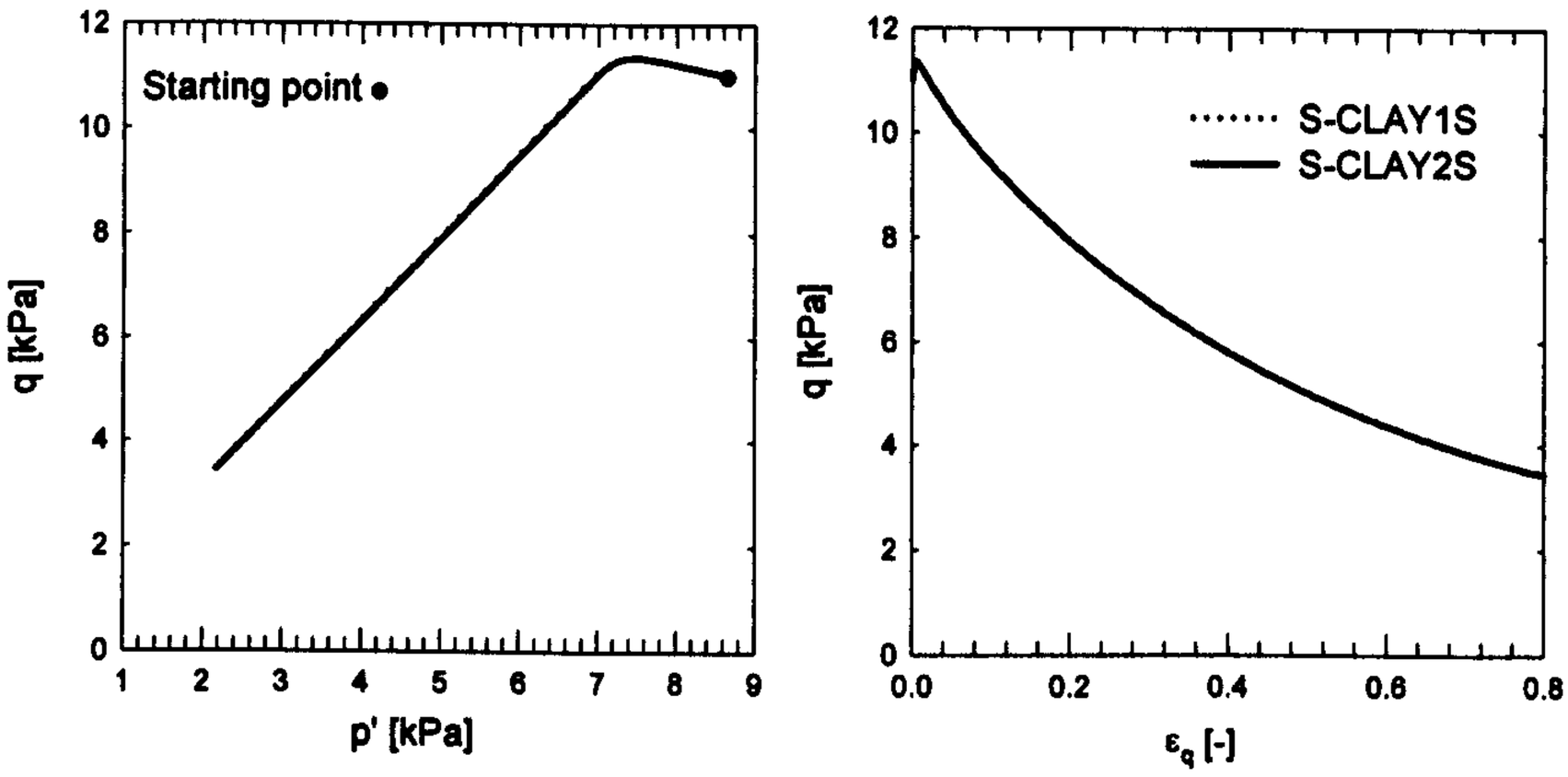

Figure 5.22: Simulation of undrained compression test: starting point η_{K0}

model. For this test the predicted strain gradients (ε_v-ε_q plot) are improved by the S-CLAY2S model.

5.3.5 Simulations of undrained tests

The following simulations are just model simulations and are not compared to test results. The simulations are used to highlight the difference in predictions by the two models. For the simulations the parameter set presented in Table 5.4 was used. Three test simulations are presented. The first test is an undrained compression test started from a normally consolidated stress state. In the normally consolidated stress state the starting point lies directly on the yield surface. No elastic loading is predicted during undrained shearing. The comparison is shown in Figure 5.22. Both models predict the same stress path and the same deviatoric strain patterns.

In Figure 5.23 simulations of a compression test with a starting point on the hydro-static axis (η=0) is shown. The soil is also slightly over-consolidated. Both models show initially an elastic loading path up to a point where both yield on the dry side as expected. The stress path then follows the shape of the yield curve towards the critical state stress ratio M. Close to M the stress path of both models slightly diverge with the

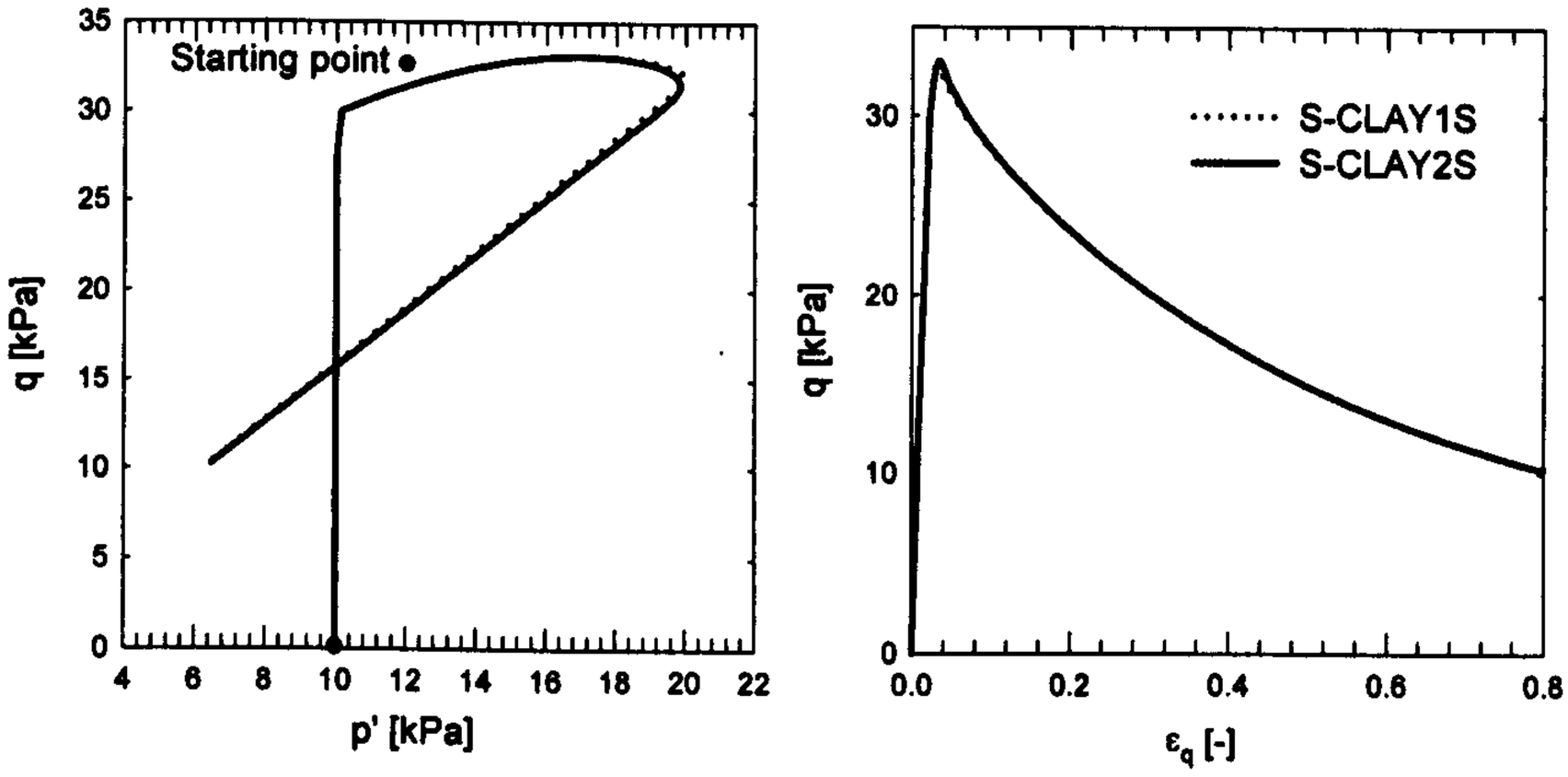

Figure 5.23: Simulation of undrained compression test: starting point η=0

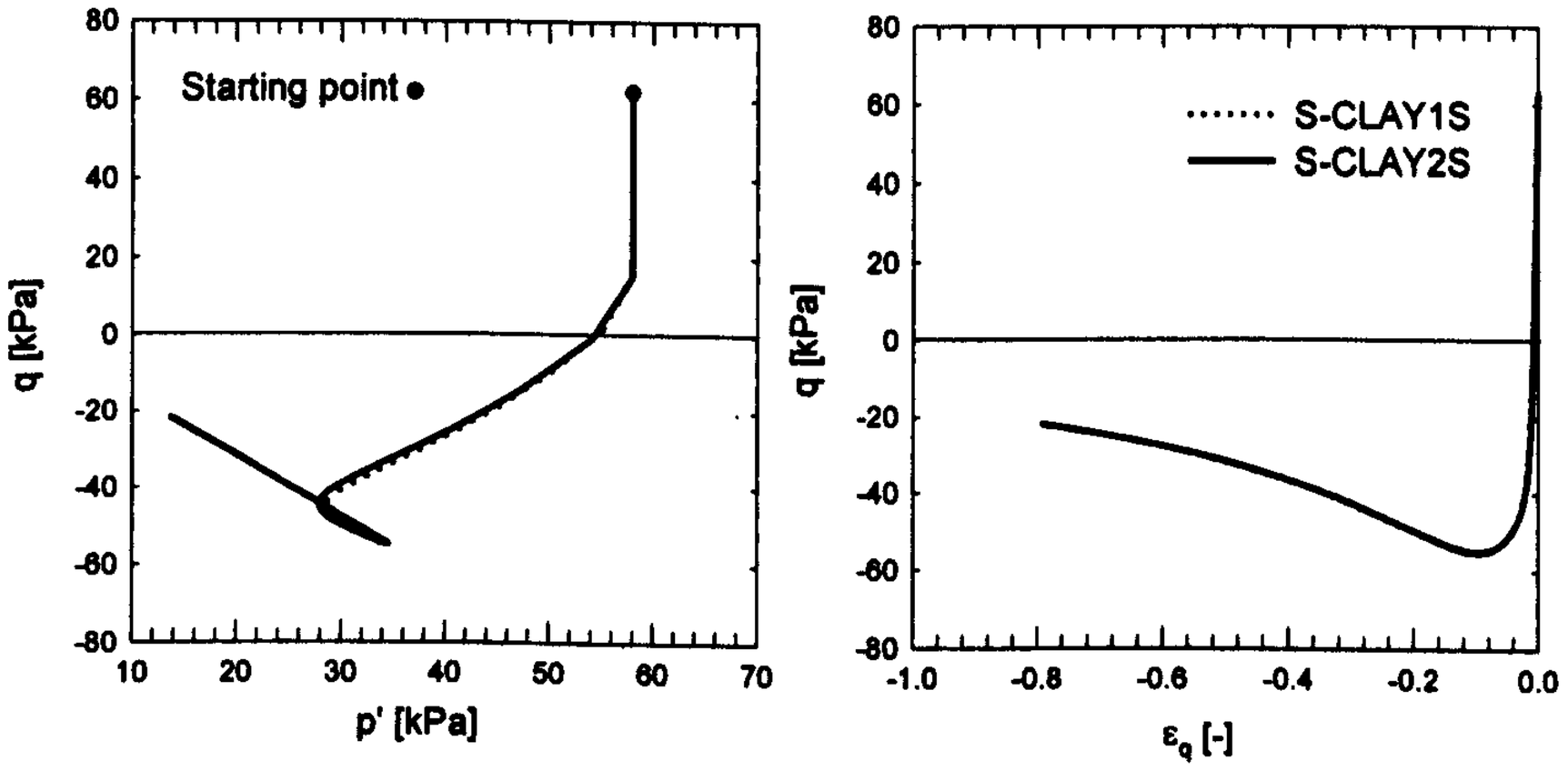

Figure 5.24: Simulation of undrained extension test: starting point η_{K0}

S-CLAY2S showing a narrower bend towards the critical state line. The same can be observed in the q-ε_q plot as both models reach the peak strength. Overall the predictions by both models are very similar.

In Figure 5.24 simulations of an undrained triaxial extension test are presented. Overall the pattern of the model predictions are similar. First an elastic unloading path is

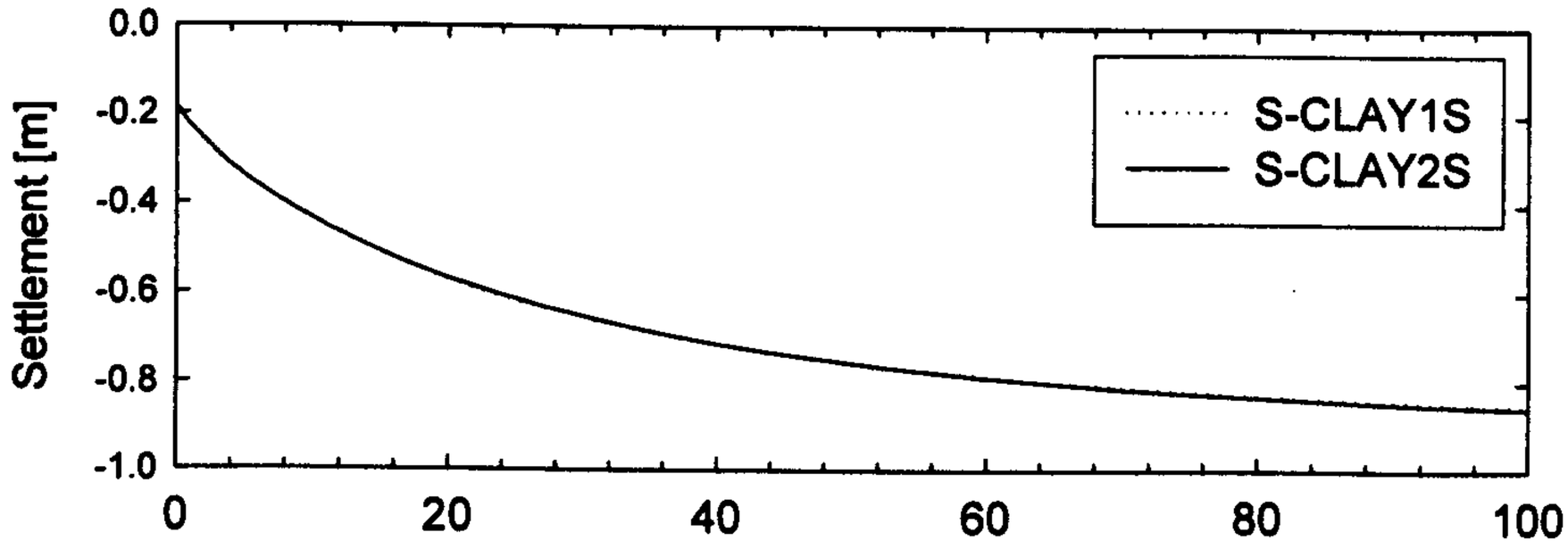

Figure 5.25: Time settlement curve

observed by both models as expected. As the stress path reaches the yield curve the two curves start diverging. The S-CLAY2S predicts marginally lower p' values than the S-CLAY1S. As both models reach a stress ratio close to M, the p' values increase again due to the continuous rotation of the natural yield surface towards its target values. After completion of the rotation, unloading (softening) is predicted by both models at the critical state stress ratio M. The same can by concluded by inspection of the q-ε_q plot.

5.3.6 Simulation of an embankment

The effect of the conditional plastic potential on the predicted settlements is studied in a simple embankment problem. The geometry and the soil layers below the embankment are the same as presented in Chapter 4. Both models use a step size of -0.01.

5.3.6.1 Vertical displacements

The predicted time settlement curves by the two models are presented in Figure 5.25. The difference in the predicted maximum displacement at a point at the centre line of the embankment is in the order of millimeters. Implementation of the non-associated flow rule does not increase the predicted settlement.

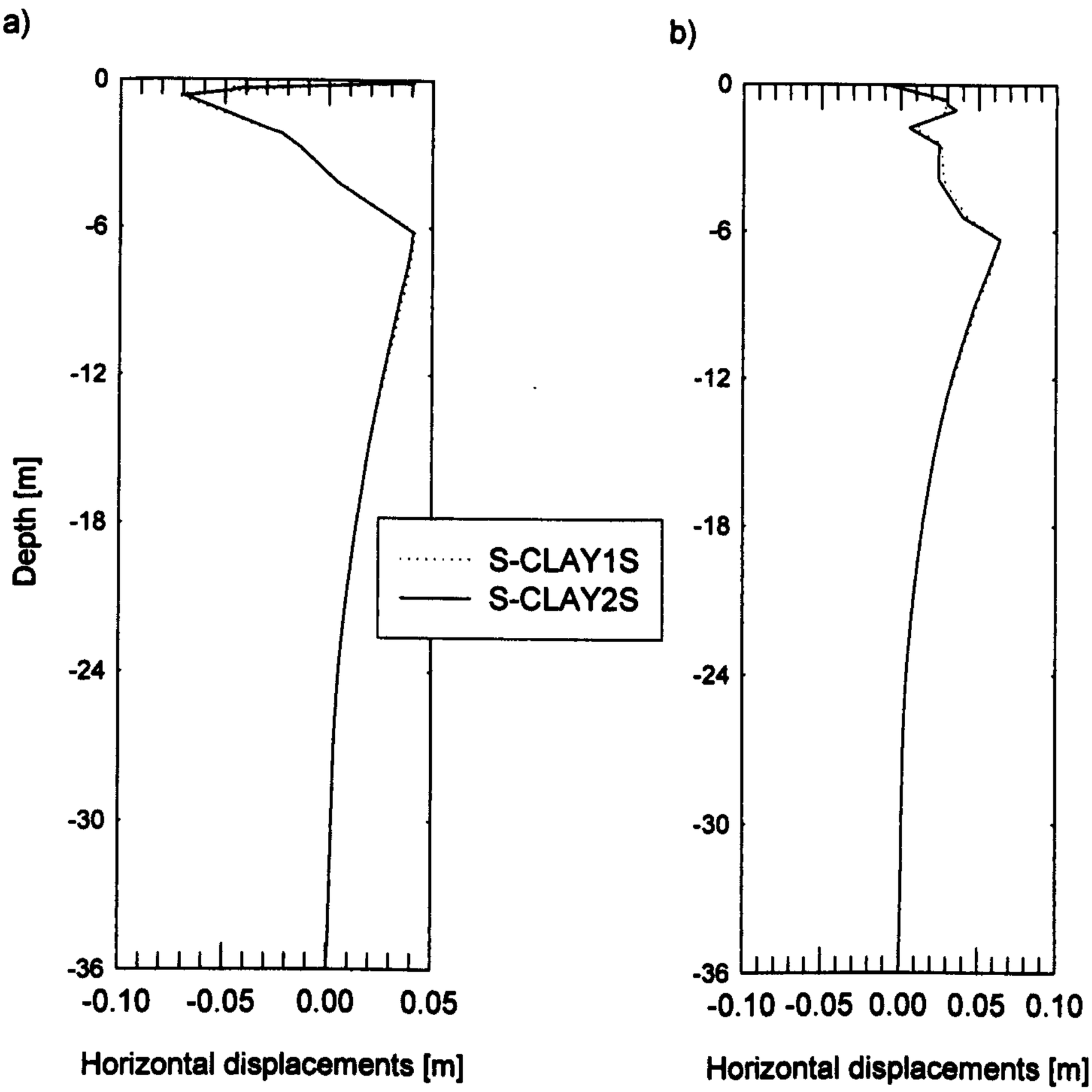

Figure 5.26: Horizontal displacements after 100 years of consolidation: a) below the crest and b) below the toe of the embankment

5.3.6.2 Horizontal displacements

The horizontal displacement profile with depth after construction is not presented but it can be concluded that the S-CLAY2S predicts the same maximum displacement in the order of 1.0 cm as the S-CLAY1S. In Figure 5.26a the horizontal displacements after 100 years of consolidation below the crest and in Figure 5.26b below the toe are presented. Below the crest both models predict the maximum at a depth of -6.2 m. S-CLAY2S estimates marginally lower displacements than S-CLAY1S which are hardly noticable in the graphs. Close to the surface both models predict the same negative horizontal movements due to the large vertical settlements. The maximum below the toe of the embankment is predicted at the same depth. Again S-CLAY2S estimates

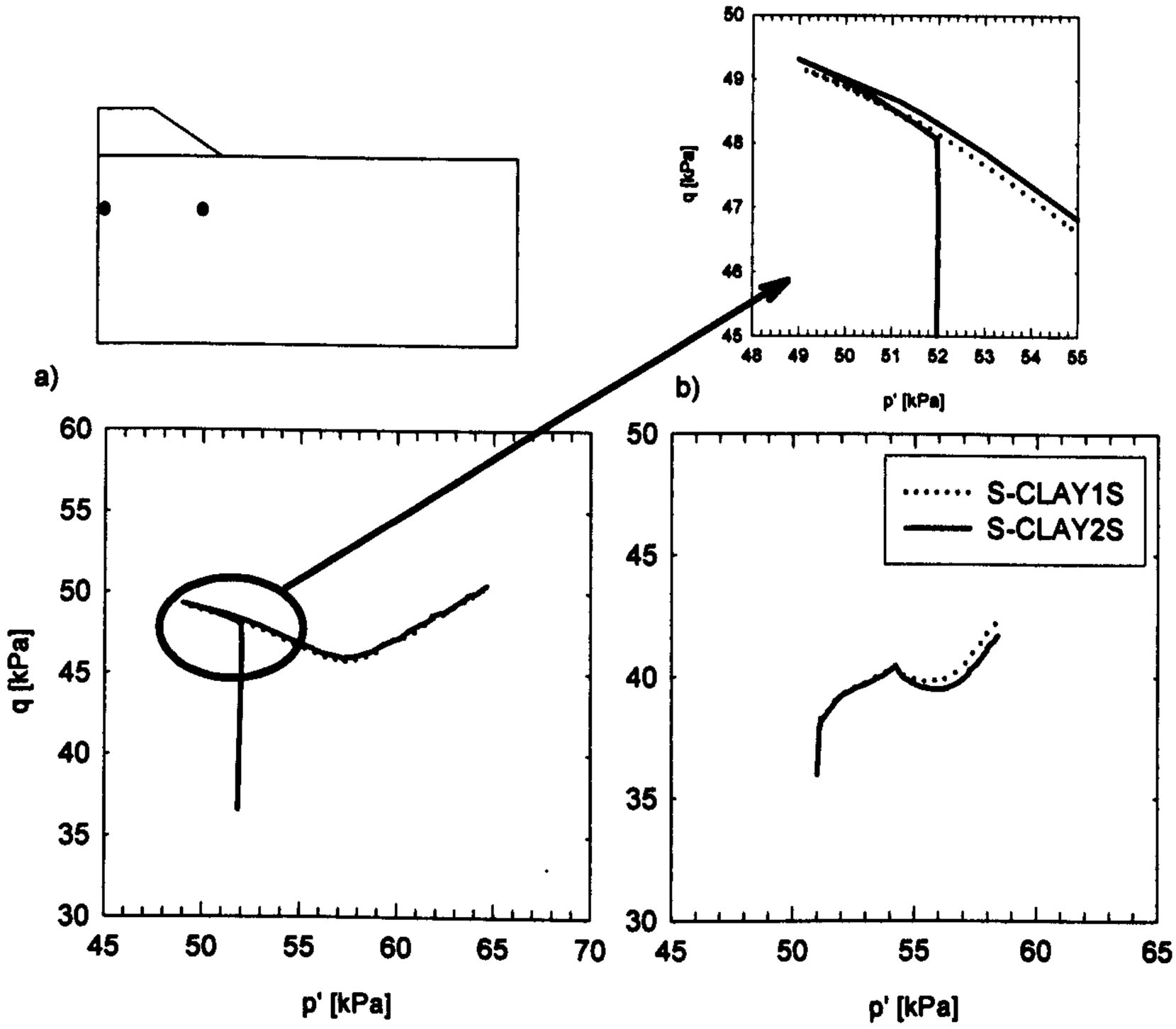

Figure 5.27: Selected stress path: a) x=0.2m y=-11.3m b) x=14.3m y=-11.0m

overall marginally smaller horizontal displacements with depth than the S-CLAY1S model.

5.3.6.3 Stress path

For comparing predictions by different constitutive models the stress paths are an informative tool. Two selected points are considered in the subsoil. A point at a depth of 11.3 m next to the symmetry line of the embankment (Figure 5.27a) and a point almost at the same depth under the toe of the embankment (x=14.3m, y=-11.0m; Figure 5.27b).

The stress paths reflect the evolution of the effective stress during the undrained construction stage of the embankment and the 100 years of consolidation. For the point at the centre line both models predict initially elastic behaviour, with a constant p' value, until some point during construction at which the soil is predicted to yield. As both

models assume the same yield surface prior to yielding, both predict yielding at the same point. As yielding continues during undrained loading the stress paths marginally diverge due to differing anti-clockwise rotation of the yield surface predicted by both models (see scaled stress path). At the beginning of consolidation the stress paths change direction towards a stress ratio η close to the normally consolidated stress ratio η_{K0}. From that point onwards both models follow almost the same stress gradient to the end of the consolidation in combination with some rotation of the yield surface.

At the same depth (of around 11m) underneath the toe of the embankment the stress pattern is different to the stress path predicted at the centre line. The difference can be attributed to the rotation of the principal stresses which is not observed for points next to the centreline of the embankment. At the end of the consolidation both models again predict a stress ratio close to η_{K0}. Before yielding on the wet side of the critical state line both follow an elastic stress path with constant p'. After yielding both paths slightly diverge.

5.3.6.4 Development of the fabric scalar α and state variable x with time

The fabric scalar α versus time for a point at a depth of 9.4m next to the centre line of the embankment is plotted in Figure 5.28a. The scalar does not represent the true rotation of the yield surface but was chosen for illustration purposes instead of the four non-zero components of the fabric tensor. During undrained loading (time =0) the α value marginally increases before it steadily increases with consolidation time up to a maximum value. The S-CLAY2S predicts marginally greater clockwise rotation of the yield surface than the S-CLAY1S model. The bonding parameter x versus time is plotted in Figure 5.28b. The x parameter gradually decreases with time from its initial value of around 12 to a lower value of 7.6. The bonds are continuously destroyed with consolidation time. Both models predict similar behaviour.

In Figure 5.28c the fabric scalar α is plotted versus time for a point at a depth of 11.0m and a distance of 14.3m from the symmetry axis of the embankment. During

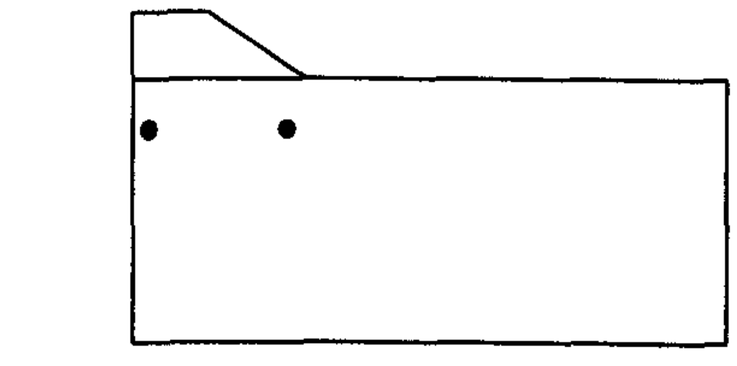

a)

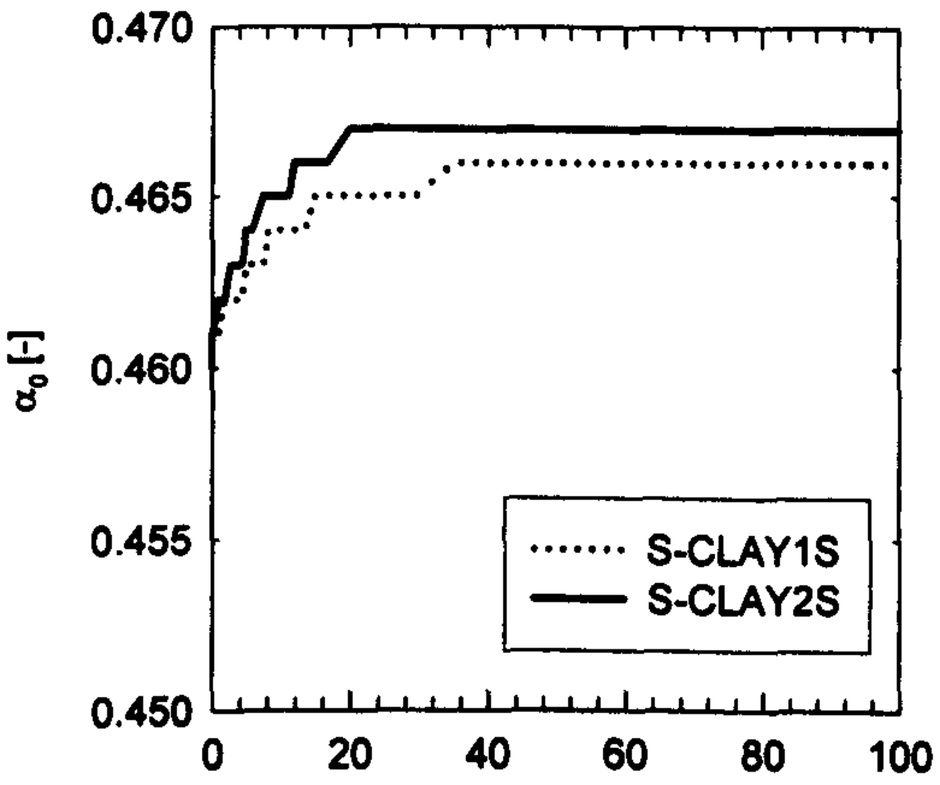

b)

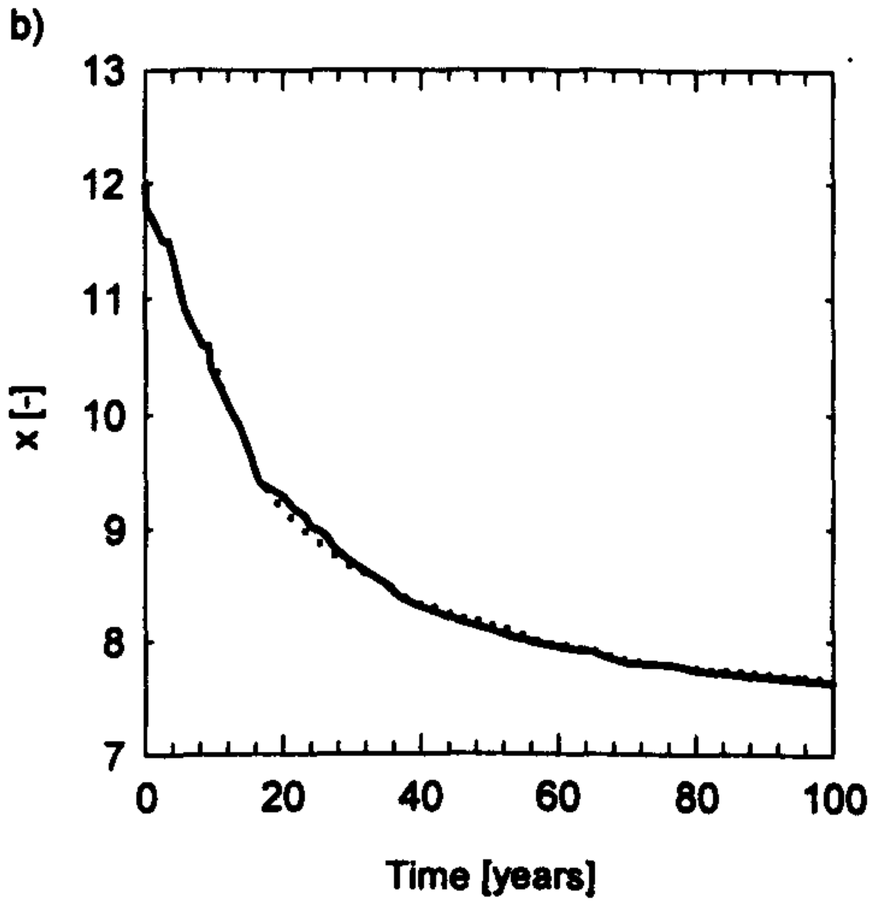

c)

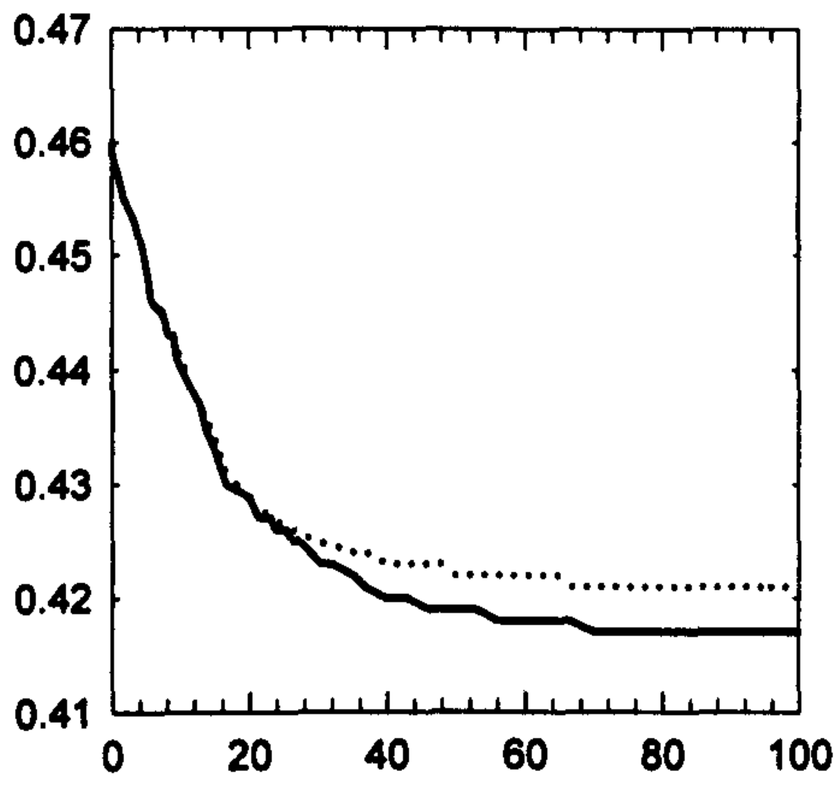

d)

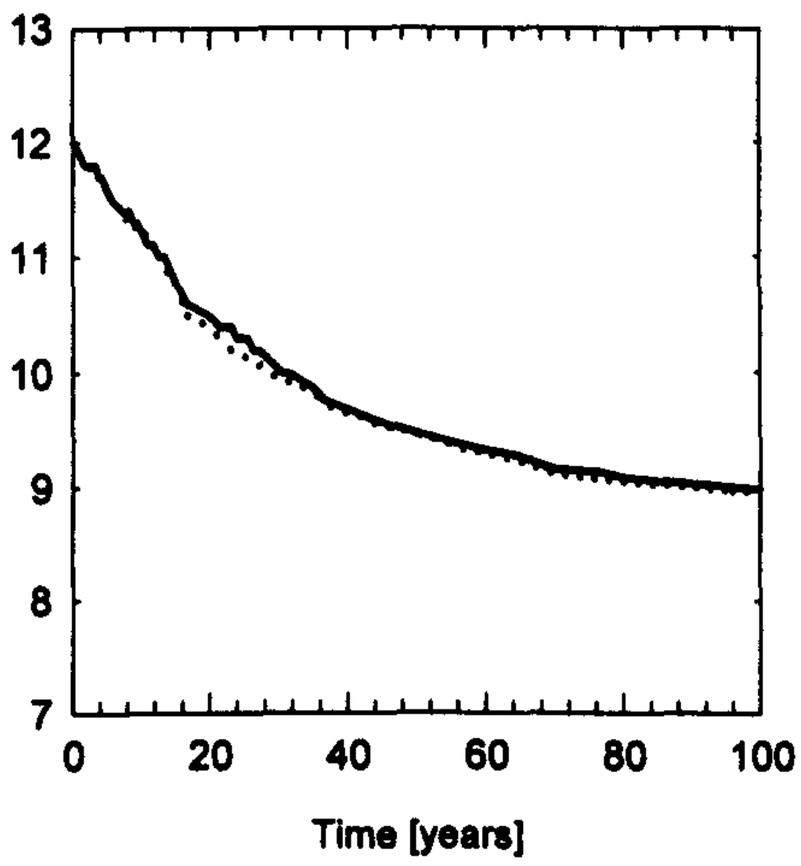

Figure 5.28: State variable α and x versus time: a and b) x=0.2m y=-9.4m c and d) x=11.4m y=-9.3m

the undrained loading (time=0) no rotation is observed by both models which is a sign that the soil element is not yielding. With consolidation both models predict a decrease in the α value with time (clockwise rotation of yield surface in p'-q plane). The S-CLAY2S predicts a bigger decrease with time than the S-CLAY1S. In Figure 5.28d the bonding parameter x versus time is plotted for the same point. A decrease of x with time is observed by both models. The x reduces from an initial 12 to 8.9.

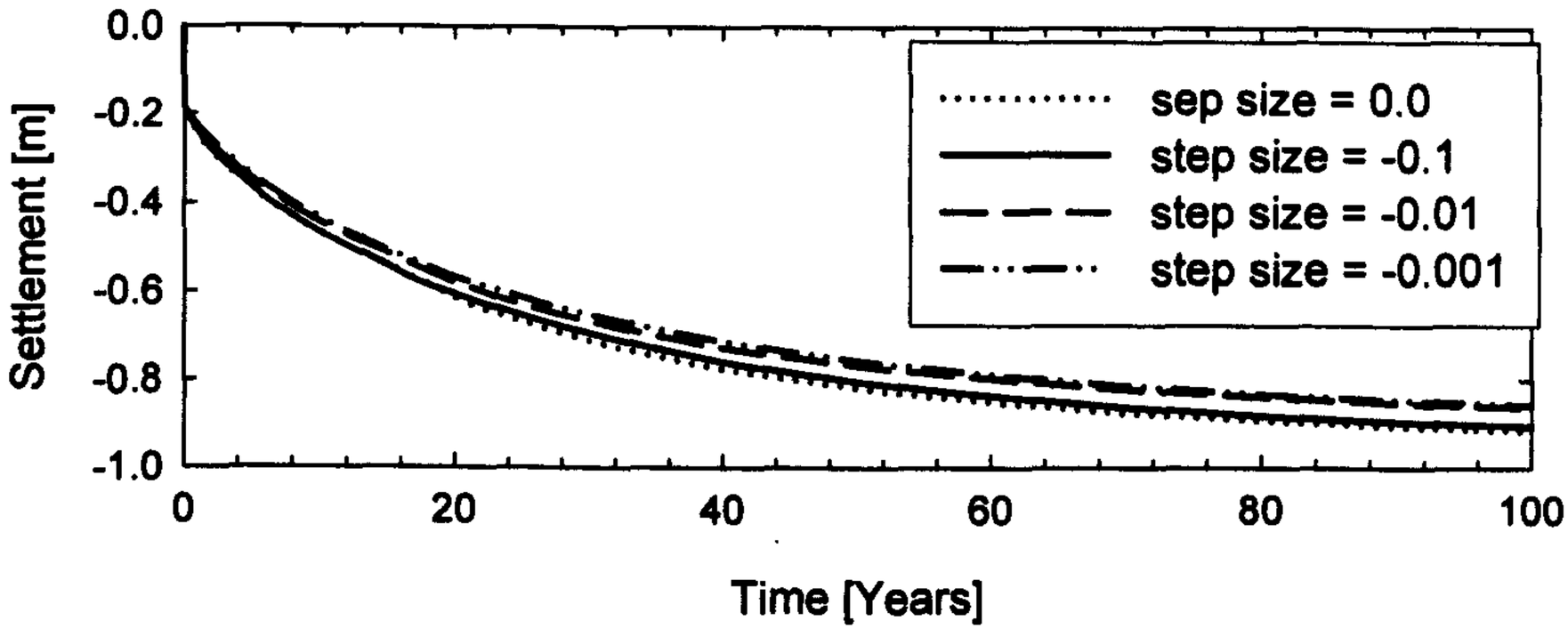

Figure 5.29: Influence of the step size on the time settlement curve

5.3.6.5 The influence of the step size on the predicted behaviour

The influence of the step size on the predicted time settlement behaviour is presented in Figure 5.29. It is clearly demonstrated that the step size is an important variable and has an influence on the predicted settlements. A smaller step size decreases the predicted settlements.

The influence of the step size on the predicted stress path is shown in Figure 5.30. Stress paths are very sensitive to the step size used. A large step size such as 0.0 or -0.1 introduces a large inaccuracy into the predicted stress path as demonstrated in the p'-q plot. Large strain increments cause the yield surface to rotated unevenly. A very smooth stress path and smooth rotation of the yield surface towards a stress ratio η_{K0} is achieved with a stress ratio of -0.001.

The step size directly influences the runtime of the simulations. The runtime for each step size is shown in Table 5.6. The runtime becomes very large in the order of 2 hours for a simple embankment problem with a very small step size.

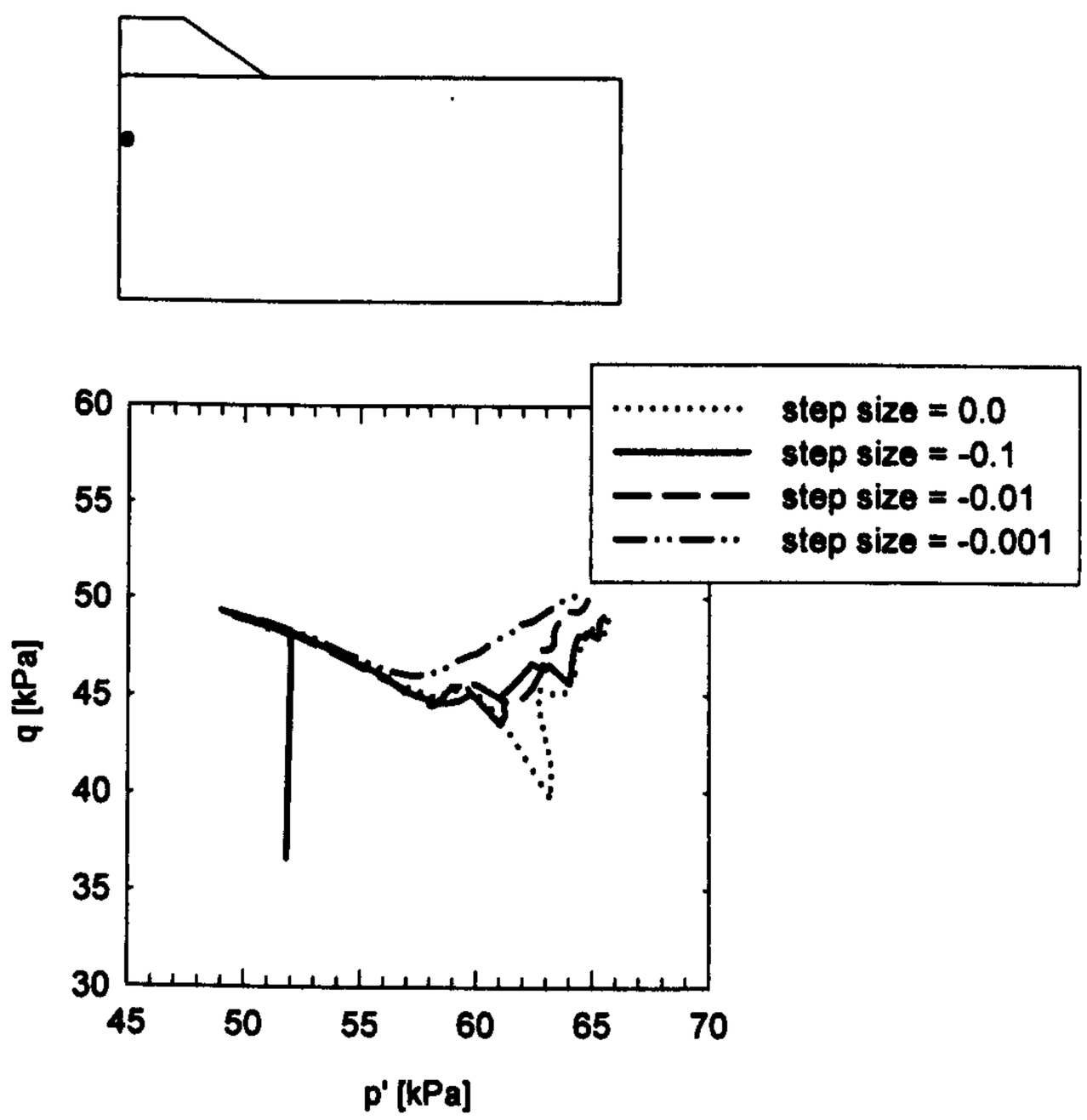

Figure 5.30: Influence of the step size on the predicted stress path

Table 5.6: Influence of stepsize on the runtime of the analysis

stepsize	runtime
0.0	8 min
-0.1	10 min
-0.01	20 min
-0.001	120 min

5.3.7 Critical review of the S-CLAY2S

The S-CLAY2S model is a simple extension of the S-CLAY1S. The aim was to introduce a non-associated flow rule without introducing further parameters or increasing complexity. A conditional plastic potential with stress ratio dependency is implemented with limitations to avoid numerical instability during simulations. Back calculation of drained multistage triaxial tests showed to some extent improvement in the prediction of the deviatoric strains ε_q compared to the S-CLAY1S model. The difference is less pronouced in the results of the simulations of undrained tests in compression and extension.

Numerical simulations of an embankment constructed on soft clay with the S-CLAY1S and S-CLAY2S models were presented. The results showed that for the embankment considered the predicted S-CLAY2S displacements with time are the same as with S-CLAY1S. Inspection of the stress path highlighted some numerical instabilities if the load increment is too big at the beginning of the calculation step when a large stepsize is used. By limiting the load increment and the maximum step size these instabilities are overcome.

Chapter 6

Murro test embankment

This Chapter investigates the influence of anisotropy and destructuration on the predicted behaviour of the Murro test embankment. The embankment has been monitored for 14 years. The construction and consolidation of the test embankment is modelled with a plane strain finite element analysis. The results of the observations are compared to the predictions of the simulations. Furthermore, the effect of bonding and destructuration on the measured undrained strength profile with depth is investigated. In the last part of the chapter the influence of Possion's ratio and the μ value on the predicted settlement behaviour is explored. Equations are proposed to estimate Poisson's ratio and the μ value based on the stress history of the soil.

6.1 Introduction and background

In 1993 the Finnish Road Administration commissioned the construction of the Murro test embankment near the town of Seinäjoki in Western Finland. Seinäjoki is close to the coast along the Gulf of Bothnia and lies between the city of Vaasa and Jyväskylä. The aim of the project was to use the information collected through site investigations, laboratory testing and measurement towards the design of new roads (e.g. Highway 18, which connects the city of Vaasa at the coast along the Gulf of Bothnia and Jyväskylä), upgrade and maintenance of roads built on soft soils in Finland. The

Figure 6.1: Murro test embankment

project was part of the Finnish Road Structures Research Programme (TPPT) (Koskinen et al. 2002b).

The test embankment is founded on a 23 m deep soft clay deposit, the so-called Murro clay deposit. Murro clay is a relatively homogeneous silty clay with a reported average undrained shear strength of less than 30 kPa (Koskinen and Karstunen, 2006). The clay is overlain by a thin dry crust. Below the soft clay there is a layer of moraine. Typically the deposits found along the coast of the Gulf of Bothnia consist of young post glacial sediments with a high organic and sulphur content. The sulphur content gives the clay a special odour and its dark black colour (Koskinen and Karstunen, 2006). The silty clays or clayey silts were sedimented in the brackish water of the Littorina Sea (Schwab, 1976). This occurred around 7000 years ago during one of the latest postglacial evolution stages of the Baltic Sea. It explains why the deposit is characterised as relatively young and typically normally consolidated. In this century the estimated isostatic uplift rate in the area of the Gulf of Bothnia is still about 1 m per century. The ground level at Murro is 37.5 m above mean sea level. The groundwater table is estimated to be at 0.8 m below ground level.

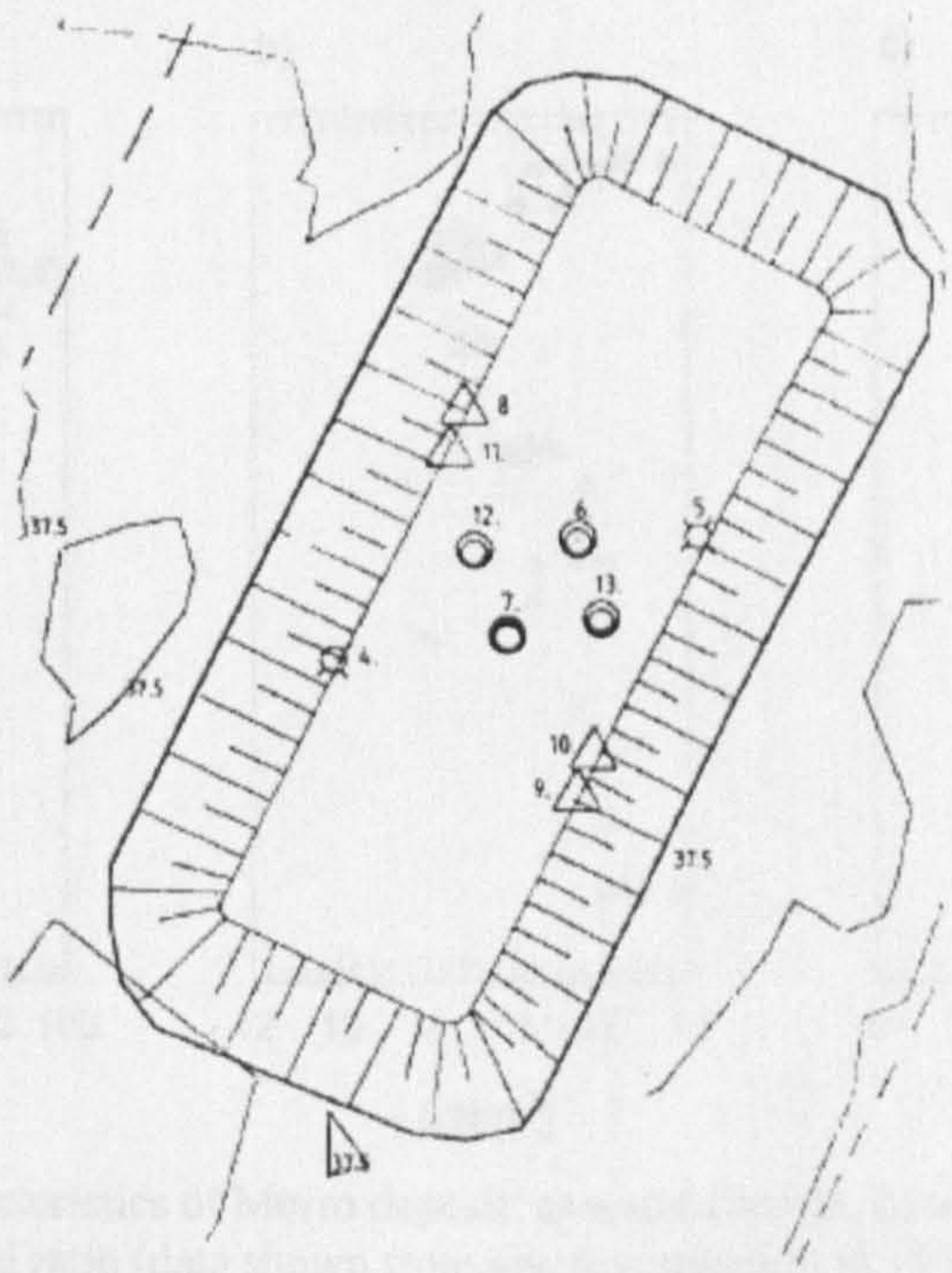

Figure 6.2: Plan view: Location of boreholes (Selkämaa, 1994)

6.2 Site and laboratory investigation

In 1993, prior to construction, the first site investigation was carried out as a routine site investigation to assess the suitability of the site itself for the construction of the proposed test embankment. This was followed by a more thorough site investigation. The field tests included Swedish weight sound testing, CPTU testing (cone penetration testing with pore water pressure), field vane testing and static dynamic penetration testing (method developed in Finland that combines piezocone testing in cohesive soils with dynamic testing in non-cohesive soils). During further soil sampling a number of undisturbed and disturbed samples were taken from boreholes (see Figure 6.2 for location of boreholes) and tested at the laboratory of soil mechanics and foundation engineering at the Helsinki University of Technology (HUT). The laboratory testing included oedometer tests, drained triaxial tests and undrained triaxial tests on undisturbed samples and various index tests. Some properties of Murro clay meas-

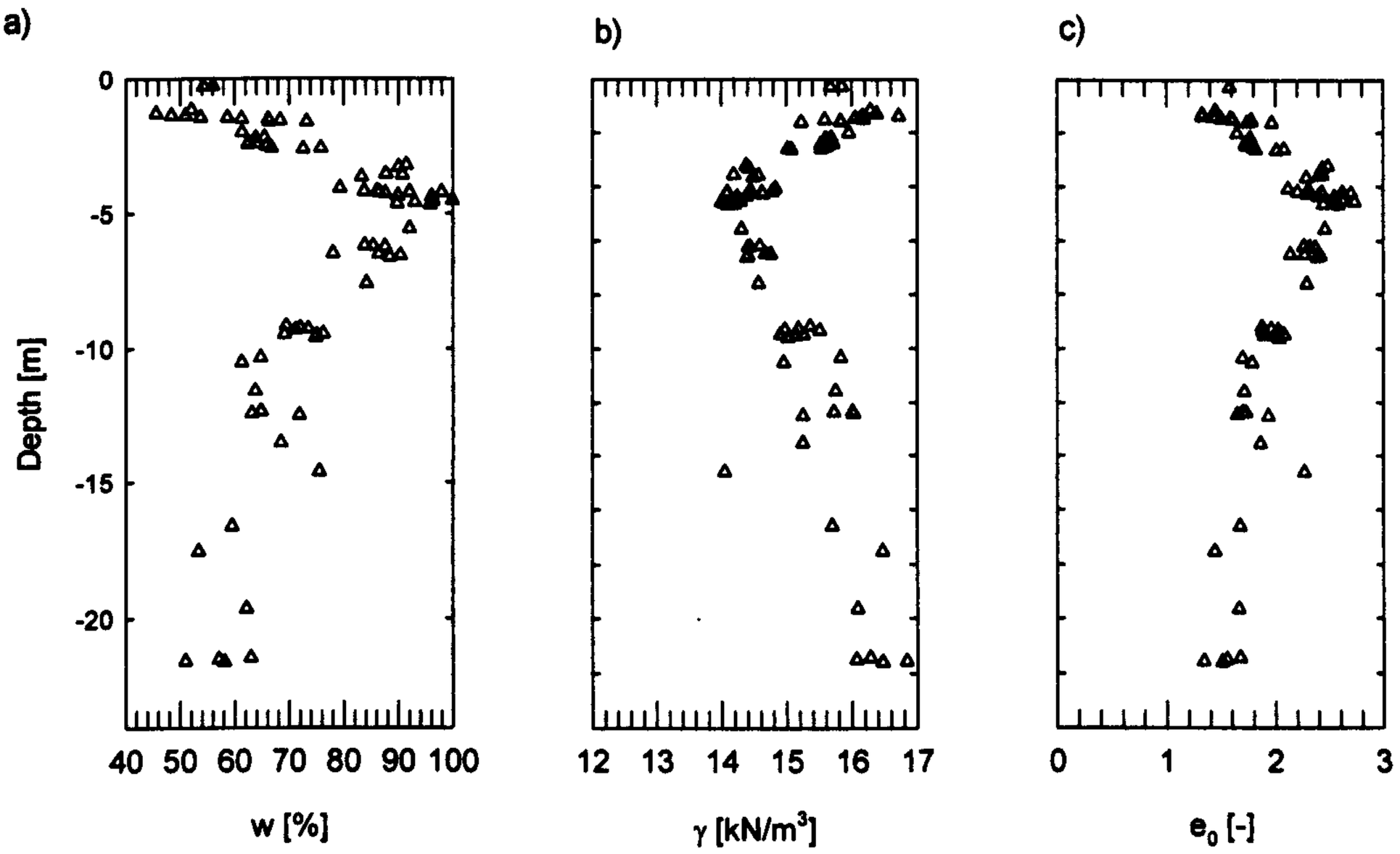

Figure 6.3: Typical characteristics of Murro deposit: a) water content, b) unit weight, and c) initial void ratio (data shown from site investigation in 1993)

ured prior to construction are shown in Figure 6.3. The water content of the soil varies between 50 and 100 %. The maximum water content is found at a depth of about -5 m and decreases with depth. A high water content at shallow depths and a decrease of the water content with depth is typical for soft Finnish clays (Karstunen, 2007). The unit weight γ varies between 15 and 17 kN/m^3. The estimated initial void ratio increases from the ground surface (e_0 in the order of 1.4) to a maximum of about 2.6 at a depth of -5m. Below -5 m the void ratio decreases and reaches a lower limit of about 1.3 to 1.5 at a depth of -22 m.

Eight years after construction of the embankment, in 2001 an additional site investigation was undertaken. The site investigation consisted of field vane tests below the embankment to estimate the increase in undrained shear strength with time due to consolidation of the subsoil. Also sampling below the embankment and in the vicinity of the embankment was performed (Koskinen et al. 2003c). The samples next to the embankment were taken to investigate the effect of the structure of the Murro clay. The investigation comprised oedometer testing and multi-stage triaxial tests of natural

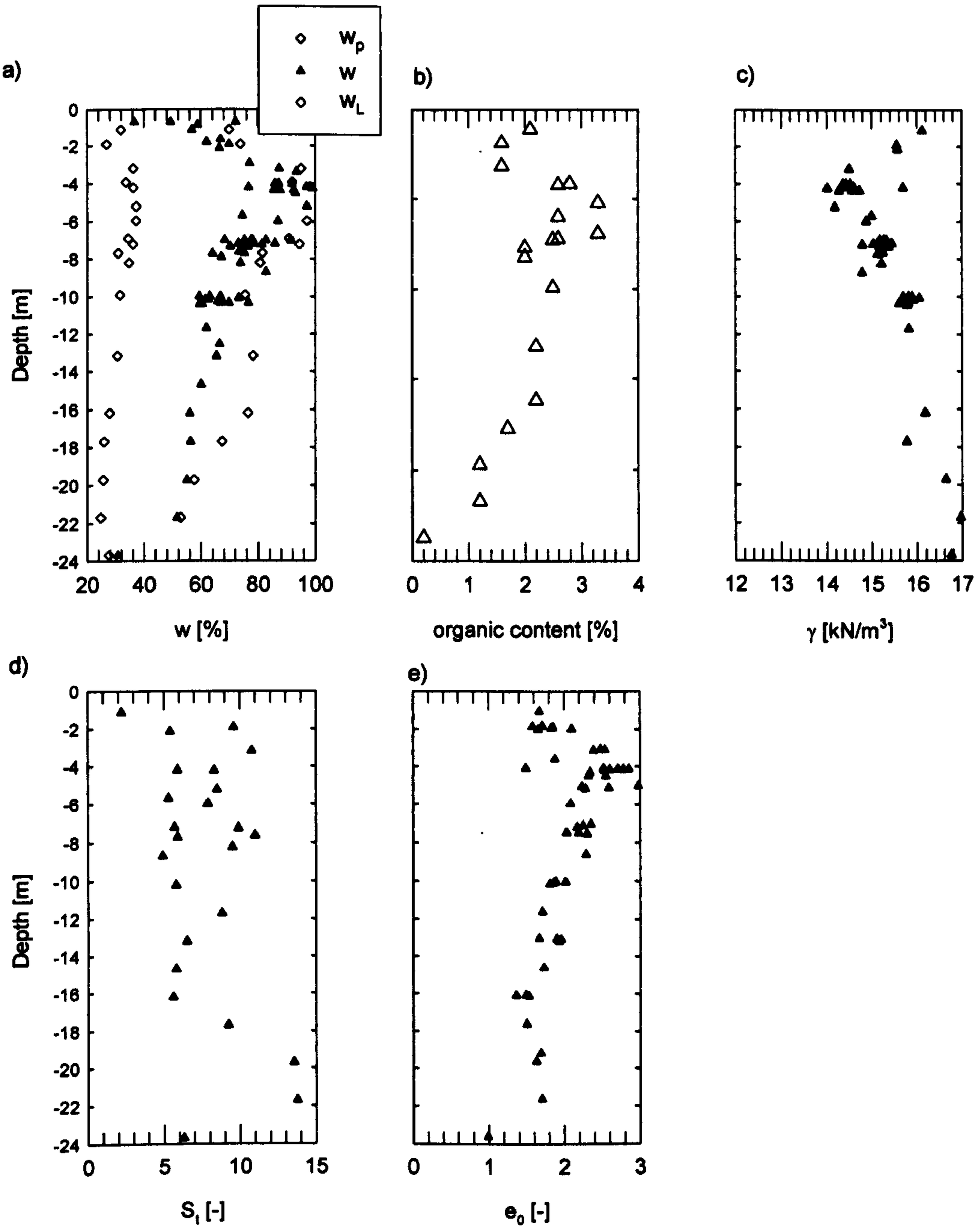

Figure 6.4: Typical characteristics of Murro deposit: a) water content, liquid and plastic limit, b) organic content, c) unit weight, d) sensitivity, and e) initial void ratio (data shown from site investigation in 2001)

and reconstituted samples (Karstunen and Koskinen, 2004; Koskinen and Karstunen, 2004). A mineralogical study in 2003 by ETH Zurich (Messerklinger et al. 2003) made it possible to identify the main minerals of the clay. It was found that Murro clay consists of 26% quarz, 46% feldspar with the clay minerals as illite (15%), choride (10%), and kaolinite (5%). The index properties from the site investigation in

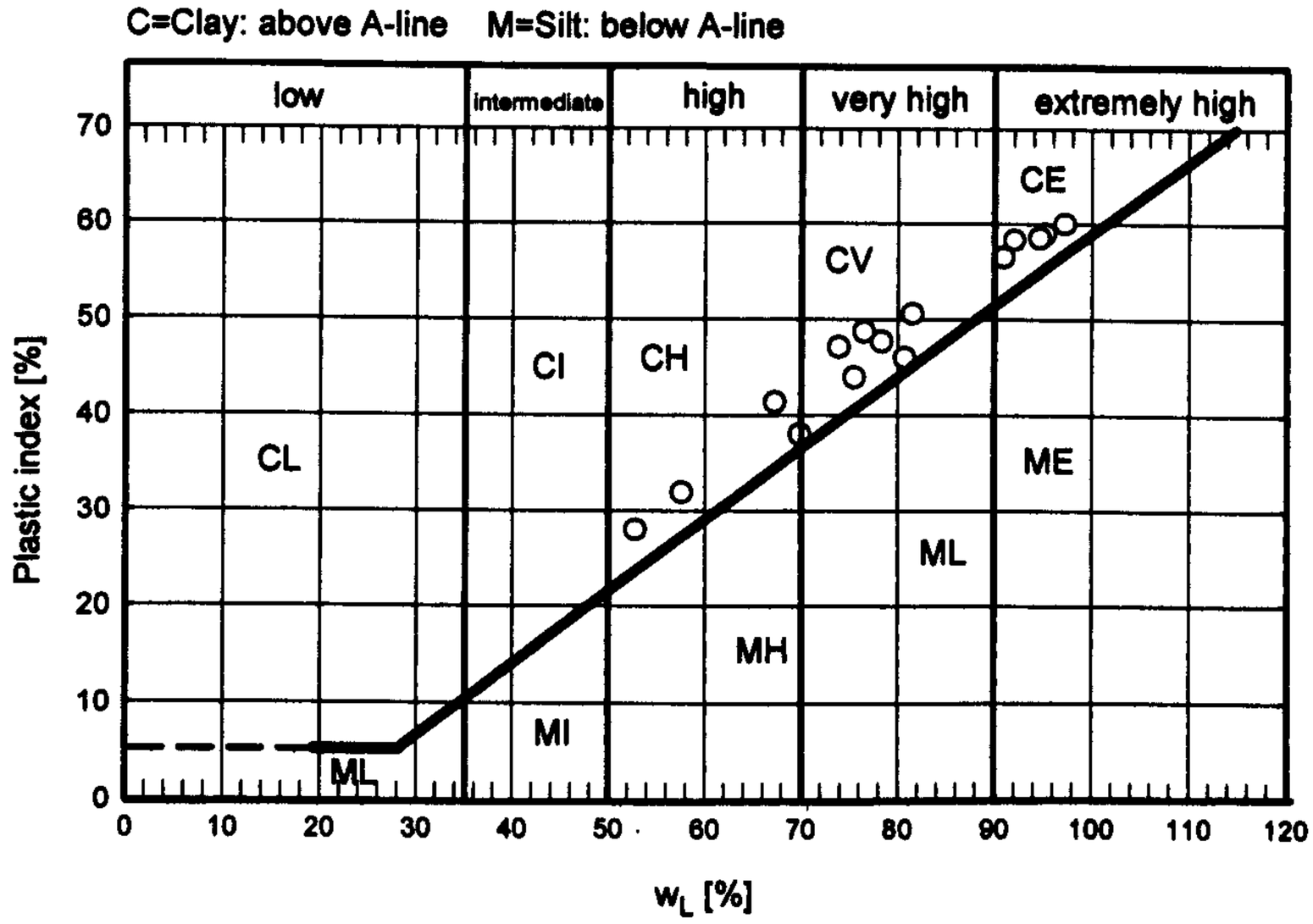

Figure 6.5: Plasticity chart for the Murro deposit

2001 are presented in Figure 6.4. The properties at shallow depths (up to -12 m) are taken from boreholes next to the embankment and the properties in the deeper areas are taken from boreholes below the embankment. To be able to present the properties in a single profile with depth (Figure 6.4) it is assumed that the properties in the deeper areas are not affected by the consolidation of the soil below the embankment.

The plastic limit of the deposit varies between 20 and 30 %. As mentioned before the water content varies with depth and is close to the liquid limit. The organic content varies between 2 to 4 % up to a depth of 15 m and decreases thereafter virtually linearly with depth to a minimum of less than 1 % at a depth of 23 m. The measured sensitivity of the Murro clay is moderate and is typically between 2 and 10 (Koskinen et al. 2002c).

In Figure 6.5 the Plasticity chart for the classification of fine soils is presented. Inspection of the chart shows that all points determined from different layers of the deposit plot above the A-line. The samples from a depth of -3.7 m to -6.0 m are characterised as extremely plastic and the rest between high and very high. Calculation of the Activity of the soil, which is defined as the degree of plasticity of the clay fraction

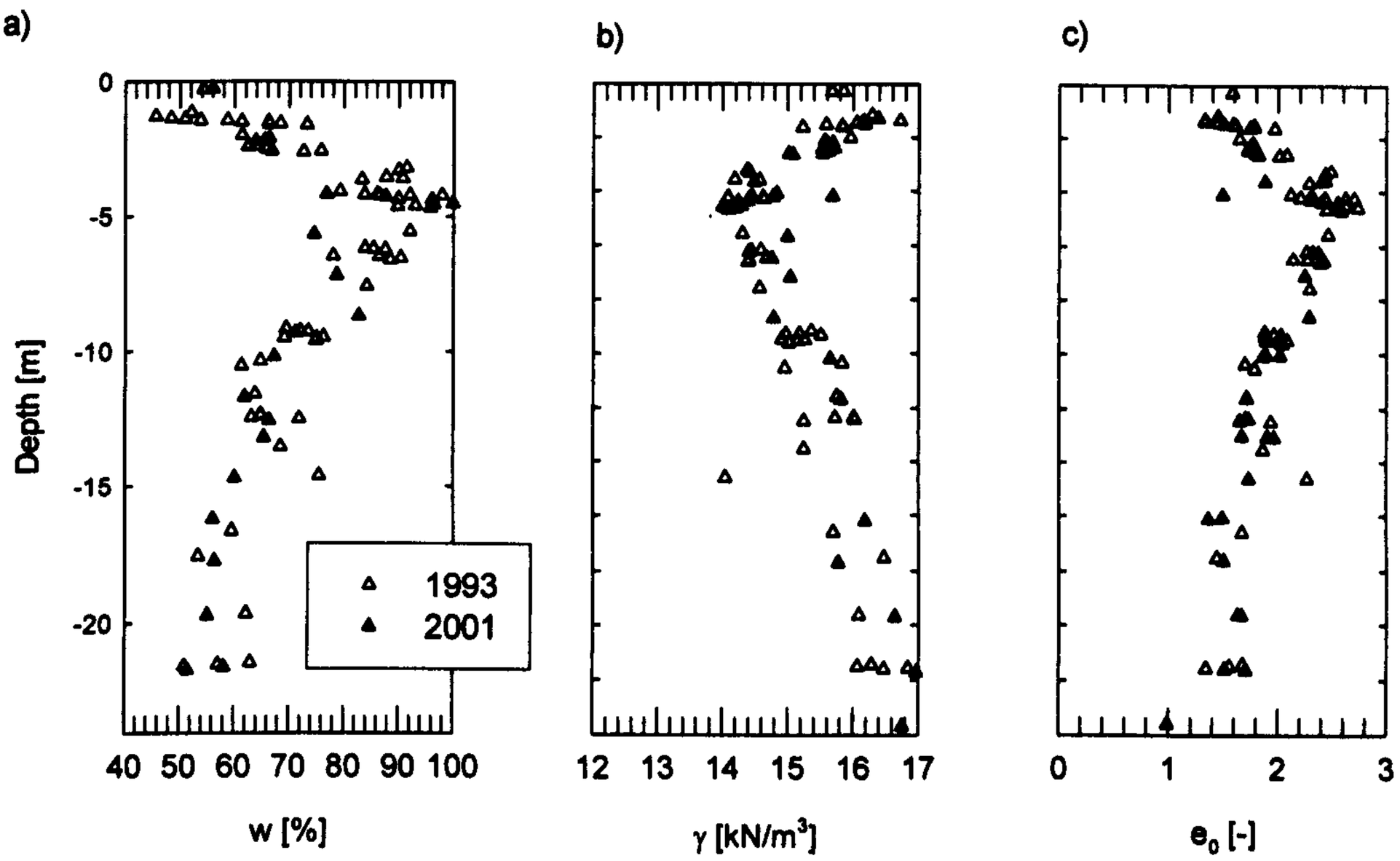

Figure 6.6: Comparison of characteristic of Murro deposit 1993 and 2001: a) water content, b) unit weight, and c) initial void ratio (data shown from site investigation in 1993 and 2001)

(Ip/clay content), showed that the Activity is greater than 1.25. Values greater than 1.25 are typical for organic estuarine clays (Whitlow, 1995). The liquidity index I_L was estimated between 0.6 to 0.95 which proves that the clay is in its plastic state.

In Figure 6.6 the properties established in 1993 prior to construction are compared to the properties derived in 2001 from the boreholes through the embankment. It is clearly shown in the water content chart that the water content in a depth of about -4 m to -7 m decreased in the order of 20% to 30%. Areas deeper than -7m do not show a visible change in water content. Also a change in the unit weight at shallow depths can be observed. A decrease in the water content is reflected in an increase in measured unit weight. The measured settlements at the ground surface below the embankment in 2001 was about 70 to 80 cm (Koskinen et al. 2002c). As a consequence part of the dry crust will be submerged under ground water. The compression of the shallow soft soil layers below the dry crust can be seen in the apparent change of the current void ratio in the shallow areas. The void ratio decreased from about 2 to 3 to less than 2.

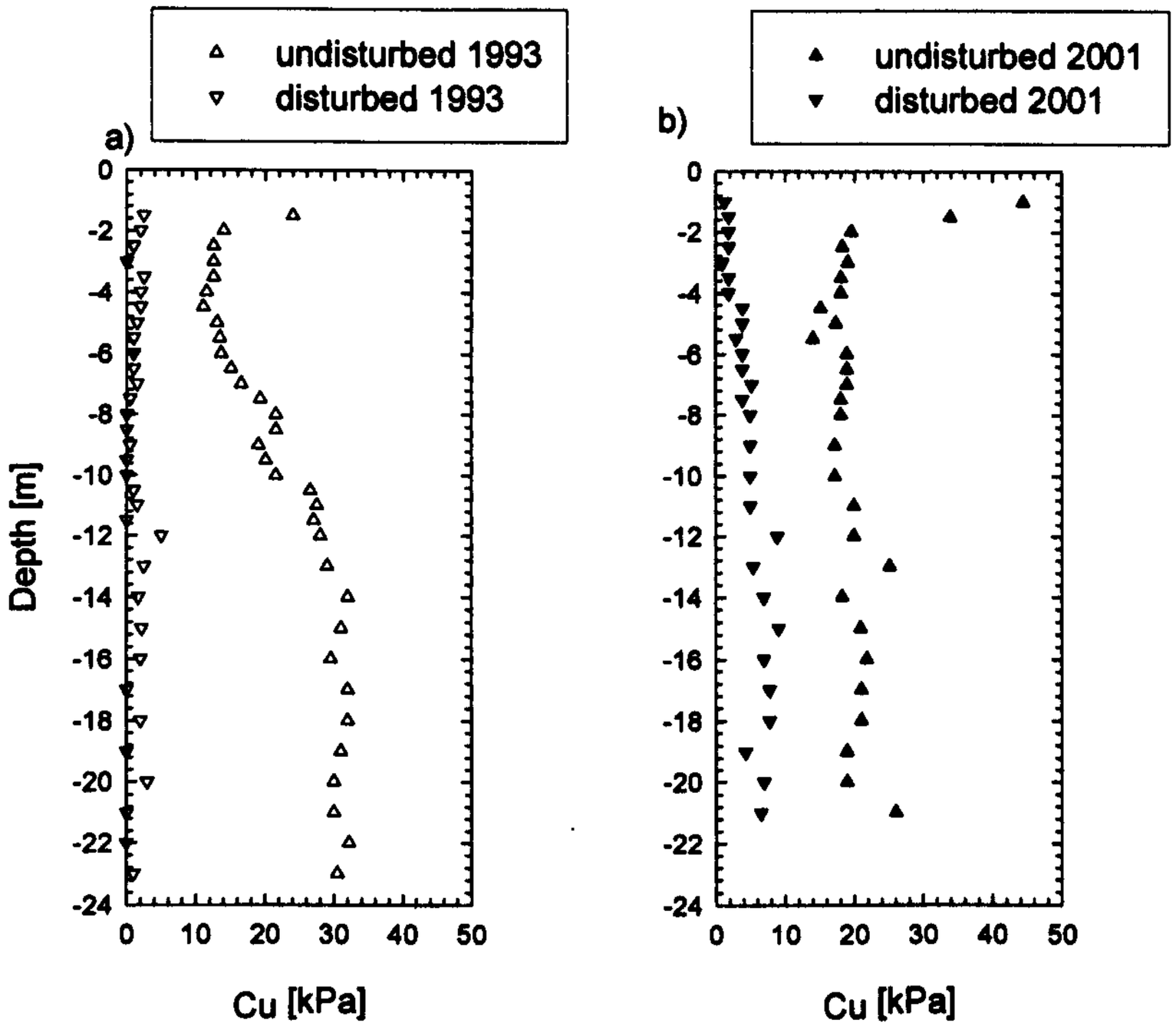

Figure 6.7: Field vane test results: a) 1993 prior construction and b) 2001 eight years after construction (in soil below embankment)

The measured undrained shear strength profile with depth prior to construction is shown in Figure 6.7a. The results of the field vane test show an undisturbed undrained strength (natural strength) in the order of 12 kPa for the 5 m thick layer underneath the dry crust. Further down, a linear increase of the strength to a maximum of 30 kPa at a depth of -15 m is shown. From -15 m to the bottom of the soft clay layer at -23 m the strength is virtually constant. The disturbed strength (remoulded strength) is almost constant to a depth of -12 m and slightly increases thereafter to an average of about 7 kPa. The results of the field vane test carried out in 2001 (eight years after construction, Figure 6.7b) showed that the disturbed strength increased over the whole depth of the deposit. The undisturbed strength of the softest layers increased from 12 kPa to 18 kPa. However, the undisturbed strength below the soft layers seemed to have decreased to 20 kPa from an initial value of about 30 kPa in 1993. This is in contrast to the common assumption that there is an increase in undrained shear strength with consolidation time.

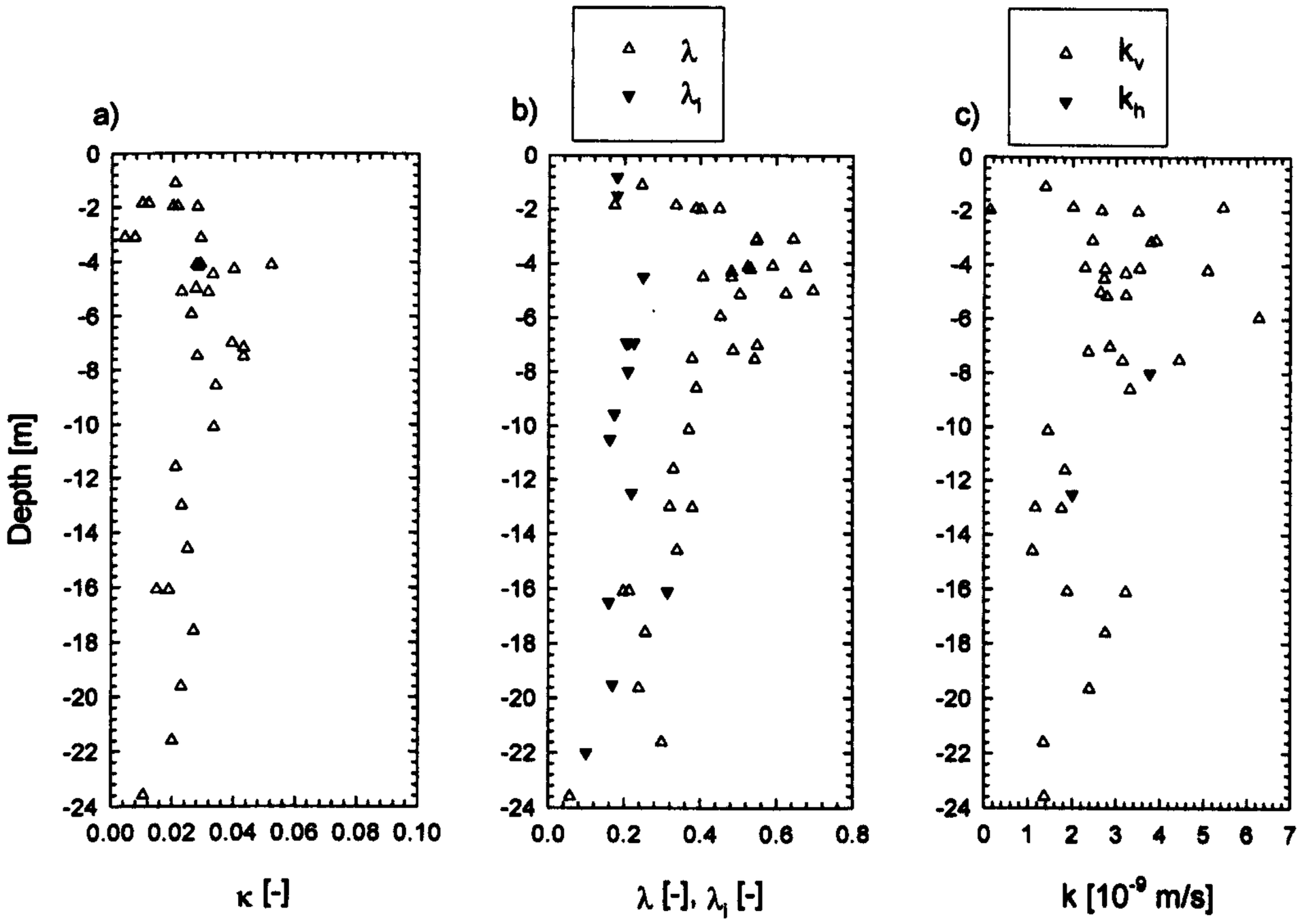

Figure 6.8: Parameters for Murro clay: a) slope of the elastic swelling line κ, b) gradient of normal compression line λ of natural soil and gradient of intrinsic compression line λ_i of reconstituted soils and c) horizontal and vertical permeability (k_h and k_v)

Stiffness parameters and permeability coefficients with depth derived from standard and constant rate strain (CRS) oedometers are shown in Figure 6.8. The distribution of κ (slope of elastic swelling line) with depth is presented in Figure 6.8a. The slope of the natural normal compression line λ and the slope of the intrinsic normal compression line λ_i are shown Figure 6.8b. λ_i is derived from oedometer tests on reconstituted samples. The λ shows a big scatter in the shallow areas which could be due to sample disturbance. Further inspection of the graph shows that the λ values are visibly decreasing with depth. However, the most compressible layers are at a depths of -1.6 m to -7 m. In contrast the estimated λ_i values are fairly constant with depth. There is no constant ratio observed between λ and λ_i as is very often assumed. The estimated permeability values k with depth are shown in Figure 6.8c. The vertical permeability k_v was estimated based on oedometer tests on vertical samples and the horizontal permeability k_h was worked out from oedometer tests on horizontal samples. The number of horizontal samples was limited to two. The lowest values of k_v

are estimated in the softer layers between -2m and -8m. Below -8m and above -16m, the vertical permeability k_v is marginally increasing with depth and shows less scatter. Between -16 m and -18 m a further decrease in permeability is observed. The ratio between k_h and k_v varies between 1.2 to 1.4, respectively.

A number of undrained triaxial tests were performed on natural samples of Murro clay from different depths. The samples were grouped into six groups (0.0 -1.6 m, 1.6 -3.0 m, 3.0 -6.7 m, 6.7 -10.0 m, 10.0 -15.0 m and 15.0 -23.0 m) which was based on the results from the index tests. To determine a strength at critical state, the test results were plotted in a diagram showing the axial strain on the x-axis and the stress ratio q/ p' on the y-axis (see Figure 6.9). The results show some scatter in the predicted critical state ratio M because each test was performed with a different strain rate.

Oedometer test results on natural samples were used to estimate the vertical preconsolidation stress σ'_p with depth. In addition, the initial effective vertical stress profile ($\sigma'_{v)}$ with depth was calculated based on average unit weights γ. For the calculation the ground water level was assumed at a depth of -0.8 m (Koskinen et al. 2003c). The σ'_p and σ'_v versus depth are plotted in Figure 6.10. The comparison of the stresses shows a heavily overconsolidated dry crust (0 -1.6 m). From -1.6 m to a depth of -10m the soil is slightly overconsolidated. Underneath a depth of -10 m the clay can be characterised as normally consolidated.

6.3 Embankment geometry and material

The Murro test embankment is 2 m high and 30 m long. The slopes of the embankment were built with a gradient of 1:2. The width of the top of the embankment is 10 m. The embankment material consists of crushed rock (biotite gneiss) with a grain size of 0 - 65 mm (Karstunen et al. 2005). Construction of the embankment was completed in two days.

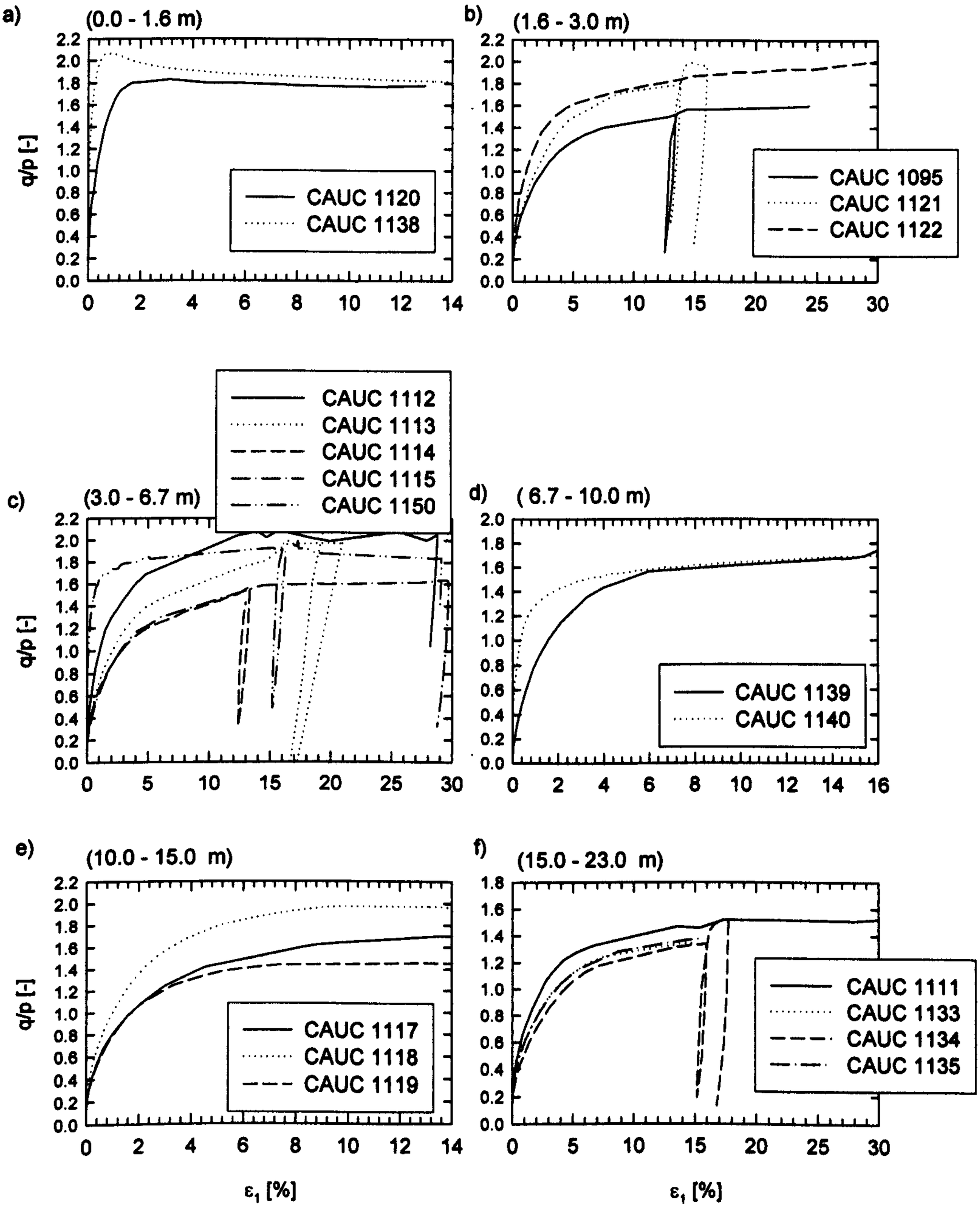

Figure 6.9: Stress ratio q/p' versus axial strain ε_1 from undrained triaxial tests on Murro clay: a) 0.0 -1.6m, b) 1.6 -3.0m, c) 3.0 -6.7m, d) 6.7 -10m, e) 10.0 -15.0 m and f) 15.0 -23.0m

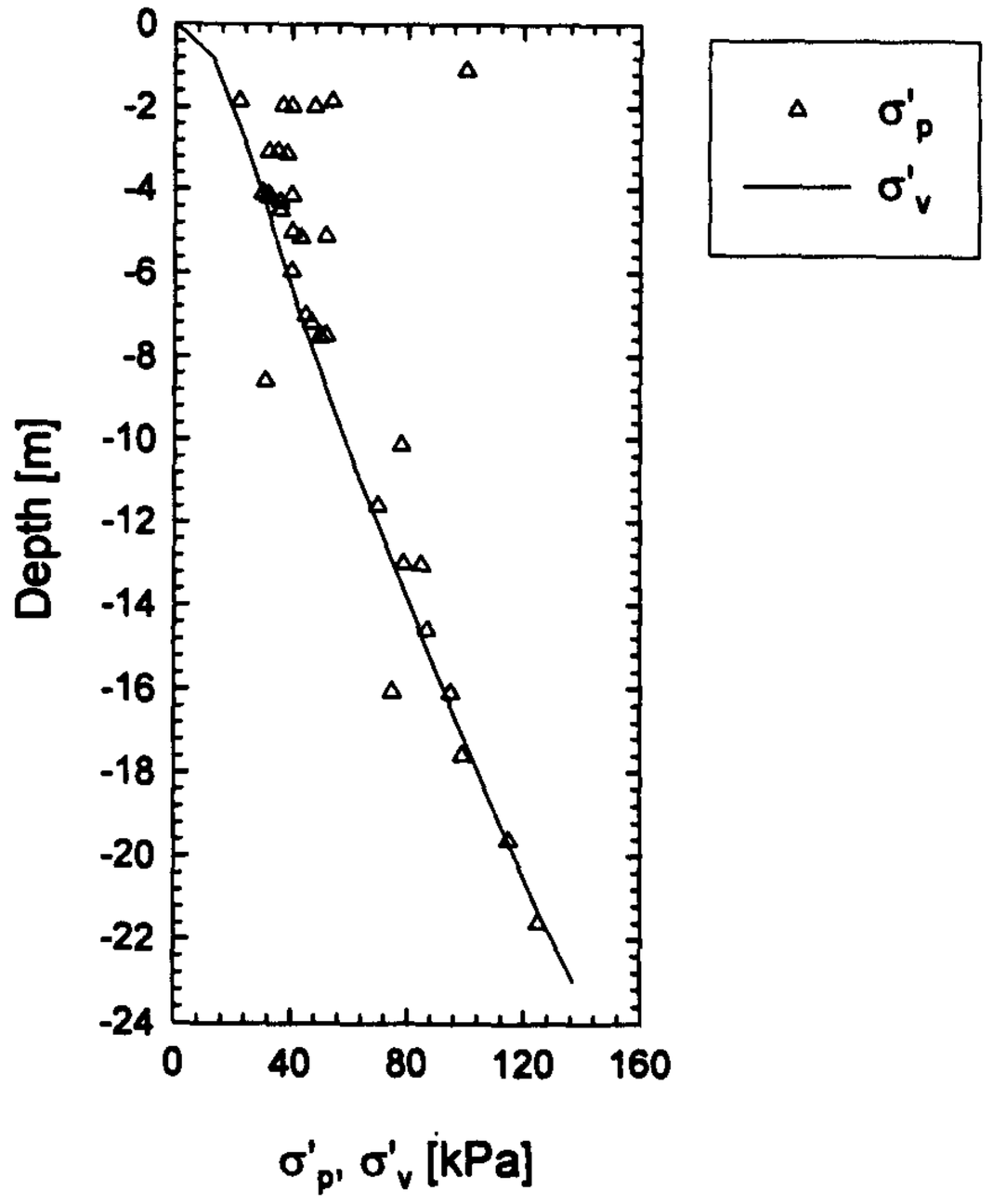

Figure 6.10: Initial vertical stress σ'_v and vertical preconsolidation stress σ'_p

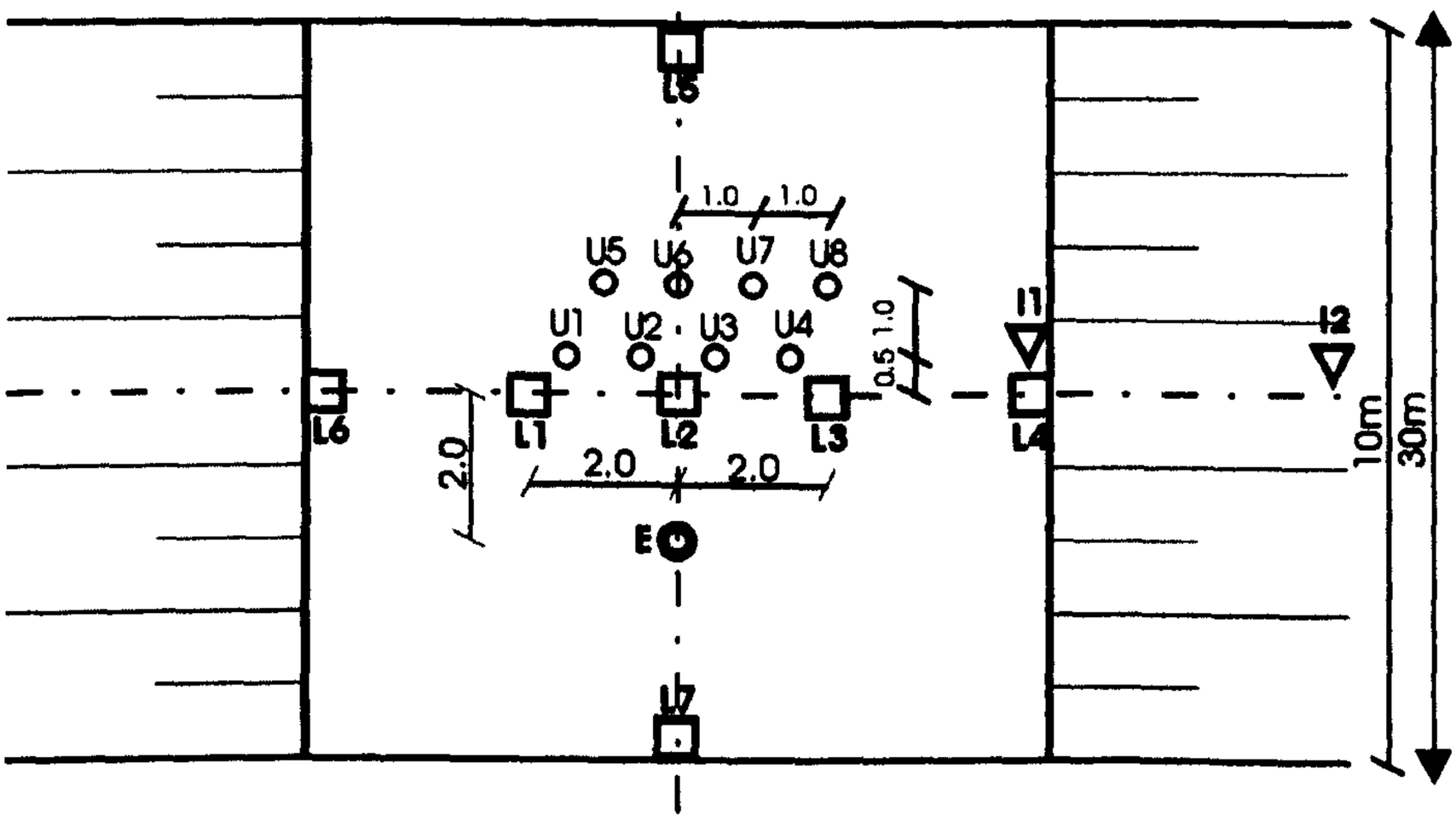

Figure 6.11: Layout of the instrumentation at the Murro test embankment

6.4 Observations

The test embankment was heavily instrumented for observation purposes. The layout of the instrumentation is shown in Figure 6.11. The instrumentation included seven

settlement plates (L1 - L7) installed at the base of the embankment along the longitutional and transversal axis of the embankment, two inclinometers (I1 - I2) for the measurement of horizontal displacements installed along the longitutional symmetry line of embankment at the crest and toe of the embankment, one extensometer (E) located next to the centre of the embankment, and ten pore pressure probes (U1 - U10) installed in a grid pattern as shown in Figure 6.11. The detailed vertical and horizontal alignment with respect to the centre point of the embankment is summarised in Table 6.1

Table 6.1: Location of the pore pressure probes

Pore pressure probes	U1	U2	U3	U4	U5	U6	U7	U8	U9	U10
Depth [m]	-15.0	-2.0	-3.5	-5.5	-7.5	-9.0	-12.0	-20.0	-2.0	-7.5
Distance from symmetry axis	1.5	0.5	0.5	1.5	1.0	0.0	1.0	2.0	19.0	20.0

The embankment was monitored and surveyed on a regular basis up to 2001. Under the sponsorship of the European research project AMGISS (Advanced Modelling of Ground Improvement in Soft Soils) a team of engineers from the Helsinki University of Technology (HUT) went back to the Murro embankment in Autumn 2007 to take some further measurements.

6.5 Numerical simulations

The Murro test embankment has been simulated in the past with different constitutive models. Koskinen et al. (2002b and 2002c) simulated the embankment with isotropic constitutive models, namely, the Modified Cam Clay model (MCC) and the Soft Soil model (SS) both which have been introduced in Chapter 2 of this work. Karstunen et al. (2005) used in addition to the MCC model, the anisotropic S-CLAY1 and the S-CLAY1S model, which incorporates destructuration in addition to anisotropy. The comparison of the simulations with the advanced models clearly showed the effect of anisotropy and destructuration on the predicted results. All of the above named performed small strain analyses either with PLAXIS or the SAGE Crisp finite element

code. Koskinen and Karstunen (2006) presented simulations with the S-CLAY1S using large strain analysis (Brinkgreve, 2002). The simulation presented in the following concentrates on the predictions of large strain simulations with the MCC, S-CLAY1, S-CLAY1S, and the S-CLAY2S model. Special focus is on the development of the undrained shear strength at depth with time. Furthermore, the latest set of measurements are presented and compared with the predictions.

6.5.1 Input data

The granular embankment fill was modelled with the simple linear elastic perfectly plastic Mohr Coulomb model implemented as a user defined soil model in the PLAXIS code. The material parameters are shown in Table 6.2.

Table 6.2: Embankment fill parameter

E [kN/m^2]	ν'	φ'	ψ'	c'	γ [kN/m^3]
40000	0.35	40	0	2	19.6

The values are typical values for crushed biotite gneiss (Koskinen and Karstunen, 2006). Parametric studies confirmed that the simulations are not sensitive to the embankment fill parameters as the response is controlled by the underlying soft soil (Karstunen et al. 2005).

In the original calculation by Karstunen et al. (2005) the deposit was divided into 5 layers because at the time only very little laboratory data was available on the intrinsic properties of the Murro clay. Based on the work by Koskinen and Karstunen (2006) the soil is divided into eight layers. The values of the soil parameters and the initial state (Table 6.3 - 6.5) for the simulations have been worked out from the laboratory test results which were presented in Section 6.2. For each layer average values have been chosen. The values of the soil parameters and initial values were all selected from the laboratory test results and not back calculations.

The initial values of the state parameters are shown in Table 6.3. e_0 is the initial void ratio of the soil. The overconsolidation of the deposit was modelled with a preover-

burden pressure (POP) profile with depth. The top layer (dry crust) was divided into two layers to model gradual decrease of the pre-consolidation stress σ'_p with depth. The in-situ K_0 values were determined using the formula by Mayne and Kulhawy (1982). The initial inclination α_0 was derived following the procedure proposed by Wheeler et al. (2003). The initial amount of bonding x_0 was estimated from the sensitivity.

Table 6.3: Initial values for state parameters

Layer	Depth [m]	e_0	POP	K_0	α_{K0}	x_0
1a	0 - 0.8	1.55	80	1.23	0.72	2.5
1b	0.8 -1.6	1.55	60	0.54	0.72	2.5
2	1.6 -3.0	1.89	10	0.48	0.63	6.5
3	3.0 -6.7	2.43	4	0.36	0.69	6.3
4	6.7 -10.0	2.12	3	0.38	0.63	6.3
5	10.0 -15.0	1.80	7	0.39	0.63	4.5
6	15.0 -18.0	1.55	2	0.44	0.54	3.1
7	18.0 -21.5	1.65	1	0.43	0.54	11.7
8	21.5 -23.0	1.3	3	0.44	0.54	4.5

The values for the conventional soil constants are shown in Table 6.4. For κ (slope of elastic swelling line) and λ (slope of normal compression line) average values for each layer were chosen. The value of ν' was taken as 0.15 which is a typical value for soft clays. Average values of M per layer were chosen based on the undrained triaxial test results presented in Figure 6.9.

Table 6.4: Values of conventional soil constants

Layer	γ [kN/m3]	κ	ν'	λ	M	k_v [m/s]	k_h [m/s]
1a	15.8	0.023	0.15	0.20	1.75	1.43E-9	8.36E-10
1b	15.8	0.023	0.15	0.20	1.75	1.43E-9	8.36E-10
2	15.47	0.028	0.15	0.36	1.60	1.26E-9	7.34E-10
3	14.47	0.041	0.15	0.56	1.70	1.37E-9	8.01E-10
4	15.07	0.039	0.15	0.36	1.60	1.26E-9	7.34E-10
5	15.66	0.030	0.15	0.32	1.60	1.26E-9	7.34E-10
6	15.93	0.027	0.15	0.22	1.40	1.06E-9	6.22E-10
7	16.24	0.028	0.15	0.22	1.40	1.06E-9	6.22E-10
8	17.29	0.012	0.15	0.15	1.40	1.06E-9	6.22E-10

The values for the additional soil constants for the S-CLAY models are presented in Table 6.5. β was determined in a manner described by Wheeler et al. (2003). Parameter μ which controls the rate of the rotation of the yield surface was estimated based on the ratio (10-15)/λ suggest by Zentar et al. (2002). The values for λ_i are average values per layer determined from tests on reconstituted samples. Parameters a and b are based on Koskinen et al. (2002a) and are typical values for soft Finnish clays.

Table 6.5: Values for additional soil constants for S-CLAY1, S-CLAY1S and S-CLAY2S

Layer	β	μ	λ_i	a	b
1a	0.98	61	0.18	10	0.2
1b	0.98	61	0.18	10	0.2
2	1.02	47	0.18	10	0.2
3	1.00	28	0.25	10	0.2
4	1.02	32	0.21	10	0.2
5	1.02	43	0.22	10	0.2
6	0.95	55	0.16	10	0.2
7	0.95	47	0.17	10	0.2
8	0.95	83	0.11	10	0.2

6.5.2 Undrained shear strength "Greenfield"

One of the goals of the simulations was to achieve a good match of the predicted undrained shear strength in plane strain compression with the shear strength estimated with the field vane tests in 1993 (prior to construction). In Figure 6.12a the undisturbed shear strength profile estimated by field vane tests is compared to the profile predicted by the MCC, S-CLAY1, S-CLAY1S and S-CLAY2S models in plane strain compression. The predicted profile gives a very good match with the estimated profile. Only at a depth of -20 m and deeper do the models overpredict the field values. The estimated profile can not be matched with the models because of the assumed state parameters which result in a certain shape of the yield surface in the normally consolidated state. Comparison of the predicted values by the models only, shows that the MCC predicts slightly lower values with depth than the S-CLAY models. This is due to the different shapes of the yield surfaces. The yield surfaces for a point at a

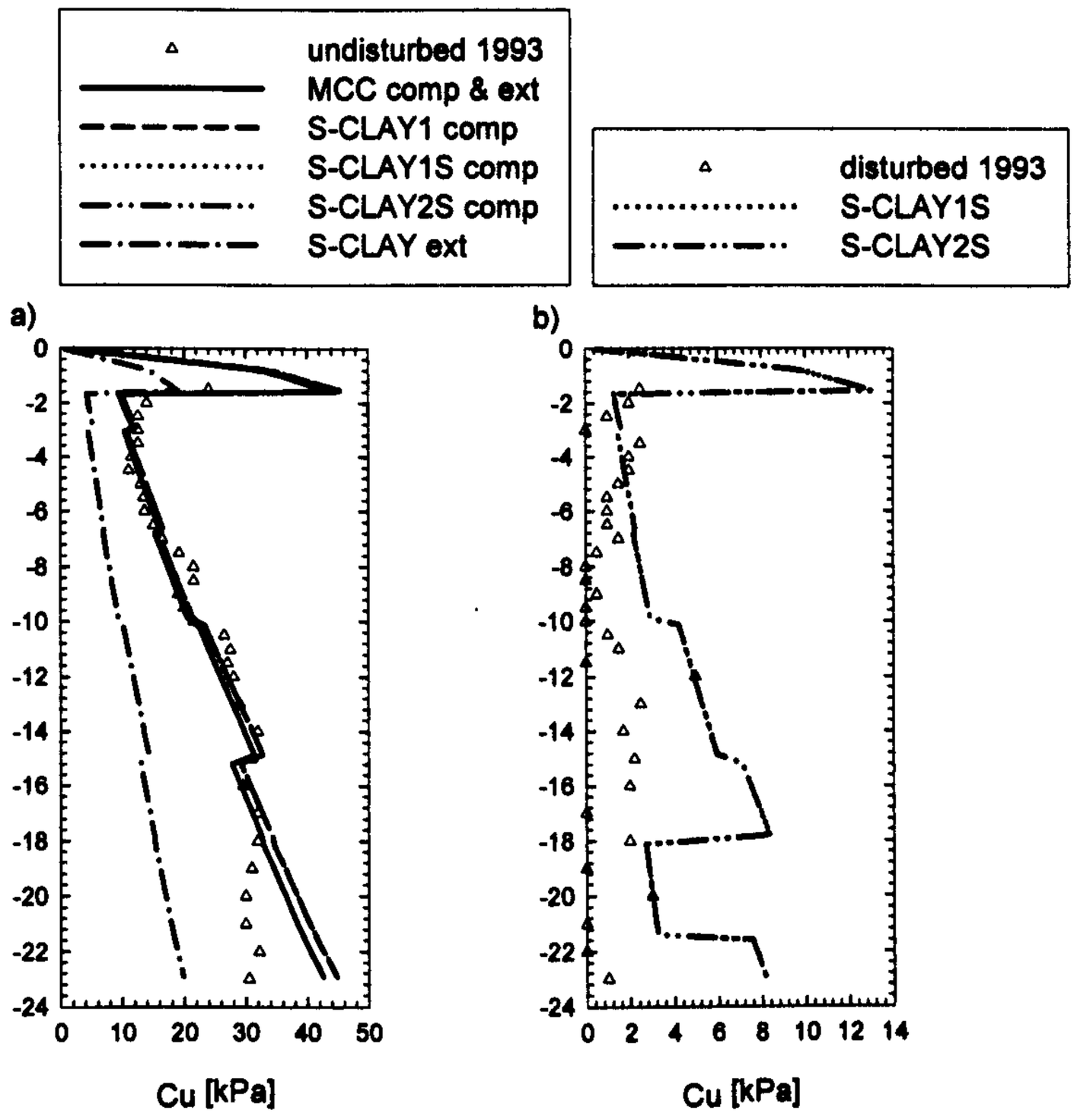

Figure 6.12: Undrained shear strength profile prior to construction: a) undisturbed strength (natural) and b) disturbed strength (remoulded)

depth of -3 m are shown in Figure 6.13. The two yield surfaces predict different maximum values of deviatoric stress q due to the different shapes of the curve. MCC predicts a lower q value in plane strain compression than the S-CLAY models. Inspection of Figure 6.13 also shows the difference in minimum q in extension for the two models. The isotropic MCC model predicts the same strength in compression and extension. In contrast the minimum value of q in extension predicted by the S-CLAY1S model is lower due to the ellipse shaped yield surface. As a consequence the undrained strength in extension predicted by the S-CLAY models is lower than in compression (see Figure 6.13a). In the following only the strength in plane strain compression is considered and compared to the field vane results.

Figure 6.12b plots the measured and predicted disturbed undrained strength. The predicted strength overestimates the strength measured in the field. The ratio between the size of the intrinsic yield surface and the natural yield surface is based on average sen-

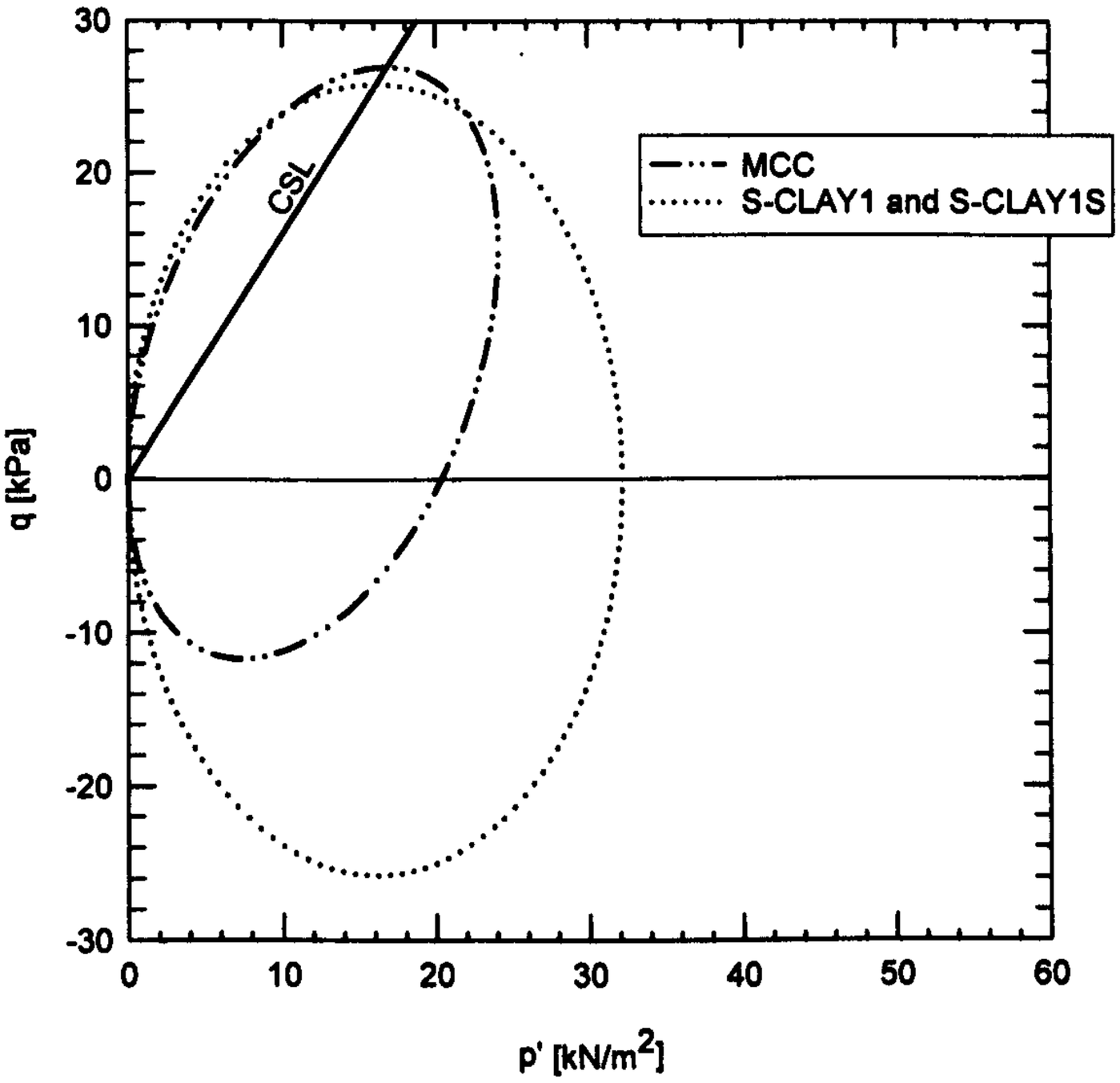

Figure 6.13: Predicted natural yield surface of the MCC, S-CLAY1 models for a point at a depth of -3 m in the p'-q plane

sitivity with depth. The sensitivity was determined with fall cone tests and may be affected by sample disturbance.

6.5.3 Numerical simulations

The Murro test embankment was modelled in plane strain with the 2D PLAXIS 8 finite element code. Due to the symmetry of the problem only half of the embankment was considered in the analyses. The problem was discretised by using a finite element mesh consisting of 693 15-noded triangular elements. In the model the symmetry axis and the lateral boundary at a distance of 36 m were fixed in the horizontal direction. The bottom boundary at a depth of -23 m was fixed in the horizontal and vertical direction. The problem was modelled as large strain analyses. Mesh sensitivity studies confirmed that the mesh was dense enough to give accurate results. The problem was analysed with the MCC, S-CLAY1, S-CLAY1S and S-CLAY2S model. The construc-

tion of the embankment was simulated as an undrained calculation phase followed by a fully coupled consolidation analysis.

The 'step size' for the user defined soil models (MCC and S-CLAY models) was set to -0.01.

6.5.4 Comparison with predictions

The comparison between the results of the finite element simulations and the field observations are presented in the following. Discrete values, shown with various symbols, correspond to the field measurements. The details are shown in the legend of each figure.

6.5.4.1 Time settlement curves

The observed and predicted surface settlements underneath the centre line of the embankment are presented in Figure 6.14. Figure 6.14a shows the results on a linear scale. The settlement plates L2, L5 and L7 are all installed along the centreline of the embankment (see Figure 6.11 for details). L2 is at the centre point of the embankment and L5 and L7 are at a distance of 5 m. Interestingly L2 settles less than L5 and L7. L7 predicts the biggest settlement with time. Due to the small distances between the settlement plates (L5 and L7) and L2 at the centre, settling the least of all, the difference can not be associated with inhomogeneous ground conditions. The difference in prediction of the plates is most likely due to problems with the compaction or other technical issues during construction. The measured settlements underneath the centre line after about 14 years of consolidation are in the order of 0.7 to 0.8 m.

The model predictions with the S-CLAY1S and the S-CLAY2S model suggest similar magnitudes for 14 year settlements. S-CLAY2S predicts marginally higher vertical settlements than S-CLAY1S. MCC predicts notably smaller settlements than the S-CLAY models. Including anisotropy only in the simulations slightly improves the predictions but still underestimates the measured values.

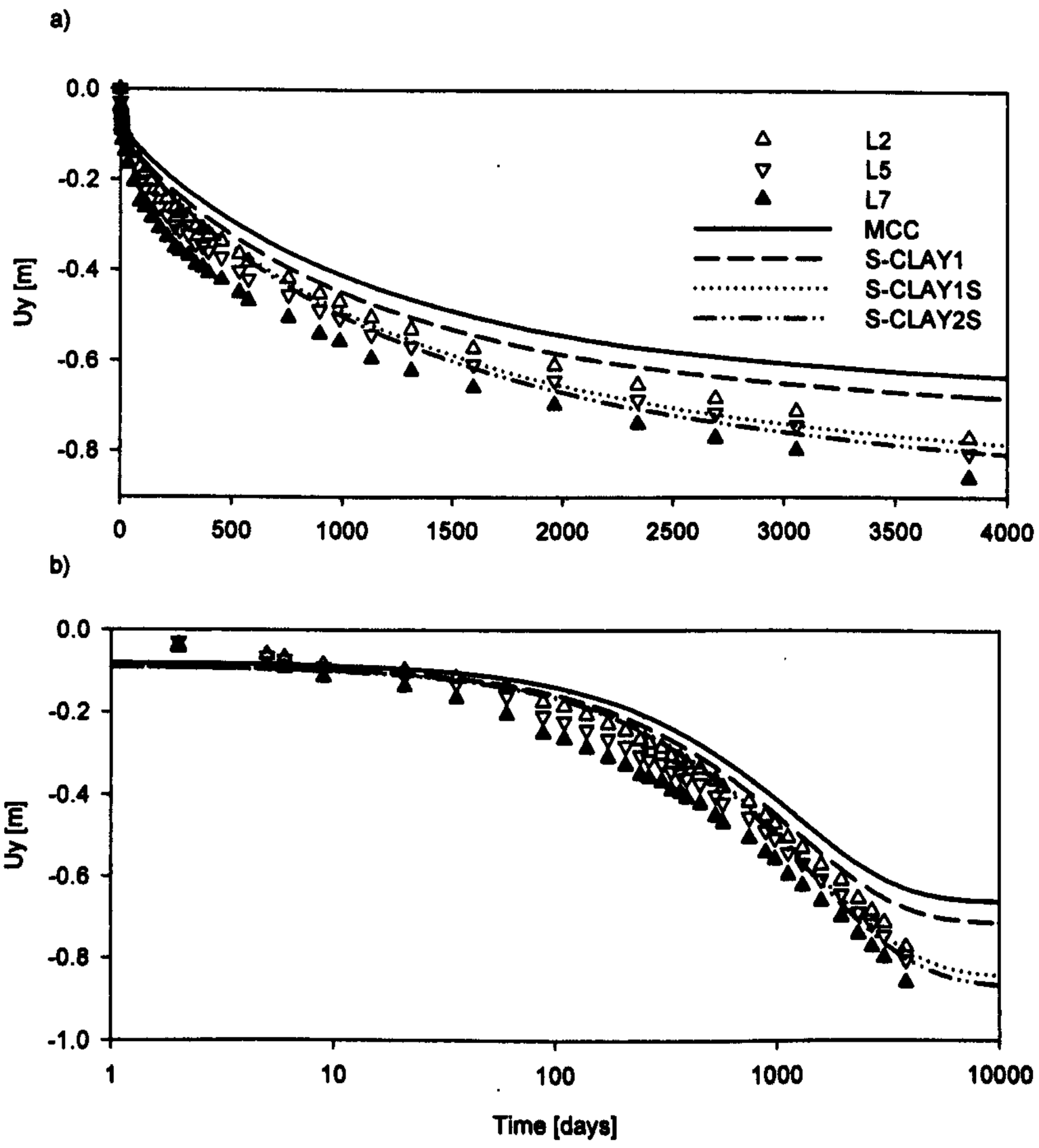

Figure 6.14: Time settlement curves: a) linear scale and b) log scale

In Figure 6.14b the time settlement curve is plotted on a semi-logarithmic scale. Inspection of the measured results suggest that the primary consolidation is still on going after 14 years. In contrast, the model simulations suggest that primary consolidation is nearly finished. The difference between the measurements and the predictions are due to creep (secondary consolidation) which is a well known characteristic in soft soils.

Vertical displacements at different levels underneath the centreline of the embankment versus time are plotted in Figure 6.15. The model predictions are compared to the results measured with the extensiometer which is installed at a location at the centre line of the embankment. Inspection of the measured results indicates that most of the vertical displacements are due to compression of the almost normally consolidated

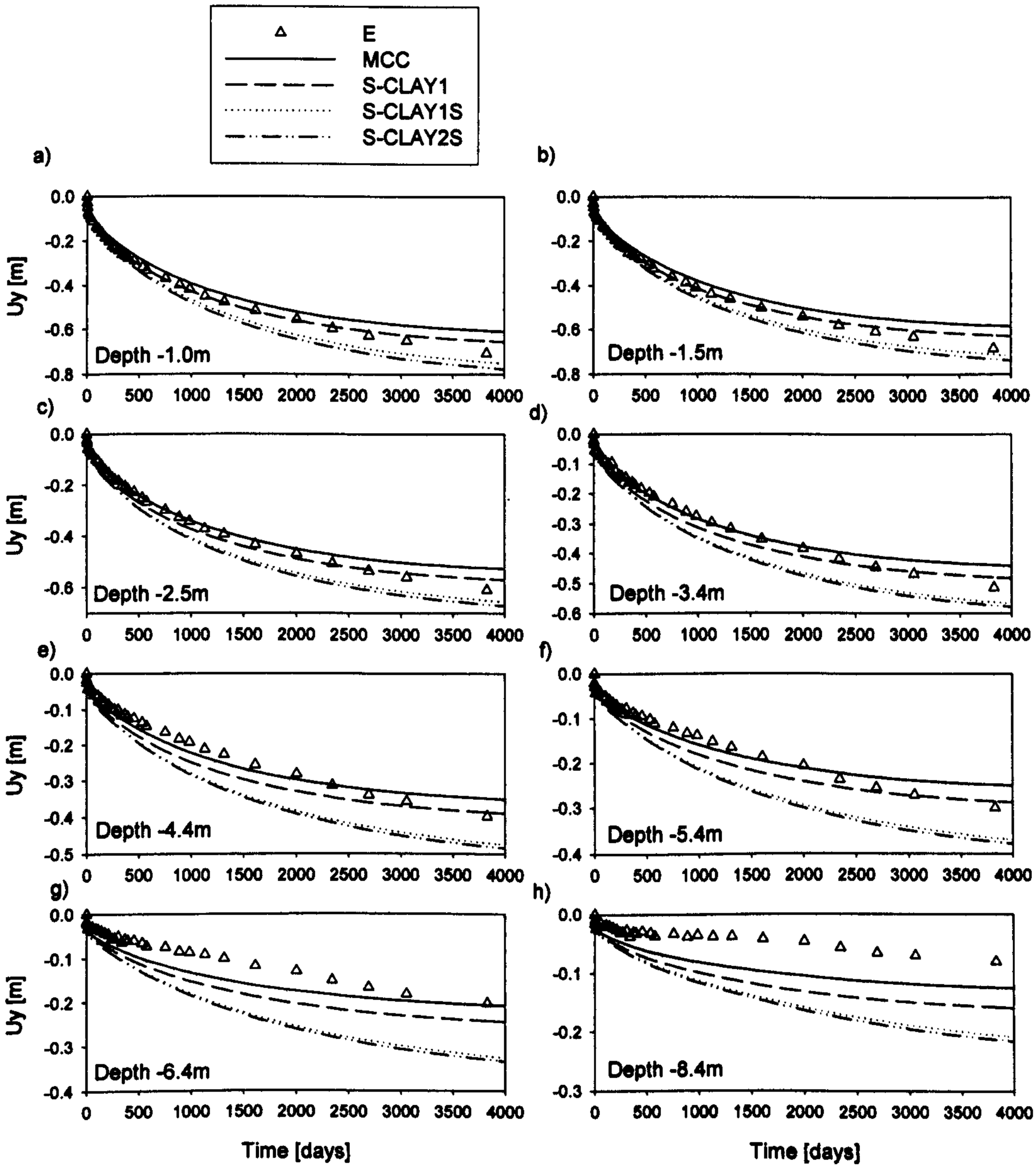

Figure 6.15: Time settlement curves for points at different depths underneath the centreline of the embankment: a) Depth -1.0m b) Depth -1.5m c) Depth -2.5m, d) Depth -3.4m, e) Depth -4.4m, f) Depth -5.4m, g) Depth -6.4m and h) Depth -8.4m

soft clay layers between a depth of -1.6 m and -6.0 m. The model predictions are in good agreement for the layers between -1.0 m and -5.0 m. For the deeper layers the simulations overestimate the observed behaviour. Either the stiffness of the soil has been underestimated or the predicted load distribution differs from the distribution in the field. Also the constant permeability used in the simulations may influence the predictions.

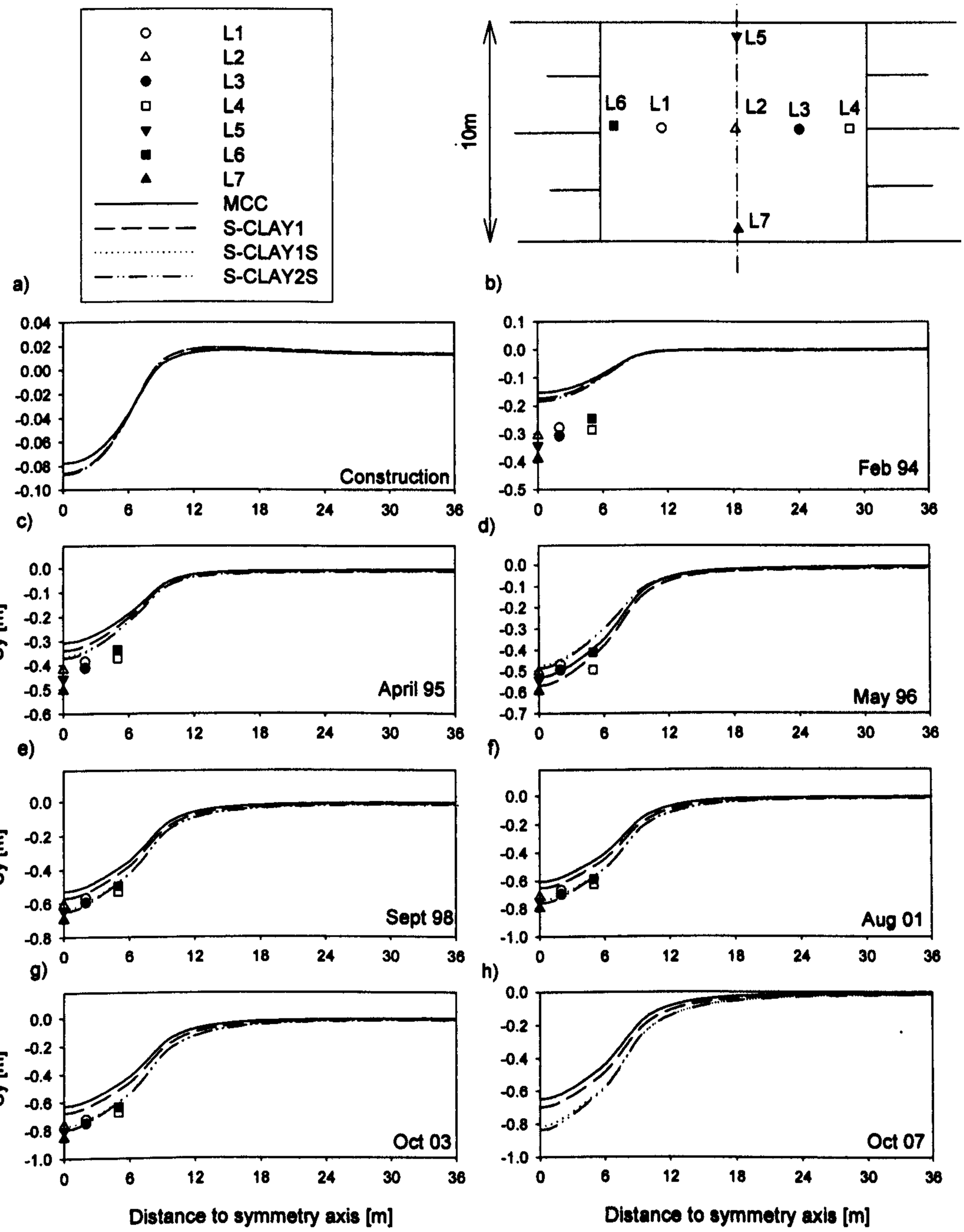

Figure 6.16: Surface settlements: a) immediately after construction b) February 1994 (1 year) c) April 1995 (2 years), d) May 1996 (3 years), e) September 1998 (5.5 years), f) August 2001 (8.5 years), g) October 2003 (10.5 years) and h) October 2007 (14.5 years)

6.5.4.2 Surface settlements

The predicted and measured surface settlements are shown in Figure 6.16. The pre-

dictions immediately after construction are shown in Figure 6.16a. All four models predict a slight surface heave outside the embankment. The anisotropic models predict slightly greater surface settlements than the isotropic MCC. There is hardly any difference in the settlement predictions for distances greater than 6m from the symmetry axis (outside the crest). In Figure 6.16b to h the predictions are compared to the field measurements (settlement plates L1 to L7). One and two years (February 1994 and April 1995) after construction of the embankment the model simulations underestimate the measured settlements at the settlement plates. With time (May 1996 to August 2001) the predictions by the model simulations are in better agreement. Overall the S-CLAY1S and S-CLAY2S model capture the measured surface settlements better with time than the MCC and S-CLAY1.

6.5.4.3 Horizontal displacements

Figure 6.17 shows the horizontal displacements at different times after construction, underneath the crest of the embankment. Immediately after construction only predictions are shown. The S-CLAY models predict slightly greater displacements than the isotropic MCC model at a depth of -3.5 m. One year after construction the S-CLAY models predict a maximum in the same order as the measured horizontal displacements. However, the measured maximum is at a slightly greater depth of -4.5 m. With increasing consolidation time the models marginally underestimate the measured maximum displacements in magnitude and depth. Overall the S-CLAY2S model predicts the magnitude of the maximum displacements slightly better than the S-CLAY1S model which uses an associated flow rule.

The horizontal displacements underneath the toe of the embankment are plotted in Figure 6.18. Immediately after construction the S-CLAY models predict greater displacements than the MCC model, in the order of 0.05 m at a depth of -3.2 m. Interestingly the maximum is at a slightly shallower depth than predicted below the crest. A year after construction the S-CLAY models overpredict the maximum which is about 0.048 m and is well predicted by the MCC. However, all the models overestimate the

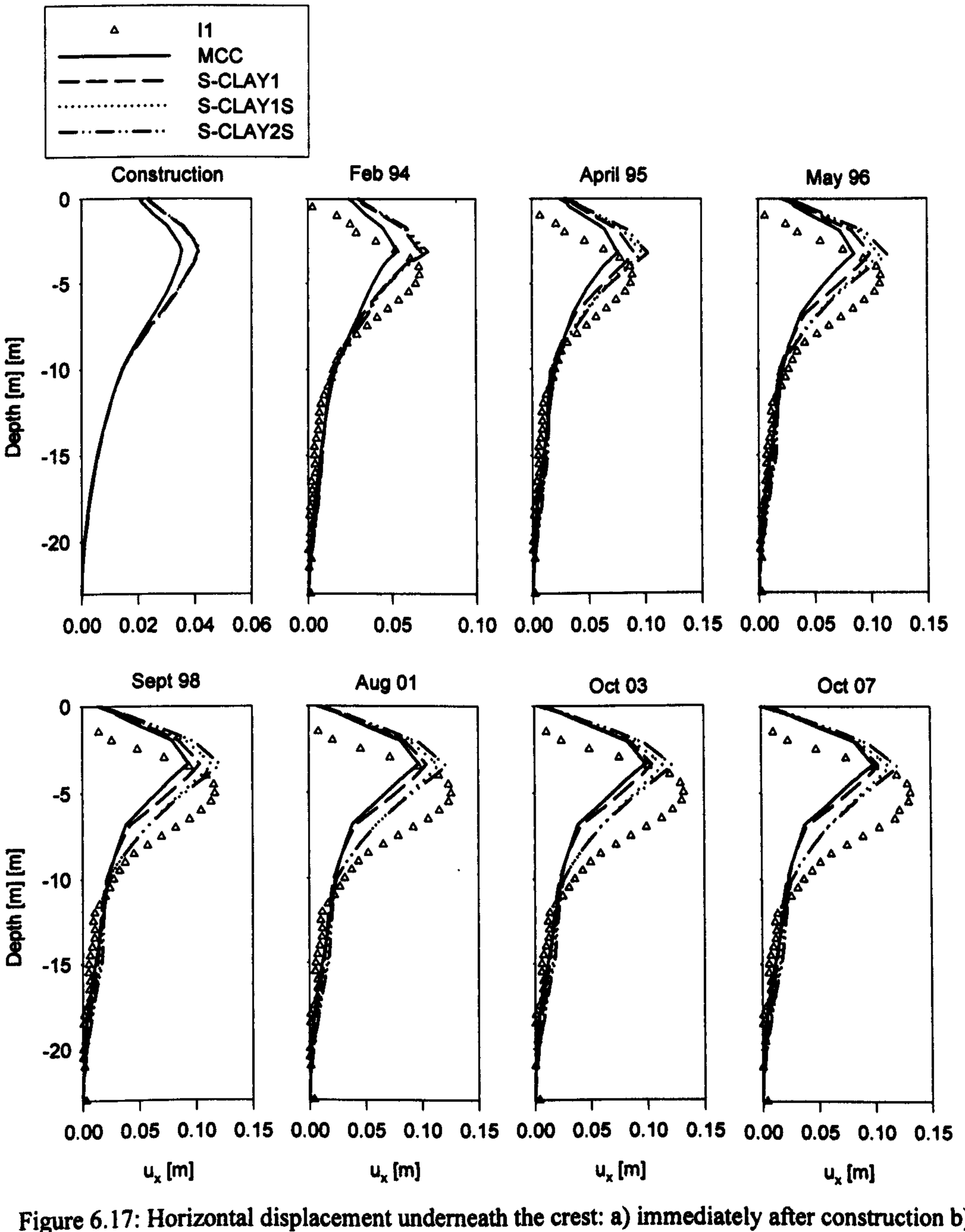

Figure 6.17: Horizontal displacement underneath the crest: a) immediately after construction b) February 1994 (1 year) c) April 1995 (2 years), d) May 1996 (3 years), e) September 1998 (5.5 years), f) August 2001 (8.5 years), g) October 2003 (10.5 years) and h) October 2007 (14.5 years)

measured profile with depth substantially by a few centimeters. With increasing consolidation time the increase in measured horizontal displacements is greater than predicted by all the models. All models predict very well the depth of the maximum displacements. With time (September 1998 and August 1991) the S-CLAY1S and S-

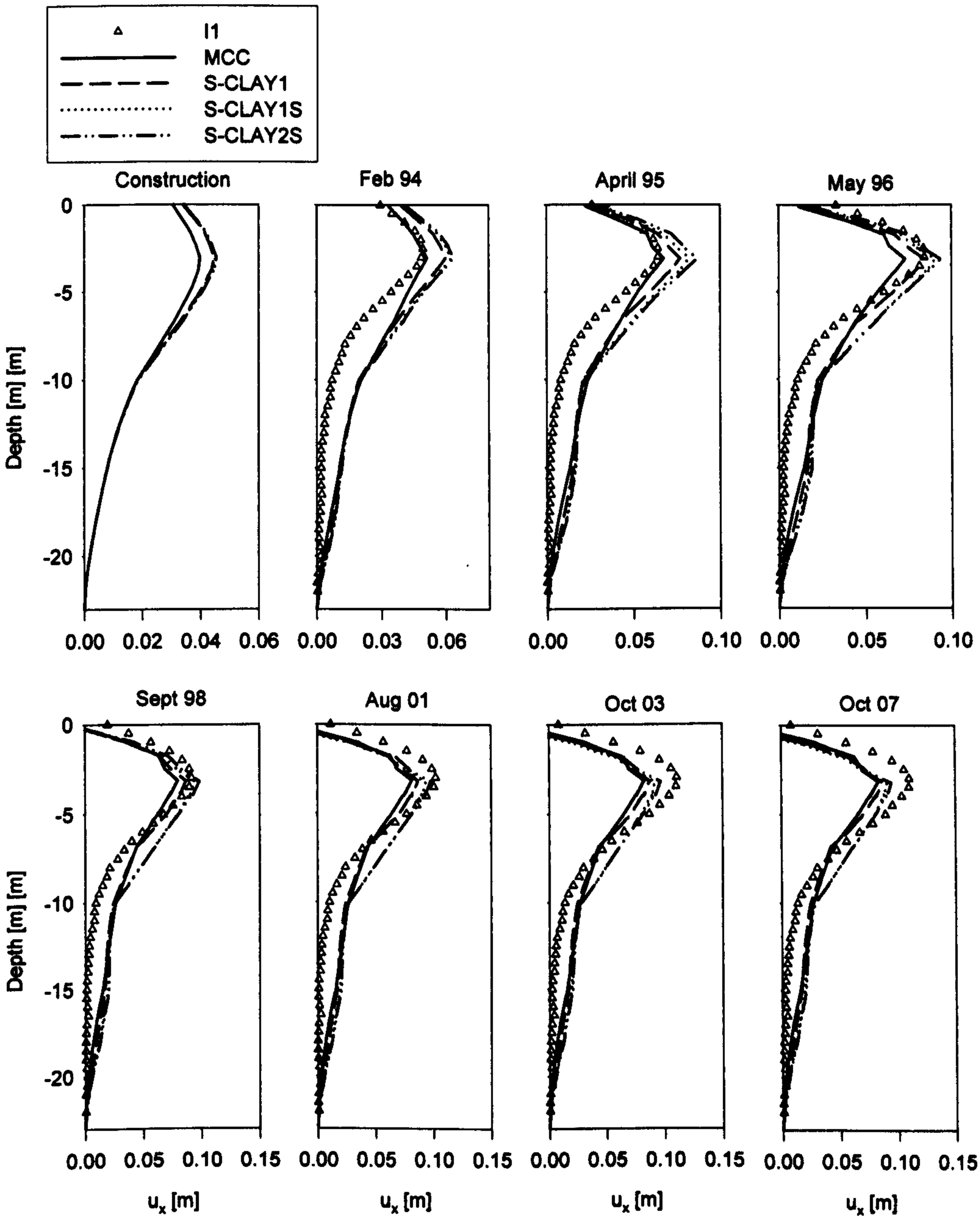

Figure 6.18: Horizontal displacement underneath the toe: a) immediately after construction b) February 1994 (1 year) c) April 1995 (2 years), d) May 1996 (3 years), e) September 1998 (5.5 years), f) August 2001 (8.5 years), g) October 2003 (10.5 years) and h) October 2007 (14.5 years)

CLAY2S simulations are in good agreement with the measured profile. Overall the S-CLAY2S model predicts the increase of horizontal displacements with time marginally better than the S-CLAY1S model. Based on the measurements from 2003 and 2007 a slow down in growth of horizontal displacements with time is observed. How-

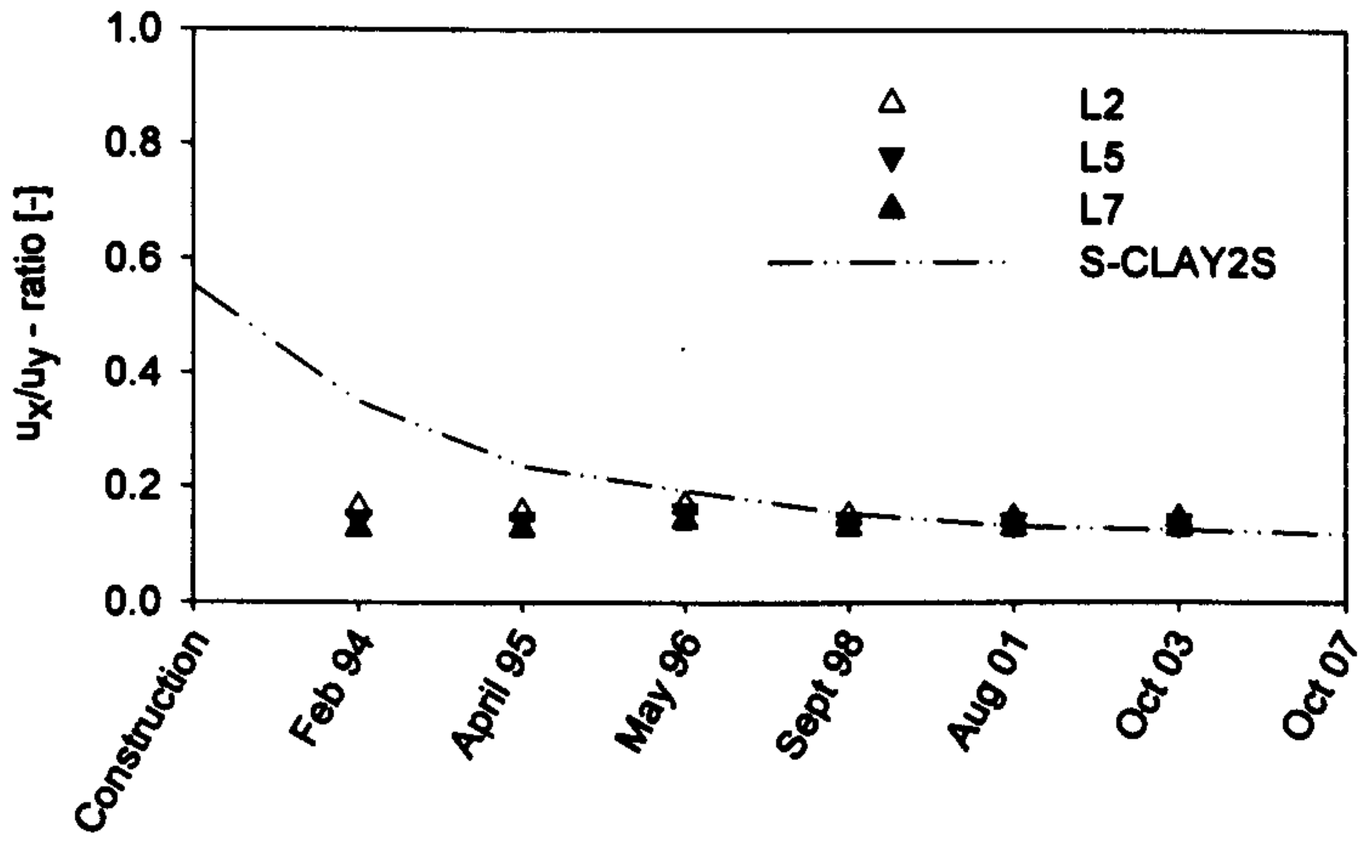

Figure 6.19: Predicted and measured u_x/u_y -ratio

ever, inspection of the u_x/u_y - ratios plotted in Figure 6.19 clearly shows that the growth in horizontal displacements to vertical displacements is rather constant and does not follow the predictions given by the simulations. The simulations suggest that the increase in horizontal displacements slows down despite an increase in vertical displacements. It is also important to mention that the maximum horizontal displacements are measured below the crest of the embankment and not below the toe. This agrees well with the simulations of test embankments and the benchmark simulations presented in Chapter 4.

6.5.4.4 Excess pore pressure

In Figure 6.20 the measured and predicted excess pore pressures (EPP) are shown. Pressure is presented as a negative value in the diagrams. In the shallow areas underneath the embankment (U2 and U3) the predicted pressures overestimated the observed pressure immediately after construction. The predictions show a decrease of EPP with time whereas the measurements show a large scatter but the trend is that EPP is almost constant with time. At locations U4, U5 and U7 the predicted values are in good agreement with the observations. Also the decrease of EPP with consolidation

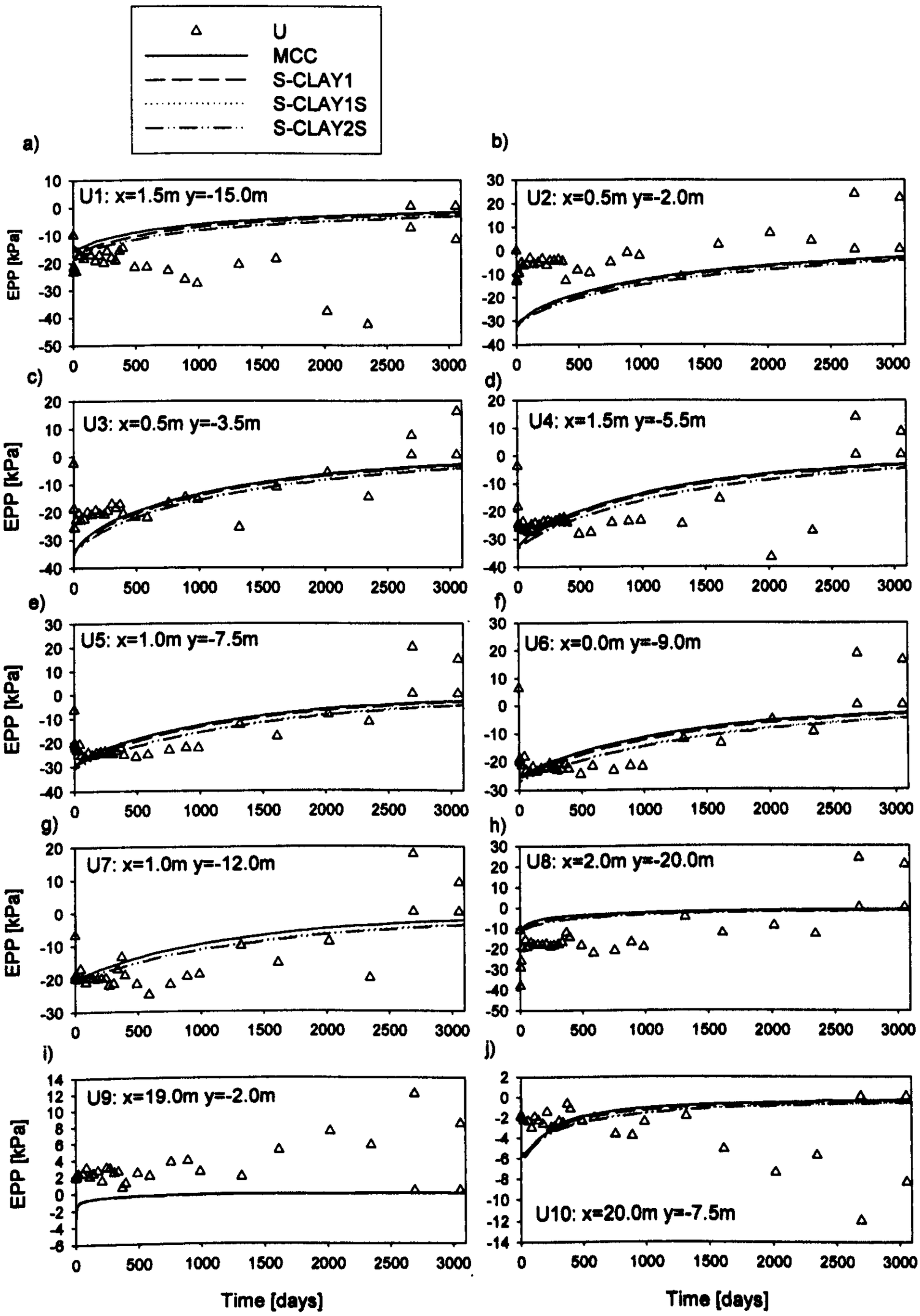

Figure 6.20: Excess pore pressure at different locations: a) U1, b) U2, c) U3, d) U4, e) U5, f) U6, g) U7, h) U8, i) U9 and j) U10

predicted by the model simulations is in good agreement with the measurements. At U8 the models marginally underestimate the measurements but the long term trend of

EPP dissipation is matched. Points U9 and U10 are reference points outside of the embankment, at a distance of 19m and 20m, respectively. The measured values are small (+/- 4kPa) and show a lot of scatter. U10 shows an increase of pressure with time and U9 suggests that some suction is apparent. At U9 the models predict a small EPP (-4kPa) after construction which dissipates fairly rapidly. At U10 the models predict an EPP of about -6kPa which is larger than the measurements suggest. The large scatter observed in the measurements might to some extent be influenced by groundwater level fluctuations and seasonal climate changes. The field observations confirm that the primary consolidation has not yet finished. Overall, according to the model simulations the anisotropic models predict marginally higher excess pore pressures underneath the embankment than the isotropic MCC model. Destructuration increases the predicted EPP by another 1 to 2 kPa.

6.5.4.5 Undrained shear strength

In Figure 6.21 the predicted and measured undrained shear strength at the symmetry axis of the embankment 8 years after construction (2001) is presented. The undisturbed strength profile (natural strength) with depth is shown in Figure 6.21a. The predictions by the MCC, S-CLAY1, S-CLAY1S and S-CLAY2S models are compared to the profile measured with the field vane test. All four models predict an increase in undisturbed shear strength of similar magnitude in the dry crust. The predicted increase is in the order of 2 to 4 kPa. At a depth from -1.6 m to about -8 m the predicted values are in good agreement with the observed increase. At a depth of -8 m and deeper the models overpredict the measured profile with depth. Overall all three S-CLAY models predict the same profile with depth. The isotropic MCC predicts marginally lower values with depth which is due to the fact that the initial profile differs from the initial profile of the S-CLAY models (see Figure 6.12).

The predicted and measured profiles of disturbed strength with depth is plotted in Figure 6.21b. The field vane results are compared to the predictions by the S-CLAY1S and S-CLAY2S model. The two models predict the same undisturbed

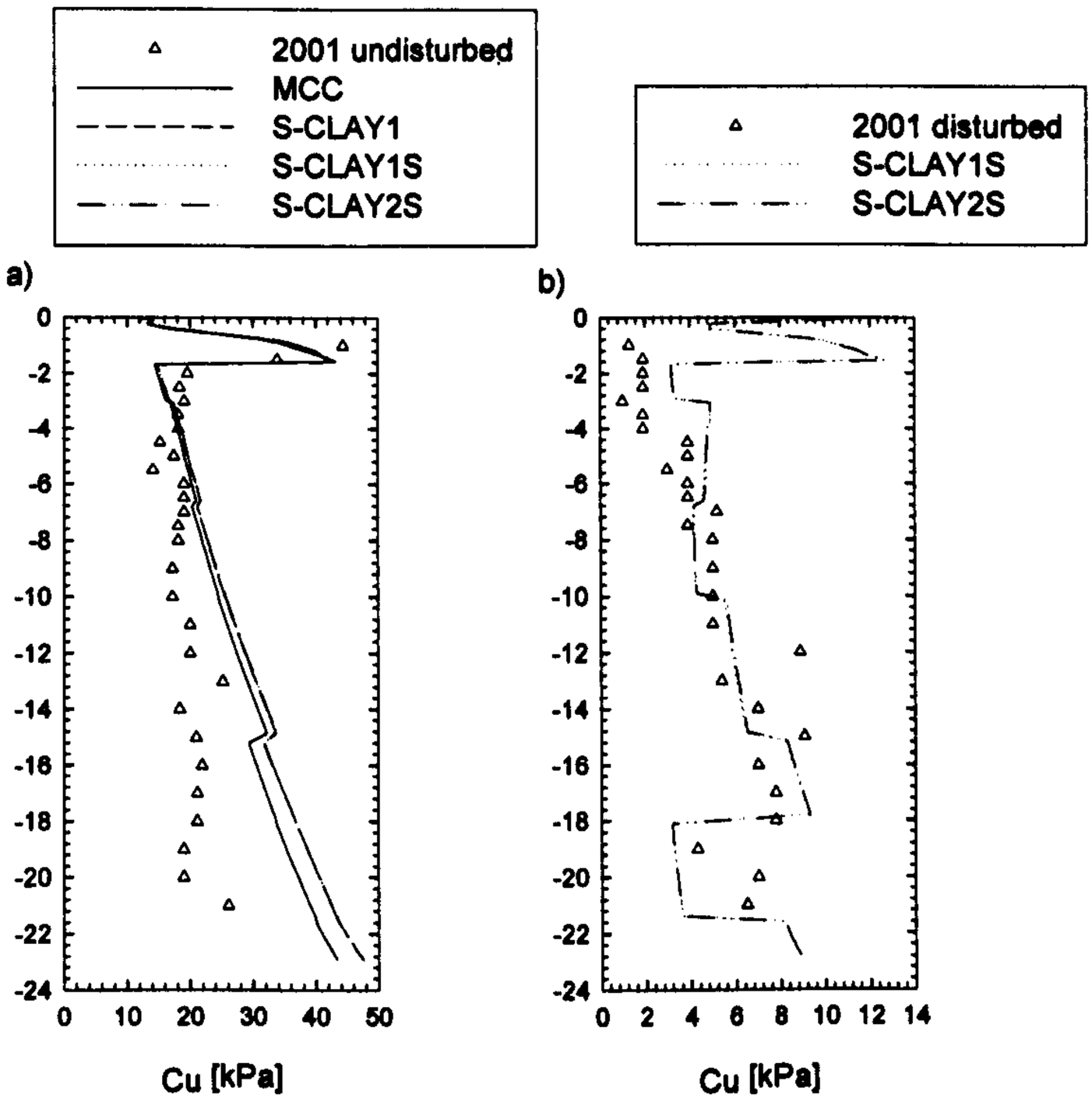

Figure 6.21: Predicted and measured undrained strength with depth at symmetry axis: a) undisturbed undrained shear strength and b) disturbed undrained shear strength

strength profile with depth. At a depth between -1.6 m and -6 m the predicted profile overestimates the measured values. Underneath a depth of -6 m the model simulation show a good match with the field vane results. In summary the predicted increase of disturbed strength with depth is of good quality.

For comparing the predictions of undrained strength with time by the model simulations it is informative to look at contour plots. The predictions by the MCC and S-CLAY1S model of undisturbed strength prior to construction, 8 years after construction and at the end of consolidation are shown in Figure 6.22. Both models predict a similar pattern of increase in undrained strength for the time 8 years after construction (August 2001). An increase of strength is not only observed in the areas directly below the embankment (toe of the embankment at x=9m) but up to a distance of 18 m from the symmetry axis (9 m from the toe). This predicted increase up to 18 m is observed over the whole depth of the deposit. At the end of consolidation (100 years after construction) the layout of the contour lines is similar to the year 2001. How-

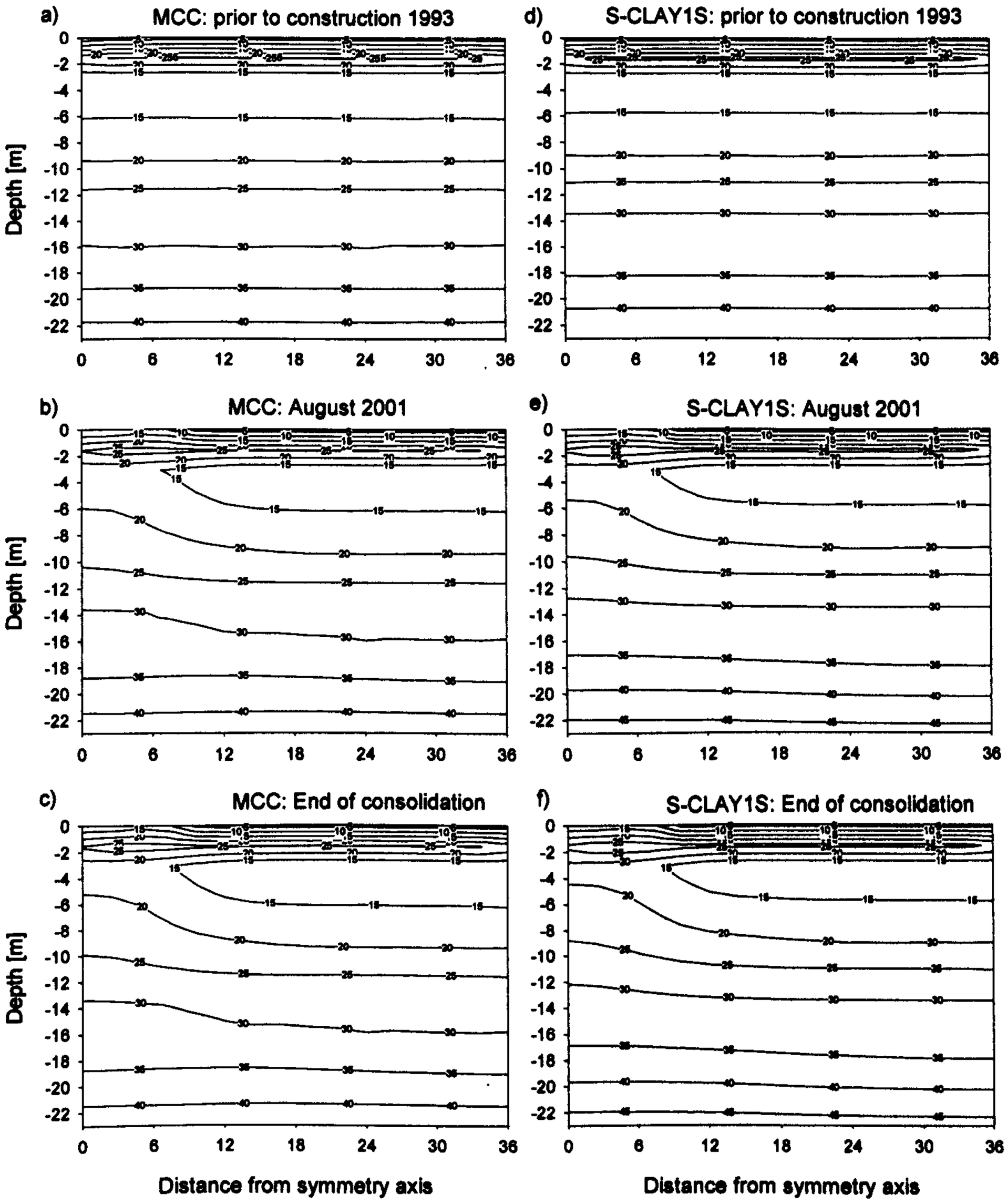

Figure 6.22: Contour plots of undisturbed undrained strength: a - c) MCC model and d - f) S-CLAY1S model

ever, the increase in strength is predicted up to a distance of 24 m from the symmetry axis. Obviously, most of the increase in strength is predicted in the first 8 years after construction, and thereafter the increase is marginal.

The contour plots of the disturbed undrained shear strength are presented in Figure 6.23. The presented results are from simulations with the S-CLAY1S model. In

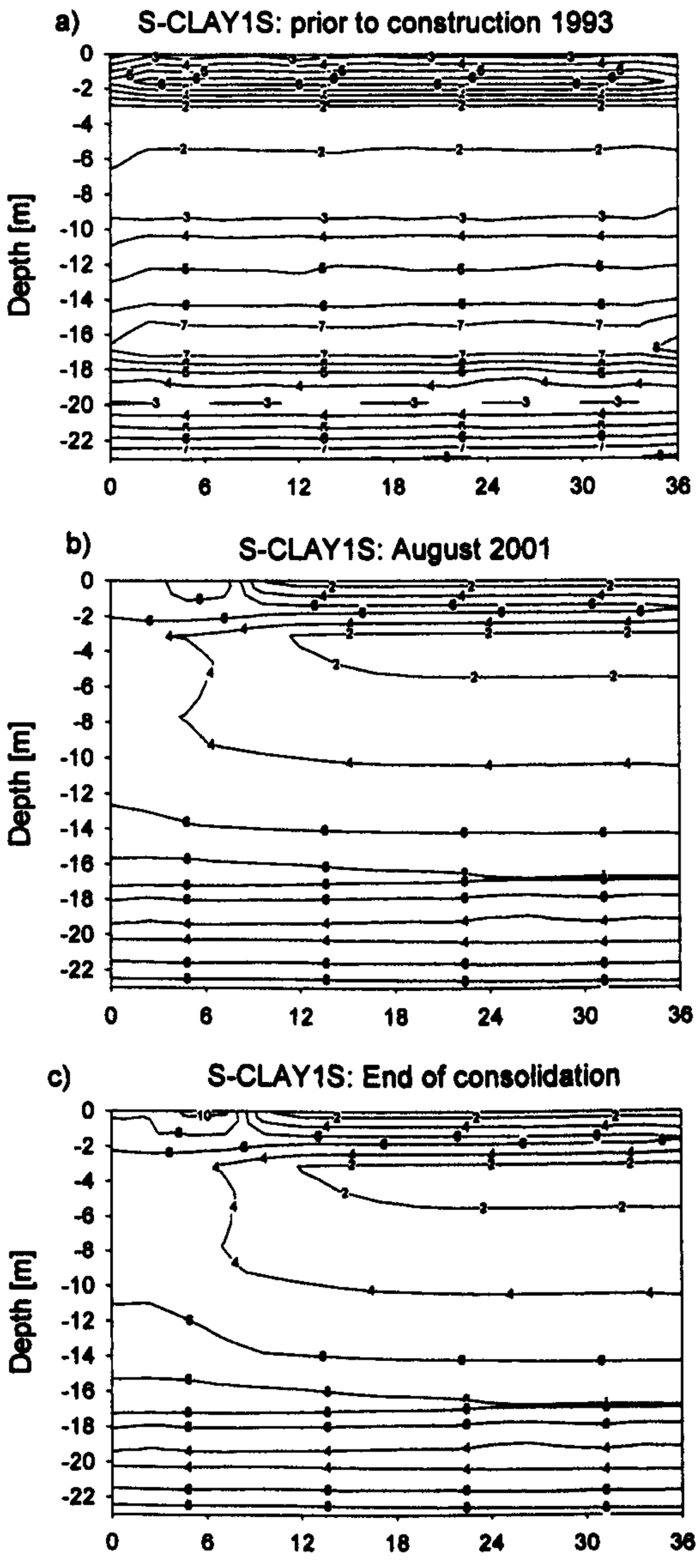

Figure 6.23: Contour plots of disturbed undrained strength

Figure 6.23a the initial profile with depth is shown. The contour lines at the vertical boundaries of the model at x=0 m and x=36 m show same scatter. The scatter is due to interpolating errors caused by the data processing programme. All lines should be horizontal at the vertical boundaries. 8 years after construction (Figure 6.23b) in August 2001 a large increase of strength in the area directly below the embankment is

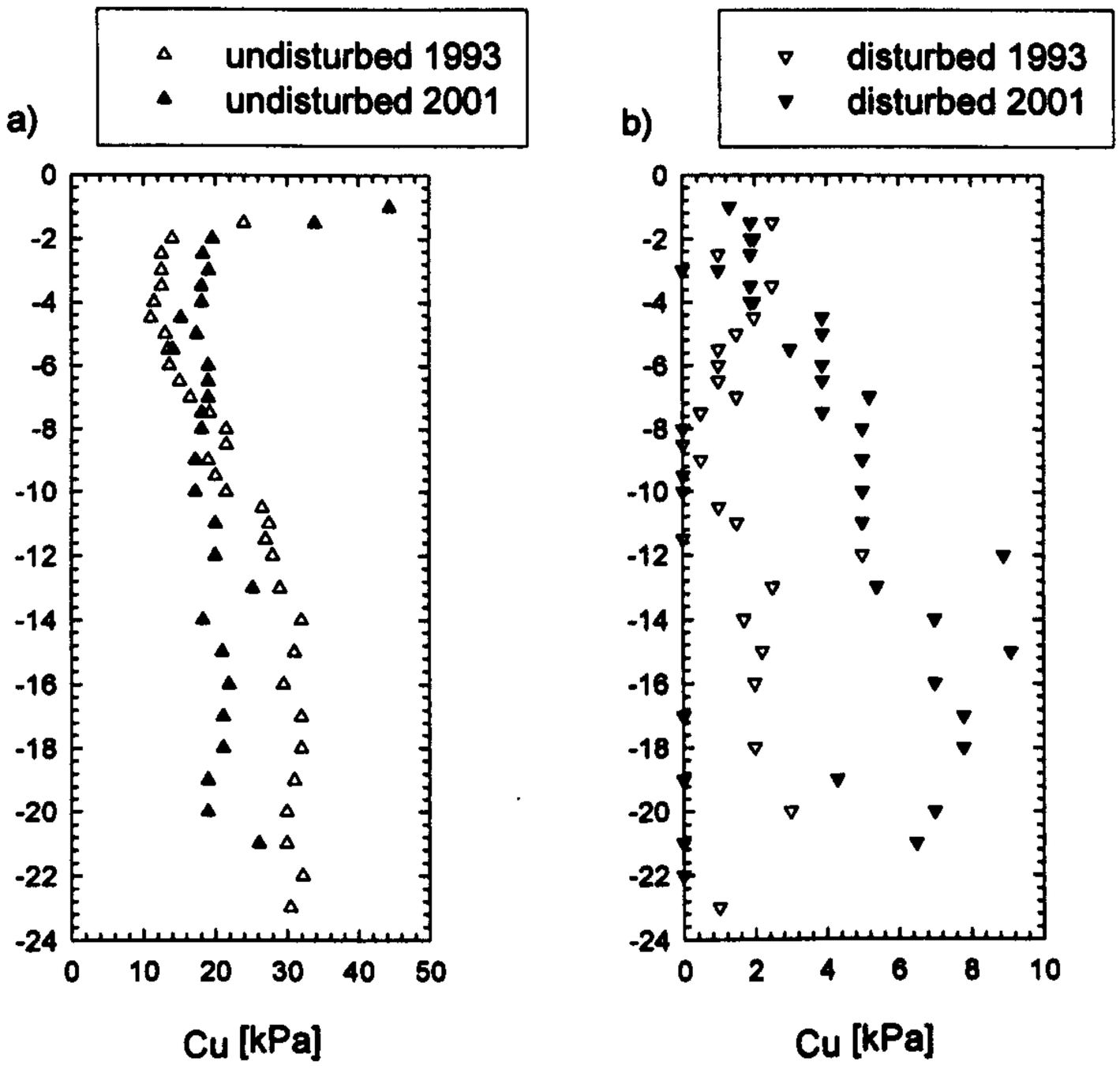

Figure 6.24: Measured undrained strength with depth: a) undisturbed undrained shear strength and b) disturbed undrained shear strength

observed. In the depth between -2 m and - 14 m, the strength is predicted to increase by about 2 to 3 kPa up to a distance of 15 m from the symmetry axis. Below -14 m the increase is marginal in the order of about 0.5 kPa. From 2001 to the end of consolidation, after about 100 years, there are only marginal changes to the predicted disturbed strength pattern.

Interestingly the models predict quantitatively the increase of undisturbed strength but overestimate the undisturbed strength below a depth of -8 m. In Figure 6.24 the field vane test results from the years 1993 and 2001 are plotted. Comparison of the undisturbed measurements (Figure 6.24a) is interesting. In the top 6 to 7m there is an increase in undrained strength as correctly predicted by the models, with a maximum increase of undrained strength of 7 to 17 kPa. However, below the depth of -7 m, the undrained strength has actually decreased, from about 30 kPa to about 20 kPa. This occurred in conjunction with an increase of disturbed strength (see Figure 6.24b). The disturbed strength increased from about 2 to 4 kPa in 1993 to 4 to 8 kPa in 2001. It

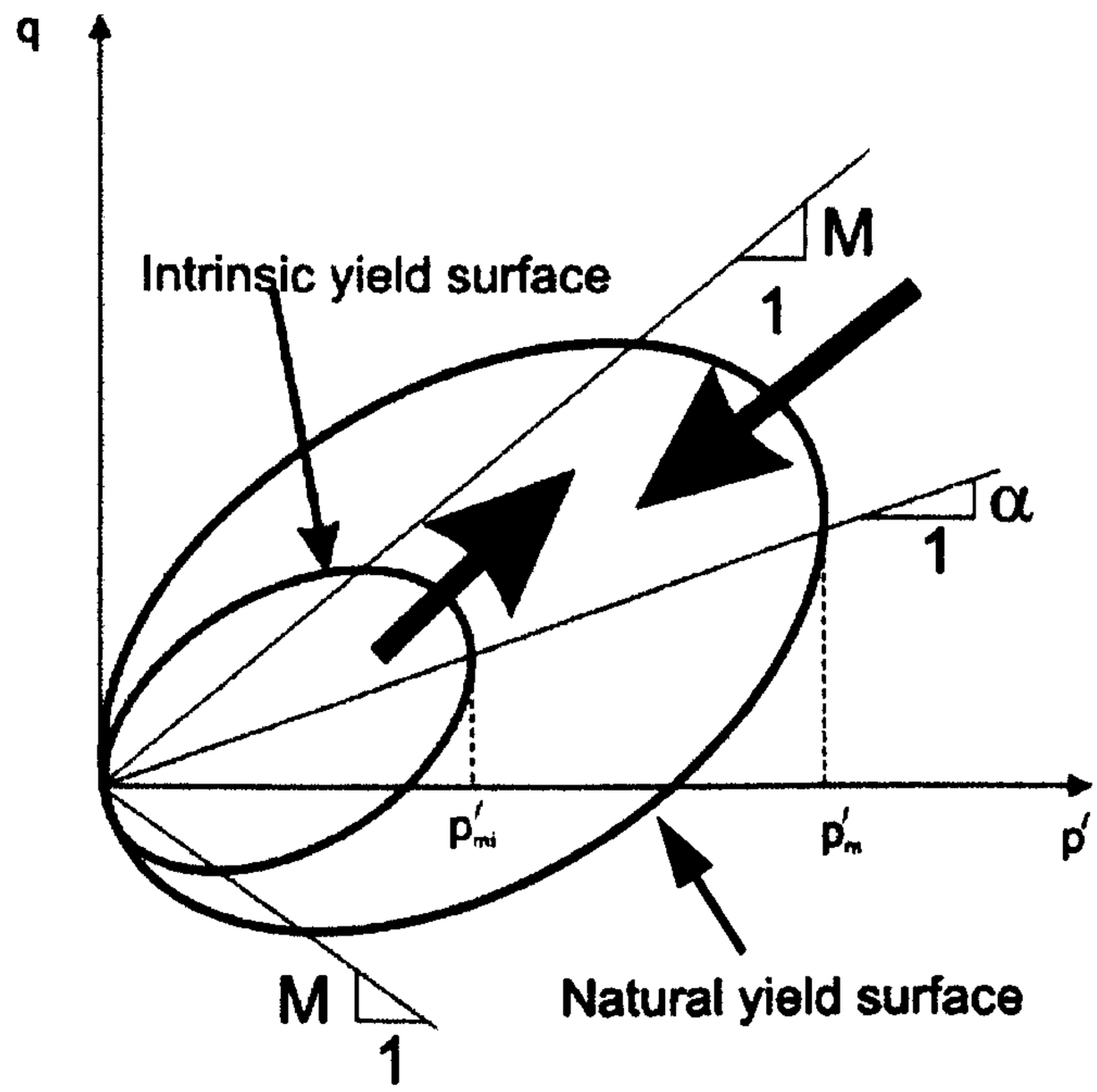

Figure 6.25: S-CLAY1S in p'-q plane: mechanism of shrinkage of natural yield surface and increase of intrinsic yield surface

shows that the sensitivity of the soil has significantly decreased throughout the depth of the deposit. This might be an indication of the gradual process of destructuration of the bonds due to plastic straining (Karstunen et al. 2005). Obviously, with a constitutive law that accounts for destructuration, such as the S-CLAY1S and S-CLAY2S, this phenomena can be explained. Theoretically, if the rate of destructuration is high, it is possible that the bonds are degrading at a high rate. This will occur in conjunction with a rapid growth of the intrinsic yield surface with consolidation time and the disturbed strength (remoulded strength) will increase. At the same time the undisturbed strength will decrease due to a reduction in size of the natural yield surface (schematic shown in Figure 6.25). With ongoing consolidation the rate of destructuration will eventually slow down and the undisturbed shear strength will increase as predicted in the top 8 m of the Murro deposit.

A parametric study was done to investigate the possibility of modelling the above mentioned phenomena with the S-CLAY1S model which accounts for destructuration of the bonds. It was thought that a high sensitivity of the deep layers of the Murro deposit would trigger such a behaviour. After several trial runs with x increased up to

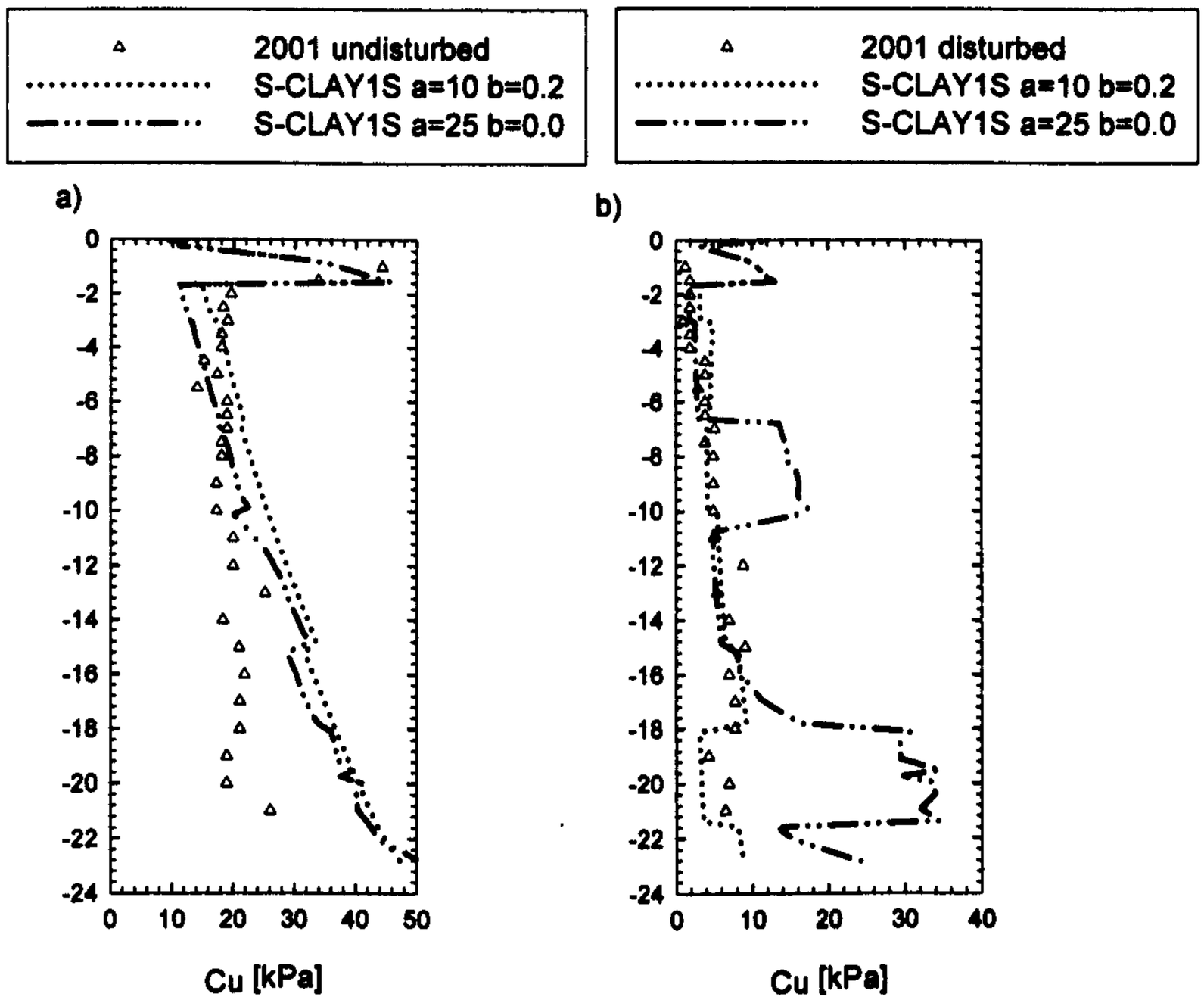

Figure 6.26: Undrained strength profile 8 years after construction: a) undisturbed strength and b) disturbed strength

500 in layer 4, 5, 6 and 7 it was found that with high a bonding parameter the phenomena cannot be simulated in a plane strain analysis. The next step was to change the parameters a and b in the destructuration law which controls the absolute rate of destructuration and relative effectiveness of plastic deviatoric strains and plastic volumetric strains in destroying the bonding. It was observed that increasing parameter a to about 20 and above in combination with an increase of parameter b to about 0.6 to 0.8, would result in a slow down of the increase of undisturbed shear strength with depth and time. As a consequence large deviatoric strains were predicted in layers 6 and 7, 8 years after construction. The predicted deviatoric strains are unrealistic at that depth and time. In order to reduce the large deviatoric strains the parameter b was set back to its original value of 0.2. Even with 0.2 the predicted shear strains were still unreasonable. As a next step the b value was set to 0. This resulted in the predicted strength profile presented in Figure 6.26. In Figure 6.26a the undisturbed strength underneath the centreline of the embankment 8 years after construction is compared

to the measured results and to the prediction of the original S-CLAY1S simulation. Inspection of the plot shows that the strength predicted with parameter a set to 25 results in a lower strength profile with depth. The predicted profile does not match the measurements but a substantial slow down in the increase of undisturbed shear strength is achieved. In Figure 6.26b the disturbed strength underneath the centreline is presented. Again the predictions are compared to the original S-CLAY1S simulations and to the measured field vane results from 2001. The increase of parameter a to 25 results in overestimating the disturbed strength at layer 4 and layer 7. Layer 4 is one of the softer layers of the deposit and the large volumetric strains cause the rapid growth of disturbed strength. The bonding parameter x used for layer 7 is 11.7 and higher than all the others used in the analysis. The x in combination with an a of 25, accelerated the growth of the intrinsic yield surface with consolidation time.

In Figure 6.27 the undisturbed strength is presented in contour plots. The current simulations are compared to the original simulations with the S-CLAY1S. Comparison of the predictions after 8 years (August 2001) clearly demonstrates the difference in the estimated strength contours. The original S-CLAY1S simulation shows an increase of strength at a depth of -2 m to -10m by an average of 5 kPa. In contrast the current simulation (S-CLAY1S with a=25 and b=0.0) hardly shows an increase of strength. Inspection of the contour plots after the end of consolidation demonstrates that the initial decrease of undisturbed strength followed by an increase in strength with time can not be modelled with S-CLAY1S. The simulation predicts a further reduction in strength with time and only a marginal increase of strength in the shallow areas.

The contour plots of disturbed strength predicted with a=25 and b=0 are shown in Figure 6.28. The results 8 years after construction and at the end of the consolidation are compared to the original S-CLAY1S simulations with a=10 and b=0.2. A large increase of strength is predicted by the simulations with a=25 and b=0.0 underneath the embankment at a depth of -5 m to -12 m. In the bottom two layers the increase in strength is predicted over the total width of the layers. The simulations predict that the strength with depth continues to increase with consolidation time. The maximum

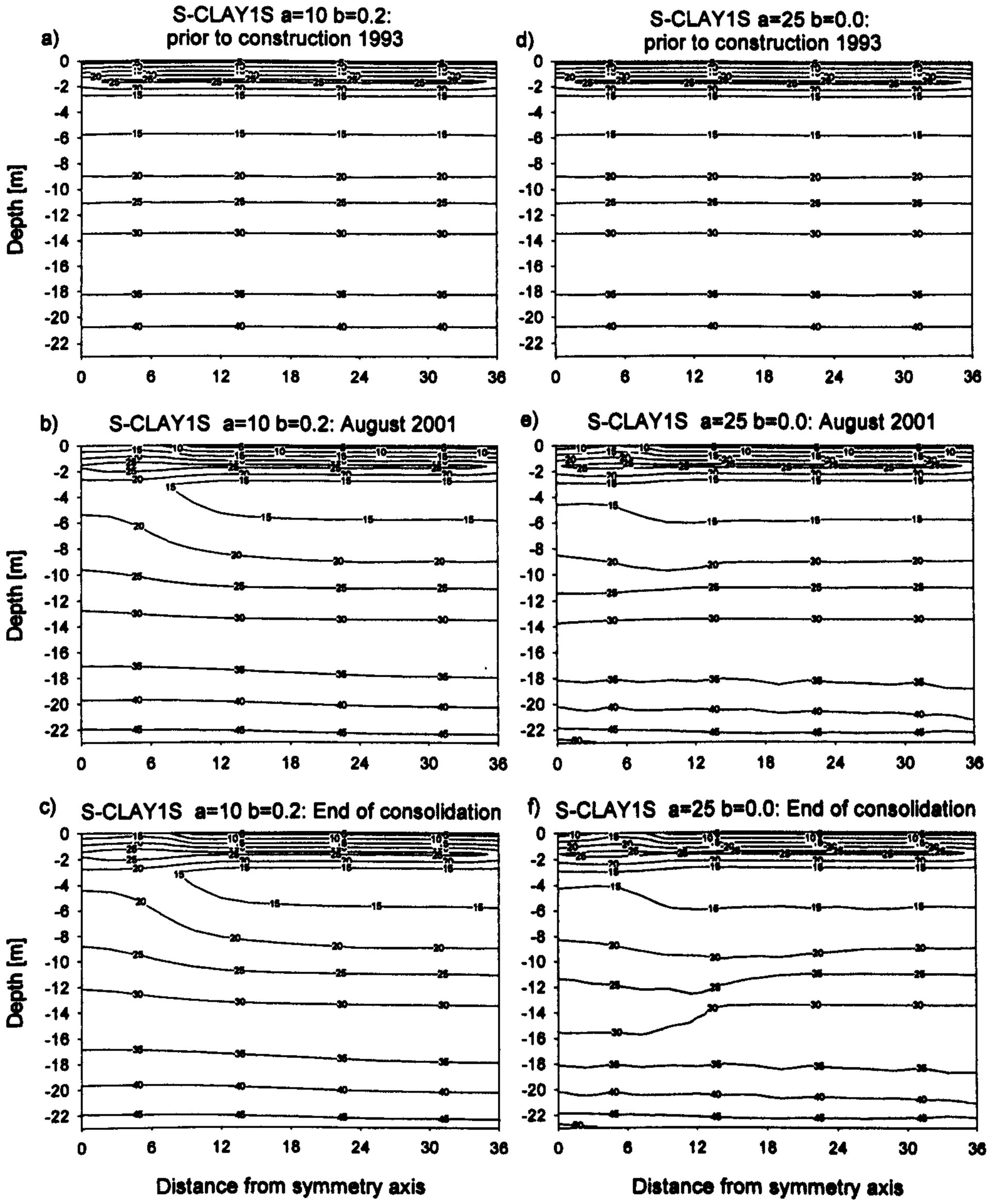

Figure 6.27: Contour plots of undisturbed undrained strength: a - c) S-CLAY1S model (a=10 and b=0.2) and d - f) S-CLAY1S model (a=25 and b=0.0)

growth rate is predicted at the end of the consolidation at a depth of about -13 m. The predicted values 8 years after construction and at the end of consolidation are far larger than the values predicted by the original simulations.

Changing parameters a and b from default values for Finnish clays (a=9-11 and b=0.2-0.3) to higher values showed that the increase of the size of the natural yield

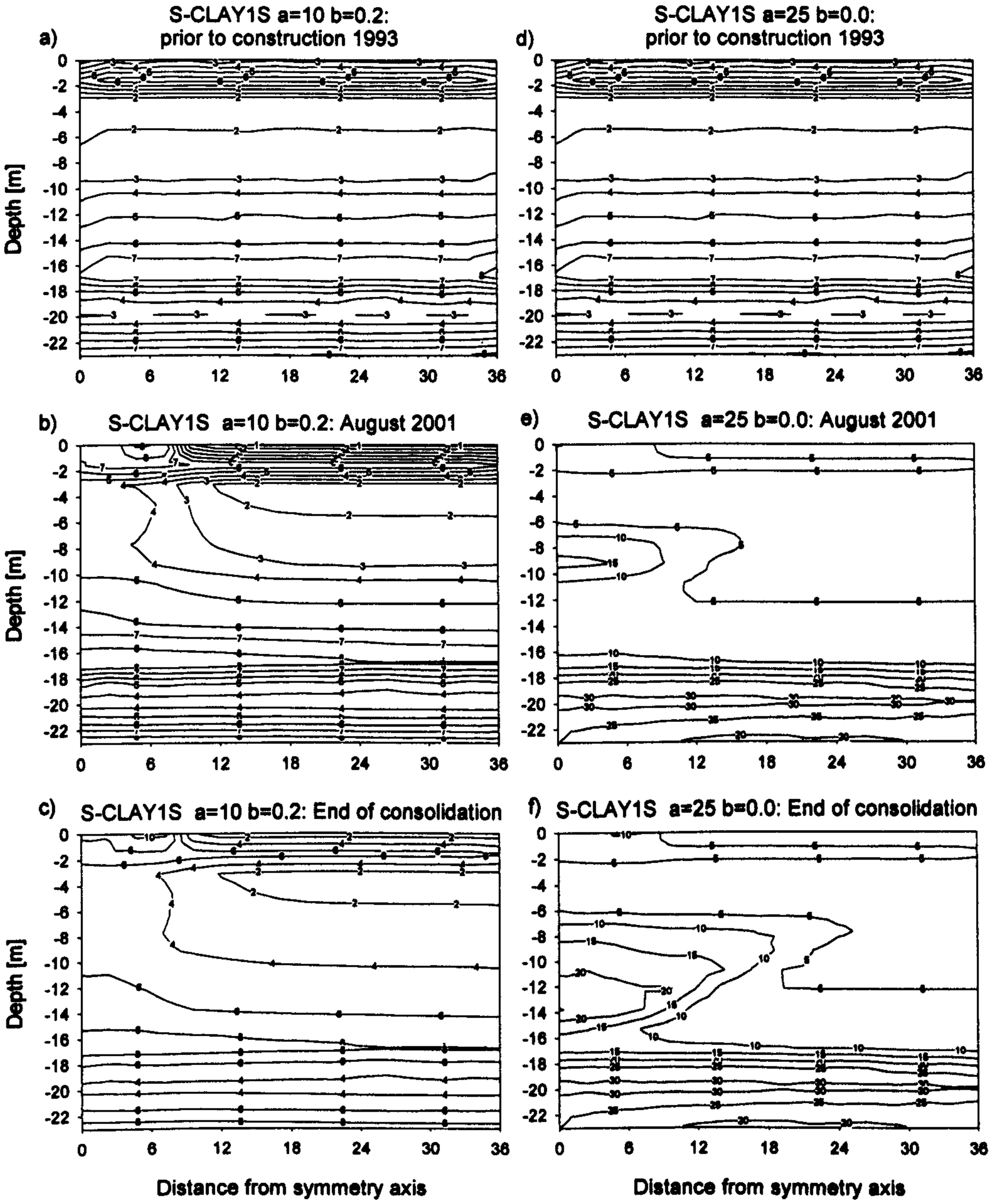

Figure 6.28: Contour plots of disturbed undrained strength: a - c) S-CLAY1S model (a=10 and b=0.2) and d - f) S-CLAY1S model (a=25 and b=0.0)

surface with consolidation time can be influenced. The increase of undisturbed strength in plane strain compression with time was slowed down. As a consequence the rate of increase of the size of the intrinsic yield surface with time was drastically increased. All of the above also influence the settlement predictions of the simulations. The maximum surface settlements at the centre line of the embankment are increased by 5 to 10 cm.

6.5.4.6 Influence of change of permeability with compression on predicted settlements

It is well known that permeability, k decreases as the void ratio decreases. In the current simulation the change of permeability with decreasing void ratio was ignored for the sake of simplicity. Koskinen et al. (2006) presented simulations of the Murro test embankment with the S-CLAY1S model where the change of permeability was accounted for. In the PLAXIS 2D finite element code the change in permeability is described by c_k which is determined by a simple relationship (Taylor, 1948):

$$\log\left(\frac{k}{k_0}\right) = \frac{\Delta e}{c_k}. \qquad [6.1]$$

Where Δe is the change in void ratio, k is the current permeability and k_0 is the initial permeability. The above relationship is used for the horizontal and vertical permeability (k_x and k_v) in the code. The gradient c_k can be determined from a void ratio versus permeability plot. Brinkgreve (2002) suggests that c_k is in the order of C_c (the compression index, which is determined in e-logσ' plot). C_c is related to λ via the simple relation:

$$\lambda = \frac{C_c}{2.3}. \qquad [6.2]$$

In Table 6.6 the c_k values estimated for the Murro deposit are shown. In the third column of the table the values suggested by Koskinen and Karstunen (2006) are presented. In the fourth column the values given are estimates based on C_c.

Table 6.6: Parameter c_k

Layer	Depth [m]	c_k (Koskinen and Karstunen, 2006)	c_k (estimated from C_c)
1a	0 - 0.8	0.25	0.46
1b	0.8 -1.6	0.25	0.46
2	1.6 -3.0	0.87	0.828
3	3.0 -6.7	1.06	1.288
4	6.7 -10.0	0.89	0.828
5	10.0 -15.0	0.64	0.736

Layer	Depth [m]	c_k (Koskinen and Karstunen, 2006)	c_k (estimated from C_c)
6	15.0 -18.0	0.47	0.506
7	18.0 -21.5	0.74	0.506
8	21.5 -23.0	0.09	0.345

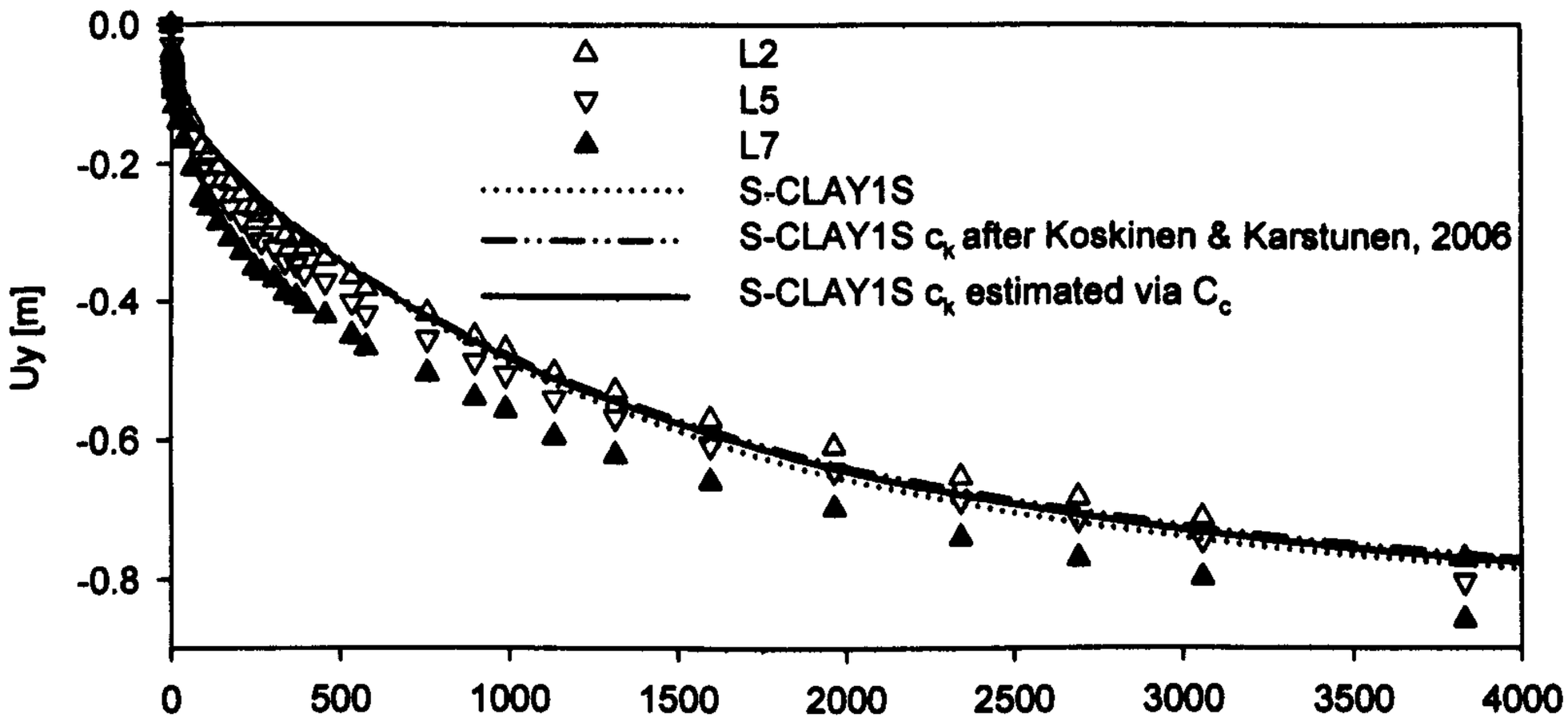

Figure 6.29: Time settlement curve: Influence of c_k

The values of c_k shown in the table are very similar except for the dry crust and for layer number 8. The effect of c_k on the predicted behaviour was studied by simulating the embankment with the S-CLAY1S model and the c_k values shown in Table 6.6. The predicted time settlement curves for a point at the symmetry axis underneath the embankment is compared to the original S-CLAY1S simulation presented previously in Section 6.5.4.1 which did not account for the change of permeability with the void ratio. The time settlement curve is shown in Figure 6.29. Accounting for the change of permeability with a decrease in void ratio marginally reduces the predicted vertical displacements with time. The magnitude of reduction is in the order of 1.5 cm (c_k after Koskinen and Karstunen, 2006) and 1.0 cm (c_k estimated via C_c).

In the absence of any data on the change of the permeability with the change in void ratio the c_k value can be reasonable well estimated via the C_c as demonstrated by the

simulations. Overall it can be concluded that neglecting the change of permeability in the simulations does not change the quality of the predicted time settlement behaviour.

6.5.4.7 Influence of Poisson's ratio

The comparison of the prediction of the horizontal displacements with the measured displacements are generally in good agreement. The underprediction of the horizontal displacements in the long term (8 - 14 years) can possibly be explained by creep. It was demonstrated in the results that one year after construction the horizontal displacements at the toe are overestimated, particularly for the displacements in the deeper layers. Despite the fact that the soil at depth is almost normally consolidated, to some extent elastic straining will influence the horizontal displacements. The predicted elastic behaviour in the MCC and the S-CLAY models is based on Hooke's law of elasticity. As mentioned in Section 6.5.1 Poisson's ratio was taken as 0.15 which is a typical value for soft clay.

Brinkgreve and Vermeer (2001) suggest a procedure to determine the initial state of the stress of overconsolidated ground by considering the stress history of the ground. Assuming one dimensional compression, loading to the maximum stress σ'_{v_max} follows a gradient of K_0^{nc} over 1, with $K_0^{nc}= 1-\sin\varphi'$ (see Figure 6.30). From point B to C the soil is unloaded. While unloading it is assumed that the soil behaves linearly elastic. The unloading gradient follows $K_0 = \nu'/(1-\nu')$ with a Poisson's ratio ν'_{ur} for unloading/reloading. The inclination of the line between point A and C can then be described by:

$$K_0^{oc} = \frac{\sigma'_h}{\sigma'_v} = (1-\sin\varphi')OCR - (OCR-1)\frac{\upsilon'_{ur}}{1-\upsilon'_{ur}}. \qquad [6.3]$$

The procedure to determine K_0^{oc} by Brinkgreve and Vermeer (2001) relies on knowing the Possion's ratio ν'_{ur} for the soil which is very often not the case. For the Murro simulations the K_0^{oc} was derived using the equation suggested by Mayne and Kul-

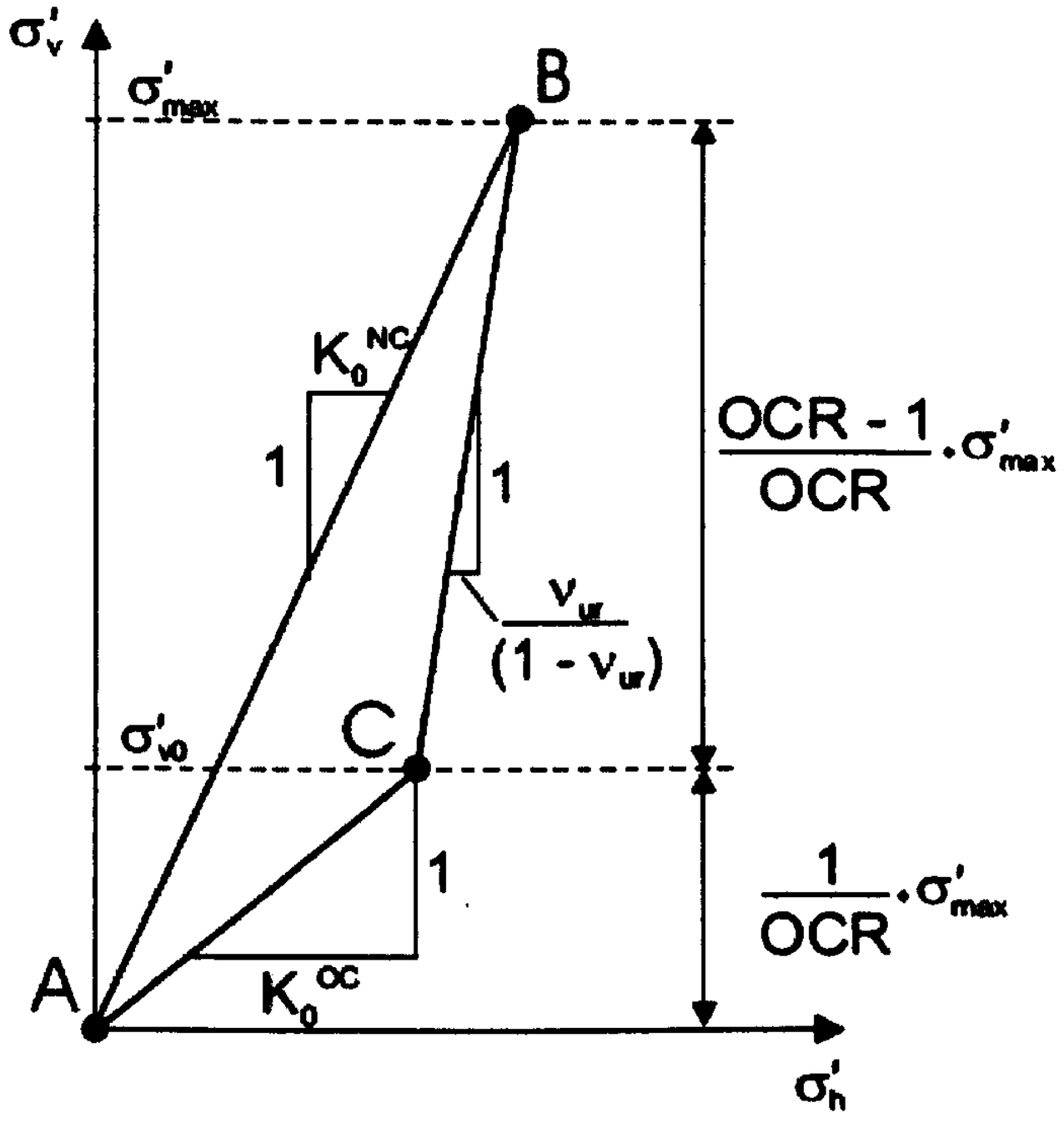

Figure 6.30: Relationship between K_0^{oc} and OCR for overconsolidated soils (Brinkgreve and Vermeer, 2001) (Figure after Moeller, 2006)

hawy (1982). Following the ideas by Brinkgreve and Vermeer (2001) presented in Figure 6.30 and replacing *Eq. 6.3* with the equation by Mayne and Kulhawy (1982) for K_0^{oc} will lead to a different inclination of the line between B and C in Figure 6.30. The different inclination will necessarily lead to a different Poisson's ratio ν'_{ur}. Poisson's ratio ν'_{ur} can be defined by:

$$\frac{\Delta\sigma'_h}{\Delta\sigma'_v} = \frac{\sigma'_{hmax} - \sigma'_h}{\sigma'_{vmax} - \sigma'_v} = \frac{K_0^{nc}\sigma'_{vmax} - K_0^{oc}\sigma'_v}{\sigma'_{vmax} - \sigma'_v} = \frac{\upsilon'_{ur}}{1 - \upsilon'_{ur}} \qquad [6.4]$$

with $K_0^{nc} = 1\text{-}\sin\varphi'$ and $K_0^{oc} = (1\text{-}\sin\varphi')OCR^{\sin\varphi'}$. Rearranging *Eq. 6.4*, Poisson's ratio ν'_{ur} can be calculated.

$$\upsilon'_{ur} = \frac{K_0^{nc}\sigma'_{vmax} - K_0^{oc}\sigma'_v}{\sigma'_{vmax}(1 + K_0^{nc}) - \sigma'_v(1 + K_0^{oc})} \qquad [6.5]$$

Inserting $\sigma'_{v\_max} = \sigma'_v * OCR$ leads to:

$$\upsilon'_{ur} = \frac{(K_0^{nc} OCR - K_0^{oc})}{(OCR(1 + K_0^{nc}) - (1 + K_0^{oc}))} \quad . \qquad [6.6]$$

The formula for deriving Poisson's ratio ν'_{ur} was used to determine Poisson's ratio ν'_{ur} for each layer in the Murro simulations. Poisson's ratios calculated based on *Eq. 6.6* are presented in Table 6.7.

Table 6.7: Poisson's ratio

Layer	Depth [m]	ν'_{ur}	ν'_{ur} estimated via *Eq. 6.6*
1a	0 - 0.8	0.15	0.18
1b	0.8 -1.6	0.15	0.13
2	1.6 -3.0	0.15	0.13
3	3.0 -6.7	0.15	0.11
4	6.7 -10.0	0.15	0.12
5	10.0 -15.0	0.15	0.12
6	15.0 -18.0	0.15	0.16
7	18.0 -21.5	0.15	0.16
8	21.5 -23.0	0.15	0.16

The Murro test embankment was recalculated with the S-CLAY1S model with the above shown values for ν_{ur} and compared to the original S-CLAY1S simulations presented previously. The predicted time settlement curve is plotted in Figure 6.31. The predicted time settlement curve is similar to the original predictions with a ν'_{ur} of 0.15, as expected. Immediately after construction the maximum settlement at the centreline is 7.4 cm compared to 8.6 cm, previously.

The effect of the ν'_{ur} on the predicted horizontal displacement with consolidation time underneath the crest of the embankment is presented in Figure 6.32. Immediately after construction the horizontal displacements are reduced due to the generally smaller ν'_{ur} used in the simulations. With increasing consolidation time the difference in predictions are becoming smaller and smaller until it is hardly noticeable. In September 1998 the difference is no longer noticeable in the predictions.

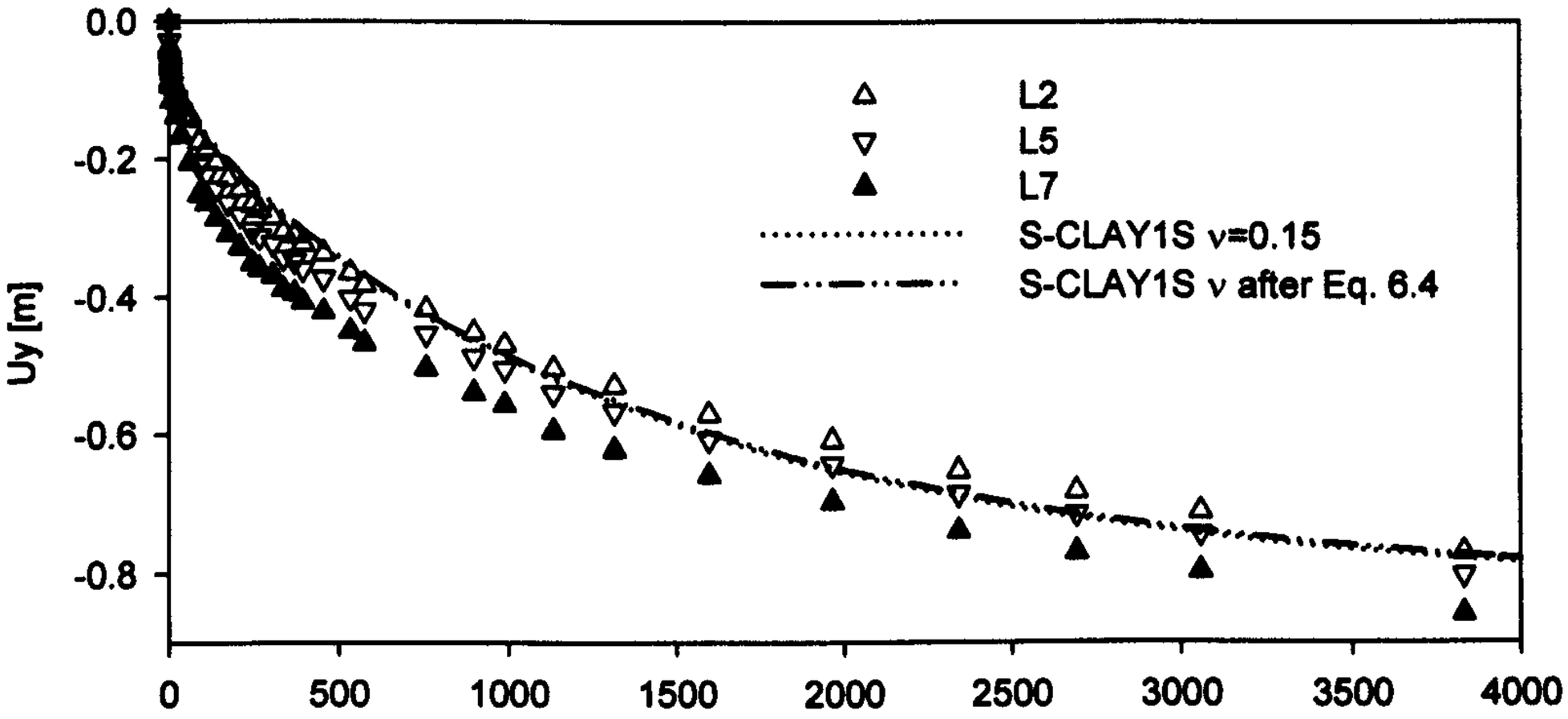

Figure 6.31: Time settlement curve: Influence of Poisson's ratio ν_{ur}

The horizontal displacements below the toe of the embankment are plotted in Figure 6.33. Again a reduction of the maximum horizontal displacement with the lower ν'_{ur} is observed. However, the measured displacements in the first two years after construction are still overestimated and underestimated with increasing consolidation time.

In the absence of any laboratory test results, the proposed method to determine ν_{ur} provides a reliable way of estimating a realistic ν'_{ur} for overconsolidated soils. One has to be aware that this method is limited to soils which are overconsolidated (OCR>1) and can not be used for normally consolidated soils.

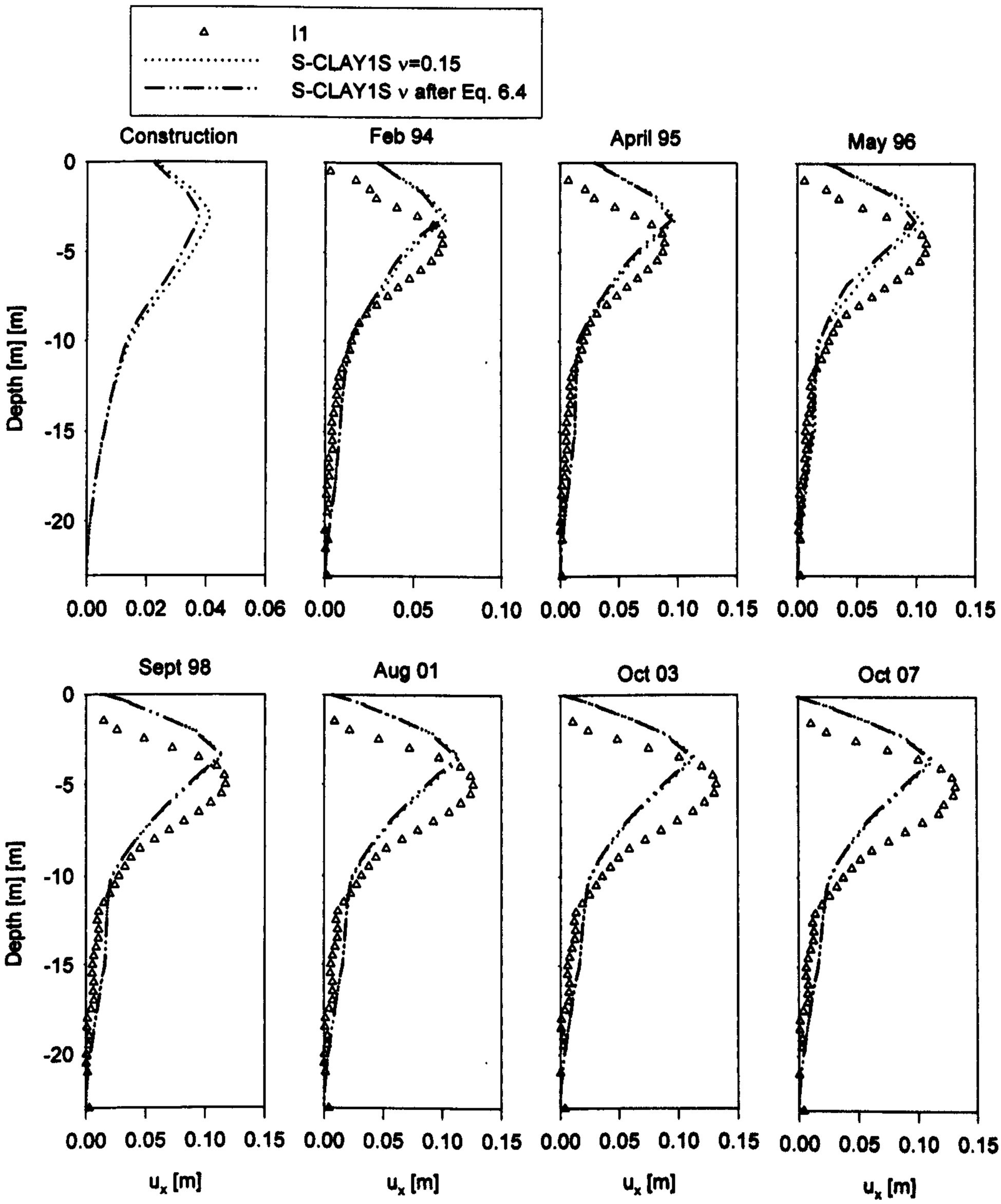

Figure 6.32: Horizontal displacement underneath the crest (influence of Poisson's ratio): a) immediately after construction b) February 1994 (1 year) c) April 1995 (2 years), d) May 1996 (3 years), e) September 1998 (5.5 years), f) August 2001 (8.5 years), g) October 2003 (10.5 years) and h) October 2007 (14.5 years)

6.5.4.8 Influence of μ

The parameter μ controls the absolute rate of rotation at which the yield surface rotates. The μ used in the simulations is estimated based on the function suggested by Zentar et al. (2002). μ is simply a function of the virgin compression index λ with 10/

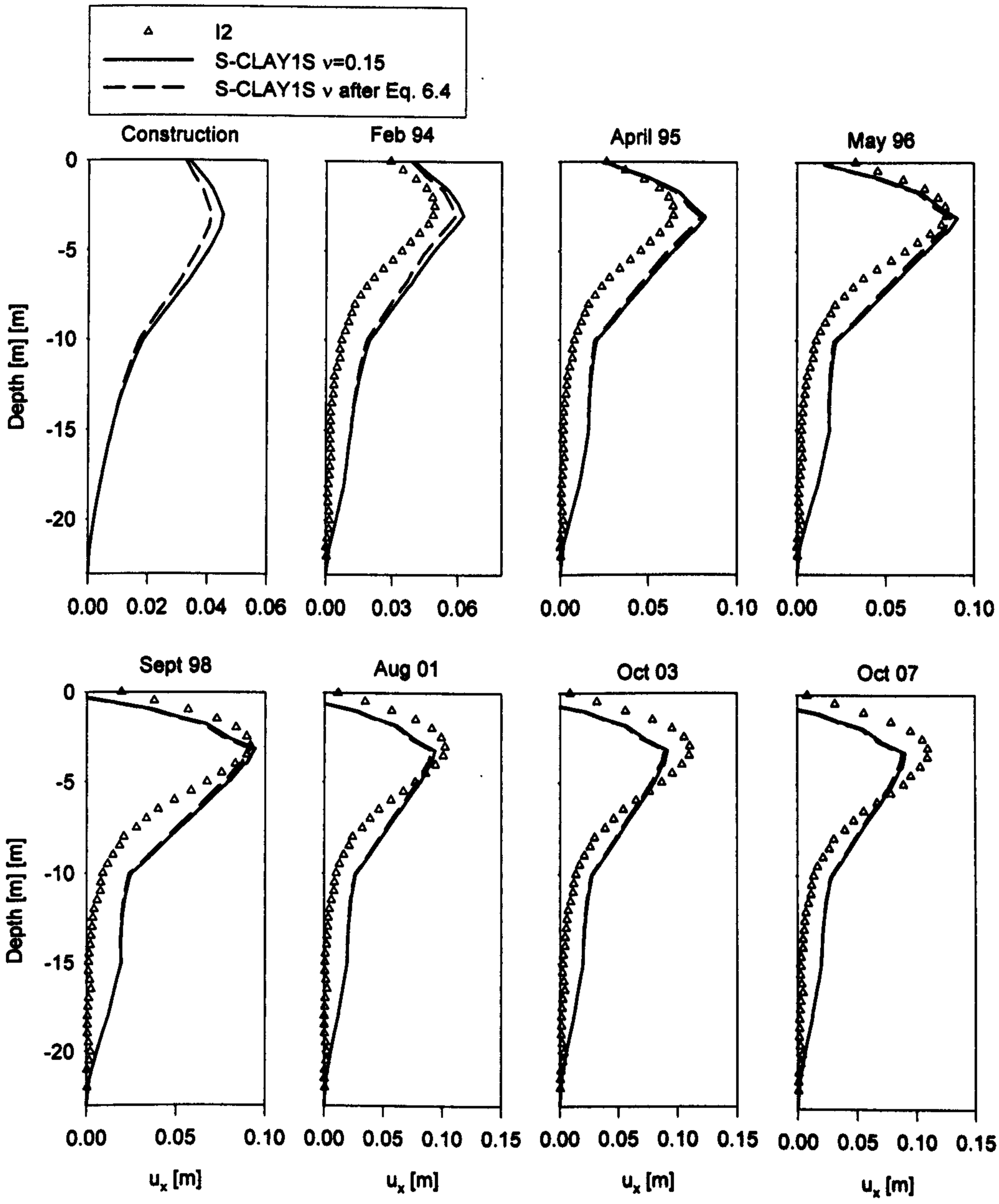

Figure 6.33: Horizontal displacement underneath the toe (influence of Poisson's ratio): a) immediately after construction b) February 1994 (1 year) c) April 1995 (2 years), d) May 1996 (3 years), e) September 1998 (5.5 years), f) August 2001 (8.5 years), g) October 2003 (10.5 years) and h) October 2007 (14.5 years)

λ to $15/\lambda$. Leoni et al. (in press) who developed the Anisotropic Creep model (see Section 2.6.2) derived a relation between ω and λ^*, where ω controls the absolute rate of rotation in their model and λ^* is the modified compression index (defined in ε_v-lnp' plot). Anandrajah et al. (1996) concluded based on experimental work that the initial anisotropy is erased if a sample is isotropically loaded to two or three times its nor-

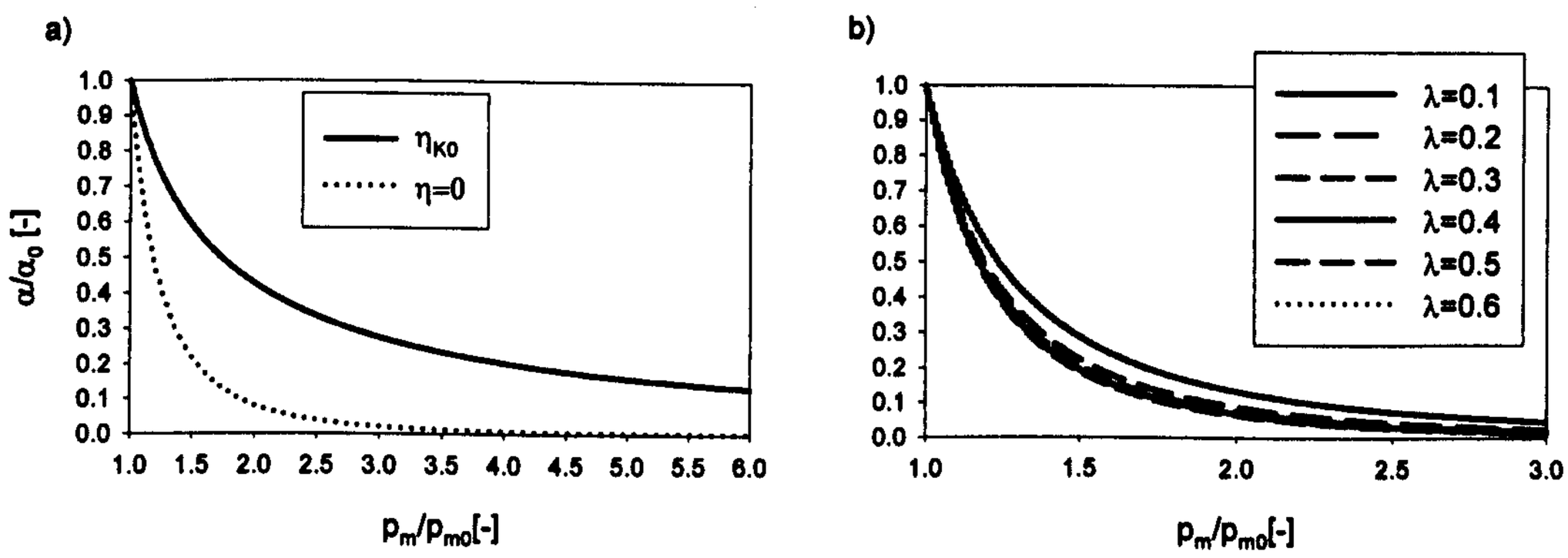

Figure 6.34: Rotation of the yield surface: a) Influence of the initial stress state and b) Influence of virgin compression index λ

mally consolidated preconsolidation pressure. They concluded that it makes a soil isotropic in terms of strain response but the soil still remains anisotropic with respect to the particle orientation. This finding allowed Leoni et al. (in press) to derive a simple relation between ω and λ^*.

$$\omega = \frac{1}{\lambda^*} \ln \frac{10M^2 - 2\alpha_0\omega_d}{M^2 - 2\alpha_0\omega_d} \qquad [6.7]$$

where α_0 and ω_d are determined by the critical state angle φ', as defined in Eq 2.23 and Eq. 2.29. ω depends soley on the modified compression index λ^* and on the critical state friction angle φ'.

The conclusions by Anandrajah et al. (1996) are investigated with the S-CLAY1 model. In Figure 6.34a the rotation of the yield surface with an increase of the size of the natural yield surface p_m is presented. The material parameters are chosen to represent Murro clay at a depth of -7 m (λ=0.42). Two simulations with the same initial stress state were performed. In the first simulation it was assumed that the sample is loaded with a stress ratio η_{K0} and in the second simulation the sample was isotropically loaded with a stress ratio η=0. Both samples were loaded until the anisotropy was almost erased or reached less than 10% of the initial value of α_0. The first sample was loaded until the ratio p_m/p_{m0} (size of the current yield surface p_m to initial yield

surface p_{m0}) was about 10 times. At this point the anisotropy reduced to about 10% of the initial anisotropy (α/α_0). In contrast in the isotropically loaded sample the ratio α/α_0 reduces to 10% or less at a ratio of p_m/p_{m0} of about 2. The model simulations are in agreement with the conclusion by Anandrajah et al. (1996) for soft soils.

In Figure 6.34b the influence of the stiffness λ of the soil on the α/α_0 and p_m/p_{m0} ratio during isotropic shearing is presented. It is clearly demonstrated that the softer the soil, the earlier the anisotropy is erased. It can be concluded that for soils with a λ equal to 0.3 or greater, the initial anisotropy is almost erased at a ratio of p_m/p_{m0} of 2.

This finding will be used to derive a relation between μ and the stiffness of the soil following the idea by Leoni et al. (in press).

The required plastic volumetric strain increment $\delta\varepsilon_v^p$ for erasing the anisotropy is:

$$\delta\varepsilon_v^p = \frac{\lambda-\kappa}{1+e}\ln\left(\frac{p'_m}{p'_{m0}}\right) = \frac{\lambda-\kappa}{1+e}\ln(2)\,. \qquad [6.8]$$

In triaxial stress space the ratio between the plastic deviatoric and plastic volumetric strain is defined by the associated flow rule:

$$\frac{d\varepsilon_q^p}{d\varepsilon_v^p} = \frac{\partial g/\partial q}{\partial g/\partial p'} = \frac{2\left(\frac{q}{p'}-\alpha\right)}{M^2-\left(\frac{q}{p'}\right)^2}. \qquad [6.9]$$

The rotational hardening law Eq. 2.16 in triaxial stress space simplifies to:

$$d\alpha = \mu\left[\left(\frac{3q}{4p'}-\alpha\right)d\varepsilon_v^p + \beta\left(\frac{q}{3p'}-\alpha\right)d\varepsilon_{vd}^p\right]. \qquad [6.10]$$

Inserting *Eq. 6.9* into *Eq. 6.10* (rotational hardening law) and assuming isotropic loading with q=0, leads to the following differential equation:

$$-\mu d\varepsilon_v^p = \frac{M^2 d\alpha}{M^2\alpha - 2\alpha^2\beta}. \qquad [6.11]$$

Eq. 6.11 can be integrated between α_0 and α_1 with $\alpha_1 = \alpha_0 + \delta\alpha$ to obtain the following equation:

$$\mu \Delta \varepsilon_v^p = \ln \frac{\alpha_0 / \alpha - 2\alpha_0 \beta}{M^2 - 2\alpha_0 \beta}. \qquad [6.12]$$

Inserting *Eq. 6.8* into *Eq. 6.12* and assuming that the anisotropy α decreases to 1/10 (α_0/α=10) the following can be obtained:

$$\mu = \frac{1+e}{(\lambda-\kappa)\ln\left(\frac{p'_m}{p'_{m0}}\right)} \ln \frac{10M^2 - 2\alpha_0\beta}{M^2 - 2\alpha_0\beta} \quad . \qquad [6.13]$$

μ depends therefore on the critical state stress ratio M, the initial inclination of the yield surface α_0, the soil constant β, the initial void ratio and the stiffness of the soil (λ and κ).

In the following study the formula for μ by Leoni et al. (in press) is compared to *Eq. 6.13* and to the relation suggested by Zentar et al. (2002). *Eq. 6.13* was used with three different ratios of p_m/p_{m0} in the study (2, 2.5 and 3). In contrast a fixed ratio of 3 was assumed by Leoni et al. (in press). In the study the virgin compression index λ was varied from 0.1 to 0.6 and a ratio of 10 was used for κ/λ. At the same time the influence of the critical state stress ratio M on the predicted value of μ was studied by varying M between 1.0 and 1.8. The results are presented in Figure 6.35. For the correlation between the modified compression index and the virgin compression index a void ratio of 1.55 was assumed. The formula suggested by Leoni et al. (in press) predicts a lower bound value for μ as does *Eq. 6.13* with a ratio of 3 for p_m/p_{m0}. It also lies outside the range suggest by Zentar et al. (2002). The μ values predicted by *Eq. 6.13* with a p_m/p_{m0} ratio of 2 are well inside the upper and lower bound suggested by Zentar et al. (2002).

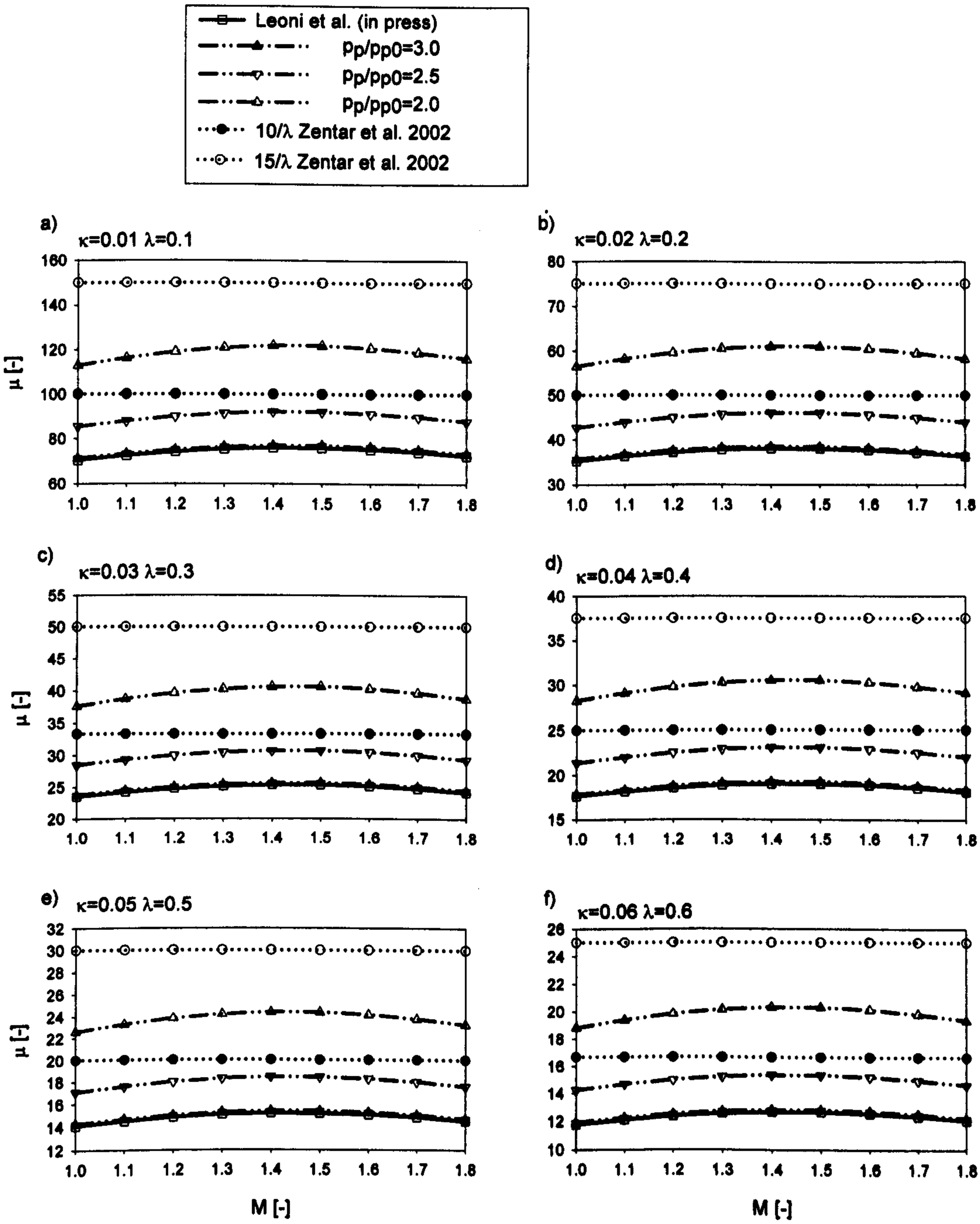

Figure 6.35: Predictions of μ with different formulas at different soil stiffness and critical state stress ratios M

The influence of the ratio of κ/λ on the predicted μ values is presented in Figure 6.36. The μ values presented were calculated by assuming a λ of 0.4 and the ratio of κ/λ

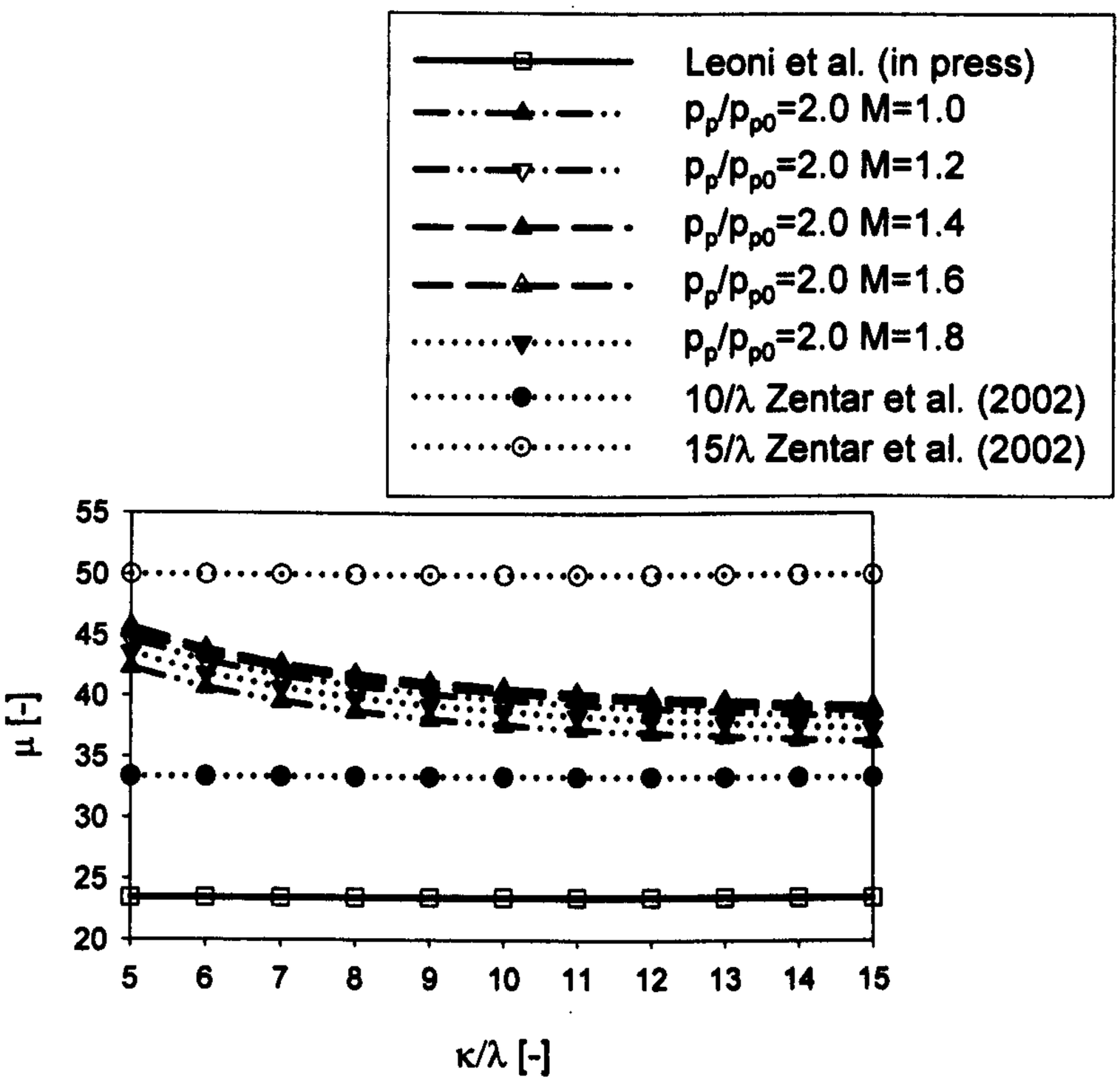

Figure 6.36: Influence on the ratio of κ/λ on the predicted μ values

was varied between 5 and 15. In addition the M was varied between 1.0 and 1.8 to demonstrate the influence of M on the μ values by *Eq. 6.13*. *Eq. 6.13* was used with a ratio p_m/p_{m0} of 2. The influence of M on Leoni et al. (in press) is not shown as it was found to be marginal if the modified compression index is kept constant. The predicted μ values decrease in a non linear manner with increasing κ/λ ratio. The influence of the κ/λ ratio is more pronounced than the influence of M on the μ values. Overall it can be seen that the μ values are still within the upper and lower bound suggested by Zentar et al. (2002). It can be concluded that *Eq. 6.13* with ratio p_m/p_{m0} of 2 is in good agreement with values suggested by Zentar et al. (2002).

The effect of calculating μ with the proposed formula rather than estimating via the relation suggest by Zentar et al. (2002) is demonstrated by the back calculation of drained triaxial test on natural Murro clay. The simulations are performed with the S-

CLAY1S model. The parameters of the tests are shown in Table 6.8 and are the same as used for the triaxial simulations in Section 5.3.4.

Table 6.8: Parameters and initial state for natural Murro Clay from a depth of 6.9-7.6 m

Model	λ_i	κ	ν'	M	μ	β	a	b	α_{K0}	x_0
S-CLAY1S μ with $10/\lambda$-$15/\lambda$	0.21	0.03	0.3	1.6	20	1.02	10	0.2	0.63	9.5
S-CLAY1S μ after *Eq. 6.11*	0.21	0.03	0.3	1.6	28	1.02	10	0.2	0.63	9.5

A λ of 0.47 (Koskinen and Karstunen, 2004) was used to estimate a μ of 20 after Zentar et al. (2002) and to calculate a μ of 28 with *Eq. 6.11*. Details of simulated tests on the natural Murro clay are summarised in Table 6.9.

Table 6.9: Simulated triaxial tests on natural Murro Clay from a depth of 6.9-7.6 meters

Test number	Depth [m]	e_0	w_0 [%]	η_1	η_2
CAD 2987	7.26-7.37	1.962	74.1	0.20	-0.87
CAE 2989	7.15-7.26	1.945	73.4	0.61	-0.66

Figure 6.37 shows the experimental data of Test CAD 2987 on natural Murro clay and the model predictions with S-CLAY1S with the different μ values of 20 and 28. The prediction of the volumetric strains are not influenced by the increase of μ from 20 to 28. During the first loading cycle at a stress ratio η_1 of 0.2 the increase of μ to 28 marginally reduces the negative deviatoric strains. Overall the predictions are similar and the μ predicted by *Eq. 6.11* is reasonable.

The results of Test CAD 2989 and the predictions by the S-CLAY1S model with different μ values are presented in Figure 6.38. Both simulations underestimate the volumetric and deviatoric strains in both loading cycles. However, the bigger μ value of 28 marginally increases the predicted deviatoric strains during the first loading cycle at η_1 of 0.61. In contrast during the second cycle with a η_2 of -0.86, the deviatoric strains are underpredicted.

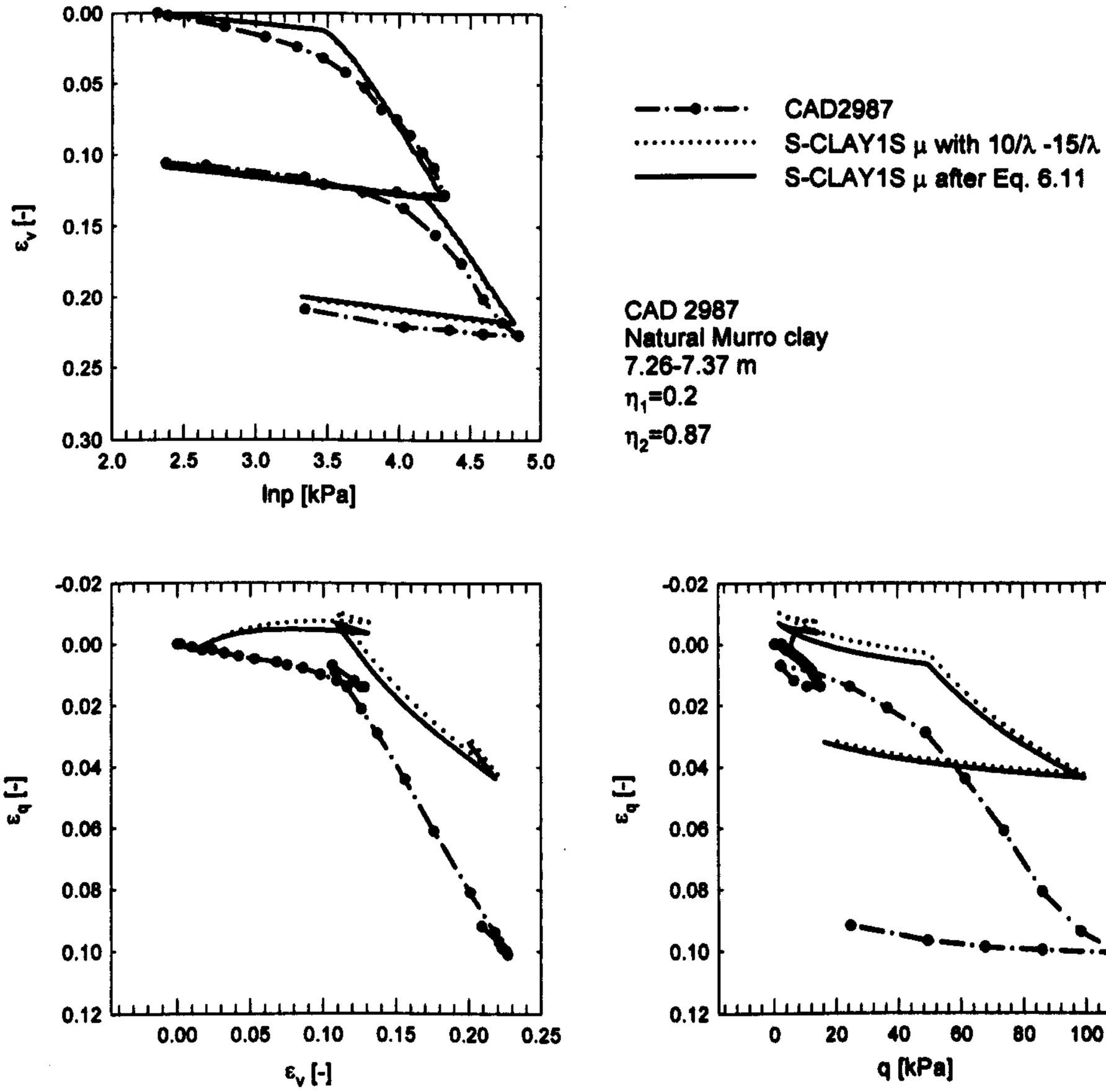

Figure 6.37: Test CAD 2987 on natural Murro clay: Influence of μ

A reasonable prediction of μ is important in situations where a lot of rotation of the yield surface can be expected. In terms of embankment simulations a large rotation of the yield surface is expected in areas below the toe of the embankment where a rotation of the principal stresses and shearing occurs. In contrast in areas below the centre line of the embankment only a small amount of rotation can be expected. As a consequence it can be expected that the reasonable μ value will not heavily influence the settlement predictions. Nevertheless, *Eq. 6.13* is used to derive μ values for the Murro test embankment simulations (Table 6.10).

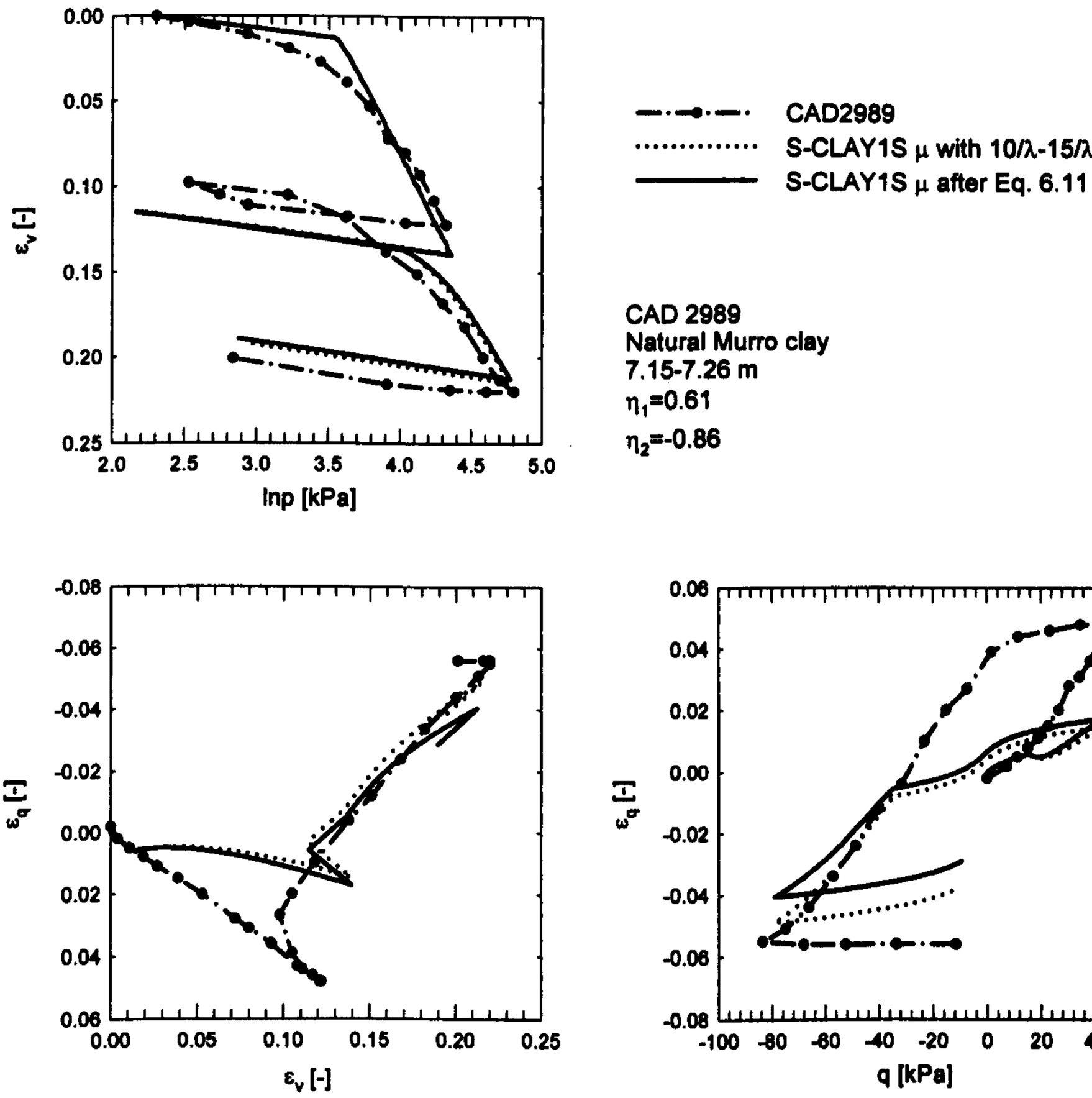

Figure 6.38: Test CAD 2989 on natural Murro clay: Influence of μ

Table 6.10: Parameter μ

Layer	Depth [m]	μ	μ estimated via *Eq. 6.13*
1a	0 - 0.8	61	61
1b	0.8 -1.6	61	59
2	1.6 -3.0	47	37
3	3.0 -6.7	28	28
4	6.7 -10.0	32	41
5	10.0 -15.0	43	41
6	15.0 -18.0	55	57
7	18.0 -21.5	47	59
8	21.5 -23.0	83	72

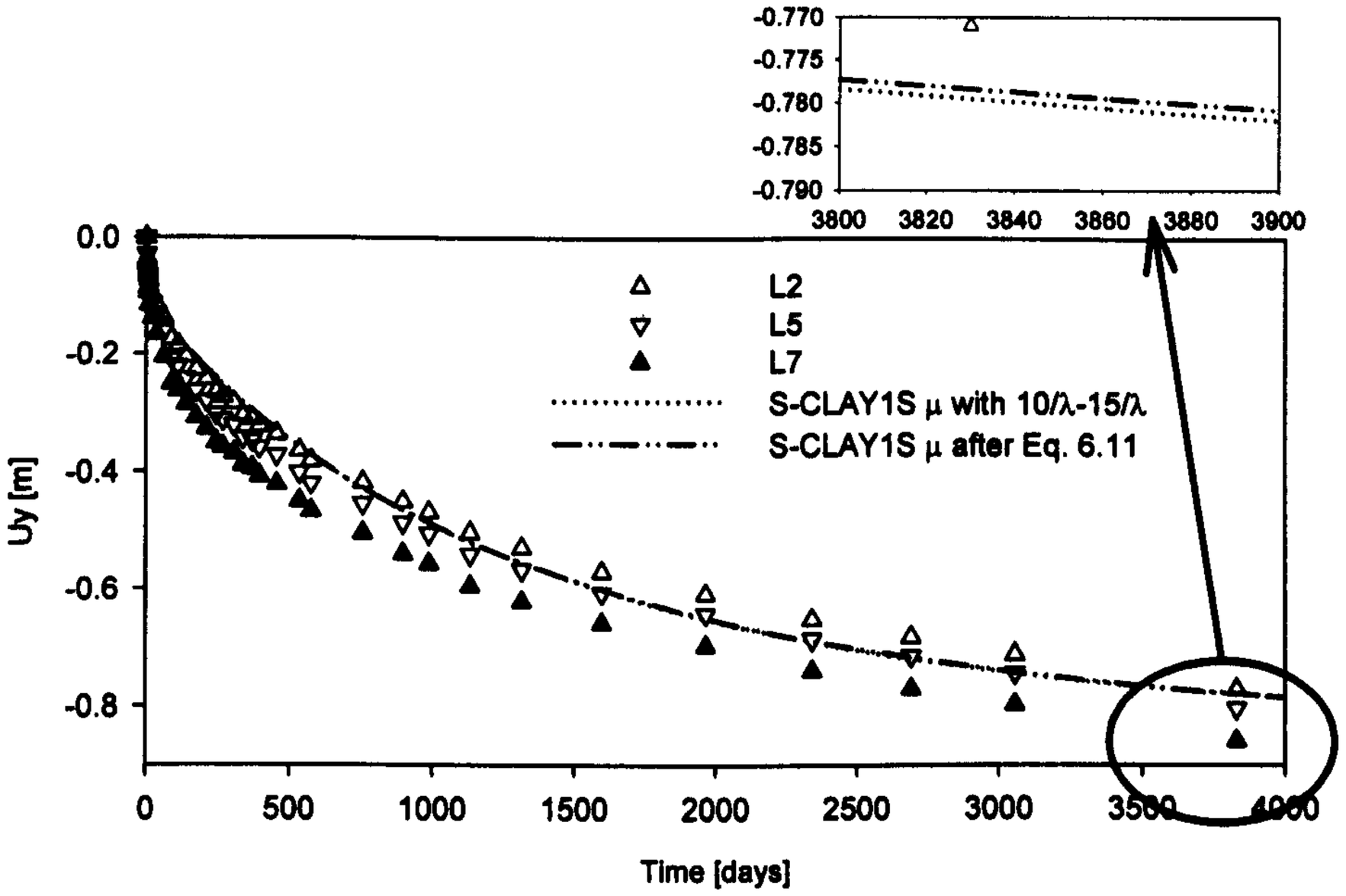

Figure 6.39: Time settlement curve: Influence of the μ values

The calculated μ values shown in the fourth column of the table have been used in a simulation of the Murro embankment with the S-CLAY1S model. The predicted time settlement curve is compared to the original S-CLAY1S simulation with the μ values estimated after Zentar et al. (2002) (see Figure 6.39). As expected the predicted time settlement curves are similar due to the fact that the μ values calculated with *Eq. 6.11* are almost of the same order. The large difference of μ in layer 8 (bottom of the model) does not influence the behaviour as the plastic volumetric and shear strains are negligible for the overall response.

Based on the experience in the back calculations of the triaxial tests and the simulations of the Murro test embankment it can be concluded that determining μ with *Eq. 6.11* is reasonable. Koskinen and Karstunen (2006) used a lower bound value of μ in their simulations. *Eq. 6.11* gives somewhat higher values which are reasonably well predicted for embankment problems.

6.5.4.9 Factor of Safety for stability

The stability of the Murro embankment was assessed at two different stages in the life time of the embankment. First the Factor of Safety (FoS) immediately after construction of the embankment was estimated using the Oasys Slope 18.2 (2007) programme. Secondly, the FoS 8 years after construction was determined. The calculations were performed in terms of a total stress analysis by assuming a circular type slip surface after Bishop. The undisturbed undrained shear strength profile with depth prior to construction is based on the profile predicted with the S-CLAY1S model and shown in Figure 6.12. In the Slope model the Murro deposit is divided into four layers. In each layer an undrained strength increasing linearly with depth was assumed based on the profile shown in Figure 6.12.

Table 6.11: Input parameters for Slope analysis: Undrained strength prior construction

	Undrained strength [kPa]	Change of undrained strength per m depth [kPa]	Reference depth [m]
Layer 1	4	25	0.0
Layer 2	10	1.9	-1.6
Layer 3	10	2.2	-3.7
Layer 4	28	0	-16.0

An isotropic undrained strength is assumed in the Slope analysis assuming the same strength in compression and in tension. The predicted slip surface is shown in Figure 6.40. The predicted FoS immediately after construction is 2.14.

To determine the increase of FoS with time the analysis was repeated for the time 8 years after construction in August 2001. The undisturbed strength profile with depth predicted by the S-CLAY1S model was used. The input is based on the contour plots of undrained strength presented in Figure 6.22e. The horizontal variation of strength over the width of the model is included in the Slope model. The non-linear contour lines presented in Figure 6.22e are simply simulated with linear non-horizontal lines

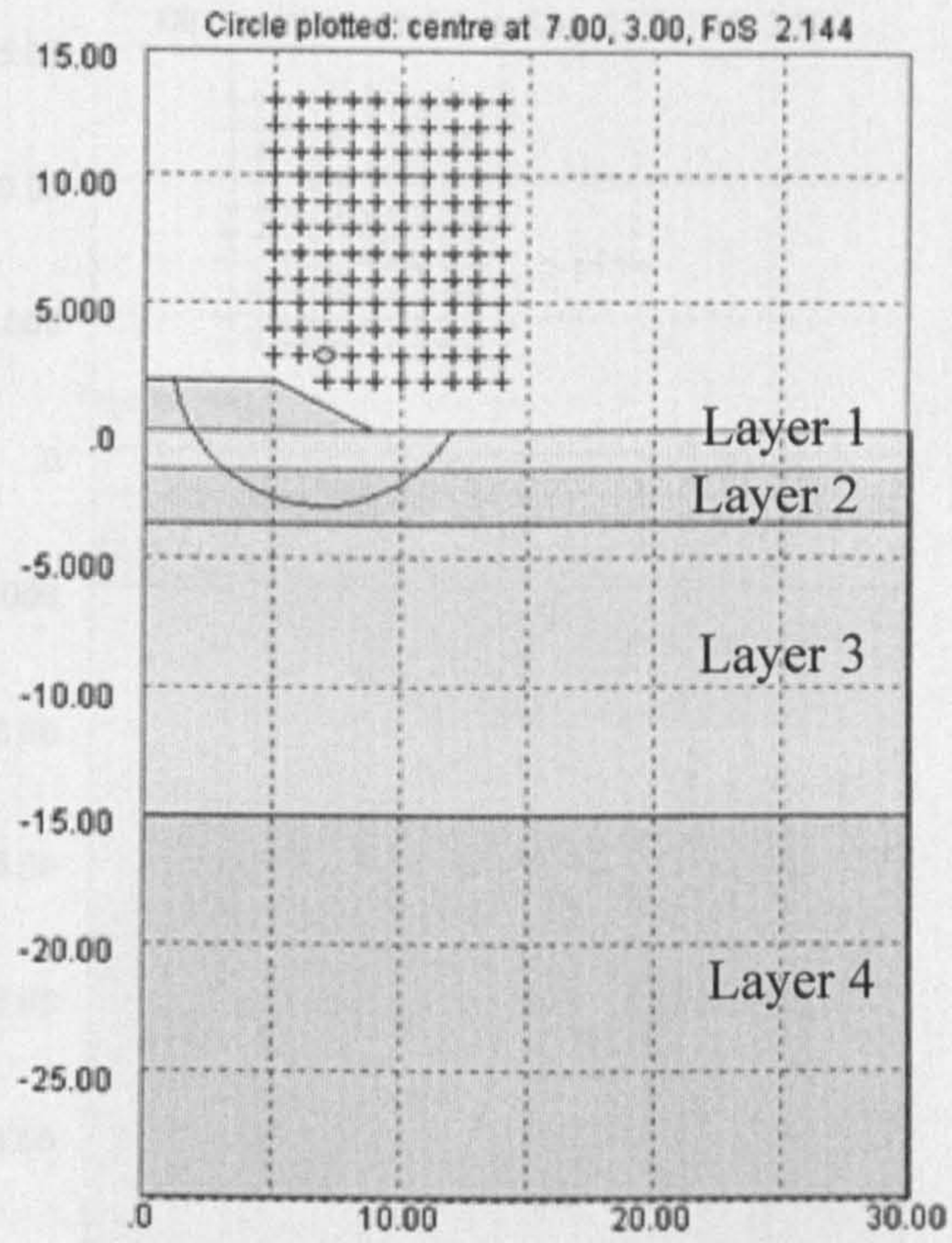

Figure 6.40: Slip surface immediately after construction of the embankment

as shown in Figure 6.41. For this simulation the Murro deposit was divided into five layers.

Table 6.12: Input parameters for Slope analysis 8 years after construction

	Undrained strength [kPa]	Change of undrained strength per m depth [kPa]	Reference depth [m]
Layer 1	4	25	0.0
Layer 2	10	1.9	-1.6
Layer 3	15	2.0	-1.6
Layer 4	19	1.6	-5.0
Layer 5	34	1.5	-16.0

In each layer a strength profile where strength increases linearly with depth was assumed. The predicted FoS is 2.96. 8 years after construction the FoS increased from the initial 2.14 to 2.96.

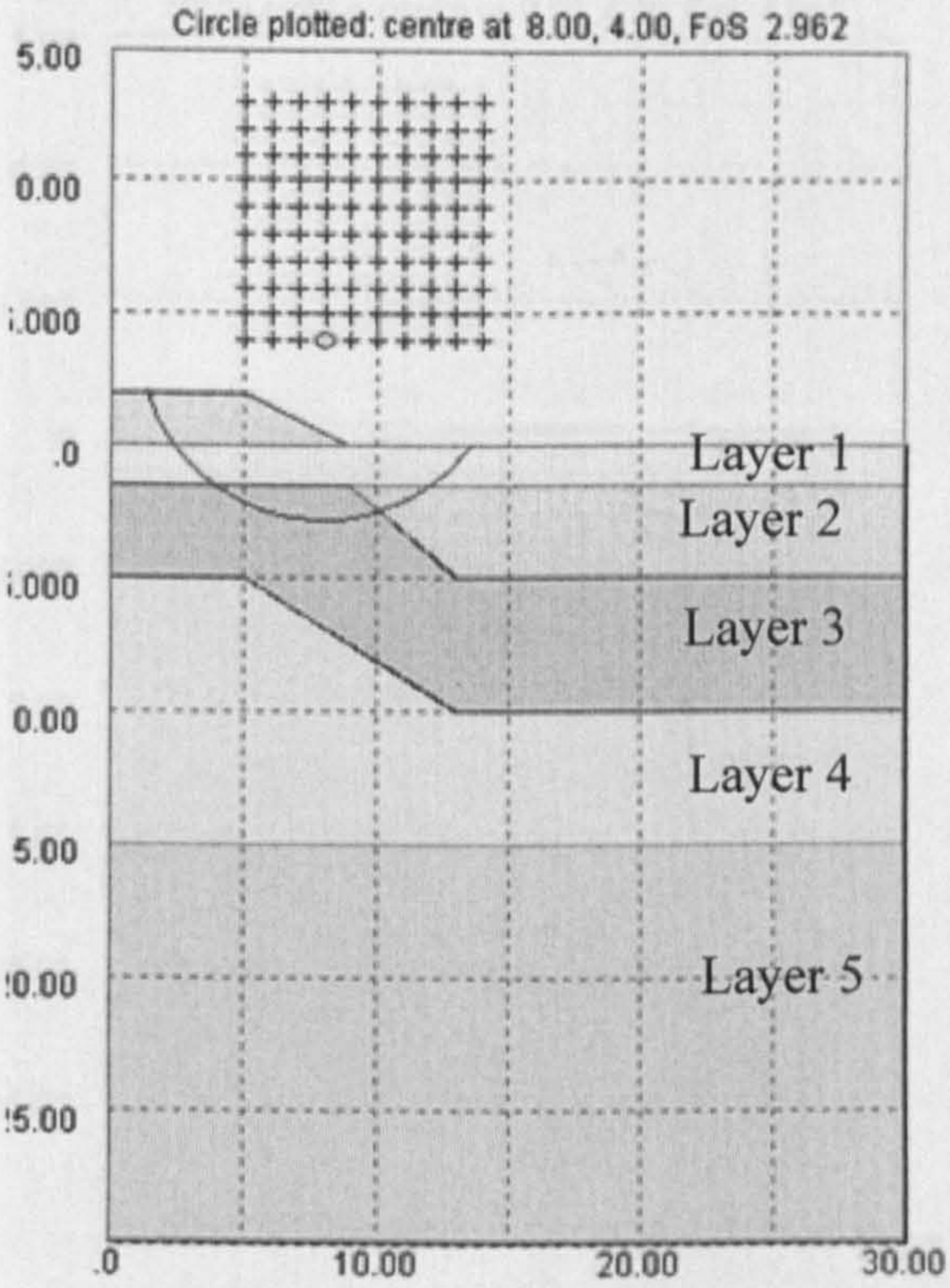

Figure 6.41: Slip surface 8 years after construction of the embankment

In the 8 years after construction the embankment settled in the order of -0.7 m to -0.8 m at the centreline. Due to the large settlements, part of the embankment fill are submerged and is below ground level. The reduction in embankment fill above ground level means a reduction of disturbing moment and an increase in shear resistance moment. One can expect an increase of FoS due to the reduced disturbing moments. In the following Slope analysis the change in surface geometry was taken into account based on the geometry estimated by the S-CLAY1S simulations 8 years after construction. The new simplified geometry is present in Figure 6.42. The predicted FoS for the reduced embankment geometry is 4.88. The FoS estimated for all three cases is summarised in Table 6.13.

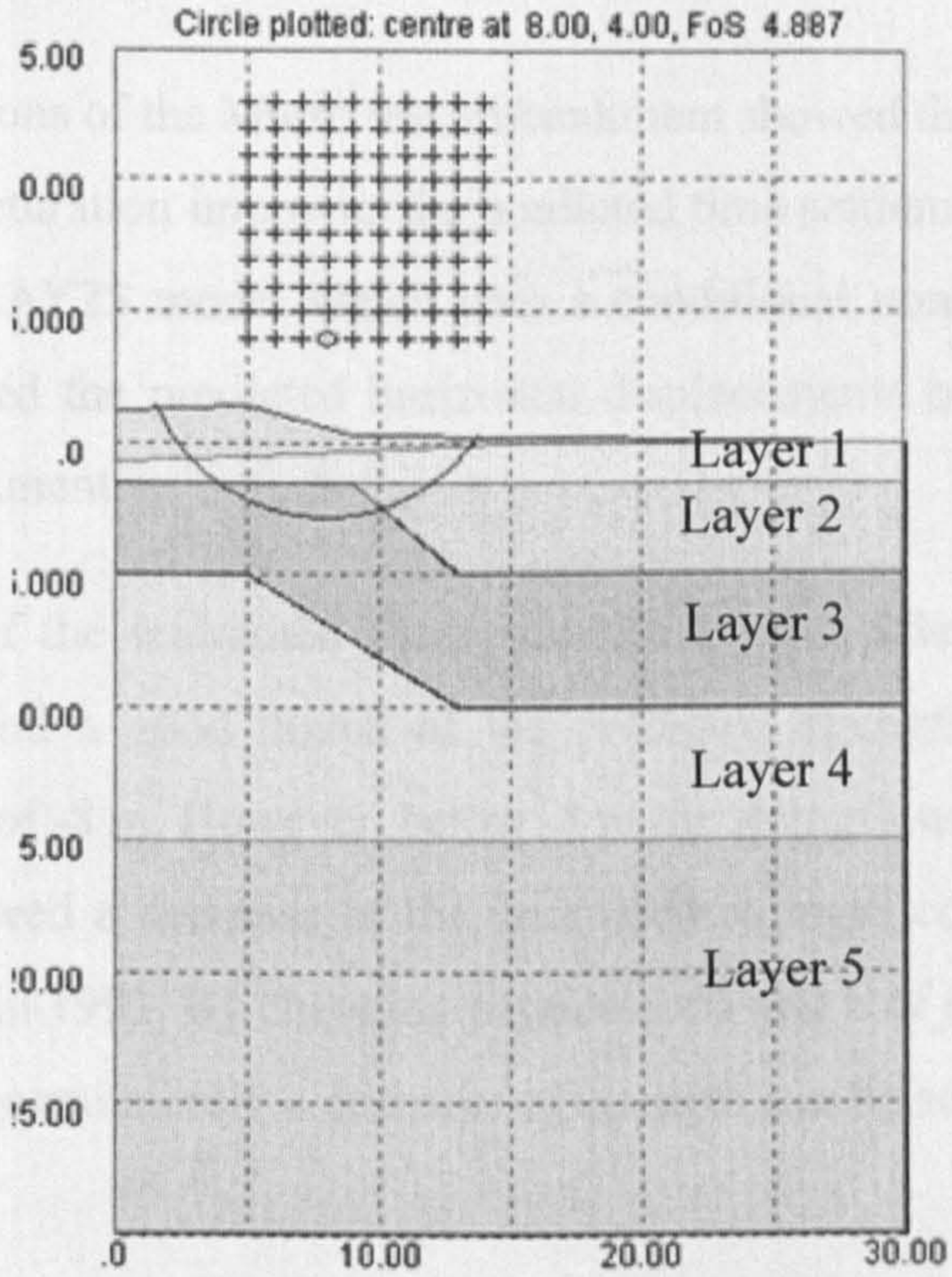

Figure 6.42: Slip surface 8 years after construction of the embankment with reduced embankment height geometry

Table 6.13: Predicted Factor of Safety

Stage	Immediately after construction	8 years after construction	8 years after construction with reduced embankment geometry
FoS	2.14	2.96	4.88
Increase in FoS	-	38 %	128 %

Comparing the increase in FoS (38 % to 128 %) for the two cases 8 years after construction clearly shows the importance of accounting for the change of the surface geometry. The finding is not so relevant for the Murro embankment because it had a safe initial FoS (2.14). However, in cases where the initial FoS is close to a minimum acceptable FoS and the growth in undrained strength is small, the true geometry might strongly influence the estimated long term stability.

6.6 Summary

Numerical simulations of the Murro test embankment showed that accounting for anisotropy and destructuration improves the predicted time settlement behaviour. Application of the S-CLAY2S model which uses a conditional non-associated flow rule marginally improved the predicted horizontal displacements below the toe and the crest of the embankment.

Back calculation of the undrained shear strength 8 years after construction of the embankment showed a good match of the predicted strength with the measured strength to a depth of -8 m. However, below -8 m the strength was overpredicted. The measurements showed a decrease of the undrained strength compared to the initial strength measured in 1993. By changing parameters a and b of the S-CLAY1S model it was shown that quantitatively a decrease of strength can be achieved in the simulations.

A formula was developed to estimated Poisson's ratio based on the stress history of the soil. Simulations with the estimated Poisson's ratios showed a good match with measured horizontal displacements. In the last part of the chapter a formula to estimate μ suggested by Leoni et al. (in press) was explored. Simulations of the Murro test embankment using values of μ calculated with the formula suggest that for numerical simulations of boundary value problems the formula gives realistic estimates of values of μ.

Chapter 7

Deep mixing

This Chapter introduces the ground improvement by the method of deep mixing. First a general introduction about the method itself is given, followed by a short review of the current design methods and guidelines. Secondly, different numerical models used to simulated deep mixed columns below embankments are reviewed and discussed.

7.1 Introduction

Deep mixing is a chemical admixture method to stabilise and improve soft soil by adding dry or wet binders. The soil mixing technology was first developed in the United States by Intrusion-Prepakt Inc. in the late 1950's (Liver et al. 1954). Between 1960 and the early 1970's a mixed-in-place stabilisation process was introduced in Sweden (Broms and Boman, 1977). They called it the "lime column method", where unslaked powered lime is mixed in-situ with soft clay using an auger type mixing tool. Broms and Boman (1977) referred to it as a giant "egg beater". The deep mixing method was continuously improved and refined especially in Scandinavia and in Japan. In the Scandinavian countries (mainly Sweden and Finland) the application concentrated mainly on onshore application, such as embankments and light foundations for housing and industrial developments. In contrast, in Japan, the development of the method was mainly focused on offshore applications, such as quay wall foundations, break waters and land reclamation. Nowadays countries worldwide increasingly

use the method in all types of civil engineering problems. Deep mixing is constantly being developed and improved as shown by recently introduced special applications such as GEOMIX, SpringSoil and Trenchmixing (Borel, 2007).

In the United Kingdom the deep mixing technique was successfully introduced in the late 80's and early 90's for ground improvement. Some recent examples include the stabilisation of the railway embankments for the Channel Tunnel Railway link. In the 90's the deep mixing was also sucessfully applied to ground remediation work (Al-Tabbaa, 2002).

The deep mixing method is extensively used in order to improve the properties of the soil, such as strength and deformation behaviour. The soil is either stabilised by forming columns (so-called column stabilisation), small wall panels, walls or by stabilising the entire volume (so-called mass stabilisation). In many cases column stabilisation is combined with mass stabilisation. With existing technical equipment the soil can be stabilised to a depth of 40 m, when using columns or walls. Mass stabilisation is limited to a depth of about 5 to 8 m (EuroSoilStab, 2001). In the following the research focuses on deep mixing in the form of column stabilisation, as this is the main area of interest in this research.

7.2 Concept of deep mixing

Deep mixing can be applied to various types of soft soils such as clays, organic soil and peat. The chemical and geotechnical properties of the soil influence the results of the deep mixing process and the choice of binders. Deep mixing can be divided into two methods, the dry method and the wet method. In the wet method a binder in slurry form is introduced with moderate water pressure and in the dry method the binder is introduced by compressed air. The dry method reduces the water content of the soil and is ideal for soil with a high water content or a water content close to the liquid limit of the soil. The dry method is commonly used in Scandinavia and the wet method in Japan. During the mixing process a rotating auger (mixing tool) is penetrated into the ground to the required depth. At this depth the direction of the rotation

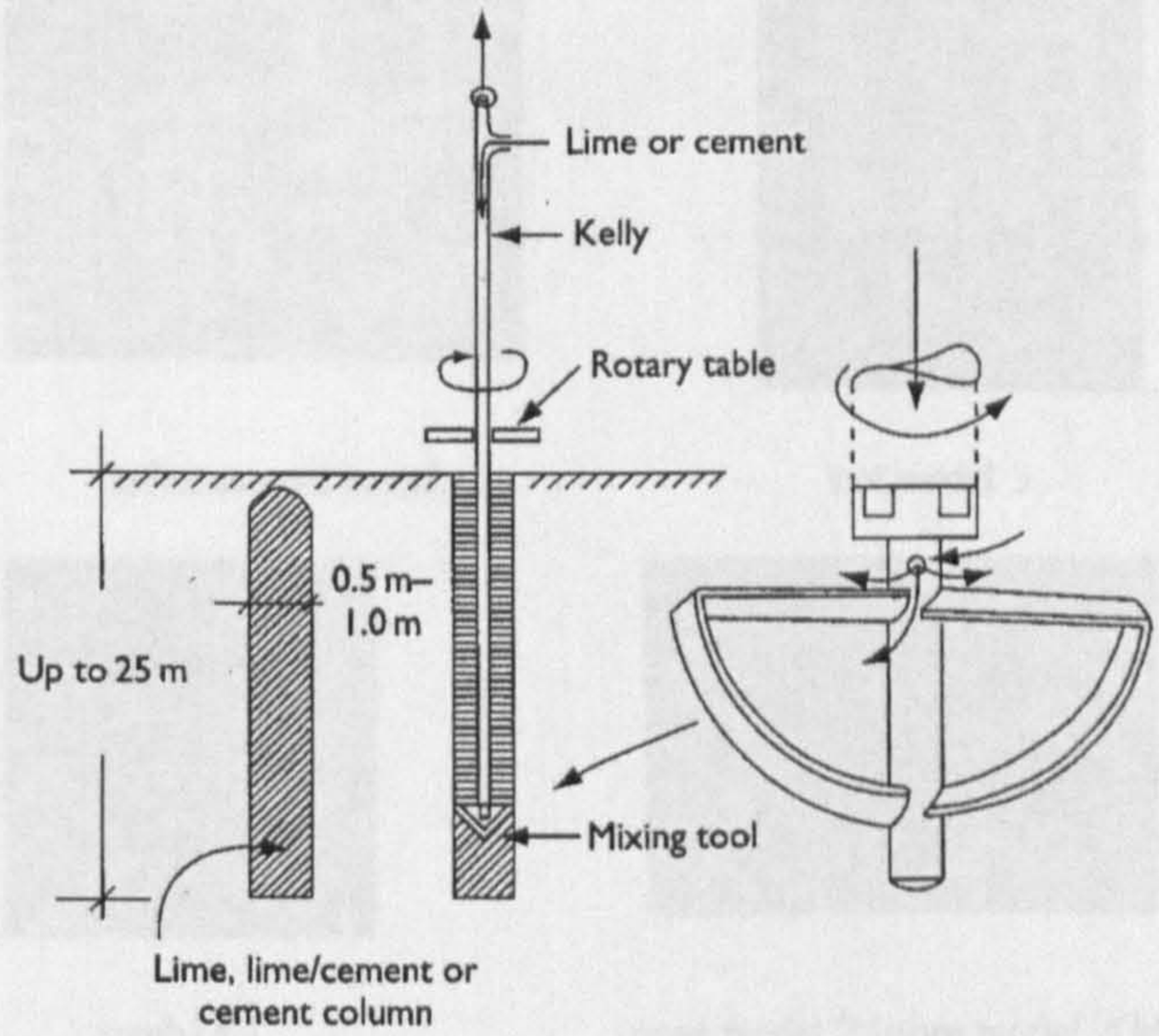

Figure 7.1: Basic concept of deep mixing (Broms, 2004)

is reversed and the nozzle opened to inject the binder. The mixing tool is lifted with a rotation speed of 100 to 200 rpm and a lift speed of 100 - 300 cm/min (Thompson, 2007; Massarsch and Topolnicki, 2004). The basic concept of the mixing process and a standard mixing tool is shown in Figure 7.1. Many different shapes of mixing tools have been developed for different applications and soils. Examples of mixing tools for dry soil mixing are shown in Figure 7.2. As it can be seen in Figure 7.1, the mixing tool has a hole in the shaft above the blades. Through this hole the binder is injected into the ground. This is standard for dry mixing tools (Thompson, 2007). Obviously as the hole is above the blade the bottom of the column is not mixed with the binder. The top of the column is also poorly mixed as the binder injection is stopped below ground surface to avoid a blow out of the binder.

Different types of binders are used. For dry mixing cement, lime, gypsum, blast furnace or pulverised fuel ash (PFA) or a combination of binders are commonly used. The powder is injected by air pressure and reacts chemically with the pore water of the soil during the curing process. In the past most of the applications used lime only. Nowadays in most projects a combination of lime and cement is used. The major

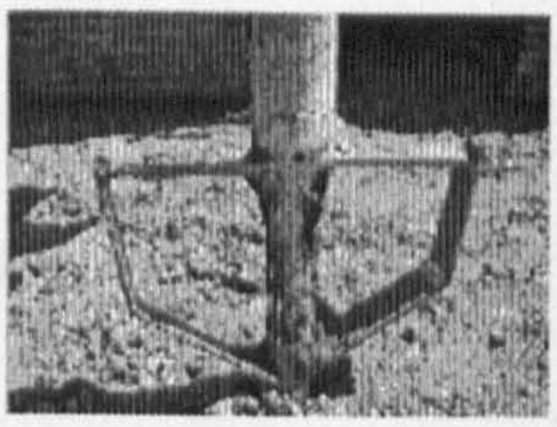

reference pot model

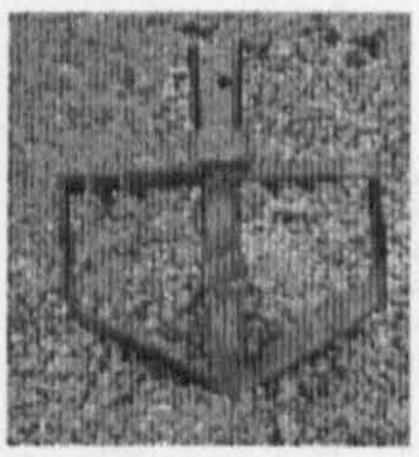

pot model 3

model K1

cone model 2 / core model 2(M)

Figure 7.2: Examples of mixing tools for dry mixing (Aalto, 2003)

advantage of cement is the high shear strength, which can be achieved. Lime columns have the advantage of a high permeability of the mixed soil compared to cement or lime/ cement combinations (Broms, 1999). In the wet method a slurry consisting of binder and water is injected. The most common binder for the wet method is cement but often various additives are added.

7.3 Applications of deep mixed columns

Typically deep mixed columns in Europe are installed below road or railway embankments. The columns will reduce the settlements and increase the stability of the embankment. It is often found that the method is more economical than other traditional ground improvement methods, such as soil replacement and small diameter piles. However, the deep mixing technique can be used for a wide range of civil engineering problems both onshore and offshore projects. The applications are settlement reduction, cut-off walls, excavation support, liquifaction mitigation, cutting and slope stabilisation and enviromental remediation. The main purposes of deep mixed columns in the different types of applications can be summarised as follows (EuroSoilStab, 2001):

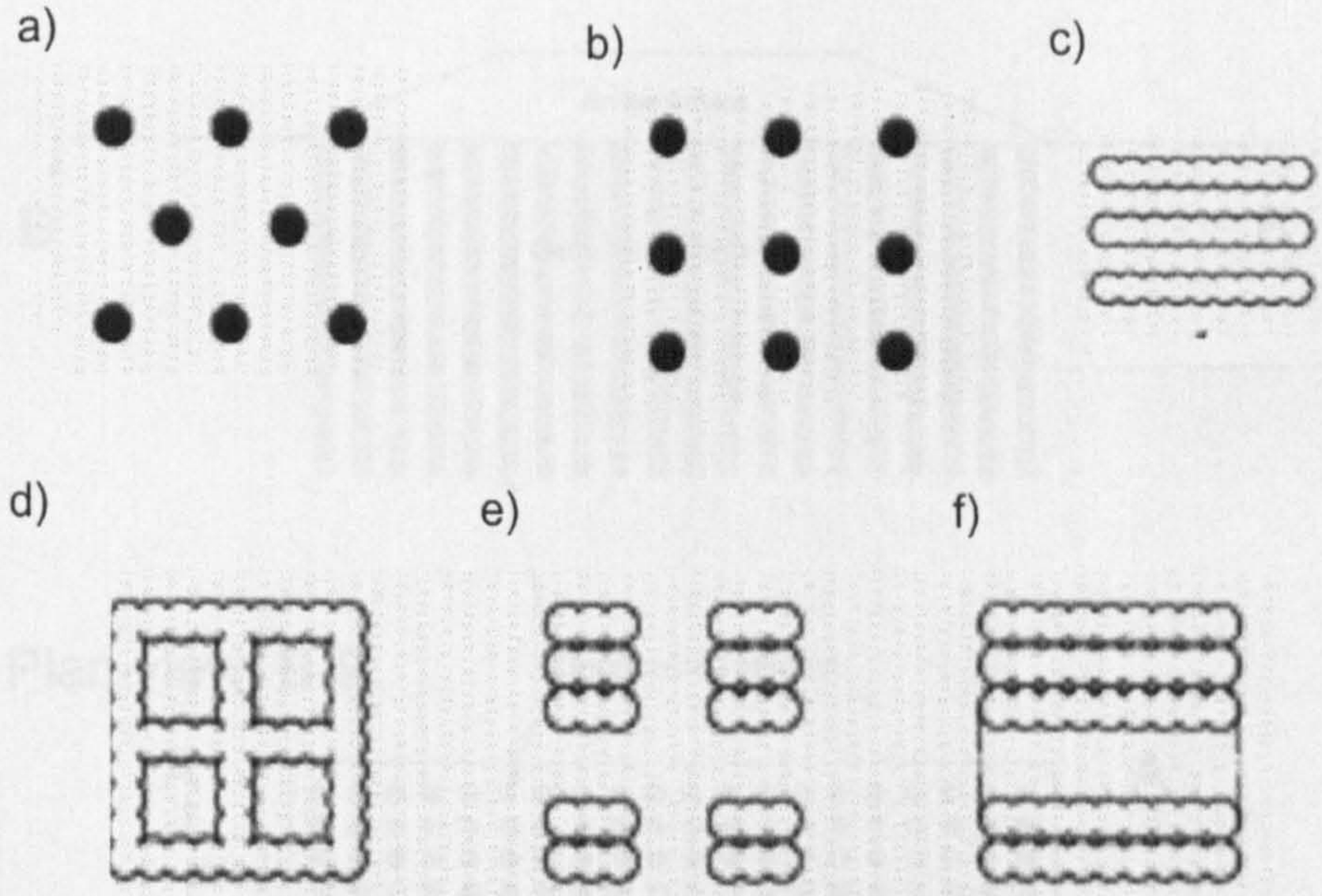

Figure 7.3: Examples of deep mixing patterns (EN 14679, 2003): a) triangular, b) square, c) wall type, d) block type, e) grid type, and f) area type

- to increase the strength of the soft soil
- to improve the deformation properties of soft soil
- to increase dynamic stiffness
- to remediate contaminated soil

Deep mixing is not suitable for all engineering problems but is most suitable where the following applies (FHA, 2000):

- the soil is not stiff or dense
- no boulders or other obstruction to the required installation depth
- a relative vibration free technology is required
- treated or improved ground volume is large
- treated soil strength has to be closely engineered (typically 0.1 to 5 MPa)

Depending on the purpose of the deep mixing application the columns can be installed in different patterns. Some typical patterns are presented in Figure 7.3. Triangular and square patterns of single columns are usually applied below embankments where a reduction of settlements is the main purpose. In this work only columns below embankments installed in a square pattern are considered due to limitations in the

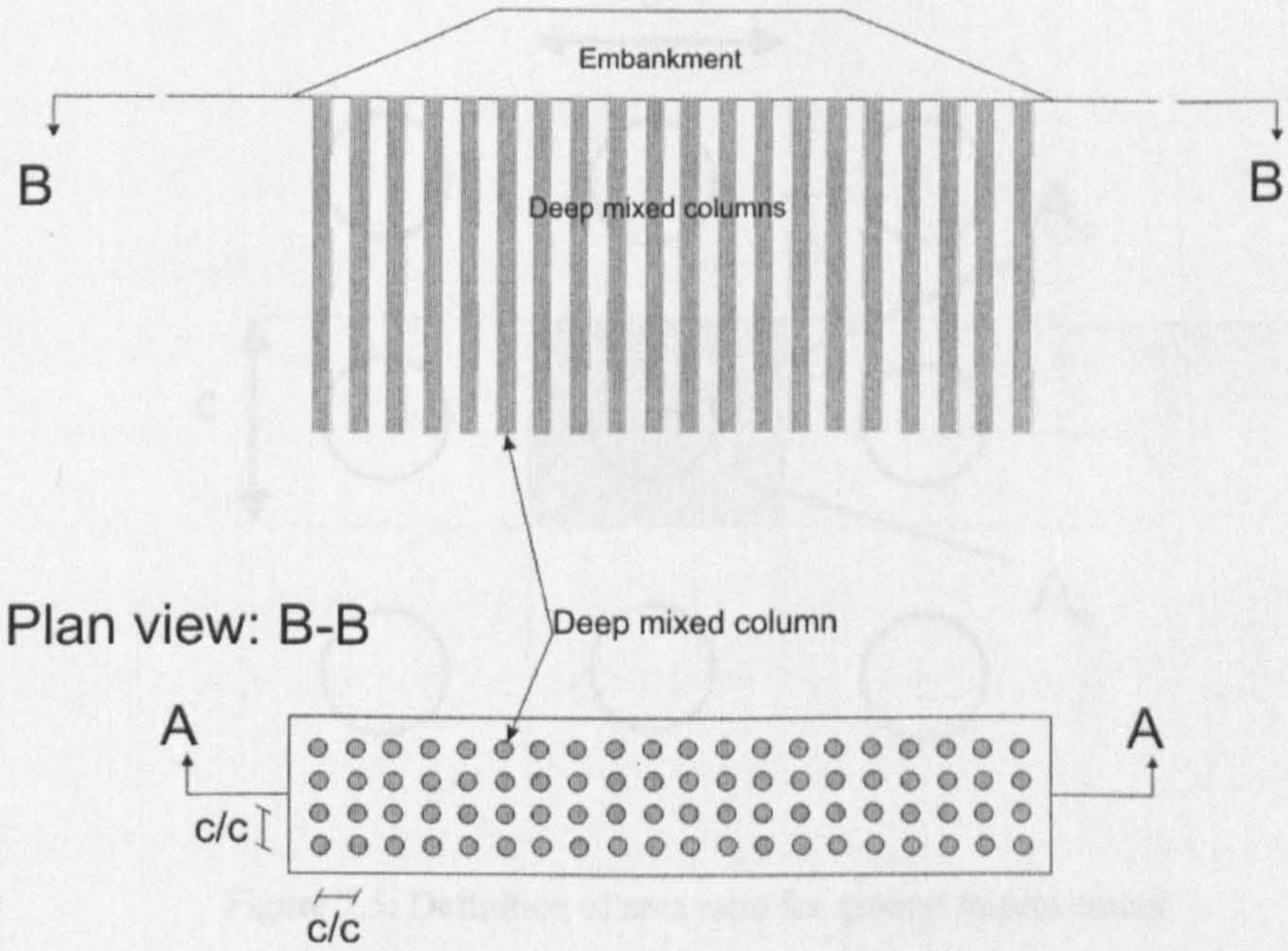

Figure 7.4: Typical arrangement of columns below an embankment

used finite element code PLAXIS 3D foundation beta. An embankment constructed on columns in a square pattern is shown in Figure 7.4. The pattern and column spacing chosen defines the area ratio of the improvement. After Broms (2004) the area ratio a for columns installed in a square pattern is defined as:

$$a = \frac{A_c}{A_s} \qquad [7.1]$$

where A_c is the area of the column and A_s the area of the soil (see Figure 7.5). A typical area ratio for columns constructed below embankments is 0.1 to 0.3 (Karstunen, 1999). The upper limit of the area ratio of improvement for a square grid is 0.79 (Broms, 2004). The diameter for the columns ranges between 0.4 and 2.4 m. In Europe a common industry standard for the diameter is 0.6 to 1.0 m, whereas in the US and Japan larger diameters are more common, depending on the type of application (Massarsch and Topolnicki, 2005; Nozu, 2005; Probaha et al. 2005).

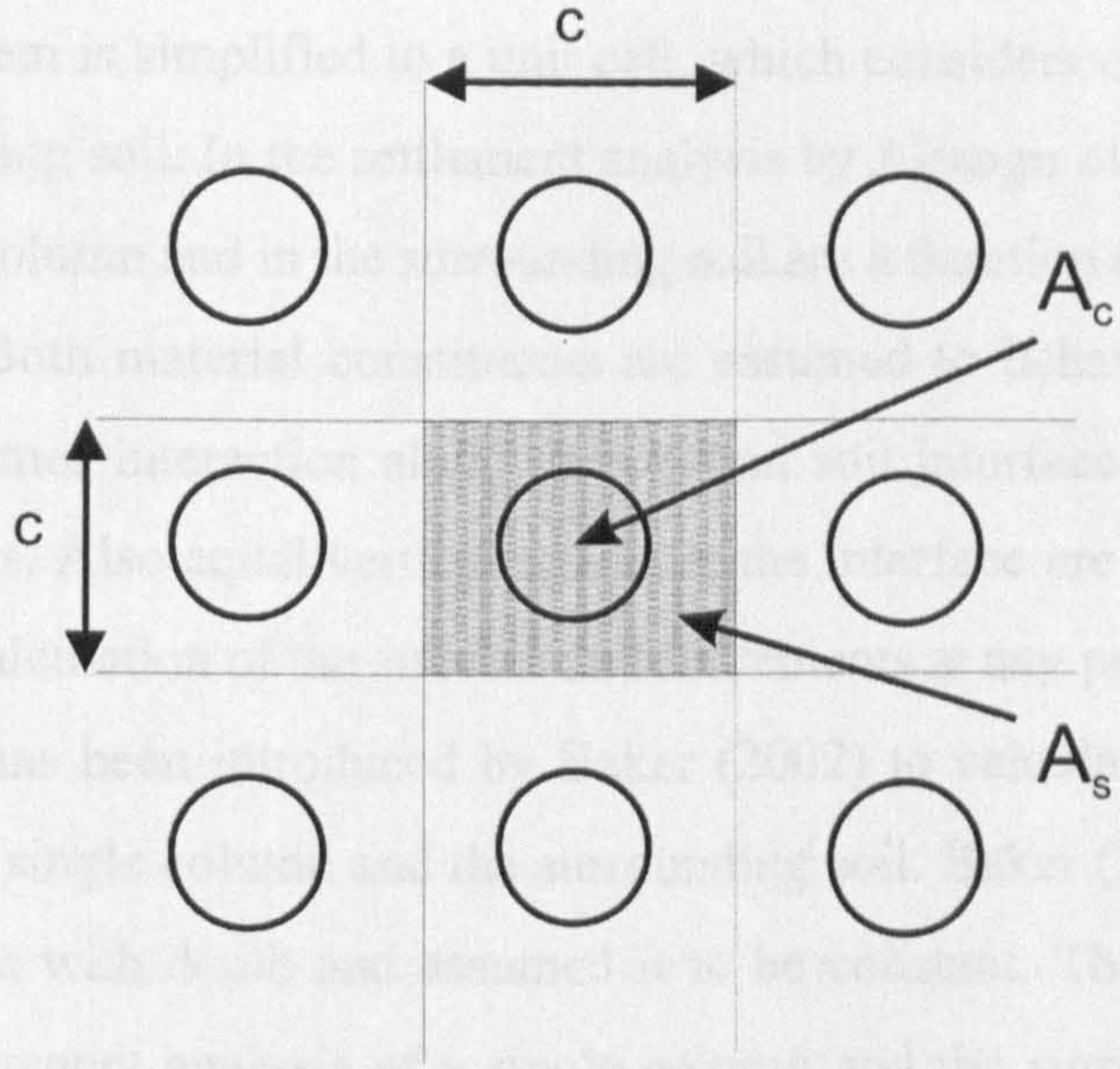

Figure 7.5: Definition of area ratio for ground improvement

7.4 Design

The design philosophy for deep mixed columns is to produce a soil-column system that mechanically fully interacts. The applied load is partly carried by the column and partly by the soil between the columns. Assuming equal strains in the column and the soil forms the basis condition for the conventional design. The empirical techniques suggested by EuroSoilStab (2001) and the recent design guidelines introduced in Sweden and Finland (Carlsten et al. 1995 and Korkiala-Tanttu, 1997) are based on ideas by Broms and Boman (1977). All guidelines rely on simple rigid-plastic solutions to predict ultimate loads. The additional stresses introduced due to embankment load are assumed to be constant with depth in the soil and in the column. The maximum load is dependent on the average allowable shear stress of the column and the soil. Empirical methods are used for settlement calculations. The settlement calculations of the deep mixed columns are based on an iterative procedure and assume an average weighted module for the column and the unstabilised soil.

More complex analytical solutions have been developed by Alamgir et al. (1996). The soil-column system is simplified to a unit cell, which considers only a single column and the surrounding soil. In the settlement analysis by Alamgir et al. (1996) the vertical strain in the column and in the surrounding soil are a function of the distance to the column centre. Both material constituents are assumed to behave linear elastically. The system assumes interaction along the column soil interface in terms of normal and shear stresses. Also equal vertical strains at the interface are assumed. The solution allows the calculation of the stresses and settlements at any point in the system. A similar method has been introduced by Baker (2002) to calculate the consolidation settlements for a single column and the surrounding soil. Baker (2002) simplified the stress distribution with depth and assumed it to be constant. The results were compared to finite element analysis of a single column and the surrounding soil, it was shown that both are in good agreement if linear elasticity is assumed for the material behaviour.

The interaction between the columns and the soft soil is very complex and may differ from the simple assumptions used in the design guidelines (EuroSoilStab, 2001) or other proposed methods (Alamgir et al. 1996; Baker 2002). Numerical methods, such as the finite element technique, are ideal to investigate the soil column behaviour. Further, by using advanced constitutive models as introduced in Chapter 2, a realistic soil and column stress-strain behaviour can be simulated (Krenn et al. 2005; Krenn and Karstunen, 2006).

7.5 Characteristics of deep mixed material

Deep mixed material is a very complex material. Its stress-strain-strength behaviour depends on a number of factors such as the binder, the binder content, the grain size of the soil, the acidity of the water, the organic content of the soil, the water content of the soil, the mixing conditions and quality (CDIT, 2002). For the analytical design methods the undrained strength of the deep mixed material is commonly required. The undrained shear strength is usually determined by unconfined compression tests,

undrained triaxial tests or by direct shear tests (Brooms, 2002). The design strength is based on the undrained strength after 28 days (EuroSoilStab, 2002), either determined by mixing in the laboratory or in the field. It is often found that the achieved field strength is 20 to 50% lower than the laboratory strength (Thompson, 2007; Broms, 2002; Aalto, 1998). The maximum undrained strength is usually 200 to 300 kPa but values of up to 1000 kPa and more are reported (Hayashi and Nishimoto, 2005). The strength also increases with time. Löfroth (2007) reported an increase from an average of 100 kPa after 1 year to about 400 kPa after 9 years based on field samples of lime/cement columns. Åhnberg (2004) concluded based on laboratory tests on deep mixed samples that undrained shear strength is not a constant as often assumed but is stress dependent. Peak friction angles of 34 to 39 degrees for deep mixed clays and 40 to 44 degrees for clayey silts are reported by Ahnberg (1996). The observed stress-strain behaviour is similar to that of an overconsolidated clay (Ahnberg, 2006: Baker, 2000). Balasubramaniam et al. (2005) made similar conclusions and suggest that after reaching the peak strength in the triaxial test, the strength decreases to the critical state strength of the untreated soil.

The tensile strength of the lime/cement columns is often found to be low, typically 10 to 20% of the unconfined compression strength (Terashi and Tanaka, 1983).

Results from anisotropic consolidation tests on deep mixed Bangkok clays plotted in a e-log(p') shows that a yield point (preconsolidation pressure) can be determined (Balasubramaniam et al. 2005, Tremblay et al. 2001). This allows the gradient of the virgin compression and the unloading/reloading line to be determined. Ahnberg (2006) concluded that the preconsolidation pressure is governed by the applied stress level and the cementation of the deep mixed material. However, it is common practice to simply determine a relation between the stiffness of the deep mixed material and the unconfined compression strength or undrained shear strength. E_{50}/c_u ratios of 150 for field samples on lime/cement columns and 200 to 300 for laboratory samples are typical. Baker (2000) reported ratios of 90 to 140 between E_{50} and the unconfined compression strength 56 days after mixing the lime/cement columns.

The permeability of the deep mixed material is dependent on the type of binder and mixing technique used. Mixing the soil with lime normally only increases the permeability, whereas mixing it with cement only, decreases the permeability (Broms, 1999, Åhnberg 1996). Baker (2000) concluded based on field samples on lime/cement columns that the permeability varies between 10 to 100 times that of the natural soil. The in-situ permeability changes with time and is dependent on the amount of binder used. Ahnberg (2004) suggests based on laboratory tests on deep mixed material that the type of binder has a minor influence on the permeability but the change of permeability can be estimated from the change of water content and strength.

7.6 Case histories of embankments constructed on deep mixed columns

About 20 to 30 years ago there were just one or two case histories reported in journal and conference papers about the use of deep mixed columns below embankments. With the continuous development of the technique over recent years, more and more case histories are being reported by geotechnical engineers and researchers.

Holm et al. (1983) summarised the findings of a full scale test of an embankment constructed on deep mixed lime columns. The test embankment was built as a part of the construction of the E4 motorway which connects Brohagen with Järna, approximately 60 km south of Stockholm, Sweden. The proposed embankment is a section of an embankment which forms a ramp to a bridge which crosses a river. The deep mixed columns were proposed as an alternative to a piling solution. The construction site is covered in soft clay, with a shear strength of about 5 to 10 kPa. On top of the soft clay is a 1.5 m thick overconsolidated dry crust. The water content ranges from 120 % at the top to about 50 % at the bottom of the clay deposit. Soil from different layers was sampled and mixed in the laboratory with lime to assess the undrained shear strength of the deep mixed material. The achieved undrained strength determined from unconfined compression tests varied with depth. It was found that about four months after mixing the shear strength of the deep mixed material increased to 10 times the in-situ

strength of the soil. The columns were installed to a depth of about 10 m with a diameter of 0.5 m and a column spacing (c/c) of 1.4 m. In addition to the columns, part of the embankment was constructed on natural ground reinforced with vertical sand drains. The maximum embankment load was 50 kPa. The embankment was instrumented to measure settlements and the measurements were taken for 2.5 years. Inspection of the time settlement curve shows that the settlements were 60% lower at the sections with the lime columns compared to the sections with the sand drains.

Another full scale test performed in the early 80's in France was reported by Soyez et al. (1983). Four embankments were constructed at the test site of Limay. One of the embankments was constructed on natural ground (embankment 0), and the other three on lime columns with different improvement ratios (embankments 1 to 3). The height of the embankment ranged from 2.5 (embankment 0 and 3), 3.75 m (embankment 1) to 5 m (embankment 2). The natural ground consisted of a 3 m deep hydraulic fill which was placed to reinstate a former gravel pit. The water content of the fill was 50 to 60 %, close to the liquid limit of the soil. The column diameter was 0.5 m. The embankments were instrumented with settlement gauges, piezometers to measure the excess pore pressure and pressure cells. Comparison of the time settlement curve of embankments 0 and 3 shows a reduction in measured maximum settlements from 0.3 m to approximately 0.1 m, respectively, about a 66 % reduction in settlements. Also a reduction in measured excess pore pressures from 30 to 40 kPa, to about 10 kPa for the improved case was observed. Overall the excess pore pressure measurements with time are inconclusive due to a lot of scatter. Results from the pressure cells for embankment 2, show how the load is shared between the columns and the soil. The measured maximum load in the column was 150 kPa and in the soil it was about 50 kPa. Inspection of the time-stress curve shows that the load in the column built up gradually with time and it took up to a year before the maximum load was reached.

As part of an extensive expansion of the transport infrastructure in Western Sweden four test embankments were built (Alen et al. 2005). Ground improvement in terms of lime/cement columns was considered to be valuable and an attractive method for the

project. Only three out of the four embankments are included in the following discussion.

At the test site, Stora Viken North the ground consists of a 15 m deep soft clay deposit with an average water content of 75 %. The maximum water content is close to the liquid limit of the soil. Columns with a diameter of 0.6 m were installed in a square pattern with a c/c-spacing of 1.5 m to a depth of -16 m. The embankment is 12 m by 25 m, and the total maximum load of the embankment is about 40 kPa. It was constructed in two stages over two years. The measurement confirmed equal settlements in the clay and the column. However, after two years of construction large settlements were measured in the top two meters of the columns and the soil (~0.18m). Below -2 m a sharp decrease in settlements was observed. Obviously the settlements with depth will increase as dissipation of excess pore pressure continues. The records of the inclinometers showed relatively small horizontal displacements in the order of 0.06 m. Similar findings are reported by Alen et al. (2005) for the test site at Surte and Nödinge. At all three embankments only small increases in excess pore pressures of about 15 kPa were measured for both construction stages. Overall, it was concluded that further investigation was needed to explain the large contribution to settlements at the top found at all three sites. The poor quality of the columns at the top or reaching the ultimate capacity of the column material have been stressed as some of the possible explanations.

The current design methods have been used sucessfully on many projects in the past 30 years. However, there have been cases where failures and large deformation of embankments constructed on deep mixed columns have occurred. Two cases are reported by Kivelö (1998). Despite the fact that the undrained shear strength of the deep mixed columns in the field was higher than assumed in the design, damage to the embankments occurred. It was speculated that the shear resistance of the group of the column was overestimated, despite the shear strength of the column being higher than the assumed design strength. Kivelö (1998) proposed an alternative method which

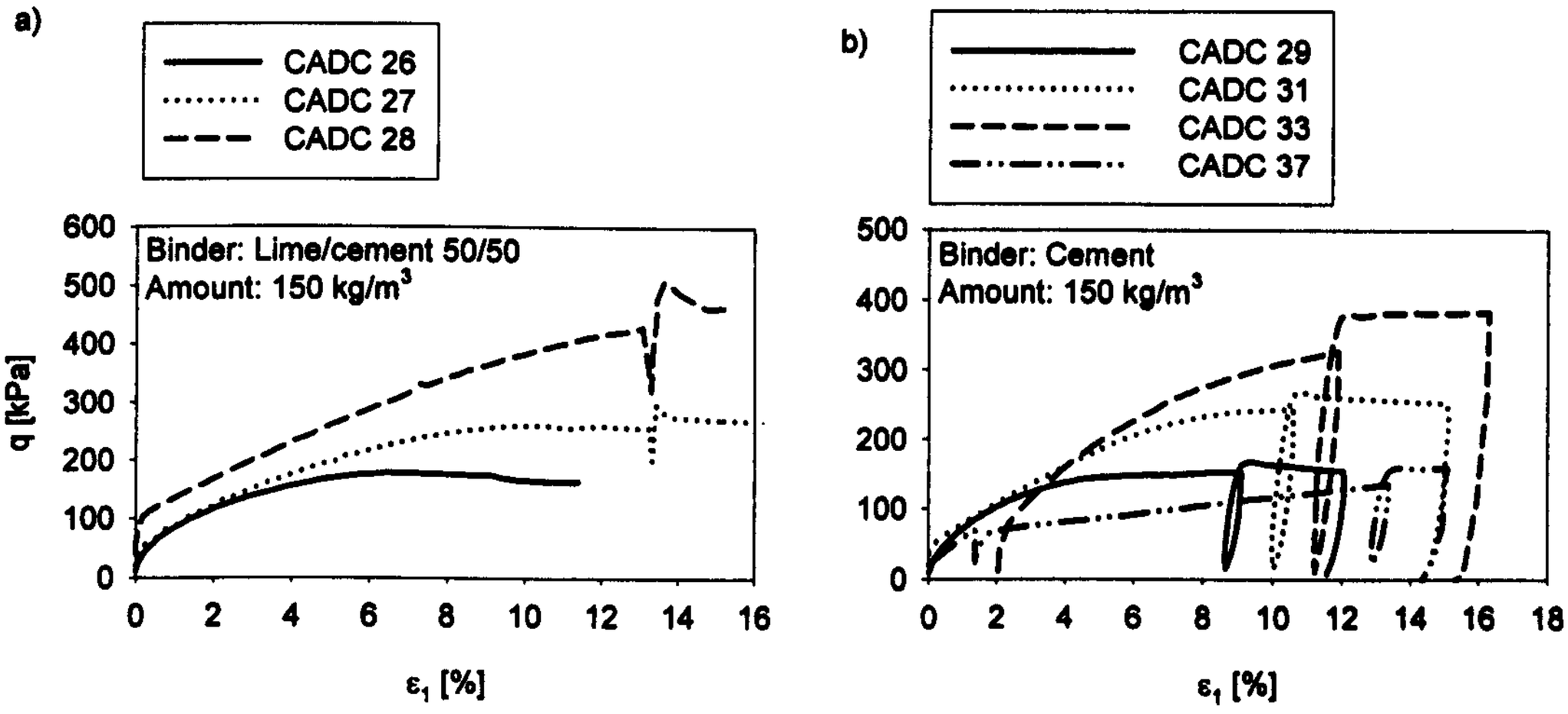

Figure 7.6: Drained triaxial test results of deep mixed Vanttila clay: a) Laboratory mixed samples and b) In-situ mixed samples

accounts for the interaction of the columns and the surrounding soil and investigates different failure modes of the columns.

7.7 Constitutive modelling of deep mixed material

It has been mentioned in Section 7.5 that the material behaviour of the deep mixed material is very complex. In Figure 7.6 the stress-strain curves of deep mixed Vanttila clay determined in drained triaxial tests are presented. Vanttila clay is a very sensitive soft clay from Finland. The sensitivity is in excess of 50 (the actual value could not be measured, Koskinen and Karstunen (2004)). The estimated undrained shear strength is between 7 and 10 kPa. The stress ratio at critical state in triaxial compression is approximately 1.2, which suggests a friction angle at critical state of 30 degrees. As part of a research project on the effect of the shape of the mixing tool on the strength properties and homogeneity of deep mixed clay, Vanttila clay was deep mixed. One partner of the project was the laboratory of Soil Mechanics and Foundation Engineering at Helsinki University of Technology (Aalto, 2003). Drained and undrained triaxial tests on laboratory and in-situ mixed samples were performed. The binder consisted of cement or a 50/50 combination of lime and cement. In the study the binder content was varied between 70 and 150 kg/m^3. In Figure 7.6a the results of the

drained test on the laboratory mixed samples are shown. The tests were performed with three different cell pressures, 30, 60 and 120 kPa, respectively. Inspection of the Figure 7.6a shows the non-linear relation between deviator stress and axial strain. The maximum deviator stress increases with increasing cell pressure. In Figure 7.6b the results of in-situ mixed samples are shown. Again a highly non-linear relation between the deviator stress and strain is observed.

Different types of constitutive models have been utilised by geotechnical engineers and researchers to represent the stress-strain behaviour of the deep mixed material. In many cases the stress-strain behaviour was simply modelled with a linear elastic model (Bergado et al. 1999; Baker, 2004; Kitazume and Maruyama, 2006). Also the linear elastic perfectly plastic Mohr Coulomb model (MC model) is a popular choice to simulate the constitutive behaviour of the deep mixed material. One of the first to apply the MC model to deep mixed columns were Lahtinen and Vepsäläinen (1983) in the early 80's. The MC model is already an improvement compared to the elastic model as it can account for the strength in compression and tension, which are both very important in numerical simulations of deep mixed material. Review of the literature shows that the MC model is the most common choice by researchers and practising engineers to represent the deep mixed material (Huang et al. 2006; Stewart et al. 2004; Han et al. 2005; Stewart and Filz, 2005; Terashi, 2005; Kurizaki et al. 2005; Ohisi et al. 2005).

In recent years more advanced models have been proposed and used to simulate the stress-strain behaviour of deep mixed material. Namikawa et al. (2005) developed an elasto-plastic model for deep mixed material which accounts for strain softening after a peak stress state. It has a bi-linear failure surface (MC criterion) to account for the shear strength in compression and extension. The model uses a stress-dependent shear modulus to account for the non-linear stress strain behaviour presented in Figure 7.6. The model was implemented in a 3D finite element code and was successfully applied to dynamic problems of deep mixed material. A similar model was proposed by Ciuhak et al. (2003). Instead of a MC criterion, the model uses a Hvorlev-surface in com-

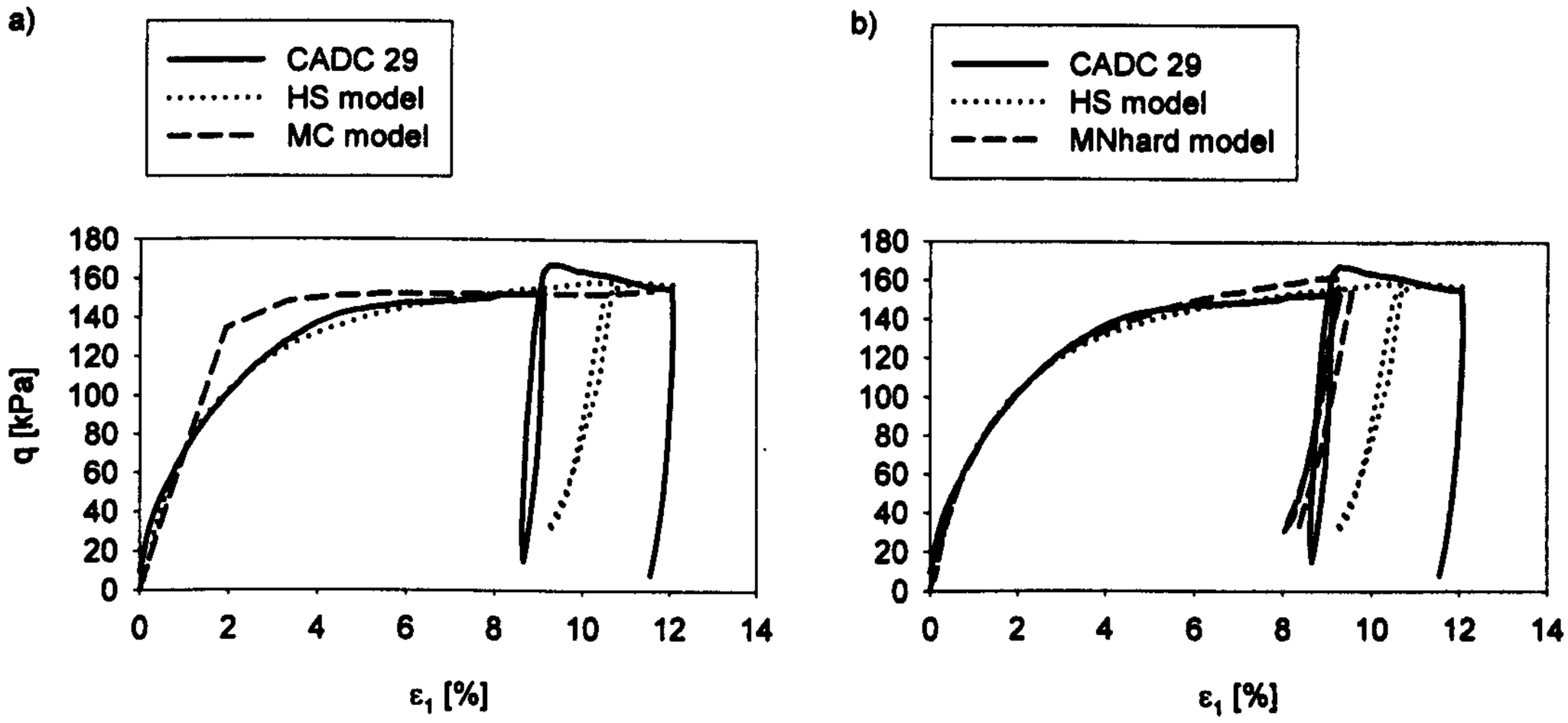

Figure 7.7: Model simulations of the CADC 29 a) MC and HS model and b) HS and MNhard model

bination with a limited tension surface. To account for post peak softening a linear residual stress surface is proposed as well.

As part of this research model simulations of drained triaxial tests of deep mixed Vanttila clay were performed. It was the aim to establish whether the MC model or the Hardening Soil model, both standard models implemented in the PLAXIS finite element code can realistically represent the observed non-linear stress-strain behaviour. In Figure 7.7 model simulations of the drained triaxial test CADC 29 on deep mixed Vanttila clay are presented. In Figure 7.7a the predicted stress-strain curves by the MC model and the Hardening Soil model (HS model, see Section 2.9.2 for details) are shown. The parameters used for the model simulations are shown in Table 7.1. Inspection of the curves shows that the simple MC model is not suitable to represent the observed non-linear stress-strain behaviour, in particular when deviations are greatest in the strain range of practical problems in serviceability. In contrast the stress-strain curve predicted by the HS model matches closely the non-linear behaviour.

Table 7.1: Model parameters for the MC and HS model

Type	E_{50}^{ref} E_{oed}^{ref} [kN/m²]	E_{ur} E_{ur}^{ref} [kN/m²]	φ'	c' [kN/m²]	ν'	m	γ [kN/m³]	p^{ref} [kN/m²]
MC model	-	12000	40	14	0.35	-	15	-
HS model	12000	27000	40	14	0.35	0.8	15	100

The model simulations were also performed with the MNhard model, which was introduced in Section 2.9.3 and is implemented as a user defined soil model into the PLAXIS finite element code. The MNhard model also accounts for a stress dependent stiffness via a hyperbolic stress-strain relationship, as used in the HS model. The parameters used for the simulations of the drained triaxial test are shown in Table 7.2.

Table 7.2: Model parameters for the MNhard model

Type	G_{50}^{ref} [kN/m²]	G_{ur}^{ref} [kN/m²]	φ'	c' [kN/m²]	ν'	m	γ [kN/m³]	p^{ref} [kN/m²]
MNhard	4444	10000	40	14	0.35	0.8	15	100

The results of the model simulations with the MNhard model are presented in Figure 7.7b. The MNhard model also shows a good match and is obviously suitable to represent the non-linear behaviour of the deep mixed material.

In this research both models, the HS and the MNhard model, will be used to represent the stress-strain behaviour of the deep mixed material.

7.8 Numerical modelling

The overall response of an embankment constructed on deep mixed columns is often dominated by the stress-strain behaviour of the soft soil (Karstunen and Krenn, 2004; Krenn et al. 2005; Karstunen et al. 2005a). Hence it is important to account for features such as anisotropy and destructuration in the soft soil. In addition to the realistic soil and column behaviour it is also important to account for the true geometry of the boundary value problem in the design. The current design methods are simple and

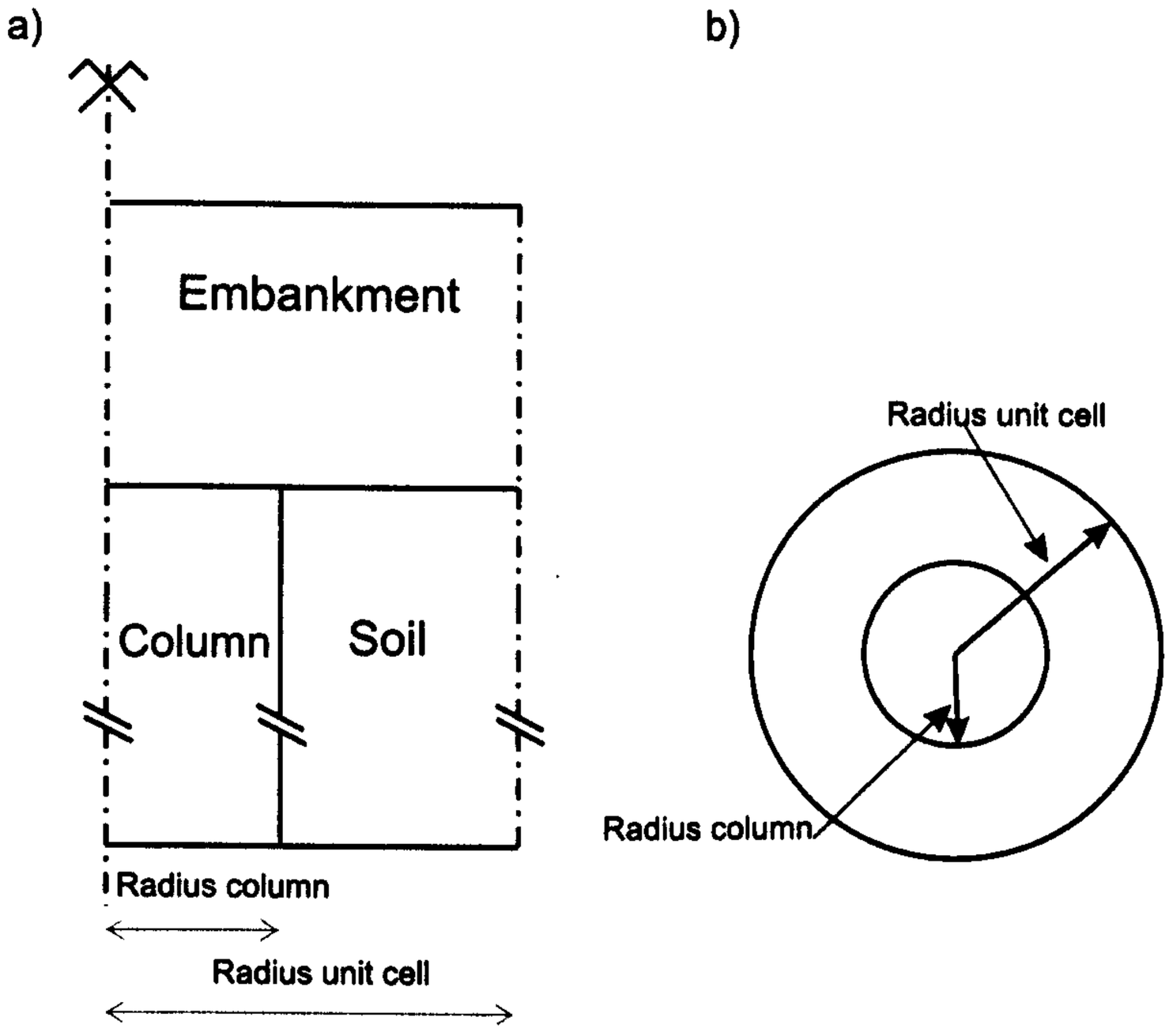

Figure 7.8: Axisymmetric unit cell a) cross section and b) plane view

semi-empirical (see Section 7.4), and are therefore limited to represent the complex mechanism of deep mixed columns below an infinite fill. Numerical tools such as the finite element method provide a suitable tool to gain understanding into the column soil interaction. In addition, the effects of column diameter, column spacing, column stiffness and the geometry of the embankment on the settlement behaviour can be investigated. Another advantage is the possibility to study the short and/or long term behaviour via fully coupled finite element analyses. In the following sections various alternatives for modelling embankments constructed on deep mixed columns will be introduced and discussed.

7.8.1 Axisymmetric unit cell

When modelling an embankment on deep mixed columns with an axisymmetric unit cell, only a single column and the surrounding soil can be simulated. This could be considered as a very crude representation of a column installed in a square pattern at the centre line under an embankment fill. An example of a cross section of a unit cell

is shown in Figure 7.8. The radius of the unit cell is dependent on the centre to centre spacing of the columns (c/c-spacing) and defined as:

$$R = \frac{c}{\sqrt{\pi}} \qquad [7.2]$$

where c is the column spacing and R, the radius of the unit cell. For model simulations the horizontal boundaries should be fixed in horizontal directions and the bottom boundary in both directions.

Lahtinen and Vepsäläinen (1983) used an axisymmetric unit cell to investigate the settlement behaviour of an embankment constructed on deep mixed lime columns. The shallow soil deposit was divided into four layers. The predicted settlements were found to be in good agreement with measurements. A unit cell was also used by Vepsäläinen and Arkima (1992) to study the Paimio test embankment. The predicted results were not in good agreement with measurements. The computed settlements actually underestimated the field measurements. Secondary compression (creep) was most likely the case of the discrepancy, which was not accounted for in the simulations (Karstunen, 1999). Maher (2006), Gardiner (2006) and Stewart and Filz (2005) utilised the unit cell approach to perform parametric studies on deep mixed columns.

7.8.2 Plane strain analysis

In a plane strain analysis the individual columns are replaced by a row of walls to represented the columns installed below the embankment. A schematic model showing the walls is given in Figure 7.9a. The centre to centre spacing of the walls in the model is the actual c/c-spacing of the columns. The width d of the wall is a function of the area of the column and can be calculated as follows:

$$d = \frac{r^2\pi}{c} \qquad [7.3]$$

where r is the radius of the deep mixed column and c is the column spacing.

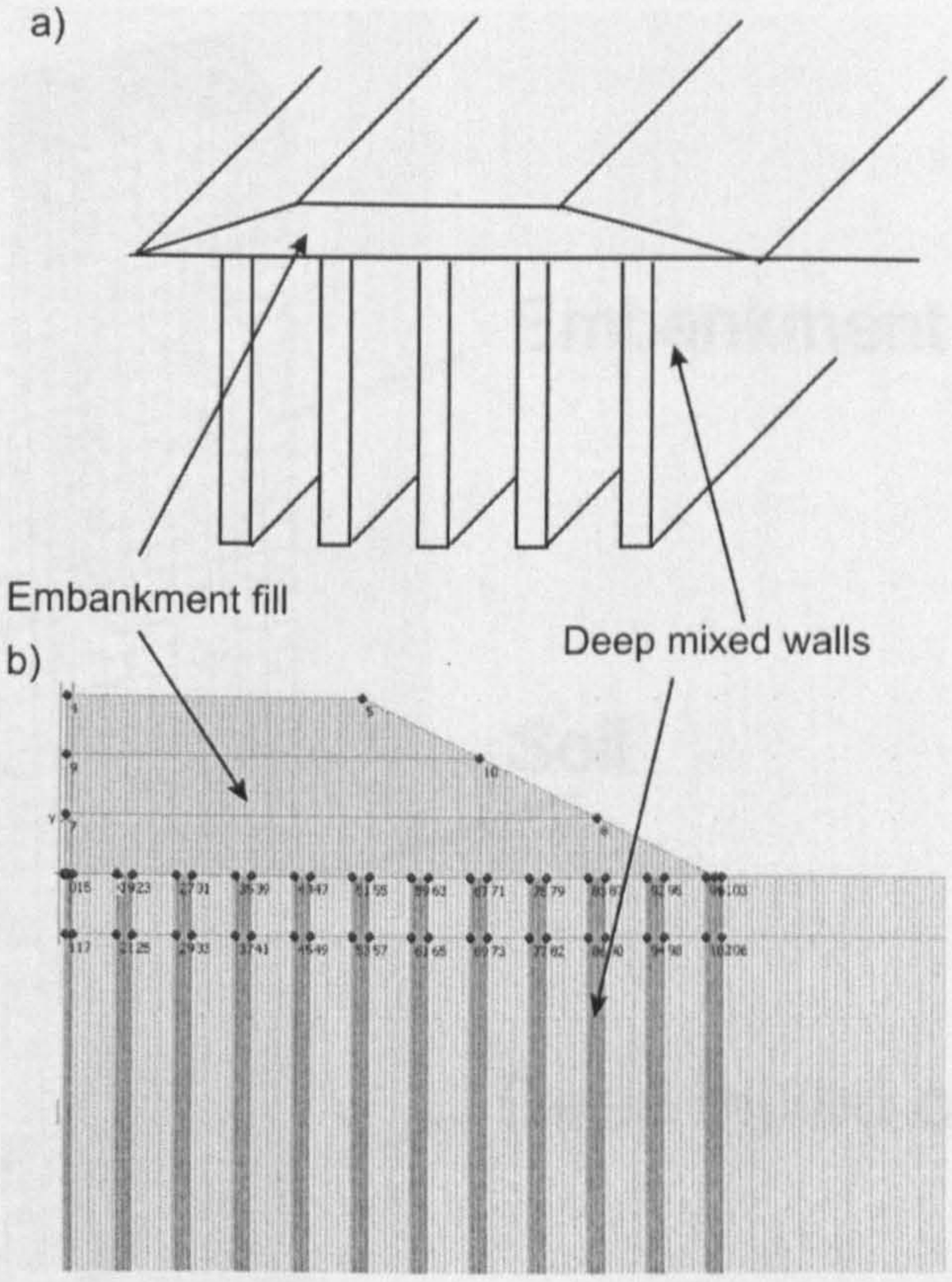

Figure 7.9: Plane strain analysis a) schematic model and b) finite element model

A plane strain model was used by Lahtinen and Vepsäläinen (1983) for the settlement analysis of the Itäkeskus test embankment. Aalto et al. (1999) used a plane strain model to simulate an embankment on soft clay constructed on deep mixed columns and reinforced with a geogrid. The model was used to compare the predictions to an embankment without reinforcement. Kitazume and Maruyama (2006) compared plane strain simulations of deep mixed columns to centrifuge tests. The model was not able to match measured settlements or horizontal displacements but the predicted stresses were in good agreement with the measurements. Huang et al. (2006) compared a plane strain analysis to a three dimensional analysis of an embankment on deep mixed columns. The settlement predictions of both models were in good agreement as long as the columns did not yield. They also compared the maximum stresses at the top of the column and found that the plane strain model underpredicts the maximum stresses compared to the three dimensional analysis.

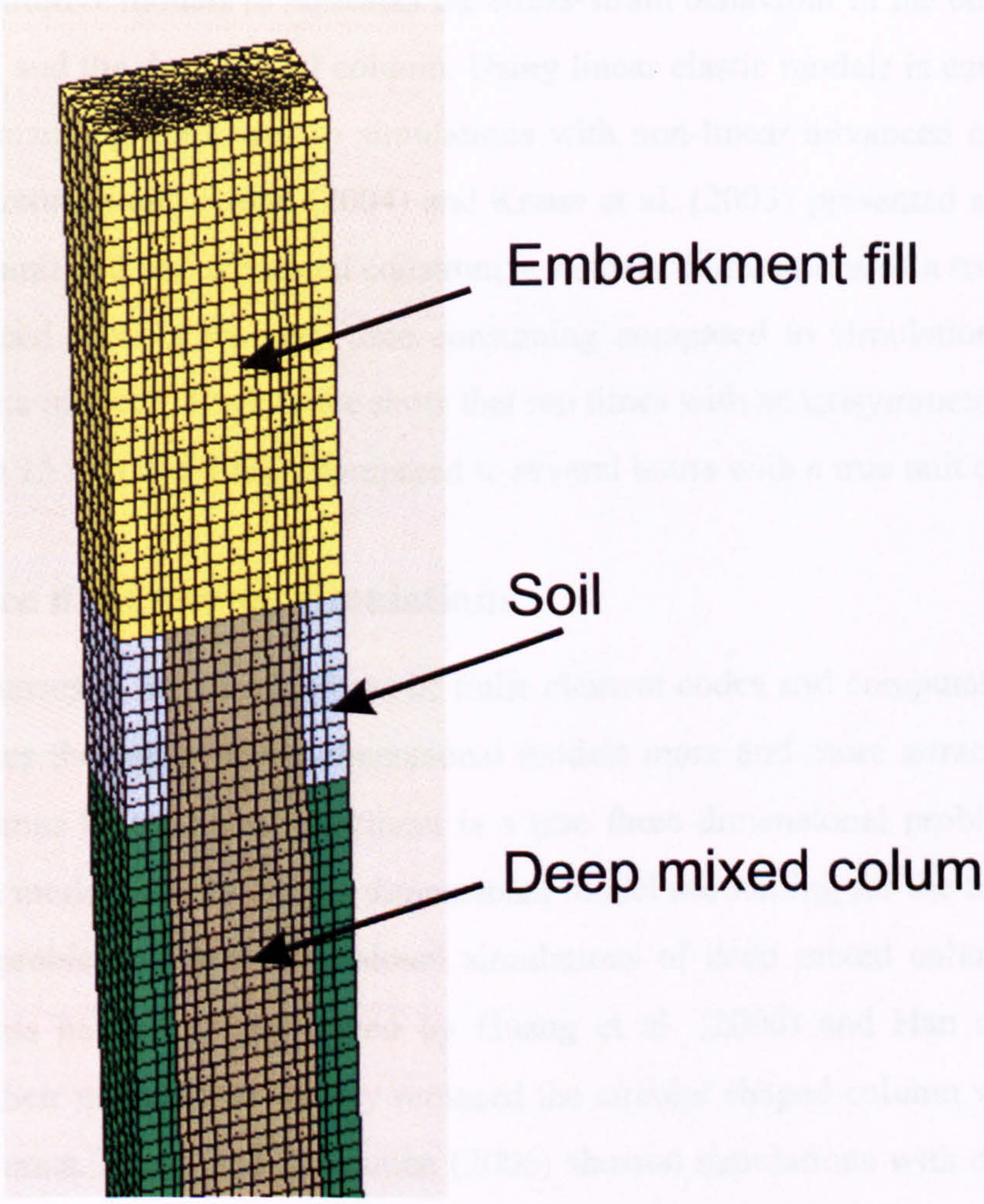

Figure 7.10: Finite element model of a true unit cell

7.8.3 Three dimensional unit cell (true unit cell)

In a three dimensional unit cell a single column and the surrounding soil are simulated. The radius and the true c/c-spacing are accounted for in the model. The advantage of the true unit cell compared to the axisymmetric unit cell is that any c/c-spacing can be modelled. The axisymmetric unit cell is limited to a square pattern. An example of a finite element model of a true unit cell is shown in Figure 7.10. The true unit cell is not widely used. Baker (2000) used a simple version of a true unit cell for a parametric study on deep mixed columns below an embankment. He modelled the column as a rectangular shape instead of the circular shape. Baker (2000) used simple

elastic constitutive models to represent the stress-strain behaviour of the embankment fill, the soil and the deep mixed column. Using linear elastic models is computationally not demanding compared to simulations with non-linear advanced constitutive models. Karstunen and Krenn (2004) and Krenn et al. (2005) presented simulations with a true unit cell and advanced constitutive models. Simulations of a true unit cell with advanced models are very time consuming compared to simulations with an axisymmetric unit cell. Experience show that run times with an axisymmetric unit cell are between 15 min and 1 hour compared to several hours with a true unit cell.

7.8.4 Three dimensional simulations

Recent advances in the development of finite element codes and computational platforms, makes the use of three dimensional models more and more attractive. Deep mixed columns below an embankment is a true three dimensional problem and as such is best modelled with a three dimensional model accounting for the true geometry of the problem. Three dimensional simulations of deep mixed columns below embankments have been performed by Huang et al. (2006) and Han and Huang (2007). In their models they simply replaced the circular shaped column with square shaped columns. Krenn and Karstunen (2006) showed simulations with deep mixed columns modelled in circular shape. An example of a three dimensional model is shown in Figure 7.11.

7.8.5 Volume averaging method

The basic idea of the volume averaging technique is to model a homogenous material in finite element simulations instead of modelling the columns and soils individually. A technique to model homogenised material was proposed by Schweiger and Pande (1986) for stone columns. An analytical volume averaging method for deep mixed material was proposed by Omine et al. (1999). The averaged model parameters were used as input for a finite element model. Both, the soil and the columns were modelled as linear elastic material combined with a Von-Mises criterion. The results of the

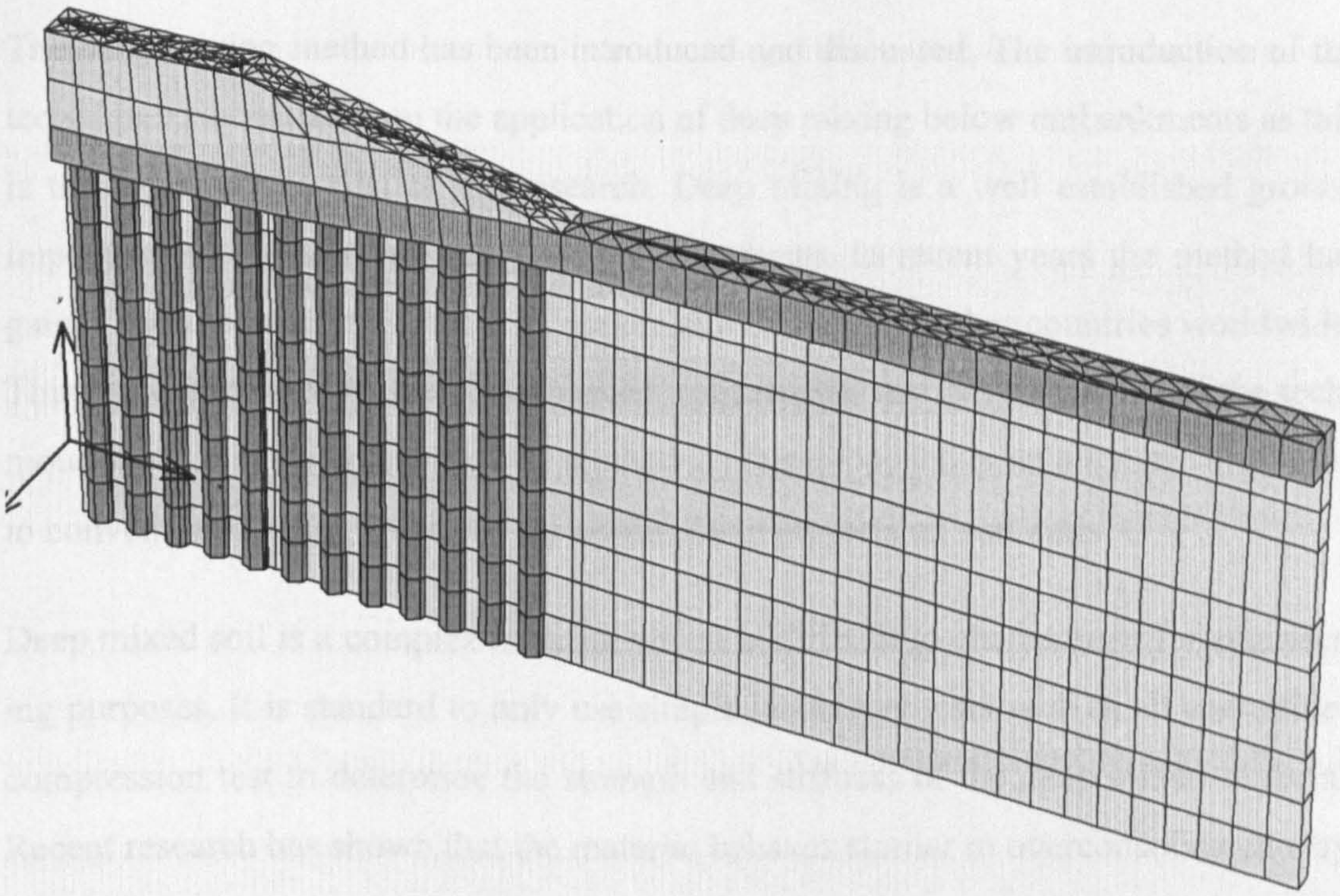

Figure 7.11: Three dimensional finite element model

simulations were then compared to 1g laboratory tests. The prediction and the tests were found to be in good agreement. Vogler (2008) proposed a volume averaging technique for deep mixed columns based on the technique proposed by Schweiger and Pande (1986) and Lee and Pande (1998). It is assumed that the deep mixed columns are installed in a square pattern below the embankment. Moreover, perfect bonding is assumed between the columns and the soil. The method proposed by Vogler (2008) allows elasto-plastic constitutive models to be adopted for the two materials using a separate constitutive model for the soil and the column. Vogler (2008) implemented the S-CLAY1S model for the soil and the MNhard model for the deep mixed material into his volume averaging technique. Comparison of the volume averaging technique with simulations using a three dimensional model shows a good match for the settlement predictions.

7.9 Summary

The deep mixing method has been introduced and discussed. The introduction of the technique concentrated on the application of deep mixing below embankments as this is the topic of this part of the research. Deep mixing is a well established ground improvement method in Scandinavia and in Japan. In recent years the method has gained more popularity in the UK, continental Europe and other countries worldwide. This has contributed to further enhanced, refinements and developments of the technique itself in many countries. The method is often proposed as an alternative solution to conventional piling solutions for construction projects on soft soils.

Deep mixed soil is a complex material which is difficult to characterise for engineering purposes. It is standard to only use simple laboratory tests such as an unconfined compression test to determine the strength and stiffness of the deep mixed material. Recent research has shown that the material behaves similar to overconsolidated clay. This finding is important for the development and application of constitutive laws to represent the stress-strain-strength behaviour.

Various alternatives of numerical modelling deep mixed columns below embankments have been introduced. The most commonly used models are the axisymmetric unit cell and the plane strain model. Axisymmetric unit cells are very useful for parametric studies. Developments of three-dimensional numerical codes and computational resources make it possible to account for the true nature of the problem. An alternative to the 3D analysis is the volume averaging technique. The method allows for both constituents to be accounted for in a plane strain analysis. In the following, however true 3D analyses have been used.

Chapter 8

Modelling of deep mixing

The objective of this Chapter is to use different approaches of modelling deep mixed columns constructed below embankments to investigate the stress distribution and settlements caused by the embankment load. The spacing of the columns is varied to demonstrate the effect of this design parameter on the overall behaviour. The influence of anisotropy and destructuration of the soft soil on the settlement behaviour is demonstrated by utilising the MCC, S-CLAY1 and S-CLAY1S models. The predicted stresses and displacements by the different models are compared to each other. In the last part of the Chapter the effect of floating columns are compared to end bearing columns. The numerical simulations have been carried out using the 2D PLAXIS V8.6 and PLAXIS 3D foundation.

8.1 Embankment on deep mixed columns

It is assumed that the embankment is constructed on soft Finnish clay improved with deep mixed columns. The deep mixed columns are installed in a periodic grid with a varied c/c-spacing. The diameter of the columns is taken to be 0.6 m, as that is a common diameter used in industry in Europe. The values of the material parameters were chosen to correspond to the soil found in Vanttila, Finland (Koskinen and Karstunen, 2004). The deposit has been idealised by representing it with only two layers

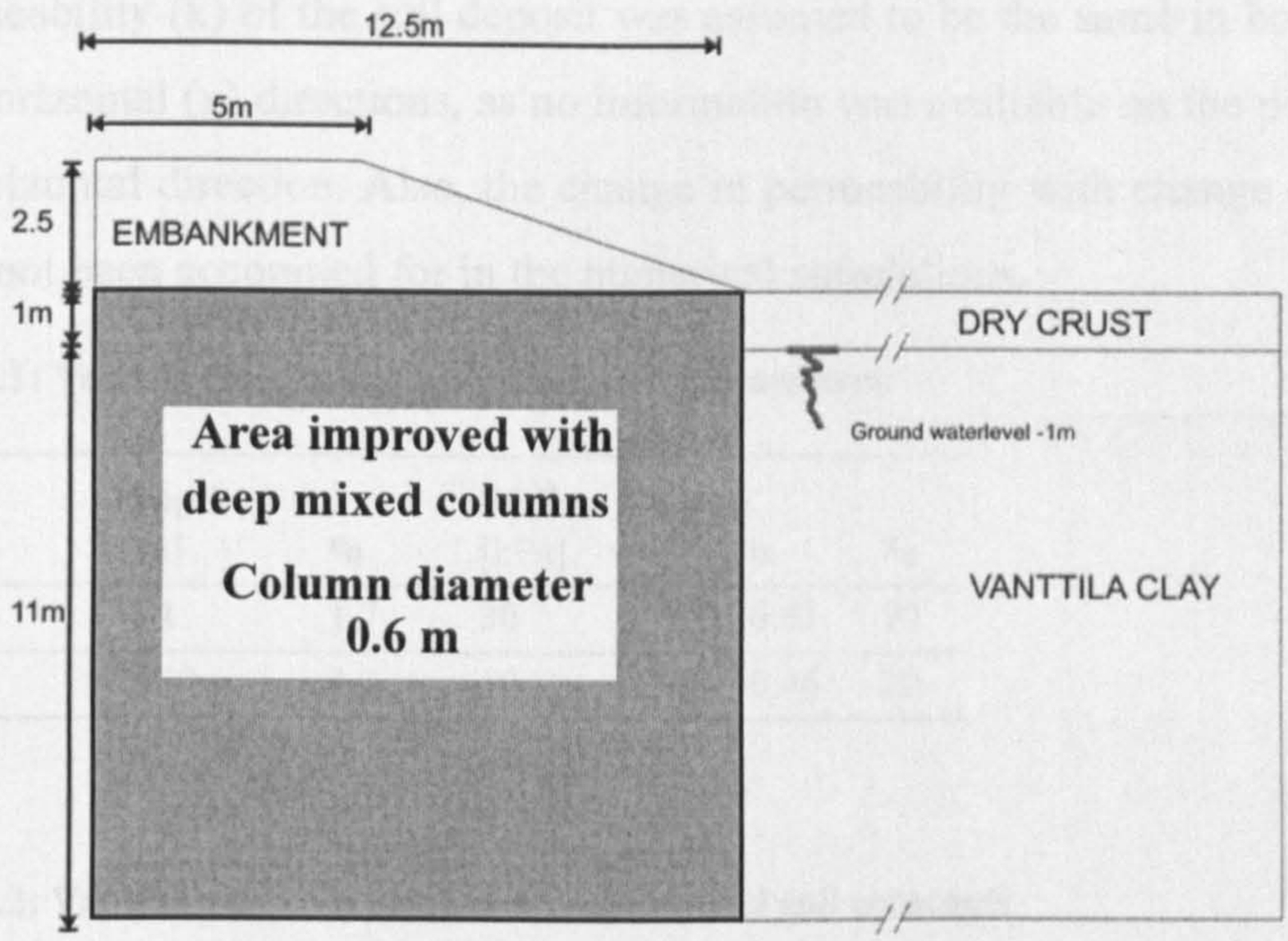

Figure 8.1: Geometry of the embankment and soil layers

(Figure 8.1): an overconsolidated dry crust of 1 m underlain by 11 m of soft, almost normally consolidated clay. The ground water level is assumed to be at 1 m below the ground level. The height of the embankment fill is assumed to be 2.5 m. The gradient of the embankment slope is assumed to be 1:3.

8.2 Soil and embankment fill parameters

The constitutive models chosen to represent the dry crust and the clay are the MCC, S-CLAY1 and S-CLAY1S models. The values for the soil parameters have been chosen to correspond to Vanttila clay. Results from oedometer tests and standard consolidated undrained triaxial tests on natural and/or reconstituted samples were used to derive the values listed in Table 8.1 to Table 8.3.

The preconsolidation of the soil is modelled by assuming the values given in Table 8.1 for the pre-overburden pressure (POP). The coefficient of the earth pressure at rest, K_0, has been computed using the formulation by Mayne and Kulhawy (1982), see Section 3.6.6 for details.

The permeability (k) of the soil deposit was assumed to be the same in both, vertical (y) and horizontal (x) directions, as no information was available on the permeability in the horizontal direction. Also, the change in permeability with change of the void ratio has not been accounted for in the numerical simulations.

Table 8.1: Vanttila clay: initial values for state parameters

Layer	Depth [m]	e_0	POP [kPa]	K_0^{oc}	α	x_0
1	0-1	1.7	30	0.76	0.63	90
2	1-12	3.2	10	0.57	0.46	20

Table 8.2: Vanttila clay: the values for conventional soil constants

Layer	γ [kN/m^3]	κ	ν'	λ	M	$k_x=k_y$ [m/day]
1	0-1	0.029	0.2	0.25	1.6	-
2	1-12	0.032	0.2	0.88	1.2	6.9E-5

Table 8.3: Vanttila clay: the values for the additional soil constants

Layer	β	μ	λ_i	a	b
1	1.07	15	0.07	11	0.2
2	0.76	40	0.27	11	0.2

The predicted undrained strength profiles for the assumed soil deposit by the MCC and S-CLAY models in triaxial compression (TXC) and extension (TXE) are shown in Figure 8.2. The isotropic MCC predicts the same strength in compression and extension. The strength in compression is marginally smaller than predicted by the S-CLAY models. The S-CLAY models predict a lower strength in TXC due to the shape of the yield surface. MCC predicts the same strength in TXC and TXE, whereas the S-CLAY models predict a lower strength in TXE.

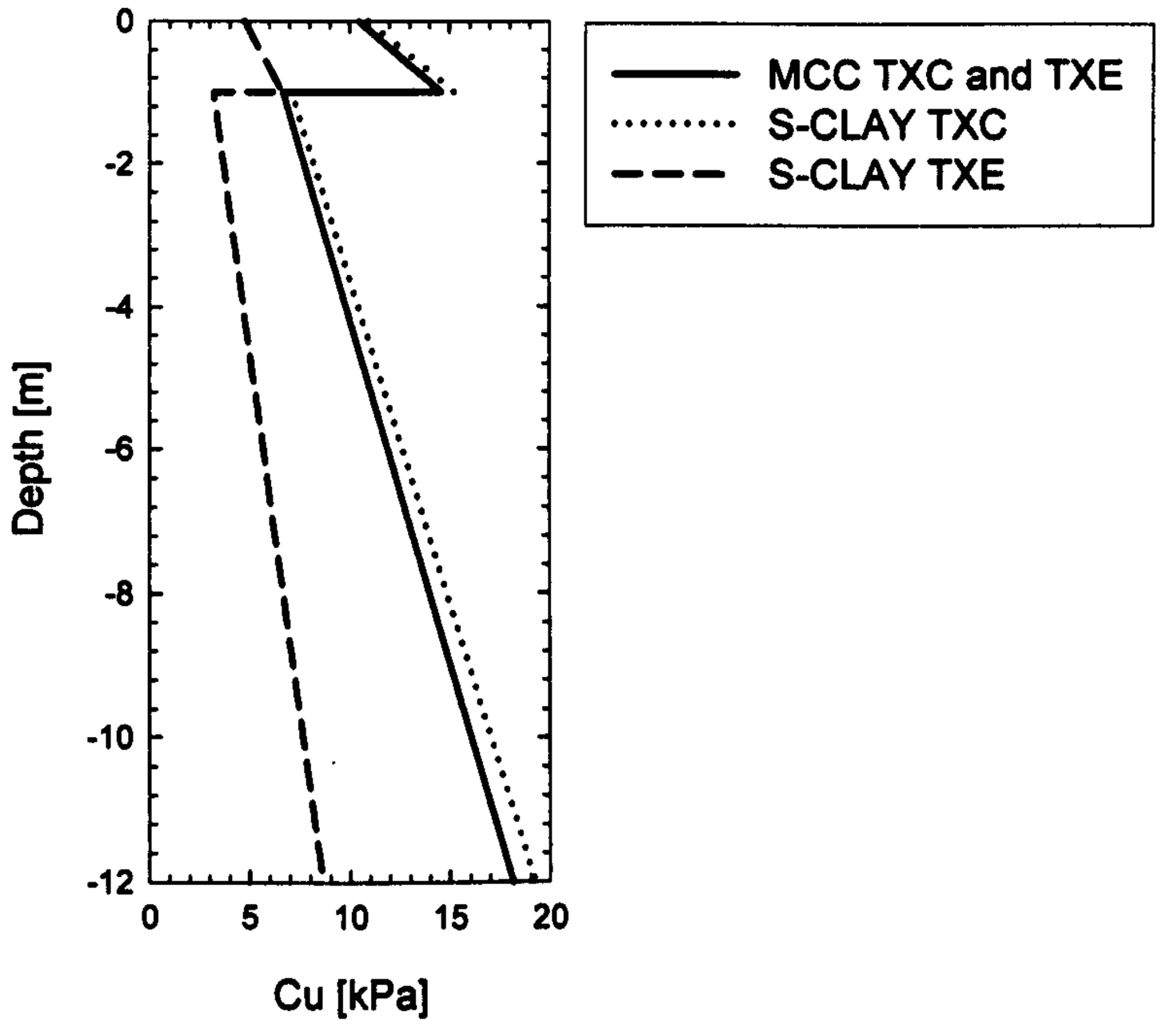

Figure 8.2: Initial undrained shear strength profile

The deep mixed Vanttila clay was modelled with either the HS model or the MNhard model. As shown in Section 7.7 both models give a good match with the experimental data on stabilised Vanttila clay, when the value for the model constants (listed in Table 7.1 and Table 7.2) were used. The stiffness values correspond to soft to medium stiff columns after Korkiala-Tanttu (1997). The design guidelines (e.g. EuroSoilStab 2002) suggest that the permeability of deep mixed material is greater than for the natural soil. However, in the simulations the permeability was assumed to be the same as for the surrounding soil. The assumption is reasonable because it is unlikely that the introduction of additional fines, in the form of cement, will notably contribute to a decrease in permeability. As no information about the tension capacity of deep mixed Vanttila clay was available, an average value of 20 kPa was assumed, which is a reasonable assumption based on CDIT (2002).

The embankment is modelled with the simple Mohr Coulomb model, assuming the parameters shown in Table 8.4. For computational stability in the three dimensional simulations a small value of cohesion was assumed.

Table 8.4: Model parameters for the embankment fill

Layer	E_{ur} [kN/m^2]	ν'	φ'	c' [kN/m^2]	ψ'	γ [kN/m^3]
Embankment fill	40000	0.3	38	2	0	20

8.3 Factor of safety of stability of the embankment

The factor of safety (FoS) of the slopes of the proposed embankment on natural ground and improved ground was computed using Oasys Slope 18.2 (2007). Two different strength profiles with depth were used in the simulations (Figure 8.3). Profile 1 is based on the TXC predicted by the S-CLAY models (see Figure 8.2). The undrained strength in Profile 1 is linearly increasing with depth in each layer. In contrast, Profile 2 has been chosen to be constant with depth per layer. The value per layer is an

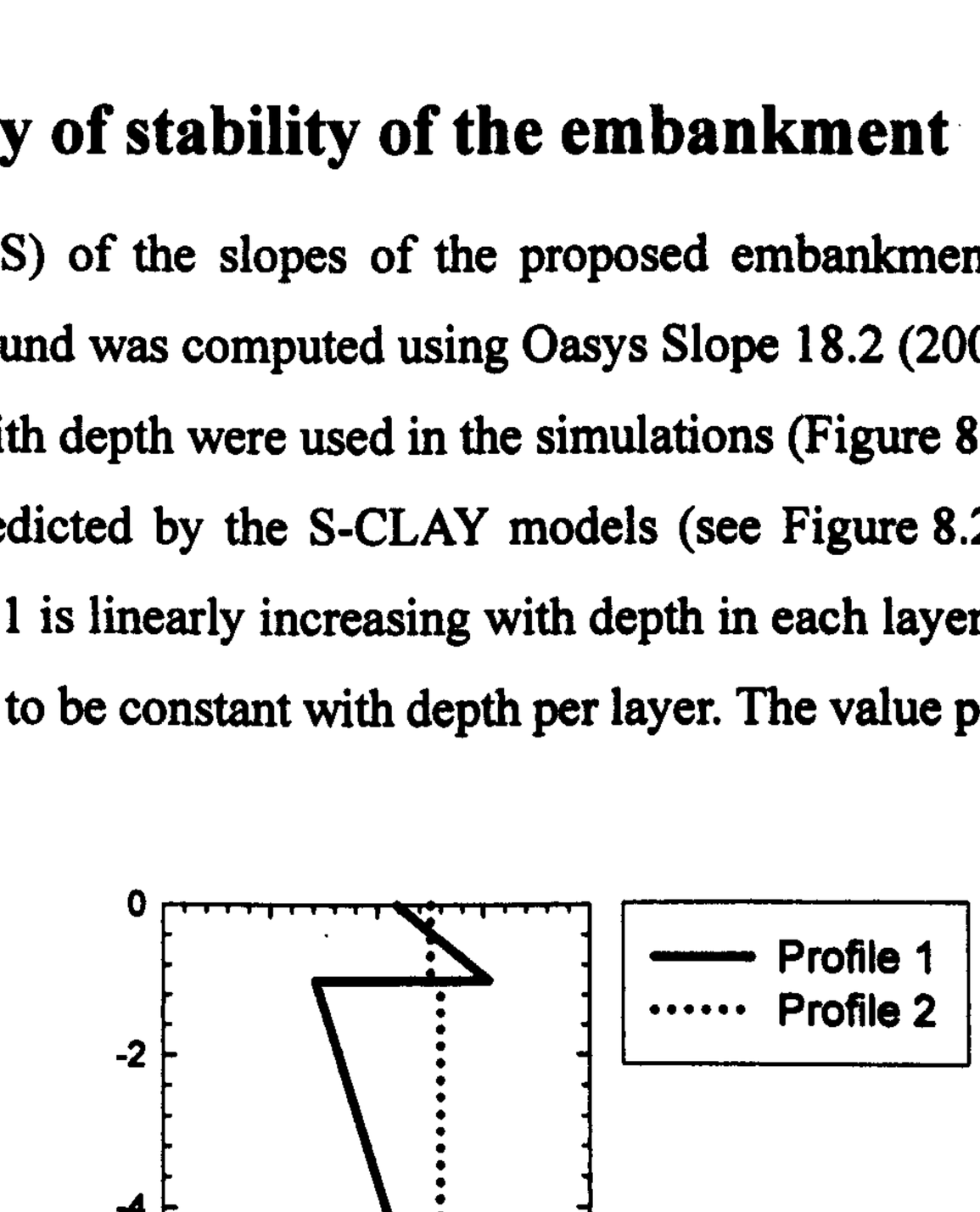

Figure 8.3: Undrained strength profile with depth

average value calculated from Profile 1. The predicted FoS for the embankment on natural ground are shown in Table 8.5.

Table 8.5: Predicted FoS for the embankment on natural ground

Cu profile	FoS
Profile 1	1.04
Profile 2	1.46

The predicted FoS for Profile 1 is 1.04. The FoS predicted with Profile 2 is larger and in the order of 1.46. The FoS was also computed for the embankment on improved ground. The c/c-spacing of the columns varied from 1.0 m to 1.6 m in 0.2 m steps. The diameter of the column is 0.6 m. The average undrained shear strength of deep mixed Vanttila clay is greater than 100 kPa. The design guidelines EuroSoilStab (2002) limits the maximum allowable undrained shear strength of the deep mixed material to 100 kPa. In the simulations a 100 kPa was chosen based on EuroSoilStab (2002). For the simulations an average undrained shear strength of the soil and the column was calculated according to EuroSoilStab (2002). The average strength is dependent on the improvement ratio a (see Section 7.3). The improvement ratios for the c/c-spacings were calculated according to *Eq. 7.1* and are shown in Table 8.6

Table 8.6: Calculated improvement ratios

c/c-spacing [m]	1.0	1.2	1.4	1.6
a	0.28	0.20	0.14	0.11

Knowing the improvement ratios for each c/c-spacing the average undrained shear strength for the improved area below the embankment (see Figure 8.1) can be calculated using the formula by EuroSoilStab (2002).

$$c_{u(av)} = a \times c_{u(col)} + (1-a)c_{u(soil)} \qquad [8.1]$$

EuroSoilStab (2002) does not assume a shear strength of the soil which increases linearly with depth. The guideline assumes that the strength of the column and the soil are constant. However, *Eq. 8.1* was used to calculate an average strength using Profile

1 for the soil. The determined average strength with depth assuming the undrained strength Profile 1 for the soil is shown in Table 8.7. The average strength in the improved area decreases with increasing c/c-spacing.

Table 8.7: Calculated average undrained shear strength for Profile 1

c/c-spacing [m]	1.0	1.2	1.4	1.6
0 m	36.1 kPa	28.4 kPa	23.8 kPa	20.7 kPa
-1 m	39.0 kPa	31.7 kPa	27.3 kPa	24.4 kPa
-1 m	33.4 kPa	25.4 kPa	20.5 kPa	17.4 kPa
-12 m	41.9 kPa	34.9 kPa	30.7 kPa	27.9 kPa

The calculated average strength for the improved area below the embankment assuming Profile 2 is shown in Table 8.8.

Table 8.8: Calculated average undrained shear strength for Profile 2

c/c-spacing [m]	1.0	1.2	1.4	1.6
0 to -1 m	37.2 kPa	29.7 kPa	25.1 kPa	22.2 kPa
-1 to -12 m	37.6 kPa	30.1 kPa	25.6 kPa	22.6 kPa

In the simulations using Oasys Slope 18.2 (2007) the calculated average strength was applied in 2/3 of the improved area below the embankment. This was done to ignore the strength of the columns in the passive area according to EuroSoilStab (2002). The predicted FoS values are presented in Table 8.9.

Table 8.9: Calculated FoS for different c/c-spacing

c/c-spacing [m]	1.0	1.2	1.4	1.6
Profile 1	2.75	2.48	2.18	2.04
Profile 2	2.75	2.58	2.30	2.11

The predicted FoS of the embankment constructed on deep mixed columns has substantially improved. For Profile 1 the FoS increased from 1.04 to a minimum of 2.04 for a c/c-spacing of 1.6 m. In the case of Profile 2 the FoS increased from 1.46 to a minimum of 2.11. Comparing the predictions of the improved embankment only it

can be seen that Profile 1 results in a lower FoS compared to Profile 2. For a c/c-spacing of 1.0 m the FoS is the same for both Profiles. Inspection of the graphical output of the simulations shows that in both cases no global failure was predicted (the predicted slip surface is within the embankment fill) and as such was not influenced by the average shear strength of the improved area.

8.4 Numerical simulations of deep mixing

This section concentrates on numerical modelling of deep mixing using two and three dimensional approaches to model the columns and the surrounding soil under an embankment fill. The simulations investigate how fabric anisotropy, interparticle bonding and the degradation of the bonds within the soft soil (between the columns) influences the stress-strain-strength behaviour of the soil-column system. The soil is modelled with different constitutive models, the isotropic MCC model, the anisotropic S-CLAY1 model and S-CLAY1S, which also accounts for bonding and degradation of bonding in addition to anisotropy. The spacing of the columns is varied to study the effect on the overall behaviour of the proposed embankment. The parameters for the soil and the columns were shown in Tables 8.1 to 8.4 and Tables 7.1 to 7.2, respectively. The geometry of the simulated embankment was introduced in Section 8.1. The construction of the embankment and the column is modelled as follows. First, the columns are installed by replacing the soil with column material. Next, the embankment material is applied as an additional layer. This occurs under undrained conditions, whilst assuming the materials above the water table to be drained. Finally, a consolidation phase is simulated via a fully coupled static consolidation analysis. All simulations are small strain simulations to allow for comparison between the different 2D and 3D models. The PLAXIS 3D foundation is limited to small strain analysis only.

8.4.1 Axisymmetric unit cell

As mentioned in Section 7.8.1 with a so-called unit cell a single column and the surrounding soil under the embankment fill can be modelled. In the simulations the col-

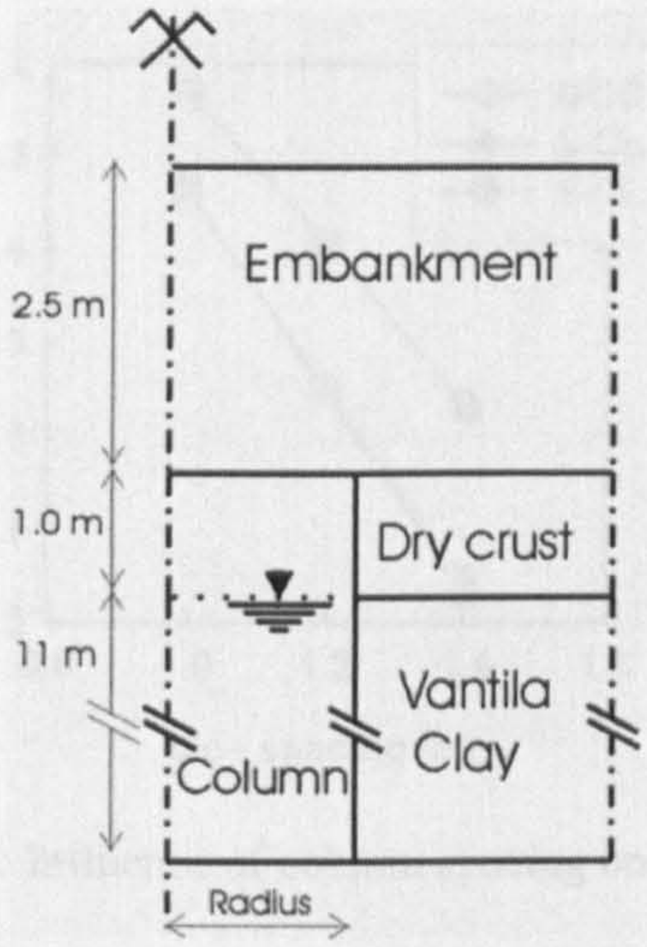

Figure 8.4: Schematic drawing of the axisymmetric unit cell

umn diameter is kept constant and the c/c-spacing is varied as 1.0 m, 1.2 m and 1.4 m. The radii of the models were calculated according to *Eq. 7.2*. The problem is idealised by using a finite element mesh with approximately 150 15-noded triangular elements (exact number of elements is dependent on the c/c-spacing). Mesh sensitivity studies using 162, 402 and 800 elements confirmed that the results are insensitive to the number of elements. The lateral boundaries of the meshes are constrained in the horizontal direction and the bottom boundaries are constrained in both directions. Drainage boundaries are assumed to be at the level of the water table at a depth of -1 m. The model is a crude idealisation of the columns installed in a square grid under the centre line below the proposed embankment (Figure 8.1). A schematic drawing of the simulated unit cell is shown in Figure 8.4.

8.4.1.1 Numerical predictions

In the following, the results of the finite element analysis of the unit cell are presented.

8.4.1.1.1 Surface settlements

Figure 8.5 presents the predicted settlements at the ground surface at the centre of the column after consolidation to a maximum excess pore pressure of 1 kPa. With

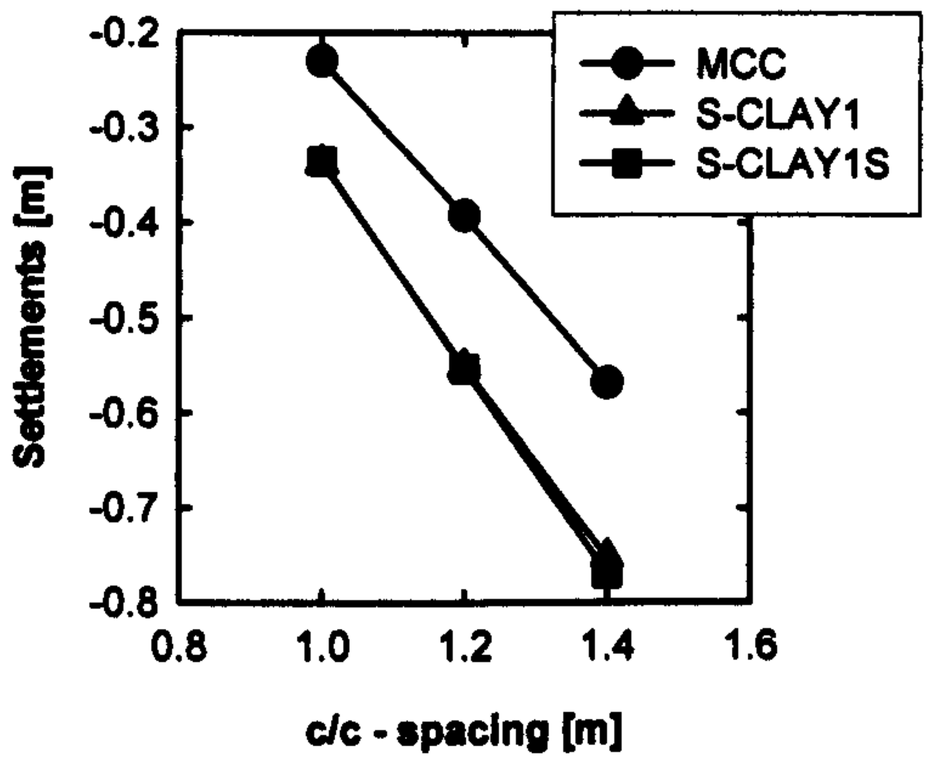

Figure 8.5: Influence of column spacing on settlements

increasing c/c-spacing the magnitude of the settlements is increasing, as expected. The smallest settlement, about -0.23 m, is predicted by the MCC model and 1.0 m c/c-spacing. The vertical displacements predicted by the S-CLAY1 and S-CLAY1S are almost identical. S-CLAY1S predicts -0.33 m compared to -0.34 by the S-CLAY1 for the case of 1.0 m c/c-spacing. That difference slightly changes with increasing c/c-spacing to -0.75 m for S-CLAY1 and -0.77 for S-CLAY1S for 1.4 m c/c-spacing. Also the difference between the predictions by MCC and the S-CLAY models increases with increasing c/c-spacing. The predicted differential settlements between soil and column at the surface are in general less than 1 mm. Thus assuming equal strains in the columns and the soil, as used in conventional design, is appropriate in the cases considered. The settlement predictions of the constitutive models suggests that the effects of bonding and destructuration are less important than the effect of anisotropy for this boundary value problem.

In Figure 8.6 the predicted time settlement response of the simulations with the three models for the different c/c-spacings is presented. The consolidation time increases with increasing c/c-spacing and the magnitudes are greater with the anisotropic models than predicted by MCC. The differences are relative minor immediately after construction of the embankment fill, but become significant during consolidation. Immediately after construction the vertical displacements predicted by all the models are the same. Typically in the order of about 2 cm for 1.0 m c/c-spacing and 3 cm for

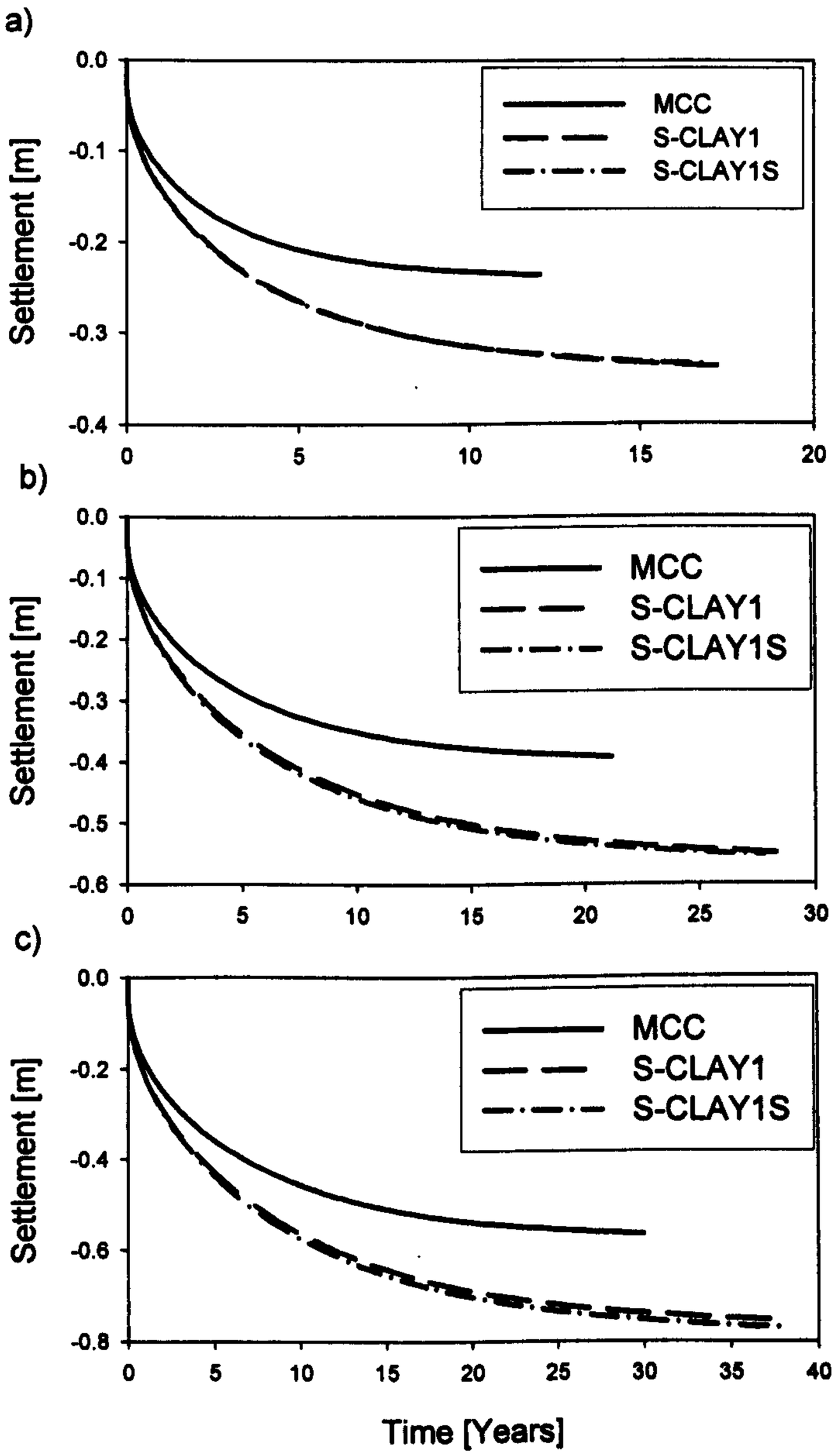

Figure 8.6: Time settlement curves: a) 1.0 m c/c-spacing; b) 1.2 m c/c-spacing; and c) 1.4 m c/c-spacing.

1.4 m c/c-spacing. According to Figure 8.6, the consolidation times predicted by the anisotropic models are in all cases longer than those by the MCC model. If the predictions of the S-CLAY models only are compared, it can be seen for 1.0 m c/c-spacing (Figure 8.6a) that both models need around 17 years to complete consolidation. With increasing c/c-spacing the time required increases to a maximum of about 39 years with the S-CLAY1S model (Figure 8.6c) for 1.4 m c/c-spacing.

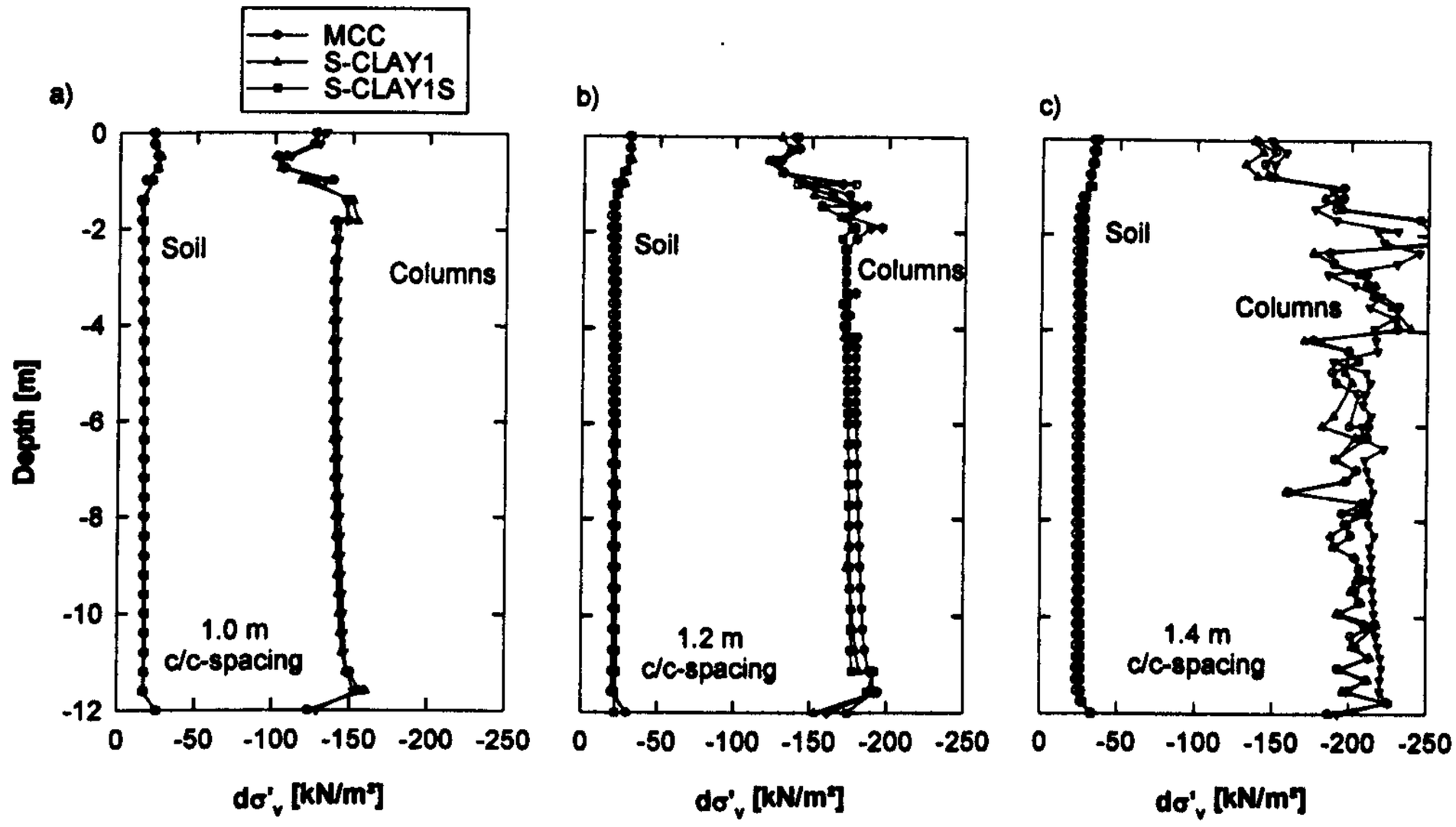

Figure 8.7: Increase in vertical stresses: a) 1.0 m, b) 1.2 m and c) 1.4 m c/c-spacing.

8.4.1.1.2 Differential vertical stresses

The predicted increase in the effective vertical stresses versus the depth are plotted in Figure 8.7, both in the soil and columns. The results correspond to the end of consolidation. The predicted increase in vertical stresses in the soil between the columns is almost constant with depth. Within the dry crust the vertical stress is slightly higher than the stress in the soft clay. This is due to the overconsolidation of the dry crust, which results in a higher apparent stiffness in the dry crust than in the underlying soft clay. All three models predict similar magnitudes of stress in the soil and columns with depth. Close to the bottom boundary a decrease of the stress in the column and a slight increase of the stress in the soil is predicted. A closer inspection reveals that the phenomenon is caused by stress rotation, associated with stress redistribution from the column back to the soil. Therefore it can be argued that the boundary conditions chosen are not ideal. The stresses in the column with 1.4 m c/c-spacing show significant scatter. This can be explained by the shear resistance of the columns. In the cases of 1.0 m and 1.2 m the shear resistance is not fully mobilised, which was confirmed by inspection of the plastic point plots. However, there is evidence of local failures with 1.4 m c/c-spacing, which is not demonstrated in the global response.

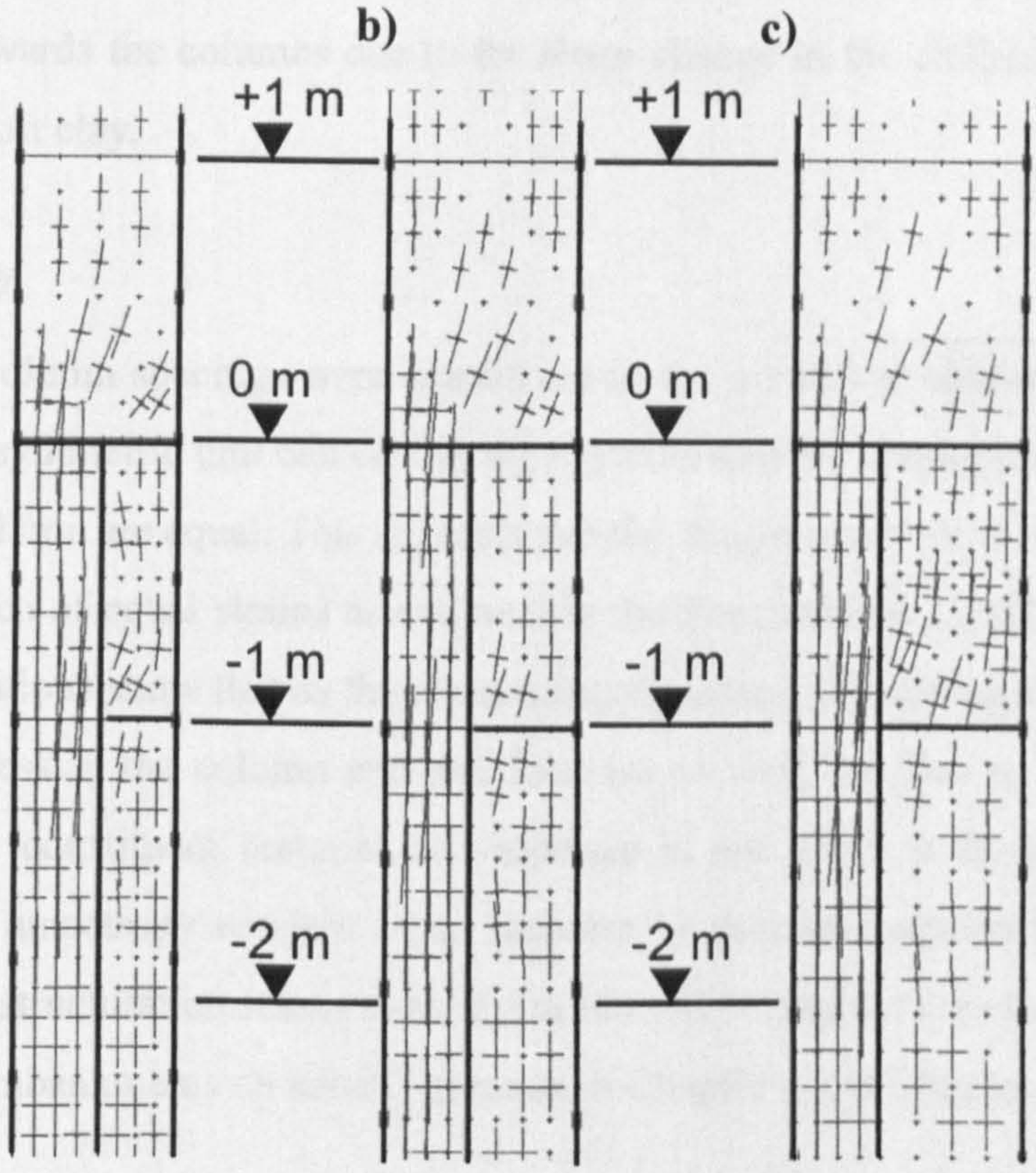

Figure 8.8: Principal effective stresses: a) 1.0 m, b) 1.2 m and c) 1.4 m c/c-spacing.

8.4.1.1.3 Principal stresses

The predicted principle effective stresses of the simulations with the S-CLAY1S model at the topmost section of the models are presented in Figure 8.8. The picture shows approximately half of the embankment height as well as the soil and the column down to a depth of -2.5 m. The arching of the embankment over the columns is clearly demonstrated by the rotation of the principle stresses. Most of the embankment load is distributed towards the columns in the bottom half meter of the embankment for the case of 1.0 m c/c-spacing (Figure 8.8a). With increasing column spacing the area within the embankment where the stress rotation occurs increases as demonstrated in (Figure 8.8b and c). Below ground level for the case of 1.0 m c/c-spacing some of the stresses are transferred back to the dry crust. This phenomenon does not seem to be apparent for the cases with bigger c/c-spacing. Close to the bottom of the

dry crust there seems to be a secondary arching mechanism, resulting in the stress redistribution towards the columns due to the sharp change in the stiffness from the dry crust to the soft clay.

8.4.1.2 Summary

Three different column spacings were considered in the numerical simulations. The results of the axisymmetric unit cell clearly demonstrate that the displacements in the soil and in the column are equal. This suggests that the design assumption for the conventional approach of equal strains as assumed in the EuroSoilStab (2002) is appropriate. All simulations show that as the c/c-spacing increases, the surface settlements increase. The stress in the column and soil increase as well, but due to non-linear behaviour of the constituent material, the increase is not linear with c/c-spacing. Incorporation of anisotropy resulted in an increase of predicted settlements in the order of 30%. Destructuration seems to have a minor effect. Similar conclusions have been drawn for embankments on natural grounds in Chapter 4 and Chapter 6.

8.4.2 Three dimensional unit cell (true unit cell)

A three dimensional model has been developed in the PLAXIS 3D foundation code for each c/c-spacing considered. The extent of the geometry in the x and y directions is dependent on the c/c-spacing (Figure 8.9a). The discretisation of the problem was extended to a real three dimensional cluster in the z direction. The model shown in Figure 8.9a served as the front plane. The cross section was copied at out-of -plane intervals (z direction) and then the three dimensional model was generated by a linear extension of the two dimensional mesh in the third dimension. A part of the 3D model is shown in Figure 8.9b. The 3D mesh consists of approximately 2000 15-noded wedge elements. Mesh sensitivity studies were done with different sizes of meshes (2000, 5000 and 12000 elements) to confirm that the meshes were dense enough to give accurate settlements predictions. Horizontal displacements were fixed on the lateral boundaries, whereas on the bottom boundaries both vertical and horizontal dis-

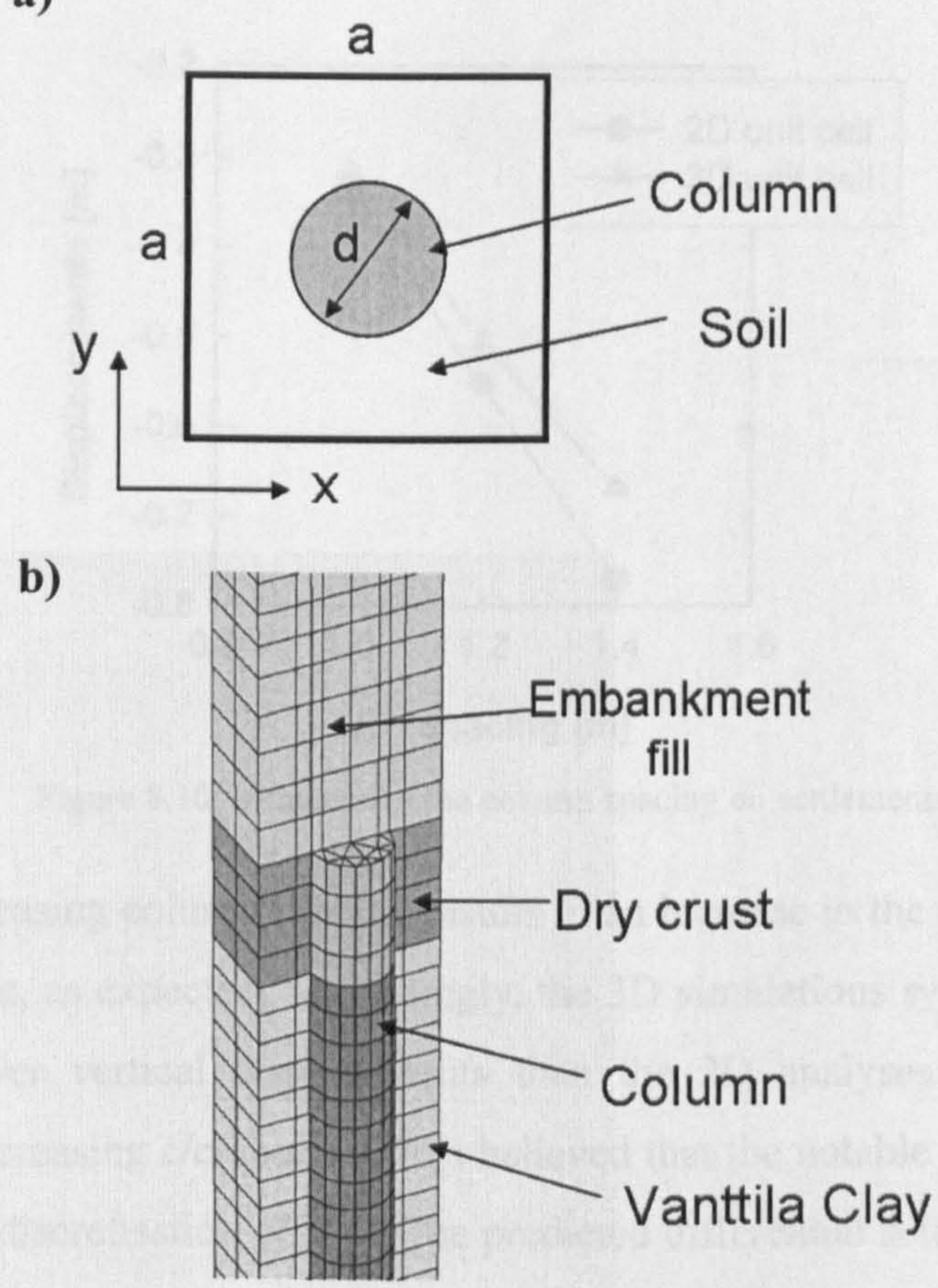

Figure 8.9: 3D unit cell: a) plane view and b) finite element model.

placements were fixed. Drainage boundaries are assumed to be at the water level and at the bottom of the mesh.

8.4.2.1 Numerical predictions

The results of the numerical simulations are presented in the following via summary diagrams that include the results of the 2D unit cell and the 3D unit cell. Only results predicted using the S-CLAY1S model for the soil are shown.

8.4.2.1.1 Surface settlements

Figure 8.10 shows the predicted final values of vertical displacements at the surface at the centre of the column. This corresponds to the end of consolidation. Based on

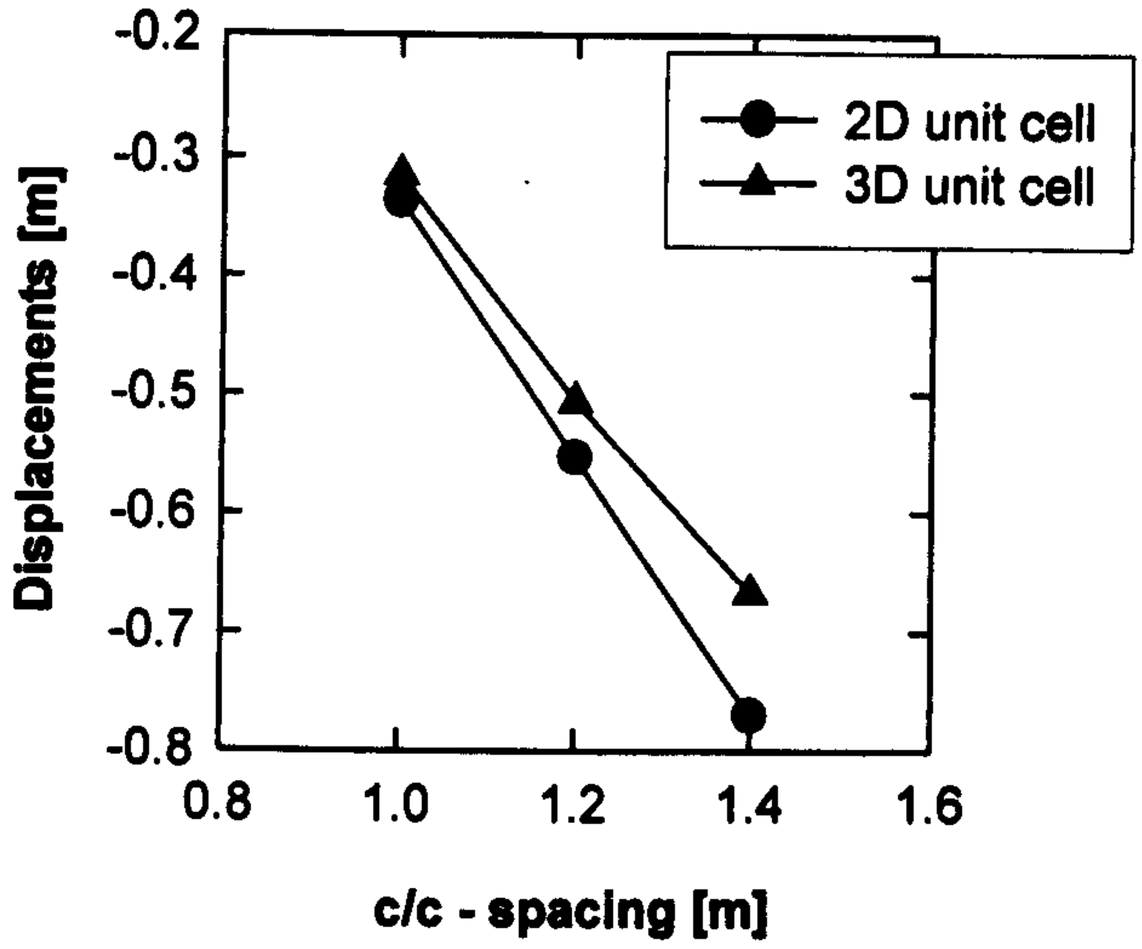

Figure 8.10: Influence of the column spacing on settlements

Figure 8.10, increasing column spacing results in an increase in the predicted magnitude of settlement, as expected. Interestingly, the 3D simulations systematically predict notably lower vertical displacements than the 2D analyses. The difference increases with increasing c/c-spacing. It is believed that the notable difference is due to geometry and discretisation effects. The predicted differential settlements between the soil and the column for the 3D simulations are in general less than 1 mm.

8.4.2.1.2 Differential vertical stresses

Figure 8.11 shows the predicted vertical stress increase in the column and the soil versus depth. There is no significant difference in the stresses in the column and in the soil predicted by the 2D and 3D simulations. For the 1.0 m c/c-spacing stress, redistribution between the column and the soil takes place in the first two meters, shown as small discontinuities in the stresses in the column in Figure 8.11a. The amount of stress redistribution is governed by the relative stiffness between soil and column. All simulations predict an almost constant stress in the soil and the column below a depth of -3 m. The shear resistance is fully mobilised in the 2D and 3D simulations with a c/c-spacing of 1.4 m close to the centre line of the column. In Figure 8.11c it is shown as a large scatter in the predicted stresses in the column. Inspection of the plastic point

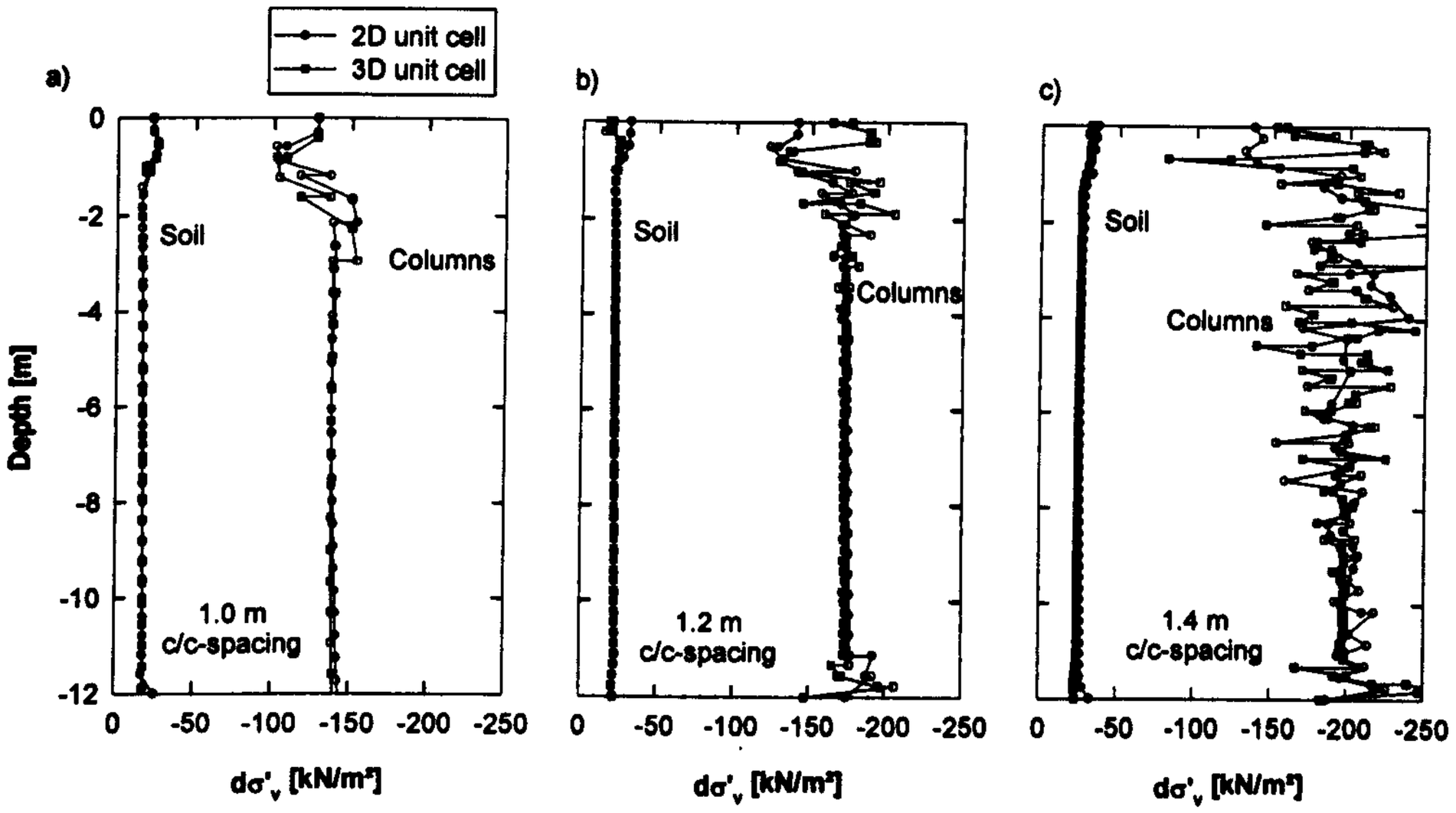

Figure 8.11: Increase in vertical stresses: a) 1.0 m, b) 1.2 m and c) 1.4 m c/c-spacing.

plots for both models confirmed that there is evidence of local failure behaviour in the column.

8.4.2.1.3 Influence of column stiffness on surface settlements

The influence of the column stiffness on the surface settlements has been studied using the S-CLAY1S model and a unit cell with a 1.0 m c/c-spacing. The results for surface settlements are shown in Figure 8.12. The reference stiffnesses used are listed in Table 8.10 below

Table 8.10: Values of the column stiffnesses

Type	E_{50}^{ref} [kN/m²]	E_{oed}^{ref} [kN/m²]	E_{ur}^{ref} [kN/m²]
Column 1	8000	8000	18000
Column 2	12000	12000	27000
Column 3	16000	16000	36000

Reference stiffness for p^{ref} = 100 kPa

The increase of the E_{50}^{ref} from 8000 kPa to 12000 kPa which is an increase in stiffness by 50 % results in a decrease of settlements for 1.0 m c/c-spacing by approximately 20 %. A further increase of stiffness to 16000 kPa which is an increase by 100

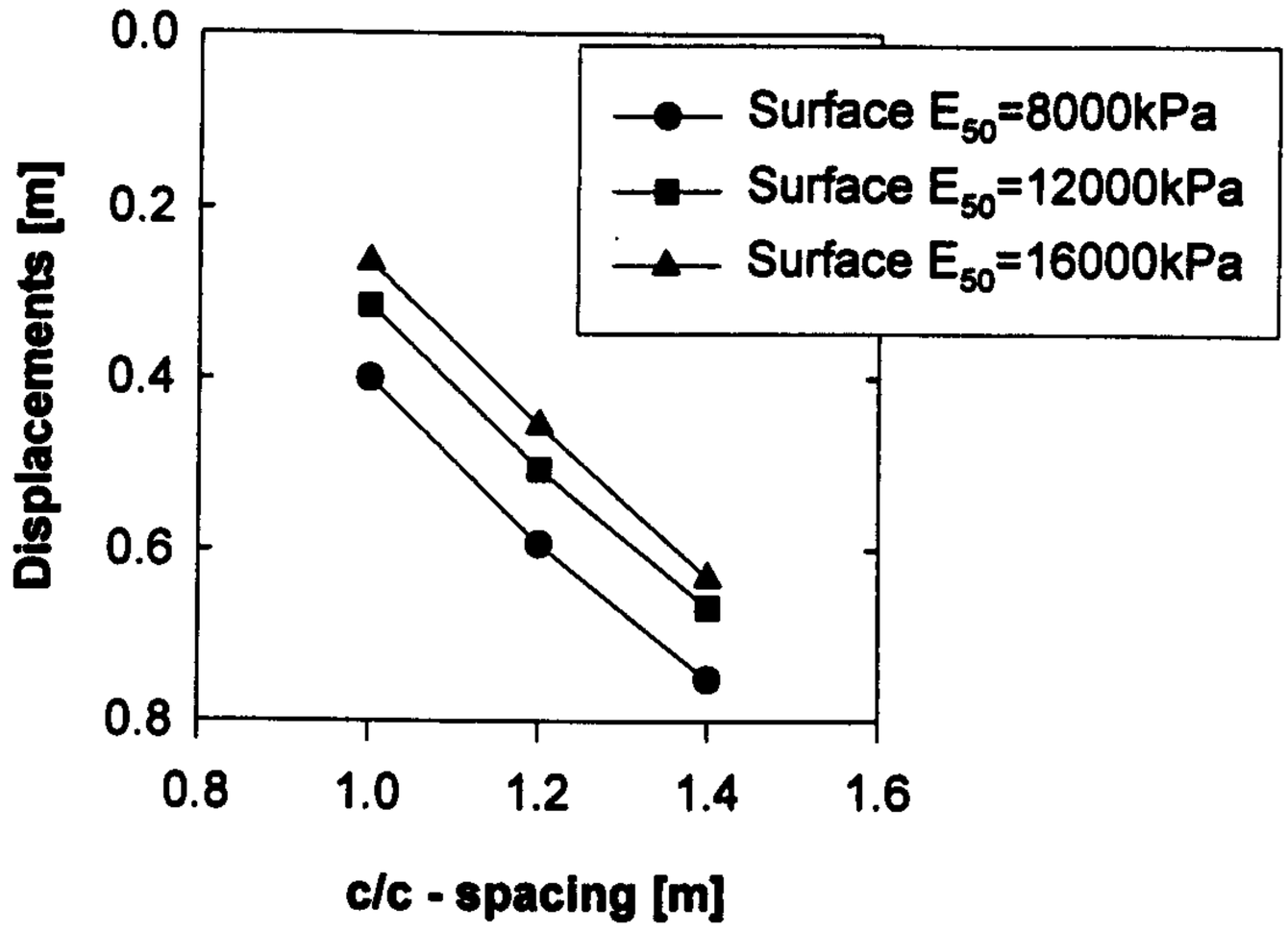

Figure 8.12: Influence of numerical model on settlements

% decreases the settlements by 44 %. This trend can also be observed for larger c/c-spacings of 1.2 m and 1.4 m. The effect of the stiffness increase is constant for the studied c/c-spacings. Comparison of Figure 8.12 to Figure 8.5 shows that the influence of the constitutive model of the soft soil is more pronounced than the column stiffness.

8.4.2.2 Summary

An axisymmetric and a true unit cell has been used to investigate the stress-strain response of deep mixed columns below an embankment fill. Based on the results the 3D simulations predict slightly less settlements than the 2D simulations. The reason for the difference in the settlement predictions is not fully understood. Similar findings were reported for simulations of stone columns with 2D and 3D models using the same finite element codes by Schweiger and Gaeb (2006) and Gaeb (2006). Despite the difference in the settlements predictions, both models predict the same stresses in the soil and the column for all three c/c-spacings investigated. Even though the predicted settlements (in the soil and the column) are uniform, the soil column system is far from a 1D problem. The difference in the apparent stiffness in the soil and the col-

umn causes stress rotation in the embankment fill but also in the soil and in the column.

From a practical point of view the 3D unit cell has a major disadvantage compared to the 2D unit cell in terms of computational run time. A fully coupled static consolidation analysis with the 2D unit cell takes about 30 minutes to an 1 hour depending on the c/c-spacing and the number of finite elements whereas simulations with the 3D unit cell takes up to several hours.

8.4.3 Full three dimensional model

Analogous to the true unit cell a full three dimensional model was developed for each c/c-spacing considered. The PLAXIS 3D foundation code was utilised for the model development and the simulations. In the 3D code, one must first design a model on a 2D plane (x-y plane) and later extend the model in the third direction (z) to achieve a full discretisation of the problem. Due to the symmetry of the embankment shown in Figure 8.1 only half of the embankment is represented in the finite element mesh. The width of the embankment strip (out of plane dimension) is dependent on the c/c-spacing. An example of a finite element mesh used can be seen in Figure 8.13. The mesh consists of approximately 6000 15-noded wedge elements. The lateral boundaries are restrained horizontally, and the bottom boundaries are assumed to be at the water level and the bottom of the model. Drainage boundaries are assumed to be at the water level and at the bottom of the model. Due to limitations in the code the undrained construction of the embankment is not modelled in stages by activating different layers of the embankment fill as in the 2D and 3D unit cell. Instead the unit weight of the fill is stepwise increased until the full load is activated.

8.4.3.1 Numerical predictions

In the following the results of the numerical simulations are presented. All the results shown have been determined using the S-CLAY1S model to simulate the stress-strain behaviour of the soil.

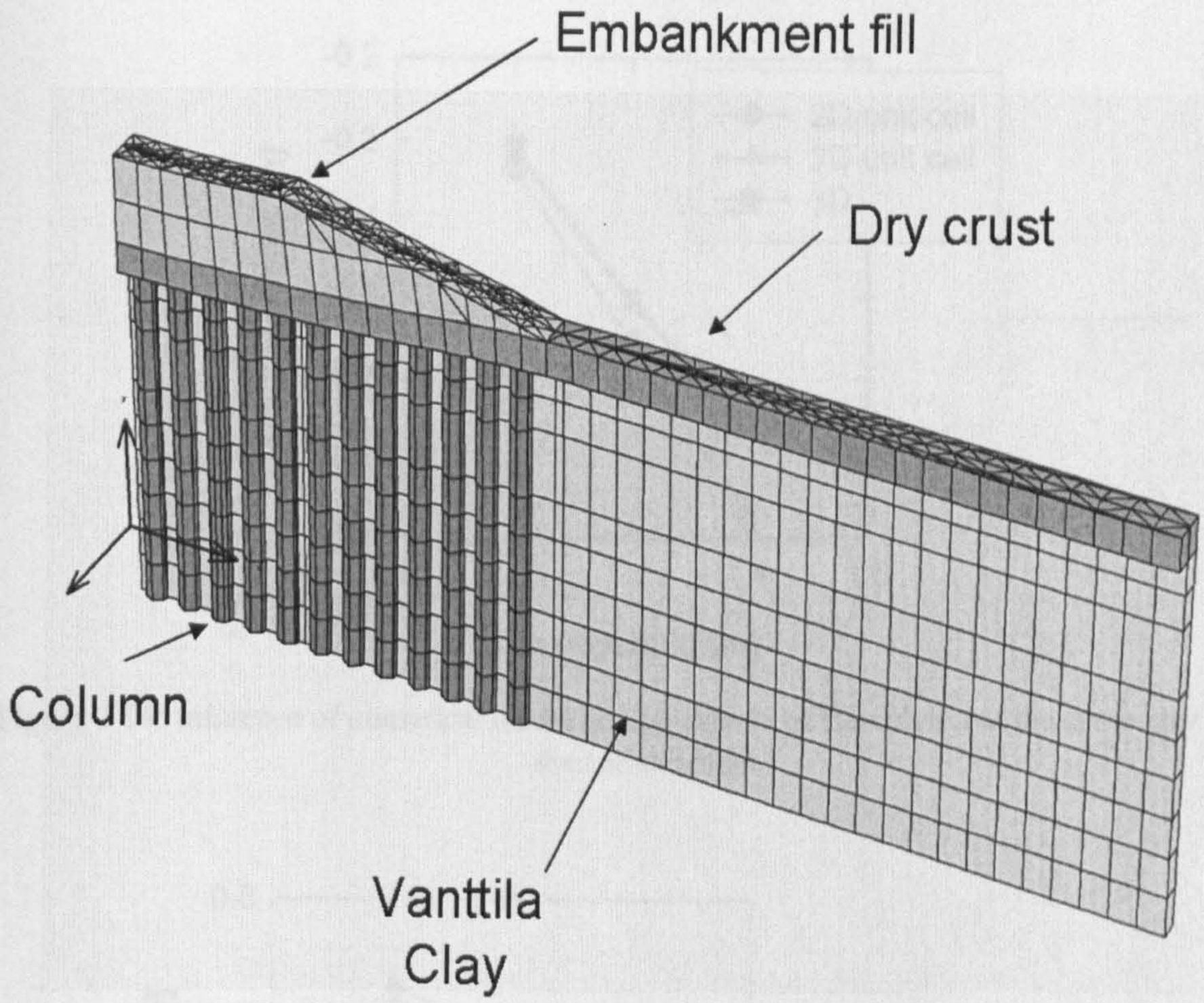

Figure 8.13: Finite element mesh of the 3D model.

8.4.3.1.1 Surface settlements

In Figure 8.14 the settlements for the column at the centreline predicted by the full 3D model are compared to the predictions by the true unit cell and the axisymmetric unit cell. Again the predictions are compared for the three c/c-spacings, 1.0 m, 1.2 m and 1.4 m. Both 3D models predict surface settlements of similar magnitude for all three c/c-spacings.

The settlements of the column at the centreline of the embankment at different depths are presented in Figure 8.15. In addition to the surface settlements, the predicted settlements at -1 m and - 5 m are presented. The results are shown only for the full 3D model and the 3D unit cell. As mentioned above both models predict similar surface settlements. The same trend can be observed for the settlements at a depth of -1 m which is the top of the soft clay deposit. At -5 m the true unit cell predicts slightly

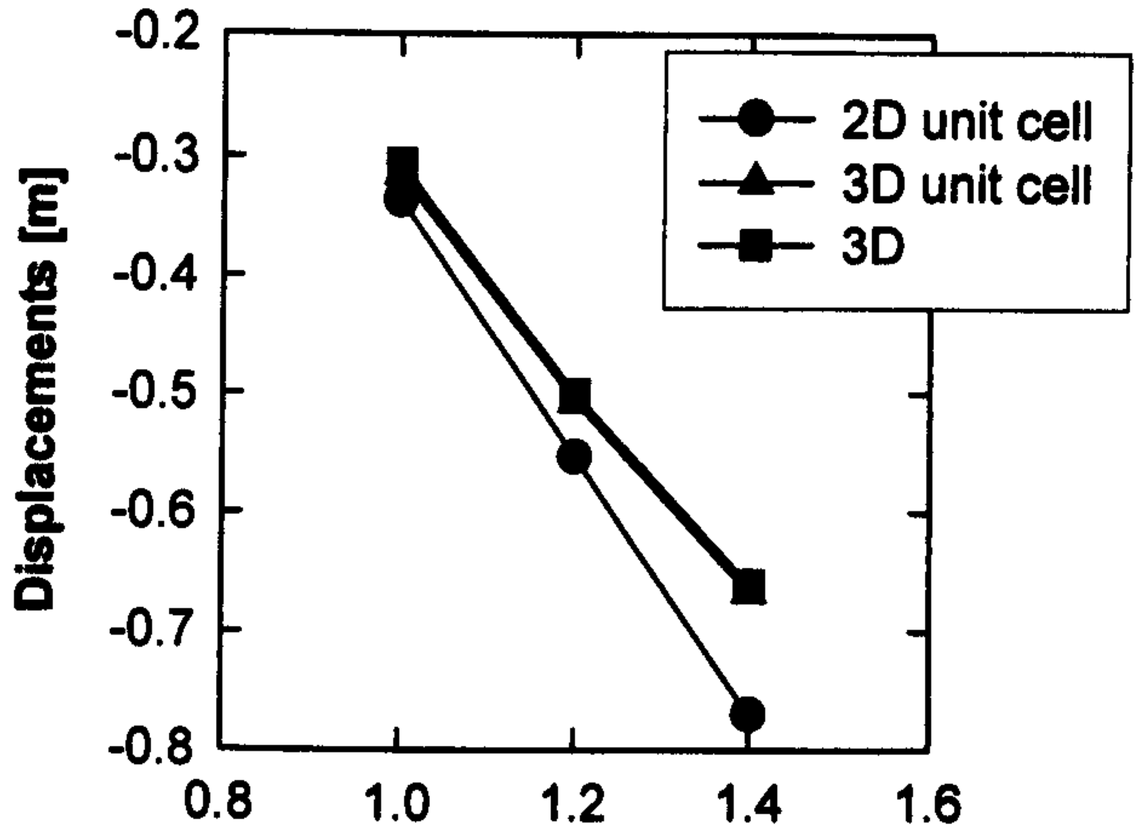

Figure 8.14: Influence of numerical model on settlements of the column at the symmetry line of the embankment

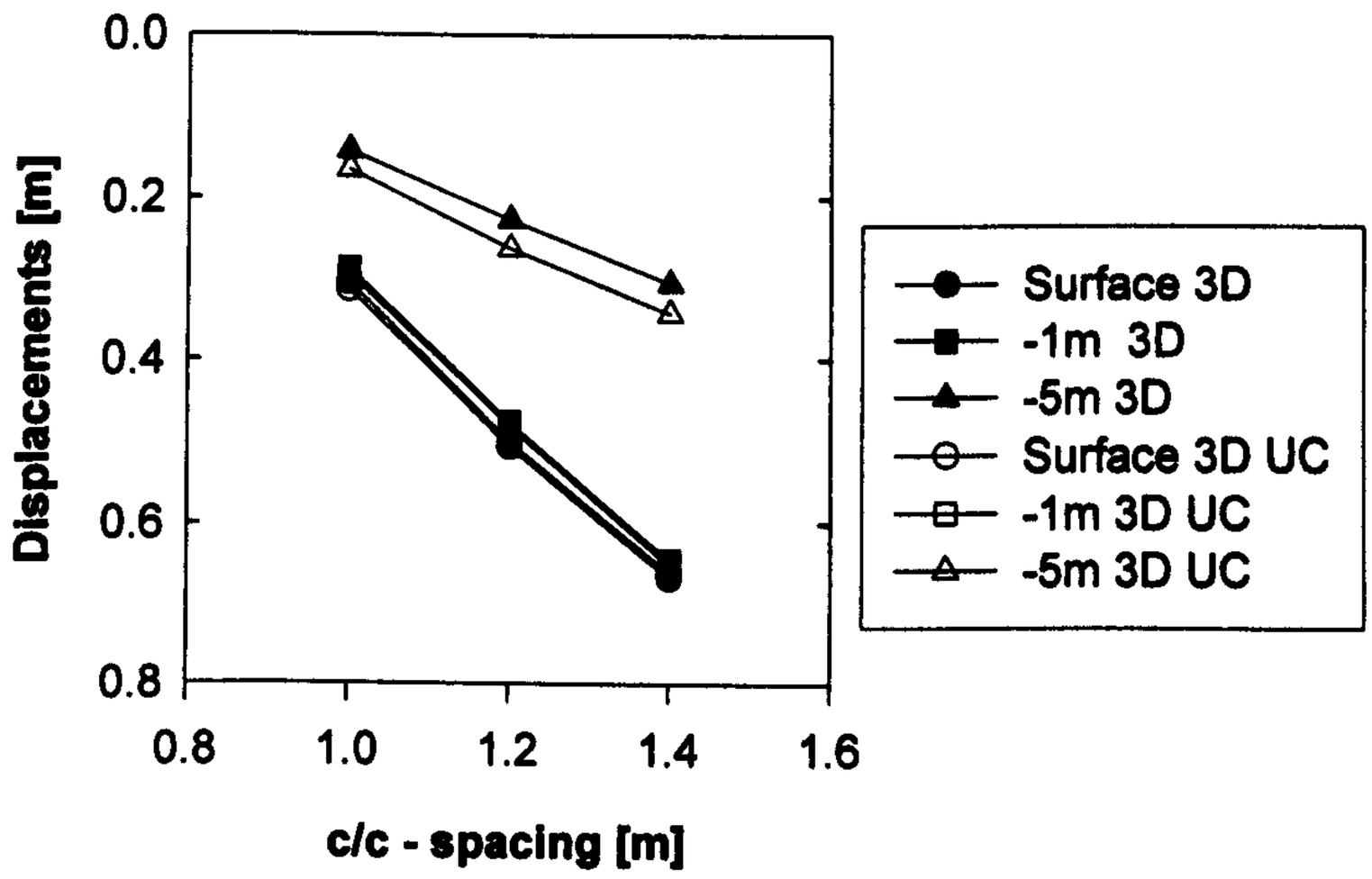

Figure 8.15: Influence of numerical model on settlements at different depths of the column at the symmetry line of the embankment

greater settlements compared to the full 3D analysis. Even at that depth the difference is marginal, in the order of 1 to 2 cm, and negligible for design purposes. If the designer is only interested in the maximum settlements at the centreline of an embankment it could be argued that a unit cell is a simple useful design tool to investigate the settlements along the centreline.

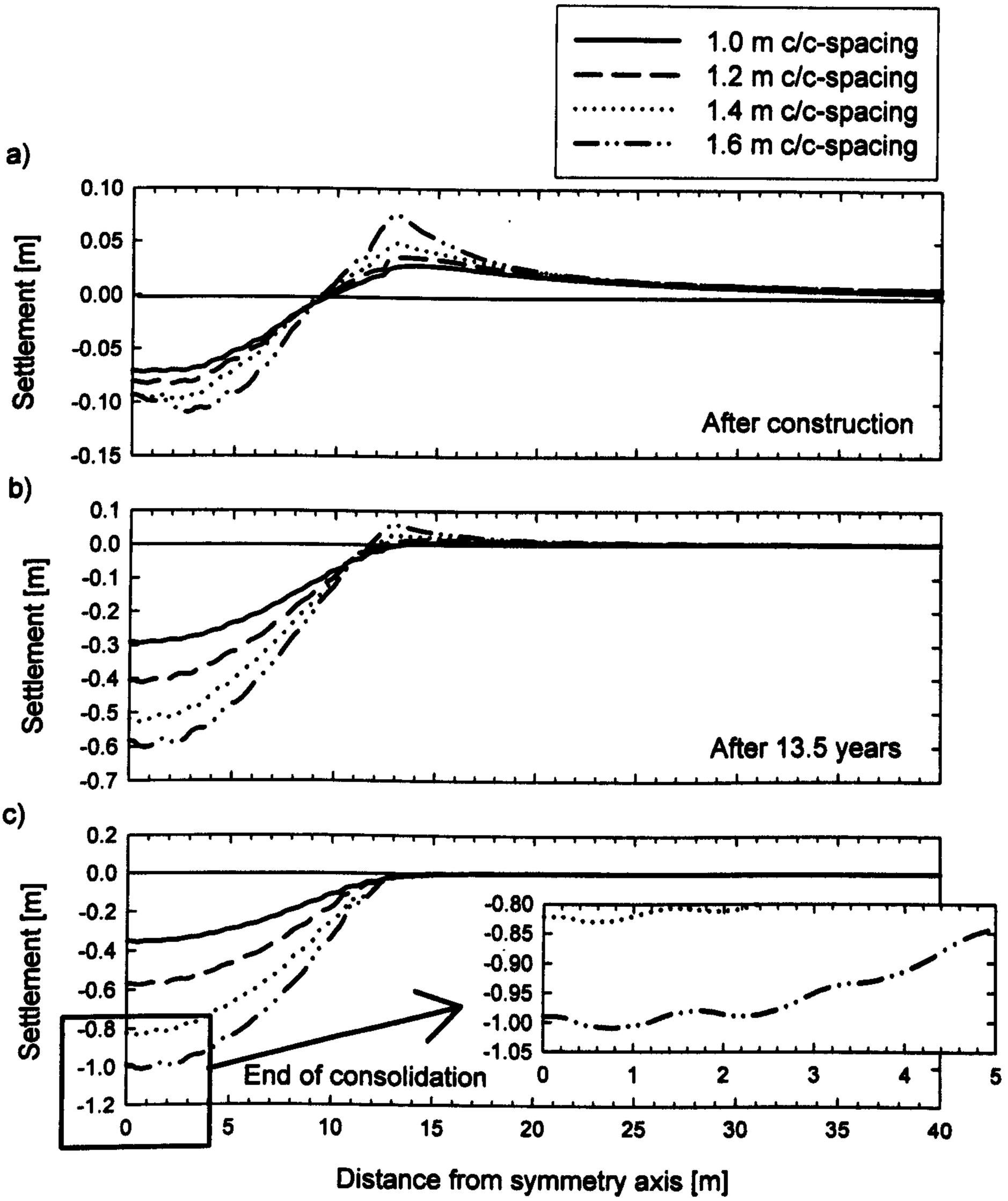

Figure 8.16: Surface settlements: a) after construction b) after 13.5 years and c) end of consolidation

The predicted surface settlement troughs for different construction stages are presented in Figure 8.16. In Figure 8.16a the surface settlements after construction of the embankment are shown. Four different c/c-spacing have been considered in the simulations, 1.0 m, 1.2 m, 1.4 m and 1.6 m. All models predict a surface heave underneath the toe of the embankment. The biggest heave in the order of 0.07 m was predicted by the model with 1.6m c/c-spacing. With decreasing c/c-spacing the heave is decreases to a minimum of about 0.03 m for 1.0 m c/c-spacing. The settlement at the centreline

for 1.0 m c/c-spacing is in the order of -0.07 m. With increasing c/c-spacing the maximum settlement increases. Interestingly, the 1.6 m model does not predict the maximum settlement at the centreline. The maximum is shown at a distance of 2 m from the centreline. Also it can be seen that the models do not predict a smooth settlement line with the distance from the centreline. The settlements decrease stepwise towards the toe of the embankment. The steps are more pronouced for the models with bigger c/c-spacing. Similar behaviour has been predicted 13.5 years after construction (Figure 8.16b). The heave at the toe of the embankment decreases but is still apparent for 1.4 m and 1.6 m c/c-spacing. The 1.0 m model predicts a maximum settlement of about -0.3 m, from -0.07 m after construction. The 1.6 m model shows the biggest increase in settlement from previously -0.12 m to -0.6 m. In Figure 8.16c the settlements at the end of consolidation are shown. The heave below the toe of the embankment is reduced to zero. The maximum settlement at the toe of the embankment is predicted by the 1.6 m c/c-spacing in the order of -1.0 m. Followed by -0.82 m for the 1.4 m c/c-spacing, -0.58 m for -1.2 m c/c-spacing and -0.38 m for 1.0 m c/c-spacing. The 1.0 m c/c-spacing shows a smooth settlement trough below the embankment, whereas the other c/c-spacings show a slight fluctuation in settlements below the embankment. The fluctuation is more pronouced with increasing c/c-spacing. The scaled picture in Figure 8.16c shows the area within 5 m of the symmetry line for the 1.6 m c/c-spacing. Inspection of the scaled picture clearly demonstrates that the columns and the soil do not settle equally. Obviously the assumption of equal strain as assumed in the conventional analysis is not true for bigger c/c-spacings. The difference in the settlements for 1.6 m c/c-spacing is in the order of 2 cm.

8.4.3.1.2 Deformed mesh

The deformed meshes of the models for each c/c-spacing after the end of consolidation are shown in Figure 8.17. In Figure 8.17a the mesh for the 1.0 m c/c-spacing is presented. Inspection of the deformed mesh shows that the columns below the middle of the slope are experiencing the most extensive shearing at a depth of about -1.2 m. With increasing c/c-spacing the shearing of the columns below the slope of the

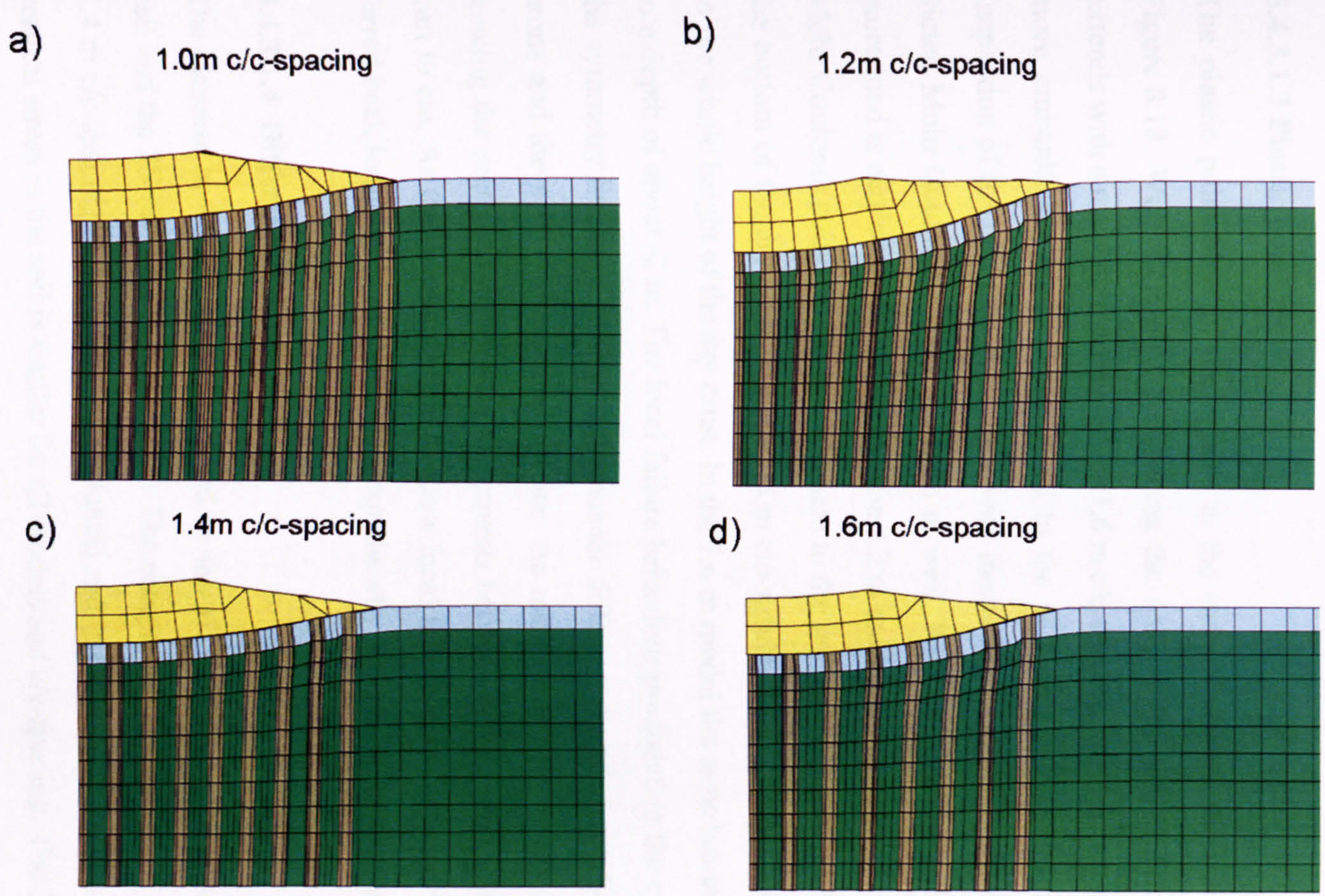

Figure 8.17: Deformed mesh at the end of consolidation: a) 1.0 m, b) 1.2 m and c) 1.4 m and c) 1.6 m c/c-spacing

embankment is more pronouced. The columns are heavily bent over a greater length. Inspection of the plots also demonstrates that the columns next to the symmetry line show some evidence of bulging.

8.4.3.1.3 Plastic point plots

The plastic point plots of the models at the end of consolidation are presented in Figure 8.18. With increasing c/c-spacing the area of the plastic points in the soil extends with a maximum predicted for 1.6 m c/c-spacing. With increasing c/c-spacing more embankment load is transferred to the soft soil next to the improved area. Inspection of the plot also shows that with increasing c/c-spacing the number of predicted Mohr Coulomb points increases as well. With the increase in the c/c-spacing more load is carried by the columns. The 1.2 m model shows only a localised zone of Mohr Coulomb points in the columns next to the symmetry line of the embankment at the bottom of the dry crust. For the 1.4 m c/c-spacing this zone has already extended to the whole height of the dry crust. In the 1.6 m model the zone has extended further to a depth of about -2 m. The local failure behaviour predicted in the columns next to the symmetry line does seem to influence the differential settlements between the columns and the soil at the ground surface. As mentioned before with increasing c/c-spacing the predicted differential settlements between column and soil increase from mm to cm. As the columns begin to show local failure behaviour more load is transferred back to the soil and that might explain why differential settlements occur.

8.4.3.1.4 Differential stresses

The increase in vertical stress predicted by the 3D model is compared to the 3D unit cell and the 2D unit cell in Figure 8.19. The comparison is made for 1.0 m, 1.2 m and 1.4 m c/c-spacing at the centreline (column) and in the soil. The predicted increase in vertical stress in the soil is similar for all models and c/c-spacing. The 3D models also predict a similar increase in vertical stress in the column in the top five meters. Below a depth of 5 m the model shows a slight reduction of the stresses in the column with depth which is not apparent in the 2D and 3D unit cells. The 2D and 3D unit cells

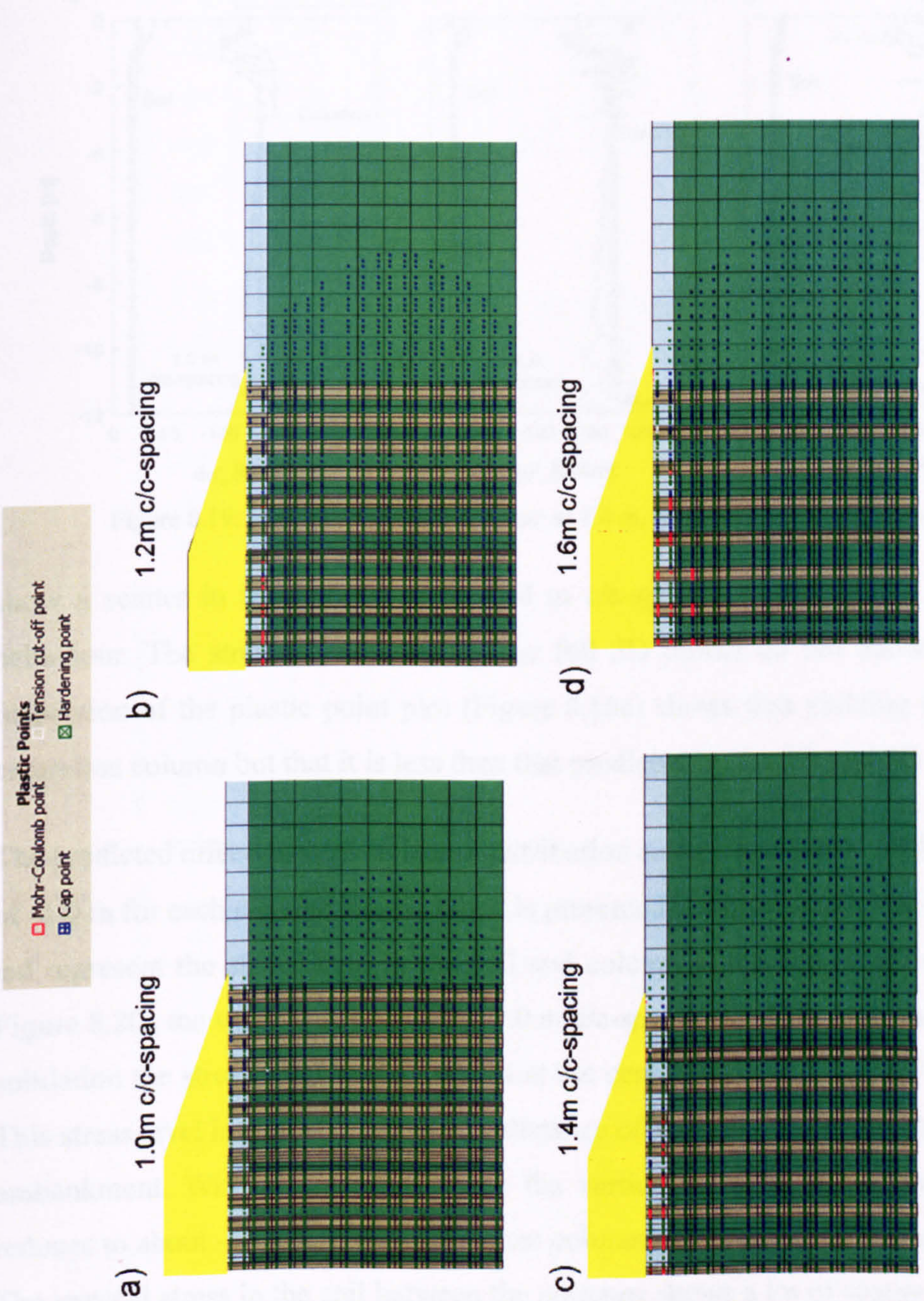

Figure 8.18: Plastic points at the end of consolidation: a) 1.0 m, b) 1.2 m and c) 1.4 m and c) 1.6 m c/c-spacing

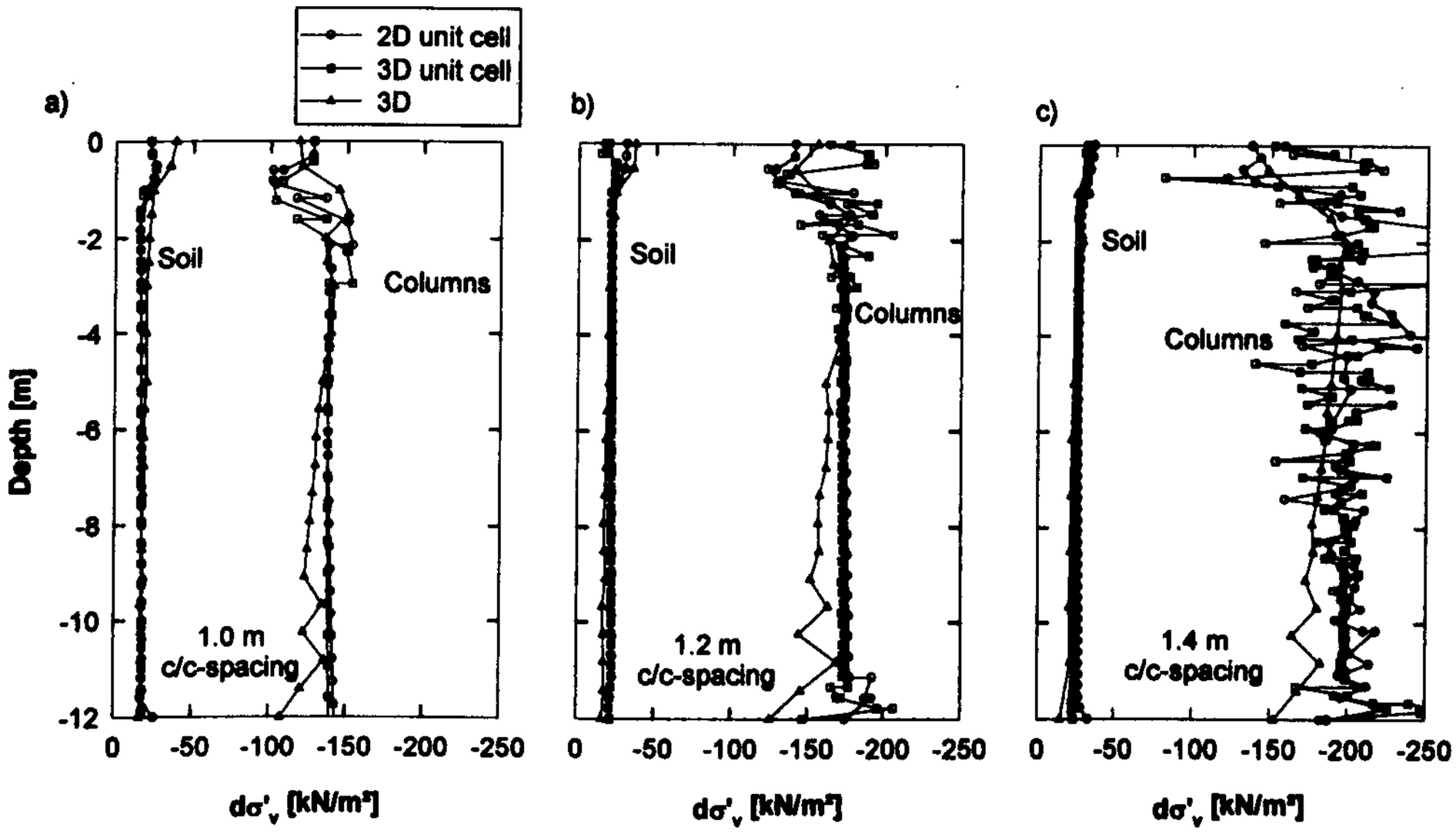

Figure 8.19: Increase in vertical stresses: a) 1.0 m, b) 1.2 m and c) 1.4 m c/c-spacing

show a scatter in the stresses of the 1.4 m c/c-spacing model due to local failure behaviour. The stresses predicted by the full 3D model do not show that scatter. Inspection of the plastic point plot (Figure 8.18c) shows that yielding occurs in the centreline column but that it is less than that predicted by the 2D and 3D unit cell.

The predicted effective vertical stress distribution along a horizontal profile at a depth of -1.0 m for each c/c-spacing modelled is presented in Figure 8.20. The stresses plotted represent the stress level in the soil and column at the end of consolidation. In Figure 8.20a the vertical stress for the 1.0 m c/c-spacing is plotted. At the end of consolidation the stress level in the column at the centreline is in the order of -160 kPa. This stress level is almost constant to a distance of 7 m from the symmetry axis of the embankment. With increasing distance the vertical stress in the column gradually reduces to about -30 kPa in the outer most column below the toe of the embankment. The vertical stress in the soil between the columns shows a lot of scatter due to interpolation errors at Gauss points. However, quantitative interpretation of the stress in the soil shows that the stress is in the order of -25 kPa or less. The ratio between the maximum stress in the column and in the soil is in the order of 6.4 close to the centreline. The column carries about 6.4 times the load of the soil.

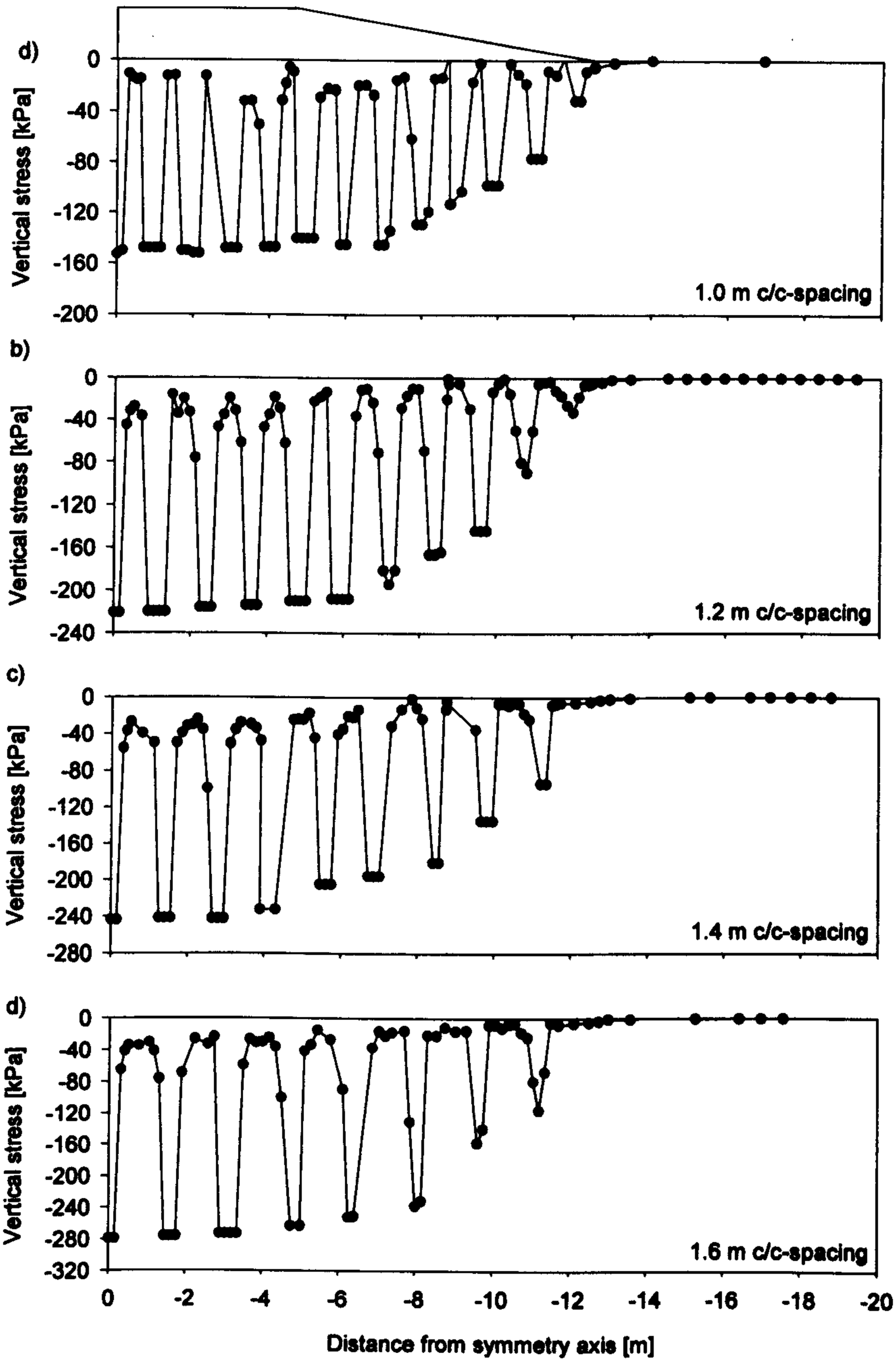

Figure 8.20: Increase in vertical stresses: a) 1.0 m, b) 1.2 m and c) 1.4 m and c) 1.6 m c/c-spacing

In Figure 8.20b the increase in vertical stress for 1.2 m c/c-spacing is shown. The maximum stress in the column at the centreline is -220 kPa. The load in the columns is almost constant to a distance of 7 m from the symmetry axis and thereafter gradually decreases with increasing distance to a minimum of about -35 kPa. The predicted

stress in the soil is in the order of -33 kPa. The ratio between the maximum load in the column and the soil is about 6.6. The maximum stress for the 1.4 m c/c-spacing is in the order of -240 kPa (Figure 8.20c). From a distance of -4 m the stress in the column gradually decreases to a minimum of about -90 kPa. The maximum stress in the soil is predicted close to the centreline in the order of -35 kPa, this results in a load ratio of 6.8.

The predicted vertical stresses for 1.6 m c/c-spacing are presented in Figure 8.20d. The maximum column load is -280 kPa. From a distance of -5 m the load in the columns decrease to a minimum of -116 kPa below the toe of the embankment. The average stress in the soil close to the symmetry line of the embankment is -40 kPa. The resulting load ratio between column and soil is about 7. The results of the simulation show that the load ratio between column and soil increases with increasing c/c-spacing, but within a small range of 6.4 to 7.

8.4.3.2 Summary

A full three dimensional model was developed to investigate the stress strain behaviour of the improved area below the embankment. The model was compared to the 3D and 2D unit cells. It was found that the full 3D model and the 3D unit cell predict similar magnitudes of vertical displacements but both give lower values than the 2D unit cell. All three modelling approaches give quantitatively the same results in terms of the predicted increase in vertical stresses in the soil and in the columns. The 3D and 2D unit cells predict local failure for 1.4 m c/c-spacing which is not observed in the full 3D model.

8.4.4 Floating columns

Floating columns are an alternative solution to end bearing columns which have been considered in the previous simulations. The minimum length of the floating columns can be estimated based on the geometry of the embankment. The length of the column should be equal to the width of the embankment or greater (Broms, 1983). Wehr

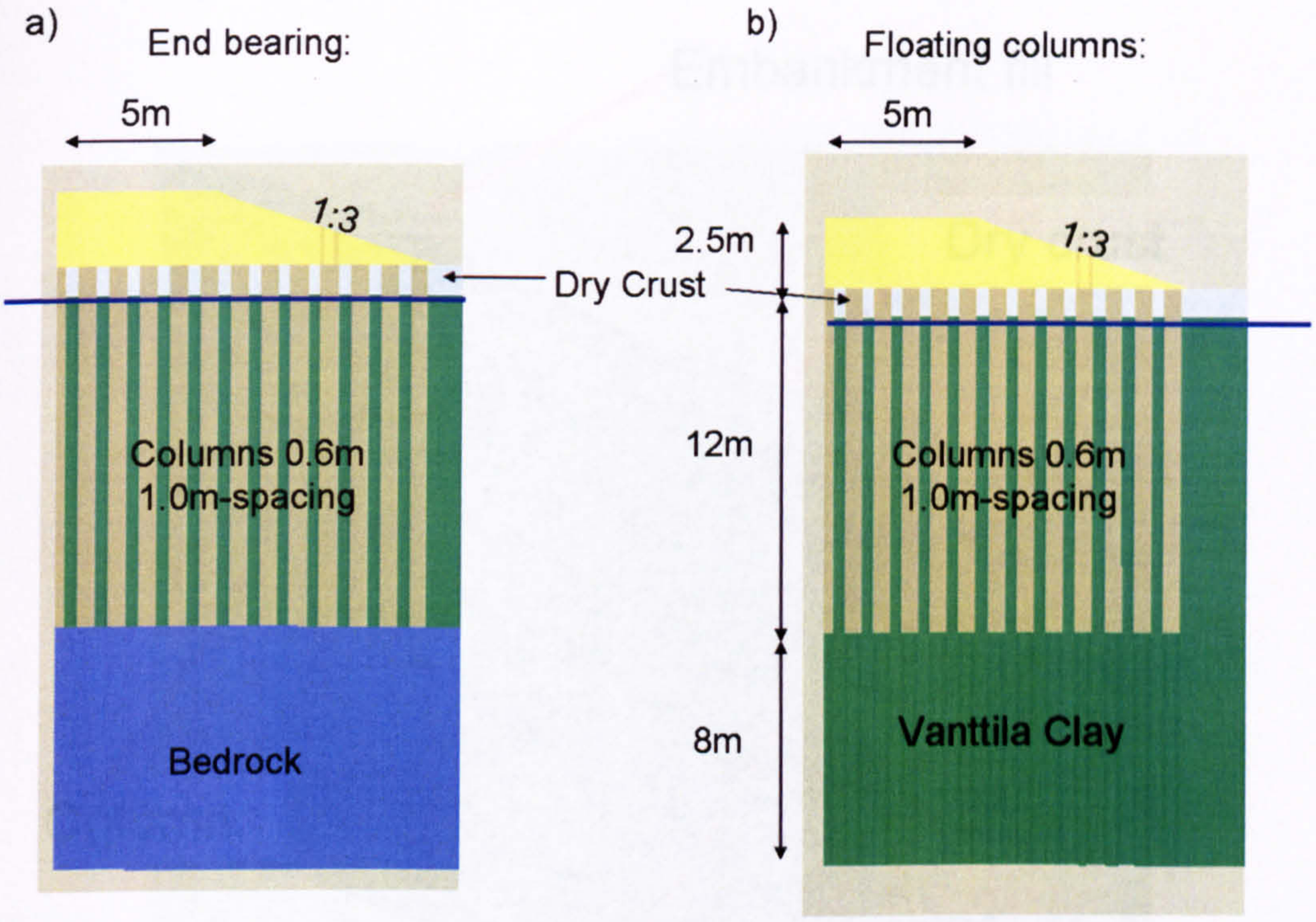

Figure 8.21: Geometry of the embankment and the improved ground

(2007) suggested the length of the floating columns can be shortened to half the width of the embankment. The latter geometry relation was used to determine the length of the columns in the finite element simulations. Two models have been created to allow comparison between an end bearing and floating solution. The geometry of the two models is shown in Figure 8.21. The geometry of the embankment is the same as considered in the previous simulations (Figure 8.1). The end bearing columns are assumed to be founded on bedrock. The length of the columns in both cases is 12 m but the floating columns are founded on Vanttila clay. The c/c-spacing is 1.0 m and the column diameter is 0.6 m. The ground water level is at a depth of -1 m. Due to the symmetry of the embankment only half of the embankment is represented in the finite element mesh. The finite element mesh consisting of about 10000 15 noded wedge elements is shown in Figure 8.22. The boundary conditions, drainage conditions and simulation stages are the same as for the full 3D model presented in Section 8.4.3.

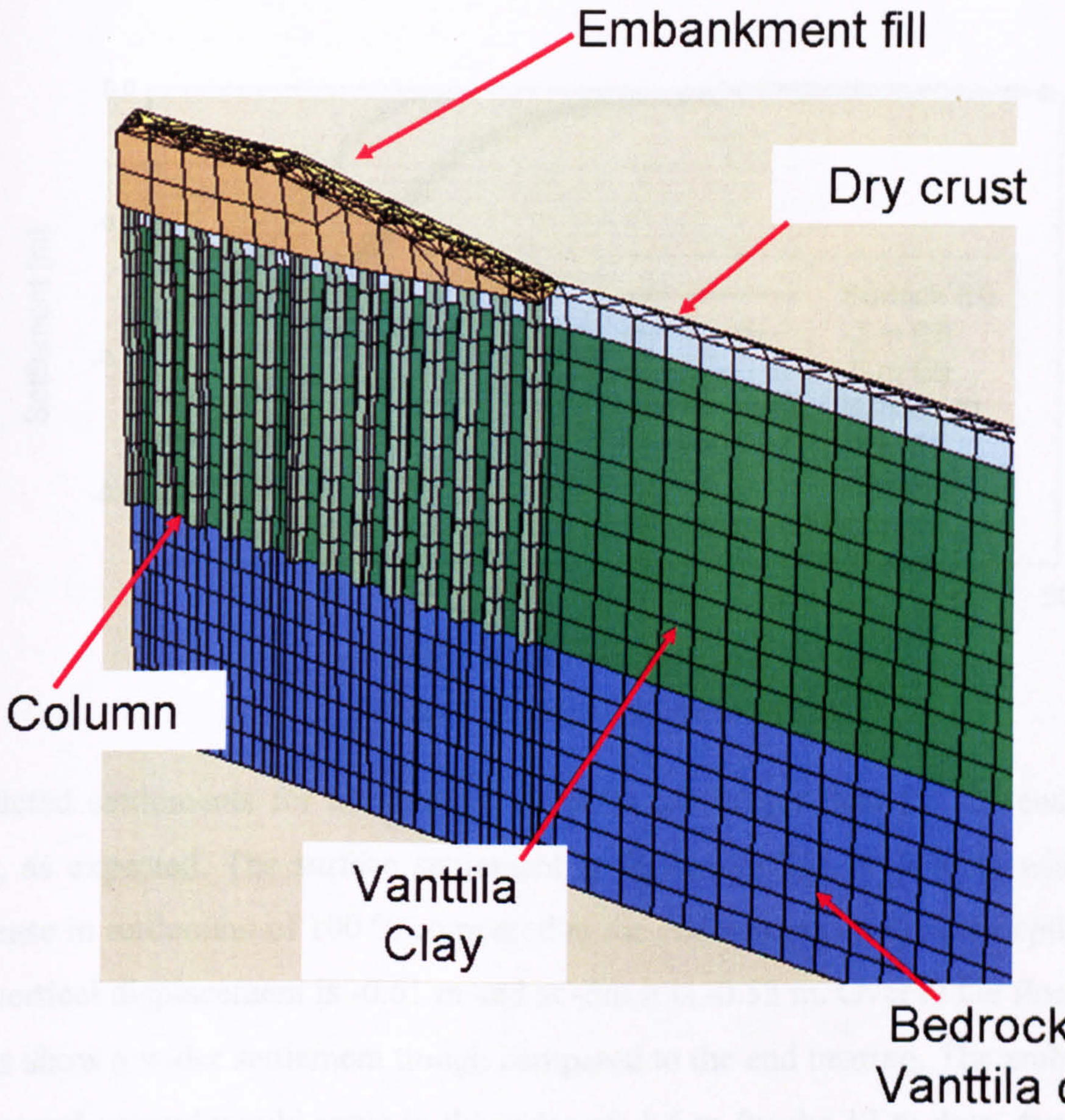

Figure 8.22: Finite element mesh

8.4.4.1 Numerical predictions

The results of the numerical simulations of the two models are discussed in the following.

8.4.4.1.1 Vertical and horizontal displacements

The predicted settlement troughs at different depth at the end of consolidation are shown in Figure 8.23. The maximum surface settlement at the centre line of the embankment is -0.33 m for the end bearing case. At a depth of -0.2 m the predicted maximum vertical displacement is -0.27 m and at a depth of -5 m it is -0.16 m. The

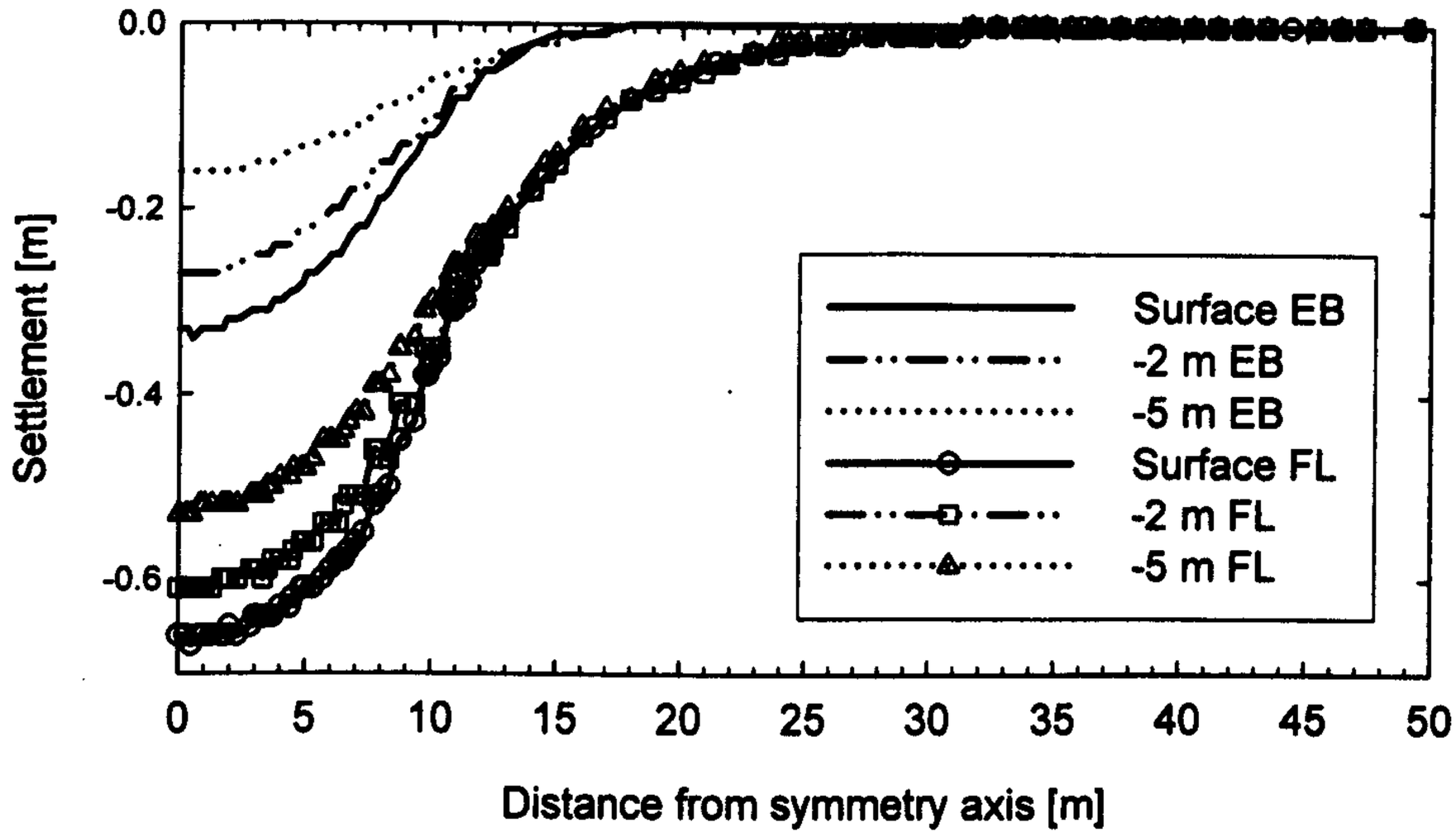

Figure 8.23: Vertical displacements

predicted settlements for the floating columns are bigger than for the end bearing case, as expected. The surface settlement at the centre line is -0.66 m which is an increase in settlement of 100 % compared to the end bearing case. At a depth of -2 m the vertical displacement is -0.61 m and at -5m it is -0.53 m. Overall the floating columns show a wider settlement trough compared to the end bearing. The embankment on natural ground would settle in the order of -1.6 m for the 12 m deep deposit (end bearing) and -1.8 m for the 20 m deep deposit (floating). The end bearing case gives an improvement ratio of 4.8 in terms of settlements and for the floating case a ratio of 2.7. The reduction of settlements calculated in percentage, is 80 % for end bearing and 63 % for floating, respectively.

The calculated horizontal displacements after the undrained construction of the embankment at the centre of each column (except centre line column) are presented in Figure 8.24. At the top of the figure a schematic drawing shows the position of the column below the embankment and its subsequent number. The column number is increasing from the centreline towards the toe of the embankment.

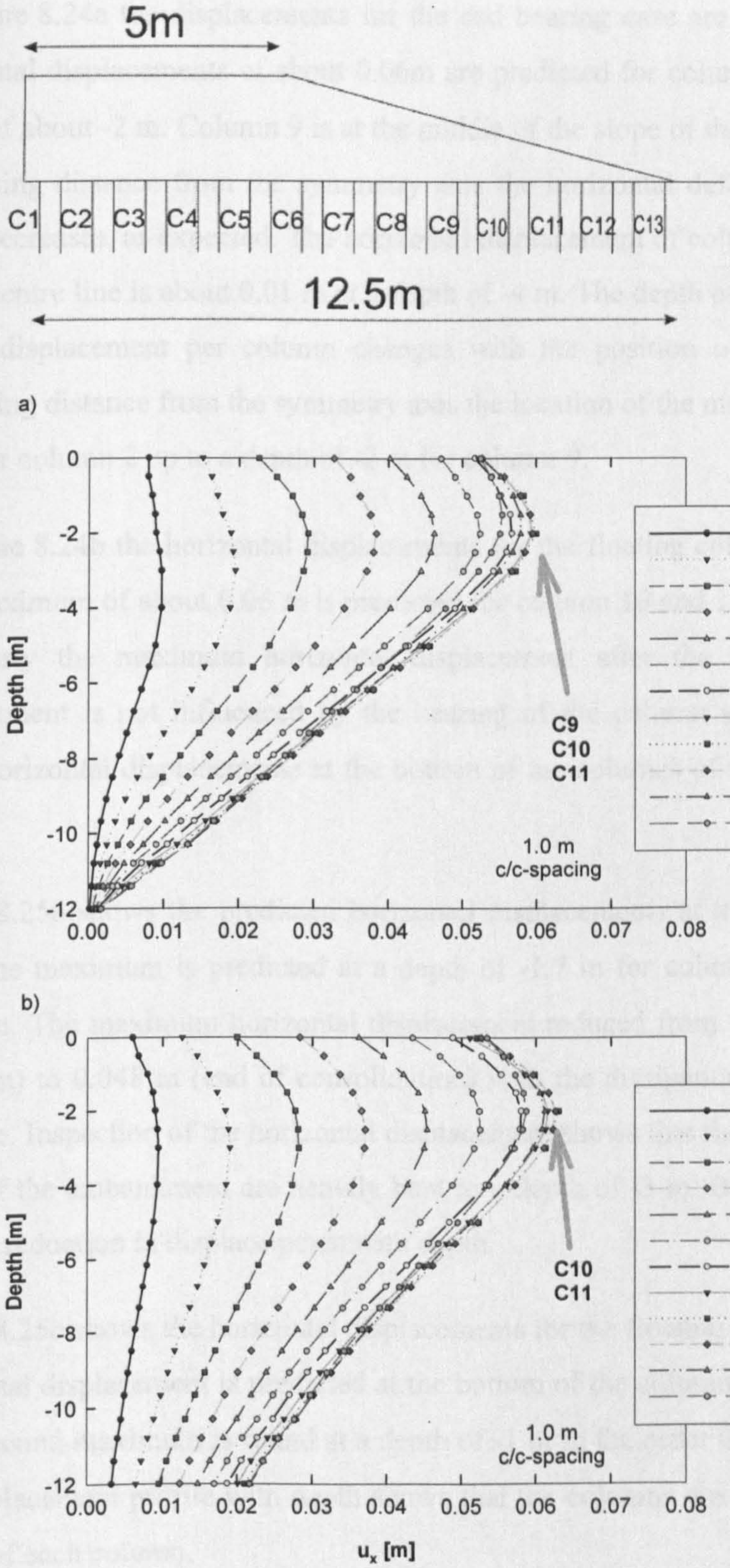

Figure 8.24: Horizontal displacements at the end of construction: a) end bearing and b) floating columns.

In Figure 8.24a the displacements for the end bearing case are shown. The biggest horizontal displacements of about 0.06m are predicted for column 9, 10 and 11 at a depth of about -2 m. Column 9 is at the middle of the slope of the embankment. With decreasing distance from the symmetry axis the horizontal deformation of the columns decreases, as expected. The horizontal displacement of column 2, which is next to the centre line is about 0.01 m at a depth of -4 m. The depth of the maximum horizontal displacement per column changes with the position of the column. With increasing distance from the symmetry axis the location of the maximum moves from -4 m for column 2 up to a depth of -2 m for column 9.

In Figure 8.24b the horizontal displacements for the floating columns are presented. The maximum of about 0.06 m is predicted for column 10 and 11 at a depth of -2 m. Obviously the maximum horizontal displacement after the construction of the embankment is not influenced by the bearing of the column system. All columns show horizontal displacements at the bottom of the columns of the order of 0.5 to 2 cm.

Figure 8.25a shows the predicted horizontal displacements at the end of consolidation. The maximum is predicted at a depth of -1.7 m for column 9 in the order of 0.048 m. The maximum horizontal displacement reduced from 0.06 m (end of construction) to 0.048 m (end of consolidation) with the dissipation of the excess pore pressure. Inspection of the horizontal displacement shows that the columns below the slope of the embankment are heavily bent to a depth of -3 m. Below -3 m there is a smooth reduction in displacements with depth.

Figure 8.25b shows the horizontal displacements for the floating case. The maximum horizontal displacement is predicted at the bottom of the column in the order of 0.06 m. A second maximum is found at a depth of -1 m in the order 0.03 m. The shape of the displacement profile with depth shows that the columns are bent over the whole length of each column.

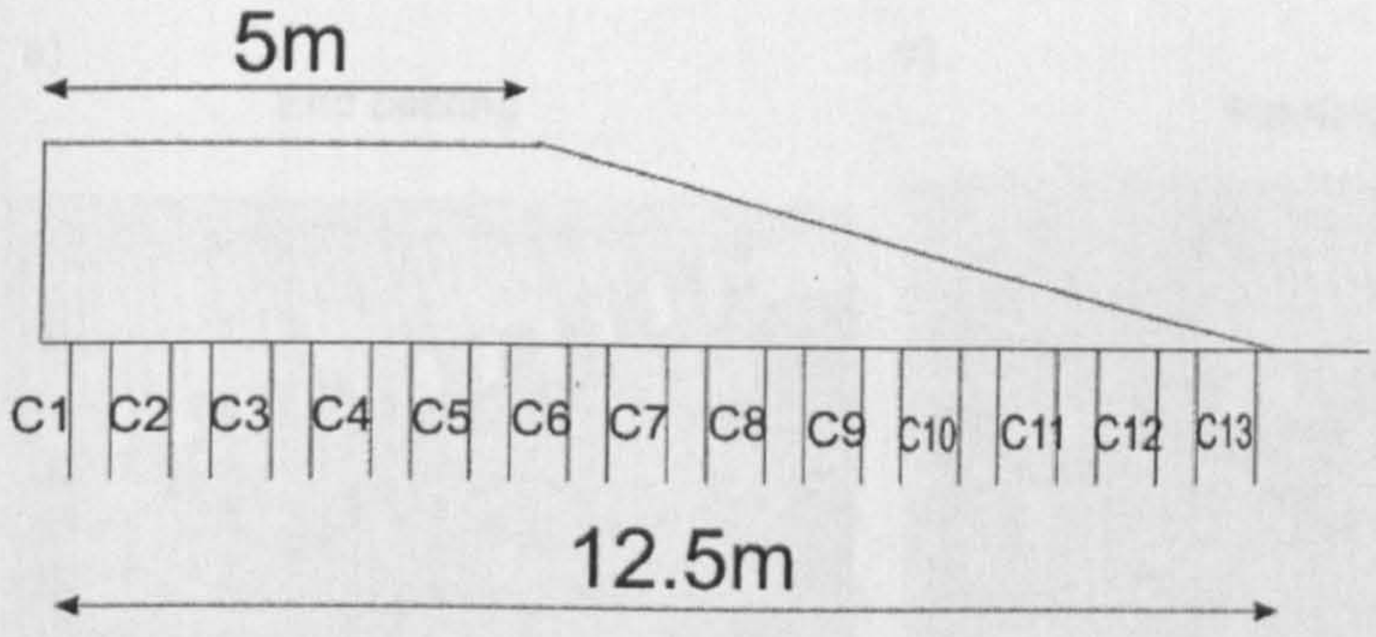

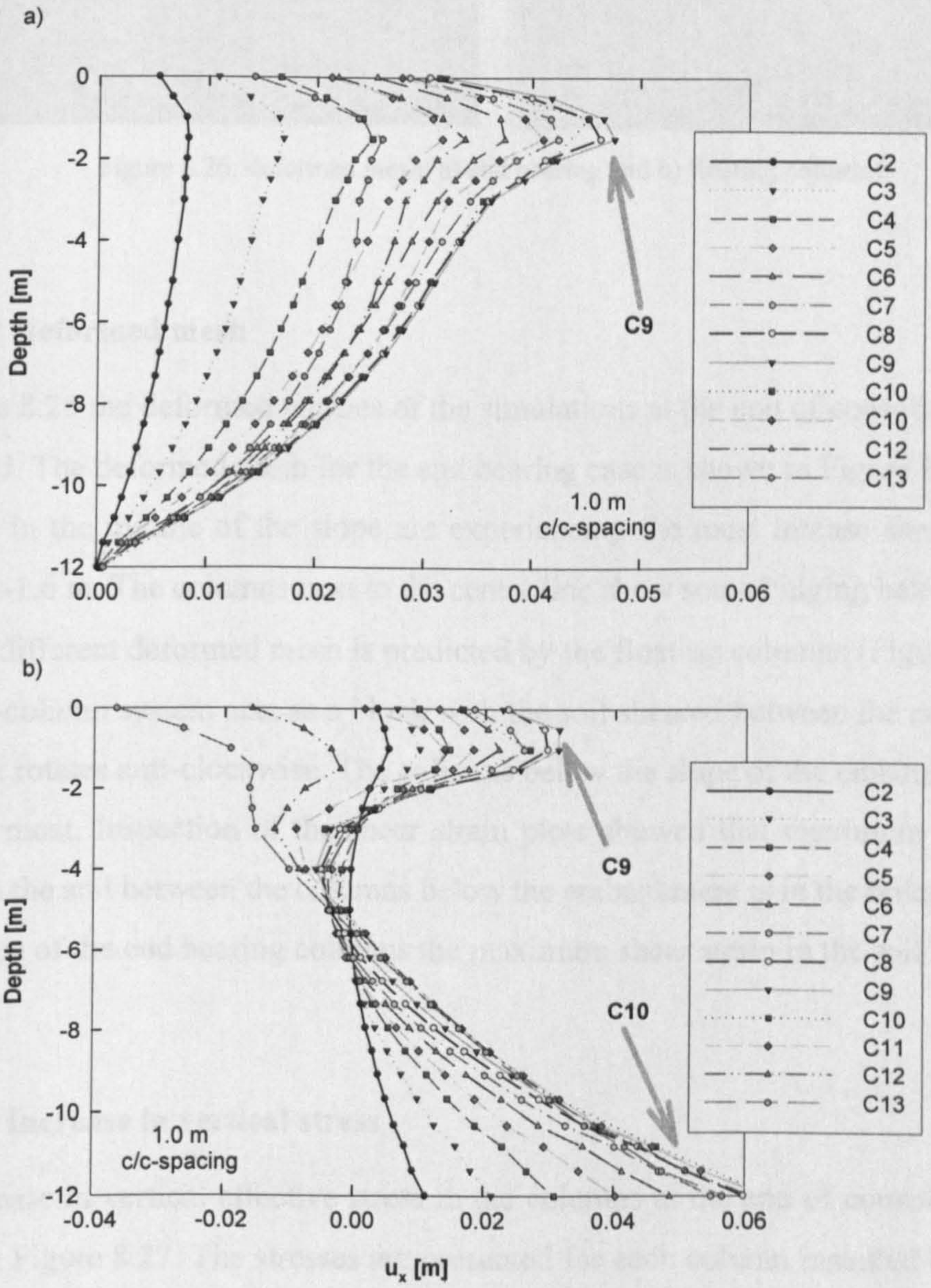

Figure 8.25: Horizontal displacements at the end of consolidation: a) end bearing and b) floating columns.

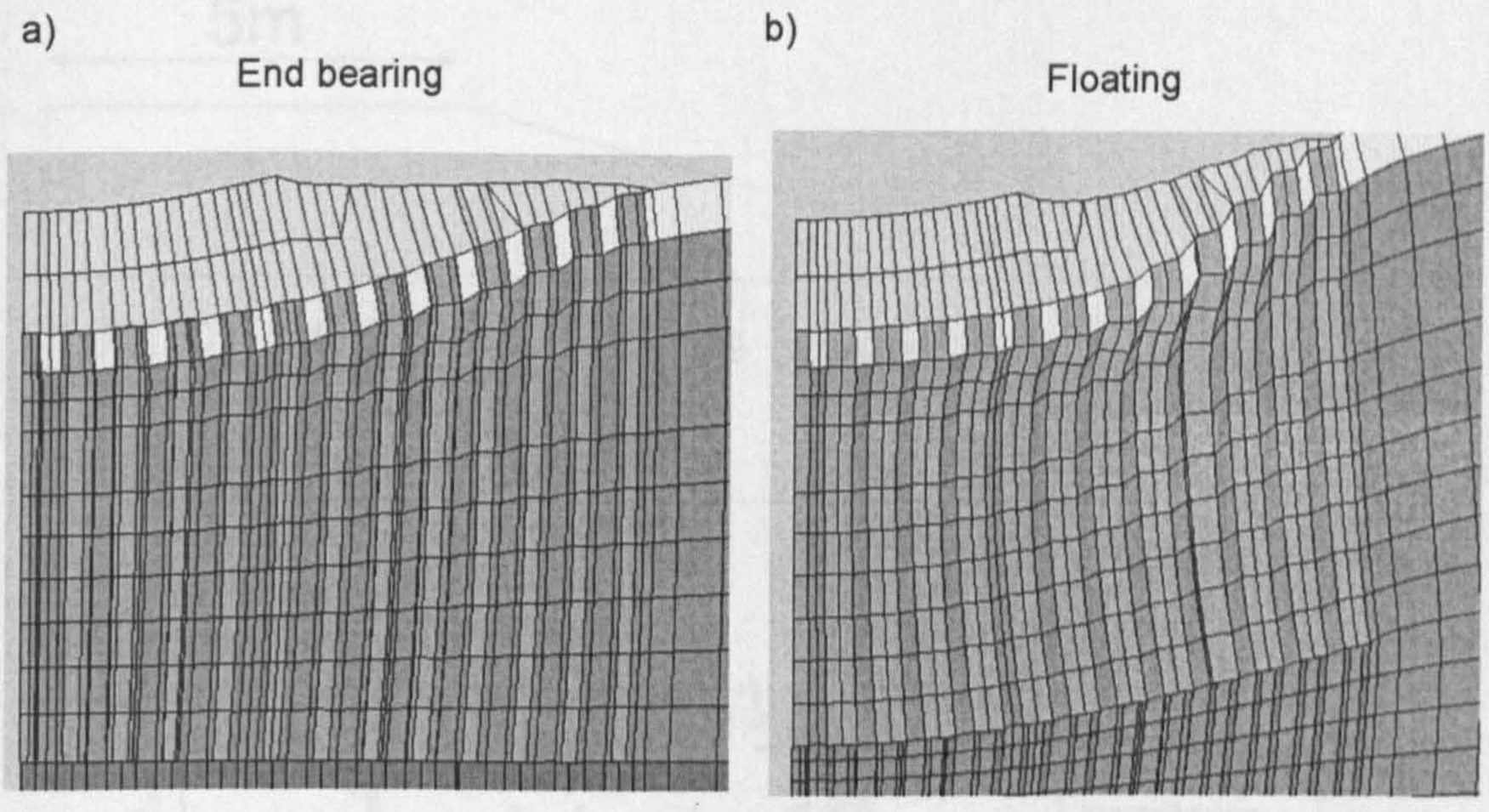

Figure 8.26: deformed mesh: a) end bearing and b) floating columns.

8.4.4.1.2 Deformed mesh

In Figure 8.26 the deformed meshes of the simulations at the end of consolidation are presented. The deformed mesh for the end bearing case is shown in Figure 8.26a. The columns in the middle of the slope are experiencing the most intense shearing at a depth of -1.6 m. The columns next to the centre line show some bulging below the dry crust. A different deformed mesh is predicted by the floating columns (Figure 8.26b). The soil-column system acts as a block with the soil sheared between the columns as the block rotates anti-clockwise. The columns below the slope of the embankment are bent the most. Inspection of the shear strain plots showed that maximum predicted strains in the soil between the columns below the embankment is in the order of 20 %. In the case of the end bearing columns the maximum shear strain in the soil is about 8 %.

8.4.4.1.3 Increase in vertical stress

The increase in vertical effective stress in the columns at the end of consolidation is shown in Figure 8.27. The stresses are presented for each column installed below the embankment. Figure 8.27a shows the stresses for the end bearing case and Figure 8.27b shows the predicted stresses for the floating columns. The maximum

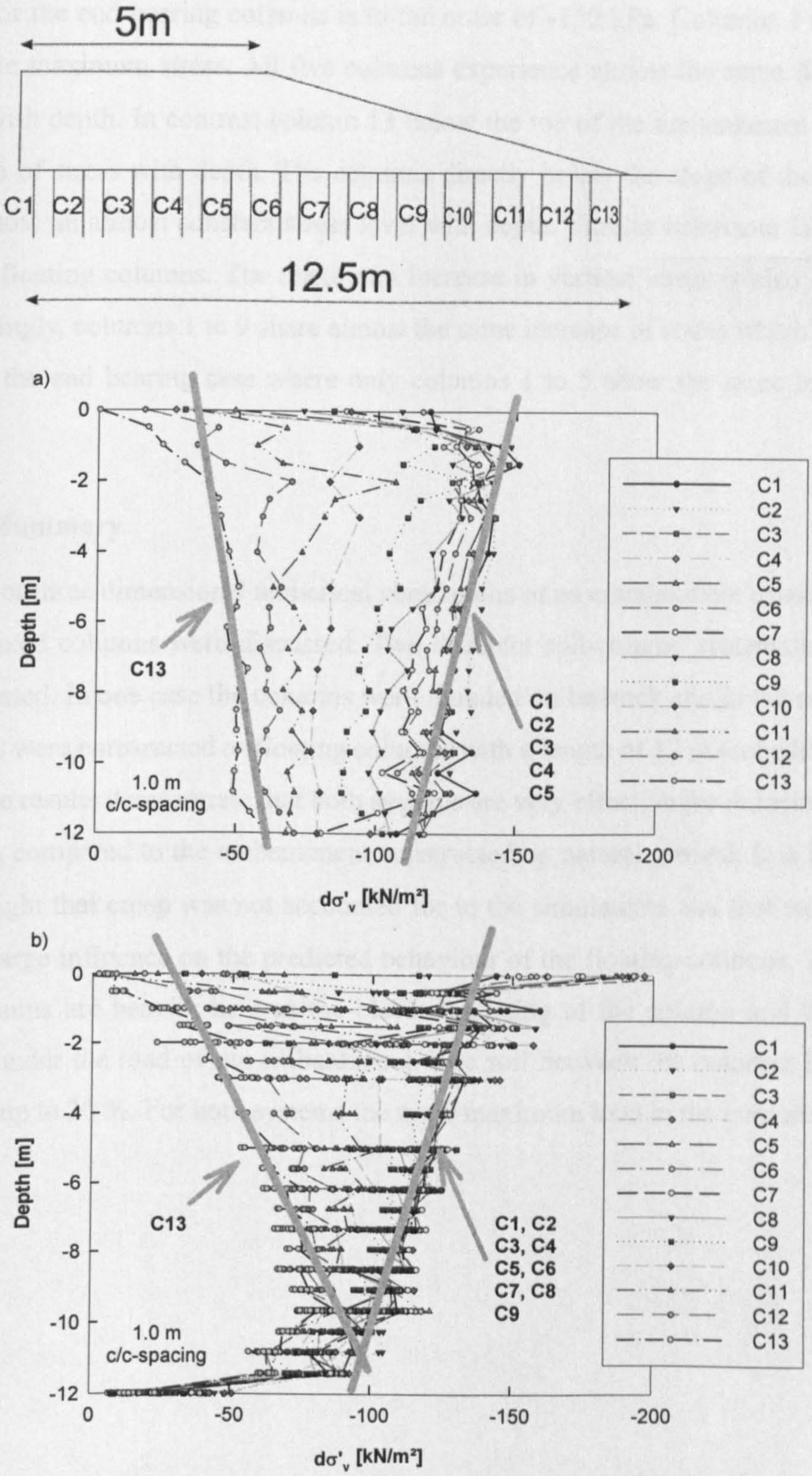

Figure 8.27:Vertical stresses in the columns: a) end bearing and b) floating columns.

stress for the end bearing columns is in the order of -150 kPa. Columns 1 to 5 show the same maximum stress. All five columns experience almost the same decrease in stress with depth. In contrast column 13 below the toe of the embankment shows an increase of stress with depth. The columns directly below the slope of the embankment show an almost constant stress level with depth. Similar behaviour is observed for the floating columns. The maximum increase in vertical stress is also -150 kPa. Interestingly, columns 1 to 9 share almost the same increase of stress which is in contrast to the end bearing case where only columns 1 to 5 show the same increase in stress.

8.4.4.2 Summary

Results of three dimensional numerical simulations of an embankment constructed on deep mixed columns were discussed. Two different soil-column systems have been investigated. In one case the columns were founded on bedrock and in the second the columns were constructed as floating columns with a length of 12 m embedded in soft clay. The results demonstrate that both systems are very effective for reducing the settlements compared to the embankment constructed on natural ground. It is important to highlight that creep was not accounted for in the simulations and that would have had an large influence on the predicted behaviour of the floating columns. The floating columns are heavily bent as the block consisting of the column and the soil is rotated under the load of the embankment. The soil between the columns is heavily sheared up to 20 %. For both systems the same maximum load in the column was predicted.

Chapter 9

Conclusions

The overall aim of this thesis was to investigate the influence of large strain anisotropy and destructuration on the stress-strain-strength behaviour of embankments constructed on either natural soft soils or soils improved with deep mixed columns through the use of advanced constitutive models. The finite element method was utilised to simulate the construction and consolidation of the embankments. At the end of each chapter individual conclusions and recommendations were presented concerning the findings. The most important conclusions are outlined in the following sections, followed by some recommendations for further research.

Chapters 3, 4 and 6 dealt with finite element modelling of embankments on natural soils, and Chapters 7 and 8 with embankments on deep mixed columns.

9.1 Settlements and horizontal displacements of embankments on natural ground

9.1.1 Influence of large strain – small strain analyses

The construction of the embankment is clearly a large strain problem. In the past, back calculation of embankments with isotropic model showed a good match with measured surface settlements. However, those analyses were carried out as small

strain analyses. Large strain analyses demonstrate that in reality it is necessary to account for anisotropy.

9.1.2 Influence of constitutive models on the surface settlements

This work demonstrated the effect of anisotropy and destructuration by simulating the construction and consolidation of an embankment on soft clay using five different constitutive models: the Soft Soil model, the Modified Cam Clay model (MCC), the S-CLAY1 model, the Multilaminate model (MMC) and the S-CLAY1S model. All the model simulations assumed an identical initial state in terms of in-situ stresses, vertical preconsolidation stress and void ratio.

The results showed that accounting for anisotropy and/or destructuration increased the predicted vertical displacements. It was found that anisotropy is more dominant than the combination of anisotropy and destructuration. Comparison of the two anisotropic models showed only that the different approaches of modelling anisotropy results in different settlement predictions. The MMC model based on the multilaminate framework predicts more anisotropic behaviour than the S-CLAY1 model. Both models however predict significantly larger displacements than the isotropic MCC model.

The isotropic Soft Soil model, which is a standard model in the PLAXIS code, gave a range of predictions depending on the shape of the yield surface. The user can control the shape of the yield surface via the input of the K_0^{nc} (normally consolidated earth pressure at rest). The two versions of the Soft Soil models used gave almost the same range in predicted vertical settlements, as the range observed between the isotropic MCC model and the anisotropic models. This suggests that the correct choice of the shape of the yield surface in the Soft Soil model is of paramount importance.

9.1.3 Influence of constitutive models on the horizontal displacements

The horizontal displacements are influenced more by the pre-yield behaviour and the shape of the yield surface than by anisotropy. The horizontal displacements predicted

by the S-CLAY models were almost identical, suggesting that the effect of bonding and destructuration is less marked than anisotropy.

All simulations showed that the maximum horizontal displacements are not below the toe of the embankment as is often incorrectly assumed. The area of maximum displacement is below the slope of the embankment and moves with time, i.e. moves deeper and marginally closer to the centerline with the dissipation of excess pore pressure. Due to practical reasons the inclinometers are often positioned at the toe of the embankment and thus should not be assumed to represent the maximum horizontal displacement. The consequence is that all previous research that aims to provide ranges of u_x/u_y-ratios (e.g. Leroueil et al. 1990) should be treated with caution.

The predicted $u_{x\text{-}toe}/u_y$-ratios decrease with consolidation time. It was found that after 10 to 20 % of the maximum consolidation the ux-toe/uy-ratio has reached its final value. This conclusion is of practical importance for the instrumentation and monitoring of an embankment. It suggests that the horizontal deformations of an embankment need only to be monitored for a certain period of time during the life time of the embankment.

9.1.4 Effect of soil permeability and Poisson's ratio

The change in permeability with compression only marginally influences the predicted time settlement curve. This suggests that for practical applications, where there is an absence of quantitative data about the change in permeability, that this can be ignored, at least for non-organic soils.

A formula was developed to estimate Poisson's ratio based on the stress history of the soil. This formula is very useful for practical applications where no information about Poisson's ratio is available. The formula should be applied with caution for normally and slightly overconsolidated soils (OCR <1.2 - 1.3). Hanzwa and Kishida (1981) showed that creep affects the stress history of the soil and consequently reduces the K_0^{oc} to K_0^{nc}.

9.2 Undrained shear strength

It is important to note that undrained shear strength can not be considered as a soil constant. It has been shown that the undrained shear strength profiles predicted by the different models are dependent on the shape of the yield surface and the chosen state parameters. Consequently different models predict a different distribution of undrained strength for the same value of preconsolidation stress.

The undrained strength predicted over consolidation time is strongly dependent on the model used. It is important that a realistic initial stress state and correct initial state parameters are assumed in order to predict a realistic initial strength profile with depth.

Model simulations of undrained triaxial and plane strain tests in compression and extension using the MCC, S-CLAY1 and S-CLAY1S models demonstrated the influence of anisotropy and destructuration on the maximum undrained strength predicted. The difference in the predictions between the MCC and S-CLAY1 is marginal for the undrained strength in compression. However, the mobilised strength prior to failure is higher for the S-CLAY1 model. In extension the S-CLAY1 predicts a much lower failure strength and ultimate strength than the MCC even though both models assume the stress ratio to be the same in triaxial compression and extension (see Figure 2.13).

Comparing only the S-CLAY1 and S-CLAY1S models showed the importance of accounting for destructuration in the undrained strength predicted in compression. S-CLAY1S predicts a reduction in mobilised undrained strength compared to the S-CLAY1 model. This can be of practical importance when designing staged construction. In extension both models predict the same strength at failure but the ultimate strength at failure predicted by S-CLAY1S is lower than that predicted by the S-CLAY1 model.

9.3 S-CLAY1, S-CLAY1S and S-CLAY2S model

9.3.1 Soil constant μ

The soil constant μ in the S-CLAY models is estimated based on an empirical formula suggested by Zentar et al. (2002). Leoni et al. (in press) suggest that for the Anisotropic Creep model the soil constant ω (equivalent to μ in the S-CLAY models) can be derived by a simple relation between ω and the modified compression index λ* and the stress history of the soil. This idea was used to develop a similar equation for the S-CLAY models.

Model simulations using the S-CLAY1 model suggest that the anisotropy is erased if the soil sample is isotropically loaded to twice its preconsolidation pressure. This is in agreement with findings by Anandrajah et al. (1996) based on laboratory tests on Kaolin clay. Model simulations demonstrate that the rate of rotation of the yield surface in an isotropically loaded test is dependent on the stiffness of the soil. However, for λ greater than 0.2 (as would be typical for most natural soft soils) the influence is marginal.

Values of μ estimated with the new equation are well within the limits suggested by Zentar et al. (2002). It was found that the formula by Leoni et al. (in press) gives lower bound estimates. Model simulations of drained triaxial tests on natural soil samples from the Murro using values of μ estimated from the new equation show a good match with the test results.

9.3.2 S-CLAY2S

A conditional non-associated flow rule has been developed without adding to much complexity and further parameters to the constitutive model. Simulations of drained multistage triaxial tests showed improvement in the predictions of the deviatoric strains ε_q for stress ratios close to hydrostatic axis. Back calculations of the Murro test embankment demonstrate marginal improvement using the S-CLAY2S in terms of predicted horizontal displacement profile.

9.4 Murro test embankment

The predicted long term behaviour of the Murro test embankment was investigated through numerical studies. The results of the finite element simulations were compared with field monitoring results.

9.4.1 Comparison of the numerical predictions to the field measurements

The agreement between the numerical simulations using the advanced constitutive models (S-CLAY1, S-CLAY1S and S-CLAY2S) and the field measurements is very good. These models show a significant improvement compared to the predictions given by the MCC model.

The simulations demonstrated that ignoring anisotropy leads to an under prediction of the measured surface settlements with time. The time settlement curves predicted by the S-CLAY models are in good agreement with the field measurements. However, plotting the time settlement curve in a logarithmic scale suggests that secondary compression contributes to the ongoing settlements. Incorporating creep in the constitutive models would improve the time settlement predictions in the long term. The horizontal displacements were better predicted by the advanced models than by the MCC. The newly implemented conditional non-associated flow rule of the S-CLAY2S model further enhanced the predictions of the horizontal displacements.

9.4.2 Undrained shear strength at Murro

The in-situ testing at Murro in 2001 included field vane tests throughout the embankment to assess the increase of undrained strength caused by 8 years of consolidation. The results showed that in the top 7 m there had been an increase in the undrained strength, but below a depth of 7 m, the measured strength decreased. This occurred in conjunction with a significant increase in remoulded strength. Obviously this is an indication of the gradual degradation of the bonds due to plastic straining.

With a constitutive model that accounts for destructuration, such as the S-CLAY1S and S-CLAY2S, this phenomenon can be simulated. If the assumed rate of destructuration is high, it is possible that the bonds are degrading at a higher rate than the intrinsic yield surface is expanding. As a result it is expected that the undrained shear strength would decrease with consolidation.

Simulations with the S-CLAY1S showed that it is quantitatively possible to simulate this behaviour. By changing the values for key model parameters (parameters a and b, see Chapter 2.5.1) in the S-CLAY1S model the increase of undrained strength with time is slowed down. In some areas under the centreline of the embankment the undrained shear strength was even found to decrease, similar to the field measurements. In nature it is expected that the rate of destructuration will eventually slow down with consolidation time and there will be eventually an apparent increase in the undrained strength. However, it was not possible to simulate this with the S-CLAY1S model and the set of soil parameters used.

The influence of the change of the geometry of the Murro test embankment and the undrained shear strength with time on the Factor of Safety (FoS) was investigated. The increase in undrained strength with time increased the FoS from initial value of 2.14 to 2.96. Accounting for the change in geometry and undrained strength increases the FoS from 2.14 to 4.88. This finding is of practical importance for assessing the FoS for embankments constructed on soft soils. It implies that the change in geometry and undrained strength with time must be related to the assessment of FoS with time. This is particularly relevant when re-using old embankment or extending existing embankments.

9.5 Embankments on deep mixed columns

The behaviour of embankments constructed on deep mixed columns was examined through numerical studies. In the absence of detailed field studies, numerical studies offer an alternative way of investigating the complex interaction between the soft soil and the deep mixed column. The major advantage of numerical modelling is that the

complex stress-strain-strength behaviour of both materials can be taken into account by advanced constitutive modelling.

9.5.1 Deep mixed Vanttila clay

The stress-strain behaviour of deep mixed Vanttila clay is non-linear and most of the strains are irreversible. Model simulations of laboratory tests on deep mixed Vanttila clay demonstrated that the Hardening Soil model (a standard model in the PLAXIS code) which accounts for stress dependency via a hyperbolic stress-strain relationship gives a good representation of the observed behaviour.

9.5.2 Axisymmetric unit cell

With an axisymmetric unit cell a single column and the surrounding soil under the embankment fill is modelled. The model is a very crude representation of a column installed in a square pattern at the centreline of an embankment.

Surface settlements predicted utilising an axisymmetric unit cell, using the MCC, S-CLAY1 and S-CLAY1S models to represent the stress-strain behaviour of the soft soil, demonstrate that it is important to account for anisotropy. However, the effect of bonding and destructuration appear to be less important.

All three models predicted quantitatively the same increase in vertical stress in the soil and column due to the embankment load. This suggests that anisotropy and destructuration do not influence the load transfer from the embankment to the column and soil.

9.5.3 3D unit cell (true unit cell)

In a 3D unit cell a single column and the surrounding soil are modelled. A major advantage of the 3D unit cell compared to the 2D unit cell is the fact that it is more flexible than a 2D model with regards to the geometry considered. The 2D model is restricted to constant c/c-spacing (the same spacing in the x and y directions) whereas with a 3D model any spacing in the x and y directions can be simulated.

Simulations using a 3D unit cell systematically predicted slightly lower settlements than the 2D unit cell. One possible reason for this is the different discretisation in the 2D and 3D unit cell. Also the shape of the finite elements and the shape functions of the elements contribute to the predicted difference.

9.5.4 Full 3D model

Comparison of the surface settlements at the centreline of the embankment predicted by the full 3D model and the 3D unit cell are in good agreement. The predictions by the unit cell suggest that the differential settlements between the column and soil are negligible. In contrast the full 3D model shows that with increasing column spacing the differential settlements at the surface are in the order of 1 to 2 cm. This suggests that the assumption of equal strain, as adopted in the conventional design, is only appropriate for small c/c-spacings and that the lateral deformations cannot be ignored.

The load transfer from the embankment to the column and the soil is dependent on the apparent stiffness ratio between the column and the soil due to the effect of arching. With increasing c/c-spacing more load is transferred to the columns and local failure was predicted in the columns. With increasing c/c-spacing the zone of local failure observed in the columns expanded, downwards and widthways.

Whilst 3D simulations are ideal for research purposes, they much more complex and time consuming than a 2D analysis. For practical applications it is recommended to undertake parametric studies on c/c-spacing, soil parameters and column parameters with a 2D unit cell and once the design is in a more advanced stage embark on a full 3D analysis. An alternative approach is the application of the volume averaging technique (Vogler, 2008). The volume averaging technique is less complex to set up and less time consuming in terms of simulation run time.

9.5.5 Floating columns

Floating columns are not embedded in a competent strata and as such do not transfer the load in terms of end bearing. However, 3D simulations of floating columns sug-

gest that floating columns are a suitable alternative solution for the settlement reduction of embankments constructed on deep mixed columns. The simulations carried out demonstrated that the soil and columns act as a block. The block is rotated outwards towards the toe due to the embankment load.

9.6 Recommendations for further research

Following the research presented in this thesis, the following areas outlined are recommended for further research.

9.6.1 Embankments on natural ground

Accounting for creep in the simulations of the Murro test embankment would potentially improve the long term predictions. The increase of undrained strength with time should be studied with a constitutive model which accounts for creep. Implementation of a non-associated flow rule into the S-CLAY1S model, with plastic potential of a different shape could improve the predictions of the horizontal displacements. The interaction between the embankment fill and the dry crust at the interface needs to be explored. The application of interface elements should be considered.

9.6.2 Embankments on deep mixed columns

Further 3D simulations are needed to demonstrate the behaviour of the soil-column interaction under working and ultimate load conditions. More parametric studies on the column material should be performed to investigate the influence of column stiffness and homogeneity on the settlement behaviour. So far creep has not been accounted in the simulations. Model simulations accounting for creep in addition to anisotropy and destructuration are recommended. More work is needed to understand the soil – column interface and the smear zone between the soil and the column. The possible application of an interface between the column and the soil should be considered in a 3D analysis.

References

Aalto, A. (2003) Full scale test in the field using dry mixing method. In: Proc. International Workshop on Geotechnics of Soft Soils - Theory and Practice, Noordwijkerhout, The Netherlands, VGE, Essen, Germany

Aalto, A., Kinani, K., Lojander, M., Vepsäläinen, P. and Tolla, P. (1999). Soil parameters and embankment modelling. In: Proc. Civil and Engineering Conference.

Adachi, T. and Okano, M. (1974). A constitutive equation for normally consolidated clay. Soils and Foundations, 14(4), p 55-73

Ahnberg, H. (1996). Stress dependent parameters of cement stabilised soil. In: Proc. 2nd international Conference on Ground Improvement Geosystems, IS-Tokya '96, Vol. 1, p 387 - 392

Alamgir, M., Miura, N., Poorooshab, H. B. & Madhav, M. R. (1996). Deformation analysis of soft ground reinforced by columnar inclusions. *Computers and Geotechnics*, Vol. 18, No. 4, 267-290.

Alen, C., Baker, C., Bengtsson, P-E. and Sällfors, G. (2005). Test Embankments on Lime/Cement Stabilized Clay. Proc. International conference on deep mixing'05, Stockholm, Vol. 1.2, p 213 - 220

Al-Tabaa, 2003. Soil mixing in the UK 1991- 2001: state of practice report. Journal of Ground Improvement, Thomas Telford, Vol. 7, No. 3, pp 117-126.

Anandarajah, A., Kuganenthira, N. and Zhao, D. (1996). Variation of Fabric Anisotropy of Kaolinite in Triaxial Loading. Journal for Geotechnical Engineering, Vol. 122, No. 8, p 633 - 640

Azizi, F. (1999). Applied Analysis in Geotechnics. London: E & FN Spon, ISBN: 0 419 25340 8

Baker, S. (2000). Deformation Behaviour of Lime/Cement Column Stabilized Clay, PhD Thesis, Report 7, Swedish Deep Stabilization Research Centre

Balasubramaniam, A.S., Buessuesco, B., Oh, E.Y.N., Bolton, M., Bergado, D.T. and Lorenzo, G.A. (2005). Strength degradation and critical state seeking behaviour of lime treated soft clay., Proc. International conference on deep mixing'05, Stockholm, Vol. 1.1, p 35 - 40

Bathe, K.J. (1982). Finite element analysis in engineering analysis. Prentice Hall, new Jersey

Banerjee, P.K. and Yousif, N.B (1986). A plasticity model for mechanical behaviour of anisotropically consolidated clay. Int. J. Numerical and Analytical Methods in Geomechanics, Vol. 10, p 521-541

Bauduin, C.M., De VOs, M. and Vermeer, P.A. (1999). Back analysis of staged embankment failure: The case study Streefkerk. In: Beyond 2000 in Computational Geotechnics - 10 Years of PLAXIS International © 1999 Balkema, Rotterdam, ISBN 90 5809 040

Baudet, B.A. and Stallebrass, S.E. (2004). A constitutive model for structured clay.s Geotechnique, v 54, n 4, p 269-278

Benz, T. (2006). Small strain stiffness of soil and its numerical consequences. PhD-Thesis, University of Stuttgart, Germany.

Bergado, D.T., Ruenkrairergsie, Taesiri, and Balasubramiam, A.S. (1999). Deep soil mixing used to reduce embankment settlements. Ground Improvement, Vol. 3. P 145 - 162

Bjerrum, J. (1967). Engineering geology of norwegian normally-consolidated clays as related to settlements of buildings. 7th Rankine Lecture. Geotechnique, Vol. 17, p 81-118

Borel. (2007). Presentation on Workshop on Ground improvement. BGA meeting, London, November 2007

Brinkgreve, R.B.J. (1994). Geomaterial models and numerical analysis of softening. Doctoral Dissertation, Delft University of Technology, 1994

Brinkgreve, R.B.J. (2002). PLAXIS Finite Element Code for Soil and Rock Analyses, 2D-Version 8. Balkema: Rotterdam

Broms, B.B. and Boman, P. (1977) Stabilisation of soil with lime columns., Ground Engineering, Vol. 12, No. 4, p 23-32

Broms, B.B. and Anttikoski, U. (1983). Soil Stabilisation., In: Proc. 8th European Conference on Soil Mechanics and Foundation Engineering. Helsinki. Vol. 3, p 933

Broms, B. (1999). Design of lime, lime/cement and cement columns. Dry Mix Methods for Deep Soil Stabilization, Holm & Broms (eds) 1999. Balkema: Rotterdam

Broms, B.B. (2004). Lime and Lime/Cement columns. Ground improvement., Spon Press, New York 2004, 2nd Edition, Chapter 8, p 254 - 330

Burland, J.B. (1990). On the compressibility and shear strength of natural clays. Geotechnique 40, No. 3, p 327-370

Carlsten, P. and Ekström, J. (1995). Kalk- och kalkcementpelare. Vägledning för projektering, utförande och kontroll, Swedish Geotechnical Society, SGF Report 4:95, Lingköping , (In Swedish).

CDIT (2003). The deep mixing method. Principal, design and construction. Coastal Development Institute of Technology. Japanese Guideline of Deep Mixing.

Chai, J.C and Bergado, D.T. (1993). Some techiques for finite element analysis of embankments on soft ground. Canadian Geotechnical Journal, Vol. 30, p 710-719

Chambon, R. (1994). Large strain computation with an incremental non-linear model. ALERT summer school 1994

Ciuhak, K. Lojander, M. and Vepsalainen, P. (2003). Constitutive modelling of deep-stabilised clay. In: Proc. International Workshop on Geotechnics of Soft Soils - Theory and Practice, Noordwijkerhout, The Netherlands, VGE, Essen, Germany, 381-390

Crawford, C.B., Fannin, R.S. and Kern, C.B. (1995). Embankment failures at Vernon, British Columbia., Canadian Geotechnical Journal, Vol. 32, No. 2, p 271 - 284

Cudny, M. and Neher, H.P. (2003). Numerical analysis of an embankment on soft grounds using an anisotropic model with destructuration., In: Geotechnics of soft soils, theory and practice. Edited by Vermeer, Schweiger, Karstunen and Cudny. Noordwijkerhout (NL),

Davies, E.H. and Poulous, H.G. (1975). Predicted and measured behaviour of an embankment on Boston blue clay. Australian Geomechanics Journal. p 1 - 9

Dafalias, Y.F. (1986). An anisotropic critical state soil plasticity model. Mechanics Research Communications 1986, 13(6), p 341-347

Dafalias, Y.F. (1987). An anisotropic critical state clay plasticity model. In: Constitutive Laws for Engineering Materials: Theory and Applications, Proc. of 2nd IC, Vol. I, Desai CS et al (eds.) Elsevier: New York, 1987, p 513-521

Dafalias, Y.F., Manzari, M.T. and Papadimitriou, G. (2006). SANICLAY: simple anisotropic clays plasticity model, Int. Journal for Numer. Anal. Meth. in Geomech., 30, p 1231-1257

Davies, M.C.R. and Newson, T.A.A. (1993). Critical state constitutive model for anisotropic soils. In: Houlsby & Schofield (eds.), Proc. Predictive soil mechanics, Oxford, UK. London: Telford, p 219-229

Diaz-Rodriguez, J.A., Leroueil, S. and Aleman, J.D. (1992). Yielding of Mexico City Clay and other natural clays. ASCE Journal of Geotechnical Engineering, 118, No. 7, p 981-995

Di Prisco, C., Nova, R. and Lanier, J. (1993). A mixed isotropic-kinematic hardening constitutive law for sand. In: Modern Approaches to Plasticity, Kolymbas D (eds.). Elsevier: Amsterdam, 1993, p 83-124

EuroSoilStab. (2002) Development of design and construction methods to stabilise soft organic soils. Design guide soft soil stabilisation. CT97-0352. Projet No. BE-96-3177. European Commission. Industrial & Materials Technologies Programme (Brite-EU-Ram III)

FHA 2000. (2000). An introduction to deep soil mixing as used in geotechnical applications. Publication No.: FHWA RD-99-138 US Department of Transportation

Gaeb, M. (2006). Unsolved issues of numerical modelling of stone column reinforced foundations. Presentation. 1st AMGISS workshop, University of Glasgow, www.ce.strath.ac.uk/amgiss

Gajo, A. and Muir Wood, D (2001). A new approach to anisotropic, bounding surface plasticity: General formulation and simulations of natural and reconstituted clay behaviour. International Journal for Numerical and Analytical Methods in Geomechanics, Vol. 25, No. 3, p 207-241

Gardiner, S. (2006). Ground improvement by deep mixing. MEng Dissertation, Dept. of Civil Engineering, University of Strathclyde, Glasgow, UK

Gens, A. and Nova, R. (1993). Conceptual bases for a constitutive model for bonded soils and weak rocks. Proc. Int. Symp. Hard Soils-Soft Rocks, Athens.

Grammatikopoulou, A. Zdravkovic, L. and Potts, D.M (2007). The effect of the yield and plastic potential deviatoric surfaces on the failure height of an embankment., Geotechnique, Vol. 57, No. 10, p 795 - 806

Han, J. and Huang. S. (2007). Validation of constitutive models for geosynthetic - reinforced column supported embankments. In: Proc. Constitutive Modelling - Development, Implementation, Evaluation and Application. Edited by J.H. Yin, X.S. Li, A.T. Yeung and C.S. Desai, Hong Kong

Hanzawa, H. and Kishida, T. (1981). Fundamental considerations on undrained strength characteristics of alluvial marine clays., Soils And Foundations, Vol. 21. No. 1, p 39 - 50

Hayashi, H. and Nishimoto, S. (2005). Strength Characteristic of Stabilized Peat using Different Types of Binders. Proc. International conference on deep mixing'05, Stockholm, Vol. 1.1, p 55 - 52

Holm, G. Tränk, R., Ekstrom, A. and Torstession, B-A. (1983). Lime columns under embankments - A full scale test., In: Proc. 8th European Conference on Soil Mechanics and Foundation Engineering. Helsinki. Vol. 2, p 909

Huang, S., Han, J. and Porbaha, A. (2006). Two and three dimensional modelling of DM columns under embankments. GeoCongress 2006, ASCE

Kamrat-Pietraszewska, D., Krenn, H., Sivasithamparam, N. and Karstunen, M. (2008). The Influence of Ansiotropy and Destructuration on a Circulat footing, Proceedings of the BGA International Conference on Foundations, Dundee, Scotland, 24 – 27 June 2008. IHS BRE Press, 2008

Karstunen, M. (2007). Personal communications

Karstunen, M. and Koskinen, M. (in press). Plastic anisotropy of soft reconstituted clays. Accepted for publication in Canadian Geotechnical Journal in September 2007.

Karstunen, M. (1999). Alternative ways of modelling embankments on deep-stabilised soil., Dry Mixing for Deep Soil Stabilisation, Bredenberg, Holm & Broms (eds), Balkema, Rotterdam ISBN: 90 5809 108 2

Karstunen, M., Wiltafsky, C., Krenn, H., Scharinger, F. and Schweiger, H.F. (2006). Modelling the stress-strain behaviour of an embankment on soft clay with different constitutive models. International Journal of Numerical and Analytical Methods in Geomechanics 30(10): 953-982. ISSN 0363-9061

Karstunen, M. and Krenn, H. (2004). Deep-stabilized columns under embankment fill: 3D finite element analysis versus unit cell approach. Invited contribution in: Geotechnical Innovations, Stuttgart 25 June, 2004. VGE, Essen. p. 337-347. ISBN 3-7739-5991-5

Karstunen, M., Krenn, H., Wheeler, S.J., Koskinen, M. and Zentar, R. (2005). The effect of anisotropy and destructuration on the behaviour of Murro test embankment. Int. J. for Geomechanics (ASCE), 5(2), p 87-97

Karstunen, M., Krenn, H. and Aalto, A. (2005a). Recent advances in numerical modelling of deep-stabilized soil. In: Proc. Stabilisation/Solidification Treatment and Remediation - Al-Tabbaa & Stegemann (eds.), Taylor & Francis Group, London, ISBN 04 1537 460 X, p 303 - 312

Kavvadas, M. and Amorosi, A. (2001). Constitutive model for structured clay. Geotechnique, v 50, n 3, Jun, 2000, p 263-273

Kitazume, M. and Maruyama, K. (2006). Internal stability of group column type deep mixing improved under embankment loading. Soil and Foundation, Vol. 46, No. 3, p 323 - 340

Kivelö, M. (1998). Stabilization of embankments on soft soil with lime/cement columns. Doctoral Thesis 1023, Division of Soil and Rock Mechanics, Dept. of Civil and Enviromental Engineering, Royal Institute of Technology, Stockholm, Sweden

Korhonen, K.H. and Lojander, M. (1987). Yielding of Perno Clay. In: Constitutive Laws for Engineering Materials: Theory and Applications, Proc. of 2nd IC, Vol. I, Desai CS et al (eds.) Elsevier: New York

Korkiala-Tanttu, L. (1997). Design Guide for Deep Mixed Columns, Finnish National Road Administration, FinnRA Report 18/1997, Helsinki, (In Finnish).

Koskinen, M. (2002). Experimental investigation on anisotropy and interparticle bonding on soft clays. In: Proc. 15th European Young Geotechnical Engineers Conference (EYGEC), Dublin, Ireland.

Koskinen, M., Zentar, R. and Karstunen, M. (2002a). Anisotropy of reconstituted Poko Clay. In: Pande & Pietruszczak (eds.) Proc. 8th Int. Symp. Numerical Models in Geomechanics (NUMOG), Rome, Italy, Rotterdam: Balkema, p 99-105

Koskinen, M., Karstunen, M. and Wheeler, S.J. (2002b). Modelling destructuration and anisotropy of a natural soft clay. In: Mestat (eds.), Proc. Numerical Methods in Geotechnical Engineering (NUMGE), Paris, France, Paris: PRESSES de l'ENPC/ LCPC, p 11-19

Koskinen, M., Vepsäläinen, P. and Lojander, M. (2002c). Modelling of anisotropic behaviour of clays, Test embankment in Murro, Seinäjoki, Finland, Finnra Reports, Vol. 16. Helsinki: Edita Prima Oy

Koskinen, M., Lojander, M., Tolla, P. and Vepsäläinen, P. (2002c). Numerical analysis on Murro test embankment. In: Mestat (eds.), Proc. Numerical Methods in Geotechnical Engineering (NUMGE), Paris, France, Paris: PRESSES de l'ENPC/LCPC, p 397-402

Koskinen, M. and Karstunen, M. (2004). Anisotropy and destructuration of Murro clay. In: Jardine, R.J. et al. (eds.) Advances in geotechnical engineering - The Skempton Conference: Vol. 1. London: Thomas Telford, p 476-487

Koskinen, M. and Karstunen, M. (2004), The effect of structure on the compressibility of Finnish clays. In: Proc. 14th Nordic Geotechnical meeting, Ystad, Sweden. Swedish Geotechnical Society, Report 3: 2004, p A11 - A 22

Koskinen, M. and Karstunen, M. (2006). Numerical Modelling of Murro test embankment with S-CLAY1S. In: Schweiger (eds.) Proc. Numerical Methods in Geotechnical Engineering. NUMGE06, p 455 - 462

Koskinen, M. and Karstunen, M. (in press). Plastic anisotropy of soft reconstituted clays. Accepted for publication in Canadian Geotechnical J.

Krenn, H. (2002). Numerical simulations of benchmark problems on soft clay. Diploma-Thesis, Department of Soil Mechanics and Foundation Engineering, Graz University of Technology

Krenn, H., Karstunen, M. and Aalto, A. (2005). 2D and 3D numerical analsyes of deep-satbilised columns. Proc. International conference on deep mixing'05, Stockholm p 547 - 554

Krenn, H. and Karstunen, M. (2006). 3D modelling of deep mixing. In: Proc: 59th Cancadian Geotechnical Conference, Vancouver 2006

Krenn, H. and Yildiz, A. (2006). Influence of anisotropy and destructuration on the settlement behaviour of an embankment and a shallow foundation constructed on soft soil. 7th International Congress on Advances in Civil Engineering, October 11-13, 2006, Istanbul, Turkey

Kurisaki, K., Sugiyama, H., Izutsu, T., Yamamoto, M., Takeuchi, G., Ohishi, K., Katagiri, M., Terashi, M. and Ishii, T. (2005). Physical and numerical simulations of deep

mixed foundations Part1: bearing capacity of treated soil., Proc. International conference on deep mixing'05, Stockholm, Vol. 1.2, p 255 - 262

Lade, P.V. and Duncan J. M. (1973). Elasto plastic stress strain theory for cohesionless soil. Proc. of ASCE, Vol. 101, p 1037-1053

Lahtinen, P.O and Vepsäläinen, P. (1983). Dimensioning deep-stabilisation using the finite element method. In: Proc. 8th European Conference on Soil Mechanics and Foundation Engineering. Helsinki. Vol. 2, p 933

Larsson, R., Bengtsson, P-E. and Eriksson, L. (1997). Prediction of settlements of embankments on soft, fine-grained soils. Calculation of settlements and their course with time. Information 13E, Swedish Geotechnical Institute

Larrson, R. and Mattsson, H. (2003). Settlements and shear strength increase below embankments - long term observations and measurement of shear strength increase by seismic cross-hole tomography. Report 63, Swedish Geotechnical Institute

Lee, J.S. and Pande, G.N. (1998). Analysis of stone column reinforced foundations. Int. J. Numer. Anal. Meth. Geomech. , Vol. 22, p 1001 - 1020

Leoni, M., Karstunen, M. and Vermeer. (in press). Anisotropic Creep Model for Soft Soils. Accepted for publication in Geotechnique

Leroueil, S. and Hight, D.W. (2003). Behaviour and properties of natural soils and soft rocks. In: Characterisation and Engineering Properties of Natural Soils - Tan et al. (eds.) © 2003 Swets & Zeitlinger, Lisse, ISBN 90 5809 537 1

Leroueil, S., Magnan, J-P. and Tavenas. F. (1990). Embankments onf Soft Clays. Ellis Horwood LtD. ISBN 0 13 275736 2

Leroueil, S., Tavenas, F., Brucy, F., La Rochelle, P., and Roy, M. (1979). Behaviour of destructured natural clays. Journal of Geotechnical Engineering, 105(6), p 759-778.

Leroueil, S. and Vaughan, P.R. (1990). The general and congruent effects of structure in natural soils and weak rocks. Geotechnique 40, No. 3, p 452-467

Liingaard, M., Augustesen, A. and Lade, P.V. (2004). Characterization of Models for Time Dependent Behaviour of Soils. International Journal of Geomechanics. p 157-177

Liver, N.L., Mardorf, E.C. and King, J.C. (1954) Developement and applications of intrusion grout Mixed in Place piles. Civil Engineering, p 56 -57

Löfroth, H.(2007). Properties of 10-year-old lime-cement columns. Poster. Swedish Geotechnical Institute. www.swedgeo.se

Magnan, J.P., Humbert, P., Belkeziz, A. and Mouratidis, A. (1982). Finite element analysis of soil consolidation, with special reference to the case of strain hardening elastoplastic stress-strain models. 4th Int. Conf. on Numerical Methods in Geomechanics. Eisenstein (eds.), Balkema, p 327-336

Maher, R. (2006). Soft Soil Stabilisation using deep mixing. BEng Dissertation, Dept. of Civil Engineering, University of Strathclyde, Glasgow, UK

Malvern, L.E. (1951). The propagation of longitudinal waves of plastic deformataion in a bar of metal exhibition a strain rate effect. Journal of Applied Mechanics, 18, p 203-208

Massarsch, K.R. and Topolnicki, M. (2005). Regional report: European practice of deep mixing technology. Proc. International conference on deep mixing'05, Stockholm p 19 - 46

Matsuoka, H. and Nakai, T. (1982). A new failure criteria for soils in three dimensional stresses. IUTAM, Conference on Deformation and Failure of Granular Materials, Delft, p 253-263

Mayne, P.W. and Kulhway, F. H. (1982). K_0-OCR relationship in soil. ASCE Journal of Geotechnical Engineering, Vol. 108, GT, p 851 - 872

Mestat, P. (2001). MOMIS: A database for the numerical modeling of embankments on soft soils and the comparison between computational results and in situ measurements. Bulletin des Laboratories des Pontes et Chausseess, 232, May-June 2001, p 45-60

Mestat, P., Bourgeois, E. and Riou Y. (2004). Numerical modelling of embankments and underground works. Computer and Geotechnics, Vol. 31, p 227-236

Mitchell, J. K. (1976). Fundamentals of soil behaviour, John Wiley, New York

Näätänen, A., Wheeler, S.J., Karstunen, M. and Lojander, M. (1999). Experimental investigation of an anisotropic hardening model for soft clays. In: M. Jamiolkowski, R. Lancellota & D. Lo Presti (eds.), Proc. 2nd Int. Symp. on Pre-Failure Deformation Characteristic of Geomaterials, Torino, Vol. 1, p 541-548. A.A. Balkema

Nakai, T. and Matsuoka, H. (1987). Elastoplastic analysis of embankment foundation. 8th ARCSMFE, p 473 - 476

Nakase, A. and Takemura, J. (1989). Prediction of behaviour of trail embankments built to failure., Int. Symp. on trial embankments on Malaysian Marine clays., Kuala Lumpur, p 3.1 - 3.13

Namikawa, T., Suzuki, Y. and Koseki, J. (2005). Seismic Response Analysis of Lattice-Shaped Ground Improvements. Proc. International conference on deep mixing'05, Stockholm, Vol. 1.2, p 263 - 272

Neher, H.P., Wehnert, M. and Bonnier, P.G. (2001). An evaluation of soft soil models based on trial embankments. Computer Methods and Advances in Geomechanics. Desai et al. (eds.), Balkema, p 373 - 378.

Neher, H.P., Vogler, U. Vermeer, P.A and Viggiani, C. (2003). 3D creep analysis of the Leaning Tower of Pisa. In: Geotechnics of soft soils, theory and practice. Edited by Vermeer, Schweiger, Karstunen and Cudny. Noordwijkerhout (NL), P 607-612

Nozu, M. (2005). Regional report: Asia. Proc. International conference on deep mixing'05, Stockholm p R3 - R18

Nova, R. (1982). A viscoplastic constitutive model for normally consolidated clays. In IUTAM Conference on Deformation and Failure of Granular Materials. Delft, p 287-295

Ohishi, K., Katagiri, M., Terashi, M., Ishii, T. and Miyakoshi, Y. (2005). Physical and numerical simulation of deep mixed foundation. Part 2: Revetment on treated soil block underlain by a sandy layer. Proc. International conference on deep mixing'05, Stockholm, Vol. 1.2, p 281 - 288

Oasys Slope Version 18.2 (2007). User manual. http://www.oasys-software.com

Pande, G. N. and Sharma, K.G. (1983). Multilaminate model of clays - numerical evaluation of the influence of rotation of principal stress axes. Int. J. Numer. Anal. Meth. Geomech., 7(4), p 397-418

Perzyna, P. 1966. Fundamental problems in viscoplasticity, New York.

Pietruszczak, S. and Pande. G. N. (1987). Multilaminate framework of soil models - plasticity formulation. Int. J. Numer. Anal. Meth. Geomech., 11(6), p 651-658

Porbaha, A., Weathereby D., Macnab, A., Lambrechts, J., Burke, G., Yang, D. and Puppala, A. J. (2005). Regional report: North American practice of deep mixing technology. Proc. International conference on deep mixing'05, Stockholm p 47 - 67

Potts, D.M. and Zdravkovic, L. (1999). Finite element analysis in geotechnical engineering: Theory. London: Telford

Potts, D.M., Axelsson, K., Grande, L., Schweiger, H. and Long, L. (2002). Guidelines for the use of advanced numerical analysis. London: Thomas Telford Ltd

Roscoe, K.H. and Burland, J.B. (1968). On the generalized stress-strain behaviour of "wet" clay. Engineering Plasticity. Editors: J. Heyman & F.A. Leckie, Cambridge University Press, p 535-609

Roscoe, K.H. and Schofield, A.N. (1963). Mechanical behaviour of an idealised "wet" clay. Proc. of the 2nd European Conf. on Soil Mechanics and Foundation Engineering, Wiesbaden, Germany, p 47-54

Rouainia, M. and Muir Wood, D.A. (2000). A kinematic hardening constitutive model for natural clays with loss of structure. Geotechnique, 50(2), p 153-164

Satibi, S., Ayman, A., Chuang, Y., Leoni, M. and Vermeer, P.A. (2007). FE Simulations of Installation and Loading of a Tube-Installed Pile. Institutsbericht 29 des Institutes fuer Geotechnik Herausgeber: P.A. Vermeer

Schanz, T. and Vermeer, P.A. (1998). Special issue on Pre-failure deformation behaviour of geomaterials. Geotechnique, 48, p 383-387

Schwab, E.F. (1976). Bearing capacity, strength and deformation behaviour of soft organic sulphide soils. Dept. of Soil and Rock Mechanics, Royal Institute of Technology, Stockholm, Sweden.

Schweiger, H.F. and Pande, G.N. (1986). Numerical analysis of stone columns supported foundations. Comp. and Geo., Vol. 2, p 347 - 372

Schweiger, H.F. and Gaeb, M. (2006). 3D modelling of ground improvement, AMGISS workshop, Helsinki, April 2006, www.ce.strath.ac.uk/amgiss

Sekiguchi, H., and Ohta, H. (1977). Induced anisotropy and time dependency in clays. In: Murayama & Schofield (eds.), Proc. 9th Int. Conf. Soil Mechanics and Foundation Engineering (ICSMFE), Tokyo, Japan, Vol. 1, p 229-238

Selkämaa, E. (1994). Test embankment Seinäjoki, Murro (in Finnish). Graduate project, Seinäjoen teknillinen oppilaitos, Rakennustekniikan osasto, p 27

Suklje, L. (1957). The analysis of the consolidation process by the isotaches method. In: Proc. 4th ICSMFE, Vol. 1, p 200 - 2006

Smith, I.M. (1993). Programming the finite element method with application to geo-mechanics. John Wiley & Sons, Chichester

Soyez, Magnan, and Delfault, (1983) Loading test on a clayey hydraulic fill stabilised by lime treated soil columns., In: Proc. 8th European Conference on Soil Mechanics and Foundation Engineering. Helsinki. Vol. 2, p 951

Stallebrass, S.E. and Taylor, R.N. (1997). The development and evaluation of a constitutive model for the prediction of ground movements in overconsolidated clay. Geotechnique, 47(2), p 235-253

Stewart, M.E. and Filz, G.M. (2005). Factors affecting load transfer to deep mixing columns from embankments without geosynthetic reinforcement. Proc. International conference on deep mixing'05, Stockholm, Vol. 1.2, p 305 - 316

Stewart, M.E., Mike, P. Navin, P.E. and Filz. G.M. (2004). Analysis of a column supported test embankment at the I-95 / Route 1 Interchange. Geotrans 2004, p 1337 - 1346.

Sun, D.A, Matsuoka, H., Yao, Y.P. and Ishii, H. (2001). An anisotropic hardening elastoplastic model for clay and sand and its application to numerical analysis. Computer Methods and Advances in geomechanics. Desai et al. (eds.), Balkema, p 407 - 412.

Tavenas, F., Leroueil, S. (1977). Effects of stresses and time on yielding of clays. In: Murayama & Schofield (eds.), Proc. 9th Int. Conf. Soil Mechanics and Foundation Engineering (ICSMFE), Tokyo, Japan, Vol. 1, p 319-326

Taylor, D.W. (1948). Fundamentals of Soil Mechanics. John Wiley and Sons, New York, USA

Terashi, M. and Tanaka (1983). Bearing Capacity and Consolidation of Improved Ground of Treated Soil Columns, Report of the Port and Harbour Research Institute, Vol. 22, No. 2 p 213 - 266

Terashi, M. (2005). Keynote Lecture: Design of deep mixed material in infrastructure application., Proc. International conference on deep mixing'05, Stockholm, Vol. 1.1, p K25

The, B.H.P.A.M., Termaat, R.J and Vermeer, P.A (1998). A viscoplastic creep model for the engineering practice., Problematic Soils, Yanagiswa et al. (eds.), Balkema, p 657 - 660.

Thomson, G. (2007). Presentation at Workshop on Ground improvement. BGA meeting, London, November 2007

Toncone, A. (2005). Numerical analysis of a landslide in soils with strain softening. Geotechnique, Vol. 55, No. 8, p 585-596

Tremblay, H., Leroueil, S. and Locat, J. (2001). Mechanical improvement and vertical yield stress predictions of clayey soil from eastern Canada treated with lime or cement., Canadian Geotechnical Journal, Vol. 38, p 567 - 579

Van Langen, H. and Vermeer, P.A. (1990). Automatic step size correction for non-associated plasticity problems. Int. J. Numer. Meth. Eng., Vol. 29, p 579-598

Vepsäläinen, P. and Arkima, O. (1992). The arching of road embankments. Final Report. Finnish National Administration, Research Report, 18/1997, Helsinki

Vermeer, P.A. and Neher, H.P. (1999) A soft soil model that accounts for creep. In: Int. Symp. "Beyond 2000 in Computational Geotechnics". Edited by R.B.J. Brinkgreve. Amsterdam. Balkema, Rotterdam, p 249-261

Vermeer, P.A. and Van Langen, H. (1989). Soil collapse computations with finite elements. Ingenieur-Archiv, 59, p 221-236

Vogler, U. (2008). Numerical modelling of deep mixing using volume averaging technique. PhD Thesis, University of Strathclyde, Scotland.

Wehr, J. (2007) Personal communications

Wheeler, S.J., Näätänen, A., Karstunen, M. and Lojander, M. (2003). An anisotropic elastoplastic model for soft clays. Canadian Geotechnical J., 40, p 403-418

Whitlow, R. (1993). Basic Soil Mechanics, Third Edition, Longman Scientific & Technical. ISBN: 0-582-23631-2

Whittle, A., J. (1987), A constitutive model for overconsolidated clays with application to the cyclic loading of friction piles. ScD thesis, Massachusetts Institute of Technology, Cambridge, Mass., USA.

Wiltafsky, C. (2003a). A multilaminate model for normally consolidated clay. Ph. D Thesis, Gruppe Geotechnik graz, Heft 18, Graz, University of Technology, Austria

Wiltafsky, C. (2003b). S-CLAY1S, User Defined Soil Model, Documentation, University of Glasgow, UK

Wiltafsky, C., Scharinger, F., Schweiger, H.F., Krenn, H. and Zentar, R. (2003). Results from a geotechnical benchmark exercise of an embankment on soft clay. Proc. International Workshop on Geotechnics of Soft Soils - Theory and Practice, Noordwijkerhout, The Netherlands, VGE, Essen, Germany, 381-390

Yin, J.H. and Graham, J. (1999). Elastic viscoplastic modelling of the time dependent stress-strain behaviour of soils. Canadian Geotechnical Journal, 40, p 403-418

Yin, Z.Y. and Karstunen, M. (2008). Influence of anisotropy, destructuration and viscosity on the behaviour of an embankment on soft clay. Accepted for publication in the 12th International Conference of International Association for Computer Methods and Advances in Geomechanics (IACMAG), 1-6 October, Goa, India

Zdravkovic, L., Potts, D.M and Hight, D.W. (2002). The effect of anisotropy on the behaviour of embankments on soft ground., Geotechnique, Vol. 52, No. 6, P 447 -457

Zienkiewicz, O.C., and Pande, G.N. (1977). Time-dependent multilaminate model of rocks - A numerical study of deformation and failure of rock masses. Int. J. Numerical and Analytical Methods in Geomechanics, Vol. 1, No. 3, p 219-247

Zienkiewicz, O.C. (1977). The Finite Element Method. McGraw-Hill, London

Appendix A

A.1 Journal paper I

Effect of Anisotropy and Destructuration on the Behavior of Murro Test Embankment

Minna Karstunen[1]; Harald Krenn[2]; Simon J. Wheeler[3]; Mirva Koskinen[4]; and Rachid Zentar[5]

Abstract: This paper investigates the influence of anisotropy and destructuration on the behavior of a test embankment on soft clay. The test embankment at Murro, Finland, was commissioned in 1993 by the Finnish Road Administration and has been monitored for over 10 years. The construction and consolidation of Murro test embankment is analyzed with finite element method using three different constitutive models to represent the soft soil. The results are compared with field observations. The constitutive models used include two recently proposed constitutive models, namely S-CLAY1 that accounts for initial and plastic strain induced anisotropy and its extension, called S-CLAY1S. The S-CLAY1S model accounts, additionally, for interparticle bonding and degradation of bonds. For comparison, the test embankment is also analyzed using the isotropic Modified Cam Clay model. The simulations demonstrate that for this type of problem, it is important to account for the anisotropy, whereas destructuration appears to have less influence on predicted deformations. However, only a model incorporating destructuration can explain the decrease in undrained shear strength during consolidation that was measured in field.

DOI: 10.1061/(ASCE)1532-3641(2005)5:2(87)

CE Database subject headings: Anisotropy; Clays; Constitutive models; Finite element method; Embankments; Finland.

Introduction

Design and construction on soft soils is still a challenge for geotechnical engineers, and yet this is becoming more common due to the lack of land available for construction in well-developed regions. The challenges involve appropriate constitutive modelling of soft soil behavior, including such fundamental features as anisotropy, destructuration, and creep.

The paper investigates how fabric anisotropy, interparticle bonding and degradation of bonds in the underlying soft clay influence the behavior of a test embankment. The analyzes use two recently proposed elasto–plastic constitutive models for soft clays, S-CLAY1 (Wheeler et al. 2003) and S-CLAY1S (Koskinen et al. 2002a). The models account for plastic anisotropy and anisotropy combined with destructuration, respectively. Both models have been implemented at Glasgow Univ. within *SAGE CRISP* and *PLAXIS 2D* V8 finite element codes. The former implementation was used for the simulations presented in this paper. For comparison, the problem is also analyzed with the isotropic Modified Cam Clay model (Roscoe and Burland 1968). First, some background information on the embankment, its location and site conditions is given. The new constitutive models are then briefly described, followed by information about the embankment geometry, material parameters and initial conditions, as necessary for the input of numerical analyzes. Finally, the results of the numerical analyzes are compared with the corresponding field observations.

Background

In 1993 the Finnish Road Administration commissioned the construction of a test embankment at Murro, with the aim of using the information for the design of Highway 18 between the cities of Vaasa and Jyväskylä. Murro is situated near the town of Seinäjoki in Western Finland close to the coast of the Gulf of Bothnia. Murro test embankment is founded on a soil deposit about 23 m deep that consists of soft silty clay overlain by a relatively thin dry crust. Underneath the soft soil there is a layer of moraine. The deposits found along the coast of the Gulf of Bothnia consist typically of young postglacial sediments with high organic and sulphur content. The soils in the area are predominantly silty clays or clayey silts that were sedimented in brackish water of the postglacial Littorina Sea (Schwab 1976), which was one of the latest postglacial evolution stages of the Baltic Sea around 7,000 years ago. The deposits are therefore relatively young and typically normally consolidated. The rate of isostatic uplift around the Gulf of Bothnia is still about 1 m per century. The ground level at the site of the test embankment is currently at 37.5 m above mean sea level and the groundwater table is estimated to be at 0.8 m depth.

The first site investigation stage in 1993 was a routine site investigation to assess the suitability of the site for a test embank-

[1]Lecturer, Dept. of Civil Engineering, Univ. of Glasgow, Glasgow G12 8LT, UK.
[2]Cormack Professor, Dept. of Civil Engineering, Univ. of Glasgow, Glasgow G12 8LT, UK.
[3]Research Assistant, Dept. of Civil Engineering, Univ. of Glasgow, Glasgow G12 8LT, UK.
[4]Research Engineer, Dept. of Civil and Environmental Engineering, Helsinki Univ. of Technology P.O. Box 2100, 02015 HUT, Espoo, Finland.
[5]Lecturer, Ecole des Mines de Douai BP 838 59508 Douai Cedex, France.

Note. Discussion open until November 1, 2005. Separate discussions must be submitted for individual papers. To extend the closing date by one month, a written request must be filed with the ASCE Managing Editor. The manuscript for this paper was submitted for review and possible publication on February 18, 2004; approved on October 25, 2004. This paper is part of the *International Journal of Geomechanics*, Vol. 5, No. 2, June 1, 2005. ©ASCE, ISSN 1532-3641/2005/2-87–97/$25.00.

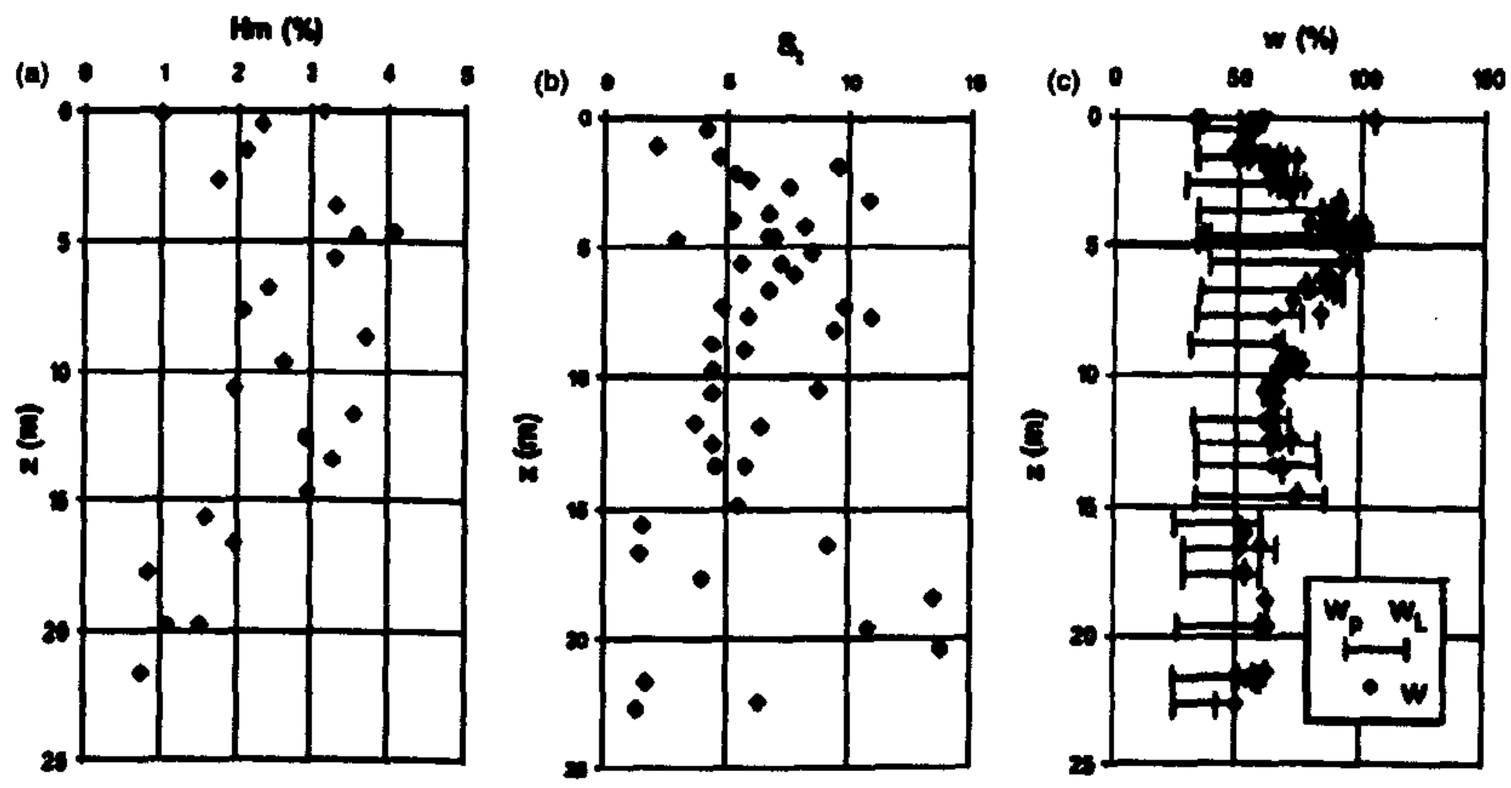

Fig. 1. Typical characteristic of Murro deposit: (a) organic content, (b) sensitivity, and (c) liquid and plastic limits and water content

ment. It was followed by a thorough site investigation, which involved four types of in situ testing methods, including Swedish weight sound testing (a routine site investigation method in Scandinavia), field vane testing, piezocone testing and static dynamic penetration testing (a method developed in Finland that combines piezocone testing in cohesive soils with dynamic testing in non-cohesive soils). In addition, a number of undisturbed and disturbed samples were taken for laboratory testing at Helsinki Univ. of Technology. These tests included drained and undrained triaxial tests and oedometer tests on undisturbed samples and various index tests. Fig. 1 shows some typical properties of Murro clay before construction of the test embankment. The undrained shear strength varied typically from 10 to 30 kPa (Koskinen et al. 2002c). The soft soil can be classified as silty clay or clayey silt with organic content of 2–3% (determined from the ignition loss). The color of the clay is black due to the presence of sulphur. The water content of the soil varies between 65 and 100%. The sensitivity of Murro clay is moderate, typically between 2 and 10 (Koskinen et al. 2002c).

An additional in situ testing and sampling exercise was performed in 2001, 8 years after embankment construction. This included field vane tests through the embankment (to assess the increase in the undrained shear strength due to consolidation of the subsoil) and sampling beneath and next to the embankment (Koskinen et al. 2002c). The samples that were taken next to the embankment were used to investigate the effect of the structure of the soil. This involved oedometer testing and specialist triaxial testing of both natural and reconstituted samples (Karstunen and Koskinen 2004; Koskinen and Karstunen 2004). A subsequent mineralogical study conducted at ETZ Zurich (Messerklinger et al. 2003) identified the main minerals of Murro clay as quartz (26%) and feldspar (46%) with the clay minerals as illite (15%), chlorite (10%), and kaolinite (5%). Overall, given the wealth of information about the soil deposit, and that the embankment has now been monitored for 10 years, it is an attractive case study for testing advanced constitutive ideas and numerical models.

The locations of the field monitoring instruments were decided based on preliminary finite element analyzes. The information available at that time was very limited. Subsequent finite element analyzes were conducted using well-known isotropic constitutive models (Koskinen et al. 2002b, c). The soil deposit in Murro is, however, characterized by a high degree of anisotropy, as shown by Karstunen and Koskinen (2004), and due to the albeit moderate sensitivity (Fig. 1), there is some natural interparticle bonding present in the soil in situ. Fabric anisotropy can influence both elastic and plastic behavior. For normally consolidated or lightly overconsolidated soft clays, however, plastic deformations are likely to dominate for many problems of practical interest, with elastic strains often being much smaller than the plastic strains. This is particularly true for problems such as embankments. The natural interparticle bonding, which originates from the mineral and pore water composition at the time of deposition, gives the soil extra strength and additional resistance to yielding. Plastic straining causes slippage and rearrangement of particles and interparticle contacts and, consequently, causes degradation of bonds (a process referred to as destructuration).

Constitutive Models

There are several different approaches to represent anisotropy of plastic behavior within a constitutive modeling framework. Alternatives include the standard elasto–plastic framework or the so-called multilaminate framework (Zienkiewicz and Pande 1977). Computationally, the standard elasto–plastic framework is much more efficient than the multilaminate framework, and consequently, there have been numerous model proposals using this framework (e.g., Banerjee and Yousif 1986; Dafalias 1986; Banerjee et al. 1988; Nova 1988; Davies and Newson 1993; Whittle and Kavvadas 1994; Pestana and Whittle 1999). The recently proposed S-CLAY1 model by Wheeler et al. (2003) has several advantages over many of the models proposed. These include the relatively simple model formulation, realistic K_0 prediction, and in addition, the values for the model parameters can be determined from standard laboratory test results by using well-defined methodologies. Furthermore, the model has been successfully validated against experimental data on several natural and reconstituted clays (Koskinen et al. 2002a, d; Wheeler et al. 2003), including Murro clay (Karstunen and Koskinen 2004). Therefore,

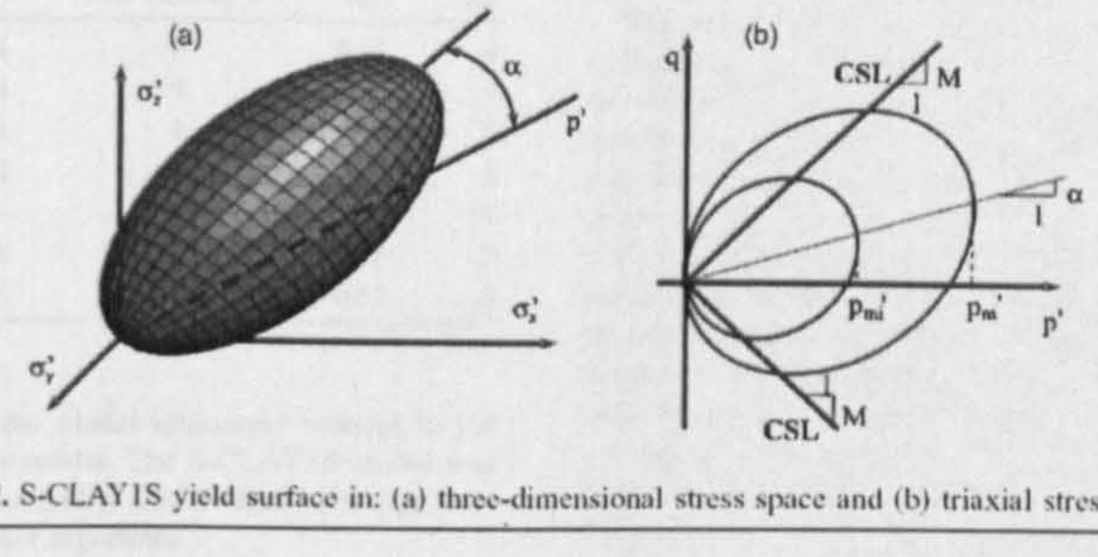

Fig. 2. S-CLAY1S yield surface in: (a) three-dimensional stress space and (b) triaxial stress space

S-CLAY1 has been chosen as one of the constitutive models used in this study.

Gens and Nova (1993) presented a general framework for incorporating bonding and destructuration within elasto–plastic constitutive models. In addition to the real yield surface for the natural material (with bonding), a notional "intrinsic yield surface" is introduced, to represent the size that the yield surface would be if there were no bonding. The difference in size of the real yield surface and the intrinsic yield surface (expressed either as a ratio or as a difference) is a measure of the bonding effect. In recent years a number of elasto–plastic constitutive models incorporating bonding and destructuration have been published (see e.g., Kavvadas and Amorosi 2000; Rouainia and Muir Wood 2000; Gajo and Muir Wood 2001; Liu and Carter 2002; Liu et al. 2003; Nova et al. 2003). Most of these models, however, do not incorporate anisotropy of large strain behavior, which is considered essential for soft clays. The S-CLAY1S model (Koskinen et al. 2002a) is an extension of the S-CLAY1 model, which accounts for bonding and destructuration, in addition to plastic anisotropy, and is the second advanced constitutive model used in this study.

In three-dimensional stress space the yield surface of the S-CLAY1S model is a sheared ellipsoid [Fig. 2(a)], given by

$$f = \tfrac{3}{2}[\{\boldsymbol{\sigma}_d - p'\boldsymbol{\alpha}_d\}^T\{\boldsymbol{\sigma}_d - p'\boldsymbol{\alpha}_d\}] - [M^2 - \tfrac{3}{2}\{\boldsymbol{\alpha}_d\}^T\{\boldsymbol{\alpha}_d\}](p_m' - p')p' = 0 \quad (1)$$

where $\boldsymbol{\sigma}_d$=deviatoric stress tensor; p'=mean effective stress; and $\boldsymbol{\alpha}_d$=dimensionless second order tensor describing the fabric anisotropy, called the deviatoric fabric tensor [as its formulation is analogous to the deviatoric stress tensor, see Wheeler et al. (2003) for details]. M=critical state value of the stress ratio in triaxial space and the state parameter p_m' defines the size of the natural yield surface of the clay. As discussed in Wheeler et al. (2003), it is possible to account for Lode angle dependency, but as the laboratory tests on Murro clay do not include any tests sheared to failure in triaxial extension, the triaxial compression value of M is used throughout. Zentar et al. (private communication 2004) explain in detail how the initial values of the terms of deviatoric fabric tensor $\boldsymbol{\alpha}_d$ are calculated.

For a special case, when the material and the stress state are both cross anisotropic, and the plane of material isotropy coincides with the plane of stress isotropy, the fabric tensor $\boldsymbol{\alpha}_d$ can be replaced with a scalar parameter α describing the inclination of the yield surface in the $p'-q$ space [Fig. 2(b)], where q is the deviator stress. This would typically be the initial in situ condition (before embankment construction).

The effect of bonding is described by an intrinsic yield surface (Gens and Nova 1993). The intrinsic yield surface is of the same shape and inclination as the yield surface for the natural soil [Fig. 2(b)], but with a size p_{mi}' that is related to p_m' (the size of the yield surface for the natural clay) by

$$p_m' = (1 + x)p_{mi}' \quad (2)$$

where x=amount of bonding.

Increase in the size of the intrinsic yield surface is related to the increments of plastic volumetric strain ($d\varepsilon_v^p$) by a hardening law for unbonded (reconstituted) soil, which is similar to that of Modified Cam Clay (MCC)

$$dp_{mi}' = \frac{v p_{mi}'}{\lambda_i - \kappa} d\varepsilon_v^p \quad (3)$$

where v=specific volume; λ_i=slope of the intrinsic normal compression line in the compression plane ($\ln p'-v$–space); and κ=slope of a swelling line in the compression plane. Ideally, the value for λ_i should be determined from an oedometer test on a reconstituted sample.

The second hardening law, describing the rotation of the yield surface (i.e., the evolution of anisotropy) due to plastic straining, is expressed as

$$d\boldsymbol{\alpha}_d = \mu\left(\left[\frac{3\boldsymbol{\eta}}{4} - \boldsymbol{\alpha}_d\right]\langle d\varepsilon_v^p\rangle + \beta\left[\frac{\boldsymbol{\eta}}{3} - \boldsymbol{\alpha}_d\right]d\varepsilon_d^p\right) \quad (4)$$

where $\boldsymbol{\eta}$=tensorial equivalent of the stress ratio, defined as $\boldsymbol{\eta} = \boldsymbol{\sigma}_d/p'$; and $d\varepsilon_d^p$=increment of plastic deviatoric strain. The new soil constants μ and β control, respectively, the absolute rate at which $\boldsymbol{\alpha}_d$ heads toward its current target value and the relative effectiveness of plastic deviatoric strains and plastic volumetric strains in rotating the yield surface [for details see Wheeler et al. (2003)].

The third hardening law of the S-CLAY1S model describes the degradation of bonding and it is assumed that both plastic volumetric strains and plastic deviatoric strains tend to reduce the bonding parameter x to zero

$$dx = -ax(|d\varepsilon_v^p| + b|d\varepsilon_d^p|) \quad (5)$$

where the new soil constant a controls the absolute rate of destructuration and b controls the relative effectiveness of plastic deviatoric strains and plastic volumetric strains in destroying the bonding [see Koskinen et al. (2002a) for details].

By setting the initial value of the state parameter x to zero and using an apparent value of λ (determined from an oedometer test on a natural clay sample), instead of the intrinsic value λ_i of a reconstituted clay, S-CLAY1S reduces to the S-CLAY1 model that accounts for plastic anisotropy only. Furthermore, if in addition the initial values of all terms of $\boldsymbol{\alpha}_d$ and the value of the soil

Table 1. Initial Values for State Parameters

Layer	Depth (m)	e_0	POP (kN/m^2)	α_0	x_0
1a	0–0.8	1.4	20	0.63	4
1b	0.8–1.6	1.4	10	0.63	4
2	1.6–3.0	1.8	1	0.63	8
3	3.0–6.7	2.4	1	0.63	8
4	6.7–10.0	2.1	1	0.63	10
5	10.0–15.0	1.8	1	0.63	9
6	15.0–23.0	1.5	1	0.63	9

constant μ are set to zero, the model ultimately reduces to the isotropic Modified Cam Clay model. The S-CLAY1S model was implemented by Zentar in the *SAGE CRISP* finite element code using an explicit forward Euler algorithm.

Geometry and Input Data

The Murro test embankment is 2 m high and 30 m long. The width of the embankment at the top is 10 m and the slopes have a gradient of 1:2. The embankment material is crushed rock (biotite gneiss) with a grain size of 0–65 mm. The construction was completed within 2 days. The embankment was modeled with a simple linear elastic–perfectly plastic Mohr Coulomb model using the following typical values for the embankment material: E=40,000 kN/m^2, ν'=0.35, ϕ'=40°, ψ'=0°, c' =2 kN/m^2, and γ=19.6 kN/m^3. Parametric studies showed that the simulations were not sensitive to the values of the parameters chosen for the embankment material, because the problem is controlled by the response of the underlying soft soil.

Based on the ground investigation data (Koskinen et al. 2002c), the 23 m thick clay deposit can be roughly divided into two main layers: a 1.6 m thick overconsolidated dry crust and an underlying thick layer of almost normally consolidated soft clay. The underlying layer can be further subdivided into five sublayers (see Table 1). The most compressible layers are at depths between 1.6 and 7 m. The groundwater level is assumed to be at approximately 0.8 m from the ground level.

The values of soil parameters and initial state (Tables 1–3) for the finite element analyzes have been worked out from laboratory results using the best practice for the determination of model and state parameters for the S-CLAY1S model and its simplifications (i.e., S-CLAY1 and MCC). Due to natural variability, there was some scatter in the values and for each layer average values have been chosen. It is important to note that with the simple exception of the preconsolidation stress in the dry crust (see next paragraph), the values for soil parameters and initial values of state variables were all selected independently from laboratory tests data and were not backcalculated to optimize the fit of numerical simulations to the observed embankment performance.

The initial values for the state parameters are shown in Table 1. Based on the oedometer test results on natural samples, only the dry crust has some evidence of overconsolidation. This is represented in Table 1 by "preoverburden pressure" (POP), defined as the difference between the vertical preconsolidation stress (σ'_{vp}) and the in situ vertical effective stress (σ'_{v0}), e.g. POP $=\sigma'_{vp}-\sigma'_{v0}$. The oedometer test results for the dry crust material had a lot of scatter, as expected, suggesting POP values between 10 and 80 kPa. Preliminary finite element analyzes suggested that values towards the bottom of the range needed to be adopted in order to get the best match (this was true with all three constitutive models). Based on this a POP of 20 kPa has been adopted for Layer 1a and a POP of 10 kPa for Layer 1b of the dry crust (see Table 1).

Based on the oedometer tests, the soft clay layer (sublayers 2–6) is practically normally consolidated. The POP values of 1 kPa were, therefore, chosen to ensure that the in situ stresses remained inside the yield surface at the start of the numerical analyzes. Sensitivity analyzes were performed to investigate the influence of the POP value of the soft clay layers, by using POP values 0.5, 1, and 5 kPa. The results of these analyzes showed that such small changes in the value of POP do not significantly influence the overall deformation behavior.

Given that the clay layers are lightly overconsolidated, the initial inclination α_0 of the yield surface (Table 1) was determined by following the procedure described by Wheeler et al. (2003), using the values of M given in Table 1 for estimating the normally consolidated K_0 values. By combining the POP values in Table 1 with normally consolidated K_0 values and the yield curve equation [Eq. (1)], the values of p'_m were calculated for the MCC, S-CLAY1, and S-CLAY1S models. The initial value for x_0, the parameter describing the amount of bonding, was estimated based on sensitivity, as suggested by Koskinen et al. (2002a). The degree of bonding is relatively low in the dry crust and nearly constant for the layers underneath varying between 8 and 10.

The values for the standard soil constants in Table 2 were determined in a conventional manner from triaxial and oedometer tests on natural samples and are the same for all models. The values for permeability were determined from CRS oedometer tests. These also included some tests on horizontal samples and based on these the ratio of horizontal to vertical permeability was taken as 1.3.

The values for the additional model parameters required for the S-CLAY1 and S-CLAY1S models are listed in Table 3. The values of λ_i, measured from oedometer tests on reconstituted samples, were worked out for two different depths (7 and 9 m) for which experimental results existed and estimated for the remaining layers assuming similar λ to λ_i ratios. It is important to

Table 2. Values for Conventional Soil Constants

Layer	γ (kN/m^3)	κ	ν'	λ	M	k_x (m/s)	k_y (m/s)
1a	15.8	0.010	0.35	0.16	1.6	2.47E−09	1.90E−09
1b	15.8	0.010	0.35	0.16	1.6	2.47E−09	1.90E−09
2	15.5	0.030	0.35	0.50	1.6	2.47E−09	1.90E−09
3	14.9	0.036	0.10	0.50	1.6	2.06E−09	1.55E−09
4	15.1	0.030	0.15	0.36	1.6	1.27E−09	1.05E−09
5	15.5	0.034	0.15	0.32	1.6	7.93E−10	6.34E−10
6	15.9	0.004	0.15	0.14	1.6	1.20E−09	9.51E−10

Table 3. Values for Additional Soil Constants for S-CLAY1 and S-CLAY1S

Layer	β	μ	λ_i	a	b
1a	1.02	45	0.07	9	0.2
1b	1.02	45	0.07	9	0.2
2	1.02	25	0.24	9	0.2
3	1.02	20	0.24	9	0.2
4	1.02	25	0.18	9	0.2
5	1.02	25	0.16	9	0.2
6	1.02	30	0.07	9	0.2

note that the simulations with MCC and S-CLAY1 employed the model parameter λ (measured from oedometer tests on natural samples), whereas the simulations with S-CLAY1S employed the model parameter λ_i (measured from oedometer tests on reconstituted samples or estimated from an assumed ratio of λ_i/λ). The values of soil parameter β were calculated using principles outlined in Wheeler et al. (2003) using estimated normally consolidated K_0 values. The values of μ were estimated based on apparent values of λ (given in Table 1), as suggested by Zentar et al. (2002). Karstunen and Koskinen (2004) determined the values of parameters a and b (that control rate of degradation of bonding) using an optimization procedure by simulating triaxial test results from the depth of 6.9–7 m on natural Murro clay. These values were used as default values throughout the deposit. Model simulations of other Finnish natural clays have indicated similar values (Koskinen et al. 2002d) for soil constants a and b.

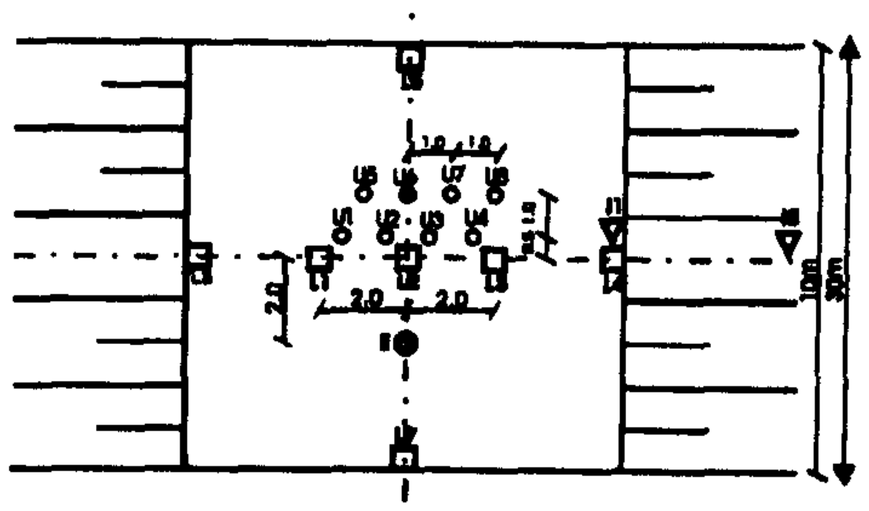

Fig. 3. Layout of instrumentation at Murro test embankment

Numerical Analyzes and Comparisons with Observations

The construction and consolidation of Murro test embankment has been modeled with the two-dimensional (2D) finite element code *SAGE CRISP*. Site investigations suggested the deposit is rather homogeneous, and furthermore, the ground surface is almost level. Given the dimensions of the embankment, it is possible to idealize it as a plane strain problem. Due to the symmetry of the problem, the analyzes considered just one half of the embankment. The problem was discretized by using a finite element mesh with about 1,400 eight-noded quadrilateral elements. The lateral boundary, at 36 m from the symmetry axis, was fixed in the horizontal direction, and the bottom boundary in both vertical and horizontal directions. Mesh sensitivity studies showed that the mesh was dense enough to give accurate results. The problem was modeled using small strain analyzes.

The initial stresses were calculated by inputting a horizontal effective stress distribution, using K_0 values estimated with equation $K_0=(1-\sin\phi')\ \mathrm{OCR}^{\sin\phi'}$ (Mayne and Kulhawy 1982), where ϕ' is the triaxial compression friction angle and OCR is the vertical overconsolidation ratio. It was assumed that the dry crust above the water table was fully saturated, and hence it was assumed initially to have negative pore pressures. The suction was assumed to increase linearly, from zero at the level of ground water table (at 0.8 m depth), to a value of −8 kPa at the ground level. All calculation phases, including the construction of the embankment, were computed as fully coupled static consolidation analyzes with additional degrees of freedom for pore pressures at the corner nodes. With *SAGE CRISP* it is not possible to allow for the decrease in the permeabilities k_x and k_y as the void ratio decreases, and therefore the constant k values listed in Table 2, were used. Drainage was allowed through the top and bottom of the clay layer, given that the permeability of the underlying moraine is likely to be orders of magnitude higher than the permeability of the clay.

It would have been possible to use the MCC model that is included in the commercial version of *SAGE CRISP* for the MCC model simulations. However, because the S-CLAY1S model reduces to S-CLAY1 and then to the MCC model, by setting certain state parameters and soil constants to zero, the same (in-house) model implementation was used for all simulations. The results are, therefore, free of any discrepancies due to differences in implementation. *SAGE CRISP* uses a fully explicit incremental (rather than incremental-iterative) solution scheme and consequently the computational results are very sensitive to the chosen load increment size; in the case of coupled consolidation analyzes this relates to the sizes of the time increments. The problem is apparent when any of the constitutive models used incorporate any type of hardening. It becomes particularly significant when a model with complex hardening laws, such as S-CLAY1S, is used. Hence, the analyzes were repeated using different time increment sizes until such a time stepping scheme was found that the global solution for the simulation with the S-CLAY1S model converged. The same time stepping scheme was then used for the S-CLAY1 and MCC model simulations.

The instrumentation of Murro test embankment included several settlement plates ($L1$–$L7$), inclinometers ($I1$, $I2$), an extensometer (E) and numerous pore pressure probes ($U1$–$U10$), as detailed in Koskinen et al. (2002c). The embankment has been monitored since 1993 and currently the measurements are taken annually or biannually. The layout of the instruments is presented in Fig. 3 and the depths and locations of the pore pressure probes are summarized in Table 4. The instrumentation has been concentrated at a 10 m section at the center of the longitudinal section. As seen in Fig. 3, the settlement plates $L2$, $L5$, and $L7$ are directly underneath the centerline of the embankment, while the rest of the settlement plates are located symmetrically along the cross section of the embankment. The pore pressure probes $U9$ and $U10$ are outside the embankment and hence act as useful reference points.

The comparisons between the results of the finite element simulations and the field observations are presented in Figs. 4–9, using different line types for the different models (MCC, S-CLAY1 and S-CLAY1S). Discrete values, shown with various

Table 4. Location of Pore Pressure Probes

Pore pressure probes	$U1$	$U2$	$U3$	$U4$	$U5$	$U6$	$U7$	$U8$	$U9$	$U10$
Depth (m)	−15	−2	−3.5	−5.5	−7.5	−9.0	−12.0	−20.0	−2.0	−7.5
Distance from symmetry axis (m)	1.5	0.5	0.5	1.5	1.0	0	1.0	2.0	19	20

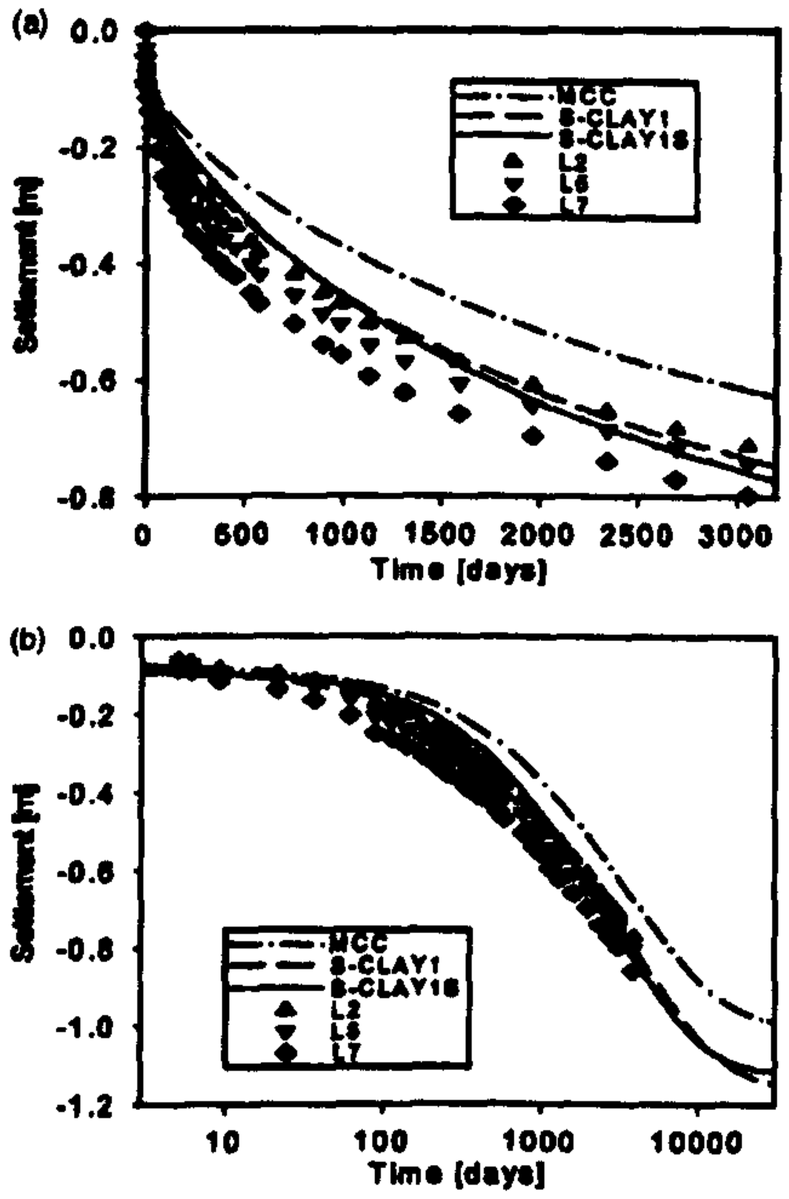

Fig. 4. Time settlement curves: (a) linear scale (for 10 years) and (b) log scale (for 100 years)

solid symbols, correspond to the field measurements, as stated in the legends of individual figures.

The observed settlements and predicted vertical displacements versus time for the node directly under the center line of the embankment are presented in Fig. 4. Fig. 4(a) shows the results with time on a linear scale. The settlement plates $L2$, $L5$, and $L7$ are all along the center line (Fig. 3), and yet Fig. 4(a) shows that they have not settled equally. The difference is about 0.1 m between $L2$ that has settled the least and $L7$ that has settled the most. Had the deposit underneath the test embankment been homogeneous, $L2$ located mid-way along the 30 m length of the embankment would be expected to settle the most. The results show, however, that $L2$ has settled the least. This could be due to small variations either in the thickness of the deposit or in the soil properties along the longitudinal section. Alternatively, it could be due to some complex three-dimensional effects that the analyzes are not accounting for. Overall, the measured settlements underneath the center line after about 10 years of consolidation vary between 0.7 and 0.8 m for this 2 m high test embankment [Fig. 4(a)].

The finite element predictions by the two anisotropic models (S-CLAY1 and S-CLAY1S) suggest similar magnitudes (about 0.75) for the 10 year vertical settlement [Fig. 4(a)]. S-CLAY1S predicts marginally higher vertical settlement than S-CLAY1, but the differences between the two model predictions are smaller that the scatter in the field measurements. The MCC model, in contrast, predicts a notably smaller 10 year vertical settlement under the center line of the embankment than the two anisotropic models, suggesting a value of around 0.6 m. The only way to improve the match of the MCC model prediction would be to assume the dry crust to be normally consolidated, which cannot be justified given the measured POP values varied from 10 to 80 kPa.

In Fig. 4(b), the results have been plotted on a semilogarithmic scale considering 100 years. The results suggest that primary consolidation is still ongoing after 10 years of consolidation (this hypothesis is supported by the measured excess pore pressures). The numerical results indicate that the average degree of consolidation is about 65% after 10 years of consolidation, if estimated based on vertical settlements. Based on the numerical analyzes it will take approximately 100 years to dissipate the excess pore water pressures completely. The final values of the primary consolidation settlement, corresponding to 100 years of consolidation, predicted by the models [Fig. 4(b)] vary from about 1 m, predicted by MCC, to about 1.15 m predicted by the S-CLAY1 model, which predicts a slightly higher final settlement than S-CLAY1S, in contrast to the 10 year predictions [see Fig. 4(a)]. The rate of destructuration is, therefore, predicted to decrease with time by the S-CLAY1S model.

All the constitutive models used ignore the effect of creep, which is a fundamental feature of soft soil behavior and the ultimate values of vertical settlement might therefore be even higher. Fig. 4 also suggests that the rate of consolidation was underpredicted by all models in the first couple of years but has been well predicted after 10 years of consolidation. This slight mismatch could be due to the constant k values assumed in the analyzes.

The predicted surface settlements are shown in Fig. 5, corresponding to a time immediately after construction [Fig. 5(a)] and after 10 years of consolidation [Fig. 5(b)]. All models predict small surface heave outside the embankment immediately after construction [Fig. 5(a)], but this is more marked for S-CLAY1 and S-CLAY1S than for MCC. The maximum vertical displacements, predicted underneath the center line, are on the order of 0.07 m (by MCC) to 0.09 m (by S-CLAY1 and S-CLAY1S) immediately after construction [Fig. 5(a)] and 0.65 m (by MCC) to about 0.77 m (by S-CLAY1S) after 10 years of consolidation [Fig. 5(b)]. Both anisotropic models are, hence, predicting higher settlements than MCC. There is a marginal difference in the predictions by the two anisotropic models immediately underneath the center line, but results are indistinguishable beyond 8 m from the symmetry axis.

As seen in Fig. 5(b), the field measurements and the numerical predictions by the two anisotropic models for the surface settlements after 10 years of consolidation are in good agreement. The measured settlements at $L1$ and $L3$ differ by less than 0.05 m and the same applies for the measurements at $L4$ and $L6$. This would suggest that the deposit is rather symmetrical along the cross section, and assuming symmetry along the center line was hence justified.

Fig. 6 shows the vertical displacements at different levels underneath the center line of the embankment against time. The model predictions are compared with the results from the extensometer, which was installed at the center line (see Fig. 3) between $L2$ and $L7$. At the time of writing, extensometer results were only available for 8 years after the construction. The measured values at 1 m depth are consistent with results from the settlement plates shown in Fig. 4(a), suggesting a vertical settlement after 8 years of the order of 0.65 m. The measurements shown in Fig. 6 indicate that most of the vertical displacements arise from compression of the normally consolidated layer (1.6–6 m beneath the ground level) and that the model predic-

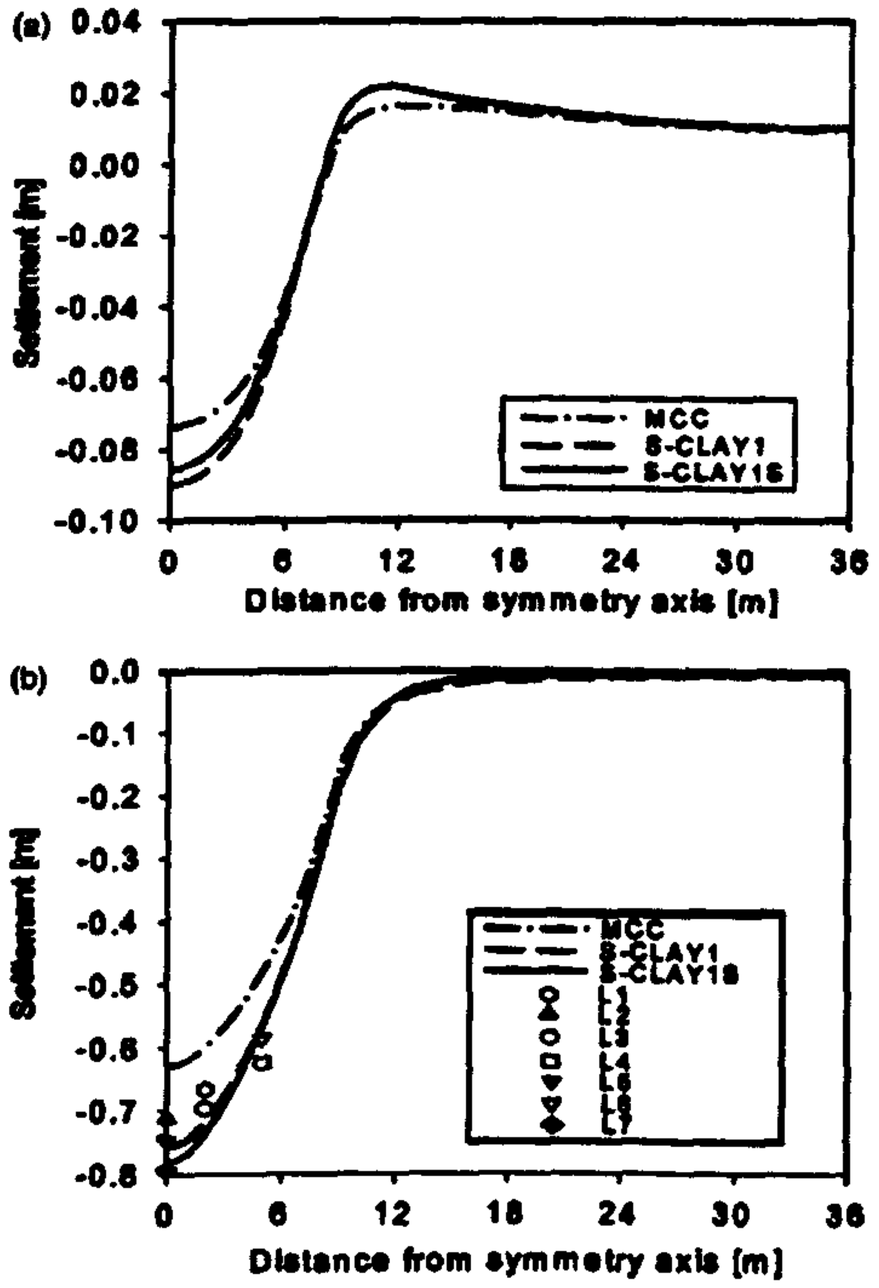

Fig. 5. Surface settlements: (a) immediately after construction and (b) after 10 years

tions within this depth range are lower than the actual observations. Thus, either the stiffness of the soil in this zone has been slightly overestimated or the vertical stresses caused by the load of the embankment are distributed in a different manner than predicted. Alternatively, the permeability of this zone in the field might be higher than assumed in the numerical analyzes. At all depths the MCC model predicts lower values of vertical displacement than the other two models, as shown by Fig. 6, and is overall in worse agreement with the field measurements than the anisotropic models.

Within the dry crust (depths −1 and −1.5 m in Fig. 6) the values of vertical displacement predicted by the anisotropic models are in excellent agreement with the field data. S-CLAY1S predicts marginally higher vertical settlements than S-CLAY1. At a depth of 2.5 m the two predictions are identical. Below that level the order changes: S-CLAY1 predicts higher settlements than S-CLAY1S. The difference between the model predictions and field measurements is greatest around 3–4 m below the surface, where the discrepancy is about 0.1 m. At a depth of 8.4 m below the surface, the numerical simulations overpredict the vertical settlements. In this case only, MCC is giving better prediction than the two anisotropic models. Overall, although the numerical simulations with the anisotropic models seem to have captured well the overall vertical displacements of the ground surface, the distribution of the vertical displacements with depth is not as well represented. Despite this, the two new models perform better than the MCC model.

Fig. 7 shows the comparison of the measured horizontal displacements (inclinometer 11 in Fig. 3) with the horizontal displacements predicted by MCC, S-CLAY1, and S-CLAY1S directly underneath the top of the embankment slope (about 4.8 m from the center line). Immediately after construction, the measured maximum horizontal displacement is about 0.042 m [Fig. 7(a)]. The measured horizontal displacements are approximately zero at 15 m depth and below. The predictions by S-CLAY1 and S-CLAY1S are much closer to the observed results than the ones predicted by the MCC model [Fig. 7(a)]. The match by the two anisotropic models is very good down to a depth of 5 m, while between 5 and 15 m depth all models seem to overpredict the horizontal displacements. The maximum displacement is predicted at the correct level, at a depth of about 2 m, by all models considered.

The results corresponding to a time of 8 years after the construction of embankment are presented in Fig. 7(b), together with the inclinometer results. Now the models that take into account plastic anisotropy overestimate the maximum horizontal displacements, by about 0.05 m, while the MCC model slightly underpredicts the maximum horizontal displacement. The measured maximum horizontal displacement is about 0.1 m and it occurs at a slightly lower level (at a depth of about 3 m) than predicted by the models (at a depth of about 2 m). S-CLAY1S predicts slightly higher horizontal displacements than S-CLAY1 up to a depth of 3 m.

The horizontal displacements directly under the toe of the embankment slope (9 m from the center line) immediately after construction and after 8 years of consolidation are shown in Figs. 8(a and b). After construction, the predicted displacements are much larger than the measured values up to a depth of 15 m [Fig. 8(a)]. Given that the MCC overall predicts lower values of horizontal displacements (and vertical settlements) than the two anisotropic models, it gives a better prediction of immediate horizontal displacements than the other two models. The maximum value measured was about 0.019 m, in contrast to the best prediction of 0.03 m (by the MCC). The maximum was predicted at a depth of about 2 m by all models, while the measured maximum was at a depth of about 5 m. Interestingly, the field measurements indicate that the dry crust initially moved horizontally as a rigid block [Fig. 8(a)].

The calculated horizontal displacements after 8 years of consolidation predicted by the S-CLAY1 and S-CLAY1S models [Fig. 8(b)] are in good agreement with the measured ones, corresponding to *I2* in Fig. 3, but the depth at which the maximum is predicted is different; the measured maximum value occurs at a depth of about 5 m, while the predicted one is at 2 m depth. Interestingly, the field measurements show negative horizontal displacements close to the ground surface underneath the toe of the embankment [Fig. 8(b)], not captured in the predictions. The former results are quite logical since the vertical deformations are so large that the surface of the soil is dragged inwards as it follows the slope of the settlement trough. The surface layer is then likely to be in tension, while the constitutive models assume zero tensile stresses. One possible cause of these interesting differences relates to representing the embankment material. Sensitivity analyzes suggested that the results are rather insensitive to the value of Young's modulus for the embankment material. Given that the problem is a soil–structure interaction problem, the friction between the soil and the embankment also plays a role. The friction angle assumed for the embankment material is rather

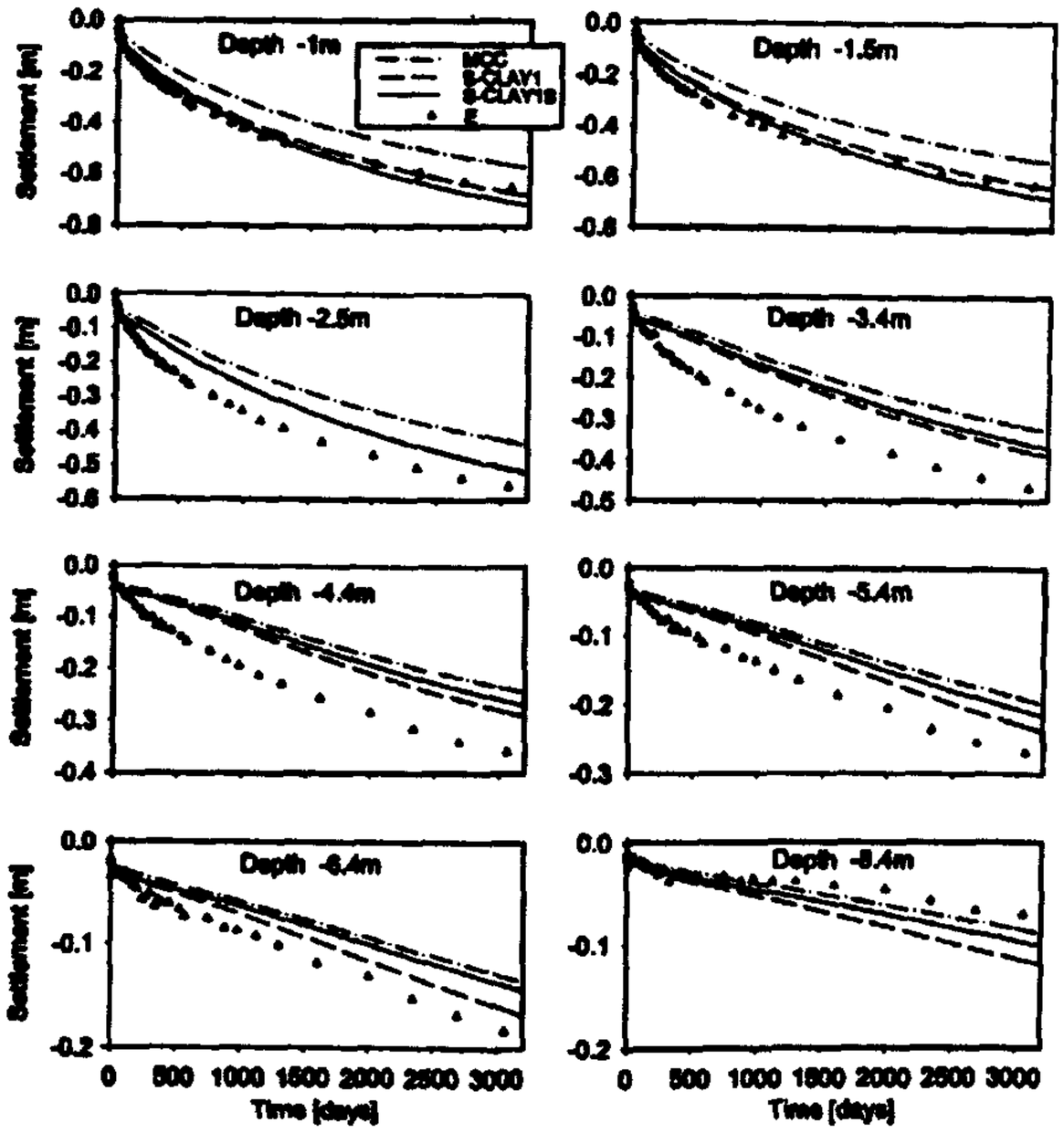

Fig. 6. Vertical displacements at different depths underneath centerline of embankment

high, and reducing this might slightly change the results. The measured behavior shown in Fig. 8(b) is, however, so extreme that it almost suggests a slippage between the embankment and the soil. Future simulations of the problem should therefore examine the influence of an interface element between the embankment and the dry crust to allow for the possibility of slippage, but then there will be the difficulty in deciding what the interface properties should be.

The predicted and measured excess pore water pressures at different locations are compared in Fig. 9. Points $U9$ and $U10$ are reference points that are outside the embankment area, at 19 and 20 m from the axis of symmetry, respectively. At these points, the

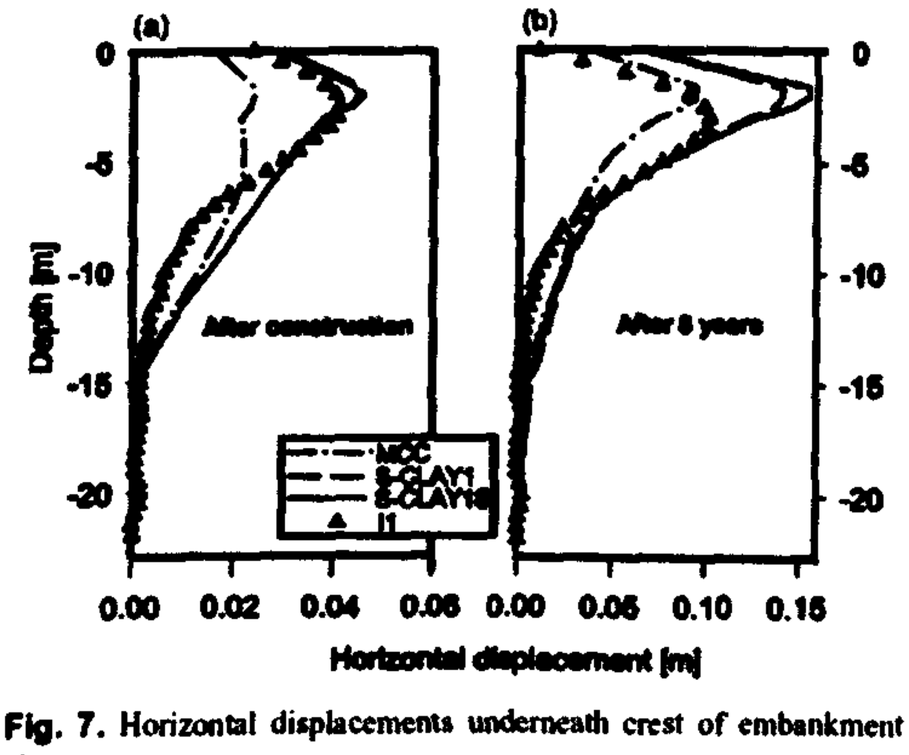

Fig. 7. Horizontal displacements underneath crest of embankment slope

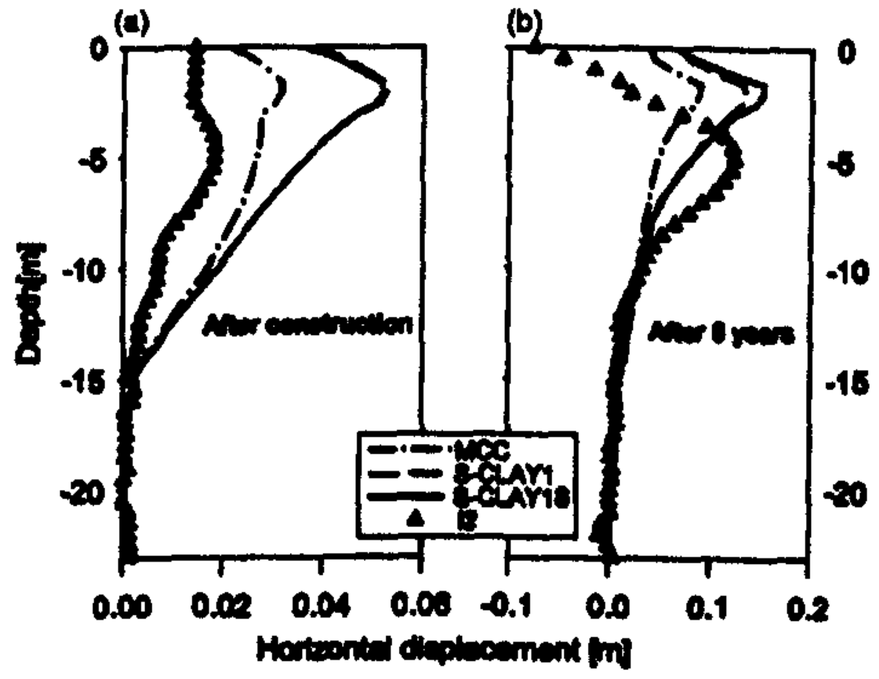

Fig. 8. Horizontal displacements underneath toe of embankment

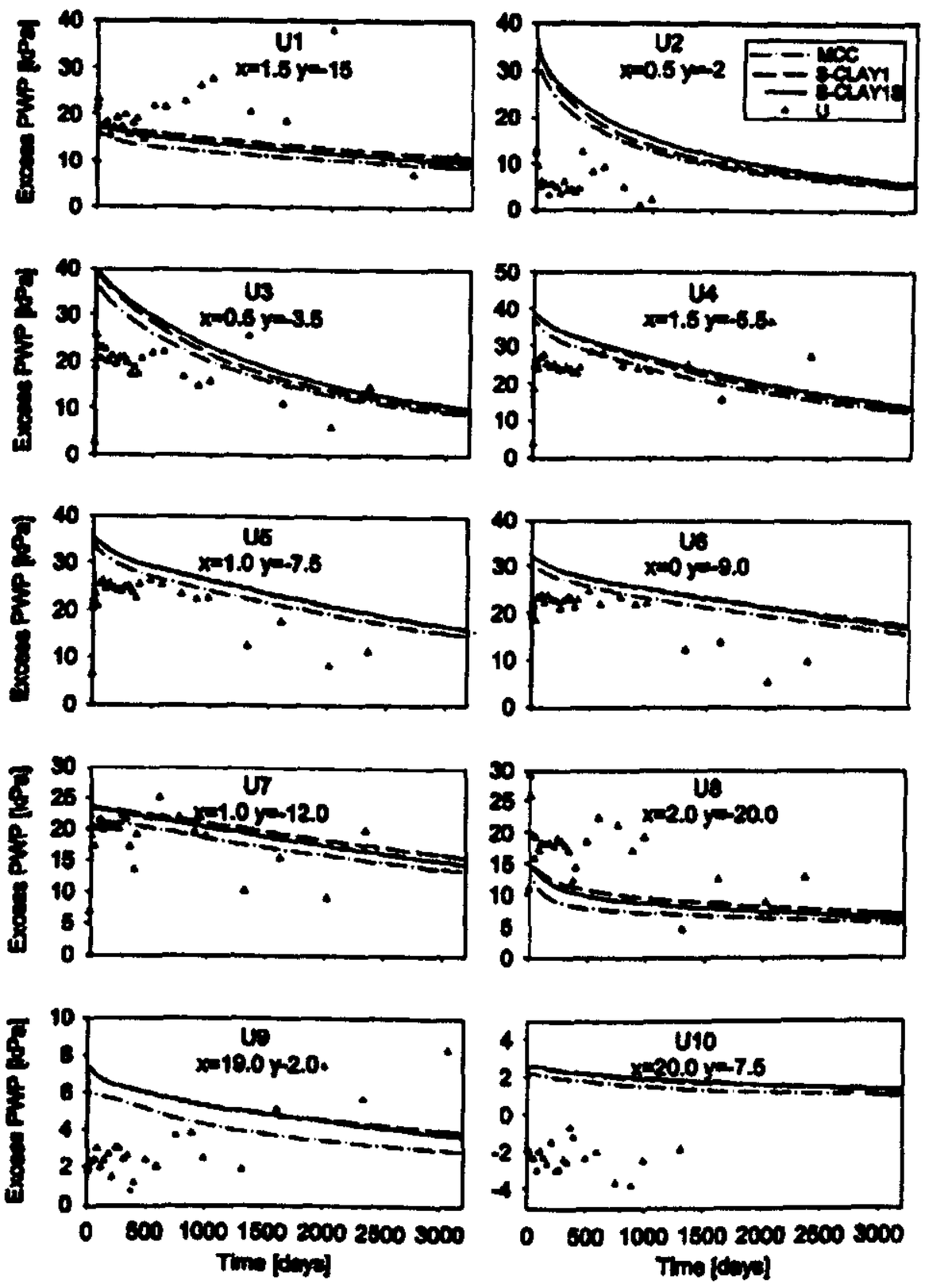

Fig. 9. Excess pore pressures at different locations [x=distance from symmetry axis (m), y=depth (m)]

measured excess pore pressures immediately after construction are small, about +2 and −2 kPa, respectively. *U*9 is suggesting an increase in the excess pore pressures with time from 2 to about 8 kPa. The predicted excess pore pressures at points *U*9 and *U*10 are notably greater than measured, but the absolute differences are about 5 kPa as a maximum, which is within the fluctuations of the measured values.

Underneath the embankment itself the predicted excess pore pressures are in general higher than the measured ones, and this is particularly marked at 2–9 m depth. At *U*2, which is located only 2 m below the ground surface (and hence very close to the actual load) and *U*3 (at y=−3.5 m), the measured excess pore pressures immediately after embankment construction are only about 15–20 kPa while the predictions by any model that assumes the soil to be saturated (with an incompressible pore fluid) would predict much higher excess pore pressures. Even if the permeability of the soil were much higher than assumed, it would not be possible to match the results. Overall, according to Fig. 9, the anisotropic models predict slightly higher excess pore pressures beneath the embankment than the MCC model. The differences between S-CLAY1 and S-CLAY1S are small. As expected, all numerical simulations show excess pore pressures gradually dissipating with time.

Although the measured excess pore pressures seem to be dissipating with time according to, e.g., *U*5 and *U*6, there have been a lot of fluctuations in the field measurements, with sudden increases and decreases on the order of tens of kiloPascals, and hence the field monitoring results need to be viewed with caution. Particularly suspicious are the results for *U*1 and *U*4 that are suggesting maximum excess pore pressures of the order of 40 kPa after 5.5 years of consolidation, in contrast to the values of about 23 and 28 kPa, respectively, measured immediately after construction. Generally, it would be difficult to estimate the average degree of consolidation based on porewater pressure measurements only. The field observations in Fig. 9, however, confirm the speculation that the primary consolidation is not yet complete, as there is still about 10–15 kPa of excess pore pressures at some layers after 8 years of consolidation.

Conclusions

Murro test embankment is a 2 m high embankment that was constructed on a 23 m thick soft clay deposit at the commission of the Finnish Road Administration in 1993. Except for a 1.6 m thick dry crust, the soft soil deposit in Murro is normally consolidated and hence very compressible. The embankment was well instrumented and has been monitored for over 10 years. The consolidation of Murro test embankment was simulated with *SAGE CRISP* finite element code using three different constitutive models. The models used were the isotropic Modified Cam Clay model (Roscoe and Burland 1968), the recently proposed S-CLAY1 model (Wheeler et al. 2003), which accounts for initial and plastic strain induced anisotropy, and its extension, the S-CLAY1S model (Koskinen et al. 2002a). The latter accounts for plastic anisotropy and interparticle bonding, as well as the degradation of the bonds due to plastic straining. The values for the parameters used in the finite element analyzes were derived using current best practice for the constitutive models adopted and were not optimized to match numerical simulations to the measured embankment behavior. Given the amount of laboratory data available, the soil constants for the advanced models could be selected with a relatively high degree of confidence.

The results of the finite element simulations were compared with the field monitoring results. Generally, the agreement between the finite element predictions using the advanced new constitutive models (S-CLAY1 and S-CLAY1S) and the field measurements is very good. The models seem to be a significant improvement compared with the MCC model. The numerical simulations demonstrate that for this particular boundary value problem ignoring the effect of anisotropy leads to underprediction of vertical displacements, and also the horizontal displacements were better predicted by the new models than by the MCC model. Considering the difficulties in estimating the coefficient of permeability in the field, the predicted time–settlement curves were in good agreement with the field observations.

The only measurements that the finite element models failed to reproduce well were the excess pore pressures, but as discussed the same would apply to any soil models that assumed the soil to be fully saturated below the water table. Furthermore, the reliability of the field measurements of pore pressures was perhaps questionable. Given that this was the first application of the two recently proposed advanced constitutive models to a real field problem, the results were encouraging. Although the analyzes presented were performed as a small strain analysis, it is expected that qualitatively the results would be similar if large strain analyzes were adopted.

The predictions by the two anisotropic models were overall very similar. Based on this study and benchmark simulations of other problems involving embankments on soft soils (Krenn et al. 2003; Wiltafsky et al. 2003), it appears that the effects of bonding and destructuration are averaged out in this type of boundary value problem. Consequently, a model that accounts only for plastic anisotropy can produce reasonable results, provided that the value for the main parameter controlling the compressibility (i.e., the apparent gradient of the normal compression line λ in $\ln p'-v$ space), is determined appropriately. In contrast to a common belief that the value of λ is a soil constant, its value for natural soils is apparently stress-ratio dependent. This stress-ratio dependence of the apparent λ value for a natural soil increases with increasing sensitivity, as demonstrated by Koskinen and Karstunen (2004) for a range of soft Scandinavian clays.

The suggestion that the effect of plastic anisotropy is more important than the effect of destructuration for the problem considered is useful from the computational point of view, because modeling of destructuration can lead to problems with nonconvergence in finite element analyzes. The reasons for this stem from the constitutive level, as the S-CLAY1S model can, for example, predict strain softening during undrained shearing of a normally consolidated sample, as shown by Zentar et al. (2002).

Modeling destructuration may, however, be important if staged construction is utilized on sensitive soft soils. The in situ testing at Murro in 2001 included a field vane test through the embankment to assess the increase in the undrained shear strength caused by 8 years of consolidation under embankment loading. These results, reported in Koskinen et al. (2002c), are rather interesting. In the top 7 m there had been an increase in the undrained shear strength due to consolidation, with a maximum increase from 7 to 17 kPa at a depth of about 4.5 m. Below the 7 m depth, however, the undrained shear strength had actually decreased from about 30 kPa to about 20 kPa. This occurred in conjunction with a significant increase in the remolded undrained strength. Overall, the sensitivity, measured with the field vane, had significantly decreased throughout the deposit. This is a clear indication of the process of gradual degradation of bonds due to plastic straining. A constitutive model that accounts for destructuration, such as S-CLAY1S, can explain these phenomena. If the assumed rate of destructuration is high, it is possible that the bonds are degrading at a higher rate than the intrinsic yield curve is expanding, and as a result the undrained shear strength of the soil may actually decrease due to consolidation. This will occur in conjunction with an increase in the remolded undrained strength. As the rate of destructuration is predicted to reduce with time, eventually there will be an apparent increase in the undrained shear strength, as indicated for the top 7 m in the case of Murro test embankment.

Prediction of deformations on soft soils is difficult and there will always be some uncertainty with regards the values of soil parameters, in particular the vertical preconsolidation stress σ'_{vp} and the permeability. Often, for the sake of simplicity simple isotropic models are adopted. Natural soils are, however, anisotropic. Given that accounting for anisotropy via S-CLAY1 model does not require any additional laboratory tests to those required for the use of an isotropic critical state model, such as the MCC model, accounting for it does not significantly increase the difficulty of performing numerical analyzes. For some problems, such as staged construction on soft sensitive soils, it is necessary to account for destructuration, in order to prevent embankment failures, which can be very costly.

The reliability of the predictions can be increased by increasing the number of boreholes and sampling locations and by investing in laboratory tests and the interpretation of the laboratory results. The application of the proposed constitutive models in an industrial environment will require development of more effective and robust algorithms than used is this work. In parallel there would be a need for advanced training to ensure the appropriate application of the models.

Acknowledgments

The work presented was carried out as a part of a Research Training Network "Soft Clay Modelling for Engineering Practice" supported by the European Community through the program "Improving the Human Research Potential and the Socio-Economic Knowledge Base." The experimental programme was funded by

the Academy of Finland (Grant Nos. 53936 and 78569) and by the Finnish Road Administration. The second author is sponsored by Donaldson Associates Ltd. (United Kingdom) and a Faculty of Engineering Scholarship at the University of Glasgow. The writers would like to thank the staff at Helsinki University of Technology, in particular, Laboratory Manager Matti Lojander, for their support. In addition, the writers would like to give credit to the staff at the Finnish Road Administration who had the foresight to finance the construction of Murro test embankment, and hence invest in fundamental geotechnical research that might, in the long term, enhance geotechnical design practice.

References

Banerjee, P. K., Kumbhojkar, A. S., and Yousif, N. B. (1988). "Finite element analysis of the stability of a vertical cut using an anisotropic soil model." *Can. Geotech. J.*, 25(1), 119–127.

Banerjee, P. K., and Yousif, N. B. (1986). "A plasticity model for the mechanical behaviour of anisotropically consolidated clay." *Int. J. Numer. Analyt. Meth. Geomech.*, 10, 521–541.

Dafalias, Y. F. (1986). "An anisotropic critical state soil plasticity model." *Mech. Res. Commun.* 13(6), 341–347.

Davies, M. C. R., and Newson, T. A. (1993). "A critical state constitutive model for anisotropic soils." *Predictive Soils Mechanics, Proc., Wroth Memorial Symp.*, G. T. Houlsby and A. N. Schofield, eds., Thomas Telford, London, 219–229.

Gajo, A., and Muir Wood, D. (2001). "A new approach to anisotropic bounding surface plasticity: General formulations and simulations of natural and reconstituted clay behaviour." *Int. J. Numer. Analyt. Meth. Geomech.*, 25, 207–241.

Gens, A., and Nova, R. (1993). "Conceptual bases for a constitutive model for bonded soils and weak rocks." *Proc., International Symp. on Hard Soils–Soft Rocks*, Athens, Greece, 485–494.

Karstunen, M., and Koskinen, M. (2004). "Anisotropy and destructuration of Murro clay." *Proc., A. W. Skempton Memorial Conf.*, R. J. Jardine, D. M. Potts, and K. G. Higgins, eds., Vol. 1, Thomas Telford, London, 476–487.

Kavvadas, M., and Amorosi, A. (2000). "A constitutive model for structured soil." *Geotechnique*, 50(3), 263–274.

Koskinen, M., and Karstunen, M. (2004). "The effect of structure on the compressibility of Finnish clays." *Proc., NGM04 (XIV Nordic Geotechnical Meeting)*, Ystad, Sweden, Vol. 1, A11–A22.

Koskinen, M., Karstunen, M., and Wheeler, S. J. (2002a). "Modelling destructuration and anisotropy of a natural soft clay." *Proc., 5th European Conf. Numerical Methods in Geotechnical Engineering*, P. Mestat, ed., Presses de l'ENPC/LCPC, Paris, 11–20.

Koskinen, M., Lojander, M., Tolla, P., and Vepsäläinen, P. (2002b). "Numerical analysis of Murro test embankment." *Proc., 5th European Conf. Numerical Methods in Geotechnical Engineering*, P. Mestat, ed., Presses de l'ENPC/LCPC, Paris, 397–402.

Koskinen, M., Vepsäläinen, P., and Lojander, M. (2002c). "Modelling of anisotropic behaviour of clays (Test embankment in Murro, Seinäjoki, Finland)." *Finnra Rep. No. 16/2002*, Finnish Road Administration, Helsinki, Finland.

Koskinen, M., Zentar, R., and Karstunen, M. (2002d). "Anisotropy of reconstituted POKO clay." *Proc., 8th International Symp. Numerical Models in Geomechanics (NUMOG) Rome*, G. N. Pande and S. Pietruszczak, eds., Balkema, Lisse, 99–105.

Krenn, H., Karstunen, M., Wheeler, S. J., and Zentar, R. (2003). "The influence of anisotropy and destructuration on an embankment on soft clay." *Proc., Int. Workshop on Geotechnics of Soft Soils—Theory and Practice*, Vermeer et al. eds., Noordwijkerhout, The Netherlands, VGE, Essen, Germany, 293–298.

Liu, M. D., and Carter, J. P. (2002). "A structured Cam Clay model." *Can. Geotech. J.* 39, 1313–1332.

Liu, M. D., Carter, J. P., and Desai, C. S. (2003). "Modeling compression behavior of structured geomaterials." *Int. J. Geomech.* 3(3/4), 191–204.

Mayne, P. W., and Kulhawy, F. H. (1982). "K_0-OCR relationship in soil." *J. Geotech. Eng. Div., Am. Soc. Civ. Eng.*, 18(6), 851–872.

Messerklinger, S., Kuhr, G., Plötze, M., Giudici, Trausch, J., Springman, S. M., and Lojander, M. (2003). "Mineralogical and mechanical behaviour of soft Finnish and Swiss clays." *Proc., International Workshop on Geotechnics of Soft Soils—Theory and Practice*, P. A. Vermeer et al., eds., Noordwijkerhout, The Netherlands, VGE, Essen, Germany, 467–472.

Nova, R. (1988). "Mathematical modelling of anisotropy of clays." *Proc., 11th ICSMFE*, San Francisco, Vol. 1, Balkema, Rotterdam, The Netherlands, 607–661.

Nova, R., Castellanza, R., and Tamagnini, C. (2003). "A constitutive model for bonded geomaterials subject to mechanical and/or chemical degradation." *Int. J. Numer. Analyt. Meth. Geomech.*, 27, 705–732.

Pestana, J. M., and Whittle, A. J. (1999). "Evaluation of a unified constitutive model for clays and sands." *Int. J. Numer. Analyt. Meth. Geomech.* 23, 1215–1243.

Roscoe, K. H., and Burland, J. B. (1968). "On the generalized stress-strain behaviour of 'wet' clay." *Engineering plasticity*, Cambridge Univ. Press, Cambridge, U.K., 553–609.

Rouainia, M., and Muir Wood, D. (2000). "A kinematic hardening constitutive model for natural clays with loss of structure." *Geotechnique*, 50(2), 153–164.

Schwab, E. F. (1976). "Bearing capacity, strength and deformation behaviour of soft organic sulphide soils." Dept. of Soil and Rock Mechanics, Royal Institute of Technology, Stockholm, Sweden.

Wheeler, S. J., Näätänen, A., Karstunen, M., and Lojander, M. (2003). "An anisotropic elasto-plastic model for soft clays." *Can. Geotech. J.*, 40(2), 403–418.

Whittle, A. J., and Kavvadas, M. J. (1994). "Formulation of MIT-E3 constitutive model for overconsolidated clays." *J. Geotech. Eng.*, 120(1), 173–198.

Wiltafsky, C., Scharinger, F., Schweiger, H. F., Krenn, H., Zentar, R., Karstunen, M., Cudny, M., Neher, H., and Vermeer, P. A. (2003). "Results from a geotechnical benchmark exercise of an embankment on soft clay." *Proc., International Workshop on Geotechnics of Soft Soils—Theory and Practice*, Noordwijkerhout, The Netherlands, VGE, Essen, Germany, 381–390.

Zentar, R., Karstunen, M., and Wheeler, S. J. (2002). "Influence of anisotropy and destructuration on undrained shearing of natural clays." *Proc., 5th European Conf. Numerical Methods in Geotechnical Engineering*, P. Mestat, ed., Presses de l'ENPC/LCPC, Paris, 21–26.

Zienkiewicz, O. C., and Pande, G. N. (1977). "Time dependent multilaminate model of rocks—A numerical study of deformation and failure of rock masses." *Int. J. Numer. Analyt. Meth. Geomech.*, 1, 219–247.

A.2 Journal paper II

INTERNATIONAL JOURNAL FOR NUMERICAL AND ANALYTICAL METHODS IN GEOMECHANICS
Int. J. Numer. Anal. Meth. Geomech., (in press)
Published online in Wiley InterScience (www.interscience.wiley.com). DOI: 10.1002/nag.507

Modelling the behaviour of an embankment on soft clay with different constitutive models

M. Karstunen[1,*,†,‡], C. Wiltafsky[2,§], H. Krenn[1,¶], F. Scharinger[3,‖] and H. F. Schweiger[3,**]

[1] *Department of Civil Engineering, University of Strathclyde, John Anderson Building, Glasgow G4 0NG, Scotland, U.K.*
[2] *Verbundplan GmbH, Branch Office Salzburg, Rainerstrasse 29, A-5020 Salzburg, Austria*
[3] *Institute for Soil Mechanics and Foundation Engineering, Computational Geomechanics Group, Graz University of Technology, Rechbauerstrasse 12, A-8010 Graz, Austria*

SUMMARY

The paper investigates the effect of constitutive models on the predicted response of a simplified benchmark problem, an embankment on soft soil. The soft soil is assumed to have the properties of POKO clay from Finland and five different constitutive models are used to model the deposit. Two of the models are isotropic models, i.e. the Modified Cam Clay model and the Soft-Soil model. The other models are recently proposed constitutive models that account for plastic anisotropy. The S-CLAY1 and S-CLAY1S models are embedded in a standard elasto-plastic framework and account for anisotropy via a rotational hardening law. In addition, the S-CLAY1S model accounts for bonding and destructuration. In contrast, the Multilaminate Model for Clay (MMC) accounts for plastic anisotropy by utilizing so-called multilaminate framework. The results of numerical simulations show that accounting for anisotropy results in notable differences in the predicted settlements and horizontal movements compared to the predictions using the isotropic models. There are also significant differences in the K_0 predictions by the different constitutive models and this has a significant impact on the results. Copyright © 2006 John Wiley & Sons, Ltd.

KEY WORDS: anisotropy; soft clay; fabric; structure; destructuration; numerical modelling; embankment

*Correspondence to: M. Karstunen, Department of Civil Engineering, University of Strathclyde, John Anderson Building, Glasgow G4 0NG, Scotland, U.K.
†E-mail: minna.karstunen@strath.ac.uk
‡Senior Lecturer.
§Geotechnical Engineer, former Research Assistant at the Institute for Soil Mechanics and Foundation Engineering, Computational Geomechanics Group, Graz University of Technology, Rechbauerstrasse 12, A-8010 Graz, Austria and the Department of Civil Engineering, Rankine Building, University of Glasgow, Glasgow G12 8LT, Scotland, U.K.
¶Research Student.
‖Research Assistant.
**Professor.

Contract/grant sponsor: EC; contract/grant numbers: HPRN-CT-1999-00049, MRTN-CT-2004-512120
Contract/grant sponsor: Donaldson Associates Ltd.
Contract/grant sponsor: Glasgow University

Received 31 March 2004
Revised 18 January 2006
Accepted 20 January 2006

1. INTRODUCTION

Building embankments and other constructions on soft natural soil deposits is still a challenge for geotechnical design. Construction on soft soils becomes increasingly important as urban areas become congested, and thus development occurs on areas that were considered unsuitable for construction just a couple of decades ago. The stress–strain behaviour of soft soils is very complex as different fundamental features of natural soil behaviour, such as anisotropy, creep and destructuration, influence the soil response to foundation loading.

A Research Training Network on Soft Clay Modelling for Engineering Practice (SCMEP) in 2000–2004, involving 5 universities in 5 European countries was funded by the EC. The research tasks of the Network covered constitutive modelling, numerical implementation and practical application. The work on constitutive modelling focused on anisotropy, destructuration and time-dependency (creep). Improved models were developed incorporating the influence of these three factors, as summarized by Wheeler *et al.* [1]. In order to ensure the possibility for widespread practical application of the constitutive models, the models were kept as simple as possible. It was also important that model parameters could be determined in a reasonably simple and robust manner, preferably from standard laboratory tests. Modelling developments were validated by experimental data from laboratory test programmes undertaken by the Network teams or published in the literature. The aim was to explore various alternative strategies and models for representing a given phenomenon. By comparing these alternatives against each other and against experimental data, the successes and limitations of different modelling approaches could be identified (see, e.g. References [1–7]). The constitutive models were implemented in commercially available finite element programs and then applied, in conjunction with conventional constitutive models, for modelling both simplified 'benchmark' boundary value problems [8,9] and real case histories [10,11]. The intention was to demonstrate the improved modelling capabilities and the practical implications for analysis and design of geotechnical structures in soft clays.

The aim of this paper is to show some of these results by simulating the construction and consolidation of an embankment on soft clay, using five different constitutive models. Two of the constitutive models are commonly used isotropic elasto-plastic models. In addition, the problem is simulated with three recently proposed constitutive models that account for plastic anisotropy. The S-CLAY1 model [4] and the S-CLAY1S model [3,11] are embedded in the standard elasto-plastic framework, and account for plastic-strain-induced anisotropy (S-CLAY1) and anisotropy combined with destructuration (S-CLAY1S). In contrast, the Multilaminate Model for Clay [6] referred to as the MMC model, accounts for plastic strain anisotropy within so-called multilaminate framework, following the ideas of Pande and his coworkers (see, e.g. Reference [12]).

First, a brief description of the constitutive models is given followed by the benchmark specification. The subsoil is modelled by using a characteristic set of parameters representing a soft Finnish clay, called POKO clay [3,13]. All models have been implemented into PLAXIS 2D Version 8.2 finite element code as user-defined soil models. The simulations aim to compare the overall response predicted by the advanced models to the results obtained using the isotropic models that are often employed in practice.

2. CONSTITUTIVE MODELS

2.1. Background and terminology

The 'structure' of a natural soil according to Burland [14] consists of two parts: the 'fabric' and the bonding between particles. The fabric refers to the spatial arrangement of soil particles and inter-particle contacts [14]. Natural soft clays tend to have significant anisotropy of fabric, developed during deposition and one-dimensional consolidation, which demonstrates as an apparent inclination of the yield surface in the p'–q-plane (where p' is the mean effective stress and q the deviatoric stress), as shown, e.g. by Diaz Rodriguez *et al.* [15] for many natural soils. During subsequent plastic straining, due to re-orientation of particles and changes in particle contacts, the fabric anisotropy can change (see, e.g. Reference [4]). Anisotropy can influence both elastic behaviour and plastic behaviour. For normally consolidated or lightly overconsolidated soft clays, plastic deformations are likely to dominate for many problems, such as the embankment loading considered in this paper. Hence, only plastic anisotropy will be considered in the following discussion.

Some of the earliest suggestions for considering both initial and plastic-strain-induced anisotropy of clays using the standard elasto-plastic framework were put forward by Nova [16] and Dafalias [17]. In this framework constitutive models that account for anisotropy incorporate hardening laws that describe, as a function of plastic strains, either the change in the orientation of the yield surface, referred to as a rotational or distortional hardening law (e.g. Reference [17]), or a shift of the centre of the yield surface in stress space via a translational (kinematic) hardening law (e.g. Reference [18]).

An alternative to the standard elasto-plastic framework is to describe anisotropy via the so-called multilaminate framework. The multilaminate framework was introduced for rocks by Zienkiewicz and Pande [19] and further extended to clays by Pande and Sharma [12] and Pietruszczak and Pande [20]. In multilaminate framework each stress integration point is associated with a certain number of sampling planes at different orientations. The elasto-plastic stress–strain relations are formulated locally on the planes (at the microscopic level). The global strains are obtained by numerical integration of the inelastic contribution from each sampling plane and the global elastic contribution. MMC [6] is an elasto-plastic constitutive model that has been embedded in the multilaminate framework.

In addition to anisotropy, natural soft soils exhibit bonding between particles. These bonds can be progressively destroyed during straining. Leroueil *et al.* [21] call the process 'destructuration'. The term destructuration is now often limited to describe the progressive damage to bonding during plastic straining, and this is the sense in which the word is used here. The presence of inter-particle bonding, demonstrated, e.g. by sensitivity in many natural clays, provides soil with additional resistance to yielding. As a consequence, oedometer tests on natural soils generally show compression curves that plot above the so-called 'intrinsic compression line' for the reconstituted material, with the post-yield compression curve for the natural soil gradually converging with the intrinsic compression line as bonding is progressively destroyed during plastic straining (see Figure 1, where v is specific volume and σ'_v is the vertical effective stress). The influence of bonding and destructuration is apparent in most natural geological materials, from soft clays to weak rocks [22].

Gens and Nova [23] were the first to suggest a general framework for incorporating bonding and destructuration within elasto-plastic constitutive models. In addition to the yield surface for

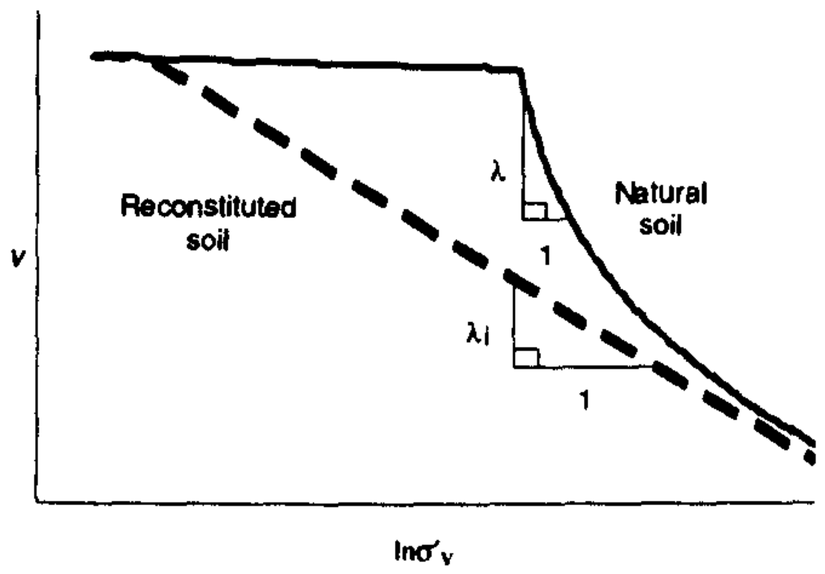

Figure 1. Oedometer curves for natural and reconstituted soil.

the natural material (with bonding), a notional 'intrinsic yield surface' is introduced, to represent the size that the yield surface would have if there were no bonding. The difference in the sizes of the yield surfaces (expressed either as a ratio or as a difference) is a measure of the amount of bonding. The increase in the size of the intrinsic yield surface is related to plastic strain increments by a conventional hardening law for unbonded (reconstituted) soil, while the reduction of bonding is related to plastic strain increments by a destructuration law.

In recent years, a number of elasto-plastic constitutive models incorporating bonding and destructuration have been published (see, e.g. References [24–29]). The various models differ in the precise form of destructuration law and in the form of the underlying reference model used for the unbonded (intrinsic) material. Several of the models involve no anisotropy due to plastic strains, although this is essential for soft clays. The S-CLAY1S model [3,11] adopted in this paper incorporates bonding and destructuration within the anisotropic S-CLAY1 model.

2.2. Isotropic models

The isotropic elasto-plastic models that have been used include the Modified Cam Clay (MCC) model [30] and the so-called Soft-Soil model implemented in the commercial version of PLAXIS 2D Version 8 finite element code [31]. The latter is a modification of the MCC model with a yield surface that can be presented in p'–q-space as shown in Figure 2. The shape of the yield surface of the Soft-Soil model is defined by soil constants c' (effective cohesion), φ' (effective friction angle) and M^*. The latter constant, M^*, is a parameter that defines the shape of the yield surface. For the case of triaxial compression the value for M^* can be calculated from the value of K_0^{NC} (the coefficient of lateral earth pressure in the normally consolidated condition) entered by the user according to equation

$$M^* = 3\sqrt{\frac{(1-K_0^{NC})^2}{(1+2^*K_0^{NC})} + \frac{(1-K_0^{NC})(1-2\nu')(\lambda^*/\kappa^*-1)}{(1+2K_0^{NC})(1-2\nu')\lambda^*/\kappa^* - (1-K_0^{NC})(1+\nu')}} \tag{1}$$

where λ^* and κ^* are the so-called modified compression indices (see below) and ν' is the Poisson's ratio (for details on the derivation of Equation (1) see Reference [32]). The size of

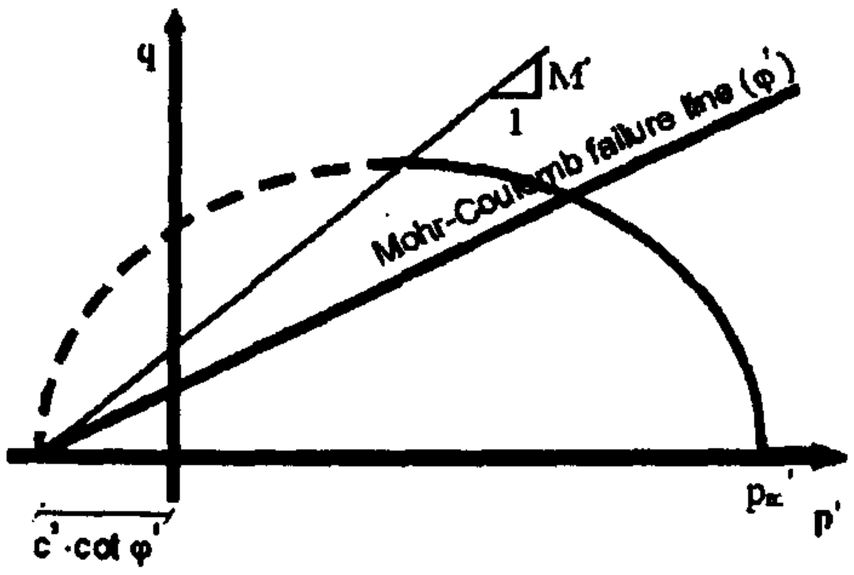

Figure 2. The Soft-Soil model.

the yield surface is defined by the state parameter p'_m in Figure 2, which can be evaluated based on the vertical preconsolidation stress. The failure surface of the Soft-Soil model is defined by a Mohr Coulomb failure criterion, with a non-associated flow rule, in contrast to the Drucker–Prager criterion of the MCC model, and the cap surface of the Soft-Soil model also has a hexagonal projection in the π -plane. Unlike in MCC, the yield surface of the Soft-Soil model is totally independent of the failure surface. On the cap surface, the flow rule is associated.

A feature of the Soft-Soil model is that the user can directly influence the K_0 prediction of the model (and hence indirectly, via Equation (1), define the shape of the yield surface). By entering a value of K_0^{NC} that approximates the value predicted by the MCC model and setting the value of c' to zero, the yield surfaces of the Soft-Soil model and MCC approximately coincide in the p'–q-plane for triaxial compression. In the model simulations (Section 4) this version of the Soft-Soil model will be referred to as the SS1 model. It is generally recognized, however, that the MCC model gives a poor prediction of the normally consolidated K_0 value. Therefore, for practical boundary value problems it is advisable to give a realistic K_0^{NC}-value, calculated, e.g. by using Jaky's simplified formula ($K_0^{NC} = 1 - \sin\varphi'$), as the input for the Soft-Soil model. In this case the line defining the apex of the cap (M^*-line in Figure 2) is above the Mohr Coulomb failure line. This version of the model will be referred to in the following as the SS2 model. Consequently, the difference between SS1 and SS2 is simply the shape of the initial yield curve, resulting from different values of M^*.

The MCC and Soft-Soil models also differ in the way they model the behaviour on the left side of the critical state line/failure line (so-called 'dry side' in the MCC model). MCC predicts quite notable strain softening on the dry side, whilst in the Soft-Soil model the behaviour is controlled by the Mohr Coulomb failure surface and is, therefore, perfectly plastic. This difference is, however, not particularly relevant for the simulations presented. In addition, the MCC model and the Soft-Soil model differ in terms of their compression relationships. In the MCC model the compression relationships are defined via parameters λ and κ, representing the slopes of the normal compression line and the swelling line in the $\ln p'$–v-plane (where v is the specific volume). In contrast, the Soft-Clay model uses the so-called modified compression

indices λ^* and κ^*, defined in $\ln p'$–ε_v-plane (where ε_v is the volumetric strain). Due to these minor differences, it is not possible to exactly match the MCC and Soft-Soil models. In the model simulations in Section 4, both the SS1 and SS2 versions of the Soft-Soil model are used to demonstrate the implications of the K_0^{NC} prediction (and the shape of the yield surface). The results are compared with the corresponding MCC model simulation.

2.3. The S-CLAY models

The S-CLAY1S model is an extension of the conventional critical state models, with anisotropy of plastic behaviour represented through an inclined yield surface and a hardening law to model the development or erasure of fabric anisotropy during plastic straining. Additionally, the model accounts for destructuration. The yield surface is defined as

$$f = \tfrac{3}{2}[\{\underline{\sigma}_d - p'\underline{\alpha}_d\}^{\mathrm{T}}\{\underline{\sigma}_d - p'\underline{\alpha}_d\}] - [M^2 - \tfrac{3}{2}\{\underline{\alpha}_d\}^{\mathrm{T}}\{\underline{\alpha}_d\}](p'_m - p')p' = 0 \tag{2}$$

where $\underline{\sigma}_d$ is the deviatoric stress tensor and $\underline{\alpha}_d$ is a deviatoric fabric tensor (a dimensionless second-order tensor that is defined analogously to the deviatoric stress tensor, see Reference [4] for details), M is the value of the stress ratio at critical state and p'_m defines the size of the yield surface of the natural clay. Equation (2) shows that the generalized version of the yield surface cannot be expressed solely in terms of stress invariants. Figure 3(a) illustrates the shape of the S-CLAY1S yield surface in three-dimensional stress space, for the case where the principal axes of both the stress tensor and the fabric tensor coincide with the x, y and z directions.

Within the yield surface there is a notional 'intrinsic yield surface' for the equivalent unbonded soil at the same void ratio and with the same fabric, which is assumed to be of the same shape and orientation as the real yield surface, but smaller in size. The size of the intrinsic yield surface is specified by a parameter p'_{mi}, and this is related to the size p'_m of the yield surface for the natural soil by a parameter x, defining the current degree of bonding:

$$p'_m = (1 + x)p'_{mi} \tag{3}$$

For the simplified conditions of a triaxial test on a previously one-dimensionally consolidated sample, it can be assumed that the horizontal plane in the triaxial sample coincides with the plane of isotropy of the sample. In this special case, the fabric tensor can be replaced by a scalar parameter α defined as

$$\alpha^2 = \tfrac{3}{2}\{\underline{\alpha}_d\}^{\mathrm{T}}\{\underline{\alpha}_d\} \tag{4}$$

which is a measure of the degree of plastic anisotropy of the soil. The yield curves of the S-CLAY1S model can then be visualized by Figure 3(b). For the sake of simplicity, the S-CLAY1S model assumes isotropic elastic behaviour, of the same form as in the conventional MCC model [30], and an associated flow rule.

S-CLAY1S incorporates three hardening laws. The first of these relates the change in the size of the intrinsic yield surface to the plastic volumetric strain increment $d\varepsilon_v^p$:

$$dp'_{mi} = \frac{vp'_{mi}}{\lambda_i - \kappa} d\varepsilon_v^p \tag{5}$$

where λ_i is the gradient of the intrinsic normal compression line (for a reconstituted soil) in the $\ln p'$–v-plane. Equation (5) is of the same form as the equivalent hardening law in S-CLAY1, but with p'_m replaced by p'_{mi} and λ replaced by λ_i.

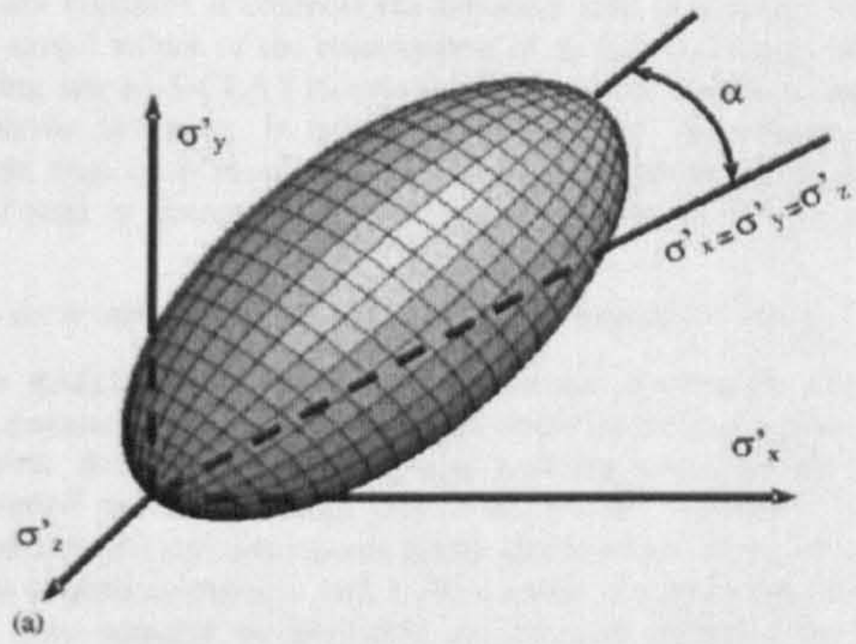

Figure 3. S-CLAY1S yield surface: (a) three-dimensional stress space (for $\tau_{xy} = \tau_{yz} = \tau_{zx} = 0$ and $\alpha_{xy} = \alpha_{yz} = \alpha_{zx} = 0$); and (b) triaxial stress space (for $\sigma'_x = \sigma'_z$, $\tau_{xy} = \tau_{yz} = \tau_{zx} = 0$, $\alpha_x = \alpha_z$ and $\alpha_{xy} = \alpha_{yz} = \alpha_{zx} = 0$).

The second hardening law (the rotational hardening law) describes the change of orientation of the yield surface with plastic straining (see Reference [4] for details):

$$d\alpha_d = \mu\left(\left[\frac{3\eta}{4} - \alpha_d\right]\langle d\varepsilon_v^p\rangle + \beta\left[\frac{\eta}{3} - \alpha_d\right]d\varepsilon_d^p\right) \tag{6}$$

where $\eta = \alpha_d/p'$, $d\varepsilon_d^p$ is the increment of plastic deviatoric strain and μ and β are additional soil constants. The soil constant β controls the relative effectiveness of plastic shear strains and plastic volumetric strains in setting the overall instantaneous target values for the components

of α_d, whereas the soil constant μ controls the absolute rate of rotation of the yield surface towards the current target values of the components of α_d (see Reference [4] for details.)

The third hardening law in S-CLAY1S (the destructuration law) describes the degradation of bonding with plastic straining. It is similar in form to the rotational hardening law (Equation (6)), except that both plastic volumetric strains and plastic shear strains (whether positive or negative) tend to decrease the value of the bonding parameter x towards a target value of zero:

$$\mathrm{d}x = a\langle[0 - x]\rangle|\mathrm{d}\varepsilon_v^p| + b\langle[0 - x]\rangle\mathrm{d}\varepsilon_d^p) = -ax(|\mathrm{d}\varepsilon_v^p| + b\mathrm{d}\varepsilon_d^p) \tag{7}$$

where a and b are additional soil constants. Parameter a controls the absolute rate of destructuration and parameter b controls the relative effectiveness of plastic deviatoric strains and plastic volumetric strains in destroying the bonding (see Reference [3] for details). Theoretically, as pointed out in Reference [33], a monotonic reduction in x implied by the hardening law (Equation (7)) can sometimes result in reduction of p'_m during hardening for certain combinations of parameters a, b and x. As a result, the peak undrained shear strength of the natural soil may actually be predicted to decrease during consolidation. There is field evidence for such behaviour on a moderately sensitive Finnish clay, as discussed in Reference [11].

By setting the initial value of the state parameter x to zero and using an apparent value of λ (determined from an oedometer test on a natural clay sample), instead of the intrinsic value λ_i of a reconstituted clay, S-CLAY1S reduces to the S-CLAY1 model that accounts for plastic anisotropy only. Furthermore, if in addition the initial value of the state parameter α (used for calculating the initial values of the components of the fabric tensor) and the value of the soil constant μ are set to zero, the model ultimately reduces to the isotropic MCC model.

The determination of the values for the state parameters and the soil constants in the S-CLAY1 model is straightforward, as described in Reference [4] and does not require any non-standard laboratory tests. For S-CLAY1S model, however, additionally an oedometer test on a reconstituted sample is needed to define the value of λ_i and a measure of sensitivity is required to estimate the initial values of x (see Reference [3] for details). For soil constants a and b, optimization simulations for a number of soft Finnish clays suggest that default values of $a = 9$ and $b = 0.2$ can often be adopted (see, e.g. References [3,7]).

The S-CLAY1 model shows excellent agreement with experimental data on several different reconstituted soils, as shown in References [3,7], and the discrepancies in simulating the behaviour of natural clays can be attributed to the effect of destructuration. S-CLAY1S has been shown to overcome some of these discrepancies and gives a reasonable representation of the stress–strain behaviour of natural clays (see References [3,7,34]).

2.4. Multilaminate Model for Clay (MMC)

The multilaminate framework, introduced for rocks by Zienkiewicz and Pande [19], was extended for clays by Pande and Sharma [12]. A formulation that enables the use of multilaminate models in combination with an elasto-plastic tangential stiffness algorithm was first presented by Pietruszczak and Pande [20]. Within the multilaminate framework each stress integration point is associated with a certain number of sampling planes at different orientations. The normal effective stress σ'_n and shear stress τ on each sampling plane are derived from the global stress tensor by a stress transformation. The stress–strain relations are formulated

locally on the planes (at the microscopic level), except for the elastic part, which is calculated at the global or macroscopic level. The global strains are obtained by numerical integration of the inelastic contribution from each sampling plane and the global elastic contribution.

When a soil element is subjected to an isotropic global stress state, the stresses on all sampling planes are identical, and therefore, the yield curves on all planes are of the same size. An anisotropic global stress state will, however, produce different combinations of σ'_n and τ on the different sampling planes, and hence an anisotropic stress history results in different sizes of yield curves on the different planes. This leads to apparent anisotropy in terms of global yield stresses, and anisotropy of the predicted stress–strain behaviour of the soil. If the anisotropy of the global stress state subsequently applied differs from the anisotropy of the previous stress state, yielding will not occur simultaneously on all sampling planes. Instead, yielding will occur progressively on an increasing number of planes, as the applied stress is increased. During this process, the anisotropy will gradually change.

In the MMC model [6], the yield curve is based on the double hardening formulation proposed by Vermeer [35]. The formulation is described in detail in Reference [6], but a brief description is included here. The yield curve in the σ'_n–τ-plane, shown in Figure 4, consists of three parts: an elliptical volumetric hardening section (f_c), a deviatoric hardening section (f) and a tension cut-off (f_t).

The equation of the elliptical 'cap' section of the yield curve is given by

$$f_c = \left(\frac{\sigma'_n}{\sigma'_{nc}}\right)^2 + \left(\frac{\tau}{M_\alpha \sigma'_{nc}}\right)^2 - 1 = 0 \tag{8}$$

where the normal preconsolidation stress σ'_{nc} defines the current size of the yield curve (see Figure 4) and the soil constant M_α defines the aspect ratio of the yield curve, and thus influences the predicted global K_0-value. M_α is not the same as the critical state stress ratio M. The value of M_α is calculated from

$$M_\alpha = \alpha(\tan\varphi') \tag{9}$$

where α is a material constant, taken as $\alpha \approx 1 - \sin(\frac{3}{5}\varphi')$ for normally consolidated clays (see Reference [6] for details). (Note: The parameter α in MMC should not be confused with the scalar α in the S-CLAY1S model.)

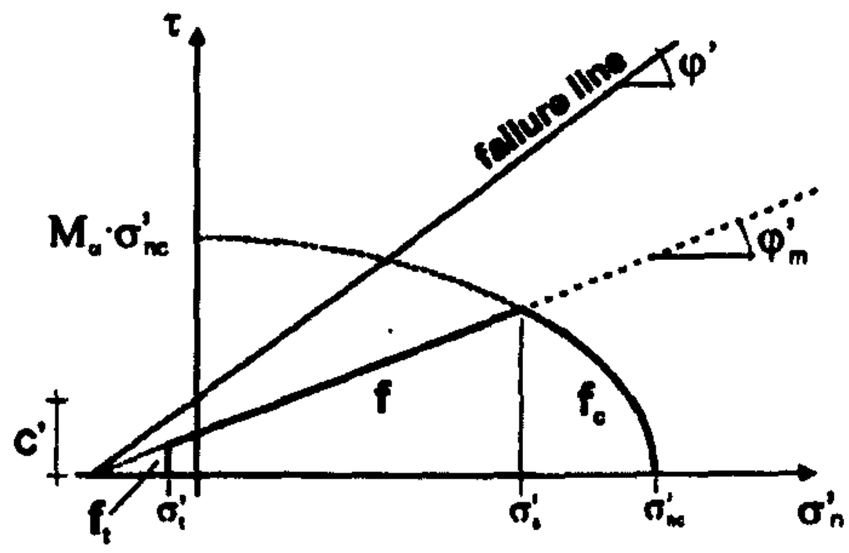

Figure 4. The yield surface of Multilaminate Model for Clay (MMC) on a sampling plane.

The hardening of the cap section of the yield curve is related solely to $d\varepsilon^{p}_{n,cap}$ (the increment of plastic normal strain on the sampling plane) in a relationship analogous to Equation (5):

$$d\sigma'_{mc} = \frac{v\sigma'_{mc} d\varepsilon^{p}_{n,cap}}{\lambda - \kappa} \tag{10}$$

For yielding on the cap section of the curve, an associated flow rule is used.

The equation of the deviatoric hardening section of the yield curve is given by

$$f = \tau - \sigma'_n \tan\varphi'_m - \frac{c' \tan\varphi'_m}{\tan\varphi'} = 0 \tag{11}$$

where φ'_m is the mobilized friction angle (a hardening parameter), c' is the cohesion and φ' is the friction angle at failure (see Figure 4). Hardening of this deviatoric section of the yield curve is related solely to $d\varepsilon^{p}_{s,cone}$ (the plastic shear strain on the sampling plane) according to

$$d(\tan\varphi'_m) = \frac{(\tan\varphi' - \tan\varphi'_m)^2}{A \tan\varphi'} d\varepsilon^{p}_{s,cone} \tag{12}$$

where A is a soil constant controlling the rate of deviatoric hardening of the cone. Plastic flow on the deviatoric hardening section of the yield curve is governed by a non-associated flow rule (see Reference [6]), using a mobilized dilation angle ψ'_m, based on the stress-dilatancy theory of Rowe [36]. This ensures that the dilatant behaviour is gradually mobilized with increasing shear strains. It differs from the original formulation in the sense that it is formulated on each contact plane rather than globally.

The third part of the yield curve provides a tension cut-off criterion and for this part of the yield curve an associated flow rule is assumed. The elastic behaviour is modelled globally, rather than locally at sampling plane level, and is assumed to be the same as in the MCC model.

The values for the input parameters of the MMC are derived in conventional manner, with the exception of parameter A, which is found by optimizing model simulations with the experimental data on triaxial compression tests to failure. Comparisons between MMC and experimental tests have been presented in References [2,6,37], albeit the validation has not been as comprehensive as for the S-CLAY-models. The results of the MMC simulations so far suggest a similar quality of match to the experimental data as S-CLAY1.

2.5. Model simulations

In order to investigate the influences of anisotropy and destructuration in the context of typical geotechnical problems, several boundary value problems (embankment, excavation and tunnel) were simulated with different constitutive models as a part of collaboration within the SCMEP network (see, e.g. References [8,9,11]). The biggest differences were predicted for the case of an embankment, which is a case where plastic straining dominates the stress–strain behaviour. Some differences could also be attributed to differences in finite element codes: in Reference [11] the MMC simulations used PLAXIS 2D Version 8.2, whilst the simulations with S-CLAY1 models (and MCC) used an implementation in SAGE CRISP. Hence, to eliminate any non-model-dependent differences, for the problem analysed in this paper (Benchmark Embankment) model implementations in PLAXIS 2D Version 8.2 are used. The specification is slightly modified from the one presented in Reference [8] to eliminate some inconsistencies in representing the initial state.

3. BENCHMARK EMBANKMENT

3.1. Numerical model

The geometry of the embankment is shown in Figure 5. The groundwater table is located 2 m below the ground surface. Drained conditions and zero initial pore pressures are assumed above the water table. The domain to be analysed (under plane strain conditions) has an extent of 60 m in the horizontal direction from the symmetry axis and 36 m in the vertical direction. The lateral boundaries are restrained horizontally, and the bottom boundary is restrained in both directions. Drainage boundaries are assumed to be at the level of the water table and at the bottom of the mesh. Due to symmetry, only half of the embankment is represented in the finite element mesh.

First, the embankment loading is applied under undrained conditions, assuming the embankment and the soil above the water table to be drained materials. Next, a consolidation phase is simulated via fully coupled static consolidation analyses. A mesh with 629 six-noded triangular elements has been used in all analyses, with extra degrees of freedom for excess pore pressures at corner nodes. Mesh sensitivity studies were done to confirm that the mesh was dense enough to give accurate results for all of the constitutive models concerned. The problem was modelled using small strain analyses, because large strain analyses, performed with some of the models, gave only marginal differences in the results.

3.2. Input values and comments about implementation

The embankment, assumed to be made of granular fill, was modelled with a simple Mohr Coulomb model assuming the following material parameters: $E' = 40\,000\,\mathrm{kN/m^2}$, $\nu' = 0.3$,

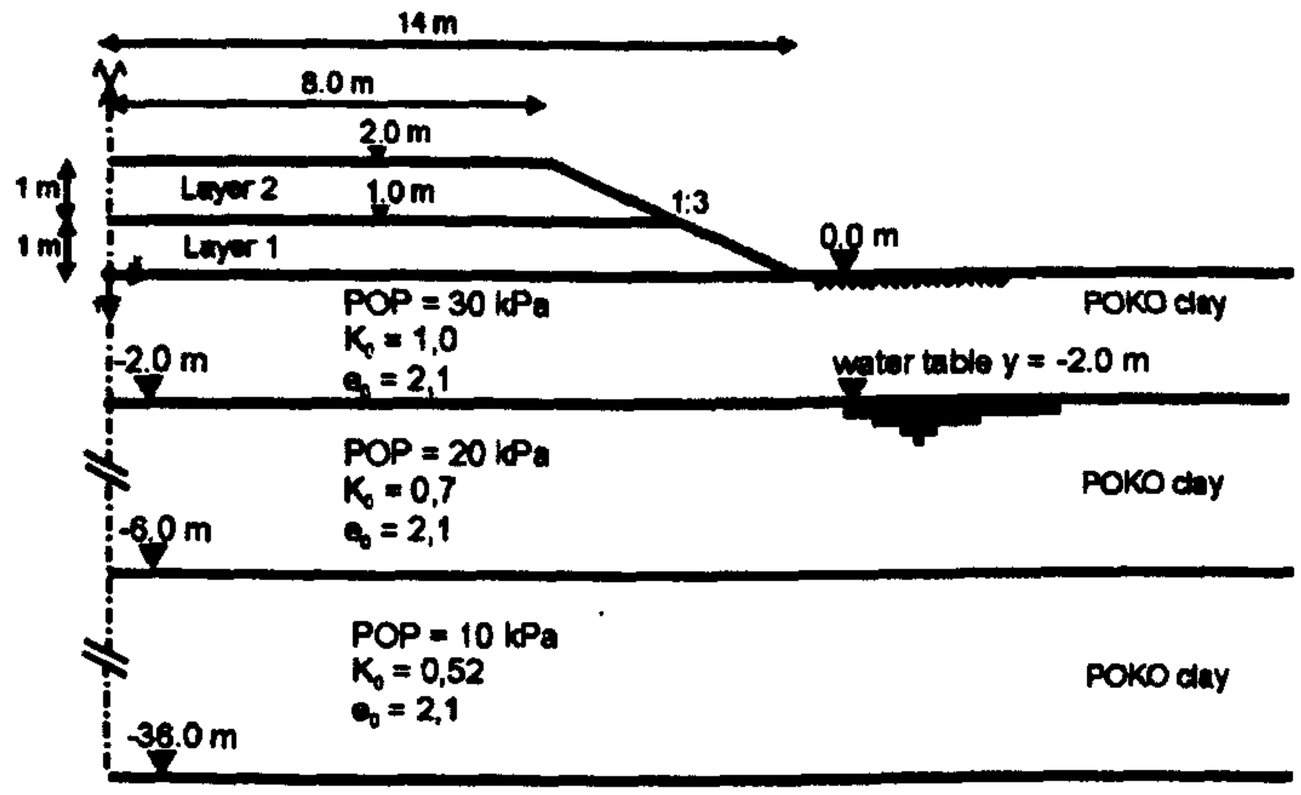

Figure 5. Geometry of Benchmark Embankment and assumed soil profile.

$\varphi' = 38°$, $\psi' = 0°$, $c' = 1\,\text{kN/m}^2$ and $\gamma = 20\,\text{kN/m}^3$, where E' is the Young's modulus, ν' is the Poisson's ratio, ψ' is the dilatancy angle and γ is the unit weight of the embankment material. The problem is dominated by the soft soil response and is hence rather insensitive to the embankment parameters.

The soft soil profile corresponds to the so-called POKO clay [3,13]. The abbreviation POKO stands for Porvoo-Koskenkylä, a 25 km long section of motorway construction near the medieval town of Porvoo, in Finland. For the benchmark simulations the deposit was idealized by using a single set of soil parameters throughout the deposit with an overconsolidation profile that approximates the conditions at the site. The deposit was modelled as a lightly overconsolidated soft clay with vertical pre-overburden pressure (POP) values and *in situ* K_0 values varying with the depth as shown in Figure 5. The vertical POP is defined as $\text{POP} = \sigma'_p - \sigma'_{v0}$ (where σ'_{v0} and σ'_p are, respectively, the *in situ* value and maximum past value of the vertical effective stress). The *in situ* stresses were estimated assuming a bulk unit weight of $15\,\text{kN/m}^3$ and the K_0 values given in Figure 5. Consequently, all model simulations have identical initial state. Because it is not possible to enter continuous distributions of POP and K_0 in PLAXIS, the assumed initial state will cause some discontinuities in the predicted local response, but as this applies equally to all models, the results are comparable. The symbol e_0 in Figure 5 stands for the initial void ratio, which has been (for simplicity) assumed to be constant with depth. Void ratio is a state variable in all models used, with the exception of the Soft-Soil models (SS1 and SS2). The permeability of the soil was assumed to be 10^{-9} m/s in both vertical and horizontal directions for all analyses.

The values of the input parameters and additional state variables for the different models are shown in Tables I–III. The values have been determined systematically from the same set of laboratory data, namely oedometer and triaxial tests on natural and reconstituted POKO clay [3,13]. Table I gives the input values for the Soft Soil models: for the SS1 model a K_0^{NC} value that corresponds to the MCC model has been given (to best match the MCC model), in contrast to the value corresponding to Jaky's simplified formula that has been assumed for the SS2 model. Based on the K_0^{NC} values, the values for M^* are calculated within the code using Equation (1), resulting in different shapes of the yield surface in the two cases, as discussed in Section 2.

For the S-CLAY1 and S-CLAY1S models (Table II) the values for the initial inclination α_{K0} of the yield surface and parameter β were determined by following the procedure described in Reference [4], using K_0^{NC} values corresponding to Jaky's simplified formula. Hence, the SS2 model and the S-CLAY models should predict approximately the same value of K_0 during plastic loading. Based on the α_{K0} value, the components of the fabric tensor are calculated within the code assuming initially cross anisotropy in the horizontal plane. This assumption is valid for the initial state of normally consolidated or lightly overconsolidated deposits with one-dimensional consolidation history, which has resulted with approximately horizontal soil layers. (Due to rotation of principal stress axis caused by the embankment loading, the orientation of the stresses and fabric are no longer predicted to coincide in some stress points during the

Table I. Input parameters and initial state for the Soft Soil models.

Model	λ^*	κ^*	ν'	c' (kPa)	φ' (°)	ψ' (°)	K_0^{NC}
SS 1	0.24	0.01	0.2	0	30	0	0.67
SS 2	0.24	0.01	0.2	0	30	0	0.5

Table II. Input parameters and initial state for MCC, S-CLAY1 and S-CLAY1S.

Model	λ (or λ_i)	κ	ν'	M	μ	β	a	b	e_0	α_{K0}	x_0
MCC	0.71	0.03	0.2	1.2	—	—	—	—	2.1	—	—
S-CLAY1	0.71	0.03	0.2	1.2	20	0.76	—	—	2.1	0.46	—
S-CLAY1S	0.26	0.03	0.2	1.2	20	0.76	9	0.2	2.1	0.46	12

Table III. Input parameters and initial state for the MMC model.

Model	λ	κ	ν'	c' (kPa)	φ' (°)	ψ' (°)	α	A	e_0
MMC	0.71	0.03	0.2	0	30	0	0.67	0.015	2.1

analyses.) The initial value for x_0 was estimated based on sensitivity, as suggested in Reference [3], and for soil constants μ, a and b typical values for POKO clay have been assumed.

Finally, the input values for the MMC model are shown in Table III. The value for A was found by optimizing simulations of drained triaxial shear tests on POKO clay. The initial anisotropic state of the soil is represented by application of an anisotropic stress state (corresponding to previous K_0 consolidation) globally and calculating the resulting different initial sizes of the yield curves on the various sampling planes.

The S-CLAY1S model and MMC were implemented to PLAXIS 2D Version 8.2 as user-defined models by Wiltafsky [6,38]. All soil constants and state variables related to the new models are input in the user-defined model interface, rather than as a part of the initial stress generation procedure. The user-defined model subroutine is called whenever information of the constitutive model is required, i.e. at initialization stage, for forming the stress–strain matrix required for assembly of the stiffness matrix, and finally to calculate the stresses and update the state variables.

For the S-CLAY1S model, 11 state variables are stored (i.e. six components of α_{ij}, the scalar value of α, p'_{mi}, x, p'_m and e), of which 9 are independent. The values of α and p'_m are only stored for the convenience of the output. For the MMC model some of the state variables need to be stored for each sampling plane, and given that a 33-plane integration rule by Bažant and Oh [39] is adopted, 4×33 state variables are stored related to individual planes (i.e. σ'_n, φ'_m, $d\varepsilon^p_{n,cap}$ and $d\varepsilon^p_{n,cone}$) whilst the rest of the state variables, such as void ratio e, are stored globally. Consequently, the multilaminate models require significantly more memory and run time than corresponding models embedded in a standard elasto-plastic framework. Typically, an analysis that takes 10 min with an anisotropic model in standard elasto-plastic framework can take several hours when multilaminate model is adopted. However, part of the additional run time can be attributed to the deviatoric hardening, which is not accounted for with the other anisotropic models. This feature is not very important for the problem considered, but plays a significant role in other boundary value problems, such as excavations [10]. The benefit of the multilaminate model is that plastic anisotropy is a natural outcome of the model formulation and no additional hardening laws are required.

The new models, i.e. the MMC and S-CLAY models, are highly non-linear models and the accuracy of the results depends on the size of the strain increment. The stress-integration

algorithm for the user-defined models adopted is based on a forward Euler algorithm with an elastic trial stress and plastic correction. The size of the elastic trial strain increment is controlled at local level within the user-defined soil model implementation by sub-stepping (via an additional input parameter 'StepSize' controlling the maximum strain increment size within the user-defined subroutine) in order to avoid inaccuracies and convergence problems. For the analyses presented, the value given for 'StepSize' (= −0.01) ensures that the norm of the trial strain increment does not exceed 1.0^{-5} (StepSize/1000). If the strain increment is greater than that, the strain increment is automatically subdivided until it is small enough to fulfil this criterion. This is a very crude approach. In future alternative approaches for error control, such as proposed by Sloan *et al.* [40], should be investigated. Convergence studies were performed with all models to ensure that the results were acceptable and MMC was found to be the most demanding. The commercial implementation of the Soft-Soil model uses a fully implicit stress integration scheme at integration point level, and therefore, no sub-stepping at integration point level is used.

At global level, the iterative procedure aims to satisfy both the equilibrium conditions and constitutive relations. PLAXIS incorporates an automatic step size procedure. The global iterative process can be controlled by the user by adjusting the appropriate control parameters, such as the tolerated error, the maximum number of iterations and furthermore, it is possible to control the global load step size by entering values for desired minimum and maximum number of iterations per step, respectively. If the step size is too small, the load is adjusted automatically by the code by multiplying it by two. If the solution fails to converge with the desired maximum number of iterations, the load increment is automatically divided by two and then the iteration procedure is continued. For the next calculation step the initial size of the load increment is made equal to the size used in the previous successful step. For these parameters recommended default values have been used (0.01 for tolerance, 60 for the maximum number of iterations, 6 for desired minimum and 15 for the desired maximum, respectively). In order to reduce the number of iterations needed for convergence, so-called over-relaxation is used (see References [41,42] for details). For the simulations shown, the parameter controlling the over-relaxation was set to 1.2.

4. RESULTS OF NUMERICAL ANALYSES

4.1. Vertical displacements

The predicted vertical displacements versus time at the node directly under the centreline of the embankment are presented in Figure 6 for 100 years consolidation time. For some of the models, the 100-year consolidation time was not enough to complete the primary consolidation. In particular, the anisotropic models required 200 years consolidation time for (almost) 100% consolidation. The final values of vertical settlement referred to in the following discussion, therefore, relate to the values corresponding to 200 years.

The isotropic MCC model gives a lower bound estimate of about 0.80 m for the final vertical settlement, whilst the highest prediction of about 1.35 m is given by the S-CLAY1S model (corresponding to 200 years). If the predictions by the isotropic models only are compared (Figure 6(b)), it can be seen that the SS1 model (that attempts to match the isotropic MCC model) gives a notably higher prediction, of about 1.23 m, for the final vertical settlement than

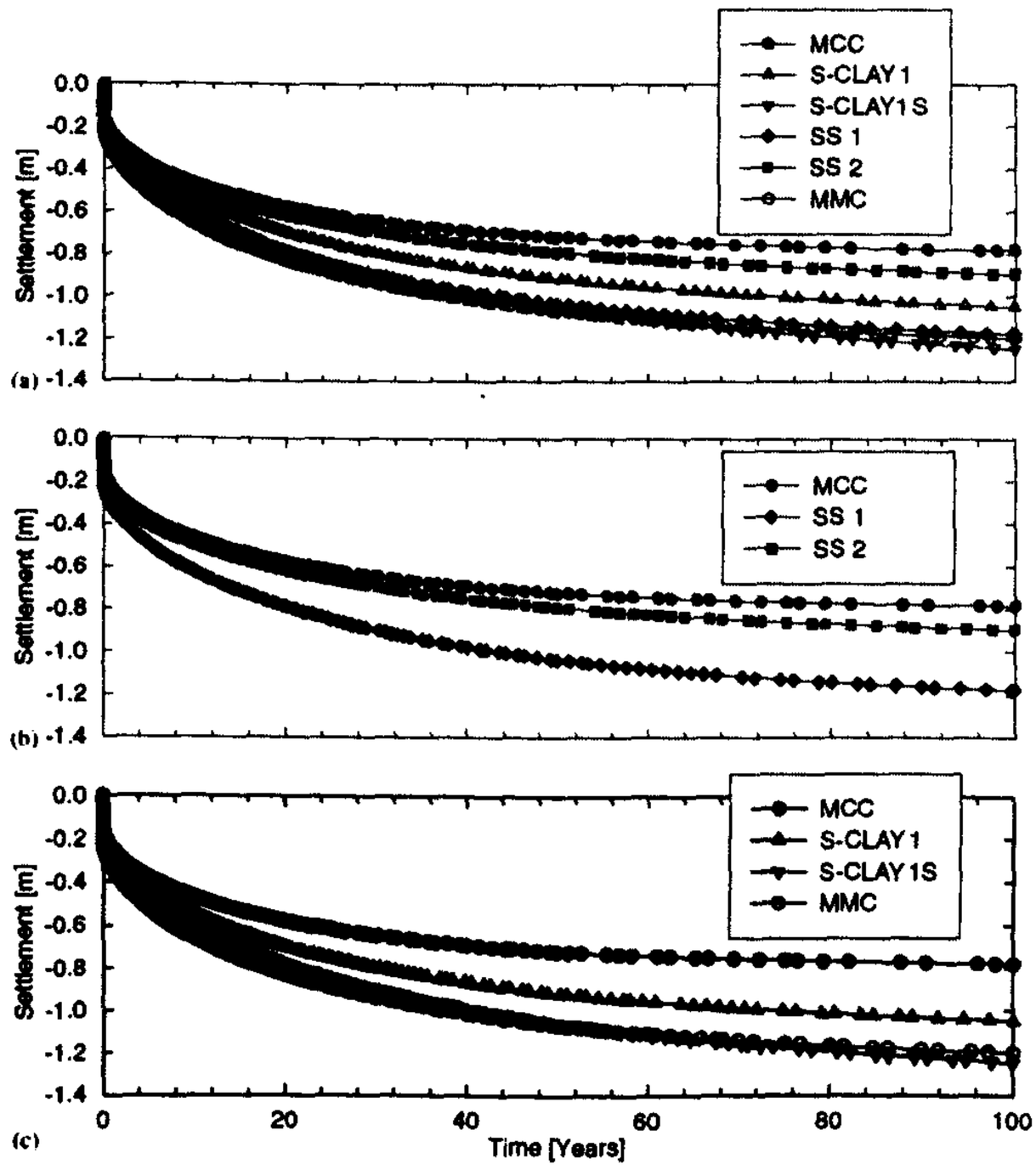

Figure 6. Time settlement curves.

the original MCC model. Investigation of void ratios predicted by the MCC model suggest that the void ratios change from the initial values of 2.1 to a minimum of about 1.9 in the soft clay layer, and from 2.1 to about 1.76 in the dry crust. The predicted void ratios are therefore not constant with depth. The predicted changes in the void ratios are notable and understandably the MCC and SS1 simulations do not match. This emphasises the importance of estimating the values of λ^* directly from soil data, at an appropriate stress range, rather than estimating it from λ by assuming a constant value for the void ratio, as often done in practice. The prediction of the SS1 model represents one of the upper bound predictions (Figure 6(a)). In contrast, if a different shape of a yield curve is adopted (by assuming a realistic value for the normally consolidated K_0 as the input for the Soft-Soil model), as was done in the case of the SS2 model, the settlement predictions are, by coincidence, relatively close to that of the original MCC

model, with a final value of about 0.94 m. This demonstrates how small differences in the shape of the yield surface (and the resulting K_0 prediction) can lead, quantitatively, to a notably different response (SS1 vs SS2) by the same constitutive model. Interestingly, two models with very different shapes for the yield surfaces (MCC and SS2) coincidentally predict quite similar vertical deformations, due to the very different K_0 predictions made by the models.

In Figure 6(c), the conventional MCC model has been taken as a reference isotropic model, given that no isotropic equivalent for the MMC model exists. Accounting for anisotropy via a rotational hardening law (S-CLAY1), results in 38% increase in the predicted final settlement (1.11 m) and incorporating additionally the effect of destructuration (S-CLAY1S) increases the value further, to the maximum value predicted (1.35 m). The MMC model predicts a final vertical settlement of about 1.25 m, and gives, therefore, very similar predictions to the S-CLAY1S models. Based on the results in Figure 6(c), there is a suggestion that incorporation of plastic anisotropy increases the predicted vertical settlements. Consequently, MMC is overall perhaps predicting overall more 'anisotropic' behaviour than the S-CLAY1 model. Furthermore, in this case the incorporation of destructuration effects seems to increase the predicted final settlement.

The predicted surface settlements are shown in Figures 7 and 8 corresponding to the time immediately after the final construction step (Figure 7) and after 100 years of consolidation (Figure 8). All models predict small amounts of surface heave outside the embankment immediately after construction, as expected (Figure 7(a)). The maximum vertical displacement immediately after construction is predicted to be directly underneath the centreline, and the zero settlement point is about 14 m from the symmetry axis for all models, corresponding to the width of the embankment base. The lowest value (about 0.14 m) is predicted by the conventional MCC model and the highest values by MMC and SS1 (about 0.19 m). The SS1 model also predicts marginally more heave than the conventional MCC and SS2 models (Figure 7(b)). MMC predicts slightly more heave than the isotropic MCC model and its anisotropic extensions, S-CLAY1 and S-CLAY1S, as shown in Figure 7(c). As all models shown in Figure 7(c) have identical elastic relationships, and yet the predictions are notably different, the plastic behaviour dominates the response during construction.

The predicted settlement troughs after 100 years of consolidation are presented in Figure 8(a). At this stage the point corresponding to zero settlement is about 30 m from the symmetry axis, extending to about twice the base width of the embankment. All models predict a rather sharp discontinuity at about 14 m from the centreline. With the multilaminate model, this is perhaps more gradual than with standard elasto-plastic models. The predictions by the isotropic MCC model and the SS2 model are only 10 cm apart (Figure 8(b)) in contrast to the SS1 model that predicts much higher values of vertical settlement than MCC and SS2. Accounting for anisotropy, as well as anisotropy and destructuration, results in a wider and steeper settlement trough at the end of consolidation than predicted by the isotropic MCC model (Figure 8(c)).

4.2. Horizontal displacements

The predicted horizontal displacements versus depth under the toe of the embankment are shown in Figures 9 and 10. Immediately after construction of the embankment (Figure 9) most models give almost identical predictions of the horizontal displacements, the two exceptions being SS1 and MMC, which predict significantly larger horizontal displacement than the other models (Figure 9(a)). Therefore, the attempt to match the yield surfaces of the isotropic MCC

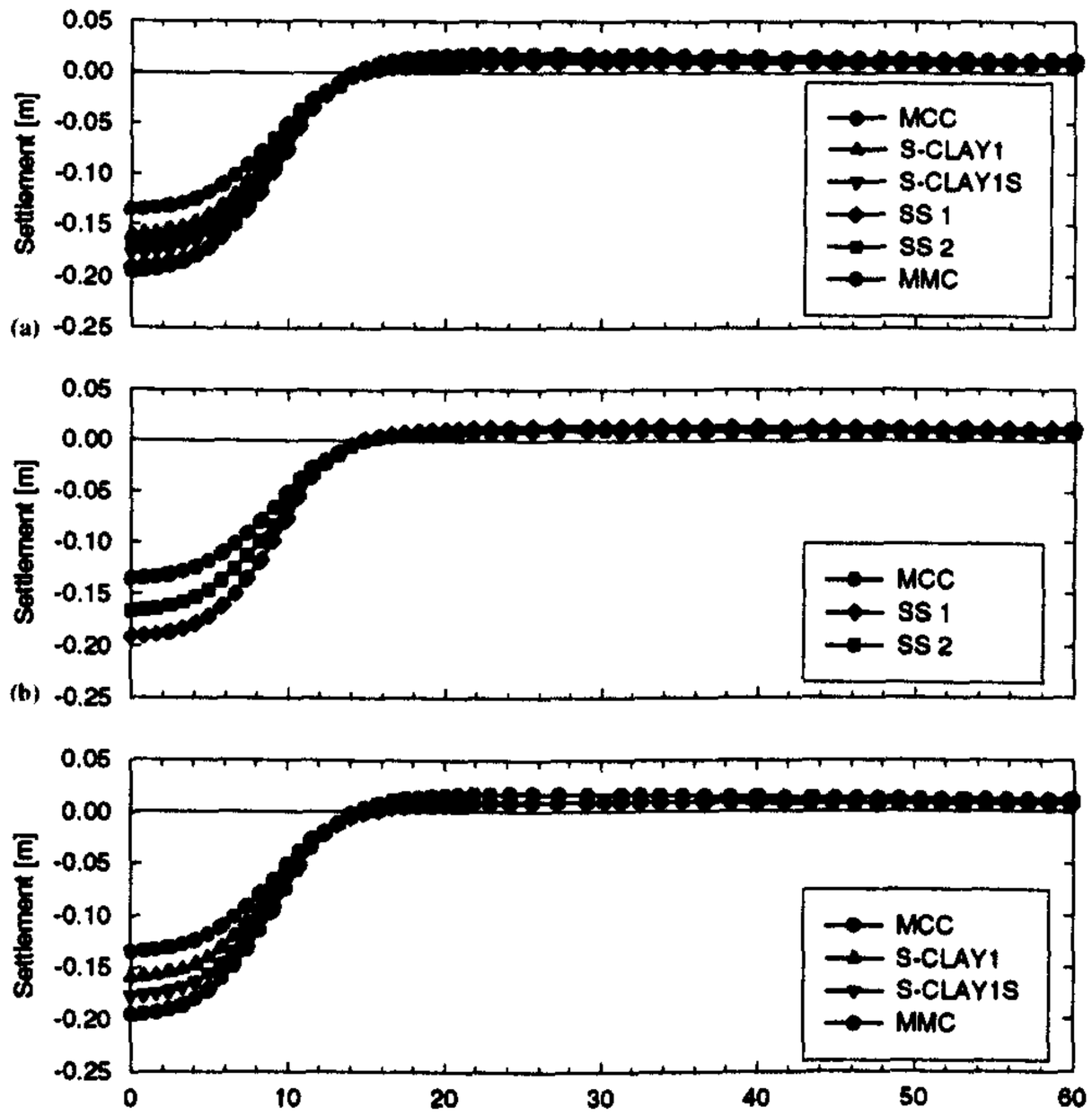

Figure 7. Surface settlements immediately after construction.

model and the Soft-Soil model (the SS1 model), results in not only very different predictions in terms of vertical displacements (Figure 6(b)), but also very different horizontal displacements (Figure 9(b)). The former is partly due to the differences in the assumed compression relationships, but in this case it may also be attributed to the differences in modelling the behaviour on the 'dry side' of the critical state (in some stress integration points) during the undrained loading. Some integration points underneath the toe exhibit a perfectly plastic behaviour predicted by the Soft-Soil model. The results, overall, clearly demonstrate that it is not possible to match MCC and the Soft-Soil model in plane strain conditions. In practise it would be best to adopt the version of the Soft-Soil model that yields a realistic K_0 prediction (SS2).

Given that all anisotropic models have the same elastic relationship as the conventional MCC model, and the two S-CLAY models give very similar predictions to the MCC model (maximum horizontal displacement u_x about 0.024 m), the significantly larger horizontal displacements

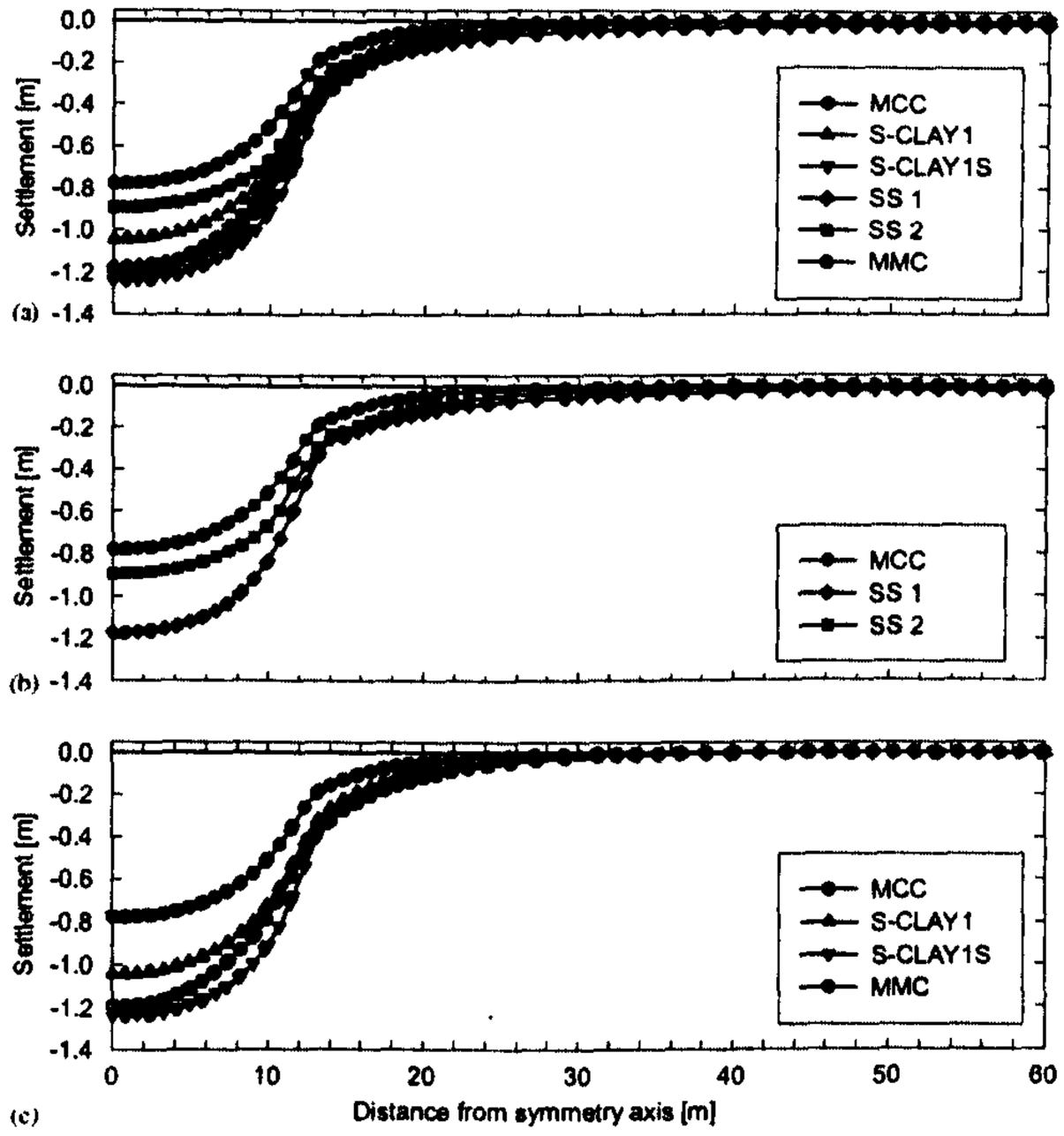

Figure 8. Surface settlements after 100 years of consolidation.

predicted by the multilaminate model (u_x about 0.042 m) in Figure 9(c) are attributed to very different plastic behaviour. It was confirmed, by plotting the plastic points predicted by the MMC model at the end of construction, that the deviatoric hardening part of the multilaminate model seems to be activated (in a number of stress integration points) during the undrained embankment construction. Consequently, this is very likely to be the main cause for differences between the two types of anisotropic models.

The ratio of the predicted maximum horizontal displacement (u_x) to the vertical settlement (u_y) at the end of construction is, consequently, very different from one model to another: u_x/u_y is about 14 and 16% for S-CLAY1 and S-CLAY1S, respectively, and much higher, i.e. 19 and 22%, respectively, for the conventional MCC model and the MMC model. The ratios of u_x/u_y immediately after construction predicted by the models used are within the range suggested by Leroueil *et al.* [43], who attributed u_x/u_y-ratio to depend on the geometry on the problem.

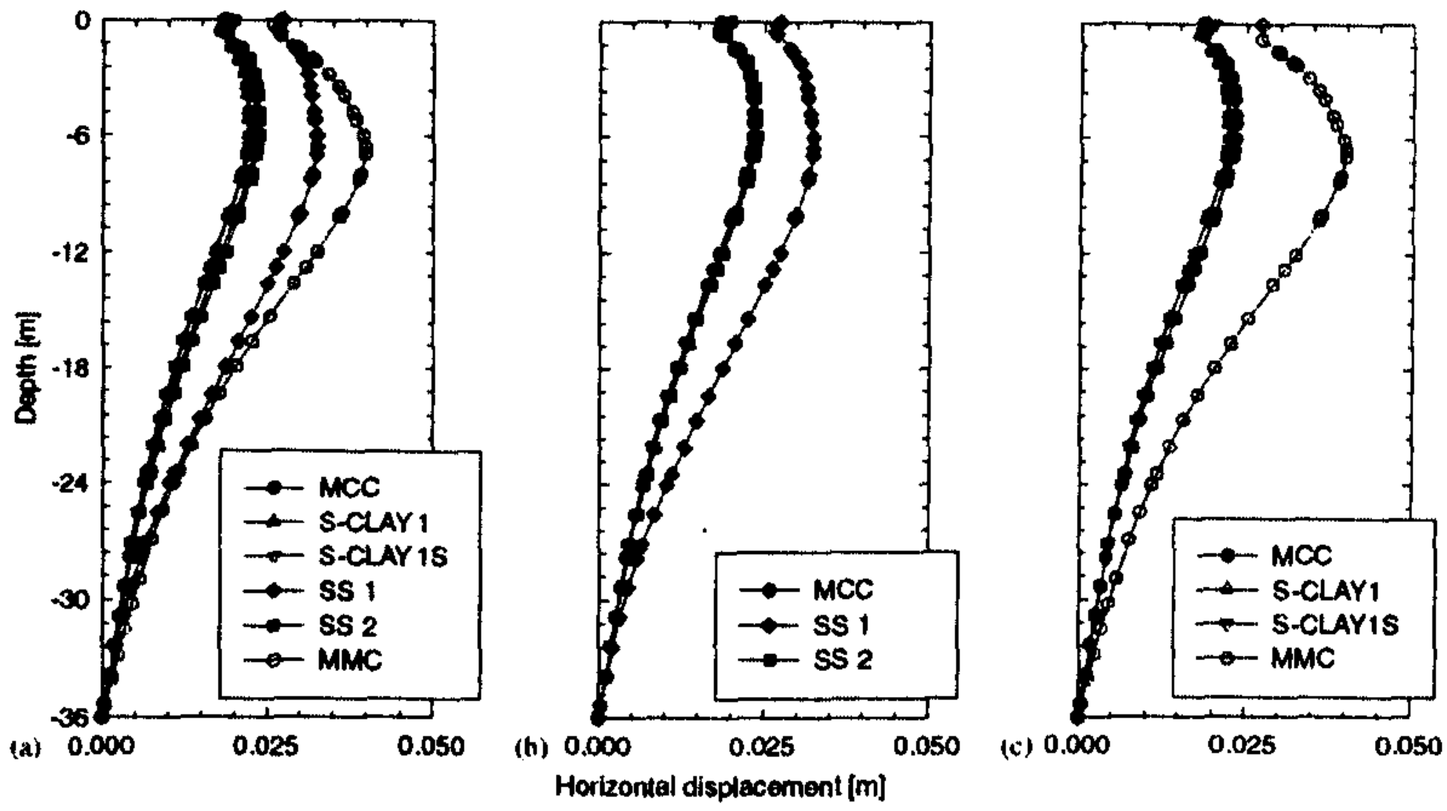

Figure 9. Horizontal displacements underneath the toe of the embankment immediately after construction.

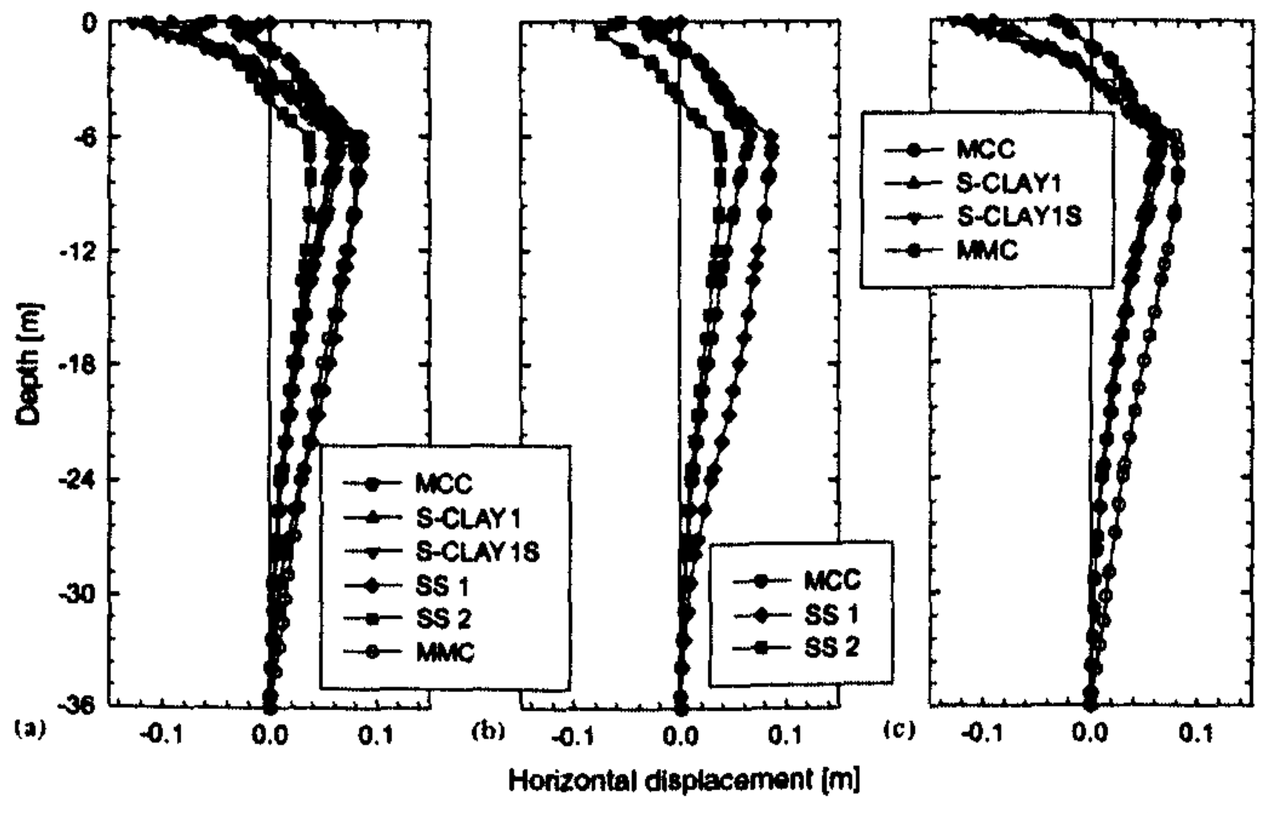

Figure 10. Horizontal displacements underneath the toe of the embankment after 100 years of consolidation.

The results of the numerical simulations shown in Figure 9 indicate that it is the predicted plastic behaviour that controls the u_x/u_y-ratio. Based on the conventional interpretation, the embankment is predicted to be much closer to failure with MMC (and SS1) at the end of construction than by the other models.

Figure 10(a) suggest that the conventional MCC model, S-CLAY1 and S-CLAY1S predict very similar values for the maximum horizontal displacement u_x within the soft clay underneath the toe of the embankment after 100 years of consolidation (about 0.06 m). The SS2 model predicts u_x of about 0.04 m. The largest horizontal displacements within the soft clay are predicted by SS1 and MMC to be about 0.08 m (Figure 10(a)). The predicted maxima within the soft clay are located at about 6 m depth coinciding with the sharp change in the *in situ* K_0 value and POP (Figure 5).

At the soil–embankment interface, all models predict some negative horizontal displacements, i.e. movements towards the symmetry axis, and the magnitudes of these are not negligible. This phenomenon is most notable in the predictions by the anisotropic models (S-CLAY1, S-CLAY1S and MMC), as shown in Figure 10(c). The predicted horizontal displacements at the surface are of the order of 0.09–0.12 m. As seen in Figure 10(b), the predictions by the conventional MCC model and SS1 are almost identical within the two topmost layers and the differences become apparent only at greater depths. Unlike for the vertical deformations (Figures 6 and 8), the S-CLAY1 and S-CLAY1S models give rather similar predictions for horizontal displacements after 100 years of consolidation, suggesting that destructuration has only a minor effect on the results. The predicted ratio of u_x/u_y within the soft clay layer is predicted to be between 5 and 6% by the anisotropic models compared to 8% by the isotropic models.

4.3. Total displacement contours

It is also useful to look at the overall displacement patterns predicted by the models. Due to restrictions with space, it is not possible to include these plots for all the models considered. In particular, it is interesting to compare the two very different formulations for predicting anisotropy. In Figure 11 the total displacement contours are shown for two of the anisotropic models: S-CLAY1 and MMC at the end of construction and after 100 years of consolidation. The same scale is used for both models in order to highlight the differences. At the end of construction, the displacements predicted by the MMC (Figure 11(a)) extend much further, both laterally and depth wise, than predicted by the S-CLAY1 model (Figure 11(c)) and overall, the predicted displacements are higher than suggested by S-CLAY1. This is likely to be attributed to the deviatoric hardening part of the model, activated during undrained embankment construction, rather than a direct consequence of the multilaminate formulation. This is confirmed when the results are compared at the end of consolidation (Figures 11(b) and (d)). The results become increasingly similar during the consolidation period, albeit still the effect of the embankment loading is seen to extend deeper in the deposit with MMC than S-CLAY1.

4.4. Excess pore pressures

The predicted excess pore water pressure distributions under the centreline of the embankment at the end of construction have been presented in Figure 12. All models predict a sharp discontinuity at the depth of about 6 m, where there is a notable change in the overconsolidation and the assumed *in situ* K_0 value (Figure 11(a)). This effect is, however, somewhat smeared out

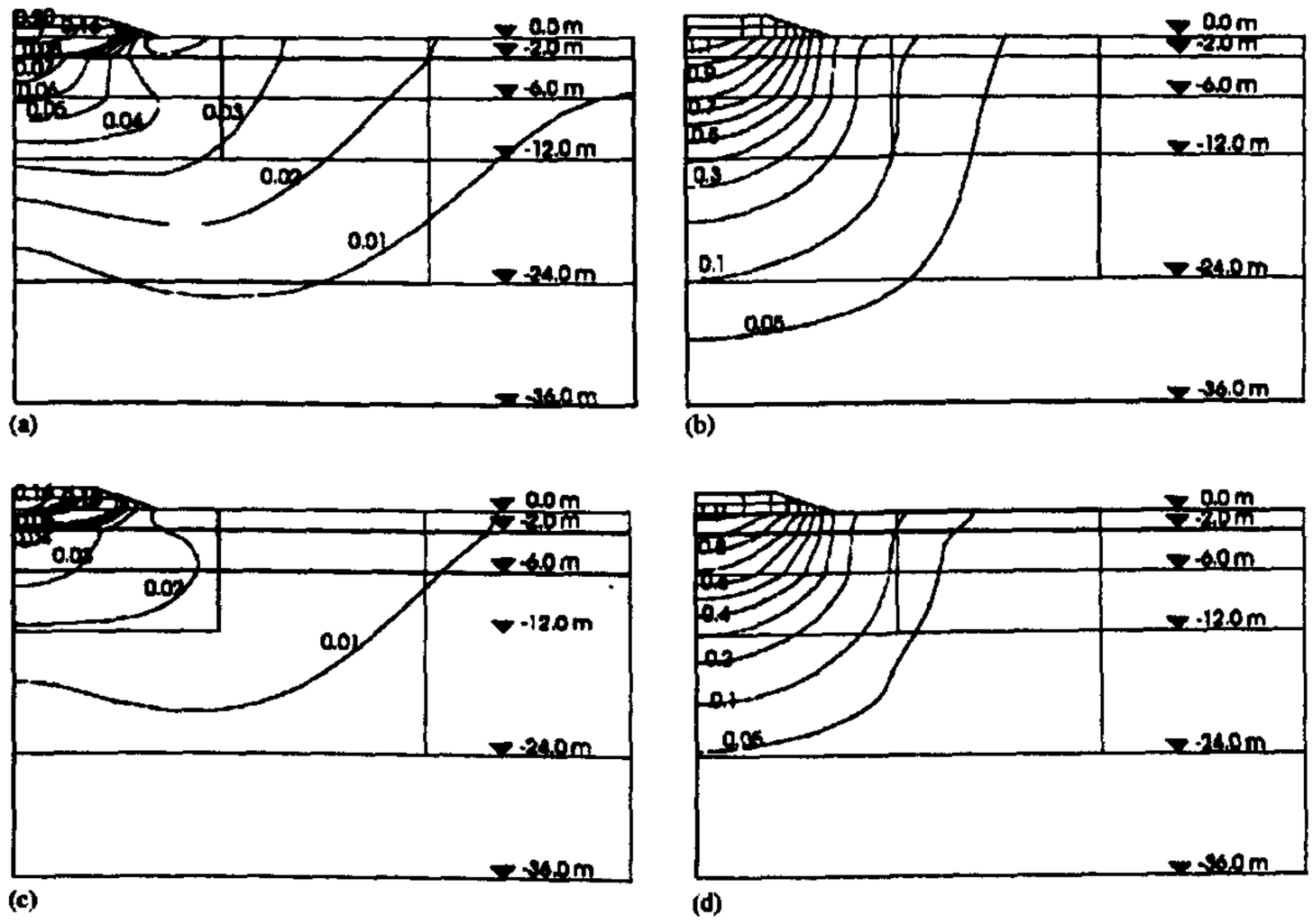

Figure 11. Total displacement contours: (a) MMC immediately after construction; (b) MMC after 100 years of consolidation; (c) S-CLAY1 immediately after construction; and (d) S-CLAY1 after 100 years of consolidation.

when the nodal results are mapped to the stress integration points. The maximum value of the excess pore pressure is predicted to occur at 6 m depth by all models. There is another apparent discontinuity at a depth of about 27 m, attributed to a sudden change in the density of the mesh. Because the construction was modelled as a fully undrained process, non-zero excess pore water pressures (10–15 kPa) are predicted at the bottom of the mesh. As soon as the coupled consolidation starts, these will become zero due to the boundary conditions imposed.

The SS2 and MCC models predict a maximum excess pore water pressure of about 30 kPa, whilst the SS1 predicts about 35 kPa (Figure 11(b)). As seen in Figure 11(c), the predictions by the MCC, S-CLAY1 and S-CLAY1S models are almost identical between 6 and 24 m. Above and below, the S-CLAY models predict marginally higher excess pore pressures than the conventional MCC model. The multilaminate model predicts notably higher excess pore water pressures than the other models, with a maximum excess pore pressure of about 39 kPa.

4.5. Strain contours

In Figure 13, the volumetric strains contours have been plotted for the two anisotropic models, MMC and S-CLAY1, respectively. During construction, all volumetric strains occur in the soil

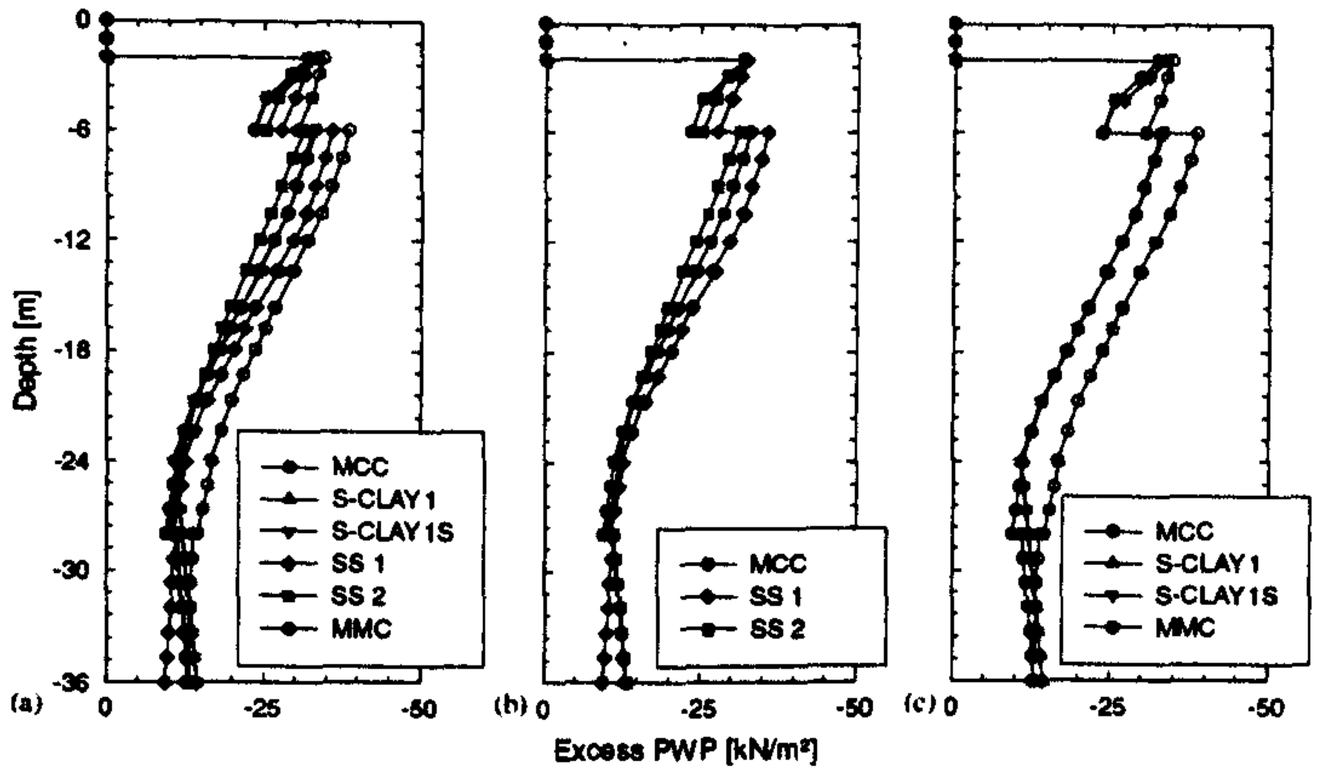

Figure 12. Excess pore pressures immediately after construction at the symmetry axis.

layer that is above the water table. As seen in Figures 13(a) and (c) the predictions by the two models are very similar. The same applies for the predicted volumetric strains at the end of consolidation (Figure 13(b) for MMC and Figure 13(d) for S-CLAY1). The patterns of volumetric strains predicted by the two models are therefore practically identical. The effects of the discontinuities in the POP values are reflected in the volumetric strain predictions by the two models as discontinuities at the interfaces. This suggests that it would be better to describe overconsolidation in terms of vertical overconsolidation ratio rather than POP, although the latter approach often matches well with the soil data.

The deviatoric strain contours are plotted in Figure 14 for MMC and S-CLAY1 at the end of construction (Figures 14(a) and (c)) and at the end of consolidation (Figures 14(b) and (d)). During the undrained loading, the deviatoric strain predictions by the two models are not dissimilar, albeit MMC (Figure 14(a)) predicts non-zero deviatoric strains up to the depth of 12 m in contrast to S-CLAY1 (Figure 14(c)). The same holds true at the end of consolidation, but overall the results are again quite similar. The differences between the deviatoric strain patterns, however, are more pronounced than those between the volumetric strain patterns, which demonstrate that globally the flow rules are not identical. Overall, the two modelling approaches, i.e. the MMC and a model incorporating rotational hardening (S-CLAY1) reproduce globally similar patterns of behaviour.

4.6. Selected stress paths

In comparing the predictions by different constitutive models it is often extremely informative to plot stress paths. For a real boundary value problem, such as the embankment considered, the

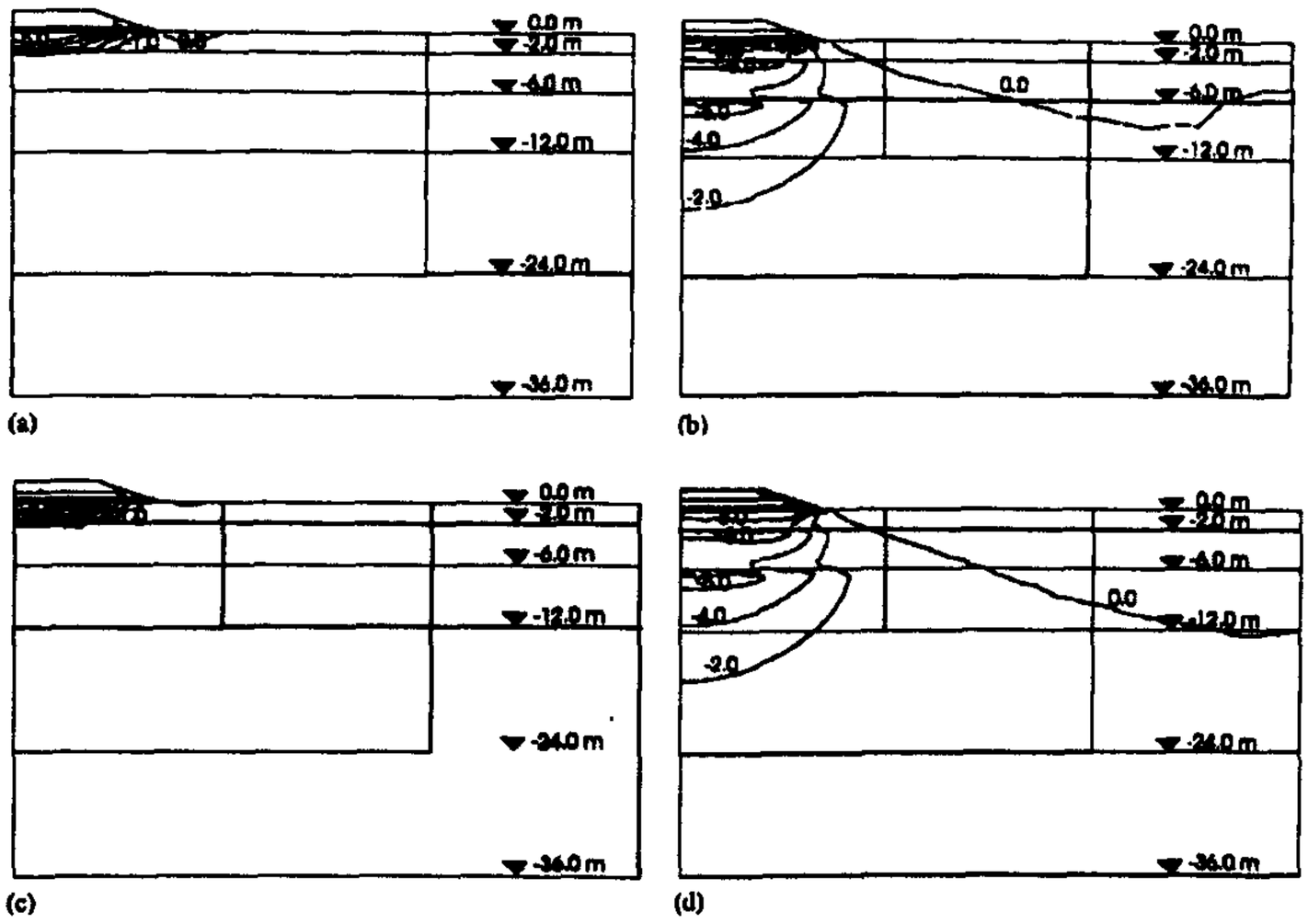

Figure 13. Volumetric strain contours: (a) MMC immediately after construction; (b) MMC after 100 years of consolidation; (c) S-CLAY1 immediately after construction; and (d) S-CLAY1 after 100 years of consolidation.

difficulty is that it is possible to present only projections of the stress paths in a two-dimensional space. In this exercise one of the key interests is to compare the K_0 predictions and the flow rules. Hence, it is convenient to look at the projections of the predicted stress paths in the p'–q-plane. Two selected points in the subsoil are considered: a point at a depth of 8 m below ground level underneath the centreline of the embankment (Figures 15(a)–(c)) and a point at the same depth under the toe of the embankment (Figures 15(d)–(f)). The stress paths reflect the evolution of effective stresses during the construction of the embankment and subsequent consolidation. Because the problem analysed is a plane strain problem, and MCC, S-CLAY1 and S-CLAY1S assume a Drucker–Prager type of failure condition, in contrast to the Mohr Coulomb assumed by SS1 and SS1, it is not possible to visualize the failure lines in Figure 15. This issue is further complicated by the fact that in the MMC model the failure surface is expressed at local level rather than at global level. Because all simulations assume the same initial stress state, all stress paths start at the same point.

Underneath the centreline of the embankment, the directions of the principal stresses stay fixed, and hence the stress paths are perhaps easier to understand. All models predict initially elastic behaviour, with a constant value of p', until at some point during construction the soil is predicted to yield. This point is different from one model to another, because of the differences

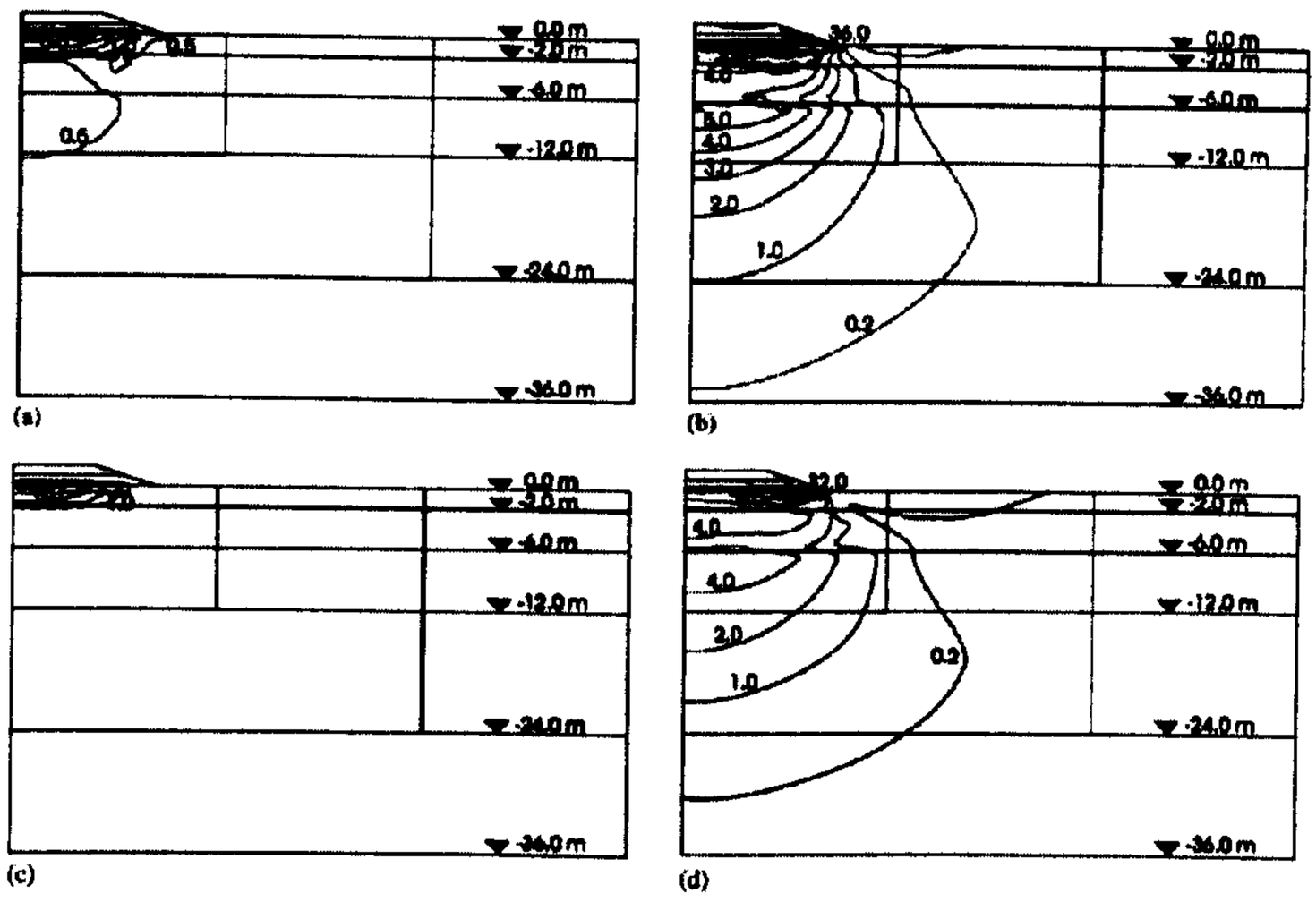

Figure 14. Deviatoric strain contours: (a) MMC immediately after construction; (b) MMC after 100 years of consolidation; (c) S-CLAY1 immediately after construction; and (d) S-CLAY1 after 100 years of consolidation.

in the yield curve shape. Figure 15(a) shows clearly the differences in the K_0 predictions by the different models. During consolidation the predictions by the SS2, S-CLAY1 and S-CLAY1S models converge towards an incremental stress ratio that is consistent with Jaky's K_0 (Figure 15(a)). The MMC predicts a slightly higher K_0 stress ratio, whilst MCC and the SS1 settle towards an incremental stress ratio that corresponds to the theoretical, albeit unrealistic, prediction by the MCC model.

Although the predictions by the SS2 model are rather similar to the ones by the S-CLAY models in terms of K_0 predictions, there are notable differences in the predicted stress paths during the undrained loading. The SS2 model predicts yielding earlier than the S-CLAY models (Figure 15(a)) and the shape of the stress path (Figure 15(b)) suggests that the soil element considered might be close to failure during the undrained loading (or that there are some numerical problems at this integration point at the start of consolidation). In contrast, the predictions by the isotropic MCC model and the SS1 model indicate no such behaviour (Figure 15(b)).

The MMC model predicts yielding much earlier than the other models (Figure 15(c)) and once consolidation starts the stress path is predicted to settle towards an incremental stress ratio that corresponds to the K_0 condition predicted by the model. As discussed earlier, the K_0 values

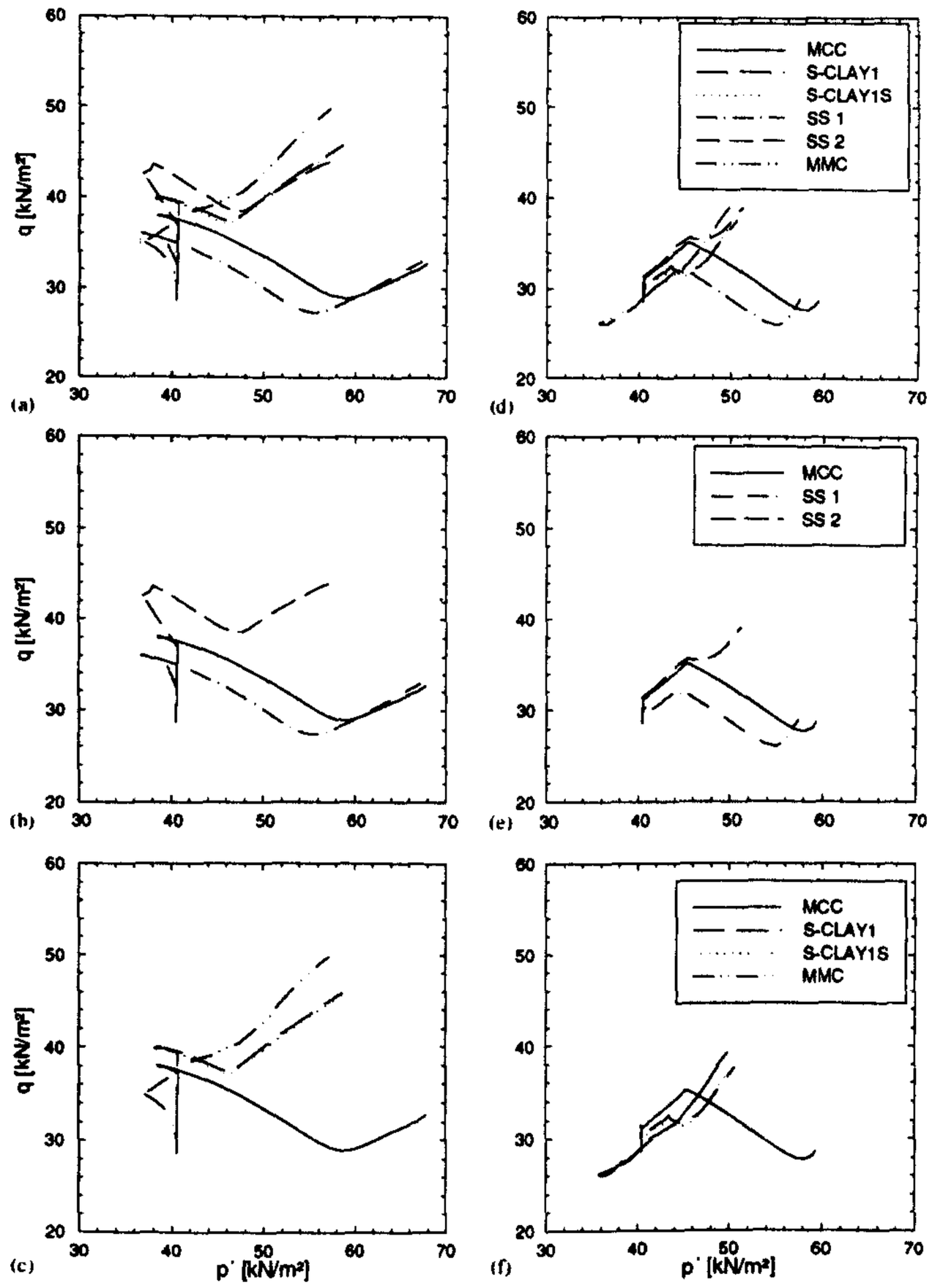

Figure 15. Stress paths at 8 m below the ground level: (a)–(c) on the centreline; and (d)–(f) under the toe of the embankment.

predicted by MMC are lower than predicted by, e.g. Jaky's simplified formula. By changing the value of the input parameter α in the MMC model, the K_0 prediction would change. The predictions by the S-CLAY1 and S-CLAY1S models, in terms of the stress paths, at the point considered are almost identical (Figure 15(e)).

At the same depth (of 8 m), underneath the toe of the embankment the projections of the stress paths in the p'–q-plane are rather complex due to the rotation of the principal stress directions. In terms of the K_0 predictions at the end of consolidation, the results are similar to those underneath the centreline (Figure 15(a) vs (d)). When considering the predictions by the isotropic models only (Figure 15(e)), both MCC and SS2 models predict very similar behaviour until, during consolidation, the stress paths deviate due to the different K_0 predictions. When considering the predictions by the anisotropic models, again S-CLAY1 and S-CLAY1S predict practically identical results (Figure 15(f)). The predictions by MMC are radically different though. The MMC model predicts a reduction in both the values of p' and q during the undrained construction, which basically implies unloading, followed by a gradually increasing gradient of the stress path. As the elastic laws are identical for all the models in Figure 15(f), this must be due to the plastic part of the model. Again, it is likely that this is caused by the deviatoric hardening part of the model and would require further investigation.

5. CONCLUSIONS

The paper studied the influence of constitutive models on the predicted stress–strain behaviour of an embankment on a soft clay during undrained construction and subsequent consolidation. The soft clay was chosen to correspond to a simplified profile of POKO clay. The benchmark example, a 2 m high embankment, was simulated using five different constitutive models to represent the soft clay. Two of these were isotropic elasto-plastic models (Modified Cam Clay and the PLAXIS Soft-Soil model). The other three models were recently proposed constitutive models that account for plastic anisotropy, either via a rotational hardening law within a standard elasto-plastic framework (S-CLAY1 and S-CLAY1S) or via a formulation embedded in the so-called multilaminate framework (the MMC model). The S-CLAY1S model additionally accounts for bonding and destructuration. These three advanced constitutive models have been implemented as user-defined models in the PLAXIS 2D V8 finite element code.

The results of the numerical simulations showed that for this particular boundary value problem, accounting for anisotropy and/or destructuration generally increased the predicted final vertical settlements (Figure 6). The highest values of the final vertical settlement (about 1.25 and 1.35 m) were predicted by the MMC and S-CLAY1S models, respectively, and the lowest values (about 0.8 m) with the isotropic MCC model.

All model simulations assumed an identical initial state in terms of *in situ* stresses and the vertical preconsolidation stress. The Soft-Soil model (the standard isotropic model in the commercial version of PLAXIS) gave a range of predictions depending on the shape of the yield curve assumed for the simulation. The shape is controlled by the user via the input value for K_0^{NC}, the coefficient of earth pressure at rest corresponding to normally consolidated condition. Therefore, the users can directly decide the predicted K_0-value during plastic loading. A lower bound, in terms of vertical settlement, of 0.94 m was predicted when the value for the K_0^{NC} was chosen to give a realistic K_0 prediction (SS2). In contrast, an upper bound of 1.23 m was predicted when K_0^{NC} was chosen to approximate the K_0 prediction by the MCC model (SS1).

Indeed, the predictions by these two versions of the Soft-Soil model (SS1 and SS2) gave almost as big a range in the predicted vertical settlements as the range between the isotropic MCC model and the anisotropic model predictions. The results were greatly influenced by the assumed K_0 prediction, and therefore, the shape of the yield surface. The simulations suggest that this may be as important as the effect of anisotropy. It is generally acknowledged that the conventional MCC model gives unrealistic predictions of K_0, and hence the predictions made by the SS2 model can be considered more realistic than those made by the SS1 model. With a realistic K_0 prediction, incorporation of anisotropy (and to a lesser extend destructuration) results in a notable increase in the predicted vertical strains. This seems logical, given the soils *in situ* are likely to have been more highly compressed in the vertical direction than in the horizontal direction during their past history. Assuming isotropy, therefore, results in underprediction of the vertical deformations. This further suggests that traditional settlement calculations, which assume one-dimensional consolidation, may be non-conservative.

The influence of the constitutive models on the predictions of the horizontal displacements under the toe of the embankment was also notable. During construction, the anisotropic models embedded in standard elasto-plastic framework (S-CLAY1 and S-CLAY1S) predicted much lower ratio of u_x/u_y (maximum horizontal displacement in the soft soil underneath the toe over the corresponding vertical displacement underneath the centreline of the embankment, respectively) than the isotropic models and the MMC model. The difference between the S-CLAY models and MMC was most likely due to the deviatoric hardening part of the multilaminate model which influenced the predicted stress–strain response during the undrained construction of the embankment, whilst having only a minor effect during consolidation. After 100 years of consolidation, the u_x/u_y ratio predicted by the anisotropic models is between 5 and 6% compared to about 8% predicted by the isotropic MCC model. Hence, when considering the long-term behaviour, accounting for anisotropy seems to reduce the predicted maximum horizontal displacements in the soft soil layer. Assuming isotropy, as is commonly done, results in over-prediction of horizontal displacements. The horizontal displacements predicted by S-CLAY1 and S-CLAY1S were almost identical, suggesting that the effect of bonding and destructuration is less marked than the effect of anisotropy. Similar conclusions were made in References [8,11] for similar boundary value problems. The comparisons between measured and predicted behaviour in Reference [11] suggested that the predictions made by the anisotropic models were more realistic than those predicted by the isotropic models.

The overall global response, in terms of displacement contours, volumetric strains and shear strains, predicted by the anisotropic models S-CLAY1 and MMC, was very similar. Consequently, the two very different model formulations, an elasto-plastic formulation with a rotational hardening law and a multilaminate formulation, predicted the global effects of anisotropy in a very similar manner. In particular, the results at the end of consolidation were practically identical. The minor discrepancies were, therefore, likely to be caused by the deviatoric hardening part of the MMC model, which activated during the undrained loading, rather than the multilaminate formulation itself.

The selected stress paths further emphasized the significant influence of the K_0 prediction, which is inherent to most constitutive models. In the case of the Soft Soil model, this can however, directly be controlled by the user (SS1 or SS2). The S-CLAY1, S-CLAY1S and SS2 models predicted very similar values of the normally consolidated K_0, whilst MCC and SS1 predicted unrealistically high K_0 values. The lowest values of normally consolidated K_0 were predicted by the multilaminate model. Although the selected stress paths (Figure 6) indicated

only small differences between the S-CLAY1 and S-CLAY1S model predictions, there was a notable difference in the predicted final consolidation settlement.

Overall, the following conclusions can be made:

- The three anisotropic models, the rotational hardening models (S-CLAY1, S-CLAY1S) and the MMC model, gave qualitatively very similar predictions of the long-term settlement behaviour.
- During construction, however, the MMC model predicted much higher horizontal displacements than the S-CLAY models. When considering the results overall, this was most likely due to the activation of the deviatoric hardening part of the model during the undrained construction rather than due to the fundamental differences between the formulations (standard elasto-plastic vs multilaminate).
- The K_0 prediction by the MMC model was slightly lower than predicted by Jaky's formula, but the user can influence this by changing the input value for the parameter α. The S-CLAY1, S-CLAY1S and SS2 models result in K_0 predictions that were similar to that of Jaky's, provided the user follows the recommendations on how the values for the relevant input parameters (α and β for the S-CLAY models (see Reference [4]) and K_0^{NC} for the Soft-Soil model, respectively (see Reference [31])) should be calculated.
- For this particular boundary value problem, the effect of anisotropy was more dominant than the effect of bonding and destructuration. A similar conclusion was derived in, e.g. Reference [11].
- At stress point level the predictions by the MMC model differed qualitatively from those predicted by the other anisotropic models, in particular underneath the toe of the embankment. At this location, MMC predicted unloading in the soil element during the undrained construction process, which seems very unlikely in reality. This will require further investigation.

Future research will concentrate on testing the validity of anisotropic models against data from real field problems, such as test embankments, in order to see if the results are as promising as shown in Reference [11] for the Murro test embankment. A parallel aim is to consider other types of geotechnical boundary value problems, including problems that involve ground improvement techniques. The application of the proposed constitutive models in an industrial environment would also require development of more effective and robust algorithms than used in this work, so that the quality of the results is not adversely affected by the experience of the user. Finally, there is a need for advanced training on the appropriate application of constitutive models for soft soils, given that a whole range of results can be predicted by a single constitutive model (Soft-Soil model) depending on the values of the input parameters chosen by the user.

ACKNOWLEDGEMENTS

The work presented was carried out as a part of a Research Training Network 'Soft Clay Modelling for Engineering Practice' supported by the EC (through the programme 'Improving the Human Research Potential and the Socio-Economic Knowledge Base'). The finalization of the manuscript benefited from the continued collaboration as a part of a Marie Curie Research Training Network on 'Advanced Modelling of Ground Improvement on Soft Soils' supported by the EC through the programme 'Human Potential and Mobility'. The third author was sponsored by Donaldson Associates Ltd. (U.K.) and a Faculty of

Engineering Scholarship at the University of Glasgow in 2003–2005. The authors would like to thank Prof. Simon Wheeler (University of Glasgow) for his useful comments during the work and the reviewers for their constructive comments. The authors would also like to thank Dr Mike Kenny (University of Strathclyde) for proofreading the final version of the manuscript. The opinions expressed are the opinions of the authors' and not the sponsors'.

REFERENCES

1. Wheeler SJ, Cudny M, Neher HP, Wiltafsky C. Some developments in constitutive modelling of soils. *Proceedings of the International Workshop on Geotechnics of Soft Soils—Theory and Practice*. Noordwijkerhout, Netherlands. VGE: Essen, 2003; 3–22.
2. Wiltafsky C, Messerklinger S, Schweiger HF. An advanced multilaminate model for clay. *Proceedings of the 8th International Symposium on Numerical Models in Geomechanics (NUMOG)*, Rome, Italy. Balkema, Rotterdam, 2002; 67–73.
3. Koskinen M, Karstunen M, Wheeler SJ. Modelling destructuration and anisotropy of a natural soft clay. *Proceedings of the 5th European Conference Numerical Methods in Geotechnical Engineering*, Paris. Presses de l'ENPC/LCPC: Paris, 2002; 11–20.
4. Wheeler SJ, Näätänen A, Karstunen M, Lojander M. An anisotropic elasto-plastic model for soft clays. *Canadian Geotechnical Journal* 2003; **40**:403–418.
5. Neher HP, Sterr C, Messerklinger S, Koskinen M. Numerical modelling of anisotropy of Otaniemi clay. *Proceedings of the International Workshop on Geotechnics of Soft Soils—Theory and Practice*, Noordwijkerhout, Netherlands. VGE: Essen, 2003; 217–224.
6. Wiltafsky C. A multilaminate model for normally consolidated clay. *Ph.D. Thesis*, Gruppe Geotechnik Graz, Heft 18, Graz University of Technology, Austria, 2003.
7. Karstunen M, Koskinen M. Anisotropy and destructuration of Murro clay. Advances in geotechnical engineering. In *The Skempton Conference*, Jardine RJ *et al.* (eds), vol. 1, London, Thomas Telford: 2004; 476–487.
8. Krenn H, Karstunen M, Wheeler SJ. Influence of anisotropy and destructuration on an embankment on soft clay. *Proceedings of the International Workshop on Geotechnics of Soft Soils—Theory and Practice*, Noordwijkerhout, Netherlands. VGE: Essen, 2003; 293–298.
9. Wiltafsky C, Scharinger F, Schweiger HF, Krenn H, Zentar R, Karstunen M, Cudny M, Neher HP, Vermeer PA. Results from a geotechnical benchmark exercise of an embankment on soft clay. *Proceedings of the International Workshop on Geotechnics of Soft Soils—Theory and Practice*, Noordwijkerhout, Netherlands. VGE: Essen, 2003; 381–390.
10. Wiltafsky C, Schweiger HF, Krenn H. Application of multilaminate model for the numerical analysis of a deep excavation problem in soft clay. *Proceedings of the International Workshop on Geotechnics of Soft Soils—Theory and Practice*, Noordwijkerhout, Netherlands. VGE: Essen, 2003; 375–380.
11. Karstunen M, Krenn H, Wheeler SJ, Koskinen M, Zentar R. The effect of anisotropy and destructuration on the behaviour of Murro test embankment. *International Journal of Geomechanics* (ASCE) 2005; **5**(2):87–97.
12. Pande GN, Sharma KG. Multilaminate model of clays—a numerical evaluation of the influence of rotation of principal stress axes. *International Journal for Numerical and Analytical Methods in Geomechanics* 1983; **7**(4): 397–418.
13. Koskinen M, Zentar R, Karstunen M. Anisotropy of reconstituted POKO clay. *Proceedings of the 8th International Symposium on Numerical Models in Geomechanics (NUMOG)*, Rome. Balkema: Lisse, 2002; 99–105.
14. Burland JB. On the compressibility and shear strength of natural clays. *Géotechnique* 1990; **40**:329–378.
15. Diaz Rodriguez JA, Leroueil S, Alemán JD. Yielding of Mexico City clay and other natural clays. *Journal of Geotechnical Engineering* 1992; **118**(7):981–995.
16. Nova R. Mathematical modelling of anisotropy of clays. *Proceedings of the 11th ICSMFE*, San Francisco, vol. 1. Balkema: Rotterdam, 1985; 607–661.
17. Dafalias YF. An anisotropic critical state soil plasticity model. *Mechanics Research Communications* 1986; **13**(6):341–347.
18. Di Prisco C, Nova R, Lanier J. A mixed isotropic-kinematic hardening constitutive law for sand. In *Modern Approaches to Plasticity*, Kolymbas D (ed.). Elsevier: Amsterdam, 1993; 83–124.
19. Zienkiewicz OC, Pande GN. time dependent multi-laminate model of rocks—a numerical study of deformation and failure of rock masses. *International Journal for Numerical and Analytical Methods in Geomechanics* 1977; **1**(3): 219–247.
20. Pietruszczak S, Pande GN. Multi-laminate framework of soil models—plasticity formulation. *International Journal for Numerical and Analytical Methods in Geomechanics* 1987; **11**(6):651–658.
21. Leroueil S, Tavenas F, Brucy F, La Rochelle P, Roy M. Behaviour of destructured natural clays. *Journal of Geotechnical Engineering* 1979; **105**(6):759–778.

22. Leroueil S, Vaughan PR. The general and congruent effects of structure in natural soils and weak rocks. *Géotechnique* 1990; **40**(3):467–488.
23. Gens A, Nova R. Conceptual bases for a constitutive model for bonded soils and weak rocks. *Proceedings of International Symposium on Hard Soils—Soft Rocks*, Athens, 1993; 485–494.
24. Lagioia R, Nova R. An experimental and theoretical study of the behaviour of a calcarenite in triaxial compression. *Géotechnique* 1995; **45**(4):633–648.
25. Rouainia M, Muir Wood D. A kinematic hardening constitutive model for natural clays with loss of structure. *Géotechnique* 2000; **50**(2):153–164.
26. Kavvadas M, Amorosi A. A constitutive model for structured soils. *Géotechnique* 2000; **50**(3):263–274.
27. Gajo A, Muir Wood D. A new approach to anisotropic bounding surface plasticity: general formulation and simulations of natural and reconstituted clay behaviour. *International Journal for Numerical and Analytical Methods in Geomechanics* 2001; **25**:207–241.
28. Liu MD, Carter JP. A structured Cam Clay model. *Canadian Geotechnical Journal* 2002; **39**:1313–1332.
29. Nova R, Castellanza R, Tamagnini C. A constitutive model for bonded geomaterials subject to mechanical and/or chemical degradation. *International Journal for Numerical and Analytical Methods in Geomechanics* 2003; **27**: 705–732.
30. Roscoe KH, Burland JB. On the generalized stress–strain behaviour of 'wet' clay. *Engineering Plasticity*. Cambridge University Press: Cambridge, 1968; 553–609.
31. Brinkgreve RBJ. *PLAXIS, Finite Element Code for Soil and Rock Analyses, 2D-Version* 8. Balkema: Rotterdam, 2002.
32. Brinkgreve RBJ. Geomaterial models and numerical analysis of softening. *Doctoral Dissertation*, Delft University of Technology, 1994.
33. Cecconi M, DeSimone A, Tamagnini C, Viggiani GMB. Constitutive model for granular materials with grain crushing and its applications to a pyroclastic soil. *International Journal for Numerical and Analytical Methods in Geomechanics* 2002; **26**:1531–1560.
34. Zentar R, Karstunen M, Wheeler SJ. Influence of anisotropy and destructuration on undrained shearing of natural clays. *Proceedings of the 5th European Conference on Numerical Methods in Geotechnical Engineering (NUMGE)*, Paris. Presses de l'ENPC/LCPC: Paris, 2002; 21–26.
35. Vermeer PA. A double hardening model for sands. *Géotechnique* 1978; **28**(4):413–433.
36. Rowe PW. Theoretical meaning and observed values of deformation parameters for soil. *Proceedings of the Roscoe Memorial Symposium*, Cambridge, U.K. Cambridge University Press: Cambridge, 1971; 143–194.
37. Zentar R, Karstunen M, Wiltafsky C, Schweiger HF, Koskinen M. Comparison of two approaches for modelling anisotropy of soft clays. *Proceedings of the 8th International Symposium on Numerical Models in Geomechanics (NUMOG)*, Rome. Balkema: Lisse, 2002; 115–121.
38. Wiltafsky C. S-CLAY1S. User defined soil model for PLAXIS. *Documentation*, University of Glasgow, October 2003.
39. Bažant ZP, Oh BH. Efficient numerical integration on the surface of a sphere. *Zeitschrift für Angewandte Mathematik und Mechanik (ZAMM)* 1986; **66**:37–49.
40. Sloan SW, Abbo AJ, Sheng D. Refined explicit integration of elastoplastic models with automatic error control. *Engineering Computations* 2001; **18**(1/2):121–154.
41. Vermeer PA, Van Langen H. Soil collapse computations with finite elements. *Ingenieur-Archiv* 1989; **59**:221–236.
42. Van Langen H, Vermeer PA. Automatic step size correction for non-associated plasticity problems. *International Journal for Numerical Methods in Engineering* 1990; **29**:579–598.
43. Leroueil S, Magnan J-P, Tavenas F. *Embankments on Soft Clays*. Ellis Horwood: Chichester, 1990.

A.3 List of publications

Journal papers:

A. YILDIZ, H. KRENN & M. KARSTUNEN Numerical modelling of a test embankment on vertical drains in Haarajoki, Finland. Submitted to Ground Improvement.

M. KARSTUNEN, C., WILTAFSKY, H., KRENN, F., SCHARINGER & H.F. SCHWEIGER (2006). Modelling the stress-strain behaviour of an embankment on soft clay with different constitutive models. International Journal of Numerical and Analytical Methods in Geomechanics 30(10): 953-982. ISSN 0363-9061

M. KARSTUNEN, H., KRENN, S.J., WHEELER, S.J., M. KOSKINEN & R. ZENTAR (2005). The effect of anisotropy and destructuration on the behaviour of Murro test embankment. ASCE International Journal of Geomechanics 5(2): 87-97. ISSN 1532-3461.

Conference papers:

D. KAMRAT-PIETRASZEWSKA, H. KRENN, N. SIVASITHAMPARAM & M. KARSTUNEN. (2008) The influence of anisotropy and destructuration on a circular footing. Proceedings of the BGA International Conference on Foundations, Dundee, Scotland, 24 – 27 June 2008. IHS BRE Press, 2008.

H. KRENN & M. KARSTUNEN (2007). 3D Modelling of footings on soft soil. Proc. Int. Workshop on Constitutive Modelling- Development, Implementation, Evaluation and application, 12-13th January 2007, Hong Kong, China. Yin et al (editors). Advanced Technovation Limited, Hong Kong. pp. 535-541.

H. KRENN, M. KARSTUNEN & A. AALTO (2006). 3D modelling of deep mixing. Proc. 4th International Conference on Soft Soil Engineering, October 4-6, Vancouver, Canada. Chan & Law (Editors). Taylor & Francis, Leiden. pp.649-656.

U. VOGLER, M. KARSTUNEN & H. KRENN (2006). Numerical modelling of deep mixing by volume averaging technique. Proc. 6th European Conf. Num. Meth. in Geotech. Eng (NUMGE), September 6-9, Graz, Austria. Schweiger (Editor). Taylor & Francis, Leiden. pp. 793-799.

H. KRENN, A. YILDIZ, (2006). Effect of anisotropy and destructuration on the settlement behaviour of an embankment and shallow footing constructed on soft soil. Advances in Civil Engineering. Istanbul, October 2006, Turkey.

A. YILDIZ, M. KARSTUNEN & H. KRENN (2006). Numerical modelling of vertical drains with advanced constitutive models. Proc. 6th European Conf. Num. Meth. in Geotech. Eng (NUMGE), September 6-9, Graz, Austria. Schweiger (Editor). Taylor & Francis, Leiden. pp. 835-841.

A. YILDIZ, M. KARSTUNEN, H. KRENN (2006). Effect of anisotropy and destructuration on the behaviour of an embankment constructed on soft soil. 11th Soil Mechanic and Foundation Engineering Turkish National Congress (ZM11) Turkey. (in Turkish)

M. KARSTUNEN, H. KRENN, U. VOGLER, H.F. SCHWEIGER, M. GÄB & G. PRIOL (2006). Numerical modelling of column-type ground improvement. Invited contribution in: Proc. ISSMGE TC36 Symposium on Rigid Inclusions in Difficult Soft Soil Conditions, 11-12 May 2006, Mexico City. Auvinet & al. (Editors). Sociedad Mexicana de Mecanica de Suelos, Mexico A.C. pp.38-43.

M. KARSTUNEN, H. KRENN & A. AALTO (2005). Recent advances in numerical modelling of deep-stabilized soil. Proc. International Conference on Stabilisation/ Solidification Treatment and Remediation. 12-13 April, Cambridge, UK. Al-Tabbaa & Stegemann (eds). Taylor & Francis Group, London. pp. 303-312.

H. KRENN, M. KARSTUNEN & A. AALTO (2005). 2D and 3D numerical analyses of deep-stabilized columns. Proc. Deep Mixing '05 (Int. Conf. on Deep Mixing – Best Practice and Recent Advances), May 23-25, Stockholm, Sweden. SD report 1 – 2,

Swedish Deep Stabilization Research Centre, c/o Swedish Geotechnical Institute, ISSN 1402-2036, Vol.1.2, 547-554.

H. KRENN, M. KARSTUNEN (2004). Influence of anisotropy and destructuration on embankment fill on deep stabilized soft soil. Proc. of IX International Symposium on Numerical Models in Geomechanics (NUMOG IX), 25-27 August, Ottawa, Canada. pp. 651-657.

M. KARSTUNEN & H. KRENN (2004). Deep-stabilized columns under embankment fill: 3D finite element analysis versus unit cell approach. Invited contribution in: Geotechnical Innovations, Stuttgart 25 June, 2004. VGE, Essen. pp. 337-347. ISBN 3-7739-5991-5

M. KARSTUNEN, F., GESTIN & H. KRENN (2003). Numerical modelling of deep-stabilized columns under embankment fill. International Workshop on Ground Improvement, Prague 29 August 2003. Satellite Conference of the 13th ECSMGE organised by the Technical Committee TC17 and TC9 of the ISSMGE (published as a CD version only).

H. KRENN, M. KARSTUNEN, S.J. WHEELER & R. ZENTAR (2003). Influence of anisotropy and destructuration on an embankment on soft clay. Proc. Int. Workshop on Geotechnics of Soft Soils- Theory and Practice, 17-19 September 2003, Noordwijkerhout, The Netherlands. pp. 293-298.

C. WILTAFSKY, F SCHARINGER, H.F. SCHWEIGER, H. KRENN, R. ZENTAR, M. KARSTUNEN, M. CUDNY, H.P. NEHER & P.A. VERMEER (2003). Results from a geotechnical benchmark exercise of an embankment on soft clay. Proc. Int. Workshop on Geotechnics of Soft Soils- Theory and Practice, 17-19 September 2003, Noordwijkerhout, The Netherlands. pp. 381-390.

C. WILTAFSKY, H.F. SCHWEIGER, H. KRENN., Application of a multilaminate model for the numerical analysis of a deep excavation problem in soft clay, In Vermeer et al. (eds.): Proc. Int. Workshop on Geotechnics of Soft Soils -Theory and Prac-